FACULTY OF SCIENCES
DEPARTMENT OF ORGANIC AND MACROMOLECULAR CHEMISTRY
LABORATORY FOR ORGANIC AND BIOORGANIC SYNTHESIS

GHENT UNIVERSITY

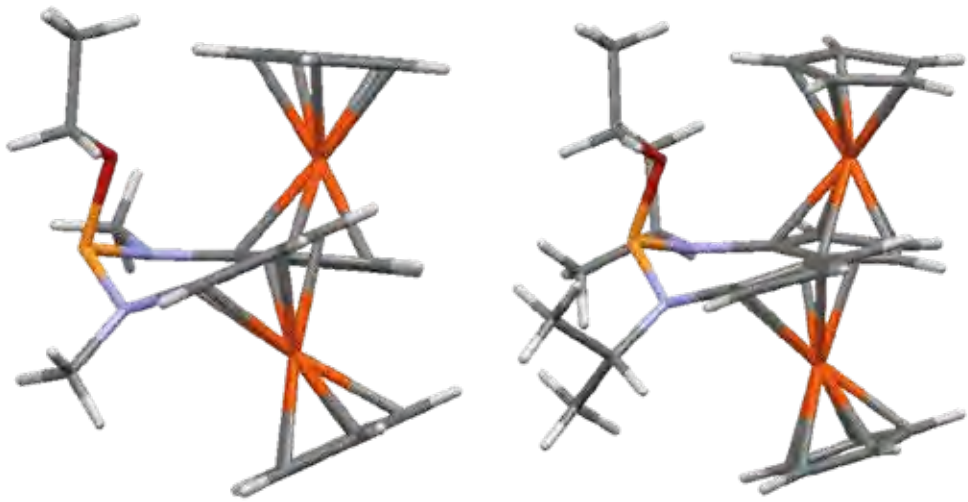

SYNTHESIS AND TESTING OF NOVEL CHIRAL BIFERROCENE-BASED LIGANDS FOR ASYMMETRIC TRANSITION METAL CATALYSIS

WIM KIMPE

Dissertation to obtain the degree of Doctor of Science: Chemistry

PROMOTOR: Prof. Dr. Johan Van der Eycken
CO-PROMOTOR: Prof. Dr. Ing. Timothy Noël

2020

FACULTY OF SCIENCES
DEPARTMENT OF ORGANIC AND MACROMOLECULAR CHEMISTRY
LABORATORY FOR ORGANIC AND BIOORGANIC SYNTHESIS

GHENT UNIVERSITY

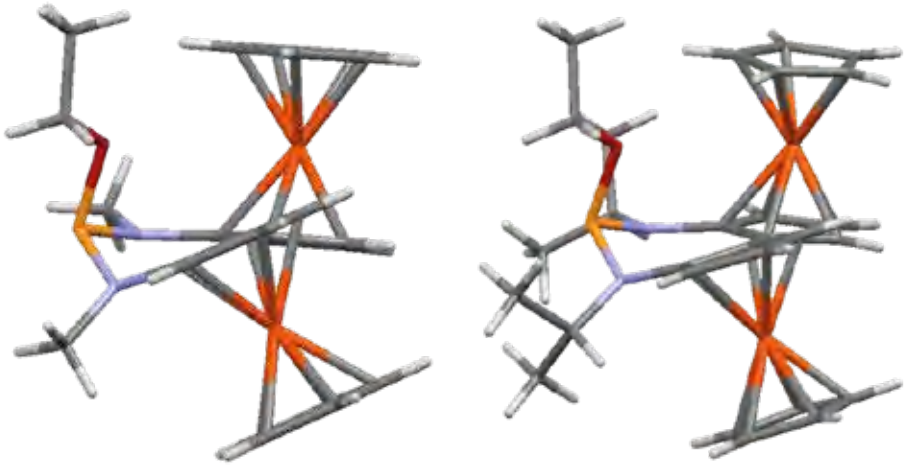

SYNTHESIS AND TESTING OF NOVEL CHIRAL BIFERROCENE-BASED LIGANDS FOR ASYMMETRIC TRANSITION METAL CATALYSIS

WIM KIMPE

Dissertation to obtain the degree of Doctor of Science: Chemistry

PROMOTOR: Prof. Dr. Johan Van der Eycken
CO-PROMOTOR: Prof. Dr. Ing. Timothy Noël

2020

Promotor:	Prof. Dr. Johan Van der Eycken (Ghent University)
Co-promotor:	Prof. Dr. Ing. Timothy Noël (Eindhoven University of Technology, Ghent University)
Examination board:	Prof. Dr. Frederic Lynen – Chairman (Ghent University) Prof. Dr. Johan Winne – Secretary (Ghent University) Dr. Jurgen Caroen (Ghent University) Prof. Dr. Ir. Matthias D'hooghe (Ghent University) Prof. Dr. Patrick Guiry (University College Dublin) Prof. Dr. Erik Van der Eycken (University of Leuven)

PREFACE - VOORWOORD

Nadat ik in 2012 mijn diploma *Master of Science in de chemie* behaalde, besloot ik om mij kandidaat te stellen als IWT-beursaal, welke mij zou toelaten een doctoraatsstudie uit te voeren. Op dat moment was het mij ook duidelijk dat ik graag het onderzoek dat ik reeds gestart was tijdens het finale jaar van mijn universitaire bachelor-master-opleiding wou verderzetten. Dit onderzoeksdomein betrof de synthese en valorisatie van nieuwe chirale liganden voor asymmetrische transitiemetaal katalyse. Bovendien was ik er eveneens van overtuigd dat ik dit onderzoek wou verderzetten aan de universiteit van Gent in het *Laboratorium voor Organische en Bioorganische Synthese* onder leiding van Professor Dr. Johan Van der Eycken. Nadat de betreffende beurs mij werd toegekend, kon ik in januari 2013 effectief beginnen met het experimentele werk van de doctoraatsstudie …

Ondertussen zijn de experimenten uitgevoerd, de resultaten geanalyseerd, verwerkt en beschreven in dit proefschrift. Dit was natuurlijk niet mogelijk zonder de aanzienlijke fundamentele bijdragen van een aantal belangrijke personen. Graag zou ik willen starten met het bedanken van Dr. Pieter Janssens en Dr. Katrien Bert. Zij introduceerden mij in de boeiende wereld van de moleculaire onderzoeks (a)symmetrie. Zij stonden mij bij met raad en daad en enkele discussies zal ik me blijven herinneren. Ook Nick Jacobs, Timoty De Cleyn en Dr. Jurgen Caroen verdienen een speciale vermelding. Zij waren gedurende de volledige vier jaar mijn naaste collega's. Daarnaast zijn er natuurlijk ook nog de andere 'afgezwaaide' doctors in de scheikunde met name Dr. Heba El Metwally, Dr. Sam Pieters, Dr. Karel-Simon Schlock en Dr. Dries Van den Bossche. In deze context verdient ook Dr. Fréderique Backaert een speciale vermelding. Gedurende lange tijd stond hij naast mijn zijde in het labo en wie, sta mij toe dit te zeggen, nogal snel begreep, hoe een bepaald experiment of reactie verliep. Naast de 'lokale' doctoraatsstudenten Bo Van de Moortel en Olivier Raes wil ik ook de talrijke bezoekende doctoraatsstudenten bedanken die een project in onze onderzoeksgroep hebben uitgevoerd. Mijn dank gaat eveneens uit naar de vele studenten die een mooie bijdrage leverden aan onze onderzoeksprojecten onder hen Christophe Pattyn, Sam Wackens, Stijn Heyndricx, Jordi Van der Gucht, Gianmarco Pisanò en Eva Papp. Zij hebben een actieve bijdrage geleverd aan de ontwikkeling van nieuwe chirale liganden binnen onze onderzoeksgroep. Bij sommige

van hen heb ik het genoegen gehad hen te begeleiden bij hun eerste ervaringen in een synthetisch onderzoekslaboratorium.

During my Ph.D. Study I had the great experience of doing research at the Laboratory of Professor Dr. Patrick Guiry at University College Dublin. During this short term exchange of eight months I worked on the same research topic with very competent researchers and other people. Special thanks in this context to my dear friends Kevin Gahan, Andrea Zanetti, and Brendán De Róiste.

Graag zou ik ook Jan Goeman bedanken voor het opnemen van tal van LC-MS-, chirale LC- en GC-stalen. Professor Dr. Kristof Van Hecke verdient een speciale vermelding omwille van de samenwerking voor XRD-analyses. Tot slot wil ik de professoren bedanken die mij tijdens mijn periode als doctoraatsstudent hebben bijgestaan, mijn promotor professor Dr. Johan Van der Eycken, mijn co-promotor Professor Dr. Ing. Timothy Noël en mijn gastheer in Dublin, Professor Dr. Patrick Guiry.

Wim Kimpe,
March, 2020

TABLE OF CONTENTS

LIST OF ABBREVIATIONS

#

2D	two dimensional
3D	three dimensional
°	degrees

A

AAA	asymmetric allylic alkylation or asymmetric allylic amination
Å	Angström
Ac	acetyl
Acac	acetylacetonate
ANDEN	anthracenyldiaminoethylene
APCI	atmospheric pressure chemical ionisation
APT	attached proton test
app	appearing
Aq	aqueous
Ar	aryl
atm	atmosphere

B

BINAP	2,2'-bis(diphenylphosphino)-1,1''-binaphthalene
BINOL	2,2'-dihydroxy-1,1'-dinaphthyl
BIFEP	2,2'-bis(dipheny1phosphino)-1,l'-biferrocene
Bn	benzyl
Boc	*tert*-butyloxycarbonyl
BPE	1,2-bis-(phospholano)ethane
br	broad
BSA	*N,O*-bis-(trimethylsilyl)acetamide
Bu	butyl
BuLi	butyllithium
Bz	benzoyl

C

C	Celsius
ca.	circa
Cbz	carboxybenzyl
CCD	charge coupled device
CDI	1,1'-carbonyldiimidazole
cf.	confer
CHIRAPHOS	2,3-bis(diphenylphosphino)butane
CE	capillary electropheresis
CIP	Cahn-Ingold-Prelog
cod	1,5-cyclooctadiene
Cp	cyclopentadiene
CSA	camphorsulfonic acid
CSP	chiral stationary phase
CuTC	copper(I)-2-thiophene carboxylate
Cys	L-cysteine

D

D	dextrorotatory (generally used for molecules)
d	dextrorotatory (generally used for minerals) or doublet
DAAA	decarboxylative asymmetric allylic alkylation
DACH	diaminocyclohexyl
DAD	diode array detector
DCC	*N,N'*-dicyclohexylcarbodiimide
DCE	dichloroethane
dba	dibenzylideneacetone
DCM	dichloromethane
DDQ	2,3-dichloro-5,6-dicyano-*para*-benzoquinone
de	diastereomeric excess
DET	diethyltartrate
DFT	density functional theory
DIAPHOX	diamino phosphinoxide
DIBAL	di-*iso*-butylaluminium hydride
DIOP	4,5-bis(diphenylphosphinomethyl)-2,2-dimethyl-1,3-dioxolane
DIPAMP	1,2-Bis[(2-methoxyphenyl)(phenylphosphino)]ethane
DIPEA	*N,N*-di-*iso*-propylethylamine
DKR	dynamic kinetic resolution
DMAP	4-dimethylaminopyridine
DMF	*N,N*-dimethylformamide
DMG	directing metalation group

DMSO	dimethyl sulfoxide
DNA	deoxyribonucleic acid
DoM	directed *ortho*-metalation
DOPA	3,4-dihydroxyphenylalanine
DPPA	diphenyl phosphoryl azide
DSM	dutch state mines

E

e^-	electron
E	electrophile
E	entgegen
E. coli	Escherichia coli
EDCI	1-ethyl-3-(3-dimethylaminopropyl)carbodiimide
ee	enantiomeric excess
e.g.	exempli gratia
EI	electron impact
er	enantiomeric ratio
ELLE	enantioselective liquid-liquid extraction
eq	equivalent(s)
ESI	electrospray ionisation
et al.	et alii
Et	ethyl
Et_2O	diethyl ether
EtOAc	ethyl acetate

F

Fc	ferrocene (or ferrocenyl)
FDA	food & drug administration
Fem	ferrocenylmethyl
FT-IR	Fourier transform infrared

G

g	gram
GC	gas chromatography

H

h	hour(s)
HATR	horizontal attenuated total reflection
HBTU	*O*-(benzotriazol-1-yl)-*N,N,N′,N′*-tetramethyluronium hexafluorophosphate (hexafluorophosphate benzotriazole tetramethyl uranium)
HIV	human immunodeficiency virus
HMDS	bis(trimethylsilyl) amide
HOBT	hydroxybenzotriazole
HOMO	highest occupied molecular orbital
HPLC	high performance liquid chromatography
HRMS	high resolution mass spectrometry
Hz	Hertz

I

INTENANT	integrated synthesis and purification of enantiomers
i-Pr	*iso*-propyl
IR	infrared
IUPAC	International Union of Pure and Applied Chemistry

J

J	Joule
J	coupling constant NMR

K

K	Kelvin
k	rate determining step or kilo
KR	kinetic resolution

L

L	liter or ligand
L	levorotatory (generally used for molecules)
l	levoratatory (generally used for minerals)
LC	liquid chromatography
L-DOPA	L-3,4-dihydroxyphenylalanine
LDA	lithium di-*iso*-propylamide
LTB_4	leukotriene B_4
LUMO	lowest unoccupied molecular orbital

M

M	metal/transition metal or molar
M	minus
m	milli or multiplet
m	meta
m/z	mass over charge

µ	micro
*m*CPBA	*meta*-chloroperoxybenzoic acid
Me	methyl
MED	male erectile dysfunction
min.	minute(s)
Mol. Sieves	molecular sieves
MS	mass spectrometry
Ms	mesyl
MTBE	methyl *tert*-butyl ether
MW	microwave

N

n	normal
na	not applicable
nd	not determined
$NaBAr_F$	sodium-tetrakis[3,5-bis(trifluoromethyl)phenyl]borate
NAD^+	nicotinamide adenine dinucleotide
NADH	nicotinamide adenine dinucleotide-H
NBS	*N*-bromosuccinimide
n.d.	not determined
NMP	*N*-methyl-2-pyrrolidone
NMR	nuclear magnetic resonance
NOE	nuclear Overhauser effect
NOESY	nuclear Overhauser effect spectroscopy
υ	frequency

O

o	ortho
ORTEP	oak ridge thermal ellipsoid plot
OTf	triflate

P

P	plus
p	page
p	para
P. pastoris	Pichia pastoris
Pa	pascal
PG	protecting group
Ph	phenyl
Ph.D.	doctor of philosophy
Phox	phenyloxazoline
Piv	pivaloyl
pKa	acid dissociation constant
ppm	parts per million
Pr	propyl
PTSA	*para*-toluenesulfonic acid
Pyr	pyridine

Q

q	quadruplet

R

R	alkyl
R	rectus
R_a	axial chiral molecule with axial rectus (*R*)-configuration
R_p	planar-chiral molecule with planar rectus (*R*)-configuration
rac	racemic
RDS	rate determining step
rel	relative
Ref	reference
R_f	ratio to front
RNA	ribonucleic acid
RT	room temperature

S

S	sinister
S_a	axial chiral molecule with axial sinister (*S*)-configuration
S_p	planar-chiral molecule with planar sinister (*S*)-configuration
s, sec	secondary
s	singlet
spt	septuplet
SALEN	*N,N'*-bis(salicylaldehydo)ethylenediamine
S/C	substrate over catalyst
SMB	simulated moving bed

T

θ_p	cone angle
TML	Trost modular ligand
t, tert	tertiary
t	triplet
TADDOL	α,α,α',α'-tetraaryl-2,2-disubstituted 1,3-dioxolane-4,5-dimethanol

TBAB	tetra-*n*-butylammonium bromide
TBAF	tetra-*n*-butylammonium fluoride
TBAI	tetra-*n*-butylammonium iodide
TBDMS	*tert*-butyldimethylsilyl
t-Bu	*tert*-butyl
Tf	triflyl
TFA	trifluoroacetic acid
TFAA	trifluoroacetic anhydride
THF	tetrahydrofuran
TLC	thin layer chromatography
TMEDA	*N,N,N′,N′*-tetramethylethylenediamine
TMM	trimethylenemethane
TMS	trimethylsilyl
TOF	turnover frequency
TOF-MS	time of flight mass spectrometry
TON	turnover number
TRAP	*trans*-chelating phosphines
t_R	retention time
Ts	tosyl
TTMS	tetramethylsilaan

U

UHP	ureum hydrogen peroxide
UV	ultraviolet

V

vs.	versus

X

XRD	X-ray diffraction
X	anionic ligand

Z

Z	zusammen

INTRODUCTION

"Dans les champs de l'observation le hasard ne favorise que les esprits préparés."

"In the field of observation, chance only favors those minds which have been prepared."

Louis Pasteur, University of Lille, France, 1854

1.1. Chirality, Enantiomers and Diastereomers

The term 'chiral' was introduced into science by Lord Kelvin (William Thompson) in 1904 during the *Baltimore Lectures on Molecular Dynamics and the Wave Theory of Light*[1]:

"I call any geometrical figure, or group of points, chiral, and say it has chirality, if its image in a plane mirror, ideally realized cannot, be brought to coincide with itself."

This means that the word chiral is used to describe an object that is non-superimposable on its mirror image. The origin of the word chirality should be found in the Greek language: χειρ (/cheir/), which is the meaning for hand. Our hands are indeed the most common examples of chiral objects. Another example of macroscopic chirality is illustrated in Figure 1.1 (a), both shells of the sea snail Neptunae Despecta exist as mirror images and can never coincide by any manual, spatial operation. Chirality is not only known in the macroscopic world but it also occurs in the microscopic world. This similarity between our hands and molecules, here amino acids, is elucidated in Figure 1.1 (b). The non-superimposable nature of chiral molecules is also exemplified in Figure 1.1 (c), which represents the image and mirror-image of chiral tartaric acid. D-Tartaric acid **1.01** occurs naturally in plants, e.g. grapes, while L-tartaric acid **1.02** is much more rare. Nowadays chirality is a very important phenomenon in (synthetic) chemistry and is defined by IUPAC as:[2]

"The geometric property of a rigid object (or spatial arrangement of points or atoms) of being non-superimposable on its mirror image; such an object has no symmetry ele-

ments of the second kind (a mirror plane, a center of inversion or a rotation-reflection axis). If the object is superimposable on its mirror image the object is described as being achiral."

Figure 1.1 (a) Macroscopic chirality illustrated by the shells of sea snails[3] **(b)** Comparison between macroscopic and molecular chirality elucidated by hands and amino acids[4] **(c)** Molecular chirality exemplified by the D- and L-enantiomers of tartaric acid

Chiral molecules which are related as image and mirror-image, such as D-tartaric acid and L-tartaric acid, are called enantiomers. The chemical composition and connectivity of the constituent atoms are the same but the spatial orientation is different. Most of the chemical and physical properties such as reactivity, enthalpy of formation, molecular weight, polarity, *etc*., are equal for both enantiomers. Nevertheless, there is one physical property that makes a distinction between two enantiomers possible: enantiomers rotate the plane of polarized light in opposite directions. This phenomenon allowed to make a differentiation between enantiomers and assign each of both with a different label. The enantiomer that rotates the plane-polarized light to the right, corresponding to a positive rotation, is called the (+)-enantiomer (or dextrorotatory enantiomer) while the enantiomer that causes a rotation to the left, corresponding to a negative rotation, is called the (-)-enantiomer (or levorotatory enantiomer). Another nomenclature method based on rotation of plane-polarized light uses stereodescriptors D and L. This methodology is based on an arbitrary convention according to glyceraldehyde, one of the simplest chiral molecules. The two enantiomers of glyceraldehyde were given the labels D (for dextro, because it was the (+)-enantiomer) and L (for Levo, because it was the (-)-negative enantiomer). Any enantiomer that could be related, by a series of chemical transformations, to D-(+)-glyceraldehyde was labelled with stereodescriptor D, although it could have a negative rotation of plane-polarized light itself. Any enantiomer that could be related to L-(-)-glyceraldehyde was labelled with stereodescriptor L. This means that there is no straight relationship between the DL-nomenclature and the (+)-(-)-nomenclature. L-tartaric acid for example causes a positive rota-

tion of plane-polarized light (or dextrorotation) and therefore it is sometimes labeled as L-(+)-tartaric acid. In the same way, D-tartaric acid causes a negative rotation of polarized light and it is labeled as D-(-)-tartaric acid. A third nomenclature was introduced 'recently' (in the '50 and '60 of last century) by Cahn, Ingold and Prelog.[5] They developed the priority rules, known as CIP-rules, which allow to denote an enantiomer with stereodescriptor *R* (rectus, right) and its opposite enantiomer as *S* (sinister, left). An equimolar mixture of both enantiomers of a certain compound is known as a racemic mixture or racemate. To indicate that a mixture is racemic the prefixes (±) or *rac* or the symbols *RS* or *SR* are used. When only one of both enantiomers is present in a sample, the compound is known to be enantiomerically pure or enantiopure. A sample of a chiral substance whose enantiomeric ratio (*er*) is greater than 50/50 but less than 100/0 is called enantiomerically enriched or enantioenriched. The optical purity of these type of mixtures is generally indicated by the enantiomeric excess (*ee*) expressed in percentage and which can mathematically be defined as:

$$ee\ (\%) = \frac{|[R] - [S]|}{[R] + [S]} * 100$$

If a molecule has two or more asymmetric (chirality) elements more stereoisomers can be formed. A maximum of 2^n different stereoisomers, with *n* the number of chiral elements present in the compound, exists. When two or more stereoisomers of a certain molecule have a different configuration at one or more, but not all, stereocenters they are called diastereomers (or diastereoisomers). These isomers are not mirror images of each other and hence are not enantiomers. Moreover, the chemical and physical properties of diastereomers are mutually different. If two diastereomers differ from each other at only one stereocenter they are called epimers.

In 1811, the mathematician-physician Arago discovered the phenomenon of optical activity by observation of colors in plane-polarized light transmitted through a quartz crystal.[6] One year later the physicist Biot confirmed that the effect was due to the rotation of the plane of polarized light.[7] He also discovered that natural quartz exists in two forms, which rotate the plane of polarization in opposite directions. Some crystals rotate the plane of polarized light to the right (dextrorotatory, *d*) while others rotated it to the left (levorotatory, *l*). Later on, Biot observed the optical activity of certain natural organic compounds in solution (including tartaric acid), in liquid and gas phase.

This was a decisive step since the observed phenomenon could no longer be explained by the molecular arrangement in the crystal but rather by an intrinsic property on the molecular level. In 1848, an explanation was established by Pasteur, based on his experiments with tartaric acid salts. He first noticed that solutions of racemic sodium ammonium tartrate did not rotate the plane of polarized light. After crystallization of the solutes he found out that two types of asymmetric enantiopure crystals were formed, of which one type rotates the polarized light in a dextrorotatory manner while the other form is levorotatory and which can be separated by hand. This is a very laborious scientific job which requires a lot of dedication, practical skills, and of course fundamental knowledge of chemistry and crystallography. This rare phenomenon is called spontaneous resolution and the salt itself is a conglomerate, which is a 50/50 mixture of two crystalline enantiomers that are mechanically separable. IUPAC defines a conglomerate as[8]:

An equimolar mechanical mixture of crystals each one of which contains only one of the two enantiomers present in a racemate.

In 1857, Kekulé published a paper on the tetravalence of carbon atoms[9] and in 1874, Le Bel and van 't Hoff found that carbon atoms have a tetrahedral arrangement of their surrounding groups.[10] Together, these two discoveries gave theoretical support on the asymmetric carbon atom and the existence of enantiomers.

Nature and biomolecules are build-up of chiral molecules. DNA and RNA for example contain chiral sugars with a uniform stereochemistry, proteins consist of chiral L-amino acids, … The word used to describe the fact that these biomolecules are made of chiral building blocks with a well-defined consistent stereochemistry is homochirality. Although its origin is still a topic of scientific discussion, it is generally accepted that it is a fundamental property of life.[11] Because of the concept of homochirality, enantiomers interact differently with these large biomolecules in biological pathways, with a different biological response as a result. This is illustrated by the thalidomide tragedy of 1954-1962, which is one of the best known examples where two enantiomers have distinctly different biological activity. Thalidomide (Figure 1.2 (a)) commercially available under the brand name Softenon®, was thought to be a wonder drug (tranquilizer) for treating insomnia, coughs, colds and headaches. It was also prescribed as an antiemetic for pregnant women against morning sickness. The (*R*)-enantiomer of thalidomide has the desired activity, while the (*S*)-enantiomer is teratogenic (which was unknown

at that time). Thalidomide was sold as a racemic mixture, and as a result children with physical disabilities were born (Figure 1.2 (b)). Unfortunately, the Softenon® tragedy could not have been avoided by selling it as the enantiopure (*R*)-enantiomer because the chiral center is unstable at low acidity (*cf*. human stomach) with *in vivo* racemization as a consequence.[12] Nevertheless this tragic story resulted in a revolution in the pharmaceutical world due to the increasing awareness of the importance of stereochemistry in biologically active compounds. Moreover, the Food and Drug Administration (FDA) improved their policy in such a way that both enantiomers of a chiral drug should be toxicologically screened *in vitro* as well as *in vivo* at an early stage in drug development.[13]

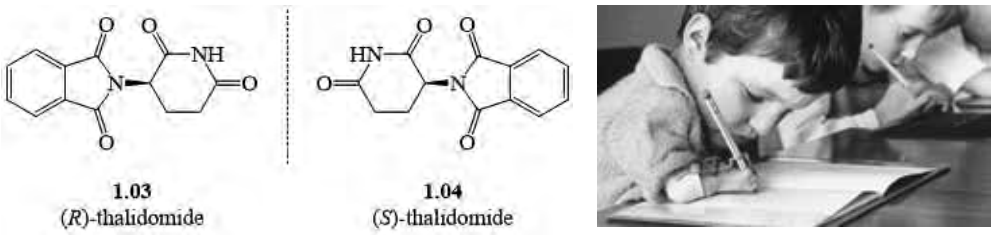

Figure 1.2 (a) (*R*)- and (S)-enantiomers of thalidomide **(b)** *'Thalidomide child'* with the typical physical disabilities[14]

Ibuprofen, a popular non-steroidal, anti-inflamatory medicine, is an example of a drug which has been sold as a racemic mixture, although only the (*S*)-enantiomer is biologically active.[15] Just like thalidomide, ibuprofen is racemized *in vivo*. Although the opposite enantiomer has no dramatic side-effects and selling the drug as a racemate is a responsible choice.

A more pleasant case of different biological activity of enantiomers are sex attractants (or pheromones) of insects, which are chiral chemical messengers. An example of such a pheromone is olean, Figure 1.3 (a), which is excreted by the olive fruit fly (*Dacus oleae*). Research has shown that males only respond to (*R*)-(-)-olean **1.05** whereas females are only attracted by (*S*)-(+)-olean **1.06**.[16]

The receptors in our nose are also made up of chiral molecules and two enantiomers of a certain compound can have a different biological response when inhaled. A 'classic example' of 'enantiomers' having a distinctive smell is limonene, Both the (*R*)- and (*S*)-enantiomers are naturally occurring terpenes (Figure 1.3 (b)). (*R*)-Limonene **1.07** extracted from orange peels has the typical sweet smell of oranges, while (*S*)-limonene

1.08 extracted from lemon peels has the typical sour lemon smell. It should be mentioned that when these compounds are obtained synthetically or via (gas) chromatographic purification, they have a piny, turpentine, wood smell. However, natural (*R*)- and (*S*)-limonene obtained via extraction from orange and lemon peels contain minor impurities giving them the typical sweet and sour smell.

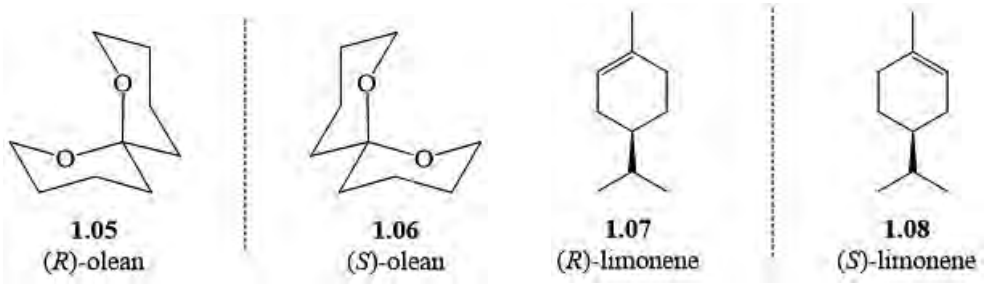

Figure 1.3 (a) Sex pheromones (*R*)-olean for female and (S)-olean for male olive fruit flies **(b)** (*R*)-limonene extracted from oranges and (S)-limonene extracted from lemons

1.2. Types of Chirality and Chirality Elements

1.2.1. Stereo-, Stereogenic-, Asymmetric- and Chiral Center

Before proceeding to a detailed description of the different types of chirality, more terminology has to be introduced. Different definitions of multiple terms in the field of stereochemistry can be found in different handbooks and some of them are indeed ambiguous. Moreover, the chirality and stereochemistry from some of the proposed ligands further on in this thesis are complex. Therefore it is necessary to define these terms precisely.

For carbon atoms, a chiral center or stereocenter is (generally) defined as a tetrahedral carbon center which is bonded to four different atoms or groups of atoms. It is important to realize that these two terms are used to describe the same phenomenon based on two different concepts. From § 1.1 it is clear that chirality, and associated with this the concept of a chiral center, is based on a fundamental property of objects and molecules itself: being non-superimposable on its mirror image. The terminology of a stereocenter is based on stereoconnectivity and the spatial arrangement of bonds around the carbon atom. A more detailed explanation makes the difference between a center that can be chirotopic or achirotopic on one side, and stereogenic or astereogenic on

the other side. A chirotopic atom is one that resides in a chiral environment. An achirotopic atom is one that is found in an achiral environment. If one wants to know if a particular atom is chirotopic or achirotopic one has to find out whether it is part of a rotation-inversion axis, S_n. If this is true, this particular center is achirotopic. If this is not the case, the center is chirotopic. On the other hand, if one wants to find out if a particular atom is stereogenic one has to check if a different stereoisomer is created by the interchange of two substituents. If this is true this center is stereogenic, otherwise it is astereogenic. This terminology can be elucidated based on the example of different stereoisomers of 2,3,4-trihydroxypentanedioic acid by using Fischer projections, shown in Figure 1.4-Figure 1.7.

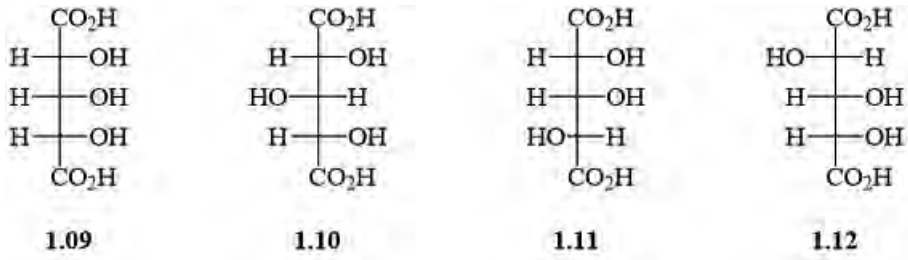

Figure 1.4 Different stereoisomers of 2,3,4-trihydroxypentanedioic acid (Fisher projections)

Figure 1.5 starts with the example of diastereomer **1.09** of 2,3,4-trihydroxypentanedioic acid. An interchange of the two ligands on the red carbon atom results into another diastereomer, which is epimer **1.10**. This means that this carbon center is definitely stereogenic. The next question is whether this center is chirotopic or achirotopic. In other words, is this center part of an S_n-axis or not. Making the mirror image of isomer **1.09** gives **1.13** as a result. After a rotation of 180° the original molecule **1.09** is obtained again which means that structure **1.13** is identical to **1.09**. Consequently, there is a mirror plane through the red carbon atom, perpendicular to the sheet, which makes that this carbon atom is found in an achiral environment. In other words, this red carbon is part of a S_1-axis. Consequently this carbon is an achirotopic center and therefore it may not be identified as a stereocenter or chiral center. Only when a specific carbon center is stereogenic and chirotopic at the same time and when it is bonded to four different atoms or atom groups, it can be correctly labeled as a stereocenter or a chiral center. Sometimes such a carbon center is also called an asymmetric carbon atom. This terminology was introduced by van't Hoff and is generally considered as old language.

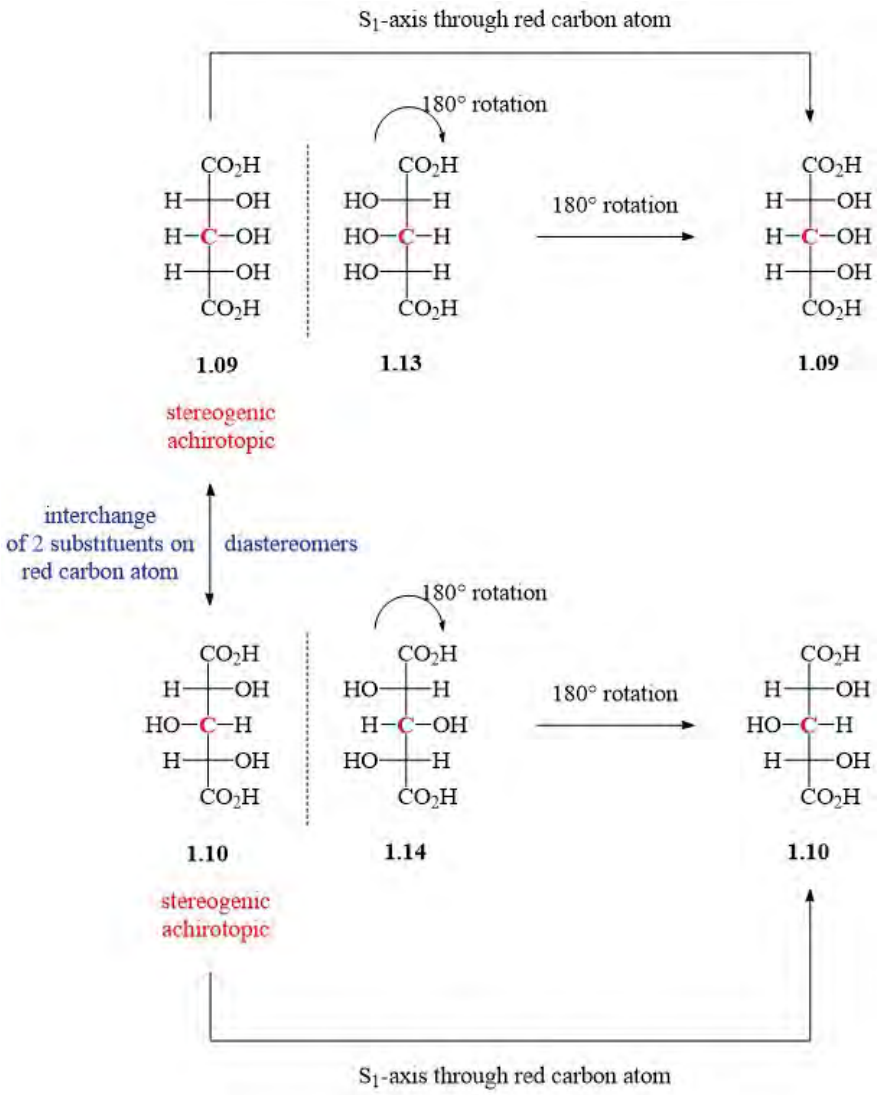

Figure 1.5 Elucidation of an achirotopic, stereogenic carbon center in 2,3,4-trihydroxypentanedioic acid

Now let us apply the same rationale for stereoisomer **1.11**, represented in Figure 1.6. Making the mirror image of **1.11** results in isomer **1.15**. Rotation of 180° for this molecule does not generate structure **1.11** again. This means that structures **1.11** and **1.15** are not identical but enantiomers. Consequently, there is no S_n-axis through the red carbon atom what makes that this atom is found in a chiral environment. Therefore it is chirotopic. The next question is whether this red carbon center is stereogenic or astereogenic. An interchange of the two substituents on this specific red carbon atom of

1.11 results in **1.12**. When studying these two molecules in more detail it can be seen that via a rotation of 180° of **1.12** the initial isomer **1.11** can be formed again. This means that these structures are identical and therefore this red carbon is astereogenic. Consequently, this carbon atom is, again, not a stereocenter or chiral center, nor an asymmetric carbon atom.

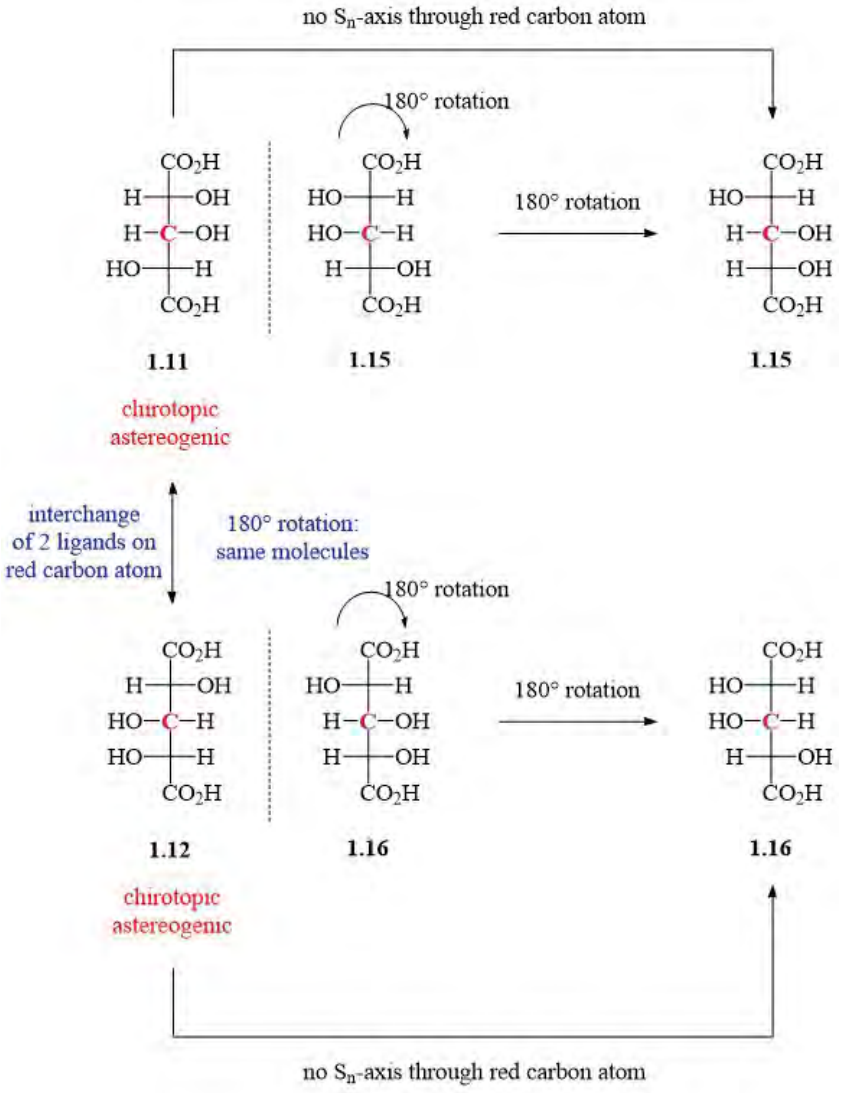

Figure 1.6 Elucidation of a chirotopic, astereogenic carbon center in 2,3,4-trihydroxypentanedioic acid

Despite the examples elucidated above, all isomers of 2,3,4-trihydroxypentanedioic acid do have stereocenters. This is explained in Figure 1.7 with structure **1.11** as an

example. Now, the focus is on the carbon atom indicated in green. This atom is bonded to four different atom groups. An interchange of the two ligands on this green carbon atom results into another diastereomer, which is epimer **1.09**. This means that this carbon center is definitely stereogenic. Making the mirror image of **1.11** results in structure **1.15**. A rotation of 180° does not result in structure **1.11**, but as already mentioned, molecules **1.15** and **1.11** are enantiomers of each other. Consequently, there is no S_n-axis through the green carbon atom what makes that this atom is found in a chiral environment. Because this carbon atom is stereogenic as well as chirotopic and bonded to four different atom groups, it is (correctly) called a stereocenter or chiral center or asymmetric carbon atom. In conclusion, for molecules **1.09**-**1.11**, the two carbon atoms next to the central one are stereogenic, chirotopic and are connected to four different atom groups. Consequently these can all be correctly identified as stereocenters.

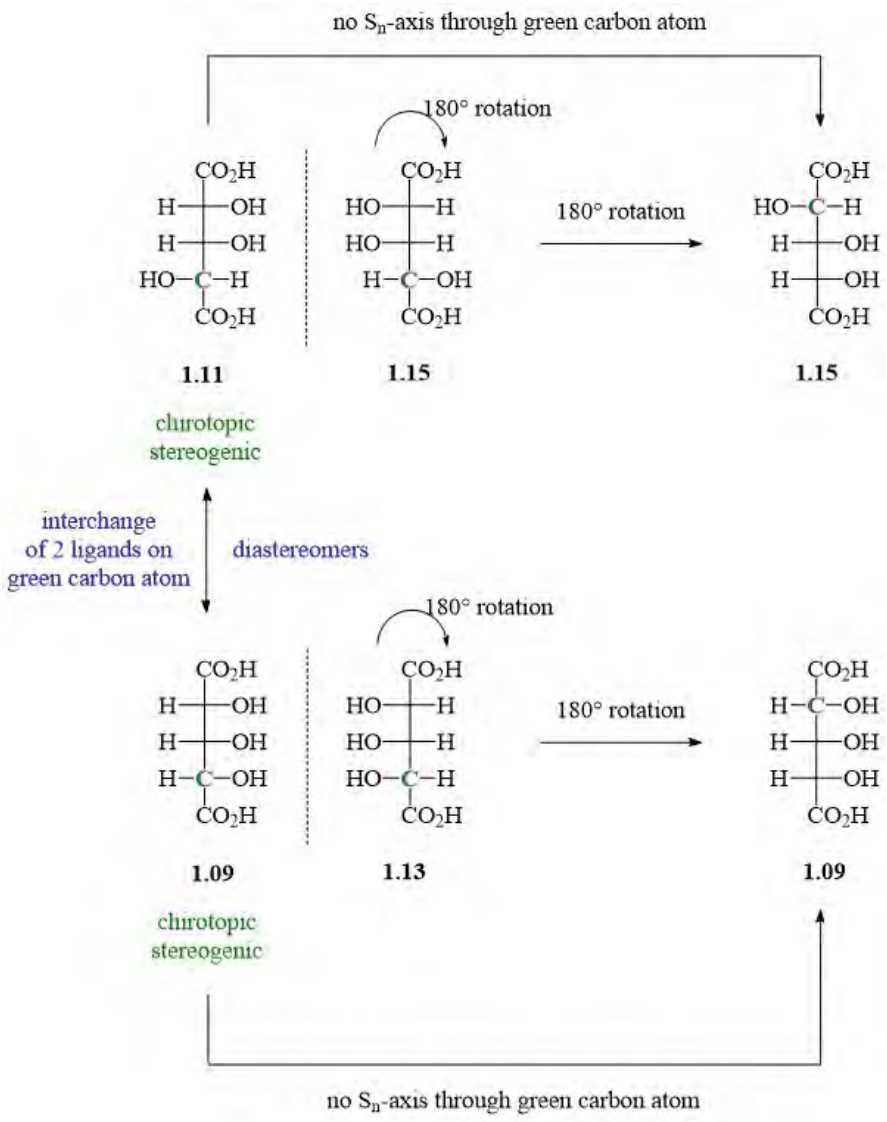

Figure 1.7 Elucidation of a stereocenter in 2,3,4-trihydroxypentanedioic acid

So far the focus of this section was on carbon centers and carbon atoms and not on chiral molecules itself. Therefore it is useful to consider structures **1.09** and **1.10** again. As said before these isomers possess a mirror plane (S_1-axis) through the central carbon atom (indicated in red in Figure 1.5) and the two carbon atoms next to this one are stereocenters. However, because of the S_1-axis, these molecules themselves are achiral (and symmetric). Therefore these molecules are optically inactive. These type

of molecules are also called *meso compounds*. They are defined by IUPAC as the achiral member (or members) of a set of diastereomers which also includes one or more chiral members.[17] On the other hand it is possible that a molecule is chiral without having a stereocenter, chiral center or asymmetric carbon atom. An example is shown in Figure 1.8, where the carbon atom highlighted in red is sp hybridized. This center is stereogenic and chirotopic but it is not bonded to four different atoms or atom groups. Other examples of chiral molecules without a stereocenter will be discussed in § 1.2.3-1.2.5. To conclude, achiral molecules are recognized by the fact that they always possess a S_n-axis and they are always symmetric. Chiral molecules, however can be asymmetric as well as symmetric. Chiral symmetrical molecules are always recognized by the presence of a C_n-axis (n>1). Examples of these type will be described later on in this thesis (*cf.* § 1.4.2). Chiral asymmetrical molecules don't possess a S_n-axis nor a C_n-axis (n>1). Examples of this type are **1.11** and **1.15**.

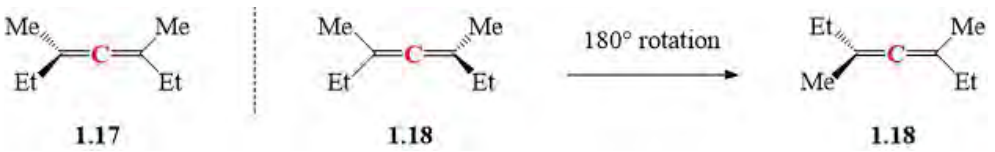

Figure 1.8 Example of a chiral molecule without a stereocenter but with a chirotopic, stereogenic carbon center

The example described in Figure 1.8 shows that there is in fact another 'phenomenon' responsible for the chirality of this molecule compared to all other chiral molecules described before in this thesis. All these previous examples possess a central point of chirality, whereas the molecule shown in Figure 1.8 possess an axis which is responsible for its chirality. Therefore it is useful to introduce the term chirality element (or an element of chirality), which can be defined as a general name for a chirality axis, a chirality center or a chirality plane. In the same way one can talk about stereogenic elements or stereogenic units. It is true that every enantiomeric molecule must possess at least one stereogenic element, although this is not sufficient to have a chiral molecule (*cf. meso compounds*). In general organic chemistry three basic types of stereogenic units, for molecular entities having not more than four substituents, are acknowledged by IUPAC[18]:

1. A grouping of atoms consisting of a central atom and distinguishable ligands, such that the interchange of two ligands leads to a different stereoisomer. *(stereogenic center)*

2. A chain of four non-coplanar atoms (or rigid groups), in a stable conformation, such that an (imaginary) rotation about the central bond leads to a different stereoisomer *(stereogenic axis)*. An example of a molecule that belongs to this type of compounds is **1.17**.
3. A grouping of atoms consisting of a double bond with substituents which give rise to *cis-trans* isomerism. *(stereogenic plane)*

However, It should be noted that these definitions are very precise and incomplete. For example, the definition of a stereogenic plane via *cis-trans* isomerism is restricted to double bonds whereas ring-systems are not included. The definition of a stereogenic axis based on a chain of four non-coplanar atoms is overly precise as well. This latter definition excludes one of the most famous molecules characterized by a stereogenic axis, BINAP (*vide infra* § 1.2.3). IUPAC defines a stereogenic unit also as a grouping within a molecular entity that may be considered a focus of stereoisomerism.[18] This definition seems to be superficial and does not focus on the main feature of molecules possessing a stereogenic unit. For these molecules stereoisomers are always created by a limited rotation caused by a stereogenic center, axis or plane present in the molecule itself.

1.2.2. Central Chirality or Point Chirality

A chiral center is a typical example to explain central chirality or point chirality. In general organic chemistry a chirotopic, tetrahedral carbon bonded to four different groups is a point (or center) responsible for chirality. In organometallic chemistry, more than four ligands can be bonded to the (transition) metal center and the concept of central chirality has to be expanded: a specific center of which none of the surrounded ligands is the same, will function as a point of chirality. Examples of molecules possessing a chiral center are shown in this thesis before like thalidomide, limonene and olean (*cf*. Figure 1.2 and Figure 1.3, § 1.1).

1.2.3. Atropisomerism and Axial Chirality

Atropisomerism is a Greek word containing *'atropos'* and *'isomerism'*. The concept of isomerism and isomers is already introduced before in § 1.1. *'Atropos'* literally means 'without turn'. As a consequence, atropisomers are formed because of a restricted rotation around a single bond. This means that atropisomers are conformational isomers

where energy differences due to steric hindrance are responsible for a rotation barrier such that isolation of the individual conformers is possible. Typically this phenomenon is observed at lower temperatures. At higher temperatures the rotation energy has reached the limit where free rotation is possible which results in an achiral molecule. Although the existence of atropisomers was described, via experiments with the tetrasubsituted biphenyl atropisomers **1.19** and **1.20** (Figure 1.9), by Christie and Kenner in 1922[19], the word atropisomerism was only introduced in 1933 by Kuhn[20]. Later on, Ōki further refined the definition of atropisomers taking into account the dependence on temperature associated with the interconversion of conformers, specifying that atropisomers interconvert with a half-life of at least 1000 seconds at a given temperature, what corresponds to an energy barrier of 93 kJ mol^{-1} at 300 K.[21]

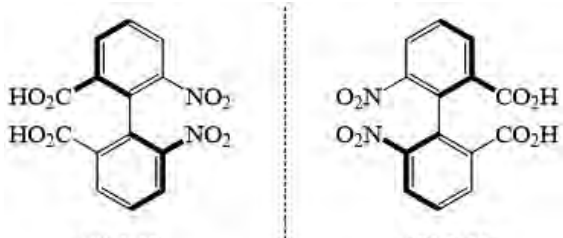

(*S*)-**1.19** (*R*)-**1.20**

Figure 1.9 First isolated atropisomers of tetrasubstituted bifenyl compounds by Christie and Kenner[19]

For those atropisomers where it is impossible to overcome the energy barrier for rotation, even at high temperatures, the term axial chirality was introduced into the field of stereochemistry. This terminology is used to refer to stereoisomerism resulting from the non-coplanar arrangement of the groups in pairs around a chirality axis. The most common stereodescriptors used to differentiate between two axial chiral enantiomers are *R* and *S*. Although sometimes R_a and S_a, where *a* stands for axial, and even the *P*, *M* nomenclature (*vide infra* § 1.2.5) are used. The best-known molecule that possesses axial chirality is BINAP, of which the enantiomers are shown in Figure 1.10 (a). These diphosphine ligands, both commercially available, have proven to be very successful in different asymmetric transition metal catalyzed reactions. Certain transition metal complexes with ferrocene ligands are known to be axial chiral as well. Therefore these ligands have to possess two substituents on two different cyclopentadienyl rings. Ferrocene ligands that are recognized by such a 1,1'-disubstitution pattern do not obtain any form of chirality. However, upon complexation with a metal, axial chiral complexes are formed due to a restricted rotation of the two cyclopentadienyl ring systems (Figure 1.10 (b)).[22]

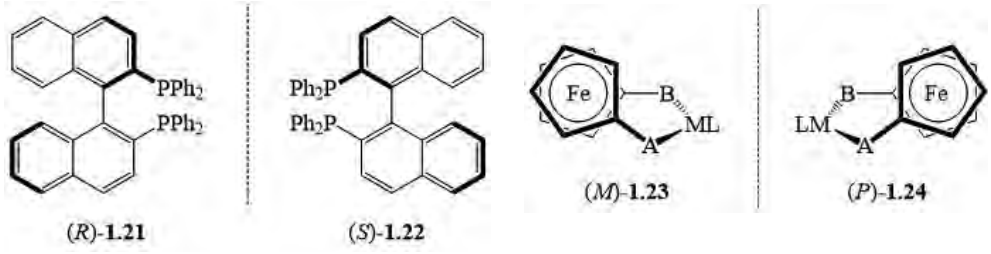

(*R*)-**1.21** (*S*)-**1.22** (*M*)-**1.23** (*P*)-**1.24**

Figure 1.10 (a) (*R*)- and (*S*)-enantiomers of axial-chiral BINAP **(b)** Axial chirality of transition metal complexes with 1,1'-disubsituted ferrocene ligands

1.2.4. Planar-chirality

Planar-chirality is important in this thesis because every novel ligand that is made during this research project possesses a planar-chirality element. These synthesized ligands are all based on ferrocene which is an extremely suitable ligand scaffold for asymmetric catalysis as described in § 1.4.3 (*vide infra*).

The term planar-chirality, or planar stereoisomerism, is used to describe chiral molecules of which the chirality arises from an out-of-plane arrangement of groups, with respect to a plane, which is called the chirality plane. The absolute configuration of a pair of planar-chiral enantiomers is indicated by stereodescriptors R_p and S_p, where p stands for planar. Different procedures to assign planar-chiral enantiomers exist but a straightforward and unambiguous method for disubstituted ferrocene compounds was developed by Schlögl.[22,23] In this thesis, all planar-chiral ferrocene compounds are assigned according this method. The principles of this procedure are illustrated in Figure 1.11 using a general 1,2-disubstituted ferrocene[1] molecule with two different substituents A and B. The ferrocene complex is oriented in such a way that the disubstituted cyclopentadiene ring is chosen as the upper ring. The observation site is now located on top of the ferrocene. Afterwards, the substituents are connected from the highest priority (here A) to the lowest one (here B) according to the shortest route. Rotation in a clockwise fashion corresponds to R_p, rotation in counter clockwise direction to S_p.

1 This 1,2-disubstituted ferrocene substitution pattern is also commonly assigned as a α,β-disubstituted ferrocene. The nomenclature of *ortho* and *meta* is generally not used for ferrocene compounds.

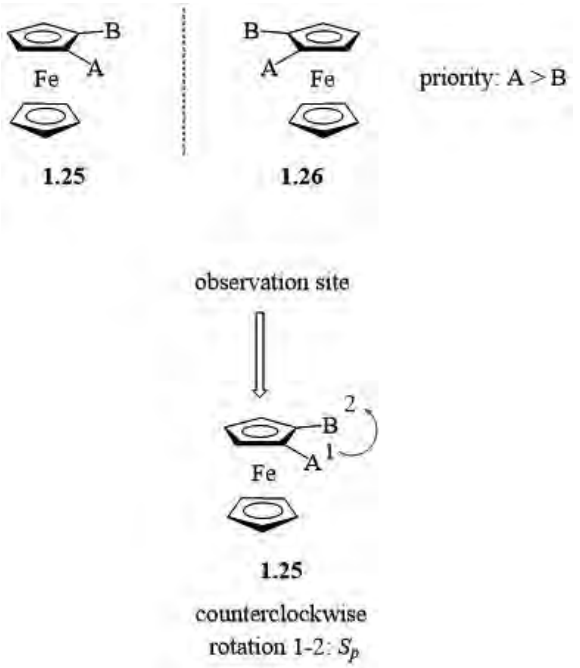

Figure 1.11 Illustration of planar-chirality with the example of a 1,2-disubstituted ferrocene molecule

1.2.5. Inherent Chirality

Chirality elements like the ones described before (centre, axis and plane) are not sufficient to describe the chirality of fullerenes, rotaxanes and other supramolecular assemblies. Therefore the terminology of *inherent chirality* was introduced in 1994 by Böhmer to describe these special chiral entities.[24] Later on, in 2004, the definition was adapted by Schiaffino *et al.*[25] and by Szumna in 2010 who designated the currently accepted definition:[26]

''Inherent chirality arises from the introduction of a curvature in an ideal planar structure that is devoid of perpendicular symmetry planes in its bidimensional representation''

To assign different enantiomers which possess inherent chirality two types of stereodescripters have been suggested. The R_c and S_c nomenclature where c stands for curvature[25]. However, the alternative *P, M* nomenclature, is recommended for this type of chirality.[27] Figure 1.12 describes the assignment of a (*M*)-calix[4]arene **1.26** as an example. The observer has to be situated at the concave site of the calixarene surface. This chirality description involves determination of the priority of the methylene bridg-

ing atoms based on the average substitution pattern of the two neighboring aromatic ring systems according to the CIP-rules. The bridging methylene carbons are labelled with 'a-b-c-d'. Molecules recognized by a clockwise a-b-c rotation are defined to have *P*-chirality (where *P* stand for *Plus*) while counterclockwise rotation is defined as *M*-chirality (*Minus*).

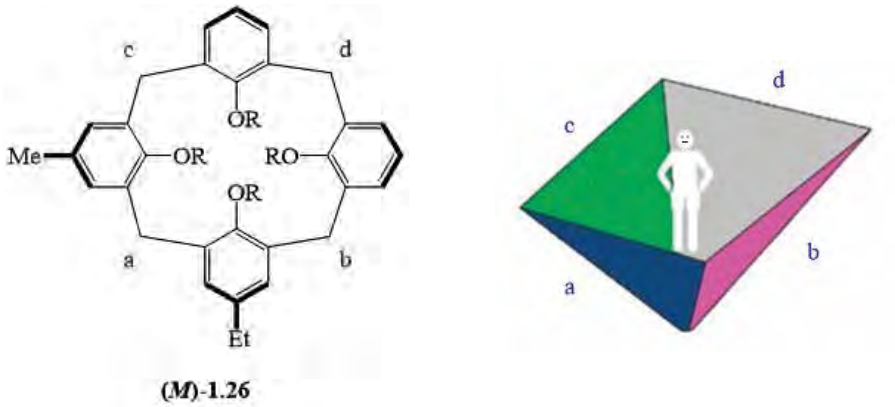

Figure 1.12 Example of an inherently chiral calix[4]arene indicated with the stereodescriptor *M*

A specific subtype of inherent chirality that is worthwhile to mention is helical chirality which is defined as the chirality of a helical-, propeller- or a screw-shaped molecular entity. A right-handed helix is described as *P* while a left-handed one has stereodescriptor *M*. DNA, of which only right-handed, double-stranded helices are naturally occurring, is off course the most straightforward example belonging to this type of compounds. Not only complex biopolymers show helical chirality but also polyaromatic hydrocarbons, known as helicenes, are helically shaped. This *P,M*-nomenclature is sometimes also used for axial chiral entities such as the ferrocenes shown in Figure 1.10 (b), § 1.2.3 (*vide supra*).

1.3. Production of Enantiomerically Pure (Enantiopure) Compounds

As described in § 1.1 enantiomeric compounds interact differently with other chiral molecules at intrinsically different rates. Therefore there is a tremendous interest in producing enantiopure compounds for specialty materials, food and agrochemical industries, fragrance industry, and especially for the pharmaceutical industry.[28-31]

For example, in 2004 allready, 9 of the top 10 drugs had chiral active ingredients and 7 of which were enantiopure.[32] A few years later, in 2010 the four top-selling drugs were on the market as pure enantiomers and 6 of the 10 top-selling small-molecule drugs were enantiopure.[33] However, in 2006 Nguyen *et.al.* posted that 56% of the commercially available drugs were chiral and 88% of these were marketed as racemates.[34] Off course, a profound evaluation of both enantiomers of a biologically active compound is necessary before its approval. Due to the superior performance of pure enantiomers, there is nowadays an increasing request by regulators to administer chiral drugs in an optically pure form.[35-38] With the need for more enantiomerically pure compounds, the academic and industrial technology to obtain these has highly improved as well. Figure 1.13 shows an overview of different pathways leading to pure enantiomers. These pathways can be divided into a 'racemic approach', which is based on the separation of a racemic (or enantioenriched) mixture and a 'chiral approach' which consists of two subclasses namely asymmetric synthesis and the chiral pool strategy. Therefore there is (theoretically) only one enantiomer involved in the chiral approach.

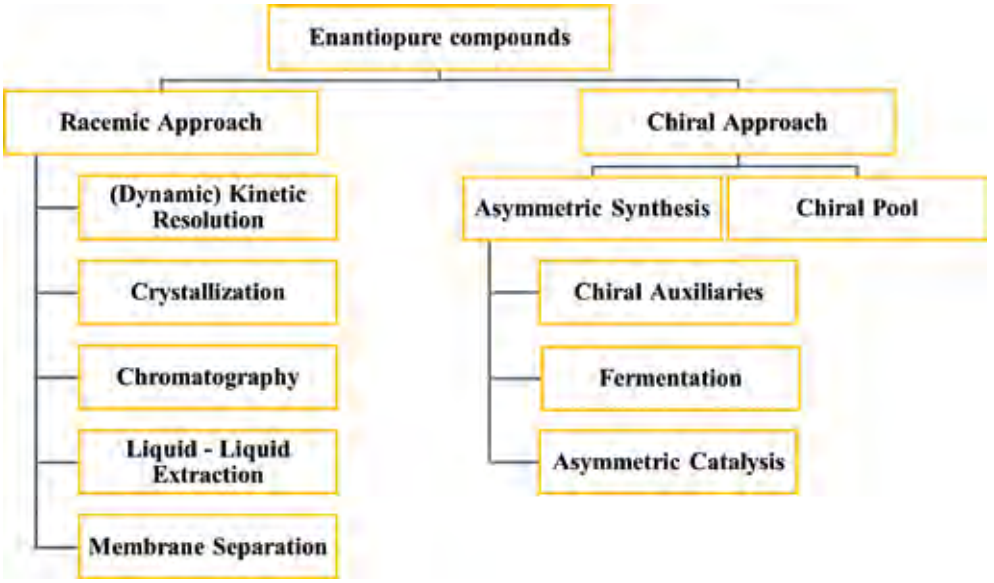

Figure 1.13 Overview of different pathways leading to enantiomerically pure compounds

The chiral pool refers to the collection of readily available, cheap enantiopure compounds like carbohydrates, amino acids, terpenes, hydroxyacids and alkaloids. These compounds are often naturally occurring or easily synthesized derivatives of these. Be-

cause often only one enantiomer of these products is available, the target molecules must have the same stereochemistry as their naturally occurring starting materials. This approach is often used in early phases of drug discovery, but it can also be used on large scale products.[38,39] tadalafil, a drug for the treatment of male erectile dysfunction (MED), commercially available as Cialis® is industrially produced by the chiral pool approach starting from (*R*)-tryptophan (Figure 1.14).[40,41]

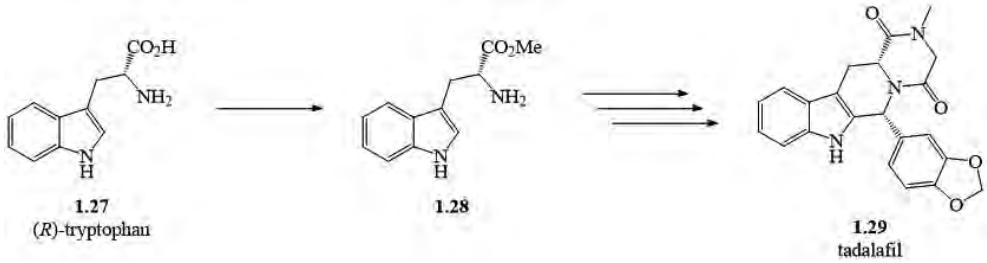

Figure 1.14 Synthesis of tadalafil starting from (*R*)-tryptophan using the chiral pool approach

Asymmetric synthesis or *stereoselective* synthesis is defined by IUPAC as a chemical reaction (sequence) in which one or more new chirality elements are formed in a substrate molecule and which produces the stereoisomeric products in unequal amounts. The synthesis of enantiopure or enantioenriched compounds from prochiral starting materials is an important subfield of asymmetric synthesis. The term prochirality is used in different ways and also the definition by IUPAC is cumbersome.[42] Based on this definition prochirality is here defined as the geometric property of an achiral object (or spatial arrangements of points or atoms) which can be made chiral in a single desymmetrization step[2]. It is important to understand that enantiomerically pure (or enantioenriched) compounds can only be synthesized, from prochiral substrates, in the presence of a chemical chiral agent. For stereoselective reactions involving the creation of a new chirality element on a prochiral substrate (enantioselective reactions), the main goal is to achieve a high enantiomeric excess. For those cases where it is impossible to reach the desired *ee*-values, purification methods described in the racemic approach can be applied to realize the required enantiomeric excess (*vide infra*).

In principle, asymmetric catalysis is the best method to introduce stereochemistry into fine chemicals like pharmaceutically active molecules.[43] This can be explained by the fact that (theoretically) a minimal amount of a chemical chiral agent (chiral catalyst),

2 This definition includes the concept of achiral molecules or entities which contain a trigonal system that can be made chiral by the addition of a new atom or achiral group to this trigonal system. This latter definition is often used to explain the concept of prochirality in student books but the general definition is not limited to these trigonal systems.

can produce a large amount of enantiopure chiral product. Subclasses of asymmetric catalysis are bio-organic catalysis and chemocatalysis. The bio-organic catalysis approach (or enzymatic catalysis approach) makes use of biocatalysts (enzymes), which can perform organic transformations with very high selectivities. Their mode of action is based on the *induced fit* model. Therefore, the main drawback is a rather limited substrate scope for some classes of a specific enzyme. For the synthesis of atazanavir (Reyataz®), an HIV protease inhibitor commercialized by Bristol-Myers Squibb, different enzyme-catalyzed reactions were used (Figure 1.15).[44,45] First, an enzymatic process has been developed for the preparation of chiral synthetic building block **1.31**. This diastereoselective reduction was carried out by oxidoreductases from the microbial cultures *Rhodococcus erythropolis* SC 13845. In this way a diastereomeric purity of 98.9% combined with a yield of 98% was obtained.[46] For the synthesis of (*S*)-*tert*-leucine **1.34**, scientists at Bristol-Myers Squibb have chosen another biocatalytic proces. This involved an enzymatic reductive amination of ketoacid **1.33** by recombinant *E. coli* expressing leucine dehydrogenase from *Thermoactinimyces intermedius*. This reaction required NADH as a cofactor. NAD^+ produced during this reaction was converted back to NADH using recombinant *E. coli* expressing formate dehydrogenase from *P. pastoris*. This afforded a conversion higher than 95% and an *ee* value higher than 99.5% for (*S*)-*tert*-leucine **1.34** at 100 g/L substrate input.[44] The production of (*S*)-*tert*-leucine as described here occurs in fact via a fermentation method (*vide supra*).

Chemocatalysis can be divided into organocatalysis, ion-pairing catalysis and transition metal catalysis. Organocatalysis uses simple chiral organic molecules as a catalyst. These compounds often belong to the chiral pool. A classic example of such a molecule is natural amino acid (*S*)-proline **1.39** which is used in different organic transformations like Aldol reactions, Mannich reactions, Michael additions, …[47] Figure 1.16 shows a general example of such a proline-catalyzed reaction with very good selectivities (*ee* up to > 99% and *anti-syn* ratios up to 24/1).[48]

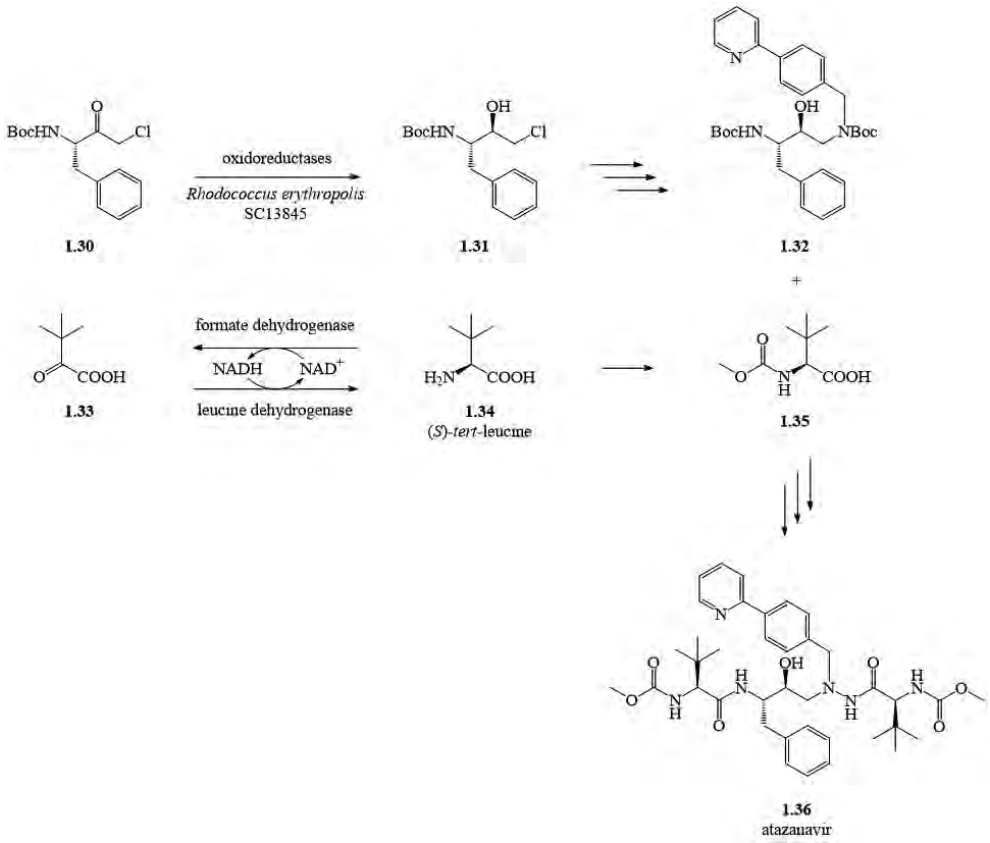

Figure 1.15 Asymmetric synthesis of HIV protease inhibitor atazanavir using different enzymatic reactions

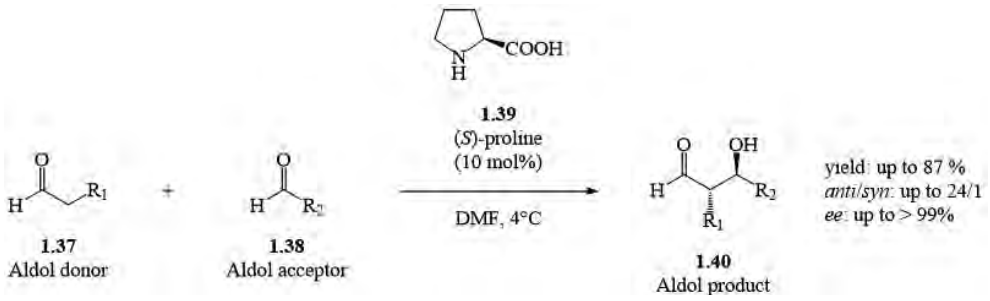

Figure 1.16 Proline-catalyzed enantioselective cross-Aldol reaction of aldehydes[48]

Ion-pairing catalysis is a rather new research topic in the field of asymmetric catalysis and the world of organic chemistry in general and its history can be traced back to 1984.[49] Asymmetric ion-pairing catalysis, in which enantioselectivity can be achieved solely through electrostatic and other noncovalent interactions, has proven to be extremely useful for those reactions where charged intermediates are involved, a challenge that is not straightforward for covalent, Lewis acid and H-bond donor catalysts. [50] Last decade, tremendous progress has been made for both chiral cationic and chiral anionic catalytic systems. One of the most successful catalysts in this research topic are the conjugate bases derived from monophosphoric acid, connected to different chiral binol-based backbones. Figure 1.17 illustrates a successful example of a counterion-mediated catalytic transfer hydrogenation of α,β–unsaturated aldehydes using a chiral phosphate anion catalyst and a Hantzsch dihydropyridine reductant **1.42**.[51] This specific catalyst **1.44** is characterized by a 2,4,6-*iso*-propyl substituent pattern on both aromatic ring systems. List *et al.* even applied this methodology for the synthesis of (*S*)-Florhydral® **1.46**, a powerful fragrance.[52]

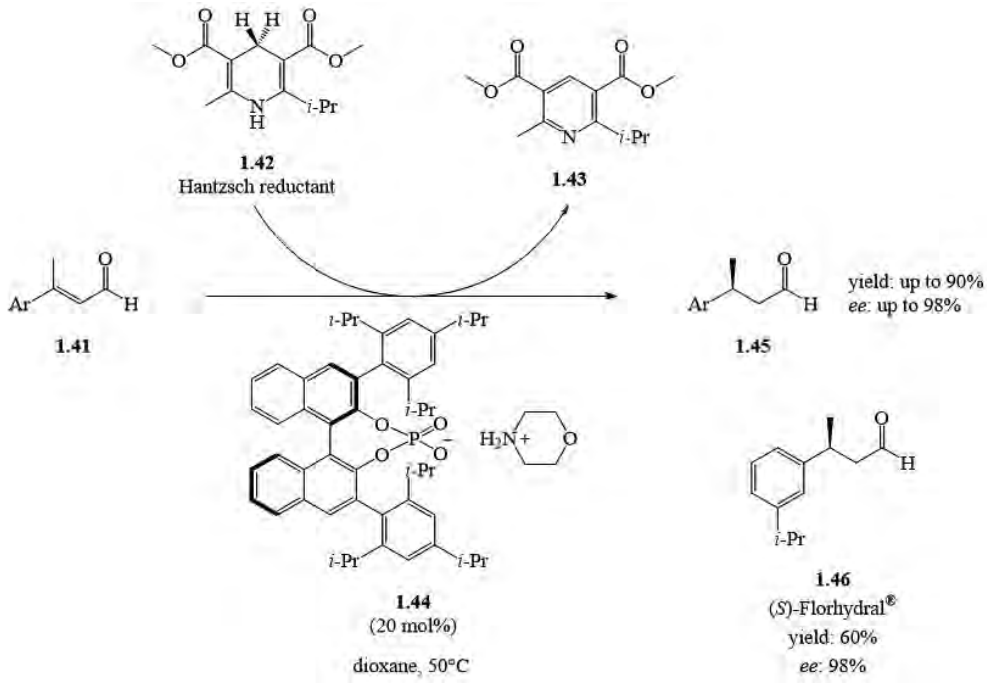

Figure 1.17 Asymmetric ion-pairing catalytic transfer hydrogenation of α,β–unsaturated aldehydes using a chiral phosphate anion catalyst and a Hantzsch reductant[51]

In the approach of transition metal catalysis, metal-ligand complexes derived from chiral ligands are responsible for chiral induction. The main advantage of asymmetric transition metal catalysis is the huge diversity of ligands combined with more or less 30 transition metals that result in an unlimited scope of asymmetric transformations. The main drawback of this approach is the potentially high cost of transition metal as well as ligand. Because the subject of this thesis is the development and testing of novel chiral ligands for asymmetric transition metal catalysis, this approach is explained in more detail in § 1.4 (*vide infra*).

Another strategy to synthesize enantiomerically pure compounds involves the use of chiral auxiliaries. The methodology of this strategy generally implicates three steps:

1. An enantiopure compound from the chiral pool, which serves as a chiral auxiliary, is attached to a prochiral substrate;
2. A diastereomeric transformation can occur: the chiral auxiliary will allow to introduce a new stereocenter (or another stereogenic element) on the prochiral substrate. In theory, two diastereomers could be formed, but due to the stereochemistry of the chiral auxiliary one will be preferred.
3. The last step of this approach is the removal of the chiral auxiliary with the formation of (ideally) an enantiopure compound. For economic reasons, a recuperation of the chiral auxiliary is recommended if possible.

Although these reactions are highly reliable and predictable, this method requires additional reaction and purification steps. Another drawback is the need for stoichiometric amounts of an (expensive) chiral auxiliary. Nevertheless, this approach is often used for the synthesis of pharmaceutically active compounds. For example, scientists at Pfizer, successfully relied on Evans' chiral oxazolidinone auxiliaries for the synthesis of the LTB_4-receptor antagonist **1.52**, an active pharmaceutical ingredient useful for the treatment of inflammatory disorders (Figure 1.18).[43,53]

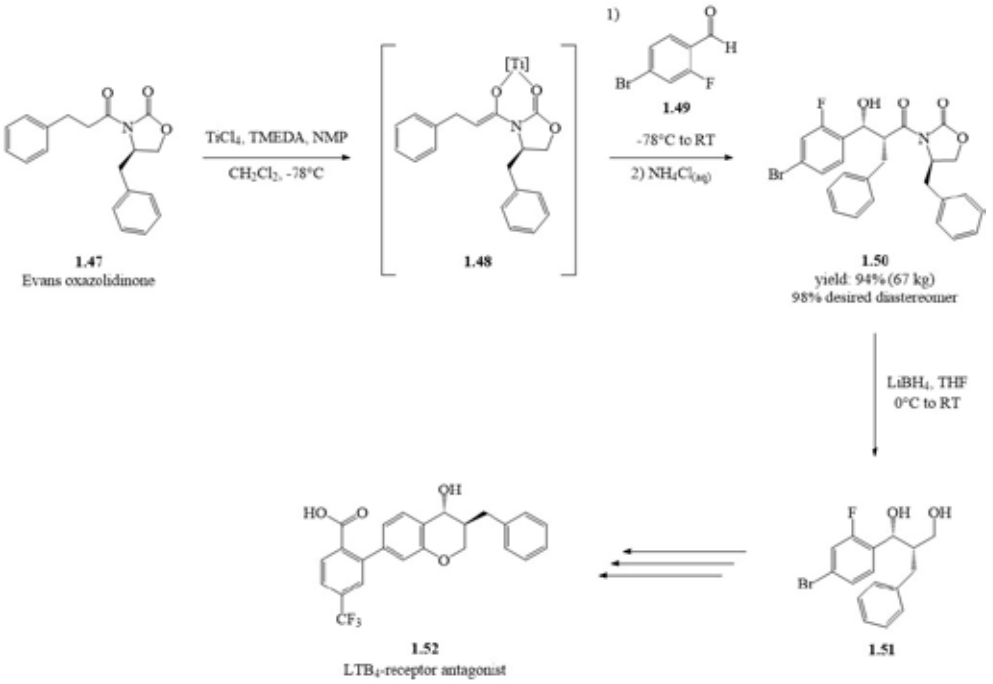

Figure 1.18 Evans' oxazolindinone chiral auxiliary for the asymmetric Aldol reaction for the synthesis of building block **1.50** to prepare LTB_4-receptor antagonist **1.52**[43,53]

Another technique for the asymmetric synthesis of enantiopure compounds is based on fermentation methods, which make use of microorganisms. They are successfully applied for the large scale production of amino acids, that are of particular interest as food additives and starting materials for chiral pool based syntheses of high-value products (*cf.* tadalafil, Figure 1.14, *vide supra*). For example, in 2012, Eggeling *et al.* communicated about the industrial production of 1.3 million ton a year of (*S*)-lysine using *Corynebacterium glutamicum* as a microorganism in this fermentation reaction. [54] For the synthesis of (*S*)-tryptophan, mutant strains of different microorganisms like *Bacillus subtilis* and *Corynebacterium glutamicum* are industrially applied.[55,56] The Bristol-Myers Squibb production of (*S*)-*tert*-leucine as described in Figure 1.15 (*vide supra*) is also an example of a fermentation process.

The other main approach to reach enantiopure compounds is the 'racemic approach' which is based on the separation of racemates (or enantioenriched mixtures). The separation of a racemate into its enantiomers is called resolution. Despite the tremendous progress achieved in asymmetric synthesis, the majority of techniques to supply pure

enantiomers on an industrially relevant scale are (nowadays) still based on the resolution of racemates.[28] One of these techniques is kinetic resolution (KR), whereby one enantiomer of a racemate (or enantioenriched mixture) via an optically active reagent or (bio)catalyst or even solvent can be selectively transformed into a new enantiopure compound, based on a difference in reaction rates of the enantiomeric starting materials. The result is a mixture of non-reacted enantiomer and a newly formed molecule derived from the other enantiomer, which can (theoretically) be separated by classical separation techniques. Figure 1.19 shows the energy profile of a kinetic resolution. For an optimal resolution, the activation energy of the fast reacting enantiomer is significantly lower than that for the slowly reacting enantiomer.[57] In other words, the higher $\Delta\Delta G^{\ddagger}$, the more easy it is to obtain high enantiomeric excesses. Although multiple examples with high *ee-values* are known in literature,[57,58] there is one major drawback: the maximal theoretical yield is only 50%.

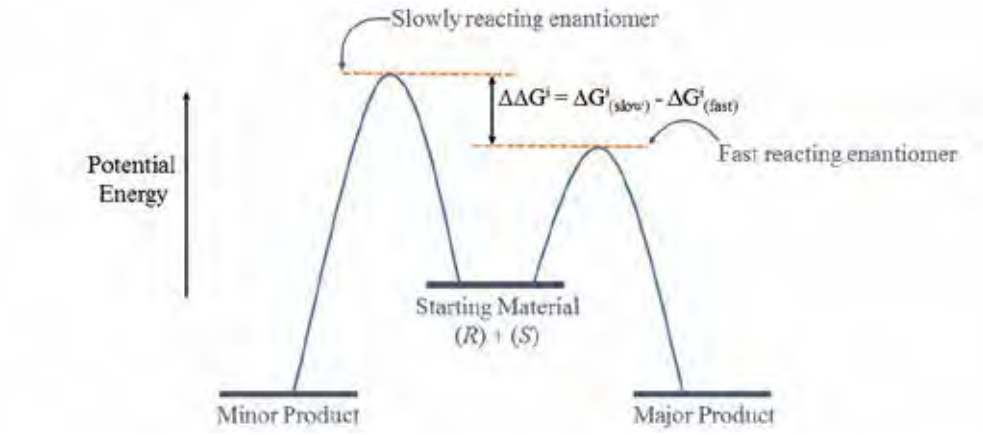

Figure 1.19 Energy profile of a kinetic resolution

Dynamic kinetic resolution (DKR), an extension to KR based on the same separation principles, was developed to obtain full conversion. In this technique the slow reacting enantiomer of a kinetic resolution is racemized spontaneously or via a (bio)chemical reaction. As a result the fast reacting enantiomer will be continuously replenished and transformed into the desired enantiopure target compound. The slowly reacting enantiomer will be consumed via the racemization reaction and very high enantiomeric excesses and yields can theoretically be obtained. An interesting example of a DKR, where the resolution qualities of an enzyme (*Candida antarctica* lipase B) are combined with a ruthenium-based racemization catalyst **1.56** (Figure 1.20), was reported by Bäckvall *et al.*[59]

The authors applied this methodology for the synthesis of (*S*)-propanolol, an anti-hypertensive drug (β-blocker) and (*R*)-denopamine **1.57**, a potent orally active β_1-receptor agonist for the treatment of heart failure (Figure 1.20).[60]

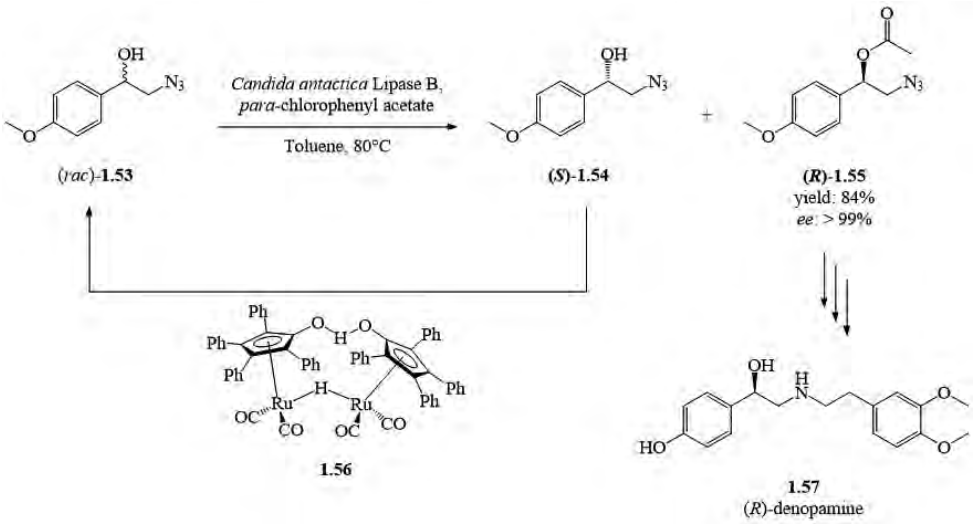

Figure 1.20 DKR of a secondary alcohol for the synthesis of (*R*)-denopamine **1.57** using a lipase for the resolution in combination with a ruthenium-based racemization-catalyst **1.56**[60]

In § 1.1 the phenomenon of spontaneous resolution of conglomerates was already mentioned, by means of the example of Pasteur's tartaric acid crystals. This preferential crystallization of enantiomers from a racemic mixture is only possible when both enantiomers form separate but pure crystals. Therefore, not more than 5 to 10% of the chiral substances belong to this type.[61] Nevertheless, spontaneous resolution is successfully applied for the large scale synthesis of high value products like L-(-)-menthol (1400 tonnes/year, Haarmann & Reimer), L-(-)-α-methyldopa (>100 tonnes/year, Merck), and (*S*)-(+)-glutamic acid (13000 tonnes/year, Ajinomoto).[28,62] For a long time spontaneous resolution was '*one of the greatest challenges in stereochemistry*'.[63] However, major breakthroughs and scientifically insights on this topic were obtained by Viedma and Blackmond.[64-70] Starting from the basic principles of a ternary phase diagram they propose that this phenomenon could be explained by the combination of thermodynamic and kinetic effects in a so-called 'thermodynamic-kinetic feedback near equilibrium' mechanism. This involves the kinetic disruption from a system in equilibrium via a dynamic crystallization/dissolution processes after which the system attempts to re-establish the equilibrium situation. Moreover, this mechanism could op-

erate in a plausible natural prebiotic scenario explaining the origin of molecular homochirality observed in nature and consequently the origin of life on earth. Another requirement necessary for the formation of conglomerates is the favorable formation of homochiral interactions over heterochiral ones.

The oldest method for the separation of a mixture of enantiomers is the so-called classical resolution. Hereby, an enantiomerically pure resolving agent is added to a mixture of enantiomers to provide diastereomeric salts which have different solubilities. Therefore they can be separated via crystallization. Traditionally, optically active acids and bases from the chiral pool have been employed as chiral resolving agents. The main drawbacks of this technique are the limitation of the maximum yield to 50% and the laborious quest for a suitable resolving agent. However, classical resolution has the advantage of being cost efficient, robust and simple to operate. Moreover, generally high *ee-values* are obtained. As a consequence, the majority of industrially produced enantiopure compounds are generated via this method and increasingly, it also becomes the method of choice for the synthesis of pharmaceutical ingredients.[71] A successful example of a classical resolution is illustrated in Figure 1.21. In the mid-seventies of last century, scientists at Hoffmann-La Roche elaborated a process for the industrial production of L-DOPA **1.62**, a therapeutic agent in the treatment of Parkinson's disease. After the racemic synthesis of **1.59**, a resolution step using (+)-dehydroabiethylamine afforded the amonium salt **1.61** of the L-enantiomer, which is the precursor for the synthesis of enantiopure L-DOPA.[72]

In theory, the resolution of racemates using a chiral solvent could be possible as well. This concept is based on the occurrence of diastereomeric interactions between both enantiomers and the solvent. The formation of these diastereomeric supramolecular assemblies should result in a preferred precipitation of one of the two enantiomers. However, due to the lack of intensive and fundamental research only a few investigations have been reported.[62]

Enantiomers can be separated via chiral high performance liquid chromatography (HPLC). In theory, chromatographic separation methods using a chiral mobile phase could be used, however these are not competent for preparative LC. In addition, the application of a chiral stationary phase (CSP) is more convenient and therefore widely used in industry at early development stages. Different types of CSPs are commercially available including polysaccharide-, synthetic polymer-, protein- and cyclo-

dextrin-based chiral stationary phases.[28] During migration of the sample through a column, diastereomeric complexes are formed and the stationary phase retains the individual enantiomers in a specific manner. Due to the development of simulated moving bed techniques (SMB), chiral separations can be done in a continuous flow mode for the large scale industrial production of enantiomerically pure compounds.[73] Nevertheless, these techniques are expensive because they require a large amount of solvent, careful design and possibly intensive optimization. Productivities between 1 to 10 kg enantiomer per kg CSP a day are achievable.[28] In 1992, Daicel Chemical Industries published the first paper about the resolution of a racemic mixture of 1-phenylethanol by SMB technology.[74,75] Since then, simulated moving beds are applied for the production of active pharmaceutical ingredients like Taxol® (paclitaxel), Zoloft® (sertraline), Zyrtec® (cetrizine), Prozac® (Fluoxetine), insulin and many others.[76,77] A cartoon picture of the principle of chiral SMB technology published by Negawa and Shoji (Daicel Chemical Industries) is shown in Figure 1.22 (a). A production scale Licosep 6-450 SMB unit, which consists of six columns with an internal diameter of 45 cm is shown in Figure 1.22 (b).

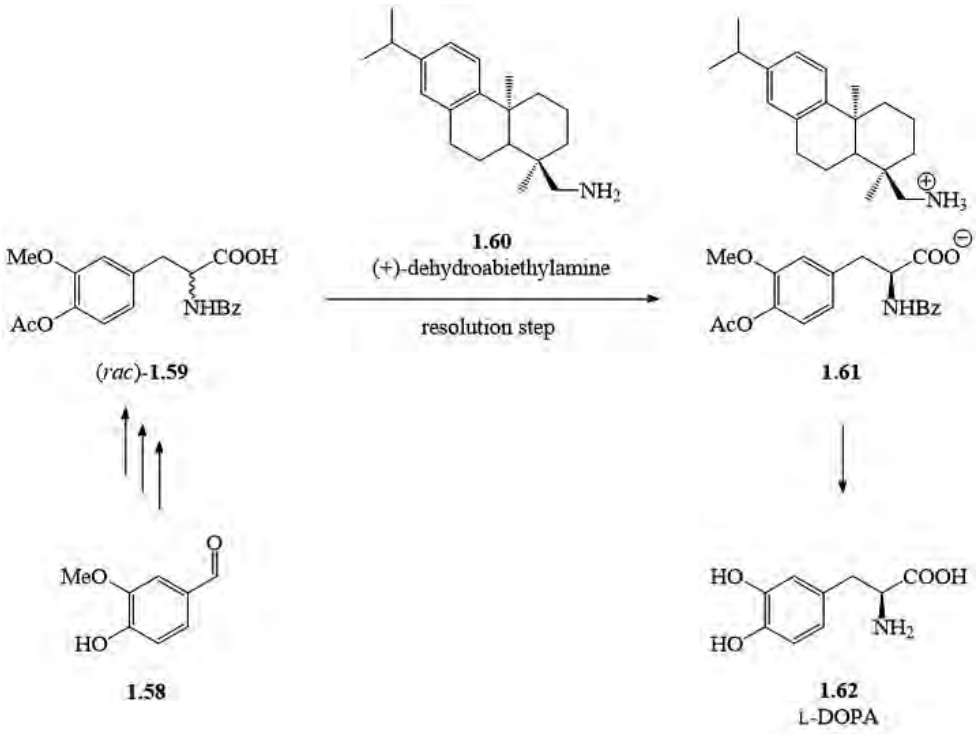

Figure 1.21 Synthetic route for L-DOPA **1.62** developed by Hoffmann-La Roche using a classical resolution step[72]

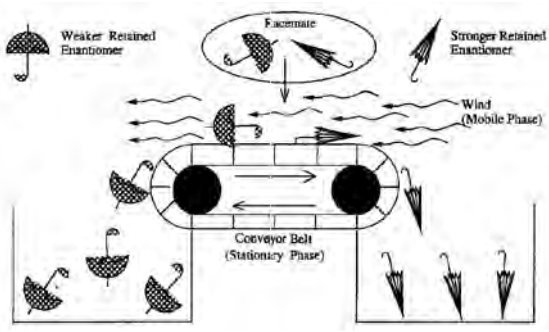

Figure 1.22 (a) Cartoon picture explaining the principle of chiral SMB technology[74] **(b)** Production scale Licosep 6-450 SMB[75]

Another technique to fractionate racemates continuously into their enantiomers is enantioselective liquid-liquid extraction (ELLE). It combines the concepts of enantiomeric recognition and solvent extraction. As a consequence this technique is closely related to the field of host-guest chemistry.[78] Some successfully used chiral extractants are cyclodextrin derivatives[79], tartaric acid derivatives[80,81], crown ethers[82], metal complexes[83] and metalloids.[84] To develop economically efficient processes, chemical industry will seek to recover the host extractants by back extraction.

The last technique that belongs to the racemic approach for the resolution of racemates is the application of membranes. Two different operation modes with membrane technology exist[28]:

1. Direct separation using enantioselective chiral membranes (which can be liquids or dense polymers).
2. Separation in which a non-selective membrane assists in an enantioselective process.

In general, crystallization methods are the most cost efficient approaches for the resolution of a racemate into its enantiomers. However, successful application of these techniques to racemic mixtures is rather difficult. On the other hand, when there is a certain enrichment of the target enantiomer, the separation of both enantiomers using these methods is simplified. Therefore it is reasonable to perform expensive chromatographic separations (or other approaches), prior to crystallization steps to achieve the required enantioenriched composition.[85,86] From 2008 to 2011, an European project called 'INTENANT' (INTegrated synthesis and purification of ENANTiomers) investigated such hybrid processes for the separation of enantiomers.[87] As such, comprehensive re-

search was carried out on the separation of a racemate of bicalutamide, an active pharmaceutical ingredient for the treatment of prostate cancer.[88] A flow sheet of the coupled processes is illustrated in Figure 1.23. In the first purification step 600 g of racemic bicalutamide is enriched by simulated moving bed chromatography, which resulted in 322 g with an enantiomeric excess of 84.76%. Afterwards two subsequent enantioselective crystallization steps, were performed. Finally, (*R*)-bicalutamide **1.63** was obtained with a yield of 45% (136 g) and an enantiomeric purity of more than 99.9%

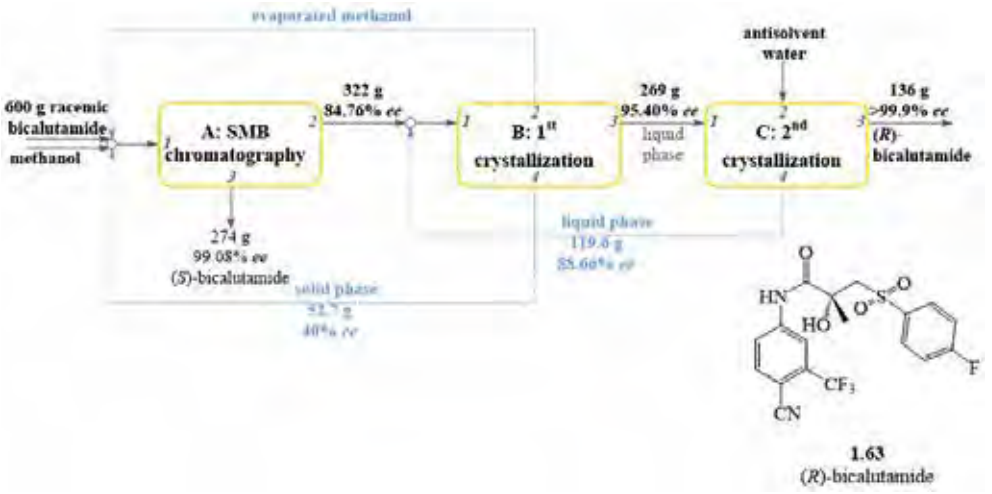

Figure 1.23 Flow sheet of the coupled processes (SMB chromatography + two crystallization steps) to isolate (*R*)-bicalutamide **1.63**, including mass balances and enantiomeric purities[28]

Now the different approaches for the production of enantiomerically pure compounds are explained, it might be useful to propose a rational, qualitative and convenient decision tree. Such a 'manual', which is based on experience gained with a large number of industrial compounds is shown in Figure 1.24.[28,33] The key question that has to be asked before a certain method can be proposed is: 'Can the compound be racemized or not?' For those molecules where this is not obvious, asymmetric synthesis approaches, potentially followed by crystallization steps, are of special interest. Only when these synthesis approaches are economically not beneficial, intensive chromatographic separation methods and subsequent crystallization have to be suggested.

If racemization of the target compound is possible, one has to find out whether the system forms a conglomerate or not. If this is the case, preferential crystallization followed by a racemization process of the unwanted enantiomer can successfully be applied.

For those systems where spontaneous resolution is not an option, one has to find out if a selective crystallization of a pre-enriched mixture, obtained via chiral chromatography, might be possible. Therefore a phase diagram has to be constructed so that the eutectic point and the eutectic composition, which is the composition at the intersection of the solubility isotherm of the single enantiomer and the solubility isotherm of the racemate, can be evaluated. To obtain an enantiopure compound after selective crystallization, the amount of the target enantiomer in the obtained mixture after the pre-enrichment step must exceed the eutectic concentration. Therefore a maximal eutectic *ee*-value of 80% is generally proposed as a reasonable eutectic composition. Afterwards, racemization of different fractions containing the undesired enantiomer will allow to increase the yield. For systems with a higher eutectic *ee*-value selective crystallization is generally not successful. For these systems, enantiopure compounds have to be obtained via intensive chromatographic separation steps. Again, racemization processes will allow to increase the yield. It is important to mention that diastereomeric salt crystallization, DKR and chiral pool synthesis are not considered as an option in this decision tree. For those processes where these approaches are a valid option, the decision tree has to be extended.

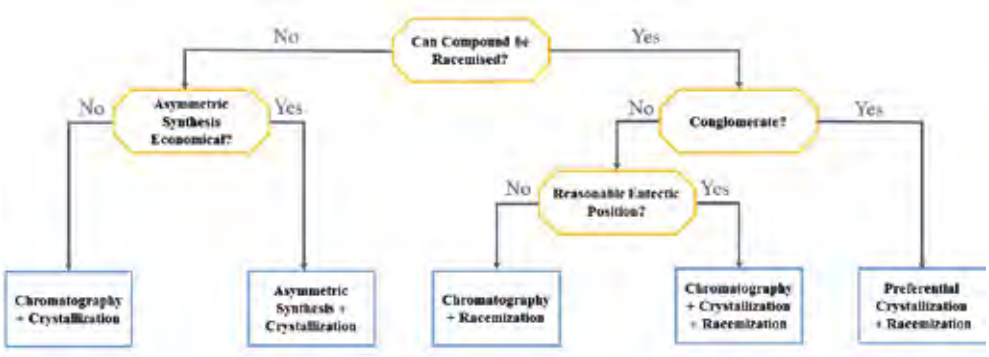

Figure 1.24 Decision tree based on simple qualitative criteria for the selection of a suitable combined or integrated process concept for the production of a pure enantiomer [33]

In conclusion, it is worthwhile mentioning that there are still challenges for the production of enantiopure compounds for industrial as well as academic applications. Therefore there is a tremendous call for more research towards all approaches to obtain enantiopure compounds since its very unlikely that one approach will herein succeed.

1.4. Chiral Ligands and Chiral Catalysts for Asymmetric Transition Metal Catalysis

1.4.1. Principles of Asymmetric Transition Metal Catalysis

The general principles of asymmetric catalysis are illustrated in Figure 1.25.[89,90] During the induction process, precatalyst **1** is converted to the active catalyst **2**, that consists of a metal (or metal ion) and a chiral ligand. Here, the active metal center is responsible for the catalytic activity whereas the ligand creates a chiral environment around the metal which allows to control the stereoinduction and stereoselectivity. The metallic center activates prochiral molecules A and B (or one of these) and transforms them into chiral molecule A-B, still coordinated to the metal center. The last step involves dissociation of A-B with regeneration of the active catalyst **2**. The mechanistic step in which catalytic species **3** is converted into **4** kinetically determines the absolute stereochemistry of final product A-B and is called the enantiodetermining step.

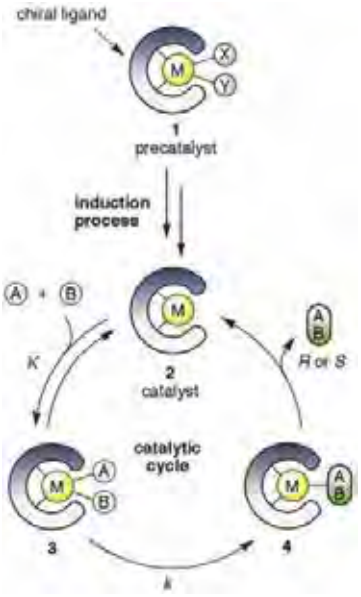

Figure 1.25 General principles of asymmetric (transition) metal catalysis with a chiral ligand[89,90]

Asymmetric catalysis is four dimensional chemistry: high efficiency can only be achieved by using a combination of both an ideal 3D structure (x,y,z) and suitable kinetics (t).[91] Outstanding asymmetric catalysis requires high *ee*-values, high turnover numbers (TON)

and high turnover frequencies (TOF). The enantiomeric excess value is still most common in the field of asymmetric synthesis, although this is an uncomfortable way to express enantiomeric purity and difficult to work with in a theoretical perspective.[92] The use of *ee*-values dates back to the 1960's when the exclusive method for determining enantiomeric composition was optical rotation, which is directly related to the enantiomeric excess.[93] Nowadays, chiral chromatography techniques are used worldwide to determine enantiomeric composition which allows to obtain *er*-values directly. The latter value is in fact preferable to represent the optical purity of a certain mixture of enantiomers. It allows to calculate *ee*-values immediately which make them easy to compare with (older) literature reports as well. In the field of organometallic catalysis, TON is defined as the number of moles of substrate that a mole of catalyst can transform (before becoming deactivated). It is a number that indicates the catalyst productivity which determines catalyst costs. Alternatively, substrate/catalyst ratios are used as well to illustrate the catalyst productivity. The TOF is the number of moles of a substrate which is converted by one mole of catalyst per unit of time. This number indicates the catalyst activity that affects the production capacity.[38,39] In general, a high TON is the minimal requirement for an ideal catalyst[94]. For other processes it is best to strive for a high catalyst activity and catalyst productivity is less important. Despite the usefulness of TON and TOF, this terminology has different definitions in different fields (e.g. chemistry vs. biochemistry). Moreover, different methodology, e.g. transition metal catalysis, organocatalysis, biocatalysis, requires different reaction conditions and are used on different scales.[95] Therefore it is not an easy task to pick the best catalyst for a certain transformation. To overcome these problems, Kozuch and Martin tried to introduce new kinetic values TON° and TOF° at standard conditions of temperature (273.15 K), pressure (10^5 Pa) and concentration (1 molar).[96,97] As an answer to these papers Lente argues for more scientifically detailed studies and for more report of rate equations and rate constants, because these include important details about reaction mechanisms.[98] To conclude, it seems that Hartwig has the most *impressing* vision on catalyst efficiency: [95]

"Everybody has their own needs to consider when judging what is the best way to compare catalysts. We just have to live with the fact that we can't distil catalyst efficiency down to a single comparative number."

Nowadays, it is well recognized that asymmetric (transition)metal catalysis is one the most efficient ways for the production of fine chemicals including pharmaceutically ac-

tive ingredients.[30,39,43] This can be explained by the huge diversity of ligands combined with the availability of many catalytically active metals, making homogeneous (transition) metal catalysis a very versatile approach for asymmetric synthesis. For noble metals as Ru, Rh, Pd, Os, Ir, Pt, ligands containing phosphorus or nitrogen coordinating atoms are preferred. For metals such as B, Ti, Mn, Fe, Co, Ni, Cu, Zn ligands with oxygen or nitrogen atoms are favored. In 2001, The Royal Swedish Acadamy of Sciences awarded the Noble Prize in Chemistry to Sharpless, for his work on chirally catalysed oxidation reactions and Knowles and Noyori, for their work on chirally catalysed hydrogenation reactions.[99-101]

1.4.2. Privileged Chiral Ligands

Enzymatic catalysis is most often characterized by a high affinity and selectivity of a certain enzyme for a specific substrate in a specific reaction. In the early stages of the development of chiral ligands for asymmetric transition metal catalysis, chemists thought this principle was valid for man-made systems as well. But later on, it seemed that certain classes of synthetic catalysts are enantioselective over a wide range of different reactions and different substrates.[99] The ligands used to build up these catalysts may be called 'privileged ligands' according to 'privileged structures', a terminology used in pharmaceutical research to describe a class of compounds that show activity against a number of different biological targets.[102-104] Examples of these privileged ligands (and complexes) are shown in Figure 1.26.

At first sight, most of these ligands are bidentate, have a rigid structure and possess C_2-symmetry. Examples of these are BINAP, BINOL, MeDUPHOS, Bis(oxazolines) and TADDOL. An important remark associated with this latter characteristic is the fact that asymmetric induction, caused by enantioface differentiation, requires only the lack of a mirror plane or inversion center as a symmetry element. In other words there is no need for chiral ligands to be asymmetric, but dissymmetry (which means the lack of a mirror plane) will do to induce chirality. Moreover, the presence of a C_2-symmetry axis can reduce the number of possible diastereomeric transition states.[105] As a consequence, this could be beneficial for enantioselection due to the possible elimination of less-selective transition states. However, there is no fundamental reason why C_2-symmetric ligands should be superior in comparison to C_1-symmetric (or asymmetric) ligands.[103] For certain reactions, the latter have experimentally proven to give higher *ee*-values compared to those ligands that possess a C_2-axis. For example, hybrid *P,N*-

Phox ligands have shown to give excellent results in asymmetric allylic alkylation reactions (Figure 1.27).[106]

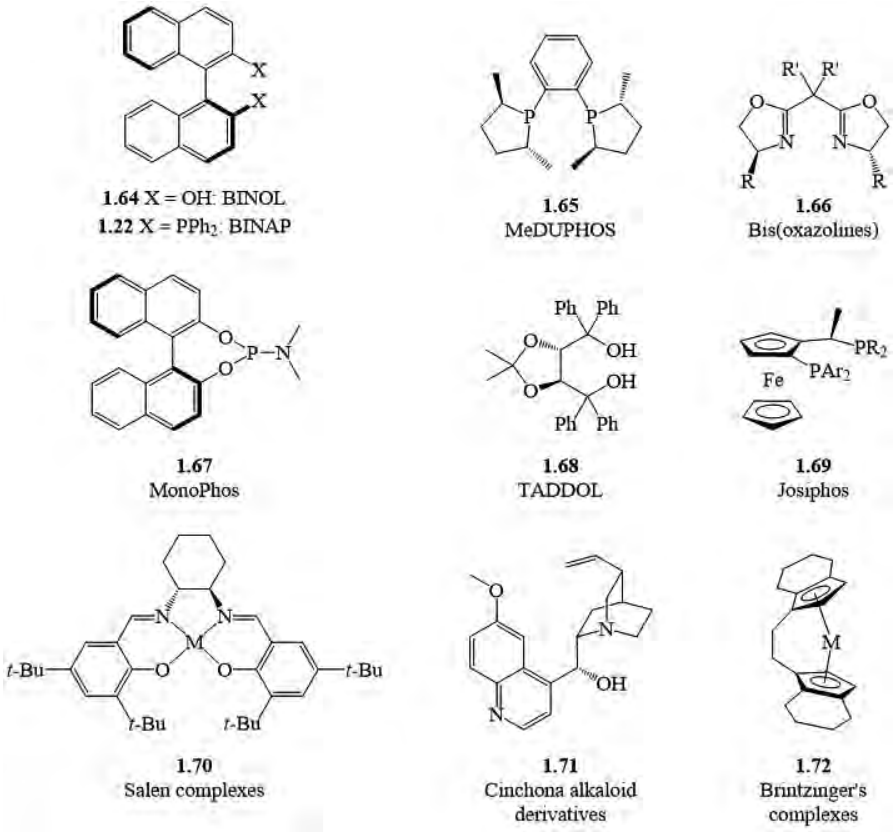

Figure 1.26 Privileged chiral ligands and catalysts

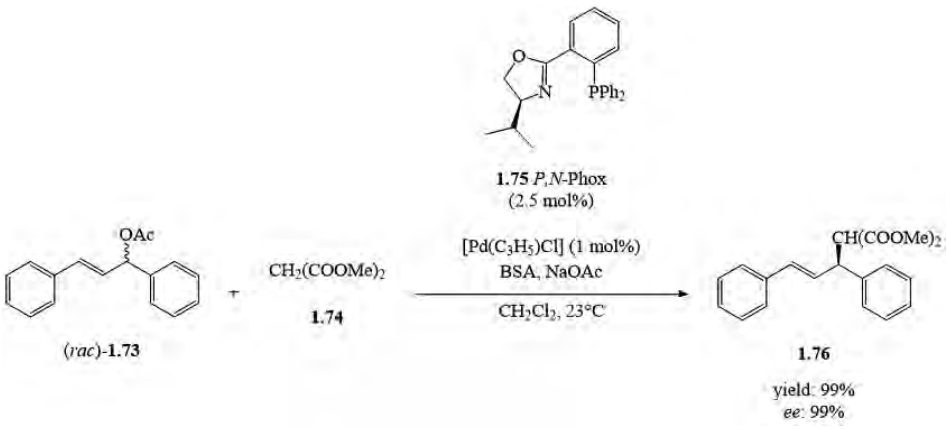

Figure 1.27 Asymmetric allylic alkylation reactions with chiral hybrid *P,N*-Phox ligands

A more or less similar philosophy is valid for the flexibility and coordination mode of ligands. Initially, the general hypothesis was that monodentate chiral ligands were too flexible and therefore detrimental for high stereocontrol.[107] But at the end of last century, Zhang commented on the future of monodentate ligands:[108]

"There have been only a limited number of monodentate chiral phosphines reported in the literature and high enantioselectivity with monodentate phosphines is difficult to obtain. However, there are many transition metal catalyzed reactions that do not work with chelating bidentate ligands. Efficient chiral monophosphines are clearly needed."

And one year later, Lagasse and Kagan, came to the same conclusion by communicating the following statement:[109]

"Chelating chiral diphosphines are especially well fitted for catalytic species involving a transition metal bond to two phosphorus atoms. However, monophosphines and more generally phosphorus derivatives where phosphorus is connected to one or several heteroatoms, may be of interest in asymmetric catalysis, even in the absence of chelate effects."

A major breakthrough came in 1996 when Feringa reported a set of binol-based phosphamidites.[110] He successfully applied these monodentate phosphorus containing ligands in the enantioselective copper-catalyzed conjugate addition of dialkylzinc reagents to enones. One of the ligands used in this study, was later called MonoPhos **1.67** and belongs nowadays to the class of privileged ligands. In this case, best results were obtained with monodentate phosphoramidite ligand **1.79** (Figure 1.28).

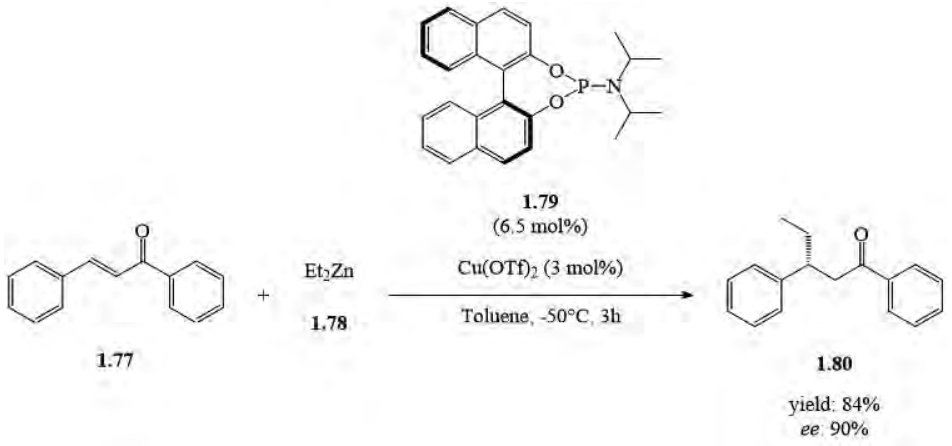

Figure 1.28 Enantioselective Cu-catalyzed Et_2Zn addition to enones with chiral monodentate phosphoramidite ligands

Due to the complexity of most catalytic processes and the lack of mechanistic details of some reactions, rational design of a chiral ligand (or catalyst) is rarely straightforward. Therefore, the successful development of novel chiral ligands and catalysts, is based on serendipity, empirical knowledge, and laborious work via parallel synthesis and high-throughput screening.[103]

1.4.3. Chiral Ferrocene Ligands

Ferrocene is undoubtedly one of the most iconic structures in chemistry. This compound, accidently discovered in the 1950's by Kealy, Pauson and Miller consists of two cyclopentadienyl rings with an iron nucleus in between.[111] It was the first example of the subclass of organometallic species we nowadays call sandwich structures. The applications of ferrocene are nowadays widespread across different research areas like medicinal chemistry (Ferroquine and Ferrocifen-type molecules)[112], supramolecular chemistry[113], polymer science[114], … But chiral ferrocenyl compounds are most prominent as ligands for asymmetric transition metal catalysis. Indeed, ferrocene is a very suitable scaffold for ligand design, what can be attributed to the following characteristics[115]:

1. Its rigidity and bulkiness are perfectly suitable to serve as a backbone for a ligand to provide a chiral environment. These are two important factors in governing stereo- and enantiocontrol.
2. The ferrocene skeleton offers the possibility to obtain complexes with additional planar and/or axial chirality besides central chirality (*cf.* § 1.2.2-1.2.4, *vide supra*). Often the combination of different types of chirality is desirable for outstanding chiral induction.
3. Ferrocene is easily derivatized via electrophilic substitution reactions or lithiations. As a consequence, most families of ferrocene-based ligands are highly modular.
4. Due to the partial negative charge on the Cp ring, ferrocene has electron donating properties.
5. Ferrocene is cheap: € 0.33/g (for 500 g, Sigma Aldrich 14/08/2017)

Since the introduction of ferrocene into the field of asymmetric catalysis, an uncountable number of ferrocene-based ligands has been designed and synthesised. All these ligands can be classified in different groups based on substitution pattern, nature of denticity or nature of their coordinating heteroatoms to metals (*P,P*; *N,N*; *P,N*; *P,S*; *P,O*;

N,O).[116] The most relevant or intriguing families of ferrocene ligands, (mainly) sorted on their substitution pattern at the ferrocene backbone, are illustrated in Figure 1.29. The majority of these ligands were given trivial names by their inventors.

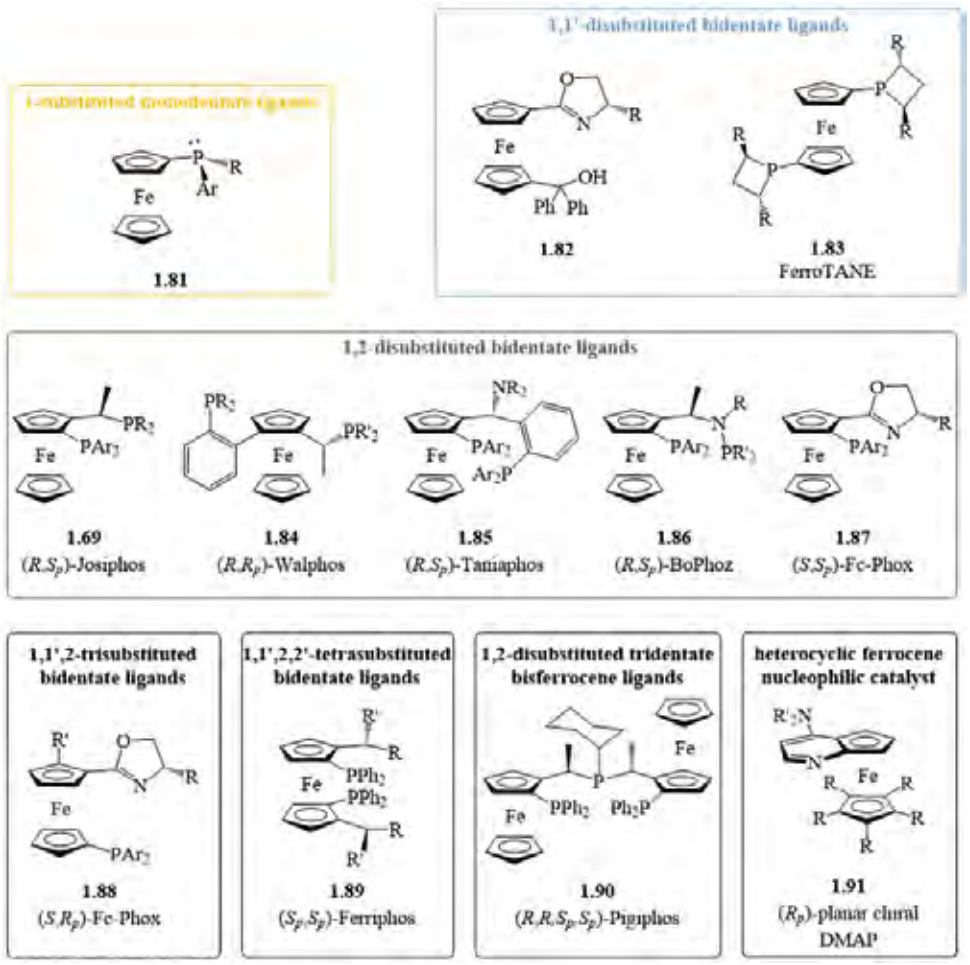

Figure 1.29 Relevant and intriguing ferrocene-based ligands

1-Substituted *P*-chiral monodentate posphines **1.81** have proven to be the ligands of choice for the nickel-catalyzed reductive coupling reaction between alkynes and aldehydes.[117] This useful method for the production of chiral allylic alcohols seemed to be very difficult to control and only moderate enantioselectivities were obtained.

Just like normal Phox ligands (Figure 1.27, § 1.4.2, *vide supra*), ferrocene-Phox ligands **1.87** and **1.88** have proven to be highly successful in palladium-catalyzed asymmetric

allylic substition reactions and palladium-catalyzed asymmetric Heck reactions.[115] FerroTANE ligands **1.83** were developed in analogy with the privileged DuPhos ligands by the research groups of Burk and Marinetti.[118] These ligands were successfully applied in rhodium-catalyzed hydrogenation reactions of a wide range of substrates. Ferrocene-based DuPhos analogue **1.93** was even applied in a hydrogenation reaction for the preparation of kilogram quantities of a potent inhibitor of thrombin fibrinolysis by Pfizer, as shown in Figure 1.30.[119]

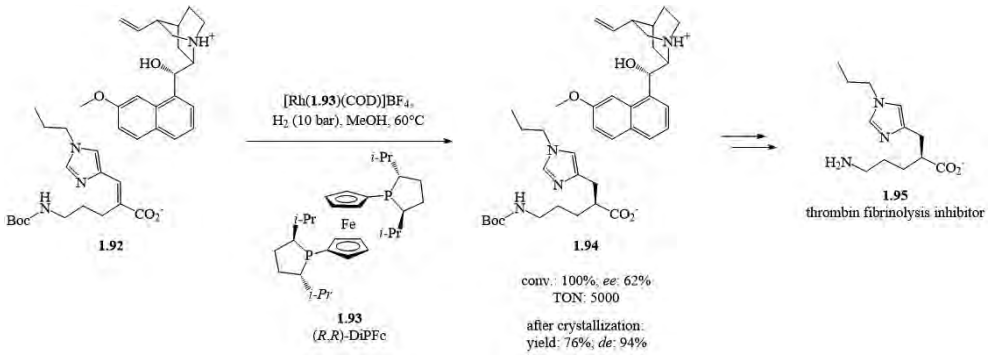

Figure 1.30 Kilogram scale production of a thrombin fibrinolysis inhibitor using a 1,1'-disubstituted ferrocene ligand **1.93**

A handful of 1,1',2,2'-tetrasubstituted ligands have been developed nowadays.[120] Besides the planar-chirality, most of them possess a stereocenter at the α-position as well. An example of these is the Ferriphos family **1.89**, developed by Knochel. These are good ligands for the rhodium catalyzed hydrogenation of dehydroaminoacids, dihydroaminoesters and enol acetates.[121]

The synthesis of nickel and palladium complexes of the tridentate Pigiphos ligands were reported by Togni and Barbaro in 1995.[122] Later on Togni applied these ligands successfully in the nickel-catalyzed enantioselective addition of secondary phosphines to methacrylonitrile.[123] This reaction is very useful for the asymmetric synthesis of novel hybrid *P,N*-ligands.

The family of 1,2-disubstituted chiral ferrocene ligands is by far the largest one. Josiphos-type ligands **1.69** (Figure 1.26, § 1.4.2, *vide supra*), which are undoubtedly the best known chiral ferrocene ligands, belong to this subclass. Several successful industrial applications of this type of ligands have already been developed.[120] The most impressive example is definitely the highly efficient Ir/Xyliphos-catalyzed enantioselective

imine hydrogenation for the production of (*S*)-Metolachlor, by Ciba-Geigy/Syngenta (Solvias) which is shown in Figure 1.31. (*S*)-Metolachlor is the active ingredient of Dual Magnum®, one of the most important grass herbicides used for the cultivation of maize and other crops.[124] The obtained enantiomeric excess of 79% was acceptable for the production of a pesticide. Moreover, the focus was on the activity of the catalyst. With a very high TON, TOF and a production of more than 10 000 tonnes per year, this is the largest known enantioselective catalytic process (on industrial scale).[38,116,125-127]

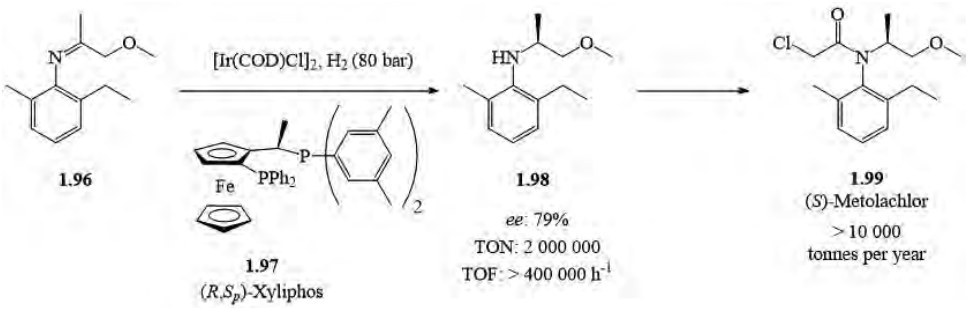

Figure 1.31 Industrial production of (*S*)-Metolachlor via enantioselective imine hydrogenation catalyzed by Ir/Xyliphos

Another example of an industrial process using a Josiphos-type ligand is illustrated in Figure 1.32. This involves the ruthenium-catalyzed enantioselective hydrogenation of **1.100** (a tetrasubstituted double bond!) for the synthesis of (+)-*cis*-methyl dihydrojasmonate **1.102**.[120,128] This fragrance is produced by Firminich on a medium scale production size of a multi hundred kilograms.[38] One of the success factors of the catalytic system is the selectivity control: besides a good enantioselectivity (88% *ee*), also a superb diastereoselectivity (*cis*/*trans* 99/1) and outstanding chemoselectivity were obtained (reduction of keto and ester functional groups was not observed).[125,129]

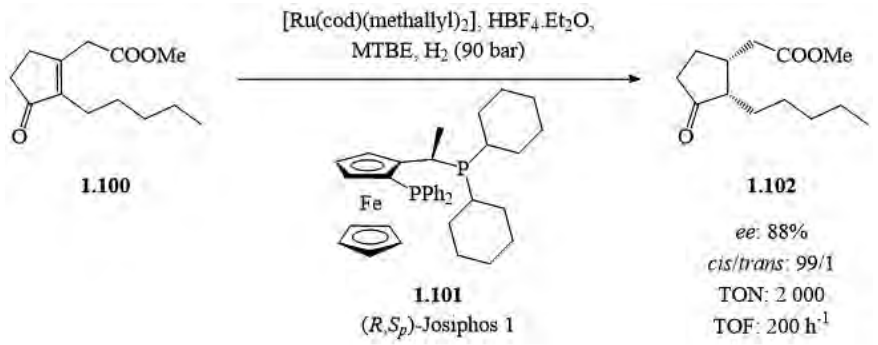

Figure 1.32 Industrial, medium scale production of (+)-*cis*-methyl dihydrojasmonate catalyzed by Ru/Josiphos 1

The use of Josiphos-type ligands in pharmaceutical industry is prominent in a large number of feasibility studies and some pilot processes for the synthesis of active pharmaceutical ingredients for example, crixivan and dextropmetorphan.[38,120,125] A rhodium-Josiphos enantioselective hydrogenation reaction was applied for the medium scale production of a precursor for the growth factor biotin. But the most impressive application of a Josiphos ligand in pharmaceutical industry is the production of MK-0431 **1.105**, used for the treatment of type II diabetes, on a multi tonnes scale per year by Merck (Figure 1.33).[128] An excellent *ee*-value of 94% and acceptable TON of 350 were obtained. Deuterium labelling experiments have shown that it is not the enamine carbon-carbon double bond that is reduced but the imine carbon-nitrogen double bond, obtained via tautomerisation.[130]

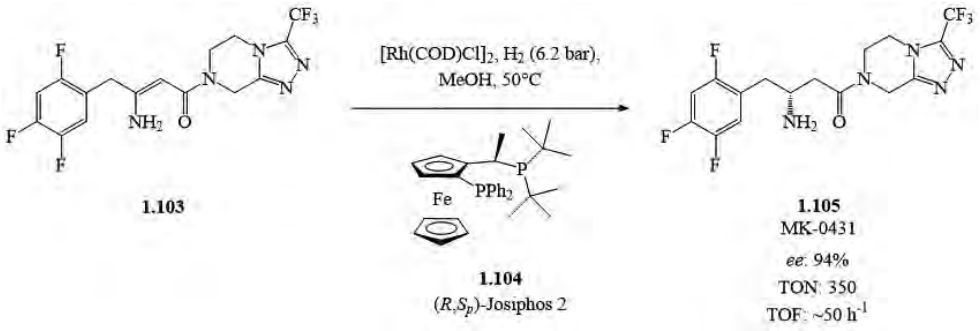

Figure 1.33 Industrially, large scale production of MK-0431 **1.105** via a Rh-catalyzed enantioselective hydrogenation using the Josiphos 2 ligand **1.104**

The success of 1,2-disubstituted planar-chiral ferrocene ligands is not limited to compounds that form 6-membered metallacycles like Josiphos **1.69** and Fc-Phox **1.87**. The large number of applications of Walphos **1.84**, Taniaphos **1.85** and BoPhoz **1.86** have proven that 7 and 8-membered metallacycles can be highly efficient catalytic systems as well. These applications include ruthenium- and rhodium-catalyzed hydrogenation of a large number of different substrates and a variety of copper-catalyzed reactions like dialkylzinc additions to activated imines, reductive additions of aldehydes and methylketones to methylacrylates and reductions of α,β-unsaturated ketones with silanes.[116,120] For several of these reactions, catalytic systems with Josiphos ligands gave inferior results in terms of enantioselectivity, productivity or catalyst activity. Rhodium/BoPhoz-catalyzed hydrogenation reactions were successfully applied (full conversion, *ee* of 98% and TON of 2000) for the synthesis of a precursor for a number of pharma-

ceutically active ingredients, by Eastman on multi-kilogram scale.[131] Moreover, a rhodium/Walphos-catalyzed hydrogenation has been realized on a multi-ton scale for the production of the renin inhibitor SPP100 against hypertension by Novartis. [120,132]

The ferrocene backbone is highly suitable for the design of a chiral DMAP-type nucleophilic catalyst. Because nucleophilic catalysis does not require intervention of transition metals, these ferrocene complexes can be used as such as a chiral catalytic system. Credits are owed to Fu for his massive contributions in this research topic. His planar-chiral ferrocene-based DMAP catalytic systems have proven to be highly successful in a variety of asymmetric inter- and intramolecular acylations, [2+2]-cycloadditions and asymmetric addition reactions to ketenes among others.[133] Of all known ligands with a planar-chiral ferrocene backbone, this is one of the few successful ligands that only possesses planar-chirality (without the presence of a stereocenter or a chirality axis). One of the success factors is attributed to the pentamethyl or pentaphenyl substitution on the Cp ring, which enhances the shielding from attack of the bottom side.[120] Other heterocyclic chiral ferrocene ligands with a nitrogen of phosphorus atom as part of the Cp ring and their applications in asymmetric transition metal catalysis are reported as well.[116,120]

1.5. References

[1] L. Kelvin, *Baltimore Lectures on Molecular Dynamics and the Wave Theory of Light*, Cambridge University Press, London, **1904**

[2] G. P. Moss, *Pure Appl. Chem,* **1996**, *68*, 2193-2222

[3] https://en.wikipedia.org/wiki/Chirality, website consulted on 20/08/2016

[4] (a) https://en.wikipedia.org/wiki/Chirality, website consulted on 20/08/2016 (b) Scanned by T. Meijer – P. H. Nyst, **1878-1881**, *Conchyliologie des terrains tertiaries de la Belgique*, Ann. Mus. r. Hist. nat. Belg., 3: 1-262 (1778), 28 pls (1881)

[5] (a) R. S. Cahn, C. K. Ingold, *J. Chem. Soc.*, **1951**, *0*, 612-621(b) R. S. Cahn, C. Ingold, V. Prelog, *Experientia*, **1956**, *12*, 81-94 (c) R. S. Cahn, C. Ingold, V. Prelog, *Angew. Chem. Int. Ed.*, **1966**, *5*, 385-415 (d) V. Prelog, G. Helmchen, *Angew. Chem. Int. Ed.*, **1982**, *21*, 567-583

[6] H. D. Flack, *Acta Cryst.*, **2009**, *A65*, 371-389

[7] A detailed chronological description of the historic events and the numerous scientists contributing to the origin of the field of stereochemistry can be found in: A. Guijarro, M. Yus, *The Origin of Chirality in the Molecules of Life*, RSC Publishing, **2009**, pp. 1-5; and references therein

[8] International Union of Pure and Applied Chemistry Compendium of Chemical Terminology Gold Book, **2014**, Version 2.2.3, pp. 1223

[9] A. Kekulé, *Annalen der Chemie und Pharmacie*, **1857**, *104*, 129-150

[10] J.-A. Le Bel, *Bull. Soc. Chim. Paris*, **1874**, *22*, 337

[11] (a) S. Pizzarello, *Acc. Chem. Res.*, **2006**, *39*, 231-237. (b) A. Cordova, M. Engqvist, I. Ibrahem, J. Casas, H. Sunden, *Chem. Commun.*, **2005**, 2047-2049. (c) J. Bailey, *Acta Astroonautica*, **2000**, *46*, 627-631. (d) W. A. Bonner, *Orig. Life Evol. Biosphere*, **1991**, *21*, 59-111. (e) S.F. Mason, *Nature*, **1985**, *314*, 400-401

[12] M. Reist, P. A. Carrupt, E. Francotte, B. Testa, *Chem. Res.Toxicol.*, **1998**, *11*, 1521-1528

[13] FDA's Policy Statement for the Development of New Stereoisomeric Drugs (Stereoisomeric Drug Policy), *Fed. Regist.*, **1992**, 57 FR22249

[14] (a) https://prezi.com/fe7lir2p8r6m/ap-chemistry-final-project-thalidomide/, website consulted on 21/08/2016; (b) http://helix.northwestern.edu/sites/helix/files/styles/16by9/public/legacy_files/image-1_2.jpeg?itok=mGmk0CGT, website consulted on 21/08/2016

[15] (a) T. S. Tracy, S. D. Hall, *Drug Metab. Dispos*, **1992**, *20*, 322-327. (b) S. S. Adams, P. Bresloff, C. G. Mason, *J. Pharm. Pharmacol.*, **1976**, *28*, 256-257

[16] G. Haniotakis, W. Francke, K. Mori, H. Redlich, V. Schurig, *J. Chem. Ecol.*, **1986**, *12*, 1559-1568

[17] International Union of Pure and Applied Chemistry Compendium of Chemical Terminology Gold Book, **2014**, Version 2.2.3, p. 911

[18] International Union of Pure and Applied Chemistry Compendium of Chemical Terminology Gold Book, **2014**, Version 2.2.3, p. 1449

[19] G. H. Christie, J. Kenner, *J. Chem. Soc. Transactions*, **1922**, *121*, 614-620

[20] https://www.revolvy.com/main/index.php?s=Atropisomerism&item_type=topic, website consulted on 15/08/2017

[21] I. Alkorta, J. Elguero, C. Roussel, N. Vanthuyne, P. Piras, *Adv. Heterocycl. Chem.*, **2012**, *105*, 1-188

[22] T. Noël, J. Van der Eycken, *Green Process. Synth.*, **2013**, *2*, 297-309

[23] K. Schlögl, *Top. Stereochem.*, **1967**, *1*, 39-91

[24] V. Böhmer, D. Kraft, M. Tabatabai, *J. Inclusion Phenom. Mol. Recognit. Chem.,* **1994**, *19*, 17-39

[25] A. Dalla Cort, L. Mandolini, C. Pasquini, L. Schiaffino, *New J. Chem.*, **2004**, *28*, 1198-1199

[26] A. Szumna, *Chem. Soc. Rev.,* **2010**, *39,* 4274-4285

[27] B. R. Buckley, J. Y. Boxhall, P. C. B. Page, Y. H. Chan, M. R. J. Elsegood, H. Heaney, K. E. Holmes, M. J. McIldowie, V. McKee, M. J. McGrath, M. Mocerino, A. M. Poulton, E. P. Sampler, B. W. Skelton and A. H. White, *Eur. J. Org. Chem.*, **2006**, *22*, 5117-5134.

[28] H. Lorenz, A. Seidel-Morgenstern, *Angew. Chem. Int. Ed.*, **2014**, *53*, 1218-1250

[29] A. M. Rouhi, *Chem. Eng. News*, **2003**, *81*, 56-61

[30] R.A. Sheldon, *Chirotechnology: Industrial Synthesis of Optically Active Compounds*, Marcel Dekker, Wiley, New York, **1993**

[31] *Chiral Drugs: Chemistry and Biological Action*, Eds: G.-Q. Lin, Q.-D. You, J.-F. Cheng, Wiley, Hoboken, **2011**

[32] A.M. Rouhi, *Chem. Eng. News*, **2004**, *82*, 47-62

[33] M. Kaspereit, S. Swernath, A. Kienle, *Org. Process Res. Dev.*, **2012**, *16*, 353-363

[34] L. A. Nguyen, H. He, C. Pham-Huy, *Int. J. Biomed. Sci.*, **2006**, *2*, 85-100

[35] S.C. Stinson, *Chem. Eng. News*, **2001**, *79*, 45-57

[36] A.M. Rouhi, *Chem. Eng. News*, **2003**, *81*, 45-55

[37] J. Blumenstein, *Chirality in Industry II, Developments in the manufacture and Applications of Optically Active Compounds*, Eds: A.N. Collins, G. Sheldrake, J. Crosby, Wiley, Chichester, **1997**

[38] H.-U. Blaser, F. Spindler, M. Studer, *Appl. Catal., A*, **2001**, *221*, 119-143

[39] H.-U. Blaser, *Chem. Commun.*, **2003**, *3*, 293-296

[40] A. C. Daugan, PCT Int. WO 9519978, **1996**, Chem. Abstr., 124, p. 55977

[41] A. C. Daugan, P. Grondin, C. Ruauld, A.-N. Le Monnier de Gouville, H. Coste, J. M. Linget, J. Kirilovsky, F. Hyafil, R. Labaudinibre, *J. Med. Chem.*, **2003**, *46*, 4533-4542

[42] International Union of Pure and Applied Chemistry Compendium of Chemical Terminology Gold Book, **2014**, Version 2.2.3, pp. 1185-1186

[43] J. M. Hawkins, T. J. N. Watson, *Angew. Chem. Int. Ed.*, **2004**, *43*, 3224-3228

[44] R. N. Patel, *Coord. Chem. Rev.*, **2008**, *252*, 659-701

[45] Z. Xu, J. Singh, M. D. Schwinden, B. Zheng, T. P. Kissick, B. Patel, M. J. Humora, F. Quiroz, L. Dong, D.-M. Hsieh, J. E. Heikes, M. Pudipeddi, M. D. Lindrud, S. K. Srivastava, D. R. Kronenthal, R. H. Mueller, *Org. Process Res. Dev.*, **2002**, *6*, 323-328

[46] R. N. Patel, L. Chu, R. Mueller, *Tetrahedron: Asymmetry*, **2003**, *14*, 3105-3109

[47] W. Notz, F. Tanaka, C. F. Barbas, *Acc. Chem. Res.*, **2004**, *37,* 580-591

[48] A. B. Northrup, D. W. C. MacMillan, *J. Am. Chem. Soc.*, **2002**, *124*, 6798-6799

[49] U.-H. Dolling, P. Davies, E. J. J. Grabowski, *J. Am. Chem. Soc.*, **1984**, *106*, 446-447

[50] K. Brak, E. N. Jacobsen, *Angew. Chem. Int. Ed.*, **2012**, *51*, 2-30

[51] S. Mayer, B. List, *Angew. Chem. Int. Ed*, **2006**, *45*, 4193-4195

[52] M. Stadler, B. List, *Synlett*, **2008**, *4*, 597-599

[53] A. Piscopio, J. M. Hawkins, S. Caron, S. E. Kelly, J. W. Raggon, M. J. Castaldi, R. W. Dugger, S. G. Ruggeri, US Patent 6096906, **2000**

[54] J. van Ooyen, S. Noack, M. Bott, A. Reth, L. Eggeling, *Biochnol. Bioeng.*, **2012**, *109*, 2070-2081

[55] J. E. Thiemann, C. Pagani, H. Pagani, US Patent 3700558, **1972**

[56] K. Nakayama, H. Hagino, US Patent 3849251, **1974**

[57] E. Vedejs, M. Jure, *Angew. Chem. Int. Ed.*, **2005**, *44*, 3974-4001

[58] J.M. Keith, J.F. Larrow, E.N. Jacobsen, *Adv. Synth. Catal.*, **2001**, *343*, 5-26

[59] B. A. Persson, A. L. E. Larsson, M. Le Ray, J.-E. Bäckvall, *J. Am. Chem. Soc.*, **1999**, *121*, 1645-1650

[60] O. Pàmies, J.-E. Bäckvall, *J. Org. Chem.*, **2001**, *66*, 4022-4025

[61] A. Collet, *Enantiomer*, **1999**, *4*, 157-172

[62] J. Jacques, A. Collet, S.H. Wilen, *Enantiomers, Racemates and Resolutions*, Krieger, Malabar, **1994**

[63] L. Pérez-Carcia, D. B. Amabilino, *Chem. Soc. Rev.*, **2007**, *36*, 941-967

[64] L.-C. Sögütoglu, R. R. E. Steendam, H. Meekes, E. Vlieg, F. P. J. T. Rutjes, *Chem. Soc. Rev.*, **2015**, *44*, 6723-6732

[65] M. Klussmann, A. J. P. White, A. Armstrong, D. G. Blackmond, *Angew. Chem. Int. Ed*, **2006**, *45*, 7985-7989

[66] C. Viedma, *Astrobiology*, **2007**, *7*, 312-319

[67] D. G. Blackmond, *Chem. Eur. J.*, **2007**, *13*, 3290-3295

[68] W. L. Noorduin, T. Izumi, A. Millemaggi, M. Leeman, H. Meekes, W. J. Van Enckevort, R. M. Kellog, B. Kaptein, E. Vlieg, D. G. Blackmond, *J. Am. Chem. Soc.*, **2008**, *130*, 1158-1159

[69] C. Viedma, J. E. Ortiz, T. de Torres, T. Izumi, D. G. Blackmond, *J. Am. Chem. Soc.*, **2008**, *130*, 15274-15275

[70] J. E. Hein, B. H. Cao, C. Viedma, R. M. Kellog, D. G. Blackmond, *J. Am.Chem. Soc.*, **2012**, *134*, 12629-12636

[71] *"From racemates to single enantiomers-chiral synthetic drugs over the last 20 years"*: H. Murakami, *Novel Optical Resolution Technologies, Top. Curr. Chem.*, *Vol 269*, Eds: K. Sakai, N. Hirayama, R. Tamura, Springer, Berlin, **2007**, pp. 273-299

[72] A. Kaiser, M. Scheer, W. Häusermann, L. Marti, US Patent 3969397, **1976**

[73] S. Mao, Y. Zhang, S. Rohani, A. K. Ray, *Can. J. Chem. Eng.*, **2014**, *92*, 1283-1292

[74] M. Negawa, F. Shoji, *J. Chromatogr.*, **1992**, *590*, 113-117

[75] J. Blehaut, R.-M. Nicoud, *Anal. Magazine*, **1998**, *26*, M60-M70

[76] P. Sá Gomes, M. Zabkova, M. Zabka, M. Minceva, A. E. Rodrigues, *AIChE J.*, **2010**, *56*, 125-142

[77] S. Abel, M. Juza, *Less common applications of enantioselective HPLC using the SMB technology in the pharmaceutical industry.* In: *Chiral Separation Techniques: A practical approach*, 3rd ed., Ed. G. Subramanian, Wiley-VCH Verlag GmbH & Co.KGaA, Weinheim, Germany, **2006**, pp. 203–273.

[78] D. J. Cram, J. M. Cram, *Container Molecules and Their Guests*, Royal Society of Chemistry, Cambridge, **1994**

[79] S. Zhao, Y.-M. Liu, *Electrophoresis*, **2001**, *22*, 2769-2774

[80] D. Kmecz, M. Simandi, E. Szekely, E. Fogassy, *Tetrahedron: Asymmetry*, **2004**, *15*, 1841-1845

[81] R. M. C. Viegas, C. A. M. Afonso, J. G. Crespo, I. M. Coelhoso, *Sep. Purif. Technol.*, **2007**, *53*, 224-234

[82] M. Togrul, Y. Turgut, H. Hosgoren, *Chirality*, **2004**, *16*, 351-355

[83] P. E. Hare, E. Gil-Av, *Science*, **1979**, *204*, 1226-1228

[84] H. Nishizawa, K. Tahara, A. Hayashida, Y. Abe, *Anal. Sci.*, **1993**, *9*, 611-615

[85] B.-G. Lim, C.-B. Ching, R. B. H. Tan, S.-C. Ng, *Chem. Eng. Sci.*, **1995**, *50*, 2289-2298

[86] H. Lorenz, P. Seehan, A. Seidel-Morgenstern, *J. Chromatogr. A*, **2001**, *908*, 201-214

[87] H. J. Federsel, *Org. Process Res. Dev.*, **2012**, *16*, 260-261

[88] H. Kaemmerer, Z. Horvath, J. W. Lee, M. Kaspereit, R. Arnell, M. Hedberg, B. Herschend, M. J. Jones, K. Larson, H. Lorenz, A. Seidel-Morgenstern, *Org. Process Res. Dev.*, **2012**, *16*, 331-342

[89] R. Noyori, *Angew. Chem. Int. Ed.*, **2013**, *52*, 79-92

[90] R. Noyori, M. Kitamura, T. Ohkuma, *Proc. Natl. Acad. Sci. U.S.A.*, **2004**, *101*, 5356-5362

[91] R. Noyori, *Asymmetric Catalysis in Organic Chemistry*, Wiley, New York, **1994**

[92] B. C. Gibb, *Nat. Chem.*, **2012**, *4*, 237-238

[93] R. E. Gawley, *J. Org. Chem.*, **2006**, *71*, 2411-2416

[94] J. A. Gladysz, *Pure Appl. Chem.*, **2001**, *73*, 1319-1324

[95] S. K. Ritter, *Chem. Eng. News*, **2013**, *91*, 46-47

[96] S. Kozuch, J. M. L. Martin, *ACS Catal.*, **2012**, *2*, 2787-2794

[97] S. Kozuch, *ACS Catal.*, **2013**, *3*, 380

[98] G. Lente, *ACS Catal.*, **2013**, *3*, 381-382

[99] W. S. Knowles, *Angew. Chem. Int. Ed.*, **2002**, *41*, 1998-2007

[100] R. Noyori, *Angew. Chem. Int. Ed.*, **2002**, *41*, 2008-2022

[101] K. B. Sharpless, *Angew. Chem. Int. Ed.*, **2002**, *41*, 2024-2032

[102] T. P. Yoon, E. N. Jacobsen, *Science*, **2003**, *299*, 1691-1693

[103] A. Pfaltz, W. J. Drury, *Proc. Natl. Acad. Sci. U.S.A.*, **2004**, *101*, 5723-5726

[104] *Chemfiles*, **2006**, *6*, 1-16

[105] J. K. Whitesell, *Chem. Rev.*, **2000**, *33*, 336-345

[106] (a) G. Helmchen, A. Pfaltz, *Acc. Chem. Res.*, **2000**, *33*, 336-345 (b) A. Pfaltz, *Acta Chem. Scand. B*, **1996**, *50*, 189-194 (c) G.Helmchen, S. Kudis, P. Sennhen, H. Steinhagen, *Pure Appl. Chem.*, **1997**, *69*, 513-518

[107] J. F. Teichert, B. L. Feringa, *Angew. Chem. Int. Ed.*, **2010**, *49*, 2486-2528

[108] X. Zhang, *Enantiomer*, **1999**, *4*, 541

[109] F. Lagasse, H. B. Kagan, *Chem. Pharm. Bull.*, **2000**, *48*, 315

[110] A. H. M. de Vries, A. Meetsma, B. L. Feringa, *Angew. Chem. Int. Ed. Engl.*, **1996**, *35*, 2374-2376

[111] (a) T. J. Kealy, P. L. Pauson, *Nature*, **1951**, *168*, 1039-1040 (b) S. A. Miller, J. F. Telboth, J. F. Tremaine, *J. Chem. Soc.*, **1952**, 632-635

[112] (a) D. R. van Staveren, N. M. Metsler-Nolte, *Chem. Rev.*, 2004, *104*, 5931-5985 (b) G. Jaouen, A. Vessières, S. Top, *Chem. Soc. Rev.*, **2015**, *44*, 8802-8817

[113] L. Xu, Y.-X. Wang, L.-J. Chen, H.-B. Yang, *Chem. Soc. Rev.*, **2015**, *44*, 2148-2167

[114] R. Pietschnig, *Chem. Soc. Rev.*, **2016**, *45*, 5216-5231

[115] L.-X. Dai, T. Tu. S.-L. You, W.-P. Deng, X.-L. Hou, *Acc. Chem. Res.*, **2003**, *36*, 659-667

[116] R. G. Arrayás, J. Adrio, J. C. Carretero, *Angew. Chem. Int. Ed.*, **2006**, *45*, 7674-7715

[117] (a) J. Chan, T. F. Jamison, *J. Am. Chem. Soc.*, **2003**, *125*, 11514-11515 (b) J. Chan, T.F. Jamison, *J. Am. Chem. Soc.*, **2004**, *126*, 10682-10691 (c) K. M. Miller, E. A. Colby, K. S. Woolin, T.F. Jamison, *Adv. Synth. Catal.*, **2005**, *347*, 1533-1536

[118] (a) A. Marinetti, F. Labrue, J.-P. Genêt, *Synlett*, **1999**, 1975-1977 (b) U. Berens, M. J. Burk, A. Gerlach, W. Hems, **2000**, *Angew. Chem. Int. Ed.*, 39, 1981-1984

[119] I. Appleby, L. T. Boulton, C. J. Cobley, C. Hill, M. L. Hughes, P. D. de Koning, I. C. Lennon, C. Praquin, J. A. Ramsden, H. J. Samuel, N. Wilis, *Org. Lett.*, **2005**, *7*, 1931-1934

[120] *Chiral ferrocenes in asymmetric catalysis*, Eds.: L.-X. Dai, X.-L. Hou, Wiley-VCH Verlag GmbH & Co. KGaA, **2010**

[121] (a) J. J. Almena Perea, A. Börner, P. Knochel, *Tetrahedron Lett.*, **1998**, *39*, 8073-8076 (b) M. Lotz, T. Ireland, J. J. Almena Perea, P. Knochel, *Tetrahedron Asymmetry*, **1999**, *10*, 1839-1842

[122] P. Barbaro, A. Togni, *Organometallics*, **1995**, *7*, 3570-3573

[123] A. D. Sadow, A. Togni, *J. Am. Chem. Soc.*, **2005**, *127*, 17012-17024

[124] T. J. Colacot, *Chem. Rev.*, **2003**, *103*, 3101-3118

[125] H.-U. Blaser, W. Brieden, B. Pugin, F. Spindler, M. Studer, A. Togni, *Top. Catal.*, **2002**, *19*, 3-16

[126] H.-U. Blaser, *Adv. Synth. Catal.*, **2002**, *344*, 17-31

[127] D. Schaarsmidt, H. Lang, *Organometallics*, **2013**, *32*, 5668-5704

[128] H.-U. Blaser, M. Lotz, A.Y. Platonov, *e-EROS Encyclopedia of Reagents for Organic Synthesis*, **2014**, 1-21

[129] D. A. Dobbs, K. P. M. Vanhessche, E. Brazi, V. Rautenstrauch, J.-Y. Lenoir, J.-P. Genêt, J. Wiles, S. H. Bergens, *Angew. Chem. Int. Ed.*, **2000**, *39*, 1991-1995

[130] Y. Hsiao, N. R. Rivera, T. Rosner, S. W. Krska, E. Njolito, F. Wang, Y. Sun, J. D. Armstrong, E. J. J. Grabowski, R. D. Tillyer, F. Spindler, C. Malan, *J. Am. Chem. Soc.*, **2004**, *126*, 9918-9919

[131] N. W. Boaz, S. E. Large, J. A. Ponasik, Jr., M.K Moore, T. Barnette, W. D. Nottingham, *Org. Process. Res. Dev.*, **2005**, *9*, 472-478

[132] T. Sturm, W. Weissensteiner, F. Spindler, *Adv. Synth. Catal.*, **2003**, *345*, 160-164

[133] (a) G. C. Fu, *Acc. Chem. Res*, **2000**, *43*, 412-420 (b) G. C. Fu, *Acc. Chem. Res*, **2004**, *37*, 542-547

DEFINITION OF THE PROBLEM, AIMS AND OUTLINE OF THIS THESIS

"Verleden heb je, toekomst moet je maken."

"What you have got is history, future you have to make."

Marc Andries

In 1966, Noyori serendipitously discovered that a chiral organometallic complex can be responsible for enantioinduction.[1] Since then the field of asymmetric (transition)metal catalysis has known a tremendous evolution. A wide variety of chiral catalysts have been developed for a comprehensive collection of enantioselective transformations in academia and industry. This gives the impression that for almost every reaction an enantioselective catalytic variant is available. However, the number of truly useful and applicable enantioselective catalysts is still limited. Many of the existing methods need to be improved and the request for new and better catalysts is still huge. Moreover, the development and applications of novel chiral catalytic systems can result in the exploration of new reactivities and new (enantioenriched) molecules. For these reasons, it is still desirable to develop efficient and operationally convenient ligands along this line with new structural motifs.

The key to efficient asymmetric catalysis is the combination of a metal with a suitable chiral organic ligand. An important characteristic of a ligand is the modularity that allows to fine-tune the electronic and steric features. The discovery and development of novel chiral catalysts is still based on serendipity, empirical knowledge and laborious work.

Different classes of chiral ligands have been synthesized and tested in a variety of asymmetric transition metal catalyzed reactions at the *Laboratory for Organic and Bioorganic Synthesis*. These ligands are shown in Figure 2.1 and a brief overview of the most important applications are summarized in Table 2.1.[2-14] Chiral imidates were developed as a new class of nitrogen-based ligands and were successfully applied in differ-

ent transformations. Bisimidate **2.01** was synthesized by Vankdyck and tested in the copper-catalyzed cyclopropanation, unfortunately without success. Later on Noël applied this ligand in the copper-catalyzed aziridination and obtained an *ee*-value of 45% in combination with a yield of 90% (entry 1, Table 2.1).[2] Noël and Bert coupled these novel imidate structures to a planar-chiral ferrocene backbone to obtain a small library of hybrid *P,N*-ligands **2.02** and successfully applied them in palladium-catalyzed asymmetric allylic alkylation reactions[3a] (entry 2, Table 2.1) and iridium-catalyzed asymmetric hydrogenations of unfunctionalized olefins.[3b] Afterwards, Janssens designed ligand **2.05** as an imidate-based Salen analogue and used it for the enantioselective epoxidation of alkenes (entry 5, Table 2.1).[4] Finally, Bert used the imidate moiety to synthesize ligand **2.06** and obtained good results in the iridium-catalyzed hydrogenation of unfunctionalized olefins (entry 6, Table 2.1).[5]

New C_2-symmetric bicyclo[2.2.1]heptadiene ligands **2.03** were synthesized by Vandyck and Noël and successfully applied in rhodium-catalyzed asymmetric 1,4- and 1,2-additions (entry 3, Table 2.1).[6] Later on Noël and Gök applied these ligands as well in the rhodium-catalyzed Mizoroki-Heck-type reaction and rhodium-catalyzed tandem conjugate addition/enantioselective protonation.[7]

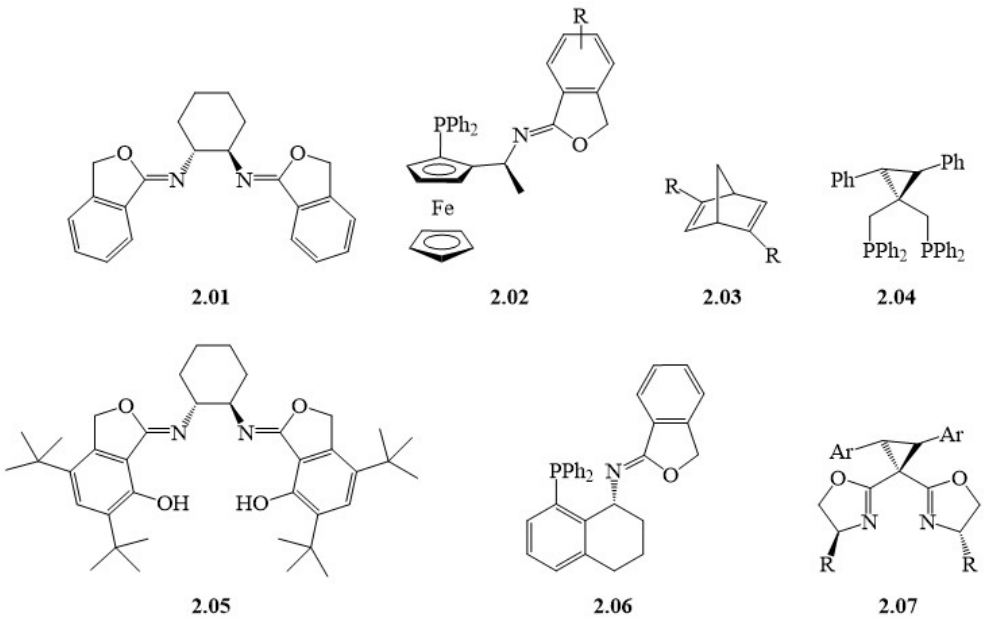

Figure 2.1 Ligands developed at the *Laboratory for Organic and Bioorganic Synthesis*

Another class of ligands developed in our research group is characterized by the presence of a chiral *trans*-2,3-diphenyl cyclopropane backbone. Diphosphane **2.04** was synthesized by Vervecken and he applied them in the rhodium-catalyzed asymmetric 1,4-addition of arylboronic acids[8,9] as well as rhodium-catalyzed hydrogenations of protected α-dehydroamino acids[8] (entry 4, Table 2.1). Gök developed a small library of C_2-symmetric Bis(oxazolines) **2.07** and tested them in palladium-catalyzed asymmetric allylic alkylation reactions (entry 7, Table 2.1), copper-catalyzed enantioselective cyclopropanations and copper-catalyzed enantioslective aziridinations.[10,11]

Ligand	Testreaction	Yield (%)	*ee* (%)
2.01	Cu(I)-catalyzed aziridination	90	45
2.02	Pd(0)-catalyzed allylic alkylation	99	99
2.03	Rh(I)-catalyzed 1,4-addition	95	96
2.04	Rh(I)-catalyzed hydrogenation	99	88
2.05	Mn(V)-catalyzed epoxidation	99	81
2.06	Ir(I)-catalyzed hydrogenation	99	90
2.07	Pd(0)-catalyzed allylic alkylation	90	96

Table 2.1 Applications of ligands developed at the *Laboratory for Organic and Bioorganic Synthesis*

In this thesis, three main classes of ligands will be studied: monodentate phosphoramidites (Figure 2.3), monodentate diamidophosphites (Figure 2.4) and bidentate Trost-type ligands (Figure 2.5). These ligands are commonly characterized by the presence of a chiral biferrocene ligand backbone. Besides the development of an efficient synthetic method to establish the ferrocene-ferrocene bond, which is supposed to be the key step, a second scientific goal is to explore the enantioinduction properties of this structural ligand motif in a benchmark test reaction. As mentioned in Chapter 1 (§ 1.4, *vide supra*), a wide variety of ferrocene ligands are already developed and successfully applied in a broad variety of asymmetric transition metal catalyzed reactions including some highly efficient large scale industrial processes. These applications indicate that ferrocene is a very suitable scaffold for designing novel chiral ligands. Indeed, diverse reasons including chemical properties, spatial orientation but also economic reasons were already highlighted. Other successful chiral ligands are characterized by the presence of an axially chiral ligand backbone. Noyori's BINAP and Feringa's MonoPhos are the most well-known examples, both belonging to the class of privileged chiral ligands

(*cf.* Figure 1.26, § 1.3, Chapter 1, *vide supra*). Despite the fact that the biferrocene-backbone generally benefits from the same properties making ferrocene a suitable ligand scaffold, in combination with its potential axially chiral properties, this structural ligand motif is remarkably a rather unexplored structural ligand motif in the field of asymmetric catalysis. Indeed, only a few examples of biferrocene-based ligands are successfully synthesized and tested in asymmetric transition metal catalyzed transformations (Figure 2.3).[15-27] Among them BIFEP-type ligands **2.08**, BIFEP (or 2,2'-bis(diphenylphosphino)-1,1'-biferrocene, R^1=Ph) itself was designed in analogy with Noyori's BINAP by substitution of the axially chiral C_2-symmetric binaphtyl backbone by the biferrocene backbone.[15-19] Bis(oxazoline) ligands **2.09** were also designed as the combination of a privileged ligand scaffold and the biferrocene structural motif.[20] Biferrocene-based ligands **2.10** belong to the family of *P,N*-type ligands.[21] The last family of successfully developed biferrocene-based ligands are the TRAP-type ligands.[22-27] They are designed in order to form a bidentate trans-chelated complex when they coordinate to a (transition) metal atom.

Consequently the chiral-biferrocene ligand scaffold clearly deserves more attention in designing novel chiral ligands and the field of asymmetric transition metal catalysis. Therefore monodentate phosphoramidite liglands **2.12-2.13**, monodentate diamidophosphite ligands **2.14** and bidentate Trost-type ligands **2.15-2.16** are proposed as novel chiral biferrocene-based ligands.

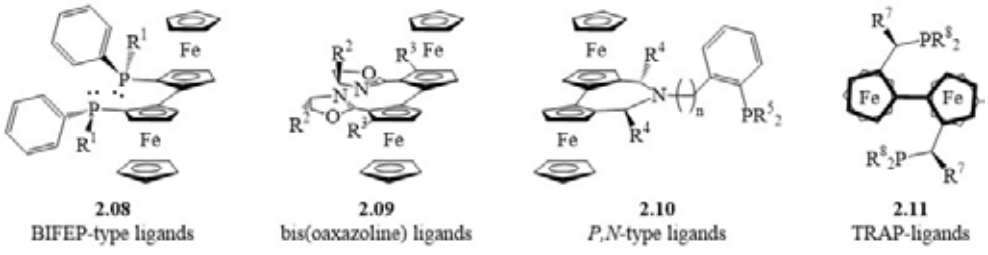

Figure 2.2 Biferrocene-based ligands successfully synthesized and tested in asymmetric transition metal catalyzed transformations

In Chapter 3, the development of two types of biferrocene-based phosphoramidite ligands will be discussed. The starting point for the proposed phosphoramidite ligands are Feringa's highly successful phosphoramidite ligands.[28] These ligands are characterized by the presence of a C_2-symmetric axially chiral binol ligand backbone which is

responsible for enantioinduction. Novel ligands **2.12** (Figure 2.3) are designed as biferrocene-based analogs of the privileged monodentate phosphoramidites. Alternative phosphoramidite ligands **2.13** were designed by incorporation of the biferrocene-backbone in the amine-substructure of the phosphoramidite functional group. For those ligands **2.13** were binol is applied as the diol-based substructure, the obtained ligands are designed by the combination of a rather unexplored chiral biferrocene backbone and privileged phosphoramidite ligand scaffold.

2.12 **2.13**

Figure 2.3 Novel chiral biferrocene-based monodentate phosphoramidite ligands

In Chapter 4, other alternatives for biferrocene-based phosphoramidite ligands **2.12** are designed by alteration of the oxygen and nitrogen atoms of the phosphoramidite functional group. These dimidophosphite ligands posses different electronic as well as steric effects what will effect their stability and coordination properties. Consequently, the chiral induction properties are totally different compared to those from phosphoramidite ligands. Different synthetic routes to obtain the proposed ligands, **2.14** (Figure 2.4) are discussed in Chapter 4.

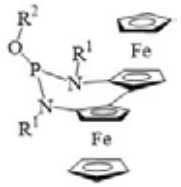

2.14

Figure 2.4 Novel chiral biferrocene-based monodentate diamidophosphite ligands

The synthesis of novel biferrocene-based Trost-type ligands **2.15** and **2.16**, which are illustrated in Figure 2.5, will be discussed in Chapter 5. These ligands are also designed by the principle of the combination of a highly successful ligand scaffold and the biferrocene ligand backbone. Indeed, bidentate Trost-type ligands have been successfully

applied in so-called Tsuji-Trost reactions of highly-demanding substrates, where other ligand-types give rather poor results in terms of enantiomeric excess and/or yield.[29]

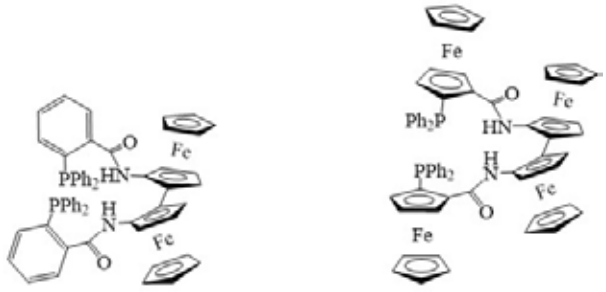

2.15 **2.16**

Figure 2.5 Novel chiral biferrocene-based Trost-type ligands

2.1. References

[1] H. Nozaki, S. Moriuti, H. Takaya, R. Noyori, *Tetrahedron Lett.*, **1966**, *7*, 5239-5244

[2] T. Noël, K. Vandyck, K. Robeyns, L. Van Meervelt, J. Van der Eycken, *Tetrahdedron*, **2009**, *65*, 8879-8884

[3] (a) T. Noël, K. Bert, E. Van der Eycken, J. Van der Eycken, *Eur. J. Org. Chem.*, **2010**, *21*, 4056-4061; (b) K. Bert, T. Noël, W. Kimpe, J. L. Goeman, J. Van der Eycken, *Org. Biomol. Chem.*, **2012**, *10*, 8539-8549

[4] P. Janssens, *Synthesis and evaluation of imidate-based ligands for asymmetric transition metal catalysis*, **2017**, Ghent University, Faculty of Sciences, Department of Organic and Macromolecular Chemistry, Laboratory for Organic and Bioorganic Synthesis

[5] K. Bert, *Synthese en valorisatie van imidaatgebaseerde liganden voor transitiemetaalkatalyse*, **2015**, Ghent University, Faculty of Sciences, Department of Organic and Macromolecular Chemistry, Laboratory for Organic and Bioorganic Synthesis

[6] T. Noël, K. Vandyck, J. Van der Eycken, *Tetrahedron,* **2007**, *63*, 12961-12967

[7] T. Noël, Y. Gök, J. Van der Eycken, *Tetrahedron: Asymmetry*, **2010**, *21*, 540-543

[8] E. Vervecken, M. Van Overschelde, T. Noël, Y. Gök, S. A. Rodríuez, S. Cogen, J. Van der Eycken, *Tetrahedron:* Asymmetry, **2010**, *21*, 2321-2328

[9] Y. Gök, T. Noël, J. Van der Eycken, *Tetrahedron: Asymmetry*, **2010**, *21*, 2768-2774

[10] Y. Gök, T. Noël, J. Van der Eycken, *Tetrahedron: Asymmetry*, **2010**, *21*, 2275-2280

[11] Y. Gök, J. Van der Eycken, *Helv. Chim. Acta.*, **2012**, *95*, 831-837

[12] T. Noël, K. Robeyns, L. Van Meervelt, E. Van der Eycken, J. Van der Eycken, *Tetrahedron: Asymmetry,* **2009**, *20*, 1962-1965

[13] T. Noël, K. Vandyck, J. Van der Eycken, *"Cyclic Imidate Ligands"*, UK Patent Application 0905995.7, PCT/EP2010/054549

[14] T. Noël, J. Van der Eycken, *Green Process. Synth.*, **2013**, *2*, 297-309

[15] M. Sawamura, A. Yamauchi, T. Takegawa, Y. Ito, *J. Chem. Soc., Chem. Commun.*, **1991**, 874-875

[16] L. Xiao, K. Mereiter, F. Spindler, W. Weissensteiner, *Tetrahedron: Asymmetry*, **2001**, *12*, 1105-1108

[17] G. Espino, L. Xiao, M. Puchberger, K. Mereiter, F. Spindler, B. R. Manzano, F. A. Jalón, W. Weissensteiner, *Dalton Trans.*, **2009**, 2751-2763

[18] U. Nettekoven, M. Wildhalm, P. C. J. Kamer, P. W. N. M. van Leeuwen, K. Mereiter, M. Lutz, A. L. Spek, *Organometallics,* **2000**, *19*, 2299-2309

[19] U. Nettekoven, M. Widhalm, H. Kalchhauser, P. C. J. Kamer, P. W. N. M. van Leeuwen, M. Lutz, A. L. Spek, *J. Org. Chem.*, **2001**, *66*, 759-770

[20] S.-G. Kim, C.-W. Cho, K. H. Ahn, *Tetrahedron: Asymmetry*, **1997**, *8*, 1023-1026

[21] L.Xiao, W. Weissensteiner, K. Mereiter, M. Widhalm, *J. Org. Chem.*, **2002**, *67*, 2206-2214

[22] M. Sawamura, H. Hamashima, Y. Ito, *Tetrahedron: Asymmetry*, **1991**, *2*, 593-596

[23] M. Sawamura, H. Hamashima, M. Sugawara, R. Kuwano, Y. Ito, *Organometallics*, **1995**, *14*, 4549-4558

[24] R. Kuwano, T. Uemura, M. Saitoh, Y. Ito, *Tetrahedron Lett.*, **1999**, *40*, 1327-1330

[25] M. Sawamura, H. Hamashima, Y. Ito, *J. Am. Chem. Soc.*, **1992**, *114*, 8295-8296

[26] M. Sawamura, R. Kuwano, Y. Ito, *Angew. Chem. Int. Ed.*, **1994**, *33*, 111-113

[27] (a) R. Kuwano, T. Uemura, M. Saitoh, Y. Ito, *Tetrahedron: Asymmetry*, **2004**, *15*, 2263-2271; (b) P. Barbaro, C. Bianchini, G. Giambastiani, S. L. Parisel, *Coord. Chem. Rev.*, **2004**, *248*, 2131-2150

[28] J. F. Teichert, B. L. Feringa, Angew. Chem. Int. Ed., **2010**, 49, 2486-2528

[29] (a) J. T. Mohr, B. M. Stoltz, *Chem. Asian J.*, **2007**, *2*, 1476-1491; (b) Z. Lu, S. Ma, *Angew. Chem. Int. Ed.*, **2008**, *47*, 258-297; (c) B. M. Trost, J. Xu, T. Schmidt, *J. Am. Chem. Soc.*, **2009**, *131*, 18343-18357 (d) B. M. Trost, D. J. Michaelis, J. Charpentier, J. Xu, *Angew. Chem. Int. Ed.*, **2012**, *51*, 204-208; (e) R. Akula, R. Doran, P. J. Guiry, *Chem. Eur. J.*, **2016**, *22*, 9938-9942

NOVEL MONODENTATE BIFERROCENE-BASED PHOSPHORAMIDITE LIGANDS

"Ik droom geregeld van mooie moleculen, van hoe je nieuwe moleculen bouwt. Daar heb je verbeeldingskracht voor nodig, maar het is zo'n prachtige wereld"

"I regularly dream of beautiful molecules, of how to build new molecules. Therefore you need imagination, but it is such a wonderful world"

Bernard Lucas Feringa, Rijksuniversiteit Groningen, 2016

3.1. The Metal-Phosphorus Bonding

In the field of asymmetric catalysis phosphorus-containing ligands are most widely used. These ligands have a lone pair on the central phosphorus atom that can be donated to empty d-orbitals of a metal, with formation of a P-M σ-bond. Figure 3.1 (a) illustrates this phosphorus-metal bonding situation. Phosphines, phosphonites, phosphites, phosphoramidites and diamidophosphites, are examples of phosphorus-containing ligands which differ in the nature of the R group on the phosphorus atom. All of them are classified as L-type ligands. Besides the σ-donating properties, these ligands are known to be π-acceptors (π-acids) as well. In contrast to classical π-acceptors, like *e.g.* CO, where an empty π^* orbital accepts electrons from a filled d-orbital of the metal, for phosphorus containing ligands, the empty σ^* orbitals of the P-R bonds plays the role of acceptor. This backbonding situation is illustrated in Figure 3.1 (b).[1] In general, it has been observed that the π-acceptor capacity increases with the electronegativity of the substituents on the phosphorus atom.[2,3] This means that electronic properties of the ligand (and the metal center) can be modified in a systematic and predictable way by variation of the R groups. Moreover, differentiation of these R groups will also allow to fine-tune the steric properties of the metal complexes. This makes phosphorus-containing ligands highly modular and allows to have full control over the most important properties of chiral ligands.

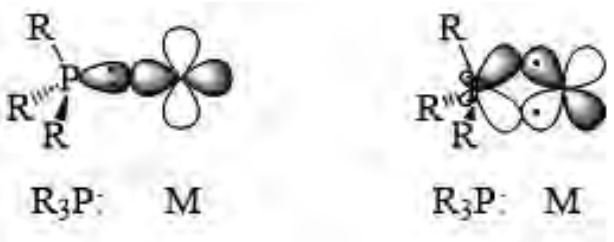

Figure 3.1 (a) (left) Bonding coordination model of phosphorus containing ligands (b) (right) Backbonding coordination model of these ligands

The steric effects of phosphorus ligands have been quantified by Tolman with his concept of the cone angle (θ_P).[4] This is obtained by taking a space-filling model of the M(PR_3) group, folding back the R subsitutents as far as they will go, and measuring the angle of the cone that will just contain all of the ligand, when the apex of the cone is at the metal (Figure 3.2). The concept of the cone angle has proven to be very useful in rationalizing the behavior of phosphorus ligands and their complexes such as the stability of a metal-ligand bond. For example, bulky ligands are known to enforce the reductive elimination step.

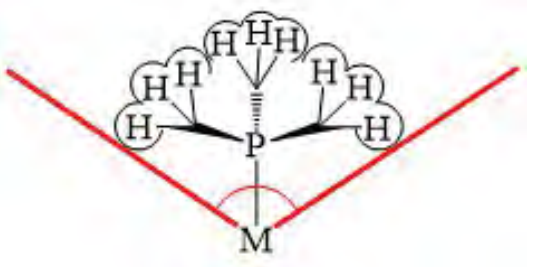

Figure 3.2 Concept of Tolman's cone angle

In his *Chemical Review* of 1977 Tolman quantified the electronic effects of various PR_3 ligands as well.[4] Therefore he compared the ν(CO) IR frequencies of a series of complexes (PR_3)Ni(CO_3) with different phosphine ligands. Stronger electron donating phosphines increase the electron density on Ni, which will be passed along to the CO ligands by back donation resulting in lower ν(CO) frequencies.

Table 3.1 shows some values of Tolman's cone angle (θ_P) and ν(CO) frequencies of (PR_3) $Ni(CO)_3$ complexes for some common monodentate phosphine, phosphite, phosphoramidite and diamidophosphite ligands. It is obvious that values of θ_P are increasing when phosphorus is substituted with more voluminous groups.

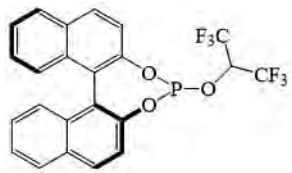

3.01

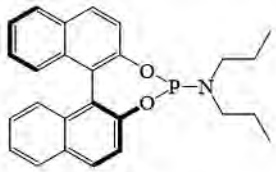

3.02

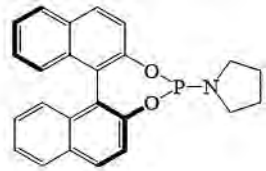

3.03

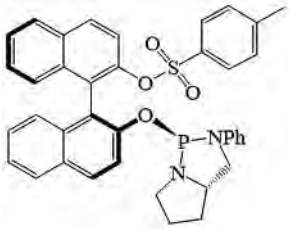

3.04

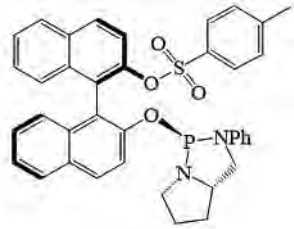

3.05

Ligand	θ_P (°)	ν_{CO} (cm^{-1})	Ref
PH_3	87	2083.2	4
PMe_3	118	2064.1	4
PEt_3	132	2061.7	4
PPh_3	145	2068.9	4
$P(i\text{-}Pr)_3$	160	2059.2	4
$P(t\text{-}Bu)_3$	182	2056.1	4
$P(OMe)_3$	107	2079.5	4
$P(NMe_2)_3$	157	2061.9	4
3.01	111[3]	-	5
3.02	140[3]	-	5
3.03	109[3]	-	5
3.04	135[3]	-	6
3.05	129[3]	-	6

Table 3.1 Steric (θ_P) and electronic (ν_{CO}) effects of $(PR_3)Ni(CO)_3$ complexes with common P-donor ligands and some interesting monodentate phosphite and phosphoramidite ligands

For alkyl substituents, ν(CO) frequencies are decreasing with increasing steric bulk of the ligands. More interesting are the ν(CO) frequencies of PMe_3, $P(OMe)_3$ and $P(NMe_2)_3$.

3 Tolman cone angles calculated via a semi-emperical quantum-mechanical method.

Trimethyl phosphite has a ν(CO) frequency larger than that of trimethyl phosphine whereas the phosphorus triamide has a ν(CO) frequency smaller than PMe_3. This means that NMe_2 substituents increase the electron density on phosphorus (and nickel), whereas OMe has net electron withdrawing properties. This has important consequences towards the stability and reactivity of these ligands. For example, $P(NMe_2)_3$ and PMe_3 are sensitive towards oxidation in air whereas, $P(OMe)_3$ is bench stable.

3.2. Monodentate Ligands for Asymmetric Catalysis

Some of the first papers published in the field of asymmetric transition metal catalysis already mention the successful use of monodentate ligands.[7] Nevertheless, the introduction of the chiral diphosphine DIOP by Kagan in 1971 was the beginning of the highly successful era of C_2-symmetric bidentate ligands.[8] Their approach of reducing many degrees of conformational freedom in the metal-ligand complexes resulted in the dogma of superiority of rigid, C_2-symmetric bidentate phosphorus ligands. However, as already mentioned in § 1.4.2 there is no fundamental reason why these ligands should be superior in comparison to others. After the rediscovery of monodentate ligands by Feringa in 1996 [9], the research groups of Reetz, Pringle and Feringa and de Vries independently reported the use of different classes of chiral monodentate phosphorus containing ligands for asymmetric hydrogenations in 2000 (Figure 3.3).[10-12] Since these publications, many more catalytic systems using monodentate phosphorus ligands have been developed. The latest developments in the field of asymmetric catalysis using these monophosphorus ligands have recently been reviewed by Fu and Tang.[13]

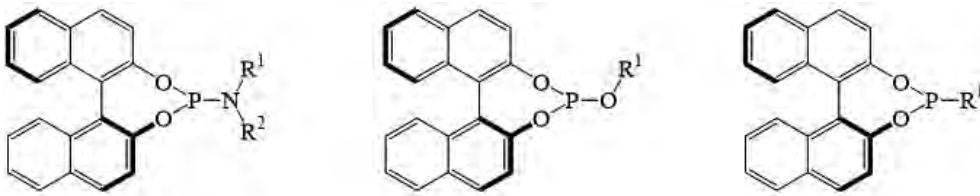

Figure 3.3 Three different classes of monodentate ligands applied in asymmetric hydrogenation reactions

Because Feringa's phosphoramidite ligands belong to the class of privileged chiral ligands, it is absolutely impossible to give an overview of all successful applications of these monodentate ligands in this thesis. An excellent review has been published in 2010 and therefore we want to refer to this publication for a detailed description of this type of ligands including structure, synthesis, properties and high-value applications.[2] Of course, there are currently still many papers being published using Feringa's phosphoramidite ligands for new asymmetric transition metal-catalyzed transformations.[13,14] In addition, novel phosphoramidites have been synthesized via advanced and/or simple modulations of the chiral diol backbone as well as the amine structure. Among them are excellent papers by prominent researchers such as Trost, Carreira, Feringa and Zhou.[15-20] This research has proven that high modularity in ligand design is an enormous advantage for diverse applications and success-level for the development of novel chiral ligands. A few examples of these modified phosphoramidite ligands are shown in Figure 3.4. Ligand **3.09** has a chiral binol backbone in combination with a modified long conjugated amine system. It was introduced into the field of asymmetric catalysis by Carreira[18] who successfully applied this ligand later on in many asymmetric transformations.[19] Based on his research, this ligand became one the most important phosphoramidites ligands. However, it is important to mention that this ligand does not belong to the class of monodentates but instead a hybrid metal-complex is formed due to coordination of the olefin bond in combination with the central phosphorus atom. Ligand **3.10**, first reported in 1998 by Feringa and co-workers for a copper-catalyzed conjugate addition of diethylzinc to cyclic enones, is characterized by a taddol chiral backbone.[17] Other common chiral alcohol backbones are the spiro-diol and bis-tetralin-diol substructures present in ligands **3.11** and **3.12** respectively. These ligands were both synthesized and tested in rhodium-catalyzed enantioselective hydrogenation reactions by the research group of Zhou.[20] For this reaction, spiro-diol based ligand **3.11** gave higher enantioselectivities than bis-tetralin-diol analogue **3.12**, 99% vs 96% *ee*. The authors attribute this to the larger dihedral angle of the aromatic planes for ligand **3.11**. More peculiar monodentate phosporamidite ligands are **3.13** and **3.14**. Both of them were introduced in the field of asymmetric transition metal catalysis by Trost. These ligands are characterized by excentric binol-based frameworks in combination with chiral, 5-membered substituted amines.[16,21] Ligand **3.13** was successfully applied in a ruthenium-catalyzed metallo-ene reaction[16] and **3.14** proved to be the ligand of choice for several palladium-catalyzed [3+2]-cycloadditions.[21]

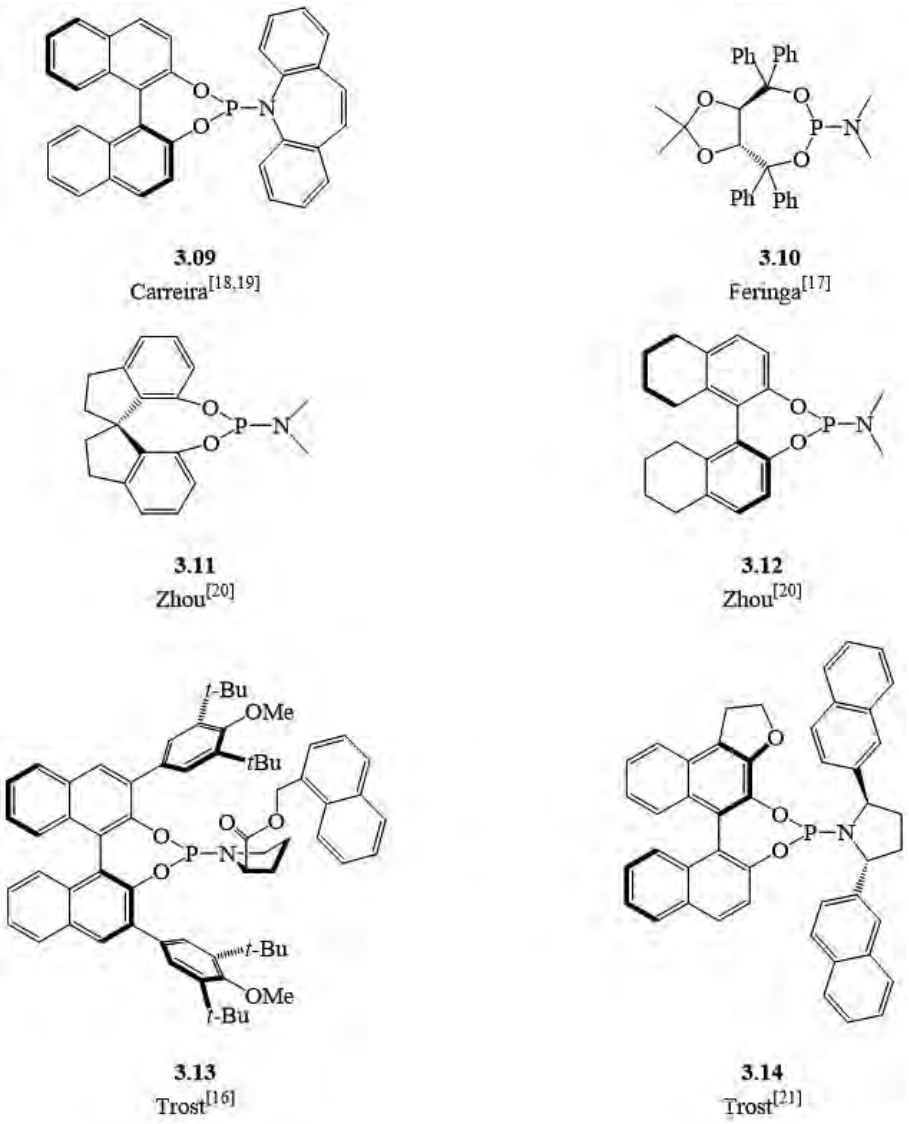

Figure 3.4 Examples of modified monodentate P-amidite ligands

3.3. Synthesis of Biferrocene-Based Ligands via Ferrocene-Ferrocene Bond Formation: Literature Overview

Although ferrocene is often regarded as an ordinary aromatic compound, it has some special features not present in common aromatics such as benzene.[22] In the same way, biferrocenes are substantially different from their non-organometallic biaryl counter-

parts. In 1959, Mayo and Goldberg already reported on the isolation and structural identification of 'diferrocenyl'.[23] A standard protocol for the synthesis of biaryl compounds is the Ullmann reaction, which is already known for more than a century. In 1960, Rausch from Monsanto used this standard protocol for the homocoupling of iodoferrocene to obtain unfunctionalized biferrocene. For this reaction he made use of activated copper bronze and temperatures of 150-160°C[4].[24] In the field of asymmetric catalysis, ligands with a 2,2'-disubstituted-1,1'-biferrocene backbone (**3.15**) are often synthesized and studied in comparison to their binaphthyl analogs (**3.16**) (Figure 3.5). Nevertheless, their conformational behavior is totally different and cannot be directly compared with binaphthyl-backbone based ligands. Chiral 2,2'-disubstituted-1,1'-biferrocene ligands are combining the elements of planar and axial chirality, whereas binaphthyl-based ligands are only characterized by axial chirality. Therefore, these biferrocene-based ligands are of considerable interest for practical as well as theoretical reasons.[25] Moreover, just like frequently used ferrocene ligands (*cf.* § 1.4.3), the presence of a chiral center at a strategic position allows to fine-tune the target ligands. All these properties make the biferrocene backbone an ideal structural ligand motif, very attractive for designing new chiral ligands.[26]

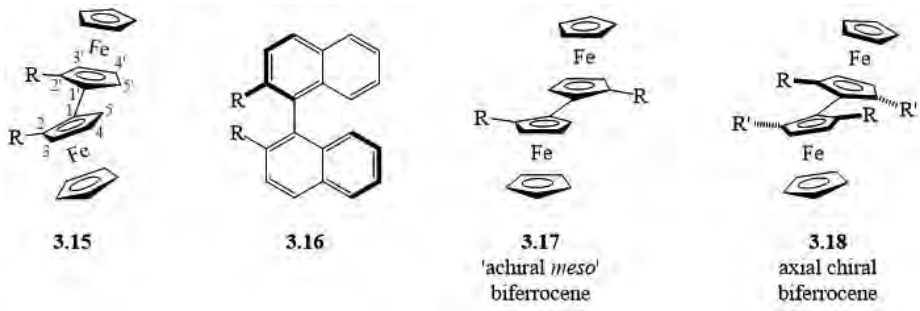

Figure 3.5 Chiral 2,2'-disubstituted-1,1'-biferrocene ligand structure (**3.15**), axial chiral binaphthyl ligand structure (**3.16**), achiral *meso* biferrocene structure (**3.17**) and axial chiral biferrocene structure due to restricted rotation (**3.18**)

In general, two useful synthetic methodologies have been developed for the formation of a ferrocene-ferrocene bond. The first approach involves a transition metal-mediated reductive coupling of halogen-substituted ferrocenes, such as the Ullmann reaction. The second procedure is based on an oxidative homocoupling of lithiated ferrocenes. In the following paragraphs the synthesis of different 2,2'-disubstituted-1,1'-biferro-

4 Using this protocol biferrocene was synthesized with a yield of 96-100%. Moreover, Mayo and Goldberg found that the reaction could be carried out at a temperature of 60° without appreciably lowering the yield of the coupling product.

cene-based compounds (mainly chiral ligands) will be illustrated, and the formation of the ferrocene-ferrocene bond will be highlighted. Enantiopure ligands with a chiral 2,2'-disubstituted-1,1'-biferrocene backbone can theoretically (statistically) only be obtained when the planar-chiral starting materials, which are iodine substituted ferrocenes or lithiated ferrocene intermediates, have a high enantiopurity. A substantial number of approaches for the stereoselective synthesis of 1,2-disubstituted planar-chiral ferrocenes are already described in full detail in the chemical literature.[22,26] Racemic starting materials will generally be converted into a racemic mixture of chiral biferrocenes and a '*meso*' biferrocene (**3.17**, Figure 3.5)[5]. However, the latter one could give rise to enantiomers, via its axial chirality (**3.18**, Figure 3.5). This is only possible when there is sufficient restriction of the torsion around the ferrocene-ferrocene axis, which depends on its substituents. For 2,2'-disubstituted-1,1'-biferrocenes, only large substituents will lead to a sufficient increase in rotational barrier.[25] The steric hindrance for 2,2',5,5'-tetrasubstituted biferrocenes is more pronounced and axial chirality is more common for this type of compounds.

The first example of a compound possessing a 2,2'-disubstituted-1,1'-biferrocene backbone was reported by Rockett *et al.* in 1968.[27] Racemic 2-(*N,N*-dimethylaminoethyl)-ferroceneboronic acid **3.19** was transformed into a mixture of two isomeric diamino-biferrocenyls using aqueous cupric acetate at 50°C (Scheme 3.1). Unfortunately, rather low yields were obtained. *Meso* biferrocene **3.20** could be isolated with a yield of 21% and a racemic mixture of diamino-biferrocene **3.21** with a yield of 27%.[28] The authors used these biferrocene structures as a scaffold to synthesize a small library of compounds characterized by a biferrocene backbone to study their conformational behavior.

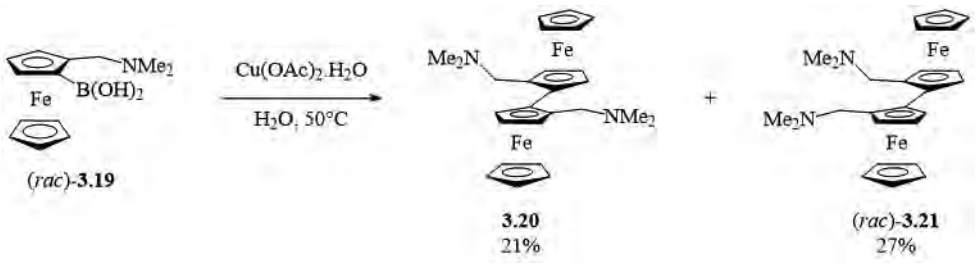

Scheme 3.1 Diamino-biferrocene synthesis via oxidative coupling using copper acetate in water

5 But exceptions exist (*vide infra*)

Later, Rockett and co-workers succeeded in the synthesis of different 2,2'-aminosubstituted-1,1'-biferrocenes, including these shown in Scheme 3.1, via an oxidative coupling of *ortho*-lithiated ferrocene with anhydrous $CoCl_2$.[29] Under these conditions, racemic (±)-diamino-biferrocene **3.21** was obtained with a yield of 24% and *meso* biferrocene **3.20** with a yield of 61%. In 1990, this methodology was applied by Widhalm *et al.* to expand the library of biferrocene amines and ethers.[25] However, the use of $CoCl_2$ (in combination with *n*-butylbromide) was already known for the direct coupling of lithioferrocene to biferrocene since the mid-sixties of last century.[30] Due to the formation of mono- as well as di-lithioferrocenes after the lithiation reaction, a mixture of bi-, ter- and higher poly-ferrocenes was obtained resulting in low yields of the desired biferrocenes.

In 1979, Davison and Rudie reported on the synthesis of 2-[(dimethylamino)methyl] biferrocene **3.24**, from a mixture of 2-lithio[(dimethylamino)-methyl]ferrocene **3.22** and lithioferrocene **3.23** (Scheme 3.2).[31] To perform this heterocoupling reaction they used tetrakis[iodo(tri-*n*-butylphosphine)copper(I)] $[CuIP(n\text{-}Bu)_3]_4$ in combination with oxygen gas and obtained a yield of 25%. This methodology also proved to be successful for the homocoupling of lithioferrocene to biferrocene, which could be isolated with a yield of 52%.[32]

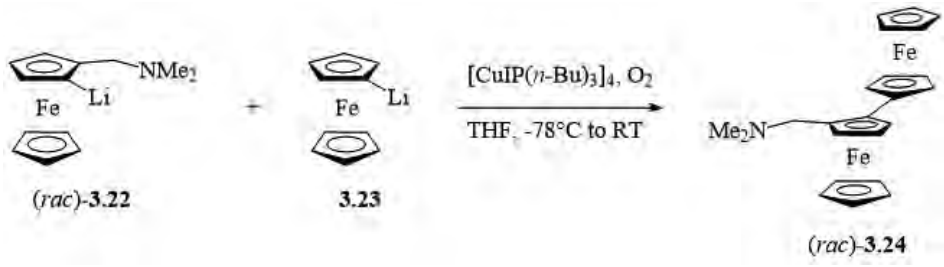

Scheme 3.2 Heterocoupling reaction between lithioferrocenes **3.22** and **3.23** using $[CuIP(n\text{-}Bu)_3]_4$ and O_2

The enantioselective synthesis of a diamino-biferrrocene was reported by Simpson *et al.* in 1994.[33] After a diastereoselective *ortho*-lithiation of Ugi's amine (**3.25**) two different oxidative homocouplings were examined (Scheme 3.3). The first one, using CuCN and oxygen gas, allowed to obtain biferrocene **3.27** with a maximum yield of 42%. The other oxidative homocoupling with iron(III)acetylacetonate ($Fe(acac)_3$) gave a yield of 27%. An interesting note is that the scientists were interested in this biferrocenylamine **3.27** because some platinum salts show potential for antitumor activity.[34]

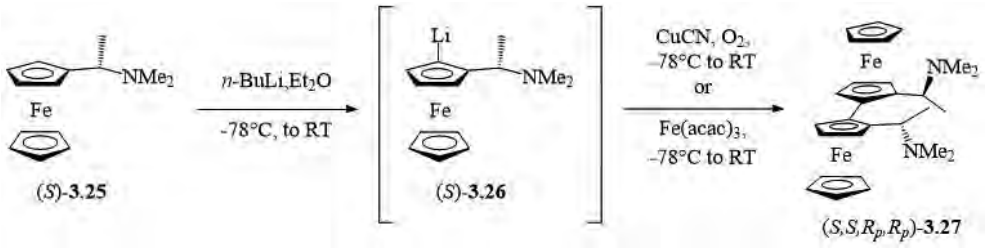

Scheme 3.3 Biferrocene synthesis of Ugi's amine via oxidative coupling using CuCN in combination with O_2 or alternatively $Fe(acac)_3$

$Fe(acac)_3$ was also used for the synthesis of phenyl-substituted diamine ligands **3.30** (Scheme 3.4).[35] The phenyl-analogue **3.28** of Ugi's amine was selectively lithiated with *t*-BuLi in a first step, and subsequently oxidatively coupled to tertiary biferrocenyl-amine **3.29**, which was transformed into target ligand **3.30** within a few steps.

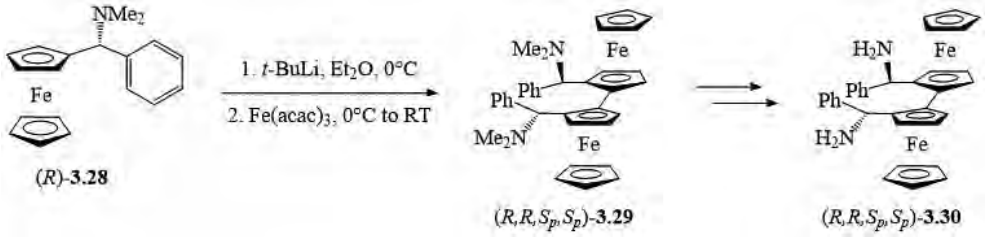

Scheme 3.4 Diamino-biferrocene synthesis via oxidative coupling using $Fe(acac)_3$

Structurally extraordinarily C_2-symmetric *bis*-phenyl-pentamethylazaferrocene **3.34**, which is a potential *N,N*-bidentate biferrocene ligand, was synthesized via an iron-catalyzed oxidative homocoupling reaction by Andersson *et al.* in 2007 (Scheme 3.5).[36] The Snieckus approach with (-)-sparteine was used for the enantioselective synthesis of phenyl substituted pentamethyl azaferrocene **3.33**.[37] The obtained lithiated species was treated with $ZnCl_2$ and a palladium(0)-catalyzed Negishi reaction with iodobezene allowed to obtain **3.33**. Regioselective deprotonation of this compound was possible with *sec*-BuLi and TMEDA. Subsequent treatment with $MgBr_2$ allowed to synthesize the corresponding Grignard reagent required for the $FeCl_3$-catalyzed oxidative homocoupling reaction towards **3.34**.

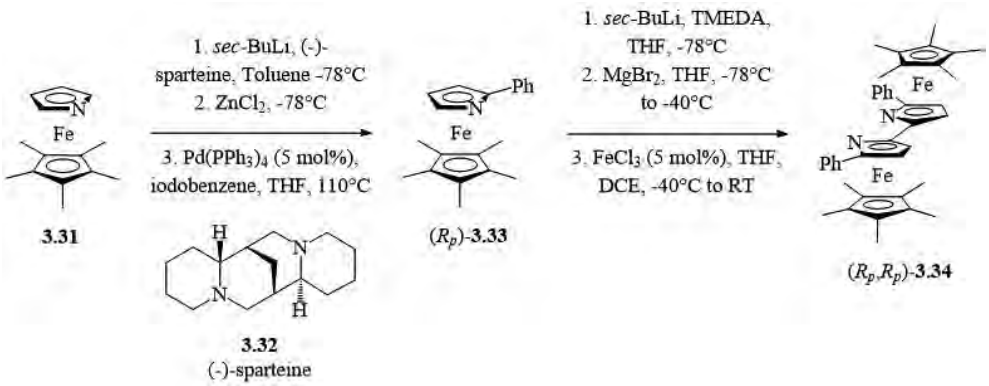

Scheme 3.5 Synthesis of *bis*-phenyl-pentamethylazaferrocene **3.33** via $FeCl_3$-catalyzed oxidative homocoupling

Phosphine ligands with a biferrocene structural backbone have been made enantiomerically pure and applied in a variety of enantioselective reactions as well. In 1991, Ito and co-workers reported already on the first member of the TRAP ligand family (with R equal to a phenyl ring, Scheme 3.6).[38] Starting from Ugi's amine **3.25**, enantiopure precursor **3.35** for the homocoupling was synthesized. Therefore a nickel(0)-complex, *in situ* generated from $NiBr_2(PPh_3)_2$ via reduction with Zn and Et_4NI was used. The homocoupling was performed in DMF at 120°C and a yield of 50% was obtained. This bidentate diphosphine ligand **3.37** forms a *trans*-chelated nine-membered metallacycle upon coordination with palladium(II) and platinum(II).

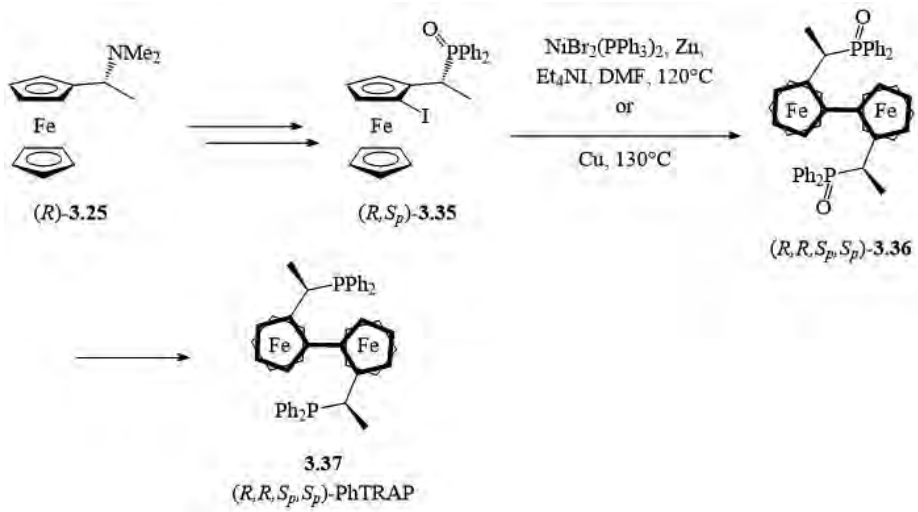

Scheme 3.6 Synthesis of (R,R,S_p,S_p)-PhTRAP ligand **3.37** where the homocoupling is catalyzed via an *in situ* formed nickel(0)-complex

A few years later Ito and co-workers were able to synthesize a library of TRAP ligands bearing diverse aryl groups on their phosphorus atoms.[39] The key step was now performed via an Ullmann-type reaction with activated copper powder without solvent at 130°C. This allowed to synthesize the C_2-symmetric biferrocene compounds with a maximum yield of 65% after crystallization. The first examples of the TRAP family class were characterized by the combination of a chirality axis, planar-chirality and two stereocenters. In 1999, Ito and co-workers published the synthesis of the (S_p,S_p)-EtTRAP-H ligand **3.41** without the presence of the two stereocenters in the side chains.[40] Therefore a new synthesis route had to be developed, starting from ferrocenyl oxazoline **3.38**, which is shown in Scheme 3.7. The copper homocoupling was now performed with activated copper powder at 80°C and allowed to synthesize the biferrocene structure with a yield of 74%. Since the development of the TRAP ligand family, they have been successfully applied in different asymmetric transition metal catalyzed reactions such as rhodium-catalyzed Michael additions of α-cyano carboxylates[41], rhodium-catalyzed asymmetric hydrosilylations of simple ketones[40,42] and rhodium-catalyzed asymmetric hydrogenations of a variety of prochiral olefins.[43]

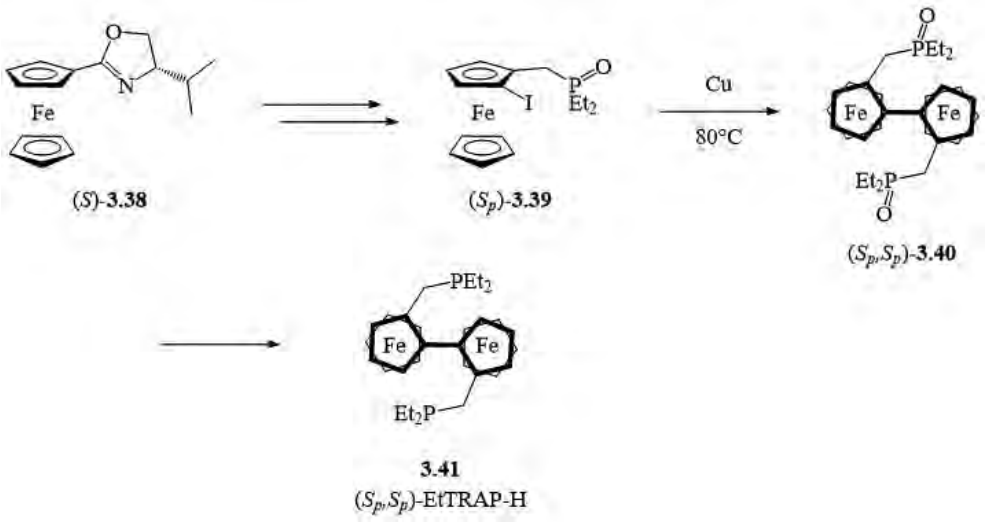

Scheme 3.7 Synthesis of (S_p,S_p)-EtTRAP-H **3.41** ligand via a metallic copper-mediated Ullmann homocoupling reaction

The biferrocene-analogue of Noyori's highly successful, axial-chiral BINAP ligand was first reported by Ito *et.al.* in 1991.[44] The original synthesis of this ligand, which is now known as BIFEP (or 2,2'-bis(dipheny1phosphino)-1,l'-biferrocene), is shown in Scheme 3.8.

Starting from ferrocene **3.42**, planar-chiral ferrocene **3.43** was synthesized as a racemate. The homocoupling was performed using nickel(0), obtained via reduction of nickel(II)-acetylacetonate with DIBAL, in benzene under reflux conditions. Phosphinoxide **3.44** was obtained as a racemic mixture with a yield of 55% and was resolved into its enantiomers by fractional recrystallization with (-)- and (+)-dibenzoyltartaric acid. Final stage reduction using trichlorosilane ($HSiCl_3$) and triethylamine (Et_3N) on both enantiomers allowed to obtain enantiopure BIFEP ligands **3.45** and **3.46**. It is important to mention that the corresponding *meso*-biferrocene compound was not observed during the coupling reaction, a phenomenon that cannot be explained statistically. Ito and co-workers also found that BIFEP chelates in a *cis*-fashion to palladium, in contrast to the TRAP ligand library.[26,38,42]

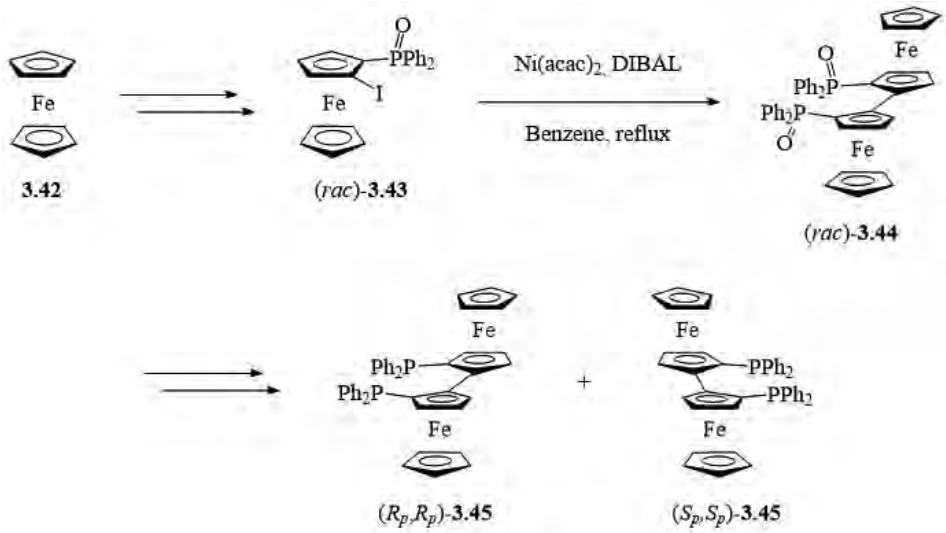

Scheme 3.8 Synthesis of BIFEP via a nickel(0)-promoted homocoupling reaction

The enantioselective synthesis of BIFEP **3.45** was described by Weissensteiner and co-workers in 2001.[45] The key step was (again) a copper-mediated Ullmann homocoupling. In a solid state reaction, iodide **3.46** was reacted with metallic copper at 130°C resulting in biferrocene **3.47** with a yield of 77% (Scheme 3.9). BIFEP **3.45** was synthesized from **3.47** in a two-step procedure using *t*-BuLi and PPh_2Cl. This ligand has been tested in the enantioselective hydrogenations of a wide, diverse range of substrates (olefins, ketones, imines) catalyzed by palladium, ruthenium, rhodium and iridium.[45,46] Although for some reactions good results were obtained, in general this ligand seemed to be inferior in comparison to BINAP.

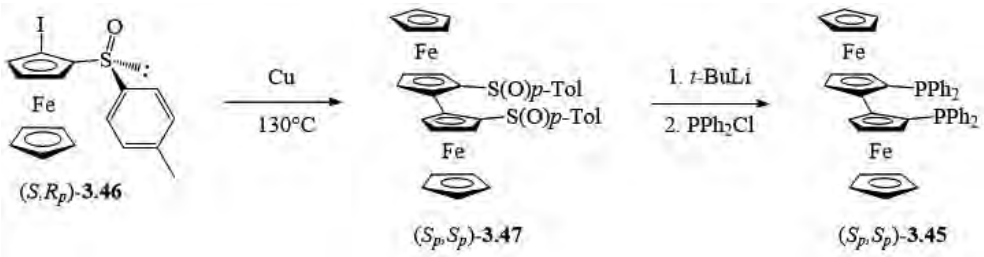

Scheme 3.9 Enantioselective synthesis of the BIFEP ligand via a copper-mediated Ullmann reaction

The first synthesis of enantiopure ligands which combine a chiral biferrocene backbone with a chiral phosphorus center was reported by Spek and co-workers.[47] Planar-chiral iodoferrocenylphosphine oxides **3.50-3.51**, respectively synthesized from **3.48-3.49**, were coupled via an Ullmann reaction at 130°C using activated copper powder with yields of 58% (R=1-napthyl) and 70% (R=2-biphenyl) (Scheme 3.10). Reduction of the phosphinoxides to the desired phosphines seemed to be difficult and required harsh reaction conditions ($HSiCl_3$, triethylamine, toluene, 130°C for 72h), which involved partial epimerization of the phosphorus stereocenters. Chromatographic separation of the diastereomers of the bis(borane) adducts was possible and stereospecific deprotection allowed to obtain the enantio- and diastereomerically pure ligands. Later, the same group applied these C_2-symmetric ligands in palladium(0)-catalyzed asymmetric allylic alkylations and aminations with a variety of substrates.[48]

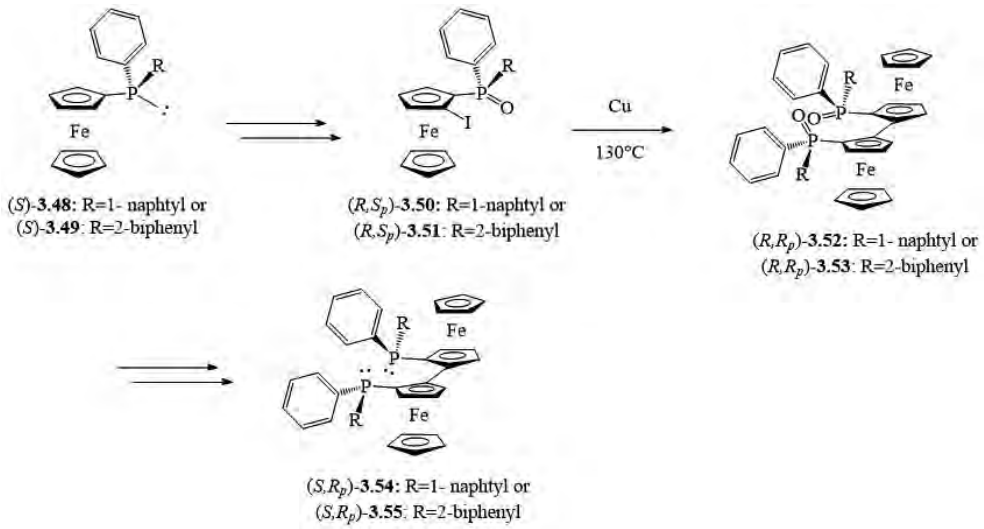

Scheme 3.10 Synthesis of biferrocene-based diphosphine ligands with chiral phosphorus centers

In 1997, Ahn *et al.* reported the synthesis of novel chiral Bis(oxazoline) ligands **3.57** and **3.58**, which are also characterized by a 2,2'-disubstituted-1,1'-biferrocene backbone (Scheme 3.11).[49] The ferrocene-ferrocene bond was formed via a three-step oxidative coupling. After diastereoselective deprotonation with *n*-BuLi, the homocoupling was performed with copper(I)bromide and oxygen gas. This methodology allowed to obtain **3.57** with a yield of 52% and **3.58** with a yield of 59%. Further optimization of the ligand-structure for **3.58**, was accomplished via regioselective lithiation followed by quenching with trialkylsilylchlorides. In this way 2,2',3,3'-tetrasubstituted-1,1'-biferrocene ligands **3.59** and **3.60** were obtained. These Bis(oxazoline) ligands were tested in the copper(I)-catalyzed asymmetric cyclopropanation of styrene with diazoacetates and, in general, better results were obtained for the tetrasubstituted ligands.

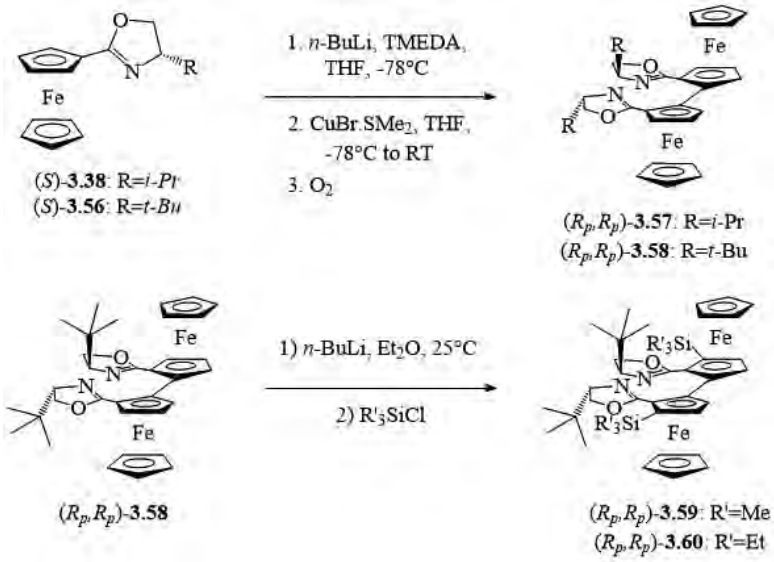

Scheme 3.11 Synthesis of chiral Bis(oxazoline) ligands with a biferrocene backbone obtained via oxidative homocoupling

In 2002 the research group of Widhalm published a very interesting and important paper on chiral biferrocene-based hybrid *P,N*-type ligands, which are shown in Figure 3.6.[50] In this paper they discuss in full detail their synthesis, their conformational behavior and their results in the palladium-catalyzed asymmetric allylic substitution of different substrates. These ligands are characterized by a biferrocene-azepine substructure, which is also present in the proposed monodentate P-amidite ligands **3.103** (*vide infra* § 3.6 or *vide supra* Figure 2.3, **2.09**). To complete the full library of the bifer-

rocenyl-azepine ligands, both synthetic approaches (oxidative and reductive coupling) for the ferrocene-ferrocene coupling reaction have been applied. Based on experimental results the authors conclude that the oxidative and reductive coupling methods are complementary to each other.

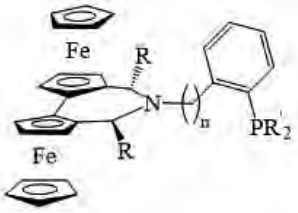

(R_p,R_p)-**3.61** n=1; R=H; R'=Ph
(R_p,R_p)-**3.62** n=1; R=H; R'=4-F-Ph
(R_p,R_p)-**3.63** n=1; R=H; R'=4-CH_3O-Ph
(R_p,R_p)-**3.64** n=0; R=H; R'=Ph
(S,S,R_p,R_p)-**3.65** n=1; R=CH_3; R'=Ph
(S,S,R_p,R_p)-**3.66** n=0; R=CH_3; R'=Ph

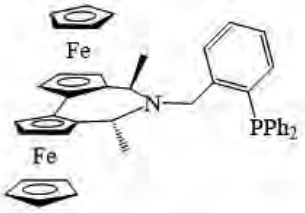

(R,R,R_p,R_p)-**3.67**

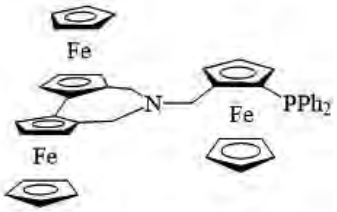

(R_p,R_p,R_p)-**3.68**

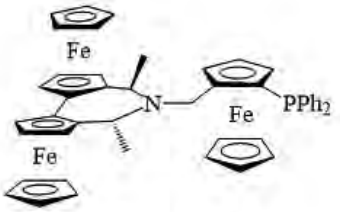

(S,S,R_p,R_p,R_p)-**3.69**

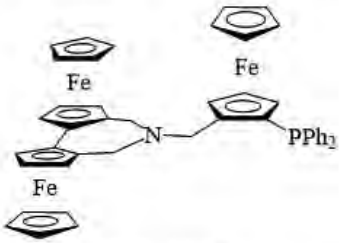

(R_p,R_p,S_p)-**3.70**

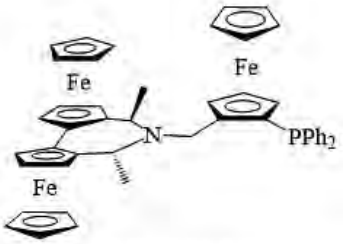

(S,S,R_p,R_p,S_p)-**3.71**

Figure 3.6 Library of hybrid *P,N*-type biferrocenyl-azepine ligands synthesized by Widhalm and co-workers[50]

For the homocoupling of α-methylated ferrocenylamines (*S*)-**3.25** and (*R*)-**3.25** the oxidative coupling of the corresponding lithiated species with $Fe(acac)_3$ showed to be a successful approach (Scheme 3.12). The synthesis of biferrocenylamine (S,S,R_p,R_p)-**3.27**

starting from (*S*)-**3.25**, using this protocol was already reported by Simpson *et.al.*[33] (Scheme 3.3). The synthesis of its diastereomer (*R,R,R*$_p$,*R*$_p$)-**3.73** was possible from (*R*)-**25** via a multistep synthesis. First, (*R,R*$_p$)-**3.72** was selectively obtained using the 'silicon trick'. This planar-chiral ferrocene compound allowed to prepare (*R,R,R*$_p$,*R*$_p$)-**3.73** via a lithium-halogen exchange, and subsequent oxidative homocoupling of the lithiated species using Fe(acac)$_3$, with a yield of 67%. The 'silicon trick' involves the introduction of a latent trimethylsilyl (TMS) group via diastereoselective *ortho*-lithiation and quench reaction with trimethylchlorosilane (TMS-Cl). An additional *ortho*-lithiation and electrophilic quench reaction allows to introduce a second substituent (here iodine), affording an intermediate trisubstituted ferrocene compound. Desilylation is generally possible via treatment with TBAF in THF, although Widhalm *et al.* used KO*t*-Bu in DMSO.

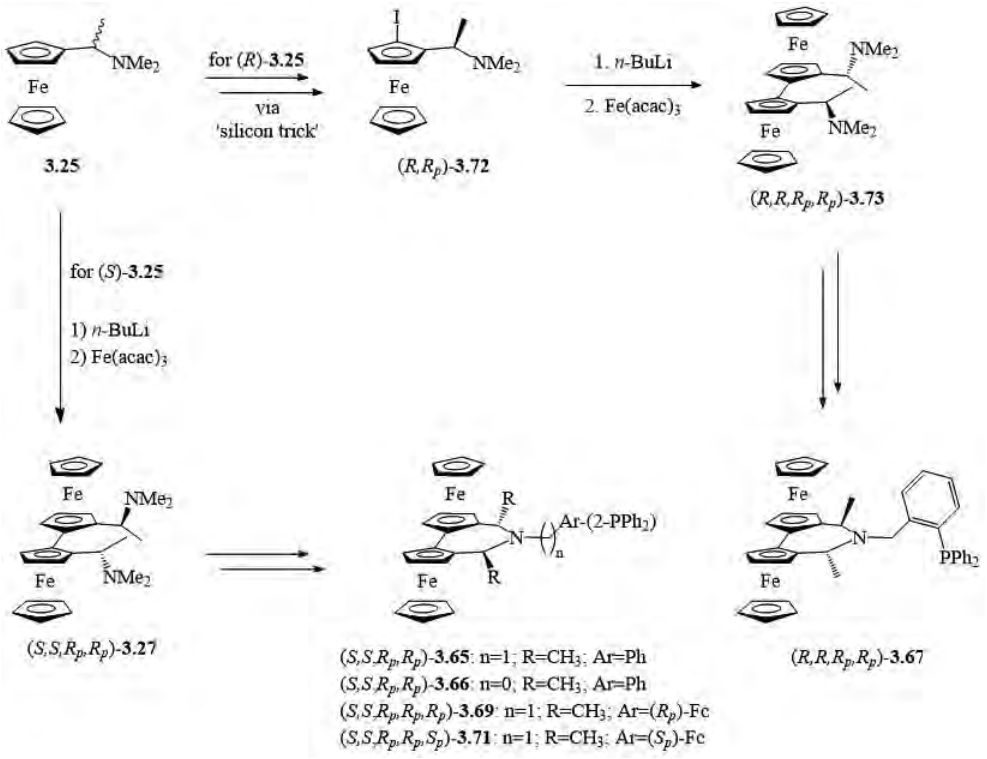

Scheme 3.12 Oxidative homocoupling of α-methylated ferrocenylamine **3.25** using Fe(acac)$_3$ for the synthesis of biferrocene *P,N*-ligands **3.65**-**3.67**, **3.69** and **3.71**

However, the conditions using Fe(acac)$_3$ failed for the homocoupling of the corresponding non α-methylated ferrocenylamines. Therefore, another synthesis based on different starting materials, which is shown in Scheme 3.13, has been developed. Planar-chi-

ral iodosubstituted ferrocenes **3.74-3.76** were reductively coupled in an Ullmann-type reaction using activated copper bronze at temperatures of 130-136°C. Yields of 72, 64 and 58% were obtained respectively.

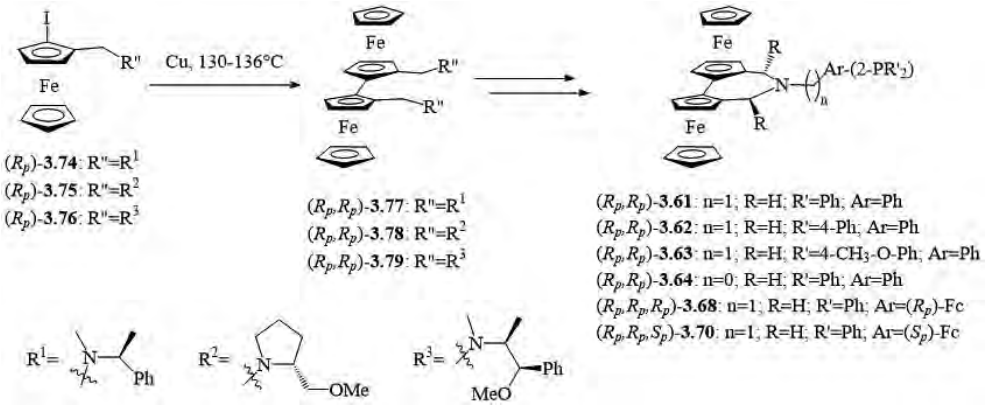

Scheme 3.13 Reductive homocoupling of non α-methylated ferrocenylamines **3.74-3.75** using metallic copper for the synthesis of biferrocene *P,N*-ligands **3.61-3.64**, **3.68** and **3.70** (see Figure 3.6 for more details of these structures)

Widhalm *et al.* succeeded in growing a single crystal of a palladium dichloride complex of ligand **3.61** suitable for X-ray analysis. Conformational comparison in the solid state with its binaphthyl analogue is possible because the same group published the corresponding cationic palladium allyl complexes earlier in 2002 (Figure 3.7).[51]

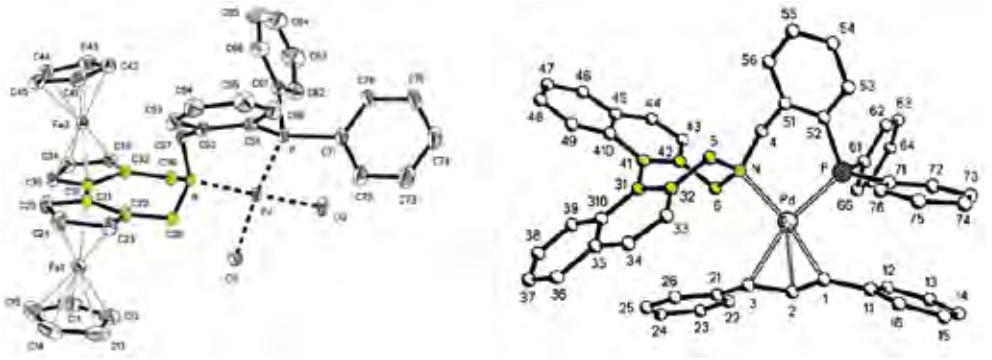

Figure 3.7 ORTEP drawings of a palladium dichloride complex with biferrocene-based *P,N*-type ligand **3.61** (left) and a palladium allyl complex with a binaphthyl based *P,N*-type ligand (*S*)-**3.80** (*vide infra*) (right)[50,51]

When analyzing these ORTEP drawings, it can easily be seen that in the solid state the dihedral angle between two connected Cp rings is totally different from the dihedral

angle between two naphthyl units. Both ferrocene units are found in a nearly coplanar arrangement (the dihedral angle C25-C21-C31-C35 is equal to 14.4°) whereas the torsion angle for its binaphthyl analogue is equal to 63°. As a consequence, the azepine subunit of the complex with the biferrocene ligand adopts an envelope-like conformation of C_1-symmetry (shown in yellow in Figure 3.7) which is significantly different from the rather strainless twist conformation of C_2-symmetry of the binaphthyl based ligand. Another observation for the biferrocene-palladium complex is the axial orientation of the benzyl substituent on the nitrogen atom of the azepine unit.

These results are supported and well-reproduced by empirical force field calculations. Figure 3.8 illustrates the conformation of the binaphthyl and biferrocenyl subunits of the corresponding *P,N*-type ligands based on the results of this empirical modeling. For palladium complexes of biferrocene-based ligands, it was found that conformers with an azepine subunit of local C_2-symmetry (twisted conformations) were always found to have the highest energy. C_1-symmetric envelope-like conformers, as illustrated in Figure 3.8, are about 25 kJ/mol energetically more favorable.

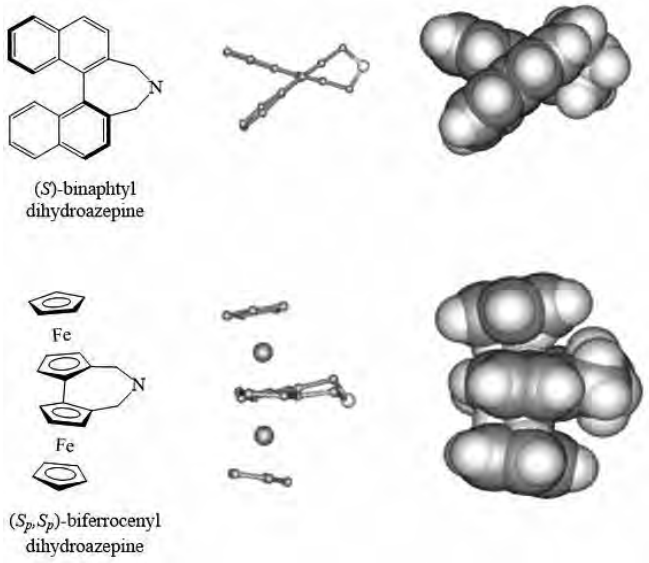

Figure 3.8 C_2-symmetric binapthyl azepines with twisted conformation (top) and C_1-symmetric biferrocenyl with envelope conformation (bottom) (models obtained via empirical force field calculations)[50]

Moreover, calculations showed that these envelope-like conformers with an axial substituent are energetically more favorable compared to envelope-like conformers with the substituent in the equatorial position. It was found that this energy difference is de-

pendent on the specific substituent. On the other hand, for biphenyl[6] derivatives, only minimum energy structures with an azepine subunit of local C_2-symmetry with a twist conformation were found to be realistic. In his paper, Widhalm reported two reasons why biferrocene envelope-like azepines are more stable:

1. Bond angles within Cp rings are smaller than in six-membered aryl rings. Therefore the bond angles within the azepine moiety necessarily increase. This enables a nearly coplanar arrangement of the ferrocene units.
2. Steric interactions between substituents at the nitrogen atom and the ferrocenyl units are reduced.

A large library of different chiral binaphthyl- and biferrocene-based ligands has been tested in palladium-catalyzed asymmetric allylic substitutions[7], which is a benchmark test reaction for *P,N*-type ligands.[50-53] A full overview of the results can be found in these references, but some of these are discussed here to illustrate the difference between a C_2-symmetric binaphthyl-based backbone, with a twisted conformation, and a C_1-symmetric biferrocene-based backbone, with an envelope like conformation. Therefore two model substrates (**3.81** and **3.84**) and six ligands, three binaphthyl-based (**3.80**, **3.86** and **3.87**) and three biferrocene-based (**3.61**, **3.68**, and **3.70**) were chosen (Figure 3.9). The results in terms of yield and enantioselectivity are shown in Table 3.2.

	Reaction 1		Reaction 2	
Ligand	**yield (%)**	***ee* (%)**	**yield (%)**	***ee* (%)**
3.80[51-53]	92	97 (*S*)	86	28 (*R*)
3.86[51]	Not reported	54 (*S*)	Not reported	49 (*S*)
3.87[51,52]	79	44 (*S*)	23	36 (*R*)
3.61[50]	97	87 (*R*)	92	50 (*S*)
3.68[50]	99	42 (*R*)	98	57 (*S*)
3.70[50]	97	69 (*R*)	97	65 (*R*)

Table 3.2 Results of palladium-catalyzed asymmetric allylic alkylation reaction of acyclic and cyclic substrates with azepine *P,N*-type ligands **3.61**, **3.68**, **3.70**, **3.80**, **3.86** and **3.87**

6 To allow for a better comparison, calculations on biphenyl rather than binaphthyl derivatives were carried out. The reason for this is that 6,6'-substituents are expected to prevent a biaryl system from adopting a coplanar arrangement of the aryl groups, an arrangement that is necessary in an envelope-like azepine structure.

7 It should be noted that for the testreactions with biferrocene-based ligands **3.61**, **3.68** and **3.70** KOAc was used as an extra additive.

For reaction 1, with acyclic diphenyl substrate **3.81**, binapthyl-based ligands resulted in the formation of (*S*)-enantiomers whereas biferrocene-based ligands resulted in the formation of (*R*)-enantiomers. The highest enantioselectivity was obtained with ligand **3.80**, that does not contain a single ferrocene unit in its structure. A similar phenomenon is observed for ligands with a biferrocene backbone: ligands **3.68** and **3.70**, characterized by a 1,2-disubstuted planar-chiral ferrocene phosphine unit show a lower enantioselectivity than ligand **3.61**, characterized by a benzylphosphine moiety (42% and 69% *ee* vs 87% *ee* respectively). Totally different results are observed for cyclohexenyl substrate **3.84**. Here, ligands with a biferrocene-based backbone gave significantly higher enantioselectivities (and yields) in comparison to their binaphthyl-based analogs (**3.61**, **3.68**, **3.70** vs **3.80**, **3.86**, **3.87**). Ligands **3.80**, **3.87** and **3.70** provided the (*R*)-enantiomer whereas ligands **3.61**, **3.86** and **3.68** resulted in the formation of the opposite enantiomer. In contrast to acyclic substrates, ligands with a planar-chiral ferrocene-phosphine unit gave higher enantioselectivities than their corresponding ligands without this extra chirality element. (49% *ee*, 36% *ee* vs 28% *ee* for binaphthyl ligands **3.86**, **3.87** and **3.80** respectively and 65% *ee*, 57% *ee* vs 50% *ee* for ligands **3.70**, **3.68** and **3.61**). Moreover, for cyclic substrates, the stereochemistry of the 1,2-disubstituted planar-chiral ferrocene phosphine unit is responsible for the observed stereochemistry of the final product. Ligands **3.86** and **3.68**, which have a (R_p) planar-chiral ferrocenyl-phosphine unit resulted in the formation of the (*S*)-enantiomer. In contrast, ligands **3.87** and **3.70** with a (S_p) planar-chiral ferrocenyl-phosphine unit delivered the (*R*)-enantiomer as major product.

Ligands with an extra chiral center due to a methyl substituent at the α-position according to the biferrocene backbone **3.65-3.67**, **3.69**, **3.71** (Figure 3.6), were also tested by Widhalm and co-workers.[50] For all tested reactions, none of these ligands gave better enantioselectivities than the ligands without this extra chirality element. Therefore, they are not discussed in detail here.

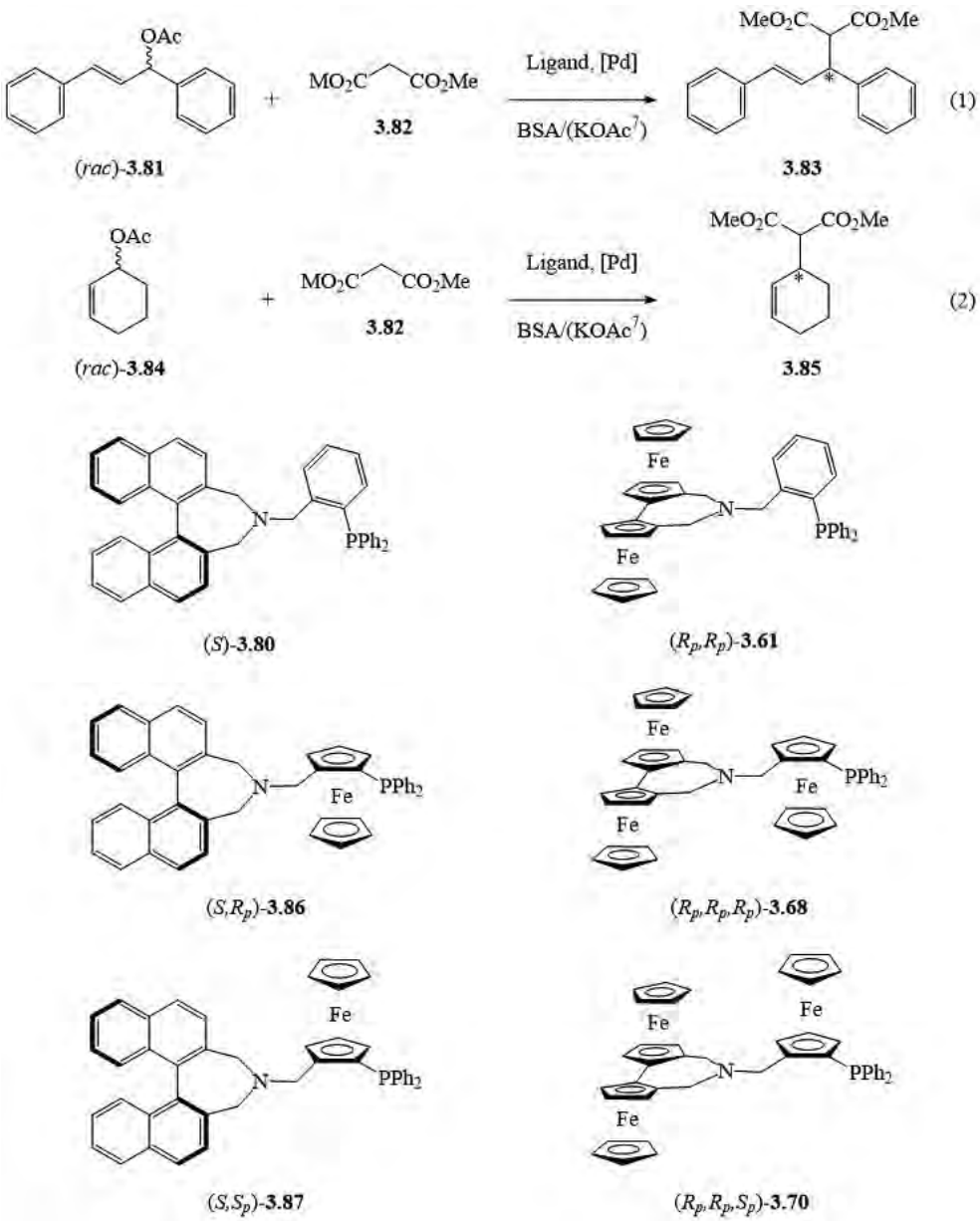

Figure 3.9 Ligands tested in asymmetric allylic alkylation reactions of acyclic and cyclic substrates. (Results shown in Table 3.2)

Two other important papers concerning this research topic were published by the research groups of Riant[54] and Gagné[55]. These will be discussed in more detail in § 3.7.1 (*vide infra*).

3.4. Retrosynthetic Analysis of Novel Phosphoramidite Ligands

The retrosynthetic analysis of ligand series **3.88** is shown in Scheme 3.14.

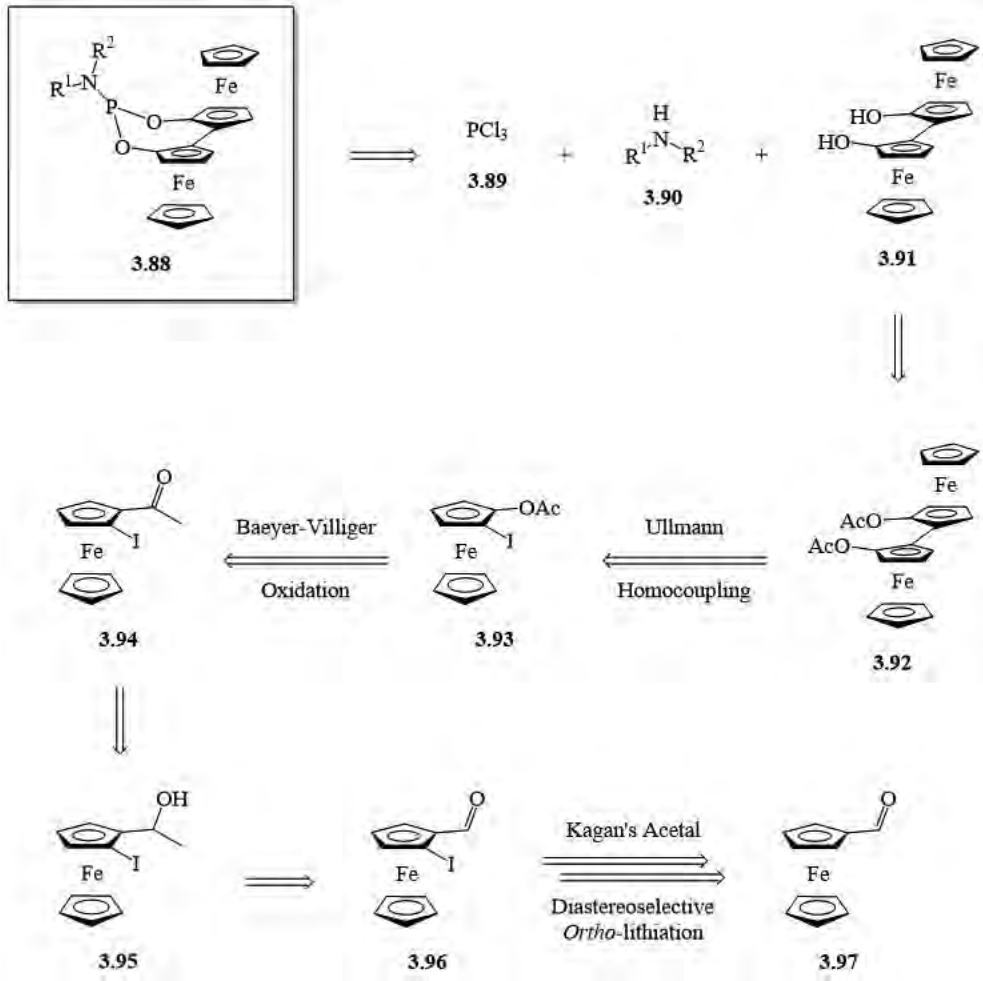

Scheme 3.14 Retrosynthetic analysis of ligand series **3.88**

Generally, the retrosynthetic analysis of phosphoramidites starts with breaking the bonds around the central phosphorus atom. This means that the proposed ligands can be synthesized from PCl_3, commercially available amines **3.90** and biferrocenol **3.91**. Consequently, the retrosynthesis can be reduced to the analysis of the latter, which can be obtained via hydrolysis of diester **3.92**. A copper-mediated Ullmann homocoupling reaction, from planar-chiral ferrocenyliodide **3.93** is proposed for the synthesis of the biferrocene backbone. As a consequence the stereoselective synthesis of a planar-chi-

ral ferrocene moiety will represent an important issue for the synthesis of the proposed ligands. To avoid substitution of the iodine by hydrogen (dehalogenation) during the coupling reaction, protection of the free alcohol as an ester is beneficial. Therefore ester **3.93** is proposed as the starting material for the Ulmann homocoupling. The latter can in principle be obtained via a Baeyer-Villiger oxidation from α-iodoketone **3.90**, which could in turn be synthesized via a Grignard addition to α-iodoaldehyde **3.96** followed by oxidation of the secondary alcohol **3.95**. In 1993 Kagan *et al.* reported on the synthesis of a few planar-chiral compounds, including α-iodoaldehyde **3.96**, via a diastereoselective directed *ortho*-lithiation using a chiral acetal.[56] This methodology was optimized later, and allowed to obtain more planar-chiral ferrocenes as well.[57]

3.5. Synthesis of Novel Phosphoramidite Ligands

3.5.1. Synthesis of planar-chiral α-iodoaldehyde **3.96** using Kagan's chiral acetal approach

Because different synthetic routes towards the preparation of novel diamidophosphite ligands were used, the synthesis of planar-chiral ferrocene compounds will be discussed in more detail in Chapter 4 (§ 4.3 and § 4.4, *vide infra*). In this chapter only Kagan's chiral acetal approach has been used for the preparation of planar-chiral α-iodoaldehyde **3.96**.[56,57] This approach involves a diastereoselective *ortho*-lithiation using a chiral auxiliairy derived from malic acid. The synthesis of aldehyde **3.96** is shown in Scheme 3.15 and was performed several times on multi-gram scale. The latter compound functions as a key-intermediate in the synthesis towards the novel chiral phosphoramidite ligands.

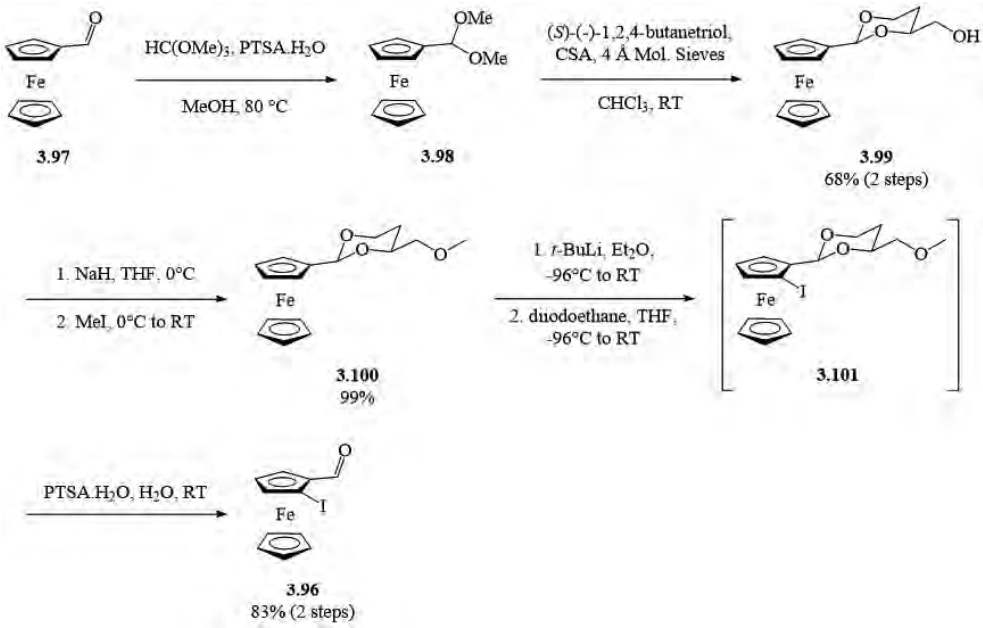

Scheme 3.15 The synthesis of planar-chiral α-iodoaldehyde **3.96** using Kagan's acetal diastereoselective *ortho*-lithiation approach

Ferrocenecarboxaldehyde **3.97** was quantitatively transformed into dimethylacetal **3.98** under reflux conditions in a mixture of trimethyl orthoformate and methanol in the presence of PTSA as an acid catalyst. Transacetalization of crude **3.98** with (*S*)-1,2,4-butanetriol, a catalytic amount of CSA and molecular sieves in chloroform at room temperature allowed the formation of *cis*-1,3-dioxane **3.99** as the major product. Isolation of this compound was achieved by subsequent silica gel chromatography and recrystallization from toluene. The mother liquor was analyzed via HPLC-MS and ^{1}H-NMR. Besides the target material **3.99**, a mixture of *cis* and *trans* dioxolanes could be identified as well. Conversions of 90% and isolated yield of 68% (2 steps) were obtained. Methylation of the free hydroxy group was then performed using NaH and MeI in THF, which resulted in desired acetal **3.100** in a quantitative yield. Diastereoselective *ortho*-lithiation was achieved using the strong, bulky base *t*-BuLi at -96°C in diethyl ether. The reaction was stirred for 10 min. at -96°C, allowed to warm up to room temperature and stirred for 1 h. The reaction was cooled again to -96°C, quenched with a solution of diiodoethane in THF and stirred for 10 min. at this temperature. Afterwards, the reaction was allowed to warm up to room temperature and the reaction flask was covered with aluminum foil as soon as this flask was removed from the cooling bath. The reaction mixture was stirred

for at least 20 h at room temperature to obtain iodo-acetal **3.101**. However, the temperature set for the quenching reaction has no influence on the conversion nor on the stereoselectivity. Separation of acetal **3.101** from **3.100** appeared to be a very difficult task. Therefore the quenched reaction mixture was treated with a deoxygenated solution of *para*-toluenesulfonic acid monohydrate (PTSA.H_2O) in water for quantitative acetal hydrolysis. Silica gel chromatography allowed to separate α-iodoaldehyde **3.96** from ferrocenecarboxaldehyde **3.97**. Planar-chiral α-iodoaldehyde **3.96** could be isolated with a yield of 83% over two steps and a maximum enantiomeric purity of 96% *ee* as determined by chiral HPLC. A chromatogram of a chiral LC analysis is shown in Figure 3.10. The major enantiomer, (S_p)-α-iodoaldehyde **3.96** eluted after 8.16 min., the minor (R_p)-enantiomer after 6.62 min. A very small amount of an uncharacterized impurity eluted after 6.30 min. Enantiomeric excess values of 93-96%, were obtained in a reproducible way.

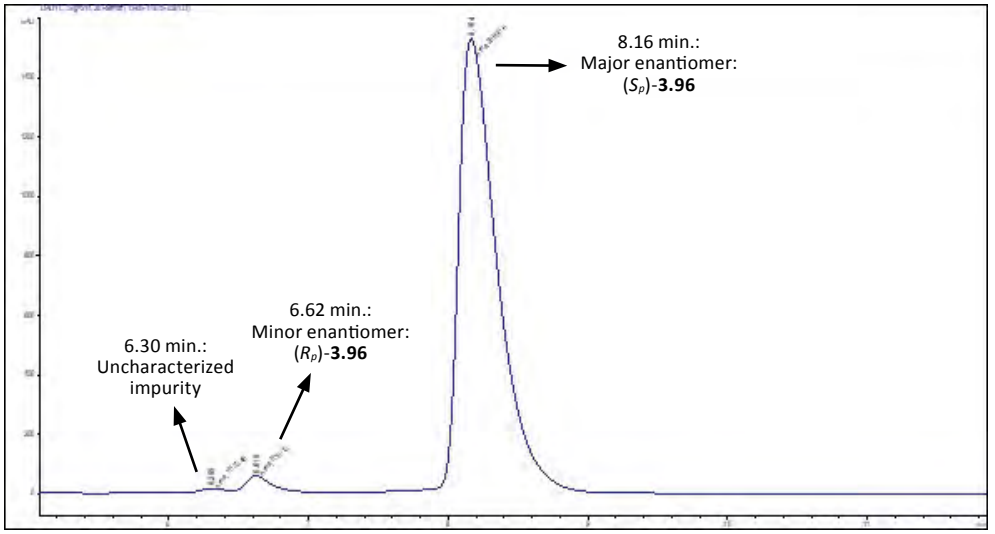

Figure 3.10 Chromatogram of a chiral HPLC analysis of α-iodoaldehyde 3.96 with an *ee*-value of 96%. (Chiralpak AS-H column, solvent: *n*-hexane/EtOH (90:10), flow rate = 1 mL/min, t = 30 min., T = 35°C)[8].

3.5.2. Two-Step Synthesis of α-iodoketone **3.94**

The synthesis of α-iodoketone **3.94** is shown in Scheme 3.16. The first step involves a Grignard addition to aldehyde **3.96** which resulted in the formation of a mixture of diastereomeric alcohols **3.95** with a yield of 88%. With the next step in mind, there was no attention for the selective synthesis of one or the other epimer nor for their separation.

8 For more experimental details see § 3.9.1 and § 3.9.5 (*vide infra*).

Several conditions for the oxidation of alcohols into their corresponding ketones are known in literature.[58] At the *Laboratory for Organic and Bioorganic Synthesis*, Swern conditions using $(COCl)_2$, DMSO and Et_3N in CH_2Cl_2 at -78°C were successfully applied for the conversion of primary ferrocenyl alcohols into their corresponding aldehydes. [59] However, oxidations of secondary ferrocenyl alcohols using MnO_2 were already described in literature.[60] When this oxidant was used in dichloromethane at room temperature, planar-chiral alcohol **3.95** was only slowly transformed into ketone **3.94**. After one week reaction, approximately 50% conversion was observed by TLC. Further optimization of this reaction was carried out, and best conditions for the oxidation of alcohol **3.95** turned out to be MnO_2 in chloroform at reflux temperature. After overnight reaction, **3.94** could be isolated with a yield of 82%.

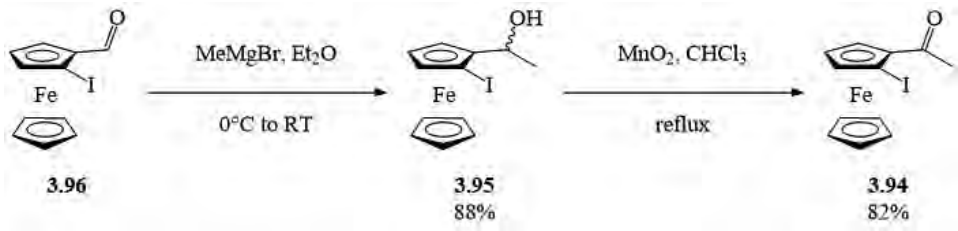

Scheme 3.16 Synthesis of planar-chiral ferrocenyl ketone **3.94** starting from aldhehyde **3.96**

3.5.3. Baeyer-Villiger oxidation towards planar-chiral α-iodoferrocenyl acetate **3.93**

In the initial experiments for the Baeyer-Villiger oxidation of ferrocenyl ketone **3.94**, classical conditions using an excess of *m*CPBA and $NaHCO_3$ in CH_2Cl_2 at room temperature were applied (Scheme 3.17). After stirring overnight, a dark reaction mixture was obtained. Neither ketone **3.94** nor ferrocenyl acetate **3.93** could be identified by HPLC-MS. TLC-analysis did not show a yellow spot indicating the presence of a ferrocene compound. Therefore it was concluded that ketone **3.94** could not be transformed into ester **3.93** using these conditions.

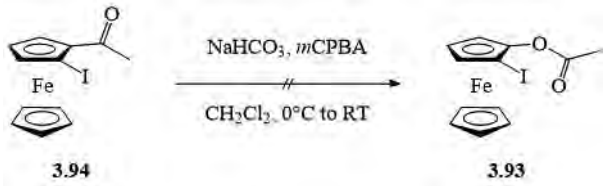

Scheme 3.17 Baeyer-Villiger oxidation towards α-iodoferrocenyl acetate **3.92**

To save highly valuable α-iodoketone **3.93** it was decided to use commercially available acetylferrocene **3.102** for further testing of other Baeyer-Villiger conditions. Table 3.3 shows an overview of all applied conditions. Several oxidants such as *m*CPBA, CH_3CO_3H, ureum hydrogen peroxide (UHP) and hydrogen peroxide were used without any success. In general, mild conditions such as ambient temperatures and shorter reaction times did not result in any conversion (entries 1-5; 9-10) whereas longer reaction times (under acidic conditions) and higher temperatures ended up in decomposition of acetylferrocene (entries 6-8). Methods using basic activation of peroxyacids with bicarbonate as well as methods using (Lewis) acids, to activate the carbonyl compound, were tested. Simultaneous activation of both reactants and the Criegee intermediate using phosphoric acids (entries 5 and 10) as a bifunctional catalyst gave no conversion either.[61]

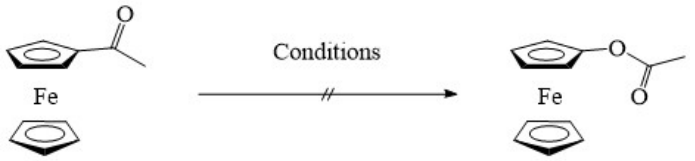

3.102 **3.103**

Entry	Conditions	Result
1	*m*CPBA, $NaHCO_3$, CH_2Cl_2, RT	no conversion
2	TFAA, $2Na_2CO_3.3H_2O_2$, CH_2Cl_2, RT	no conversion
3	CH_3CO_3H, $NaHCO_3$, CH_2Cl_2, reflux	no conversion
4	UHP, $ZrCl_4$, CH_2Cl_2, RT	no conversion
5	H_2O_2, H_3PO_4, CH_2Cl_2, RT	no conversion
6	CH_3CO_3H, CH_3CO_2H, 80°C	decomposition
7	CH_3CO_3H, CH_3CO_2H, RT, 4 days	decomposition
8	TFAA, $2Na_2CO_3.3H_2O_2$, $CHCl_3$, 65°C, 4 days	decomposition
9	UHP, Zr.2THF, CH_2Cl_2, RT	no conversion
10	H_2O_2, (*n*-BuO)$_2$P(O)OH, CH_2Cl_2, RT	no conversion

Table 3.3 Overview of the tested conditions for the Baeyer-Villiger oxidation of commercially available acetyl ferrocene **3.102**

Unfortunately, failure of this Baeyer-Villiger oxidation implicates that the synthesis of the proposed biferrocene-based phosphoramidite ligands **3.88** could not be performed successfully. Therefore, alternative phosphoramide ligands with a biferrocene backbone in the amine part are proposed. Their synthesis and applications in asymmetric transition metal catalysis will be discussed in the following parts of this chapter.

3.6. Retrosynthetic Analysis of Alternative, Novel Phosphoramidite Ligands

Despite the fact that phosphoramidite ligands **3.88**, characterized by a biferrocenol backbone could not be obtained, this synthesis route offers the possibility to develop a new (small) library of phosphoramidite ligands **3.104** (Scheme 3.18). For these ligands the aim is to use a fixed, novel biferrocene-based secondary amine **3.106** in combination with different commercially available achiral and chiral diols **3.105**. The use of an achiral alcohol allows to study the influence of the chiral biferrocene-backbone as such, whereas the combination of chiral amine **3.106** and a chiral diol allows to explore the matched and mismatched situations. The retrosynthetic analysis of this ligand series is shown in Scheme 3.18.

The retrosynthetic analysis of ligand series **3.104** starts again by cleavage of the bonds around the central phosphorus atom. This means that the proposed ligands can be synthesized from PCl_3, commercially available diols **3.105** and biferrocenyl-amine **3.106**. As a consequence, this retrosynthetic analysis can be reduced to the synthesis of the latter. Disconnection of the C-N bonds in this compound with reductive amination in mind reveals dialdehyde **3.107** and ammonia as precursors. Because this type of reactions with ammonia are known to be problematic in many cases, an alternative strategy which uses a primary amine, as a 'protected' alternative for ammonia is a better prognosis. A variety of protecting groups such as benzyl, *para*-methoxybenzyl, allyl, … are known in literature.[62] However, selectivity issues have to be taken into account: the *N*-ferrocenylmethylamine moiety is used as a protecting group for the amino group as well, and can be cleaved using similar conditions as, for example, the benzyl protecting group.[63] A copper mediated Ullmann biaryl reaction, from planar-chiral α-iodoaldehyde **3.96** is proposed for the synthesis of the biferrocene backbone. The stereoselective synthesis of **3.96** using Kagan's chiral acetal approach is described earlier in § 3.5.1.

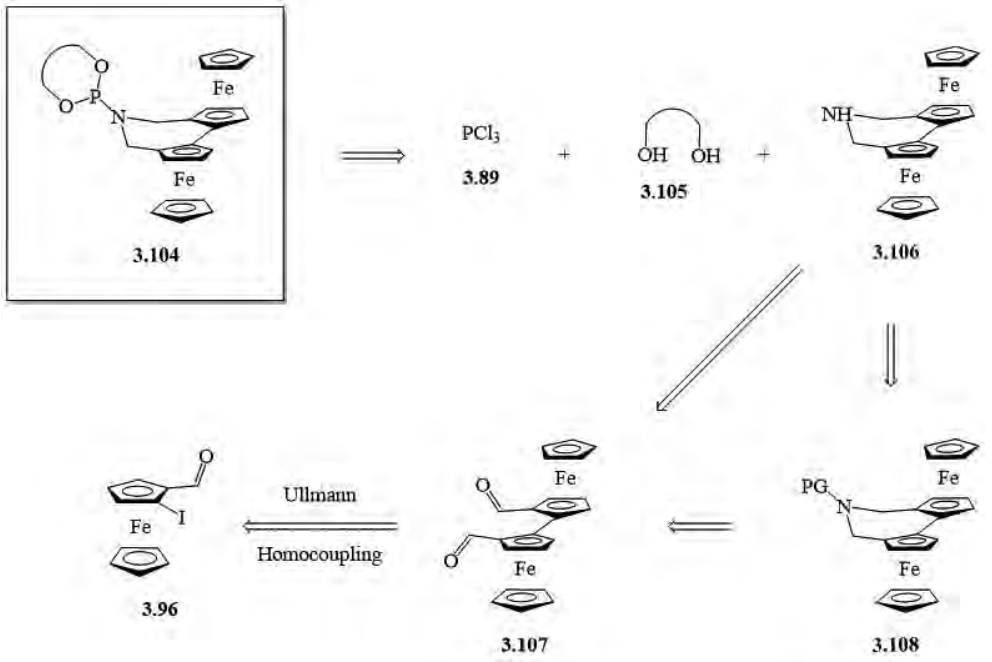

Scheme 3.18 Retrosynthetic analysis of ligand series **3.104**

3.7. Synthesis of Alternative, Novel Phosphoramidite Ligands

3.7.1. Synthesis of dialdehyde **3.107**

In the retrosynthetic analysis, the synthesis of biferrocene-dialdehyde **3.107** is described by using an Ullmann-type homocoupling of aldehyde **3.96** in order to obtain the biferrocene skeleton. However, dialdehyde **3.107** was already known in literature and its synthesis was described independently by Riant[54] and Gagné.[55] Both methodologies are based on Kagan's chiral acetal approach: after the diastereoselective *ortho*-lithiation of chiral acetal **3.100** the oxidative coupling was achieved by adding neat $Fe(acac)_3$ (Riant) or a solution of $Cu(OPiv)_2$ (Gagné). Yields of 70% and 62% have been reported respectively, and in both cases the formation of the *meso* isomer was not mentioned.

Therefore, the initial experiments towards the synthesis of dialdehyde **3.107** were performed using these methods (Scheme 3.19). Unfortunately, very low conversions (< 5% based on TLC-analysis) were obtained when $Fe(acac)_3$ was used. Disapointing results

were also obtained for the exeperiments with $Cu(OPiv)_2$: diacetal **3.109** could only be isolated with yields <10%. For both oxidative coupling methods, the major product was starting material **3.100**.

Hydrolysis of diacetal **3.109** under acidic conditions allowed the synthesis of dialdehyde **3.107**, which could be isolated with a yield of 83%. A side product, containing one aldehyde and one acetal function was formed due to incomplete hydrolysis. The hydrolysis step could also be performed during work-up in a separation funnel using HCl (1M) as the aqueous phase. A drawback of this *modus operandi* is the formation of ferrocenecarboxaldehyde due to hydrolysis of acetal **3.100** making recovery of this precious starting material impossible. Again low yields for dialdehyde **3.107** were obtained due to inefficient homocoupling.

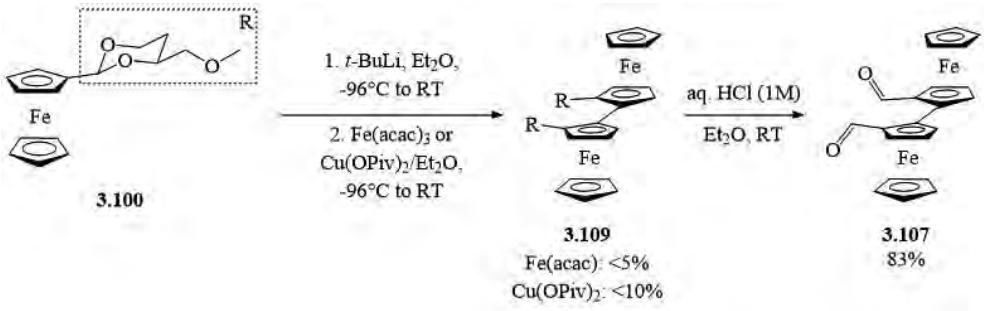

Scheme 3.19 Oxidative homocoupling of acetal **3.100** using $Fe(acac)_3$ and $Cu(OPiv)_2$ followed by acidic hydrolysis

Because the synthetic methods developed by Riant and Gagné for the preparation of dialdehyde **3.107** couldn't be reproduced successfully, more research was necessary. A typical reaction for the synthesis of biaryl compounds is the copper-mediated Ullmann coupling.[64] In general, this reaction requires high temperatures (>200°C) and the order of reactivity is I>Br>>Cl. Electron withdrawing groups (such as CHO) located in the *ortho* position with respect to the halogen atom are beneficial for the reactivity of the aryl halide, whereas bulky groups at this position are detrimental for the formation of the biaryl compound due to steric hindrace. Moreover, the presence of substituents in the *ortho* position which have a lone pair seem to increase the reactivity regardless whether they are electron donating or electron withdrawing. In 1997, Liebeskind *et al.* described a method for the synthesis of a variety of biaryl compounds at ambient temperature.[65] This procedure uses copper(I)-2-thiophene carboxylate (CuTC) in NMP for the reductive coupling of different arylhalides (not including ferrocenes).

In this research project, the reaction conditions from Liebeskind were applied for the first time for the synthesis of the biferrocene skeleton. Homocoupling of α-iodoaldehyde **3.96** using CuTC in NMP at room temperature allowed to isolate biferrocene **3.107** with a yield of 50%. When the temperature was increased to 70°C a yield of 59% was obtained (Scheme 3.20). Hence, a relatively efficient, novel, and easily accessible method for the synthesis of biferrocenes has been developed in this research project[9]. It is also important to note that biferrocene dialdehyde **3.107** is a light-sensitive compound. Therefore all flasks as well as purification columns should be wrapped in aluminum foil in order to obtain the reported yields.

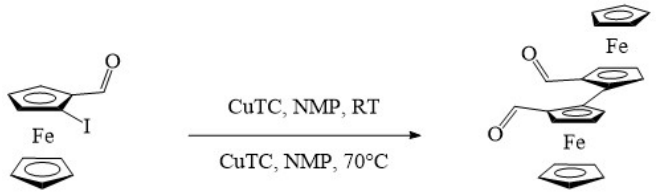

3.96 **3.107**
RT: 50%
70°C: 59%

Scheme 3.20 Ullmann biferrocene synthesis using CuTC

Classical reductive copper mediated Ullmann reactions for the synthesis of dialdehyde **3.107** have been studied here as well. The reaction was performed at 105°C without solvent by adding metallic copper to α-iodoaldehyde **3.96**. It was noticed that a red product was found on the wall and top of the reaction flask, indicating partial sublimation of α-iodoaldehyde **3.96**. Sublimation is a phenomenon that is observed more common for ferrocene compounds, and ferrocene itself can be purified via sublimation.[66] This metallic copper mediated method allowed to synthesize dialdehyde **3.107** with a yield of 67% on 2.6g scale. It is important to notice that this reaction is scale dependent: in general higher yields are obtained on a larger scale. For small scale reactions (generally less than 500 mg), dialdehyde **3.107** was isolated in higher yields via the solution phase methodology with CuTC at 70°C in NMP. Full conversions were never obtained for this homocoupling reaction. Besides starting material **3.96**, which could be recovered, a low percentage of dehalogenated compound (ferrocencarboxaldehyde) was also observed. The presence of trace amounts of (protic) solvents and/or impurities increased the formation of ferrocenecarboxaldehyde.

9 The novel reductive method for the preparation of the biferrocene skeleton using CuTC and NMP was actually developed and optimised using ferrocene carbamate **4.69** as described in § 4.6 (*vide infra*).

Another phenomenon that absolutely needs a discussion in this chapter is the experimentally observed stereoselectivity for the homocoupling reactions, using metallic Cu as well as CuTC in NMP. In general, the homocoupling reactions of chiral ferrocenes can serve as an 'intrinsic chiral resolution' step if the diastereomeric *meso* form can be separated from the other 2 diastereomers (which are enantiomers of each other). This can be explained in more detail based on a fictive transformation, of which all reactions are reversible and chemical equilibrium is reached.

Consider two enantiomers A and B in a ratio of 70/30. A homocoupling reaction will result in three products:

- Enantiomer 1: A-A (as a result of homocoupling between two A enantiomers). This enantiomer will be formed with a percentage of 49% (0.70 x 0.70)
- Enantiomer 2: B-B (as a result of homocoupling between two B enantiomers). This enantiomer will be formed with a percentage of 9% (0.30 x 0.30)
- *Meso*-form: A-B which is the same as B-A (as a result of coupling between enantiomer A an enantiomer B). This *meso* compound will be formed with a percentage of 42% (0.70 x 0.30 x 2)

Enantiomers 1 and 2 can (theoretically) be separated from the *meso* compound via classical separation techniques. Therefore, the ratio of enantiomers 1 and 2 is now 49/9 or 84.5/15.5. As a consequence the enantiomeric excess after homocoupling (which is 69%) is significantly higher than the enaniomeric excess before coupling (which was only 40%).

Of course when a racemic mixture of two enantiomers is reacted in a homocoupling reaction there is no enrichment and a 1/1/2 ratio is expected for enantiomer 1, enantiomer 2 and *meso*-form respectively. However, if racemic α-iodoaldehyde **3.96** was homocoupled to afford dialdehdyde **3.107** using CuTC or metallic copper, this statistical ratio was not observed. A chromatogram resulting from a chiral HPLC analysis of this reaction is shown in Figure 3.11. The observed ratio of the three expected isomers (with retention times of 12.68, 14.28 and 15.90 min.) is almost equal to 1/1/1, which is significantly different from the expected, theoretical ratio. UV-spectra of compounds corresponding to 14.28 and 15.90 min. are identical which means that they are enantiomers of each other. The UV-spectrum of the compound corresponding to 12.68 min. is different, although similar, and assumed to be the *meso* compound (**3.110**) of **3.107**. These results were confirmed by achiral reversed phase HPLC-MS analysis: The ratio

of the enantiomers 1 and 2 versus the *meso* compound is approximately equal to 2/1, instead of the expected 1/1. These analyses are shown in Figure 3.12. The peak at a retention time of 6.13 min. corresponds to the racemic mixture of dialdehyde **3.107**, whereas the peak at a retention time of 6.20 min. corresponds to the *meso* compound. The mass-spectra of both signals prove that both compounds are diastereomers of each other because the same mass-to-charge ratio was found (426.9 Da corresponding to $[M+H]^+$).

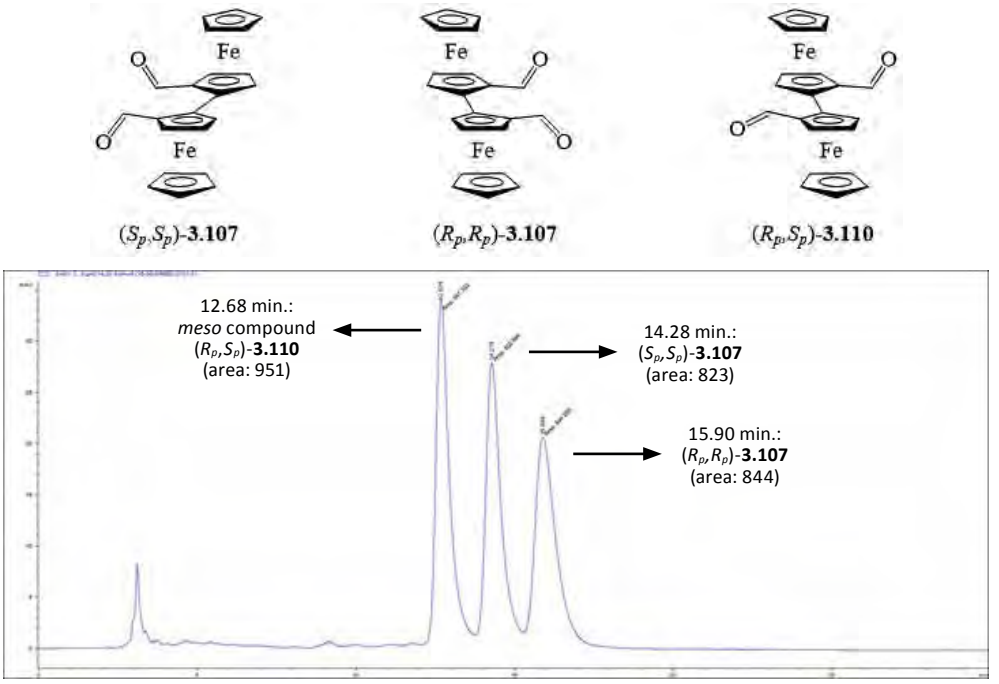

Figure 3.11 Chromatogram chiral HPLC analysis showing an almost 1/1/1 ratio (Chiralpak AS-H column, solvent: *n*-hexane/EtOH (80:20), flow rate = 1 mL/min, t = 30 min., T = 35°C)[10]

Further experiments for the homocoupling reaction where performed with a scalemic mixture of 84% (S_p)-**3.96** and 16% of (R_p)-**3.96**. Similar to TLC-analysis of the homocoupling of racemic α-iodoaldehyde **3.96**, two bright red spots could be detected corresponding to the homocoupled products. After chromatographic separation, both compounds were analyzed via HPLC-MS and chiral HPLC. The HPLC-MS analysis of the first compound, which is shown in Figure 3.13, shows a single peak at a retention time of 6.13 min. The HPLC-MS analysis of the second compound (Figure 3.14) shows a major

10 For more experimental details see § 3.9.1 and § 3.9.5 (*vide infra*).

signal at 6.20 min. corresponding to the *meso*-form (only a very tiny peak at 6.13 min. is observed for its diastereomers). These observations are confirmed in the chiral HPLC analyses, of which the chromatograms are shown in Figure 3.15 and Figure 3.16. But the most important conclusion of the analysis represented in Figure 3.15 is that there is only one enantiomer present! Or in other words with a mixture of (S_p)-**3.96** and (R_p)-**3.96** with an *ee*-value of 68%, (S_p,S_p)-**3.107** was synthesized as an enantiopure compound!

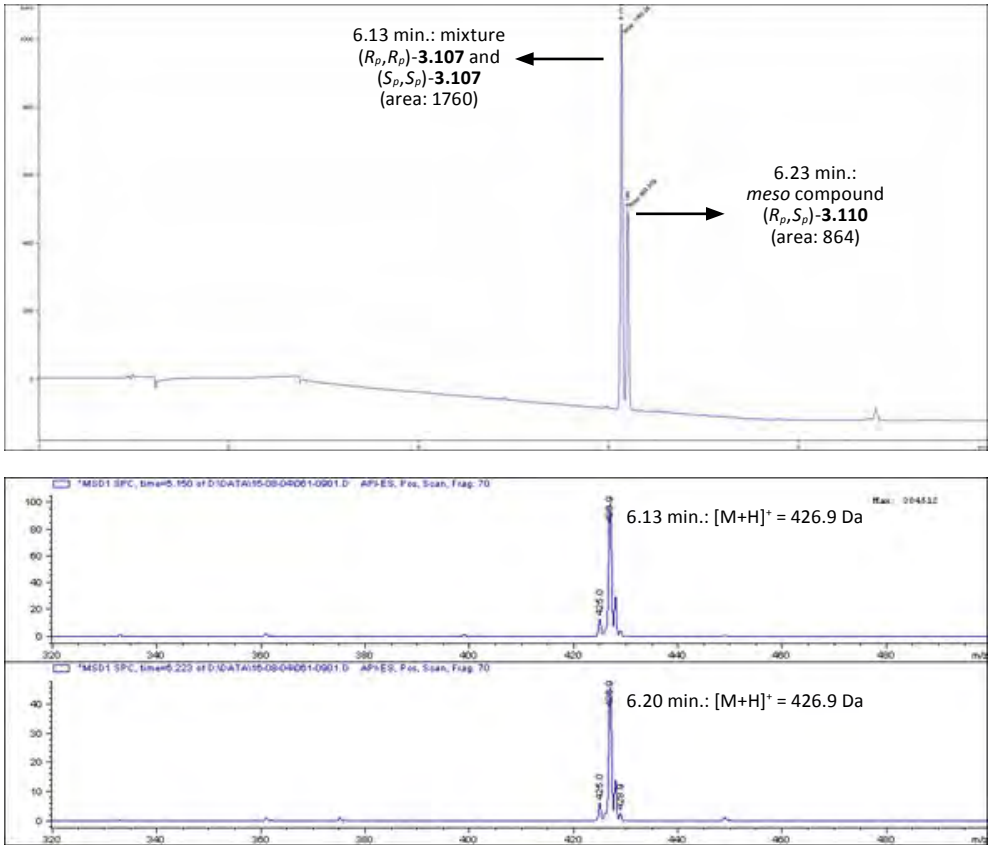

Figure 3.12 Upper: chromatogram achiral HPLC-MS analysis showing two peaks in a 2/1 ratio Lower: identical mass spectra of both peaks of the chromatogram (Phenomenex Kinetex C18, solvent: method 3, flow rate = 1 mL/min., T = 35°C)[11]

A similar phenomenon, and even more pronounced is already reported in literature (and mentioned in § 3.3, *vide supra*) for the synthesis of BIFEP ligands.[44] However, a generally accepted explanation for these observations is not known and also during this thesis there were no further experiments performed to explain these results. It

11 For more experimental details see § 3.9.1 and § 3.9.5 (*vide infra*).

was just accepted as a great advantage for the enantiomerically pure synthesis of the target ligands. It is obvious that enantiomerically pure (S_p,S_p)-dialdehyde **3.107** can be obtained from a mixture of 96% *ee* of α-iodoaldehyde **3.96** as well (*cf.* § 3.5.1). Moreover, the observed yield was higher due to the fact that significantly less *meso*-compound **3.110** was produced.

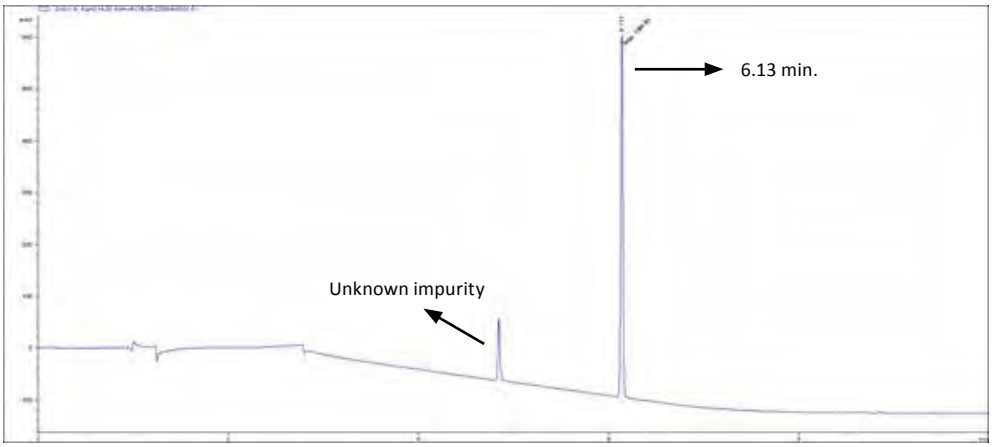

Figure 3.13 Chromatogram of achiral HPLC analysis showing only one signal. There is no signal observed corresponding to the *meso*-compound 3.110 (Phenomenex Kinetex C18, solvent: method 3, flow rate = 1 mL/min., T = 35°C)[12]

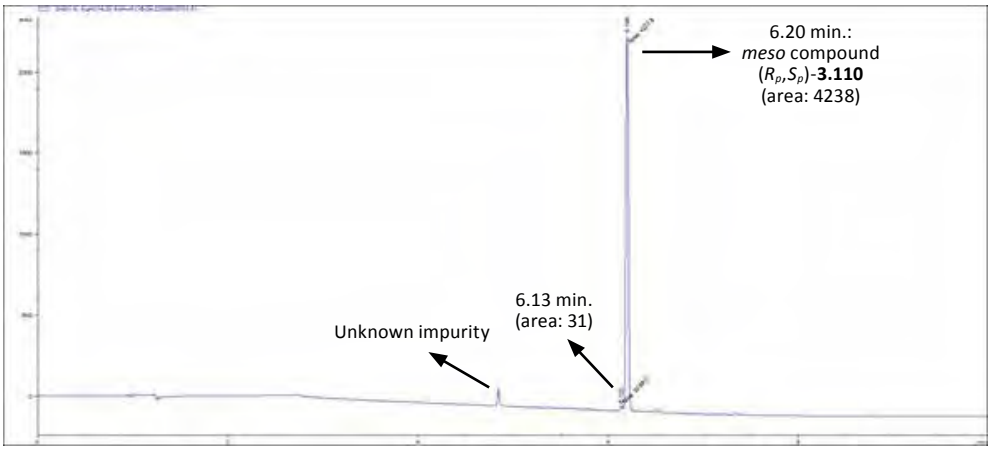

Figure 3.14 Chromatogram of achiral HPLC analysis with a major signal corresponding to the *meso*-form 3.110 and a tiny peak corresponding to its diastereomer (Phenomenex Kinetex C18, solvent: method 3, flow rate = 1 mL/min., T = 35°C)[12]

12 For more experimental details see § 3.9.1 and § 3.9.5 (*vide infra*).

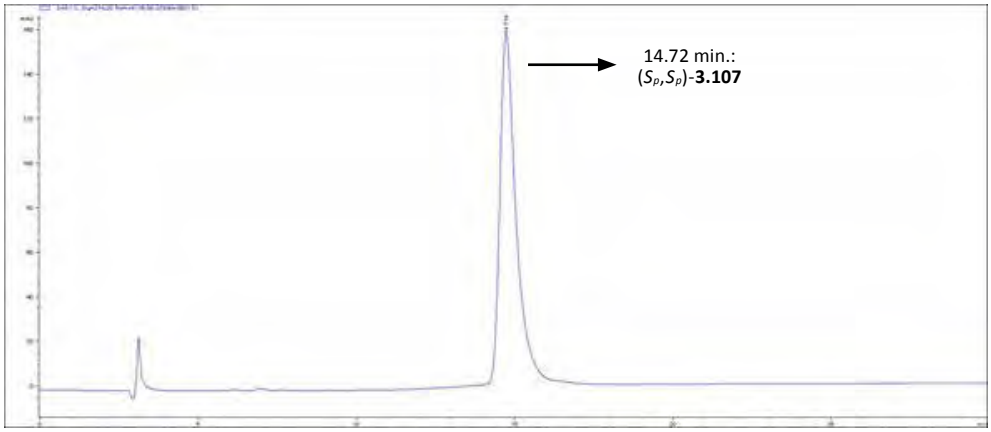

Figure 3.15 Chromatogram of chiral HPLC analysis showing only one signal meaning that (S_p,S_p)-dialdehyde 3.107 could be obtained as a single enantiomer (Chiralpak AS-H column, solvent: *n*-hexane/EtOH (80:20), flow rate = 1 mL/min, t = 30 min., T = 35°C)[13]

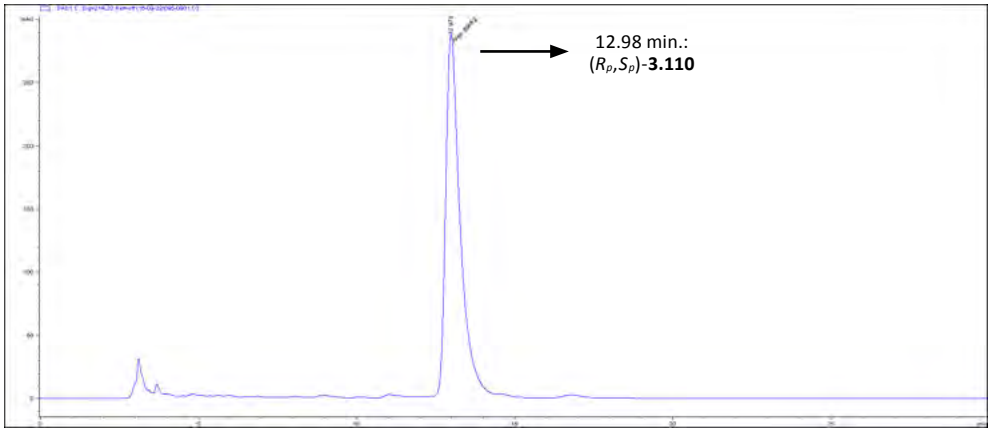

Figure 3.16 Chromatogram of chiral HPLC analysis showing one signal corresponding to the *meso*-form 3.110 enantiomer (Chiralpak AS-H column, solvent: *n*-hexane/EtOH (80:20), flow rate = 1 mL/min, t = 30 min., T = 35°C)[13]

The exact mechanism of the reductive Ullmann coupling is not known and two pathways are theoretically possible.[64,67] The first one involves the formation of aryl radicals whereas arylcopper intermediates are formed in the second pathway. Nevertheless, the latter mechanism is most widely accepted since the intermediate arylcopper species could be isolated.[68-73] This mechanism is illustrated in Scheme 3.21 for the synthesis of dialdehyde **3.107** starting from α-iodoaldehyde **3.96** as an example. The oxidation level, represented as x, is equal to 0 when the homocoupling reaction is considered

13 For more experimental details see § 3.9.1 and § 3.9.5 (*vide infra*).

with metallic copper and +I when CuTC is applied as copper source. The first step of the mechanism is a reversible oxidative addition of the aryl halide to the copper source.[70] The next step involves the formation of the active copper species with a second equivalent of the initial copper source via a disproportionation step. During this step the oxidation level of arylcopper intermediate **3.111** gets reduced whereas the oxidation state of the second equivalent of copper increases with formation of $[Cu]^{x+1}I$. A second oxidative addition of a subsequent equivalent of arylhalide **3.96** results in the formation of copper species **3.113**. Reductive elimination with the formation of an aryl-aryl carbon bond, here the bond between two ferrocene moieties and (again) one equivalent of $[Cu]^{x+1}I$, is the last step. This mechanism involves the formation of high valent copper intermediates: Cu^{III} species when metallic copper has been used as initial copper source and a Cu^{IV} intermediate when CuTC has been applied. Although these high valent copper species are known, they are considered to be very rare.[74] The efficiency of CuTC as copper source for reductive Ullmann couplings is explained by an inherent ability of carboxylate as a ligand to stabilize the oxidative addition product as implied by the position of the equilibrium depicted in Scheme 3.22, and not to the internal coordination of the sulfur atom to the metal.[65,73]

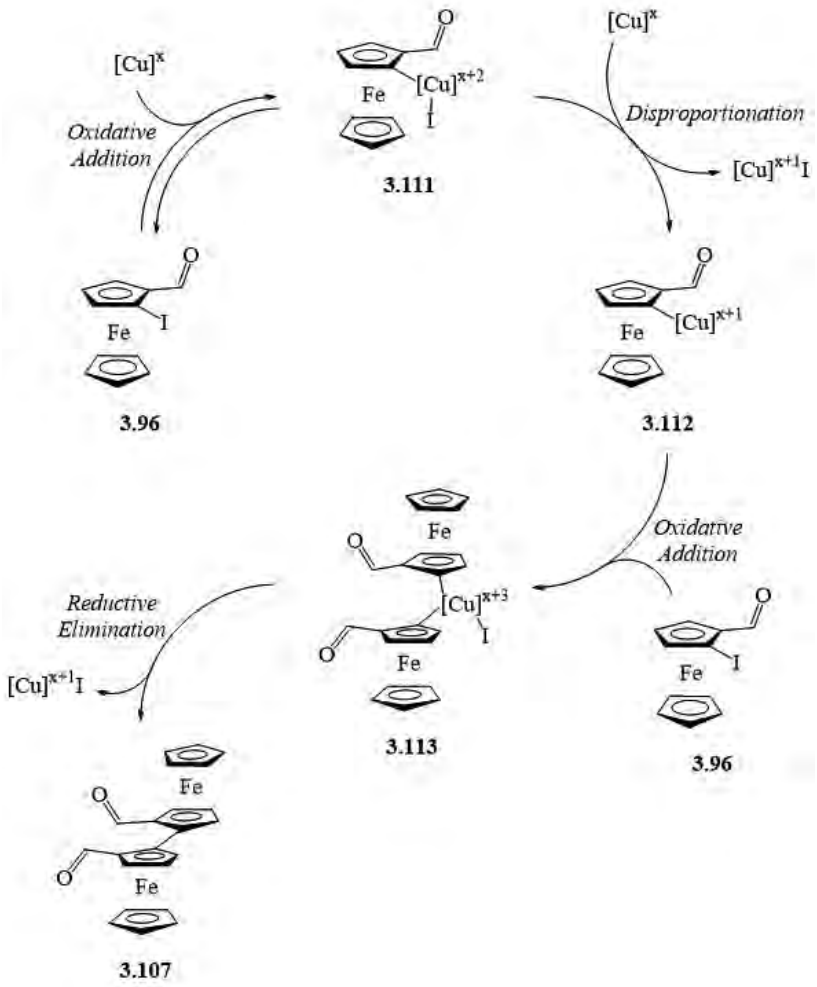

Scheme 3.21 Generally accepted mechanism of the Ullmann homocoupling reaction

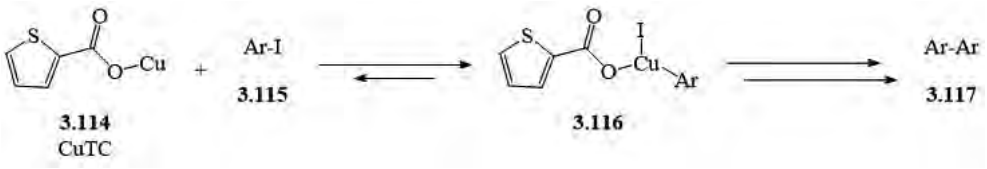

Scheme 3.22 Explanation of the efficiency of CuTC as a copper source

3.7.2. Reductive aminations for the synthesis of biferrocene-based dihydroazepines

The synthesis of ligand precursor **3.106** from dialdehyde **3.107** should theoretically be possible via a reductive amination with a solution of liquid ammonia in a suitable organic solvent. Nevertheless, it is known that this type of reactions is problematic, and this was indeed observed for the conversion of **3.107** into **3.106** with $NaBH_3CN$ as a mild, selective reducing agent, in MeOH or MeCN or DCE (0% yield, Scheme 3.23). Therefore, reductive amination with a primary amine which simultaneously functions as a protecting group was proposed. As already mentioned in § 3.5 selective cleavage is an important challenge because the ferrocenylmethyl (Fem) group is known to be a protecting group for amines and aminoacids as well.[63,75] For that reason the synthesis of multiple biferrocene-based dihydrozaepines **3.118**-**3.120** was proposed.

Reductive amination of **3.107** with an excess of $NaBH_3CN$ and the primary amines benzylamine, *para*-methoxybenzylamine and allylamine in DCE allowed to prepare the corresponding biferrocene dihydroazepines **3.118**-**3.120** with yields of 76-88% (Scheme 3.23). Accidently, it was found that the addition of anhydrous K_2CO_3 accelerates the reaction. The formation of side-products, due to incomplete dihydroazepine ring closure, or double amination of both aldehyde functional groups, or reduction of the carbonyl group to the alcohol was not observed.

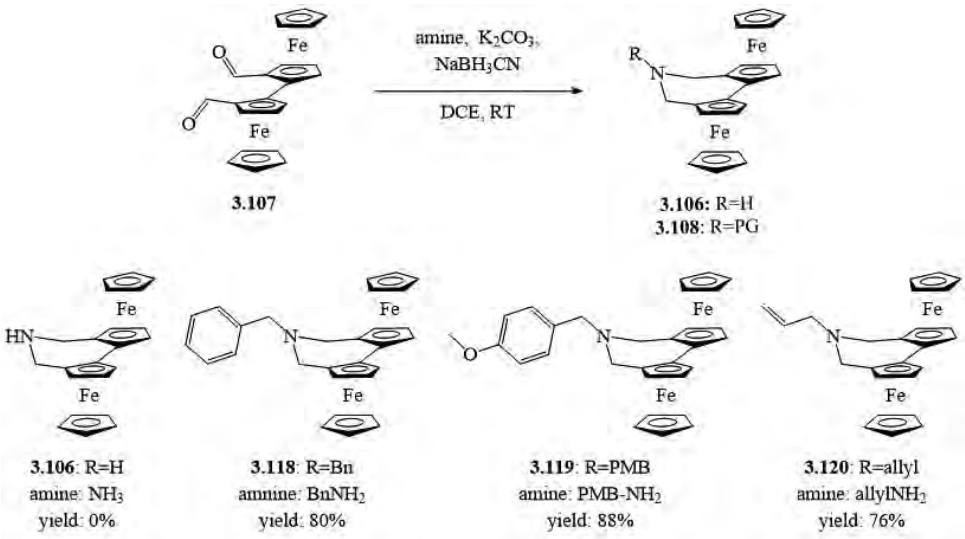

Scheme 3.23 Reductive aminations of dialdehyde **3.107** for the synthesis of different biferrocene-based dihydroazepines **3.106**, **3.118-3.120**

3.7.3. Deprotection reactions: synthesis of biferrocene-based dihydroazepine **3.106**

The mildest method for the deprotection of benzyl amines is catalytic hydrogenolysis using a transition metal (palladium or platinum) and hydrogen gas. Unfortunately, when these conditions were applied for the deprotection of *N*-benzyl-substituted dihydroazepine **3.118**, target amine **3.106** could not be identified (Scheme 3.24). TLC-analysis showed the formation of a hydrophobic yellow compound. Although no further analysis for the identification of the latter was accomplished, it is presumed that this compound might be identified as 2,2'-dimethyl-1,1'-biferrocene. This means that catalytic hydrogenolysis is a possible method for the cleavage of the ferrocenylmethyl (Fem) group, similar to the hydrogenolysis of benzylamines. In their publication, Eckert and Seidel mention that the Fem group can be cleaved with TFA as well and therefore these conditions have to be avoided.[75] Selective removal of p*ara*-methoxybenzylamines can be accomplished under oxidative conditions. A standard procedure involves the use of 2,3-dichloro-5,6-dicyano-1,4-benzoquinone (DDQ) in phosphate buffered (pH=7) dichloromethane. However, when these conditions were applied for the deprotection of **3.119**, amine **3.106** was not formed. Moreover, there were no yellow spots characteristic for ferrocene compounds observed by TLC analysis. Here it is postulated that strong oxidative agents like DDQ might oxidize ferrocene itself resulting in the formation of decomposition products. Isomerization of allylamine with KO*t*-Bu in DMSO at elevated temperatures with subsequent mild acidic hydrolysis is one of the most common methods for the deprotection of allylamines. Indeed, the deprotection of the allyl group of **3.120** was performed successfully via a isomerization reaction with KO*t*-Bu in DMSO at 100°C and subsequent work-up with NH_4Cl. This allowed to obtain biferrocen dihyroazepine **3.106** with a yield of 97%.

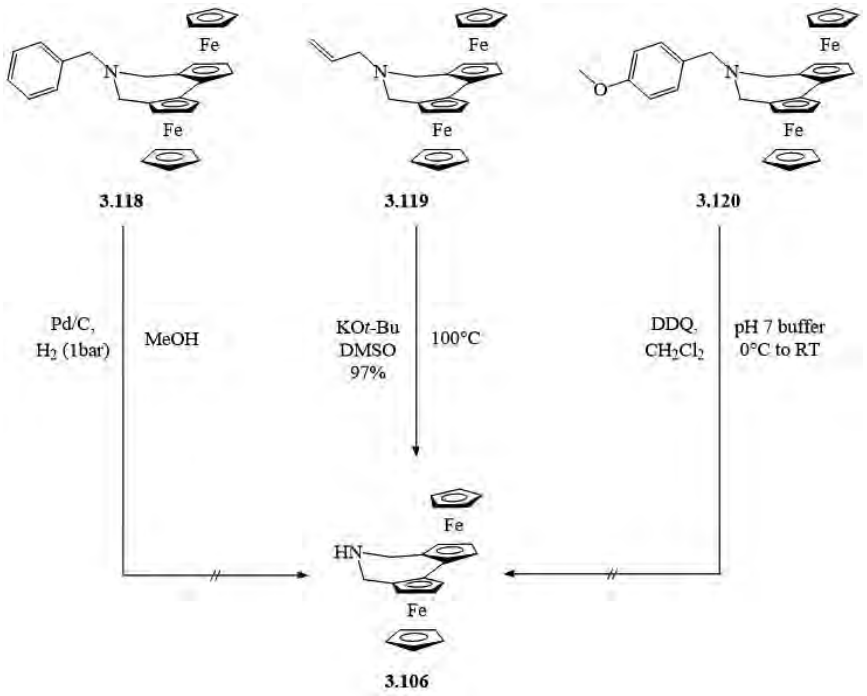

Scheme 3.24 Deprotection methods for the synthesis of dihydroazepine **3.106** from different substituted dihydroazepines

3.7.4. Synthesis of alternative novel biferrocene-based phosphoramidite ligands

Different synthetic routes for the preparation of phosphoramidite ligands have already been developed, depending on which of the key bonds, P-O or P-N are established first.[2,76] Three of these methods are shown in Scheme 3.25. In route A diol **3.105** is treated first with phosphorus trichloride in the presence of a base (typically Et_3N, DIPEA, pyridine) to yield intermediate chlorophosphite **3.121**. Afterwards, amine **3.90** is added together with extra equivalents of base.[76-79] Route B generally has a higher success rate when more sterically hindered amines are used. Here, dichloroaminophosphine **3.123** is initially formed by reacting amine **3.90** with phosphorus trichloride in the presence of a base. Diol **3.105** is added afterwards.[80] Pathway C starts with the reaction of diol **3.105** with $P(NMe_2)_3$ (hexamethylphosphorus triamide) to give a dimethylamine derived phosphoramidite ligand **3.124**. This can either be applied as a ligand itself or it can undergo subsequent amine exchange under basic conditions to obtain a number of other phosphoramidite ligands.[12,81,82]

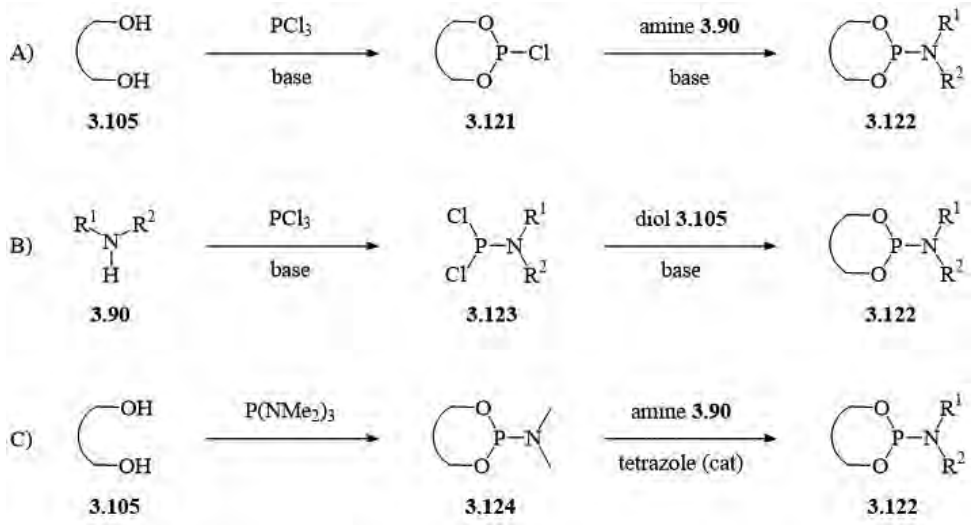

Scheme 3.25 General approaches for the synthesis of diol-based phosphoramidites ligands

Phosporamidite ligands with an axial chiral dihydroazepine backbone, which represent analogs of the target ligands **3.104** (*cf.* § 3.6, Scheme 3.18, *vide supra*) have already been synthesized by different groups (Figure 3.17). For the synthesis of both diastereomers of spiro-diol-based ligands **3.125**, Zhou reported a yield of 43% and 47% using pathway A.[83] This protocol was also applied by Moberg *et al.* to obtain monodentate phosphoramidite ligands **3.126**-**3.127** with an aromatic diol scaffold.[84] Unfortunately there were no yields reported. But, in 2007 Matt *et al.* described in full detail the synthesis of the same ligands using the same approach and yields between 65% and 85% were reported.[85]

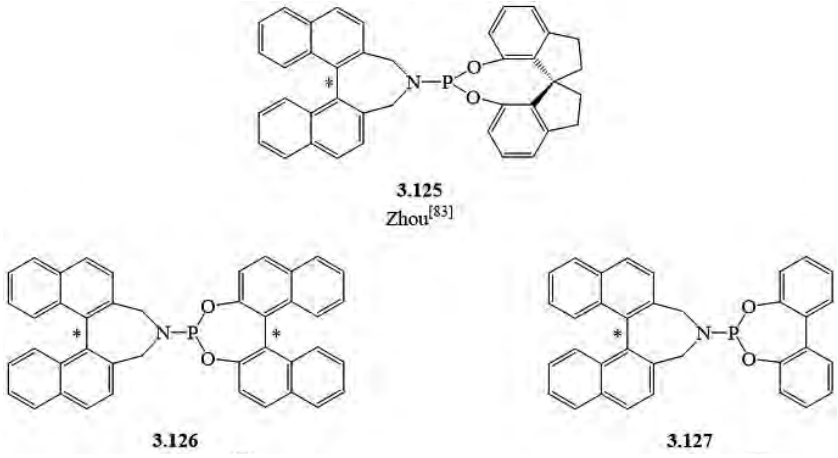

Figure 3.17 Phosphoramidite ligands with an axial chiral amine backbone

The experiments of Matt *et al.* showing good to excellent results were obtained via approach A. However, biferrocene-based dihydroazepine **3.106** is more sterically hindered than the corresponding axial chiral binaphthyl-based dihydroazepine. Therefore route B is considered to be the best route for the synthesis of target phosphoramidite ligands **3.104** (Scheme 3.26). Practically, amine **3.106** was dissolved in anhydrous toluene, cooled to 0°C and 10 equivalents of Et_3N as a base were added. Afterwards, a solution of freshly distilled PCl_3 (1 eq) in anhydrous toluene was carefully added. Because these reactions were carried out at small scale (30-75mg of **3.106**) it is important to purify PCl_3 via distillation to avoid the formation of hydrolyzed and oxidized side products. The reaction mixture was stirred for 15 min. at 0°C, allowed to warm up to room temperature and stirred for 2 h before it was cooled again to 0°C. A solution of the desired aromatic diol in anhydrous toluene was added together with another 2.6 equivalents of Et_3N, and the reaction was stirred overnight. After work-up and purification via column chromatography, monodentate phosphoramidite ligands **3.129**-**3.131** were obtained with yields of 29-44%. Compared to the results reported by Matt *et al.*, these yields are significantly lower. It is therefore important to mention that these reactions were not optimized. For example, Matt and co-workers used *N,N*-di-*iso*-propylethylamine as a base, despite the fact that triethylamine is more frequently used for the synthesis of phosphoramidites. A longer reaction time for the formation of dichloroaminophosphane **3.128** can be beneficial to obtain higher yields as well and sometimes, temperatures are even gradually increased to reflux conditions for the synthesis of dichloroaminophosphanes.[82] But the most important reason for the moderate yields is the fact that these reactions were carried out on a small scale (30-75mg of **3.106**) due to the limited amount of dihydroazpine **3.106** that was available.

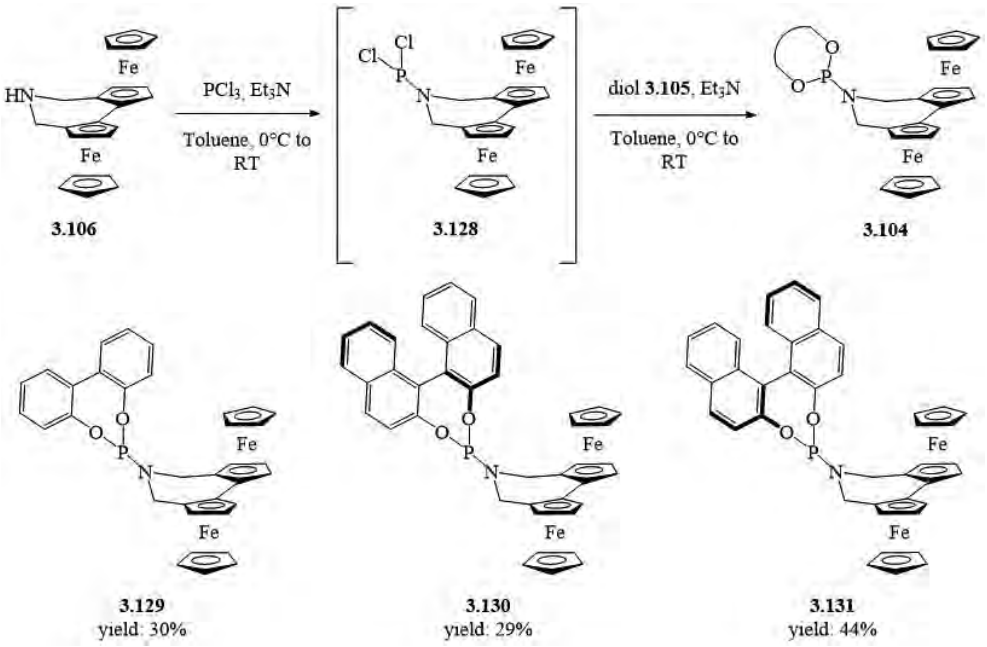

Scheme 3.26 Synthesis of biferrocene-based phosphoramidite ligands **3.129**-**3.131** with a 1,1'-diaryl-2,2'-diol backbone

3.8. Rhodium(I)-Catalyzed Asymmetric Hydrogenations

3.8.1. General considerations: mechanism and origin of Stereoselectivity

Catalytic asymmetric hydrogenations of prochiral substrates such as olefins, ketones and imines are one of the most powerful and most studied transformations in the field of asymmetric catalysis.[86] Rhodium, ruthenium, iridium and palladium are transition metals frequently used for this type of reactions, often in combination with chiral (bidentate) phosphine ligands.

In general, the results of transition-metal catalyzed enantioselective hydrogenations are dependent on multiple parameters like solvent, temperature, pressure, substrate, catalyst (precursor), catalyst loading and ligand. Because these parameters are able to influence more steps in a catalytic cycle (or mechanism in general), it is not always obvious to explain their impact on the outcome of a certain reaction. For example, higher enantioselectivities are generally obtained when lower temperatures are applied.

However, this negatively affects reaction kinetics and therefore better enantioselectivities could be obtained at higher temperatures with some catalysts for certain reactions.[87]

The substrate scope of rhodium(I)-catalyzed hydrogenations is limited to those compounds possessing a second functional group that can coordinate to the metal. Among these belong *N*-acyl-enamides, α- or β- dehydro-amino acids and –esters, itaconic acids and –esters. The mechanism of Rh-catalyzed hydrogenations has been extensively studied by the research groups of Halpern[88] and Imamoto.[89] Halpern postulated the 'unsaturated' mechanism whereas Imamoto and co-workers came up with a 'dihydride' mechanism. Initial mechanistic studies by both research groups were carried out using bidentate diphosphine ligands.

The catalytic cycle of the Halpern mechanism, valid for diphosphine ligand systems, is illustrated in Scheme 3.27.[88,90] Catalytic sources such as $[Rh(cod)_2]BF_4$ generally represented as $[Rh(diene)_2]^+X^-$ are mostly used. After ligand exchange chiral cationic precatalyst $[RhL_2(diene)]^+X^-$ is formed (in this complex L_2 is a chiral bidentate diphosphine ligand). The diene ligand is removed by hydrogenation and the free coordination sites formed in this step are occupied by solvent molecules S. The new rhodium(I)-complex $[RhL_2(S)_2]^+X^-$ **3.132** is able to enter the catalytic cycle. Here, the first step includes the coordination of substrate **3.133**[14] in a bidentate fashion, displacing two solvent molecules. Because the substrate can bind in two different ways, with either its *Si* or its *Re*-face oriented to the metal, two diasteomeric complexes $\mathbf{3.134}_{major}$ and $\mathbf{3.134}_{minor}$ can be formed. The coordination of the substrate molecule is reversible, and therefore both diastereomeric complexes are in equilibrium with each other. As their thermodynamic stability is different, the energetically more stable diastereomer will be present in larger amounts. However, the diastereomeric complex which is present in minor amounts results in the formation of the major final product (*S*)-$\mathbf{3.137}_{major}$, (anti lock-and-key postulate). This is because the next step in the catalytic cycle is the oxidative addition of hydrogen to rhodium, which is supposed to be the rate determining step in the Halpern mechanism (rate constant k_2). The latter reaction step is faster for the diastereomeric complex $\mathbf{3.134}_{minor}$ than for $\mathbf{3.134}_{major}$. This explains why the major final product (*S*)-$\mathbf{3.137}_{major}$ is formed from the minor diastereomeric rhodium complex $\mathbf{3.134}_{minor}$.

14 One of the benchmark substrates for these hydrogenations, methyl-2-acetamido acrylate **3.133,** is chosen as an example for further discussion.

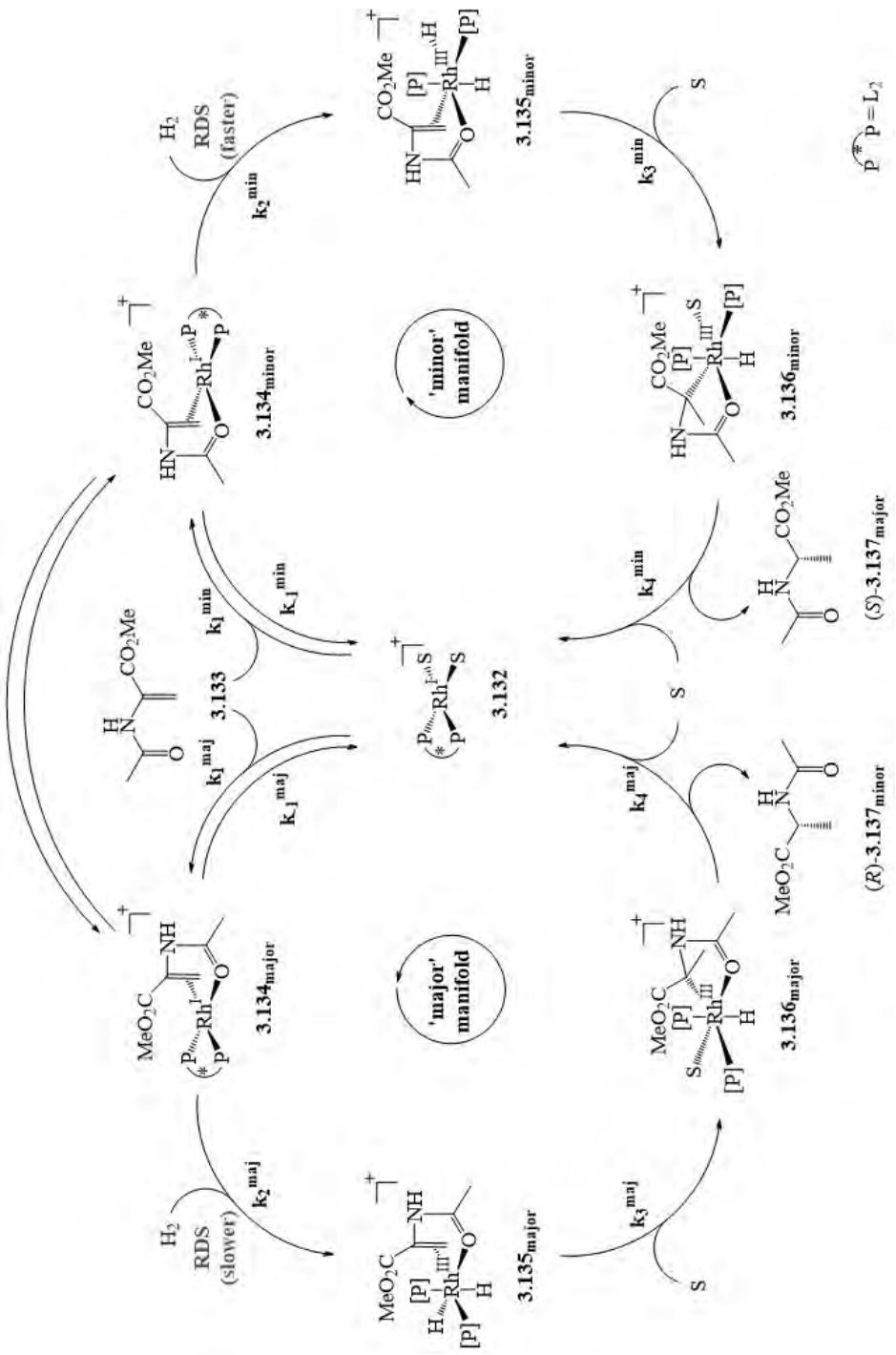

Scheme 3.27 Halpern mechanism for Rh-catalyzed hydrogenations of activated olefins

Migratory insertion which involves addition of one of the hydrogen atoms to the double bond occurs simultaneously with the formation of a rhodium-carbon bond. Reductive elimination with release of the chiral amino acid derivative **3.137** and the rhodium complex $[RhL_2(S)_2]^+X^-$ **3.132** is the last step of the catalytic cycle.

The discussion of the stereochemistry of the rhodium-catalyzed asymmetric hydrogenation using bidentate diphosphine ligands starts with the complexation of the substrate (methyl-2-acetamido acrylate **3.133**), (*vide supra*). Two diastereomeric complexes, each will give final products with opposite configuration, can be formed. In order to predict the stereochemical outcome of these rhodium(I)-catalyzed hydrogenations, empirical rules have been proposed. The representation via quadrant diagrams, which is based on results of XRD (X-ray diffraction) experiments, is the most frequently used approach and has been developed by Knowles.[91] In this model, shown in Figure 3.18, chiral C_2-symmetric ligands are creating a chiral environment around the central rhodium atom. Two out of four quadrants are sterically more hindered via the arrangement of the substituents on phosphorus, directing the coordination of the substrate. These substituents are oriented in such a way that two of the P-aryl rings occupy axial positions in the chelate ring and are torsionally forced to be 'face-on' to the substrate. The other pair of P-aryl rings occupy the equatorial positions and are forced to be 'edge-on'. In the example, shown in Figure 3.19, the approach of the substrate with its *Si*-face is less hindered and as such lower in energy which results in the major complex. However as discussed in the Halpern mechanism above, the minor complex will undergo a faster oxidative addition of hydrogen gas. Consequently, the major product (*S*)-**3.137**$_{major}$ will be formed from the minor complex where the substrate binds in a *Re*-face fashion. The quadrant diagram empirical rules have proven to predict the stereochemical outcome correctly for the bidentate diphosphine ligands DIPAMP and CHIRAPHOS. Nevertheless, this approach has led to wrong predictions for other highly-successful bidentate diphosphine ligands such as the DuPhos ligand family and BPE[15] ligands.[91,92]

15 BPE: 1,2-bis-(Phospholano)ethane

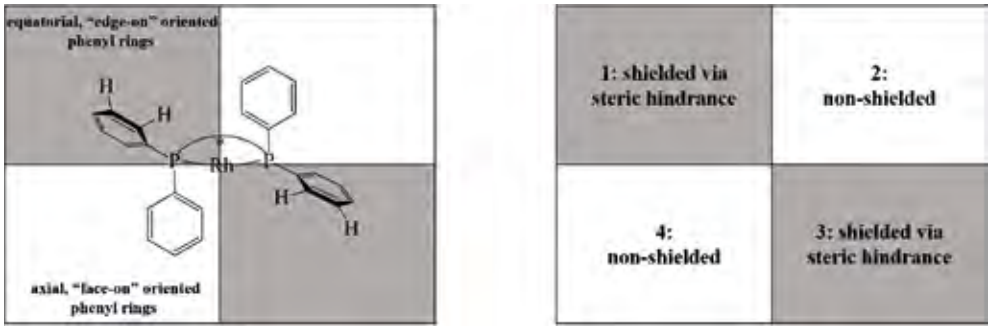

Figure 3.18 Quadrant diagrams for bidentate diphosphine ligands

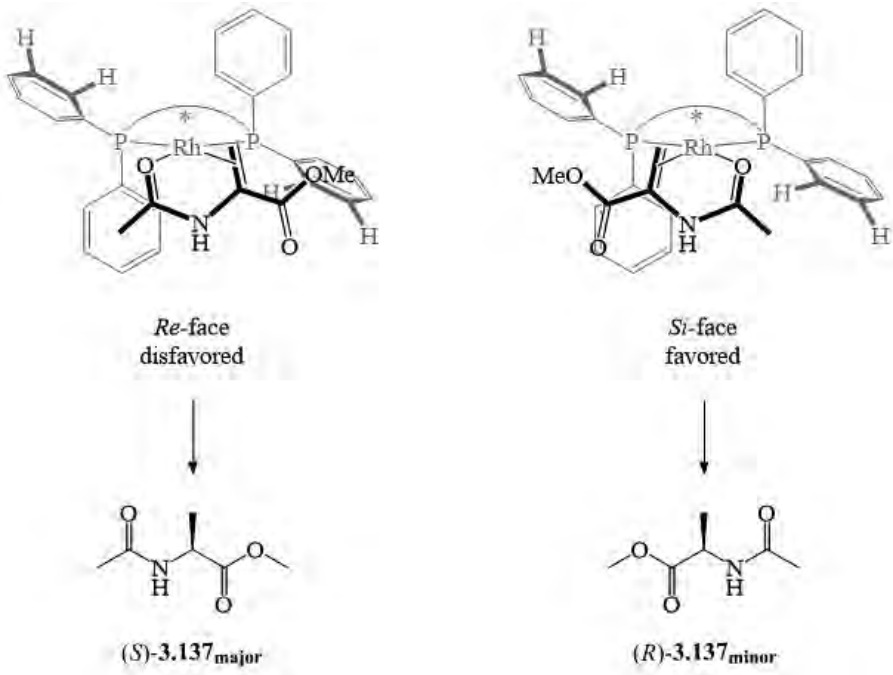

Figure 3.19 Quadrant diagrams explaining the observed stereoselectivity using bidentate diphosphine ligands

For a long time is it was generally accepted that the enantioselectivity of the rhodium-catalyzed hydrogenation was solely dictated by steric effects, based on XRD-analysis of solid state complexes, as described above.[93] But one always has to keep in mind that the observed stereoselectivity depends on the 3D structure of the catalyst in solution. For that reason XRD-based rationales are not always valid. Moreover, molecular dynamics and NOE (Nuclear Overhauser Effect) investigations of (intermediate) struc-

tures in solution have shown that the enantioselectivity of the Rh-catalyzed hydrogenation is not solely dictated by steric effects.[94] Oxidative addition of H_2 to the major or minor complex plays a major role in the enantioselectivity in this type of transformations. The electronic barrier for H_2-addition is a two-orbital, four electron repulsion between a filled, metal based d_z-like molecular orbital and the incoming filled H_2 σ-molecular orbital.[95] This repulsion is influenced by the amount of shielding of the rhodium atom induced by all coordinating ligands. Both the chiral diphosphine ligand and the coordinated substrate determine the total shielding of the rhodium and consequently the ease of H_2 additions. In conclusion, the enantioselectivity of the rhodium(I)-catalyzed hydrogenation is controlled both by steric factors, which control the ratio between the two dynamically equilibrating diastereomeric complexes, and the electronic properties of the ligands which influence the relative rates of oxidative addition of hydrogen to the rhodium complexes.

Extensive mechanistic research was performed by van den Berg and Feringa for the enantioselective hydrogenation using MonoPhos as a chiral monodentate ligand.[96] Kinetic analysis experiments in combination with spectroscopic data (NMR and UV-VIS), X-ray analysis, EI-MS measurement and a non-linear effect experiment can be statistically modelled adequately using the 'Halpern mechanism' proposed for bidentate ligands. However, when the mechanism was expanded with a resting state **3.139**, the model performance resulted in higher statistical correlations between measured and modeled data. The resting state, which is formed after coordination of one extra substrate molecule to the 16-electron complex **3.138**, is a 20-electron rhodium complex and is catalytically inactive (Scheme 3.28). The existence of this 20-electron complex could be confirmed via EI-MS experiments and even single crystal X-ray analysis. The existence of the resting state **3.139** in combination with the fact that excellent *ee*-values are obtained with the MonoPhos ligand allows to modify the mechanism presented in Scheme 3.27 to the one shown in Scheme 3.28.

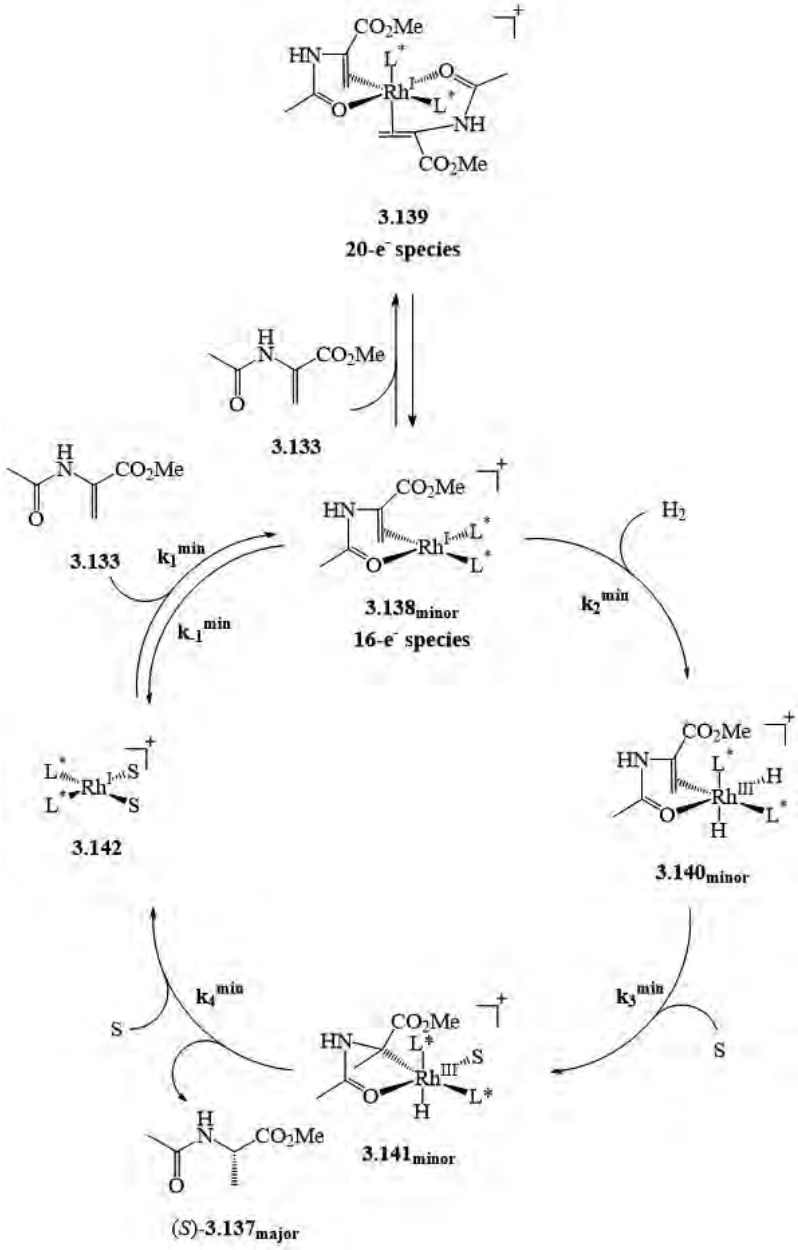

Scheme 3.28 Catalytic cycle expanded with the resting state **3.140**

Unfortunately, the comprehensive studies of van den Berg could not rule out whether the mechanism is Halpern or anti-Halpern for MonoPhos as a monodentate ligand. In this latter mechanism the anti lock-and-key concept is not valid but here the pre-

dominant enantiomer of the product arises from the most stable diastereomeric complex **3.138**$_{major}$. An extensive experimental and theoretical mechanistic study including NMR analysis, kinetic measurements, experiments on non-linear effects and DFT calculations were carried out by a collaboration of the research groups of Reetz and Blackmond.[97] Two important conclusions have emerged from this study. Firstly, kinetic studies revealed that the catalytically active species has indeed two monodentate ligands bonded to rhodium. In this study, monodentate phosphite ligands were used. The second conclusion, about the stereochemistry and mechanism, needs more explanation. Therefore DFT calculations were performed with itaconic acid dimethyl ester **3.143** (dimethyl itaconate) as olefin substrate and chiral monophosphite (*R*)-binol-based ligand **3.144**, shown in Figure 3.20.

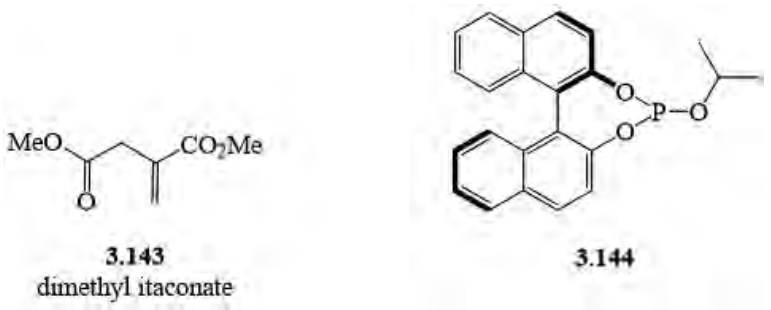

Figure 3.20 Dimethyl itaconate **3.143** and monodentate phosphite ligand **3.144** used in the DFT calculation by Reetz and Blackmond

For the traditional Halpern mechanism with C_2-symmetric bidentate disphosphine ligands, two diastereomeric rhodium complexes are formed after complexation of olefin substrate (*cf.* Scheme 3.27: **3.134**$_{minor}$ and **3.134**$_{major}$). However, for rhodium-catalyzed hydrogenations using more flexible monodentate ligands, this C_2-symmetry is no longer present. Consequently, four cationic rhodium-complexes $[Rh(L)_2(olefin)]^+$ ($[Rh(\mathbf{3.144})_2(\mathbf{3.143})]^+$ in the study from Reetz and Blackmond), in two diasteromeric pairs can be formed. In each pair, the metal coordinates with one enantioface of the prochiral olefin (*Re*-face and *Si*-face), Figure 3.21. If conformational differences are considered, which arise from rotations around chemical bonds such as the rhodium-ligand bond, additional species have to be considered. Theoretical, unconstrained DFT calculations of the full system showed that the three conformers with the lowest energy were $[Rh(\mathbf{3.144})_2(\mathbf{3.143})]^+$ complexes with a *Re*-face complexation mode, which will give the (*S*)-product. However, experimentally the (*R*)-enantiomer was obtained in 98%

enantiomeric excess. Thus for monodentate phosphite ligands, the classical Halpern mechanism involving the anti lock-and-key concept is not valid. Asymmetric rhodium-catalyzed hydrogenations using this type of ligands obey the lock-and-key concept and therefore the anti-Halpern mechanism. This means that the major diastereomeric rhodium complex $[Rh(L)_2(olefin)]^+$ leads to the experimentally observed enantiomer.

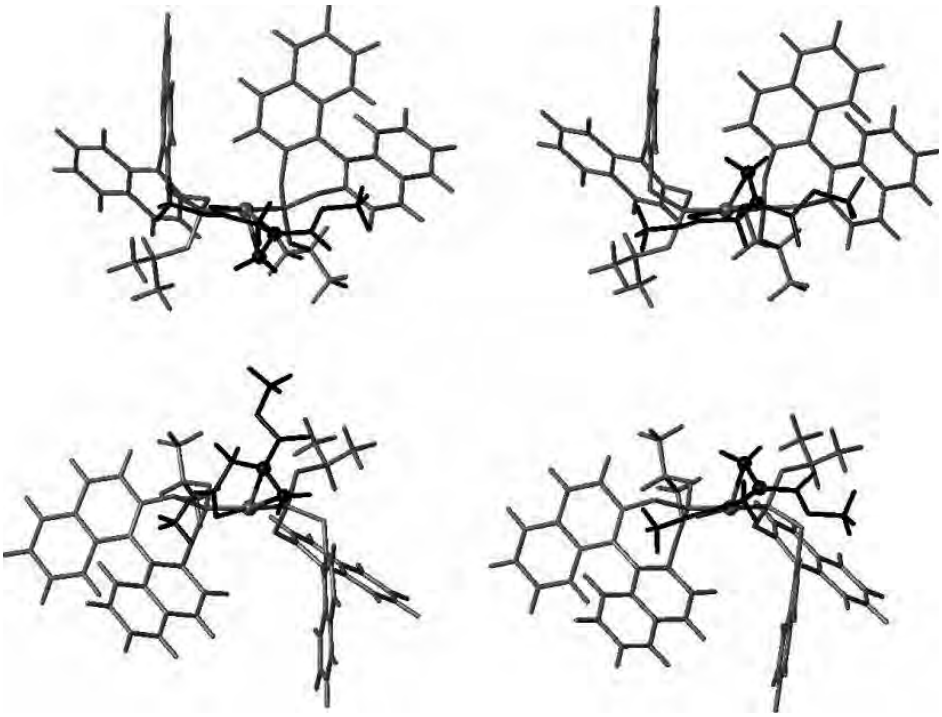

Figure 3.21 Coordination modes of olefin **3.143** in [Rh(**3.144**)$_2$**3.143**]$^+$. Left: conformers involving *Re*-face complexation, right: conformers involving *Si*-face complexation.[97]

Despite the fact that the mechanistical study of Reetz and Blackmond was of significant importance, the theoretical study is incomplete because the transition state at every stage of the catalytic cycle has not been considered. This, however, requires extensive DFT calculations, a process very hard to fulfill successfully for this type of complicated reactions …

To conclude, the (simplified) Anti-Halpern mechanism for the asymmetric Rh-catalyzed hydrogenation of itaconic acid dimethyl ester **3.143** with monodentate phosphite ligands is illustrated in Scheme 3.29. This mechanism is simplified because only two diastereomeric complexes instead of four $[Rh(L)_2(olefin)]^+$ cationic species are considered.

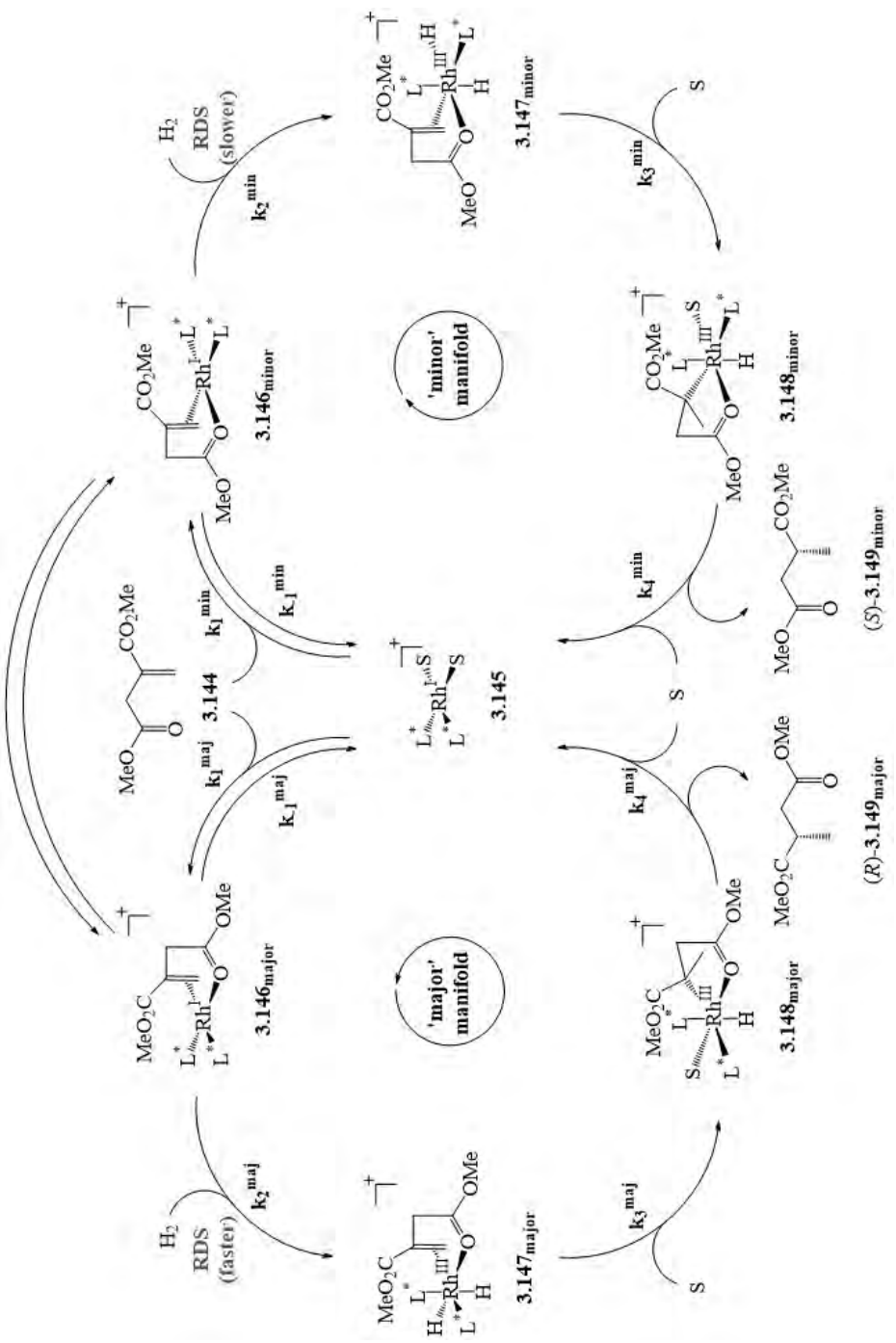

Scheme 3.29 Simplified anti-Halpern mechanism for the asymmetric Rh-catalyzed hydrogenation of dimethyl itaconate with monodentate phosphite ligands (mechanism simplified because only two instead of four $[Rh(L)_2(olefin)]^+$ complexes are considered)

In 2003 a new concept in the area of combinatorial enantioselective transition metal catalysis was described independently by the research groups of Reetz and Feringa. [98,99] The basic idea concerned the use of mixtures of chiral monodentate ligands to improve the enantioselectivity and/or catalyst activity. Indeed, for the hydrogenation of methyl-2-acetamido acrylate **3.133**, enhanced enantioselectivities were obtained when a proper combination of ligands was applied (Scheme 3.30). This particular ligand combination involves the use of a bulky phosphonite **3.151** and the least sterically demanding phosphite **3.150** (Reetz). Similar results were obtained by the research group of Feringa using mutual mixtures of monodentate phosphoramidite ligands in the hydrogenation of (*Z*)-β-(acylamino)acrylates.

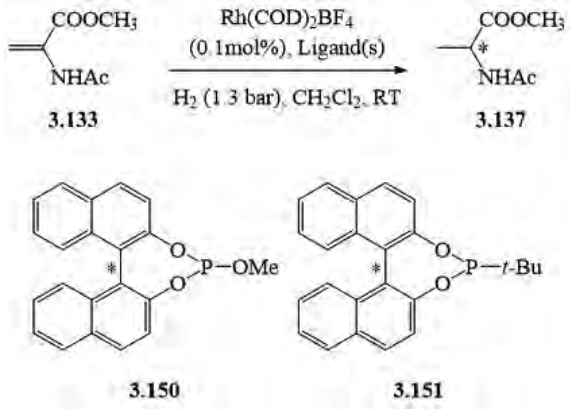

Ligand System	Conversion (%)	*ee* (%)
(*S*)-**3.150** (0.2 mol%)	100	76.6 (*R*)
(*R*)-**3.151** (0.2 mol%)	100	93.3 (*S*)
(*R*)-**3.150** (0.1 mol%) + (*R*)-**3.151** (0.1 mol%)	100	98.0 (*S*)

Scheme 3.30 Mixed ligand approach for the Rh-catalyzed hydrogenation of enamide **3.133** using monophosphite and monophosphonite ligands

Later on, both research groups expanded the idea of the mixed-ligand approach by using the combination of a chiral and an achiral monodentate ligand. In 2003, experiments by Reetz showed that the reversal of enantioselectivity was possible for the Rh-catalyzed asymmetric hydrogenation of methyl-2-acetamido acrylate **3.133**.[100] Therefore, he compared the results of a hydrogenation reaction performed with two equivalents of a chiral phosphite ligand and the combination of one equivalent (com-

pared to Rh) of the same chiral phosphite ligand and one equivalent of an achiral phosphine ligand. Unfortunately, the *ee*-values for the mixed ligand approach were rather low. In 2005, Feringa and co-workers showed that a catalyst complex based on the heterocombination of a chiral and an achiral monodentate ligand gave significantly higher enantioselectivities in the rhodium-catalyzed asymmetric hydrogenation of cinnamic acid derivatives, compared to homocomplexes.[101] This methodology has been applied on an industrial multi-ton scale production of a key intermediate for the renin inhibitor aliskiren **3.155** by DSM (Scheme 3.31). Cinnamic acid derivative **3.152** was hydrogenated with full conversion, high TON and TOF, and 90% enantiomeric excess using the mixed-ligand approach consisting of bulky phosporamidite **3.153** and ordinary PPh_3 as the chiral and achiral ligands respectively.[2,102]

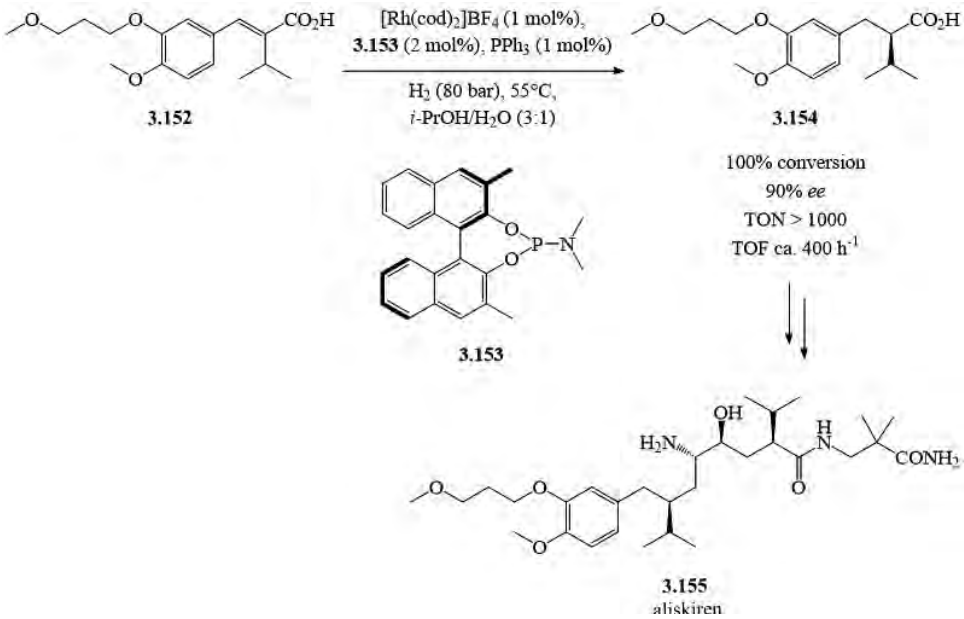

Scheme 3.31 Mixed ligand approach using phosphoramidite **3.153** and PPh_3 for the hydrogenation of **3.152**, applied in the industrial synthesis of aliskiren by DSM

3.8.2. Results of historical monodentate ligands and novel monodentate biferrocene-based P-amidite ligands

Two benchmark olefin substrates for the rhodium-catalyzed asymmetric hydrogenation reaction are methyl-2-acetamido acrylate **3.133** and methyl-(*Z*)-acetamidocinnamate **3.156** (Scheme 3.32). Among other olefins, these enamides were the initial substrates

used by pioneer researchers Pringle, Reetz and Feringa in the field of asymmetric hydrogenations using monodentate ligands.[10-12] Their obtained results in terms of conversion and enantioselectivities are shown in Table 3.4. In general, full conversions are reported for both substrates and all ligand subclasses. The enantioselectivities reported for Feringa's phosphoramidites are excellent (entries 10-12) and these ligands can compete with bidentate diphosphine ligands.[103] Although the *ee*-values obtained with monodentate phosphite ligands developed by Reetz are lower compared to Feringa's phosphoramidites, these results are still good (between 73 and 95% *ee*, entries 1-3). The results reported for Pringle's phosphonite ligands are variable. When methyl-2-acetamido acrylate **3.133** was used as substrate, full conversion was only observed for phenyl based ligand **3.07-b** (entry 5). The *ee*-values are variable between 73 and 92% (entries 4-6). For both the phosphite ligands developed by Reetz as well as Pringle's phosphonites its best result was obtained for the ligand with the bulky *t*-Bu substituent (95 and 92% *ee* respectively, entry 3 vs. entry 6). The enantioselectivities for the hydrogeenation of methyl-(*Z*)-α-acetamidocinnamate **3.156** are significantly lower for Pringle's phosphonite ligand series compared to Feringa's phosphoramidites (entries 7-9 vs. entries 11-12). With an enantiomeric excess of only 10%, the lowest *ee*-value was now obtained *t*-Bu substituted ligand **3.07-c**.

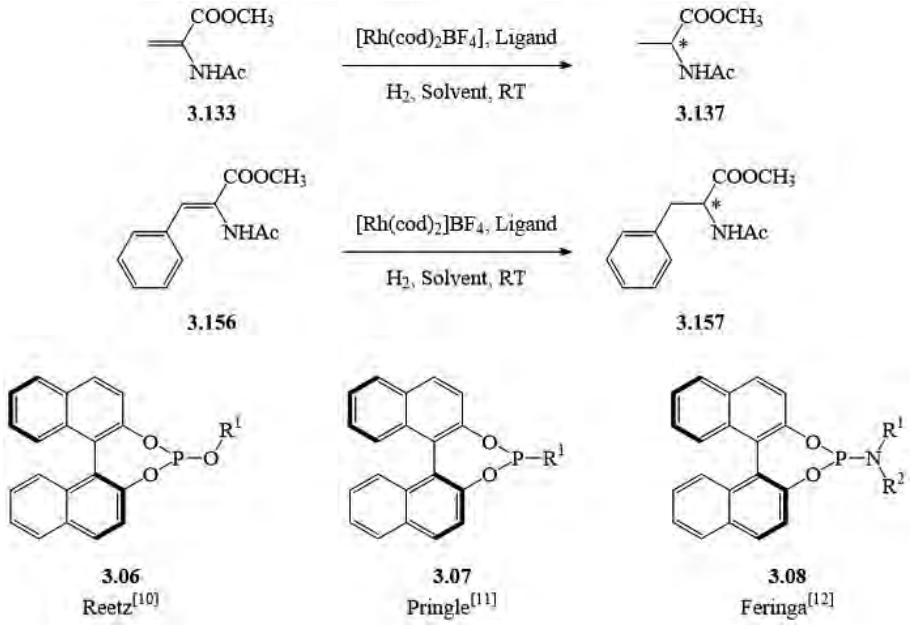

Scheme 3.32 Benchmark enamide substrates for rhodium-catalyzed asymmetric hydrogenation with monodentate ligands

Entry	Research Group	Substrate	Ligand, R^1, R^2	Conversion (%)	*ee* (%)
1	Reetz	**3.133**	**3.06-a**, Me	100	73
2	Reetz	**3.133**	**3.06-b**, Ph	100	81
3	Reetz	**3.133**	**3.06-c**, *t*-Bu	100	95
4	Pringle	**3.133**	**3.07-a**, Me	76	78
5	Pringle	**3.133**	**3.07-b**, Ph	100	73
6	Pringle	**3.133**	**3.07-c**, *t*-Bu	73	92
7	Pringle	**3.156**	**3.07-a**, Me	100	80
8	Pringle	**3.156**	**3.07-b**, Ph	100	63
9	Pringle	**3.156**	**3.07-c**, *t*-Bu	100	10
10	Feringa	**3.133**	**3.08-a**, Me, Me	100	99
11	Feringa	**3.156**	**3.08-b**, Me, Me	100	95
12	Feringa[16]	**3.156**	**3.08-c**, Et, Et	100	98

Table 3.4 Results of rhodium-catalyzed hydrogenation of enamide substrates **3.133** and **3.156** with monodentate phosphorus ligands

Other interesting monodentate phosphoramidite ligands that were applied in the rhodium-catalyzed asymmetric hydrogenation of enamides were developed by Matt and co-workers (Figure 3.22) and were already mentioned in § 3.7.4 (*vide supra*).[85] These binaphthyl-based dihydroazepine ligands **3.126**-**3.127** are analogues of the novel biferrocene-based dihydroazepine ligands **3.129-3.131** synthesized in this thesis. Therefore, the study of the influence of the biferrocene dihydroazepine residue is not limited to mutual comparison of these ligands, but can be expanded to the comparison of the biferrocene backbone against the binaphthyl backbone. Catalytic reactions as described by Matt and co-workers were performed at room temperature, using 1 mol% of $[Rh(cod)_2]BF_4$, 2.2 mol% of ligand, dichloromethane as solvent, and a hydrogen pressure of 5 bar. In general, full conversions were obtained after 1 h, as shown in Table 3.5. For ligands **3.126**, consisting of two axial chiral binaphthyl units, it can be seen that the chirality of the binol backbone determines the stereochemical outcome of the final product. Ligands **3.126-a** and **3.126-b** possessing the (*S*)-binol will provide (*R*)-**3.157**, whereas ligands containing (*R*)-binol are favoring the (*S*)-product. Further, excellent *ee*-values of 99% and 96% were obtained for ligands **3.126-a** and **3.126-d**. Interestingly, the counterparts of these ligands, **3.126-b** and **3.126-c** gave *ee*-values which are almost 20%

16 The results obtained with this ligand are not reported by the research group of Feringa but by Chan *et* al. [104]

lower. This means that there is respectively a matched and mismatched effect between those diastereomeric pairs. As a consequence, the chiral information provided by the dihydroazepine residue undoubtedly plays a significant role in the enantiodiscrimination process. Overall, best enantioselectivities were obtained for ligands having the opposite configuration of the binaphthyl units, while identical configuration resulted in a drop of selectivity. The influence of the dihydroazepine substructure was further investigated by the application of ligands **3.127** in the rhodium-catalyzed hydrogenation of enamide **3.156**. These ligands, solely characterized by an axial chiral dihyroazepine backbone, provided (equivalent) *ee*-values of 50 and 51%. As expected from the matched and mismatched situations for ligands **3.126**, axial chiral (*R*)-dihydroazepine containing ligand **3.127-a** resulted in the formation of (*R*)-**3.157** and an excess of (*S*)-**3.157** was observed for (*S*)-dihydroazepine containing ligand **3.127-b**.

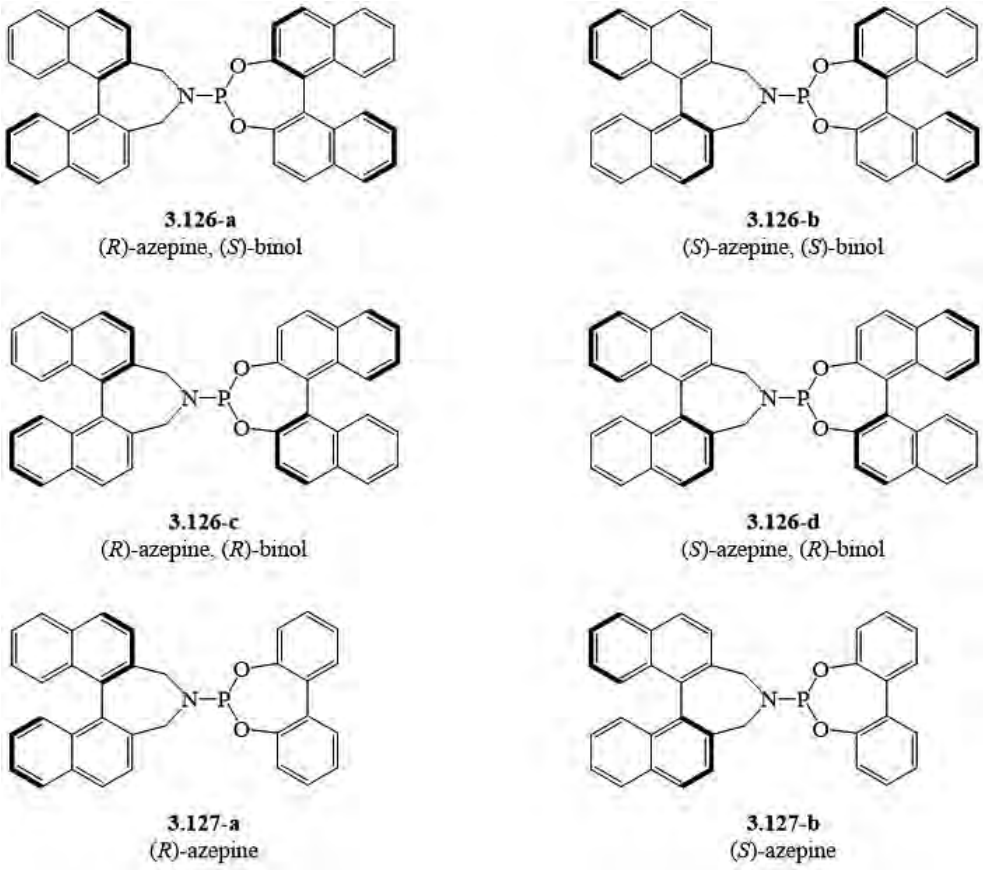

Figure 3.22 Monodentate binapthyl-based azepine phosphoramidite ligands developed by Matt *et al.*[85]

Substrate	Ligand	Time (h)	Conversion (%)	*ee* (%)
3.156	**3.126-a**	1	100	99 (*R*)
3.156	**3.126-b**	1	100	82 (*R*)
3.156	**3.126-c**	1	100	83 (*S*)
3.156	**3.126-d**	1	100	96 (*S*)
3.156	**3.127-a**	1	97	51 (*R*)
3.156	**3.127-b**	1	98	50 (*S*)

Table 3.5 Results for the Rh(I)-catalyzed asymetric hydrogenation of enamide **3.156** using monodentate dihydroazepine phosphoramidite ligands **3.126**-**3.127**

As already mentioned before, multiple parameters have an influence on the conversion and enantioselectivity in the rhodium-catalyzed hydrogenation. Extensive research on these parameters for phosphoramidite ligands was performed by the research group of Feringa and discussed in different publications.[12,81,105-107] The general features which emerge from these studies can be summarized as follows:

- $[Rh(cod)_2]BF_4$ is generally applied as the catalytic source
- Non-protic solvents are recommended and best results are obtained with dichloromethane and ethyl acetate
- Increasing the hydrogen pressure has little effect on the enantioselectivity but accelerates the reaction
- Lowering the reaction temperature is beneficial for the enantioselectivity but decreases the reaction rate
- Enantioselectivities, TON and TOF are generally high (up to 6000 and 1667 respectively); Successful hydrogenations of enamides with 0.015 mol% Rh are reported[105]

In addition to the synthesis of the novel biferrocene-based phosphoramidite ligands **3.129-3.131**, the subsequent goal of this research was the testing of these ligands in a benchmark test reaction. This means that two research questions have to be examined. First, can these ligands catalyze a reaction? Second, is there any chiral induction obtained for these ligands? A fully detailed, extensive study to optimize the enantioselectivities, TON or TOF is beyond the scope of this thesis. The Rh-catalyzed asymmetric hydrogenation of protected α- and β-dehydroaminoacids is the benchmark testreaction which is most often applied for novel mondontate ligands. These substrates allow to efficiently synthesize aminoacid precursors, which in turn allow to obtain natural,

as well as unnatural aminoacids. Because only small amounts of ligands **3.129**-**3.131** were obtained, only one substrate could be tested. Enamide **3.156** functions a a precursor for the synthesis of phenylalanine and is one of the most used substrates within this class of test reactions. Moreover, at the *Laboratory of Organic and Bioorganic Synthesis* the Rh-catalyzed hydrogenation of enamide **3.156** was already selected as a test reaction by Vervecken to evaluate his bidentate diphosphane ligand.[110] Consequently, experimental details including analytical chromatographic separation methods in order to determine conversion and enantiomeric excess are already well-known in our research group. The applied standard conditions for the test reactions performed in this research project involve 1 atmosphere of hydrogen pressure, room temperature as reaction temperature, dichloromethane as solvent and a catalyst loading of 5 mol% Rhodium as $[Rh(cod)_2]BF_4$ in combination with 10 mol% of ligand. An overview of the results is shown in Table 3.6. Excellent conversions of 100% and 95% were obtained for ligands **3.129** and **3.130**. For ligand **3.131** it turned out that the conversion was lower since a value of 84% was obtained. However, it has to be said that these experiments were only performed once and therefore, this can be explained by experimental errors. A rather low *ee*-value of 26.2% was obtained for ligand **3.129** which possesses only the chirality of the biferrocene moiety. Just like the (*S*)-azepine based ligand **3.127-b**, ligand **3.129** characterized by a (S_p,S_p)-biferrocene backbone is responsible for the major formation of the (*S*)-enantiomer of **3.157** (*cf.* Table 3.5). Unfortunately, biferrocene-based ligand **3.129** was not able to surpass the axial chiral analogous ligand since an *ee*-value of 50% was obtained with ligand **3.127-b**. The experiment performed with (*R*)-MonoPhos seemed to be superior since full conversion in combination with an *ee*-value of 95.4%, favoring the (*S*)-enantiomer, was obtained. It is important to note that for this ligand the axially (*R*)-chiral backbone is responsible for the major production of the (*S*)-enantiomer.

Based on the results of ligand **3.129** and (*R*)-MonoPhos, ligand **3.130** characterized by the (S_p,S_p)-biferrocene backbone in combination with the axial chiral (*R*)-binol should allow to obtain the highest *ee*-value for the biferrocene ligand series. This was confirmed experimentally because an enantiomeric excess of 67.6% was obtained. Again, this ligand provided a lower *ee*-value compared to the double axial chiral azepine-based ligand **3.126-d** reported by Matt and coworkers.[85] (The latter one provided a *ee*-value of 96% favoring the (*S*)-enantiomer (*cf.* Table 3.5)). Ligand **3.131** characterized by the (S_p,S_p)-biferrocene backbone in combination with axial chiral (*S*)-binol backbone pro-

vided an enantiomeric excess of only 4.0% favoring the (*R*)-enantiomer. Based on the previous experiments with ligands **3.129**, **3.130** and MonoPhos it was expected that this ligand represents the mismatched combination with formation of the (*R*)-enantiomer of **3.157** as the major compound. Here as well, biferrocene-based ligand **3.131** gave a lower enantiomeric excess compared to binaphthyl-based azepine ligand **3.126-b**, of which an *ee*-value of 82% for the (*R*)-enantiomer was reported by Matt *et al.*

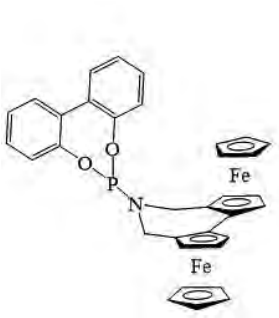

3.129

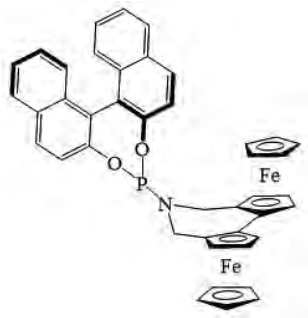

3.130

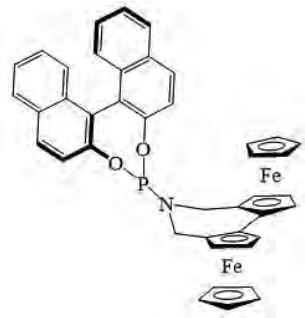

3.131

Substrate	Ligand	Time (h)	Conversion (%)	*ee* (%)
3.156	**3.129**	24	100	26.2 (*S*)
3.156	**3.130**	24	95	67.6 (*S*)
3.156	**3.131**	24	84	4.0 (*R*)
3.156	None (blanco)	24	0	-
3.156	(*rac*)-BINAP	24	80	0
3.156	(*R*)-MonoPhos	24	100	95.4 (*S*)

Table 3.6 Results for the Rh(I)-catalyzed asymmetric hydrogenation of enamide **3.156** using novel biferrocene-based phosphoramidites ligands **3.129**-**3.131**

Based on the experiments performed in this thesis with and the experiments performed by Matt and coworkers, it can be concluded that the biferrocene backbone is a less efficient chiral enantiodiscriminating backbone compared to the binaphthyl azepine backbone for the rhodium-catalyzed hydrogenation of enamide substrate **3.156**.

3.9. Experimental

3.9.1. General Considerations

All reactions were carried out under argon atmosphere using a balloon in dry solvents under anhydrous conditions, unless otherwise noted. All reagents were purchased and used without further purification unless otherwise stated. CH_2Cl_2, Et_3N, DIPEA and *n*-hexane were dried via distillation over CaH_2. $CHCl_3$ and 1,2-dichloroethane were dried via distillation over P_2O_5. Toluene, THF and Et_2O were dried over sodium with benzophenone indicator. All other dry solvents (DMF, DMSO, CH_3CN, …) were purchased as anhydrous solvents. When needed, solvents were deoxygenated prior to use by three freeze-pump-thaw cycles on an argon Schlenk line. Microwave irradiations were performed in a CEM Discover LabMate microwave oven. Analytical TLC was performed using Macherey-Nagel SIL G-25 UV254 (0.25 mm) plates. Visualization was performed using UV (254 nm) and/or staining with potassium permanganate, cerium ammonium molybdate or ninhydrin. Flash chromatography was carried out on Rocc silica gel (0.040-0.063 mm) and solvents were HPLC grade quality.

^{1}H, ^{13}C and ^{31}P-NMR spectra were recorded on a Bruker Avance 300 or a Bruker Avance 400 or a Bruker AM 500 spectrometer as indicated, with chemical shifts reported in ppm relative to TMS, using the residual solvent signal as a standard for ^{1}H and ^{13}C, and relative to 85% aqueous phosphoric acid for ^{31}P NMR.

IR-spectra were recorded on a Perkin-Elmer-1000 FT-IR spectrometer with Pike Miracle Horizontal Attenuated Total Reflectance (HATR) module.

Optical rotations were recorded on a Perkin-Elmer polarimeter 241 at a wavelength of 589 nm (sodium D line) and a temperature of 20°C.

Melting points were measured with a Kofler melting point apparatus.

ESI-MS was performed on an Agilent 1100 series with a single quadrupole MS detector G1946C (type VL) equipped with an API-ESI source. High Resolution Mass Spectrometry (HRMS) was performed on an Agilent 1100 series connected to a 6220A TOF-MS detector equipped with an APCI-ESI multimode source or a Kratos MS50TC mass spectrometer (EI). For all MS-analysis the standard solvent was a 50:50 mixture of MeOH: 5 mM aqueous NH_4OAc and a sample volume of 5 µL was injected.

LC-MS analyses were performed on an Agilent 1100 series HPLC connected to a UV-DAD detector and a single quadrupole MS detector G1946C (type VL) equipped with an API-ESI source. Detection of positive and negative ions was accomplished separately. Standard columns used for LC-MS were Phenomenex Kinetex C18 (150 x 4.6 mm, 5 µm) and Phenomenex Luna C18(2) (250 x 4.6 mm, 5 µm). All measurements were performed at 35°C and a flow rate of 1 mL/min. A sample volume of 15 µL was injected on a Phenomenex Kinetex C18 column and 25 µL on Phenomenex Luna C18 column. Milli-Q water and HPLC quality grade CH_3CN were used. Different solvent gradient systems were used which will be explained in more detail below:

- **Method 1**
  Phenomenex Luna C18 column; 5 mM aqueous NH_4OAc/CH_3CN solvent system
- **Method 2**
  Phenomenex Luna C18 column; 5 mM aqueous NH_4OAc/CH_3CN solvent system

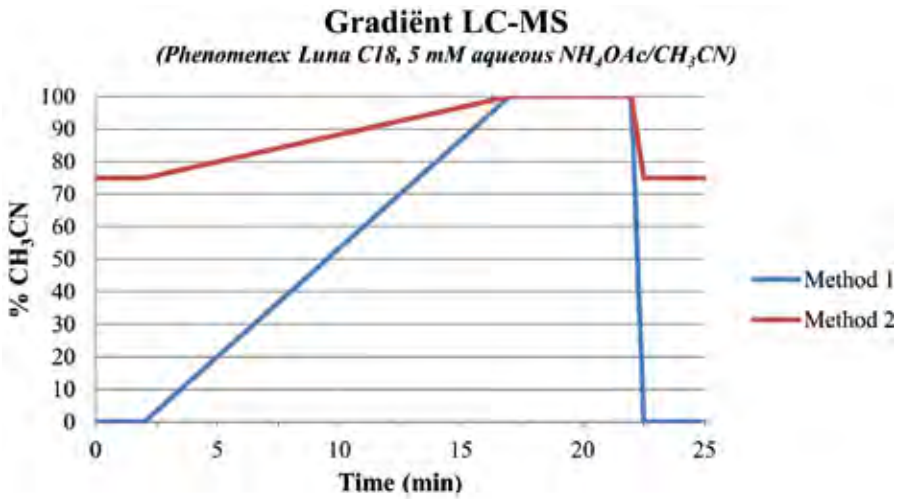

- **Method 3**
  Phenomenex Kinetex C18 column; 5 mM aqueous NH_4OAc/CH_3CN solvent system
- **Method 4**
  Phenomenex Kinetex C18 column; 5 mM aqueous NH_4OAc/CH_3CN solvent system
- **Method 5**
  Phenomenex Kinetex C18 column; 5 mM aqueous NH_4OAc/CH_3CN solvent system

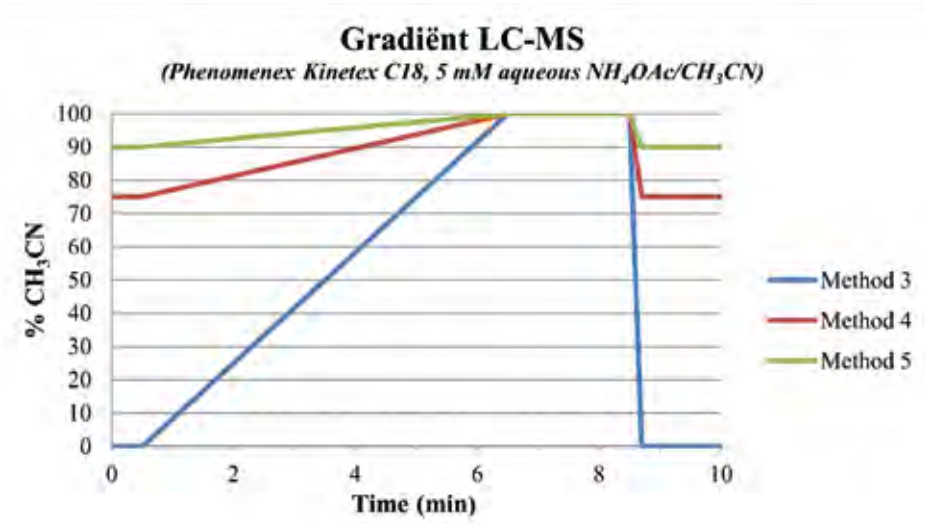

Analytical chiral separations were performed on an Agilent 1100 series HPLC system connected to a UV-DAD detector. HPLC quality grade solvents were used for all measurements.

X-ray intensity data were collected on an Agilent Supernova Dual Source (Cu at zero) diffractometer equipped with an Atlas CCD detector using Cu Kα radiation (λ = 1.54178 Å) and ω scans.

All experiments were performed according the general laboratory safety rules and personal protective equipment such as goggles, lab coat and gloves were always worn in the laboratory. All reactions, work-ups and purifications were performed in a well-ventilated fume hood. A detailed overview for the identification of the hazards of the most dangerous chemicals that were used in this chapter is given in Appendix I.

3.9.2. Synthesis of dimethoxyferrocenyl methane **3.98**

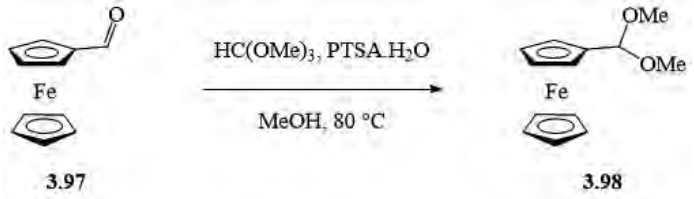

3.97 **3.98**

An oven-dried, 500 mL two-neck round bottom flask was charged with a magnetic stirring bar, a reflux condenser, ferrocenecarboxaldehyde **3.97** (25 g, 116.8 mmol) and PTSA.H_2O (1.24 g, 6.5 mmol, 5 mol%). Trimethyl orthoformate (150 mL) and anhydrous methanol (100 mL) were added. The dark solution was stirred overnight at 80°C. The reaction mixture was allowed to cool down to room temperature. Anhydrous K_2CO_3 (2.5 g, 18.1 mmol) was added and stirring was continued for 10 min. The suspension was diluted with Et_2O and filtered over Celite. The filter cake was washed with Et_2O until the filtrate was colorless. Solvents were removed under reduced pressure and crude acetal **3.98** was obtained with a quantitative yield, as a dark oil.

Formula: $C_{13}H_{16}FeO_2$ (260.11 g/mol).
R_f (*n*-hexane/EtOAc: 2/1): 0.58.
^{1}**H-NMR:** (300 MHz, $CDCl_3$): δ = 3.30 (s, 6H), 4.15-4.19 (m, 2H), 4.16 (s, 5H), 4.31 (app. t, *J* = 1.79 Hz, 2H), 5.41 (s, 1H) ppm.
^{13}**C-NMR:** (75.4 MHz, $CDCl_3$): δ = 52.2 (CH_3), 67.2 (CH), 67.8 (CH), 68.8 (CH), 84.9 (C), 102.3 (CH) ppm.
IR (HATR): ν_{max} = 3929, 3091, 2923, 2835, 2766, 2255, 1986, 1677, 1665, 1489, 1452, 1409, 1395, 1368, 1352, 1329, 1244, 1200, 1104, 1030, 1001, 927, 880, 824, 743 cm^{-1}.
ESI-MS m/z (rel. intensity %): 260.0 (17, $[M+H]^+$), 230.0 (15), 227.0 (6), 229.0 (100).
Retention time HPLC: 6.74 min. (method 2)

3.9.3. Synthesis of (2*S*,4*S*)-4-(hydroxymethyl)-2-ferrocenyl-1,3-dioxane **3.99**

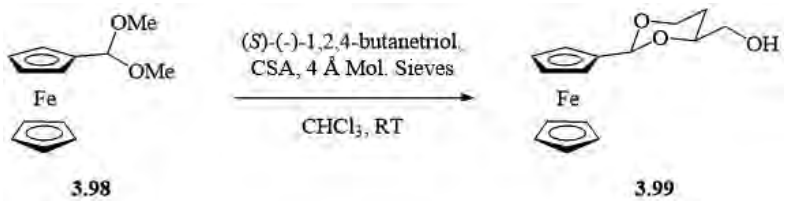

3.98 **3.99**

An oven-dried, 500 mL round-bottom flask was charged with (*S*)-(-)-1,2,4-butanetriol (14.1 g, 133.8 mmol). The triol was dried via dissolving it in anhydrous toluene, followed

by azeotropic distillation on a rotary evaporator (three times) and dried overnight under high vacuum. The triol was dissolved in $CHCl_3$ (150 mL), activated 4 Å molcular sieves (70 g) and racemic camphorsulfonic acid (1.23 g, 5 mmol, 5 mol%) were added. Crude acetal **3.98** was dissolved in $CHCl_3$ (50 mL) and added to the mixture using a cannula. The reaction mixture was stirred overnight at room temperature. Anhydrous K_2CO_3 (2.5 g, 18.1 mmol) was added and stirring was continued for 10 min. The suspension was diluted with CH_2Cl_2 and filtered over Celite. The filter cake was washed until the filtrate was colorless. Solvents were removed under reduced pressure and the resulting residue was filtered over silica gel (*n*-hexane/EtOAc: 50/50) to remove ferrocenecarboxaldehyde and polar impurities. Purification of the desired dioxane from the dioxolane was accomplished via recrystallization: the obtained solid was dissolved in hot toluene (100 mL) and then placed in a freezer (-20°C) for 2-3 days. Yellow crystals were formed, filtered off, washed with a minimal amount of cold toluene and *n*-hexane and dried under high vacuum. **3.99** was obtained as yellow crystals with a yield of 67.8% over two steps, calculated from ferrocenecarboxaldehyde **3.97**.

Formula: $C_{15}H_{18}FeO_3$ (302.15 g/mol).

R_f (*n*-hexane/EtOAc: 1/1): 0.25.

^{1}**H-NMR:** (300 MHz, $CDCl_3$): δ = 1.41 (app dtd, *J* = 13.2 Hz, *J* = 2.6 Hz (x2), *J* = 1.5 Hz, 1H), 1.86 (dddd, *J* = 13.2 Hz, *J* = 12.4 Hz, *J* = 11.7 Hz, *J* = 5.3 Hz, 1H), 2.04 (dd, *J* = 7.7 Hz, *J* = 5.3 Hz, 1H), 3.63 (ddd, *J* = 11.7 Hz, *J* = 6.5 Hz, *J* = 5.3 Hz, 1H), 3.70 (ddd, *J* = 11.7 Hz, *J* = 7.7 Hz, *J* = 3.4 Hz, 1H), 3.92 (ddd, *J* = 12.4 Hz, *J* = 11.5 Hz, *J* = 2.6 Hz, 1H), 3.96 (dddd, *J* = 11.7 Hz, *J* = 6.5 Hz, *J* = 3.4 Hz, *J* = 2.6 Hz, 1H), 4.15 (app t, *J* = 1.9 Hz, 2H), 4.18 (s, 5H), 4.25 (ddd, *J* = 11.5 Hz, *J* = 5.3 Hz, *J* = 1.5 Hz, 1H), 4.33-4.37 (m, 2H), 5.42 (s, 1H) ppm.

^{13}**C-NMR:** (75.4 MHz, $CDCl_3$): δ = 26.9 (CH_2), 65.8 (CH_2), 66.5 (CH_2), 66.5 (CH x2, Fc), 66.6 (CH), 68.0 (CH x2, Fc), 68.9 (CH x5, Fc), 77.2 (CH), 85.8 (C), 100.2 (CH) ppm.

IR (HATR): ν_{max} = 3459, 3415, 3331, 3231, 3197, 3095, 2965, 2939, 2919, 2856, 2717, 2667, 2619, 2581, 2525, 2485, 2444, 2351, 2308, 2258, 2212, 1121, 2035, 1992, 1950, 1899, 1859, 1813, 1758, 1731, 1682, 1622, 1599, 1357, 1033, 903, 792, 699 cm^{-1}.

ESI-MS m/z (rel. intensity %): 304.0 (18), 303.0 (100, $[M+H]^+$]), 302.0 (34), 301.0 (5), 215.0 (29), 117.1 (7)

HRMS (ESI): calculated for $C_{15}H_{19}FeO_3$ $[M+H]^+$: 303.0678; found: 303.06085

Retention time HPLC: 15.10 min. (method 1); 3.90 min. (method 2); 5.48 min. (method 3) (KP, 5.480 min); 1.23 min. (method 4)

Chiral HPLC: Chiralcel OD-H column, solvent: *n*-hexane/EtOH (95:5), flow rate = 1 mL/

min, t = 30 min., T = 35°C, retention times: 12.09 min. for (*R,R*)-**3.99** and 13.85 min. (*S,S*)-**3.99**

Optical rotation: $[\alpha]_D^{20}$ = +0.84 (c 0.96, $CHCl_3$)

Melting point: 59°C

3.9.4. Synthesis of (2*S*,4*S*)-4-(methoxymethyl)-2-ferrocenyl-1,3-dioxane **3.100**

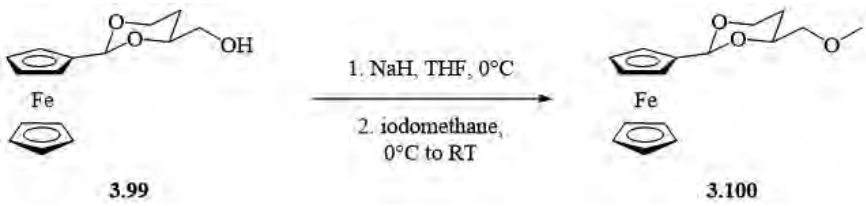

An oven-dried, 500 mL two-neck round-bottom flask was charged with a magnetic stirring bar, a dropping funnel,. NaH (3.33 g, 137.7 mmol, 1.5 eq) and anhydrous THF (30 mL). The reaction flask was cooled to 0°C using an ice-water bath and a solution of dioxane **3.99** (27.7 g, 91.8 mmol) in THF (300 mL) was added dropwise within 2 h using the dropping funnel. Neat iodomethane (8.57 mL, 137.7 mmol, 1.5 eq) was injected to the reaction mixture which was allowed to warm up to room temperature and stirred overnight at room temperature. Excess NaH and iodomethane were destroyed at 0°C by slow addition of methanol until the formation of hydrogen gas stopped. The reaction was quenched with water and the organic solvents were removed under reduced pressure. The residue was taken up in Et_2O (350 mL) and washed with water (350 mL) and brine (350 mL). The organic phase was dried over anhydrous $MgSO_4$ and filtered. The organic solvents were removed under reduced pressure and the resulting residue was purified by flash chromatography (*n*-hexane/EtOAc: 95/5) affording acetal **3.100**, with a quantitative yield, as a brown oil which became an orange solid upon standing in a freezer (-20°C).

Formula: $C_{16}H_{20}FeO_3$ (316.17 g/mol).

$\mathbf{R}_f$ (*n*-hexane/EtOAc: 1/1): 0.56.

^{1}**H-NMR:** (300 MHz, $CDCl_3$): δ = 1.49 (app dtd, *J* = 13.2 Hz, *J* = 2.6 Hz (2x), *J* = 1.5 Hz), 1.78 (dddd, *J* = 13.2 Hz, *J* = 12.4 Hz, *J* = 11.5 Hz, *J* = 5.2 Hz, 1H), 3.43 (dd, *J* = 10.4 Hz, *J* = 4.6 Hz, 1H), 3.44 (s, 3H), 3.54 (dd, *J* = 10.4 Hz, *J* = 6.1 Hz, 1H), 3.91 (ddd, *J* = 12.4 Hz, *J* = 11.5 Hz, *J* = 2.6 Hz, 1H), 4.00 (dddd, *J* = 11.5 Hz, *J* = 6.1 Hz, *J* = 4.6 Hz, *J* = 2.6 Hz, 1H), 4.10-4.13

(m, 2H), 4.19 (s, 5H), 4.24 (ddd, *J* = 11.5 Hz, *J* = 5.2 Hz, *J* = 1.5 Hz, 1H), 4.33-4.58 (m, 2H), 5.37 (s, 1H) ppm.

^{13}C-NMR: (75.4 MHz, $CDCl_3$): δ = 28.1 (CH_2), 59.5 (CH_3), 66.7 (CH_2), 66.7 (CH, Fc), 66.8 (CH, Fc), 66.9 (CH, Fc), 67.9 (CH, Fc), 69.0 (CH x5, Fc), 75.7 (CH_2), 76.1 (CH), 86.1 (C), 100.1 (CH) ppm.

IR (HATR): ν_{max} = 3091, 3051, 2924, 2850, 2808, 2763, 2717, 1370, 1322, 1294, 1239, 1198, 1145, 1104, 1070, 1039, 1016, 1001, 896, 840, 810, 749, 701 cm^{-1}.

ESI-MS m/z (rel. intensity %): 317.1 (100) $[M+H]^+$, 315.1 (6), 215.0 (10), 103.1 (46)

HRMS (ESI): calculated for $C_{16}H_{21}FeO_3$ $[M+H]^+$: 317.0835; found: 317.0845

Retention time HPLC: 17.89 min. (method 1), 6.38 min. (method 3); 1.67 min. (method 4) **Chiral HPLC:** Chiralcel OD-H column, solvent *n*-hexane/EtOH (98:2), flow rate = 1 mL/min, t = 30 min., T = 35°C, retention times: 7.21 min. for (*R,R*)-**3.100** and 9.53 min. for (*S,S*)-**3.100**

Optical rotation: $[\alpha]_D^{20}$ = -31.3 (c 1.0, $CHCl_3$); literature: -32.5 (c 1.14, $CHCl_3$)[57]

3.9.5. Synthesis of (S_p)-α-Iodoferrocenecarboxaldehyde **3.96**

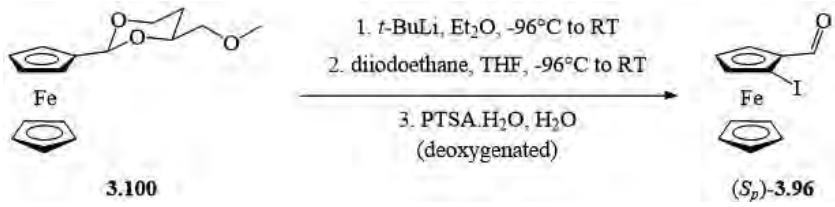

An oven-dried, 250 mL two-neck round-bottom flask was charged with a magnetic stirring bar and **3.100 (**4.036 g, 12.6 mmol). Freshly distilled Et_2O (70 mL) was added and the solution was cooled to -96°C. Afterwards *t*-BuLi (1.7 M in hexanes, 8.18 mL 13.9 mmol, 1.1 eq) was added dropwise within 30 min. The reaction mixture was stirred for an additional 15 min. at -96°C and allowed to warm up to room temperature and stirred for 1 h. The reaction was cooled to -96°C and a solution of diiodoethane[17] (4.279 g, 15.2 mmol, 1.1 eq) in THF (19 mL) was cautiously added. After 5 min., the reaction was allowed to warm up to room temperature. The reaction flask was wrapped in aluminum foil and the reaction mixture was stirred for 20 h at room temperature. A deoxygenated solution of PTSA.H_2O (2.914 g, 15.2 mmol, 1.2 eq) in water (20 mL) was added to the reaction

17 Diiodoethane was purified before use via the following procedure: 5.00 g of diiodoethane was dissolved in Et_2O (100 mL), washed 5 times with a saturated solution of $Na_2S_2O_3$ (25 mL) and one time with water (25 mL). The organic phase was dried over $MgSO_4$ and filtered. The solvents were removed under reduced pressure with the flask carefully covered in aluminum foil. Diiodoethane was obtained as white solid.

mixture and stirred for 1.5 h at room temperature. The reaction was quenched with water (100 mL) and the aqueous phase was extracted 3 times with Et_2O (75 mL). The combined organic phases were washed with a saturated solution of $Na_2S_2O_3$-solution (50 mL), water (50 mL) and brine (50 mL). The organic phase was dried over anhydrous $MgSO_4$ and filtered. The solvents were removed under reduced pressure and the resulting residue was purified by flash chromatography (toluene/Et_2O: 99/1) affording (S_p)-**3.96**, with a yield of 84.7 % as a dark red-brown solid (after removal of solvents under reduced pressure via an azeotrope with dichloromethane and pentane respectively).

Formula: $C_{11}H_9FeIO$ (339.94 g/mol).
R_f (toluene/diethyl ether: 95/5): 0.38
^{1}**H-NMR:** (300 MHz, $CDCl_3$): δ = 4.27 (s, 5H), 4.69 (app t, *J* = 2.3 Hz, 1H), 4.82 (dd, *J* = 2.3 Hz, 1.4 Hz, 1H), 4.88-4.90 (br m, 1H), 10.03 (s, 1H) ppm.
^{13}**C-NMR:** (75.4 MHz, $CDCl_3$): δ = 41.9 (C), 67.6 (CH), 72.6 (CH x5), 73.7 (CH), 76.6 (C), 79.6 (CH), 194.4 (CH) ppm.
IR (HATR): ν_{max} = 3330, 3085, 2853, 2792, 2775, 1726, 1670, 1430, 1408, 1363, 1348, 1246, 1219, 1105, 1066, 1039, 999, 976, 859, 826, 745, 612 cm^{-1}.
ESI-MS m/z (rel. intensity %): 340.9 (100) $[M+H]^+$, 338.9 (6), 304.2 (24), 283.2 (16), 282.3 (78), 280.2 (9), 247.1 (6), 215.0 (15), 214.0 (92)
HRMS (ESI): calculated for $C_{11}H_{10}FeIO$ $[M+H]^+$: 340.9120; found: 340.9115
Retention time HPLC: 17.31 min. (method 1), 6.28 min. (method 3).
Chiral HPLC: Chiralpak AS-H column, solvent: *n*-hexane/EtOH (90:10), flow rate = 1 mL/min, t = 30 min., T = 35°C, retention times: 6.62 min. for (R_p)-**3.96** and 8.16 min. for (S_p)-**3.96**.
Optical rotation: $[\alpha]_D^{20}$ = +555 (c 0.4, $CHCl_3$, 92% *ee*); literature: +558 (c 0.35, $CHCl_3$, 98% *ee*)[57]
Melting point: 82°C

3.9.6. Synthesis of 1-[(S_p)-α-Iodoferrocenyl]ethanol **3.95**

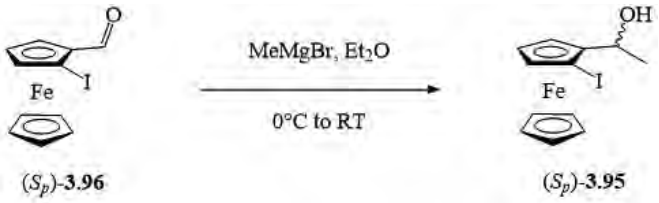

(S_p)-**3.96** (S_p)-**3.95**

An oven-dried 50 mL round-bottom flask was charged with a magnetic stirring bar and (S_p)-**3.96** (264 mg, 0.776 mmol). Freshly distilled Et_2O (10 mL) was added and the reac-

tion mixture was cooled to 0°C using an ice-water bath. MeMgCl (3.0 M in Et_2O, 285 µL, 0.854 mmol, 1.1 eq) was slowly added. The reaction mixture was stirred for 15 min. at 0°C, allowed to warm up to room temperature and stirred for an additional 2 h at room temperature. The reaction was carefully quenched with a saturated solution of NH_4Cl-solution (30 mL) and extracted 3 times with Et_2O (30 mL). The combined organic phases were dried over anhydrous $MgSO_4$ and filtered. Et_2O was removed under reduced pressure and the resulting residue was purified by flash chromatography (cyclohexane/EtOAc: 85/15) affording a diastereomeric mixture of (S_p)-**3.95**, with a yield of 87.6% a yellow-orange solid.

Formula: $C_{12}H_{13}FeIO$ (355.98 g/mol).
R_f (toluene/diethyl ether: 95/5)**:** 0.26
Retention time HPLC: 6.08 min. and 6.51 min. (method 3).
ESI-MS m/z (rel. intensity %): 356.9 (12) $[M+H]^+$, 355.9 (80), 339.8 (15), 338.9 (100).

Due to the fact that a mixture of diastereomers was obtained, full characterization was not accomplished.

3.9.7. Synthesis of (S_p)-α-Iodo-acetylferrocene **3.94**

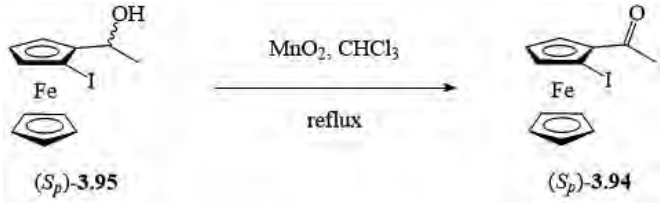

An oven-dried, 50 mL round-bottom flask was charged with a magnetic stirring bar, a diastereomeric mixture of (*R,S*$_p$)-**3.95** and (*S,S*$_p$)-**3.95** (276 mg, 0.776 mmol) and MnO_2 (2.249 g, 23.28 mmol, 30 eq). $CHCl_3$ (15 mL) was added and the suspension was stirred overnight at 65°C. The reaction mixture was allowed to cool to room temperature, diluted with CH_2Cl_2 and filtered over Celite. The solvents were removed under reduced pressure and the resulting residue was purified by flash chromatography (gradient: cyclohexane/Et_2O: 9/1 to 6/4) affording (S_p)-**3.94**, with a yield of 82.3%, as a red solid.

Formula: $C_{12}H_{11}FeIO$ (353.96 g/mol).
R_f (*c*-hexane/acetone: 8/2)**:** 0.48
^{1}**H-NMR:** (400 MHz, $CDCl_3$): δ = 2.53 (s, 3H), 4.24 (s, 5H), 4.53 (app t, *J* = 2.7 Hz, 1H), 4.78 (dd, *J* = 2.7 Hz, *J* = 1.4 Hz, 1H), 4.79 (dd, *J* = 2.7 Hz, *J* = 1.4 Hz, 1H), ppm.

^{13}C-NMR: (125 MHz, $CDCl_3$): δ = 28.8 (CH_3), 38.2 (C), 70.2 (CH), 72.8 (CH x5), 73.0 (CH), 77.3 (C), 80.9 (CH), 200.9 (C) ppm.

IR (HATR): ν_{max} = 3926, 3328, 3093, 2921, 2851, 1668, 1426, 1411, 1372, 1351, 1318, 1262, 1248, 1130, 1106, 1038, 1001, 974, 904, 824, 623 cm^{-1}.

ESI-MS m/z (rel. intensity %): 354.9 (100) $[M+H]^+$, 355.9 (17), 100.2 (15), 228.1 (8), 352.9 (8)

HRMS (ESI): calculated. For $C_{12}H_{12}FeIO$ $[M+H]^+$: 354.9277; found: 354.9279

Retention time HPLC: 6.24 min. (method 3)

Optical rotation: $[\alpha]_D^{20}$ = -137° (c 0.33, $CHCl_3$)

3.9.8. Synthesis of (S_p,S_p)-[1,1'-biferrocenyl]-2,2'-dicarboxaldehyde **3.107**

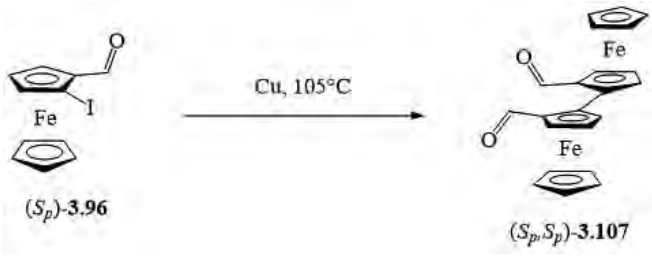

(S_p)-**3.96** (S_p,S_p)-**3.107**

An oven-dried, 50 mL round-bottom flask was charged with (S_p)-**3.96** (2.610 g, 7.68 mmol). Metallic copper (1.950 g, 30.71 mmol, 4 eq) was carefully added in such way that all of the starting material was covered with copper. A heavy, egg-shaped stirring bar was carefully added and the reaction flask was wrapped in aluminum foil. The reaction was stirred overnight at 105°C. The crude reaction mixture was taken up in CH_2Cl_2 and filtered over Celite, while the filtrate was collected in a round-bottom flask which was wrapped in aluminum foil. The solvent was removed under reduced pressure and the resulting residue was purified by flash chromatography[18] (gradient *n*-hexane/EtOAC: 8/2 to 6/4) affording (S_p,S_p)-**3.107**, with a yield of 66.8%, as a red solid.

Formula: $C_{24}H_{18}Fe_2O_2$ (426.07 g/mol).

R_f ((S_p,S_p)-**3.101**) (*n*-hexane/EtOAc: 7/3): 0.25

R_f ((R_p,S_p)-**3.101**, *meso*-form) (*n*-hexane/EtOAc 7/3): 0.40

R_f (**3.92**) (*n*-hexane/EtOAc 7/3): 0.69

^{1}H-NMR: (500 MHz, $CDCl_3$): δ = 4.31 (s, 10H), 4.74 (dd, *J* = 2.8 Hz, *J* = 2.4 Hz, 2H), 4.94 (dd, *J* = 2.4 Hz, *J* = 1.6 Hz, 2H), 4.95 (dd, *J* = 2.8 Hz, *J* = 1.6 Hz, 2H), 9.94 (s, 2H) ppm.

18 Because **3.107** is light sensitive, the column was wrapped in aluminum foil as well. First a mixed fraction of ferrocenecarboxaldehyde **3.97** and α-iodoferrocenecarboxaldehyde (S_p)-**3.96** was collected. The polarity of the eluent system was raised to *n*-hexane/EtOAC: 7/3 and the *meso*-form (R_p,S_p)-**3.110** was collected. The polarity of the eluent system was raised to *n*-hexane/EtOAC: 6/4 and (S_p,S_p)-[1,1'-biferrocenyl]-2,2'-dicarboxaldehyde (S_p,S_p)-**3.107** was collected in a round bottom flask which was wrapped in aluminum foil.

^{13}C-NMR: (125 MHz, $CDCl_3$): δ = 68.8 (CH x2), 71.0 (CH x10), 71.9 (CH x2), 76.6 (CH x2), 78.6 (C x2), 85.3 (C x2), 192.2 (CH x2) ppm.

IR (HATR): ν_{max} = 3921, 3561, 3315, 3101, 3009, 2941, 2840, 2778, 2764, 1661, 1652, 1426, 1409, 1395, 1289, 1208, 1106, 998, 990, 825, 774, 733, 679 cm^{-1}.

ESI-MS m/z (rel. intensity %): 426.9 (100) $[M+H]^+$, 428.0 (23), 425.0 (10)

HRMS (ESI): calculated for $C_{22}H_{19}Fe_2O_2$ $[M+H]^+$: 427.0078; found: 427.0079

Retention time HPLC: 6.13 min. (for (S_p,S_p)-**3.107**) (6.20 min. for *meso*-form (R_p,S_p)-**3.110**) (method 3)

Chiral HPLC: Chiralpak AS-H column, solvent: *n*-hexane/EtOH (80:20), flow rate = 1 mL/min, t = 30 min., T = 35°C, retention times: 12.68 min. for (R_p,S_p)-**3.110**, 14.28 min. for (S_p,S_p)-**3.107**, 15.90 min. for (R_p,R_p)-**3.107**.

Optical rotation: $[\alpha]_D^{20}$ = -257° (c 0.1, CH_2Cl_2); literature: $[\alpha]_D^{25,4}$ = -12.6 (c 1.02, CH_2Cl_2)[55]

Melting point: 175-176°C

3.9.9. Synthesis of (S_p,S_p)-[1,1'-biferrocenyl]-2,2'-dicarboxaldehyde **3.107**

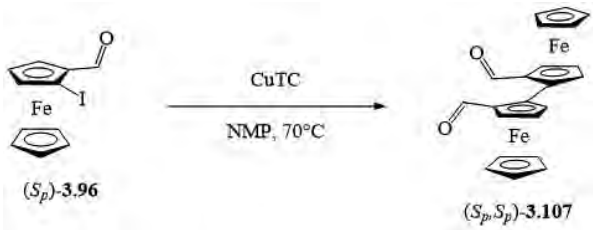

(S_p)-**3.96** (S_p,S_p)-**3.107**

An oven-dried 5 mL round-bottom flask was charged with a magnetic stirring bar, (S_p)-**3.96** (68 mg, 0.20 mmol) and CuTC (114 mg, 0.60 mmol, 3 eq). Anhydrous NMP (1 mL) was added and the reaction flask was wrapped in aluminum foil. The reaction mixture was heated to 70°C and stirred overnight. Then, the reaction mixture was allowed to cool to room temperature, diluted with Et_2O and filtered over Celite. Et_2O was removed under reduced pressure. The residue was taken up in Et_2O (10 mL) and washed 3 times with water (10 mL). The organic phase was dried over anhydrous $MgSO_4$ and filtered. Et_2O was removed under reduced pressure and the resulting residue was purified by flash chromatography[19](gradient: *n*-hexane/EtOAC: 8/2 to 6/4) affording (S_p,S_p)-**3.107**, with a yield of 59.0%, as a red solid.

19 Because **3.107** is light sensitive, the column was wrapped in aluminum foil as well. First a mixed fraction of ferrocenecarboxaldehyde **3.97** and α-iodoferrocenecarboxaldehyde (S_p)-**3.96** was collected. The polarity of the eluent system was raised to *n*-hexane/EtOAC: 7/3 and the *meso*-form (R_p,S_p)-**3.110** was collected. The polarity of the eluent system was raised to *n*-hexane/EtOAC: 6/4 and (S_p,S_p)-[1,1'-biferrocenyl]-2,2'-dicarboxaldehyde (S_p,S_p)-**3.107** was collected in a round bottom flask which was wrapped in aluminum foil.

Formula: $C_{24}H_{18}Fe_2O_2$ (426.07 g/mol).

R_f ((S_p,S_p)-**3.101**) (*n*-hexane/EtOAc: 7/3): 0.25

R_f ((R_p,S_p)-**3.101** *meso*-form) (*n*-hexane/EtOAc 7/3): 0.40

R_f (**3.92**) (*n*-hexane/EtOAc 7/3): 0.69

^{1}**H-NMR:** (500 MHz, $CDCl_3$): δ = 4.31 (s, 10H), 4.74 (dd, *J* = 2.8 Hz, *J* = 2.4 Hz, 2H), 4.94 (dd, *J* = 2.4 Hz, *J* = 1.6, 2H), 4.95 (dd, *J* = 2.8 Hz, *J* = 1.6, 2H), 9.94 (s, 2H) ppm.

^{13}**C-NMR:** (125 MHz, $CDCl_3$): δ = 68.8 (CH x2), 71.0 (CH x10), 71.9 (CH x2), 76.6 (CH x2), 78.6 (C x2), 85.3 (C x2), 192.2 (CH x2) ppm.

IR (HATR): ν_{max} = 3921, 3561, 3315, 3101, 3009, 2941, 2840, 2778, 2764, 1661, 1652, 1426, 1409, 1395, 1289, 1208, 1106, 998, 990, 825, 774, 733, 679 cm^{-1}.

ESI-MS m/z (rel. intensity %): 426.9 (100) $[M+H]^+$, 428.0 (23), 425.0 (10)

HRMS (ESI): calculated for $C_{22}H_{19}Fe_2O_2$ $[M+H]^+$: 427.0078; found: 427.0079

Retention time HPLC: 6.13 min. (for (S_p,S_p)-**3.107**) (6.20 min. for *meso*-form (R_p,S_p)-**3.107**) (method 3)

Chiral HPLC: Chiralpak AS-H column, solvent: *n*-hexane/EtOH (80:20), flow rate = 1 mL/min, t = 30 min., T = 35°C, retention times: 12.68 min. for (R_p,S_p)-**3.110**, 14.28 min. for (S_p,S_p)-**3.107**, 15.89 min. for (R_p,R_p)-**3.107**.

Optical rotation: $[\alpha]_D^{20}$ = -257° (c 0.1, CH_2Cl_2); lit: $[\alpha]_D^{25,4}$ = -12.6 (c 1.02, CH_2Cl_2)[55]

Melting point: 175-176°C

3.9.10. Synthesis of (S_p,S_p)-*N*-benzyl-3,5-dihydro-4*H*-diferrocenyl-[c,e]-azepine **3.118**

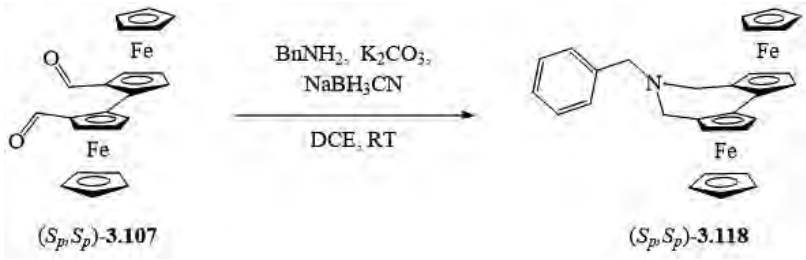

An oven-dried, 25 mL two-neck round-bottom flask was charged with a magnetic stirring bar, (S_p,S_p)-**3.107** (118 mg, 0.28 mmol). Freshly distilled 1,2-dichloroethane (8.0 mL) was added followed by a solution of benzylamine in 1,2-dichloroethane (1.3 M, 850 µL, 1.1 mmol, 4 eq). The reaction mixture was stirred for 5 min. at room temperature and $NaBH_3CN$ (609 mg, 9.69 mmol, 35 eq) and anhydrous K_2CO_3 (153 mg, 1.11 mmol, 4 eq) were added. The reaction was stirred overnight at room temperature and quenched

with a saturated solution of $NaHCO_3$ (30 mL). The aqueous phase was extracted 3 times with CH_2Cl_2 (30 mL). The combined organic phases were dried over anhydrous $MgSO_4$ and filtered. The solvents were removed under reduced pressure and the resulting residue was purified by flash chromatography (*n*-hexane/EtOAc/Et_3N: 8/2/0.2) affording (S_p,S_p)-**3.118**, with a yield of 79.9%.

Formula: $C_{29}H_{27}Fe_2N$ (501.22 g/mol).
R_f (*n*-hexane/EtOAc 7/3): 0.14
^{1}**H-NMR:** (500 MHz, $CDCl_3$): δ = 3.72 (d, *J* = 15.0 Hz, 2H), 3.88-3.89 (m, 2H), 3.89 (d, *J* = 15.0 Hz, 2H), 3.95 (s, 10H), 3.99-4.00 (m, 2H), 4.11 (dd, *J* = 2.4 Hz, *J* = 2.2 Hz, 2H), 4.39 (dd, *J* = 2.4 Hz, *J* = 1.4 Hz, 2H), 7.28-7.41 (m, 5H) ppm.
^{13}**C-NMR:** (125 MHz, $CDCl_3$): δ = 56.4 (CH_2 x2), 60.4 (CH_2), 65.8 (CH x2), 66.3 (CH x2), 67.7 (CH x2), 69.9 (CH x10), 82.6 (C x2), 84.5 (C x2), 127.0 (CH), 128.3 (CH), 128.9 (CH), 139.3 (C) ppm.
IR (HATR): ν_{max} = 3920, 3087, 2923, 2852, 1731, 1493, 1453, 1357, 1265, 1130, 1104, 1028, 999, 815, 804, 734, 698 cm^{-1}.
ESI-MS m/z (rel. intensity %): 502.0 (100) $[M+H]^+$, 503 (35)
HRMS (ESI): calculated. for $C_{29}H_{28}Fe_2N$ $[M+H]^+$: 502.0915; found: 502.0917
Retention time HPLC: 6.81 min. (method 4)
Optical rotation: $[\alpha]_D^{20}$ = -508° (c 1.2, $CHCl_3$)

3.9.11. Synthesis of (S_p,S_p)-*N*-4-methoxybenzyl-3,5-dihydro-4*H*-diferrocenyl-[c,e]-azepine **3.119**

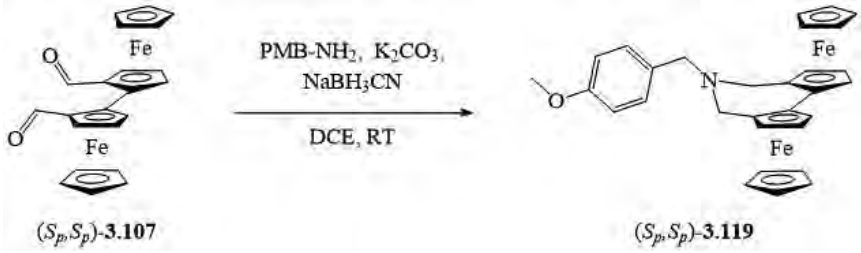

An oven-dried, 25 mL two-neck round-bottom flask was charged with a magnetic stirring bar, (S_p,S_p)-**3.107** (118 mg, 0.28 mmol). Freshly distilled dichloroethane (8.0 mL) was added followed by a solution of *para*-methoxybenzylamine in dichloroethane (1.3 M, 850 µL, 1.1 mmol, 4 eq). The reaction mixture was stirred for 5 min. at room temperature and $NaBH_3CN$ (609 mg, 9.69 mmol, 35 eq) and anhydrous K_2CO_3 (153 mg, 1.11 mmol, 4 eq) were added. The reaction was stirred overnight at room temperature and

quenched with a saturated solution of $NaHCO_3$ (30 mL). The aqueous phase was extracted 3 times with CH_2Cl_2 (30 mL). The combined organic phases were dried over anhydrous $MgSO_4$ and filtered. The solvents were removed under reduced pressure and the resulting residue was purified by flash chromatography (*n*-hexane/EtOAc/Et_3N: 8/2/0.2) affording (S_p,S_p)-**3.119**, with a yield of 88.2%.

Formula: $C_{30}H_{29}FeNO$ (531.25 g/mol).
R_f (*n*-hexane/EtOAc: 7/3): 0.14
^{1}**H-NMR:** (500 MHz, $CDCl_3$): δ = 3.70 (d, *J* = 14.9 Hz, 2H), 3.80-3.82 (m, 2H), 3.83 (s, 3H), 3.86 (d, *J* = 14.9 Hz, 2H), 3.95 (s, 10H), 3.98-4.01 (m, 2H), 4.10 (dd, *J* = 2.4 Hz, *J* = 2.2 Hz, 2H), 4.38 (dd, *J* = 2.2 Hz, *J* = 1.4 Hz, 2H), 6.89 (br d, *J* = 8.5 Hz, 2H), 7.3 (br d, *J* = 8.5 Hz, 2H) ppm.
^{13}**C-NMR:** (125 MHz, $CDCl_3$): δ = 55.3 (CH_3), 56.2 (CH_2 x2), 59.8 (CH_2), 65.8 (CH x2), 66.2 (CH x2), 67.7 (CH x2), 70.0 (CH x10), 82.6 (C x2), 84.5 (C x2), 113.7 (CH), 130.1 (CH), 158.7 (C) ppm. *1C not observed*.
IR (HATR): ν_{max} = 3916, 3090, 2925, 2833, 1610, 1584, 1455, 1440, 1357, 1300, 1170, 1130, 1104, 1031, 999, 814, 733, 703 cm^{-1}.
ESI-MS m/z (rel. intensity %): 532.0 (100) $[M+H]^+$, 533.0 (36)
HRMS (ESI): calculated for $C_{30}H_{30}Fe_2NO$ $[M+H]^+$: 532.1021; found: 532.1032
Retention time HPLC: 5.79 min. (method 4)
Optical rotation: $[\alpha]_D^{20}$ = -454° (c 1.0, $CHCl_3$)

3.9.12. Synthesis of (S_p,S_p)-*N*-allyl-3,5-dihydro-4*H*-diferrocenyl-[c,e]-azepine **3.120**

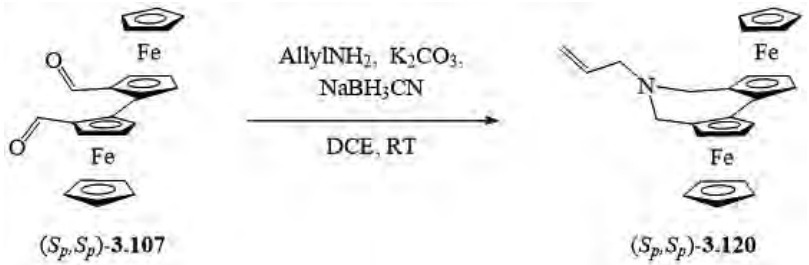

An oven-dried, 25 mL two-neck round-bottom flask was charged with a magnetic stirring bar, (S_p,S_p)-**3.107** (118 mg, 0.28 mmol). Freshly distilled dichloroethane (8.0 mL) was added followed by a solution of allylamine in dichloroethane (1.3 M, 850 µL, 1.1 mmol, 4 eq). The reaction mixture was stirred for 5 min. at room temperature and $NaBH_3CN$ (609 mg, 9.69 mmol, 35 eq) and anhydrous K_2CO_3 (153 mg, 1.11 mmol, 4 eq) were

added. The reaction was stirred overnight at room temperature and quenched with a saturated solution of $NaHCO_3$ (30 mL). The aqueous phase was extracted 3 times with CH_2Cl_2 (30 mL). The combined organic phases were dried over anhydrous $MgSO_4$ and filtered. The solvents were removed under reduced pressure and the resulting residue was purified by flash chromatography (*n*-hexane/EtOAc/Et_3N: 8.5/1.5/0.2) affording (S_p,S_p)-**3.120**, with a yield of 75.6%.

Formula: $C_{25}H_{25}Fe_2N$ (451.16 g/mol).
R_f (*n*-hexane/EtOAc: 7/3): 0.19
^{1}**H-NMR:** (400 MHz, $CDCl_3$): δ = 3.31 (dd, *J* = 13.7 Hz, *J* = 6.8 Hz, 1H), 3.37 (dd, *J* = 13.7 Hz, *J* = 5.8 Hz, 1H), 3.72 (d, *J* = 14.9 Hz, 2H), 3.86 (d, *J* = 14.9 Hz, 2H), 3.96 (s, 10H), 4.06 (br dd, *J* = 2.3 Hz, *J* = 1.3 Hz, 2H), 4.10 (br dd, *J* = 2.3 Hz, *J* = 2.1 Hz, 2H), 4.36 (br dd, *J* = 2.1 Hz, *J* = 1.3 Hz, 2H), 5.20 (dd, *J* = 10.3 Hz, *J* = 1.4 Hz, 1H), 5.21 (dd, *J* = 17.1 Hz, 1.4 Hz, 1H), 5.96 (dddd, *J* = 17.1 Hz, *J* = 10.3 Hz, *J* = 6.8 Hz, *J* = 5.8 Hz, 1H) ppm.
^{13}**C-NMR:** (100 MHz, $CDCl_3$): δ = 56.3 (CH_2 x2), 59.4 (CH_2), 65.7 (CH x2), 66.2 (CH x2), 67.6 (CH x2), 69.9 (CH x10), 82.2 (C x2), 84.6 (C x2), 117.5 (CH_2), 136.3 (CH) ppm.
IR (HATR): ν_{max} = 3081, 2928, 2797, 2362, 2336, 1636, 1452, 1432, 1406, 1316, 1219, 1130, 1102, 1076, 1026, 997, 975, 922, 846, 810, 804, 757 cm^{-1}.
ESI-MS m/z (rel. intensity %): 452.1 (100) $[M+H]^+$, 453.0 (86), 450.0 (60), 451 (46)
HRMS (ESI): calculated for $C_{25}H_{26}Fe_2N$ $[M+H]^+$: 452.0759; found: 452.0751
Retention time: 5.14 min. (method 4)
Optical rotation: $[\alpha]_D^{20}$ = -659° (c 1.7, $CHCl_3$)
Melting point: 108-109°C

3.9.13. Synthesis of (S_p,S_p)-*N*-H-3,5-dihydro-4*H*-diferrocenyl-[c,e]-azepine **3.106**

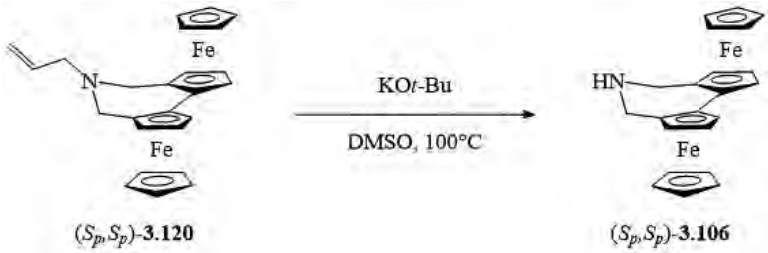

An oven-dried pressure tube was charged with a magnetic stirring bar, (S_p,S_p)-**3.120** (90 mg, 0.20 mmol) and KO*t*-Bu (112 mg, 1.00 mmol, 5 eq). Anhydrous DMSO (7.0 mL) was

added and the pressure tube was closed with a stopper. The reaction mixture was heated to 100°C for 2 h. The reaction was allowed to cool to room temperature. The dark suspension was diluted with Et_2O (30 mL) and carefully quenched with a saturated solution of NH_4Cl (30 mL). The organic phase was separated and washed 3 times with water (30 mL) and once with brine (30 mL). The organic phase was dried over anhydrous $MgSO_4$ and filtered. Et_2O was removed under reduced pressure and pure (S_p,S_p)-**3.106** was obtained as a yellow solid with a yield of 96.2%.

Formula: $C_{22}H_{21}Fe_2N$ (411.10 g/mol).
R_f (*n*-hexane/EtOAc/Et_3N: 2/7/1): 0.33
^{1}**H-NMR:** (500 MHz, $CDCl_3$): δ = 3.92 (d, *J* = 16.0 Hz, 2H), 3.96 (s, 10H), 4.05 (d, *J* = 16.0 Hz, 2H), 4.11-4.13 (m, 4H), 4.30 (app t, *J* = 1.9 Hz, 2H) ppm.
^{13}**C-NMR:** (125 MHz, $CDCl_3$): δ = 51.6 (CH_2 x2), 65.4 (CH x2), 66.4 (CH x2), 67.6 (CH x2), 69.6 (CH x10), 82.0 (C x2), 88.0 (C x2) ppm.
IR (HATR): ν_{max} = 3075, 2909, 2851, 2359, 2331, 1616, 1442, 1406, 1354, 1307, 1212, 1115, 1102, 1030, 998, 809, 780, 737, 674 cm^{-1}.
ESI-MS m/z (rel. intensity %): 412.0 (100) $[M+H]^+$, 413.0 (28), 411.0 (20), 410.0 (13)
HRMS (ESI): calculated for $C_{22}H_{22}Fe_2N$ $[M+H]^+$: 412.0446; found: 412.0448
Retention time HPLC: 6.74 min. (method 3); 2.80 min. (method 4)
Optical rotation: $[\alpha]_D^{20}$ = -399° (c 0.09, $CHCl_3$)
Melting point: 145°C (decomposition).

3.9.14. Synthesis of bifenol-based phosphoramidite ligand **3.129**

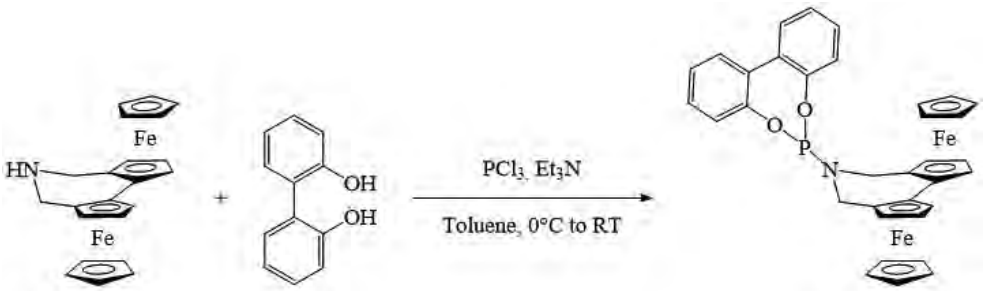

An oven-dried Schlenk tube charged with a magnetic stirring bar and (S_p,S_p)-**3.106** (73 mg, 0.18 mmol) was cooled to 0°C using an ice-water bath. A solution of Et_3N in toluene (0.36 M, 5.0 mL, 1.80 mmol, 10 eq) was added, followed by dropwise addition of a solu-

tion of freshly distilled PCl_3 in toluene (0.57 M, 316 µL, 0.18 mmol, 1 eq). The reaction mixture was stirred for 10 min. at 0°C, allowed to warm up to room temperature and stirred for an additional 2 h. The reaction was cooled again to 0°C and a suspension of 2,2'-biphenol **3.158** (33 mg, 0.18 mmol, 1.0 eq) in toluene (3.0 mL) was added, followed by addition of a solution of Et_3N in toluene (0.36 M, 1.2 mL, 0.44 mmol, 2.5 eq). The reaction mixture was stirred for 10 min. at 0°C, allowed to warm up to room temperature and stirred overnight. The reaction was quenched with water (70 mL) and extracted 3 times with CH_2Cl_2 (70 mL). The combined organic phases were washed with brine (100 mL), dried over anhydrous $MgSO_4$ and filtered. The organic solvents were removed under reduced pressure and the resulting residue was purified by flash chromatography (*n*-hexane/EtOAc: 98/2) affording **3.129**, with a yield of 30.2%, as a yellow solid.

Formula: $C_{34}H_{28}Fe_2NO_2P$ (625.06 g/mol).
R_f (*n*-hexane/EtOAc: 7/3): 0.78
^{1}**H-NMR:** (400 MHz, $CDCl_3$): δ = 3.90 (dd, *J* = 2.3 Hz, *J* = 1.5 Hz, 2H), 4.01 (s, 10H), 4.09 (app t, *J* = 2.3 Hz, 2H), 4.22 (dd, $^2J_{HH}$ = 15.8 Hz, $^3J_{PH}$ = 7.4 Hz, 2H), 4.36 (dd, *J* = 2.3 Hz, *J* = 1.5 Hz, 2H), 4.37 (dd, $^2J_{HH}$ = 15.8 Hz, $^3J_{PH}$ = 8.4 Hz, 2H), 6.87-6.92 (m, 1H), 7.24-7.33 (m, 4H), 7.41 (td, *J* = 7.7 Hz, *J* = 1.8 Hz, 1H), 7.48-7.53 (m, 2H) ppm.
^{13}**C-NMR:** (100 MHz, $CDCl_3$): δ = 49.6 (CH_2 x 2, d, J_{CP} = 22.7 Hz), 65.6 (CH x 2), 66.2 (CH x 2), 67.8 (CH x 2), 69.8 (CH x 10), 81.9 (C x 2), 86.3 (C x 2, d, J_{CP} = 4.4 Hz), 122.0 (CH), 122.6 (CH), 124.3 (CH), 124.7 (CH), 129.2 (CH), 129.3 (CH), 129.5 (CH), 129.7 (CH), 130.5 (C, d, J_{CP} = 2.9 Hz), 131.2 (C, d, J_{CP} = 3.7 Hz), 151.0 (C, d, J_{CP} = 6.6 Hz), 151.2 (C, d, J_{CP} = 3.7 Hz) ppm.
^{31}**P-NMR** (162 MHz, $CDCl_3$): 144.57 ppm.
IR (HATR): ν_{max} = 3083, 2953, 2922, 2854, 1474, 1433, 1365, 1245, 1225, 1189, 1123, 1097, 1042, 1031, 1005, 882, 846, 818, 793, 762, 732, 702, 676 cm^{-1}.
ESI-MS m/z (rel. intensity %): 625.0 (100), 626.0 (56) $[M+H]^+$, 627.0 (16)
HRMS (ESI): calculated for $C_{34}H_{29}Fe_2NO_2P$ $[M+H]^+$: 626.0629, found: 626.0617; calculated for $C_{34}H_{28}Fe_2N_2OP$ $[M]^{\cdot+}$: 625.0551, found: 625.0527
Retention time HPLC: 4.24 min. (method 5)
Optical rotation: $[\alpha]_D^{20}$ = -396° (c 0.10, $CHCl_3$)

3.9.15. Synthesis of (*R*)-binol-based phosphoramidite ligand **3.130**

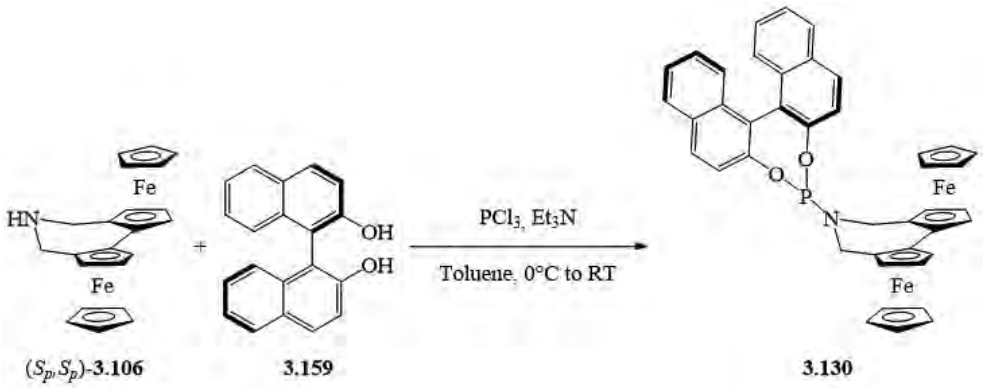

An oven-dried Schlenk tube charged with a magnetic stirring bar and (S_p,S_p)-**3.106** (30 mg, 0.073 mmol) was cooled to 0°C using an ice-water bath. A solution of Et_3N in toluene (0.36 M, 2.0 mL, 0.73 mmol, 10 eq) was added, followed by dropwise addition of a solution of freshly distilled PCl_3 in toluene (0.57 M, 128 µL, 0.073 mmol, 1 eq). The reaction mixture was stirred for 10 min. at 0°C, allowed to warm up to room temperature and stirred for an additional 2 h. The reaction was cooled again to 0°C and a suspension of (*R*)-binol **3.159** (21 mg, 0.073 mmol, 1.0 eq) in toluene (1.0 mL) was added, followed by addition of a solution of Et_3N in toluene (0.36 M, 0.5 mL, 0.18 mmol, 2.5 eq). The reaction mixture was stirred for 10 min. at 0°C, allowed to warm up to room temperature and stirred overnight. The reaction was quenched with water (25 mL) and extracted 3 times with CH_2Cl_2 (25 mL). The combined organic phases were washed with brine (40 mL), dried over anhydrous $MgSO_4$ and filtered. The organic solvents were removed under reduced pressure and the resulting residue was purified by flash chromatography (*n*-hexane/EtOAc: 98/2) affording **3.130**, with a yield of 28.7%, as a yellow solid.

Formula: $C_{42}H_{32}Fe_2NO_2P$ (725.37 g/mol).

R_f (*n*-hexane/EtOAc: 7/3): 0.75

^{1}**H-NMR:** (500 MHz, $CDCl_3$): δ = 3.79 (dd, *J* = 2.3 Hz, *J* = 1.5 Hz, 2H), 3.97-4.01 (m, 2H), 3.98 (s, 10H), 4.00-4.02 (m, 2H), 4.26 (dd, $^2J_{HH}$ = 15.7 Hz, $^3J_{PH}$ = 8.7 Hz, 2H), 4.29 (dd, *J* = 2.4 Hz, *J* = 1.5 Hz, 2H), 7.24-7.28 (m, 1H), 7.32-7.37 (m, 2H), 7.39-7.52 (m, 5H), 7.89-7.91 (m, 2H), 7.99-8.03 (m, 2H) ppm.

^{13}**C-NMR:** (125 MHz, $CDCl_3$): δ = 49.6 (CH_2 x 2, d, J_{CP} = 21.8 Hz), 65.5 (CH x 2), 66.3 (CH x 2), 67.4 (CH x 2), 69.8 (CH x 10), 81.9 (C x 2), 86.4 (C x 2, d, J_{CP} = 3.6 Hz), 121.9 (CH), 122.1 (CH), 123.9 (C, d, J_{CP} = 5.5 Hz), 124.6 (CH), 124.8 (CH), 126.1 (CH), 126.1 (CH), 127.0 (CH

x 2), 128.3 (CH), 128.3 (CH), 130.1 (CH), 130.2 (CH), 130.7 (C), 131.4 (C), 132.7 (C), 132.8 (C), 132.8 (C), 149.6 (C), 150.1 (C, d, J_{CP} = 4.5 Hz) ppm.

^{31}**P-NMR** (162 MHz, $CDCl_3$): 145.23 ppm.

IR (HATR): ν_{max} = 3088, 2954, 2921, 2852, 1589, 1506, 1463, 1431, 1326, 1227, 1202, 1124, 1103, 1061, 1039, 1004, 951, 932, 913, 820, 799, 747, 697, 683, 626 cm^{-1}.

ESI-MS m/z (rel. intensity %): 725.0 (100), 726.1 (68) $[M+H]^+$, 727.0 (26)

HRMS (ESI): calculated for $C_{42}H_{33}Fe_2NO_2P$ $[M+H]^+$: 726.0942, found: 726.0922; calculated for $C_{42}H_{32}Fe_2N_2OP$ $[M]^{\cdot+}$: 725.0864, found: 725.0862

Retention time HPLC: 5.79 min. (method 5)

Optical rotation: $[\alpha]_D^{20}$ = -549° (c 0.10, $CHCl_3$)

3.9.16. Synthesis of (*S*)-binol-based phosphoramidite ligand **3.131**

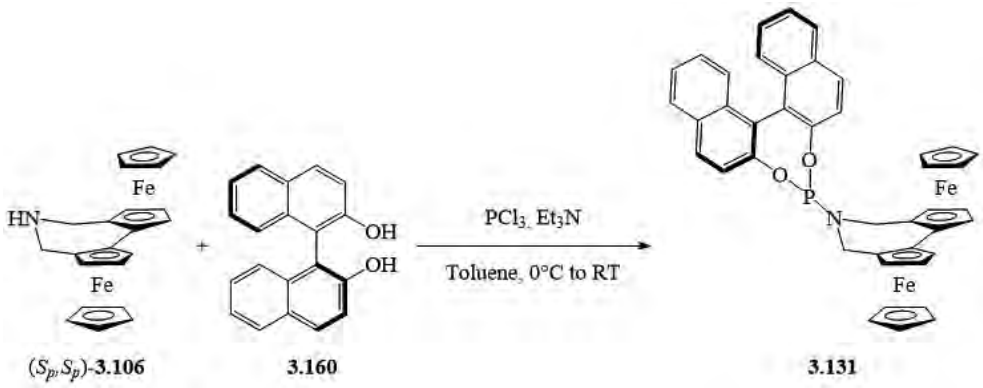

An oven-dried Schlenk tube charged with a magnetic stirring bar and (S_p,S_p)-**3.106** (60 mg, 0.15 mmol) was cooled to 0°C using an ice-water bath. A solution of Et_3N in toluene (0.36 M, 4.1 mL, 1.46 mmol, 10 eq) was added, followed by dropwise addition of a solution of freshly distilled PCl_3 in toluene (0.57 M, 256 µL, 0.15 mmol, 1 eq). The reaction mixture was stirred for 10 min. at 0°C, allowed to warm up to room temperature and stirred for an additional 2 h. The reaction was cooled again to 0°C and a suspension of (*S*)-binol **3.160** (42 mg, 0.15 mmol, 1.0 eq) in toluene (2.0 mL) was added, followed by addition of a solution of Et_3N in toluene (0.36 M, 1.0 mL, 0.36 mmol, 2.5 eq). The reaction mixture was stirred for 10 min. at 0°C, allowed to warm up to room temperature and stirred overnight. The reaction was quenched with water (50 mL) and extracted 3 times with CH_2Cl_2 (50 mL). The combined organic phases were washed with brine (80 mL), dried over anhydrous $MgSO_4$ and filtered. The organic solvents were removed un-

der reduced pressure and the resulting residue was purified by flash chromatography (*n*-hexane/EtOAc: 98/2) affording **3.131**, with a yield of 43.6%, as a yellow solid.

Formula: $C_{42}H_{32}Fe_2NO_2P$ (725.37 g/mol).
R_f (*n*-hexane/EtOAc: 7/3): 0.71
^{1}**H-NMR:** (400 MHz, $CDCl_3$): δ = 3.83 (m, 2H), 4.00 (s, 10H), 4.12 (app t, *J* = 2.4 Hz, 2H), 4.14 (dd, $^{2}J_{HH}$ = 15.9 Hz, $^{3}J_{PH}$ = 7.5 Hz, 2H), 4.35 (dd, $^{2}J_{HH}$ = 16.0 Hz, $^{3}J_{PH}$ = 8.3 Hz, 2H), 4.39 (dd, *J* = 2.4 Hz, *J* = 1.5 Hz, 2H), 7.05 (d, *J* = 8.7 Hz, 1H), 7.22-7.26 (m, 1H), 7.28-7.36 (m, 2H), 7.40-7.50 (m, 3H), 7.55 (d, *J* = 8.8 Hz, 1H), 7.82 (d, *J* = 8.7 Hz), 7.90-7.97 (m, 2H), 7.99 (d, *J* = 8.8 Hz, 1H) ppm.
^{13}**C-NMR:** (100 MHz, $CDCl_3$): δ = 49.7 (CH_2 x2, d, J_{CP} = 23.5 Hz), 65.5 (CH x2), 66.1 (CH x2), 68.2 (CH x2), 69.9 (CH x10), 82.0 (C x2), 85.9 (C x2, J_{CP} = 4.4 Hz), 121.9 (CH), 122.9 (CH), 124.0 (C, J_{CP} = 5.1 Hz), 124.5 (CH), 124.9 (CH), 125.9 (CH), 126.1 (CH), 127.1 (CH x2), 128.3 (CH), 128.3 (CH), 130.2 (CH), 130.4 (CH), 130.6 (C), 131.4 (C), 132.5 (C), 132.8 (C), 132.8 (C), 149.1 (C), 149.3 (C, J_{CP} = 7.3 Hz) ppm.
IR (HATR): ν_{max} = 3089, 3054, 2958, 2923, 2853, 2359, 2341, 1619, 1590, 1506, 1462, 1431, 1366, 1328, 1261, 1229, 1204, 1124, 1104, 1043, 1066, 1031, 1007, 982, 951, 927, 820, 800, 750, 737, 696 cm^{-1}.
^{31}**P-NMR**: (162 MHz, $CDCl_3$): 143.47 ppm.
ESI-MS m/z (rel. intensity %): 726.0 (100) $[M+H]^+$, 727.0 (45), 725.0 (43), 724.0 (13), 728.1 (11)
HRMS (ESI): calculated for $C_{42}H_{33}Fe_2NO_2P$ $[M+H]^+$: 726.0942, found: 726.0899; calculated for $C_{42}H_{32}Fe_2N_2OP$ $[M]^{\cdot+}$: 725.0864, found: 725.0867
Retention time HPLC: 6.11 min. (method 5)
Optical rotation: $[\alpha]_D^{20}$ = -60.7° (c 0.14, $CHCl_3$)
Melting point: 152-153°C.

3.9.17. Synthesis of Methyl *Z*-2-acetamido-3-phenylacrylate **3.156**

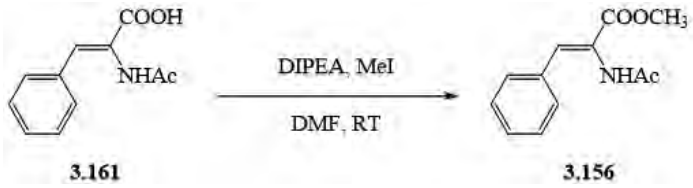

An oven-dried 50 mL round-bottom flask was charged with a magnetic stirring bar and α-acetamidocinnamic acid **3.161** (2.21 g, 10.7 mmol). Anhydrous DMF (20 mL), anhydrous DIPEA (3.7 mL, 21.5 mol, 2 eq) and iodomethane (2.7 mL, 43.1 mmol, 4 eq) were added. The reaction mixture was stirred overnight at room temperature, quenched with a saturated solution of NH_4Cl (100 mL) and extracted three times with EtOAc (100 mL). The combined organic phases were washed with a 10 mol% solution of $KHCO_3$ (100 mL) and a 10 mol% solution of citric acid (100 mL) and dried over Na_2SO_4. After filtration and removal of the organic solvents under reduced pressure, the obtained solid was washed with Et_2O and *n*-hexane. Methyl *Z*-2-acetamido-3-phenylacrylate **3.156** was obtained as a white solid with a yield of 82.3%.

Formula: $C_{12}H_{13}NO_3$ (219.24 g/mol).
R_f (CH_2Cl_2/EtOAc: 85/15): 0.19
^{1}**H-NMR:** (400 MHz, $CDCl_3$): δ = 2.15 (s, 3H), 3.86 (s, 3H), 6.98 (br s, 1H), 7.10-7.7.85 (m, 6H) ppm.
^{13}**C-NMR:** (100 MHz, $CDCl_3$): δ = 23.5 (CH_3), 52.7 (CH_3), 124.2 (C), 128.6 (CH x 2), 129.5 (CH), 129.6 (CH x 2), 132.2 (CH), 133.7 (C), 165.7 (C), 168.7 (C) ppm.
ESI-MS m/z (rel. intensity %): 242.1 (100) $[M+Na]^+$, 220.1 (25) $[M+H]^+$.
Melting point: 123°C; literature: 122-124°C [86]

3.9.18. General procedure Rhodium(I)-catalyzed asymmetric hydrogenation of **3.156**

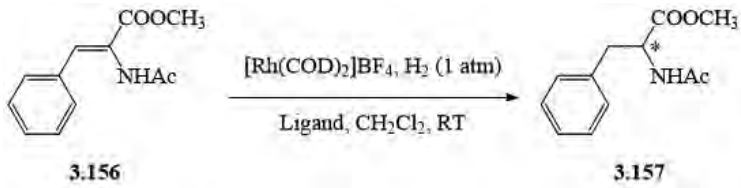

An oven-dried Schlenk tube was connected to an argon Schlenk line, charged with a magnetic stirring bar, $Rh(cod)_2BF_4$ (2.8 mg, 6.89 µmol, 1 mol%) and a ligand (**3.129**,

3.130, **3.131**) (13.8 µmol, 2 mol%). Degassed[20] CH_2Cl_2 (3 mL) was added to the catalyst mixture and stirred for 30 min. at room temperature. Methyl *Z*-2-acetamido-3-phenylacrylate **3.156** (151 mg, 689 µmol) was added and hydrogen gas was bubbled through the reaction mixture for 10 min. The reaction was stirred overnight at room temperature under a hydrogen atmosphere using a balloon. The reaction mixture was filtered over a short plug of silica gel and eluted with EtOAc. The solvents were removed under reduced pressure and **3.157** was obtained as a white solid. Conversion and enantiomeric excess were determined by chiral LC analysis on a OD-H column. The absolute configuration of **3.157** was assigned via correlation of its specific rotation with literature values.[108,109]

Formula: $C_{12}H_{15}NO_3$ (221.25 g/mol).
R_f (CH_2Cl_2/EtOAc: 90/10): 0.18
^{1}**H-NMR:** (500 MHz, $CDCl_3$): δ = 1.98 (s, 3H), 3.09 (dd, *J* = 13.9 Hz, *J* = 5.8 Hz, 1H), 3.14 (dd, *J* = 13.9 Hz, *J* = 5.8 Hz, 1H), 3.73 (s, 3H), 4.83 (app dt, *J* = 7.8 Hz, *J* = 5.8 Hz, 1H), 5.95 (br s, 1H), 7.07-7.11 (m, 2H), 7.22-7.32 (m, 3H) ppm.
^{13}**C-NMR:** (125 MHz, $CDCl_3$): δ = 23.3 (CH_3), 38.0 (CH_2), 52.5 (CH), 53.2 (CH_3), 127.3 (CH), 128.4 (CH), 128.8 (CH), 135.9 (C), 169.8 (C), 172.2 (C) ppm.
ESI-MS m/z (rel. intensity %): 222.1 (74) $[M+H]^+$, 180.1 (92), 162.1 (100), 120.1 (50)
Retention time HPLC: 4.73 min. (method 3)
Chiral HPLC: Chiralcel OD-H column, solvent: *n*-hexane/EtOH (95:5), flow rate = 1 mL/min, t = 30 min., T = 35°C, retention times: 11.20 min. for (*R*)-**3.157**, 12.80 min. (*S*)-**3.157** and 20.81 min. for starting material **3.156**.
Melting point: 64°C

Part of this research has been published:

W. Kimpe, P. Janssens, K. Bert, S. Wackens, J.L. Goeman, J. Van der Eycken,

Tetrahedron, 2019, *75*, 130416

20 Degassing was accomplished by bubbling of H_2-gas through the solvent for 10 min. using a balloon.

3.10. References

[1] R. H., Crabtree, *The Organometallic Chemistry of the Transition Metals*; Wiley, New Jersey, **1988**

[2] J. F. Teichert, B. L. Feringa, *Angew. Chem. Int. Ed.*, **2010**, *49*, 2486-2528

[3] P. B. Dias, M. E. Minas de Piedade, J. A. Martinho Simões, *Coord. Chem. Rev.*, **1994**, *135*, 737-807

[4] C. A. Tolman, *Chem. Rev.*, **1977**, *77*, 313-348

[5] K.N. Gavrilov, S. E. Lyubimov, S. V. Zheglov, E. B. Benetsky, V. A. Davankov, *J. Mol. Catal. A: Chem.*, **2005**, *235*, 255-260

[6] K.N. Gavrilov, S. V. Zheglov, E. A. Rastorguev, N. N. Groshkin, M. G. Maksimova, E. B. Benetsky, V. A. Davankov, M. T. Reetz, *Adv. Synth. Catal.*, **2010**, *352*, 2599-2610

[7] (a) L. Horner, H. Siegel, H. Büthe, *Angew. Chem. Int. Ed.*, **1968**, *7*, 942-943 (b) L. Horner, H. Büthe, H. Spiegel, *Tetrahedron Lett.*, **1968**, *9*, 5889-5892 (c) W. S. Knowles, M. J. Sabacky, *Chem. Commun.*, **1968**, 1445-1446 (d) W. S. Knowles, M. J. Sabacky, B. D. Vineyard, *J. Chem. Soc. Chem Commun.*, **1972**, 10-11

[8] (a) T. P. Dang, H. B. Kagan, *J. Chem. Soc. D Chem. Commun.*, **1971**, 481 (b) H. B. Kagan, T. P. Dang, *J. Am. Chem. Soc.*, **1972**, *94*, 6429-6433

[9] A. H. M. de Vries, A. Meetsma, B. L. Feringa, *Angew. Chem. Int. Ed.*, **1996**, *35*, 2374-2375

[10] (a) M. T. Reetz, G. Mehler, *Angew. Chem. Int. Ed.*, **2000**, *35*, 3889-3890 (b) M. T. Reetz, T. Sell, *Tetrahedron Lett.*, **2000**, *41*, 6333-6336

[11] C. Claver, E. Fernandez, A. Gillon, K. Heslop, D. J. Hyett, A. Martorell, A. G. Orpen, P. G. Pringle, *Chem. Commun.*, **2000**, 961-962

[12] M. van den Berg, A. J. Minnaard, E. P. Schudde, J. van Esch, A. H. M. de Vries, J. G. de Vries, B. L. Feringa, *J. Am. Chem. Soc.*, **2000**, *122*, 11539-11540

[13] W. Fu, W. Tang, *ACS Catal.*, **2016**, *6*, 4814-4858

[14] (a) M. Fañanás-Mastral, R. Vitale, M. Pérez, B. L. Feringa, *Chem. Eur. J.*, **2015**, *21*, 4209-4212; (b) M. Chen, J. F. Hartwig, *Angew. Chem. Int. Ed.*, **2014**, *53*, 8691-8695

[15] W.-J. Shi, L.-X. Wang, Y. Fu, S.-F. Zhu, Q.-L. Zhou, *Tetrahedron: Asymmetry*, **2003**, *14*, 3867-3872

[16] B. M. Trost, M. C. Ryan, *J. Am. Chem. Soc.*, **2016**, *138*, 2981-2984

[17] E. Keller, J. Maurer, R. Naasz, T. Schader, A. Meetsma, B. L. Feringa, *Tetrahedron: Asymmetry*, **1998**, *9*, 2409-2413

[18] C. Defieber, M. A. Ariger, P. Moriel, E. M. Carreira, *Angew. Chem. Int. Ed.*, **2007**, *46*, 3139-3143

[19] (a) M. Roggen, E. Carrerira, *Angew. Chem. Int. Ed.*, **2011**, *50*, 5568-5571 (b) M. A. Schafroth, D. Sarlah, S. Krautwald, E. M. Carreira, *J. Am. Chem. Soc.*, **2012**, *134*, 20276-20278 (c) J. Y. Hamilton, S. L. Rösseler, E. M. Carreira, *J. Am. Chem. Soc.*, **2017**, *139*, 8082-8085; and references therein

[20] (a) Y. Fu, J.-H. Xie, A.-G. Hu, H. Zhou, L.-X. Wang, Q.-L. Zhou, *Chem. Commun.*, **2002**, 480-481 (b) A.-G. Hu, Y. Fu, J.-H. Xie, H. Zhou, L.-X. Wang, Q.-L. Zhou, *Angew. Chem. Int. Ed.*, **2002**, *41*, 2348-2350

[21] (a) B. M. Trost, D. A. Bringley, S. M. Silverman, *J. Am. Chem. Soc.*, **2011**, *133*, 7664-7667; (b) B. M. Trost, D. A. Bringley, *Angew. Chem. Int. Ed.*, **2013**, *52*, 4466-4469

[22] D. Schaarsmidt, H. Lang, *Organometallics*, **2013**, 32, 5668-5704

[23] S. I. Goldberg, D. W. Mayo, *Chem. Ind.*, **1959**, 671-672 (issue: 22)

[24] M. D. Rausch, *J. Am. Chem. Soc.*, **1960**, *82*, 2080-2081

[25] P. Krajnik, C. Kratky, K. Schlögl, M. Widhalm, *Monatsh. Chem.*, **1990**, *121*, 945-953

[26] *Chiral ferrocenes in asymmetric catalysis*, Eds.: L.-X. Dai, X.-L. Hou, Wiley-VCH Verlag GmbH & Co. KGaA, **2010**

[27] G. Marr, R. E. Moore, B. W. Rockett, *Tetrahedron Lett.*, **1968**, *21*, 2517-2520

[28] G. Marr, R. E. Moore, B. W. Rockett, *Tetrahedron*, **1969**, *25*, 3477-3484

[29] D. J. Booth, G. Marr, B. W. Rockett, *J. Organomet. Chem.*, **1971**, *32*, 227-230

[30] (a) K. Hata, I. Motoyama, H. Watanabe, *Bull. Chem. Soc. Jap.*, **1964**, *37*, 1719-1720; (b) H. Watanabe, I. Motoyama, K. Hata, *Bull. Chem. Soc. Jap.*, **1966**, *39*, 790-801

[31] A. Davison, A. W. Rudie, *J. Organomet. Chem.*, **1979**, *169*, 69-76

[32] A. Davison, A. W. Rudie, *Synth. React. Inorg. Met-Org. Chem.*, **1980**, *10*, 391-395

[33] M. Spescha, N. W. Duffy, B. H. Robinson, J. H. Simpson, *Organometallics*, **1994**, *13*, 4895-4904

[34] B. H. Robinson, J. Simpson, D. J. Wilson, *Acta. Cryst.*, **1996**, *C52*, 2196-2198

[35] S.-I. Fukuzawa, M. Yamamoto, S. Kikuchi, *J. Org. Chem.*, **2007**, *72*, 1514-1517

[36] J. C. Anderson, J. D. Osborne, T. J. Woltering, *Org. Biomol. Chem.*, **2008**, *6*, 330-339

[37] (a) M. Tsukazaki, M. Tinkl, A. Roglans, B. J. Chapell, N. J. Taylor, V. Snieckus, *J. Am. Chem. Soc.*, **1996**, *118*, 685-686 (b) R. S. Laufer, U. Veith, N. J. Taylor, V. Snieckus, *Org. Lett.*, **2000**, *2*, 629-631 (c) C. Metallinos, H. Szillat, N. J. Taylor, V. Snieckus, *Adv. Synth. Catal*, **2003**, *345*, 370-382

[38] M. Sawamura, H. Hamashima, Y. Ito, *Tetrahedron: Asymmetry*, **1991**, *2*, 593-596

[39] M. Sawamura, H. Hamashima, M. Sugawara, R. Kuwano, Y. Ito, *Organometallics*, **1995**, *14*, 4549-4558

[40] R. Kuwano, T. Uemura, M. Saitoh, Y. Ito, *Tetrahedron Lett.*, **1999**, *40*, 1327-1330

[41] M. Sawamura, H. Hamashima, Y. Ito, *J. Am. Chem. Soc.*, **1992**, *114*, 8295-8296

[42] M. Sawamura, R. Kuwano, Y. Ito, *Angew. Chem. Int. Ed.*, **1994**, *33*, 111-113

[43] (a) R. Kuwano, T. Uemura, M. Saitoh, Y. Ito, *Tetrahedron: Asymmetry*, **2004**, *15*, 2263-2271; (b) P. Barbaro, C. Bianchini, G. Giambastiani, S. L. Parisel, *Coord. Chem. Rev.*, **2004**, *248*, 2131-2150 (and references therein).

[44] M. Sawamura, A. Yamauchi, T. Takegawa, Y. Ito, *J. Chem. Soc., Chem. Commun.*, **1991**, 874-875

[45] L. Xiao, K. Mereiter, F. Spindler, W. Weissensteiner, *Tetrahedron: Asymmetry*, **2001**, *12*, 1105-1108

[46] G. Espino, L. Xiao, M. Puchberger, K. Mereiter, F. Spindler, B. R. Manzano, F. A. Jalón, W. Weissensteiner, *Dalton Trans.*, **2009**, 2751-2763

[47] U. Nettekoven, M. Wildhalm, P. C. J. Kamer, P. W. N. M. van Leeuwen, K. Mereiter, M. Lutz, A. L. Spek, *Organometallics,* **2000**, *19*, 2299-2309

[48] U. Nettekoven, M. Widhalm, H. Kalchhauser, P. C. J. Kamer, P. W. N. M. van Leeuwen, M. Lutz, A. L. Spek, *J. Org. Chem.*, **2001**, *66*, 759-770

[49] S.-G. Kim, C.-W. Cho, K. H. Ahn, *Tetrahedron: Asymmetry*, **1997**, *8*, 1023-1026

[50] L.Xiao, W. Weissensteiner, K. Mereiter, M. Widhalm, *J. Org. Chem.*, **2002**, *67*, 2206-2214

[51] M. Widhalm, U. Nettekoven, H. Kalchhauser, K. Mereiter, M. J. Calhorda, V. Félix, *Organometallics*, **2002**, *21*, 315-325

[52] M. Widhalm, K. Mereiter, M. Bourghida, *Tetrahedron: Asymmetry*, **1998**, *9*, 2983-2986

[53] P. Wimmer, M. Widhalm, *Monatsch. Chem.*, **1996**, *127*, 669-681

[54] A. Gomez Neo, A. Gref, O. Riant, *Chem. Commun.*, **1998**, 2353-2354

[55] A. O. Larsen, R. A. Taylor, P. S. White, M. R. Gagné, *Orgnanometallics*, **1999**, *18*, 5157-5162

[56] O. Riant, O. Samuel, H.B. Kagan, *J. Am. Chem. Soc.*, **1993**, *115*, 5835-5836

[57] O. Riant, O. Samuel. T. Flessner, S. Taudine, H.B. Kagan, *J. Org. Chem.*, **1997**, *62*, 6733-6745

[58] G. S. Zweifel, M. H. Nantz, *Modern Organic synthesis: An introduction*, *First edition*, W. H. Freeman, **2010**, p 88-97

[59] K. Bert, *Synthese en valorisatie van imidaatgebaseerde ligandin voor transitiemetaalkatalyse*, **2015**, Ghent University, Faculty of Sciences, department of Organic and Macromolecular Chemistry, Laboratorium for Organic and Bioorganic Synthesis

[60] S. Barriga, C. F. Marcos, O. Riant, T. Torroba, *Tetrahedron*, **2002**, *58*, 9785-9792

[61] S. Xu, Z. Wang, X. Zhang, K. Ding, *Eur. J. Og. Chem.*, **2011**, 110-116

[62] P. G. M. Wuts, T. W. Greene, *Greene's Protective Groups in Organic Synthesis, Fourth edition*, John Wiley & Sons, Inc, **2006**, p 803-827

[63] P. G. M. Wuts, T. W. Greene, *Greene's Protective Groups in Organic Synthesis, Fourth edition*, John Wiley & Sons, Inc, **2006**, p 823

[64] L. Kürti, B. Czakó, *Strategic Applications of Named Reactions in Organic Synthesis*, Elsevier, **2005**, p 466-467

[65] S. Zhang, D. Zhang, L. S. Liebeskind, *J. Org. Chem.*, **1997**, *62*, 2312-2313

[66] G. Wilkinson, *Org. Synt.*, **1956**, *36*, 31-33

[67] T. D. Nelson, R. D. Crouch, *Org. React.*, **2004**, *63*, 265-555

[68] A. H. Lewin, *Tetrahedron Lett.*, **1965**, *50*, 4531-4536

[69] T. Cohen, T. Poeth, *J. Am. Chem. Soc.*, **1972**, *94*, 4363-4364

[70] T. Cohen, I. Chrisea, *J. Am. Chem. Soc.*, **1976**, *98*, 748-753

[71] G. W. Ebert, R. D. Rieke, *J. Org. Chem.*, **1988**, *53*, 4482-4488

[72] S. E. Douglass, S. T. Massey, S. G. Woolard, R. W. Zoellner, *Transition Met. Chem.*, **1990**, *15*, 317-324

[73] J. Hassan, M. Sévignon, C. Gozzi, E. Schulz, M. Lemaire, *Chem. Rev.*, **2002**, *102*, 1359-1469

[74] E. Sperotto, G. P. M. van Klink, G. van Koten, J. G. de Vries, *Dalton Trans.*, **2010**, *39*, 10338-10351

[75] H. Eckert, C. Seidel, *Angew. Chem. Int. Ed.*, **1986**, *25*, 159-160

[76] B. L. Feringa, *Acc. Chem. Res.*, **2000**, *33*, 346-353

[77] A. H. M. de Vries, A. Meetsma, B. L. Feringa, *Angew. Chem. Int. Ed.*, **1996**, *35*, 2374-2376

[78] B. L. Feringa, M. Pineschi, L. A. Arnold, R. Imbos, A. H. M. de Vries, *Angew. Chem. Int. Ed.*, **1997**, *36*, 2620-2623

[79] C. R. Smith, D. Mans, T. V. RajanBabu, *Org. Synth.*, **2008**, *85*, 238-247

[80] A. Alexakis, D. Polet, S. March, *J. Org. Chem.*, **2004**, *69*, 5660-5667

[81] D. Peña, A. J. Minnaard, J. G. de Vries, B. L. Feringa, *J. Am. Chem. Soc.*, **2002**, *124*, 14552-14553

[82] L. Eberthardt, D. Armspach, J. Harrowfield, D. Matt, *Chem. Soc. Rev.*, **2008**, *37*, 839-864

[83] W.-J. Shi, L.-X. Wang, Y. Fu, S.-F. Zhu, Q.-L. Zhou, *Tetrahedron: Asymmetry*, **2003**, *14*, 3867-3872

[84] M. Gerdin, M. Penhoat, R. Zalubovskis, C. Pétermann, M. Moberg, *J. Organomet. Chem.*, **2008**, *693*, 3519-3526

[85] L. Eberhardt, D. Armspach, D. Matt, L. Toupet, B. Oswald, *Eur. J. Org. Chem.*, **2007**, 5395-5403

[86] W. Tang, X. Zhang, *Chem. Rev.*, **2003**, *103*, 3029-3063

[87] Y. Sun, J. Wang, C. LeBlond, R. A. Reamer, J. Lasuidara, J. R. Sowa, D. G. Blackmond, *J. Organomet. Chem.*, **1997**, *548*, 65-72

[88] (a) J. Halpern, *Science*, 1982, *217*, 401-407; (b) C. R. Landis, J. Halpern, *J. Am. Chem. Soc.*, **1987**, *109*, 1746-1754

[89] (a) I. D. Gridnev, N. Higashi, K. Asakura, T. Imamoto, *J. Am. Chem. Soc.*, **2000**, *122*, 7183-7194; (b) I. D. Gridnev, Y. Yamanoi, N. Higashi, H. Tsuruta, M. Yasutake, T. Imamoto, *Adv. Synth. Catal.*, **2001**, *343*, 118-136; (c) I. D. Gridnev, M. Yasutake, N. Higashi, T. Imamoto, *J. Am. Chem. Soc.*, **2001**, *123*, 5268-5276; (d) I. D. Gridnev, T. Imamoto, *Acc. Chem. Res.*, **2004**, *37*, 633-644

[90] T. Schmidt, W. Baumann, H. –J. Drexler, A. Arrieta, D. Heller. H. Buschmann, *Organometallics*, **2005**, *24*, 3842-3848

[91] W. S. Knowles, *Acc. Chem. Res.*, **1983**, *16*, 106-112

[92] M.J. Burk, J.E. Feaster, W.A. Nugent, R.L. Harlow, *J. Am. Chem. Soc.*, **1993**, *115*, 10125-10138

[93] (a) B. Bosnich, *Pure Appl. Chem.*, **1990**, *62*, 1131-1134; (b) P.L. Bogdan, J.J. Irwin, *Organometallics*, 1989, *8*, 1450-1453; (c) J.M. Brown, P.L. Evans, *Tetrahedron*, **1988**, *44*, 4905-4916

[94] J.S. Giovannetti, C.M. Kelly, C.R. Landis, *J. Am. Chem. Soc.*, **1993**, *115*, 4040-4057

[95] B. R. Bender, M. Koller, D. Nanz, W. von Philipsborn, *J. Am. Chem. Soc.*, **1993**, *115*, 5889-5890

[96] M. van den Berg, *Rhodium-Catalyzed Asymmetric Hydrogenation using Phosphoramidite Ligands*, **2006**, University of Groningen

[97] M. T. Reetz, A. Meiswinkel, G. Mehler, K. Angermund, M. Graf, W. Thiel, R. Mynott, D. G. Blackmond, *J. Am. Chem. Soc.*, **2005**, *127*, 10305-10313

[98] M. T. Reetz, T. Sell, A. Meiswinkel, G. Mehler, *Angew. Chem. Int. Ed.*, **2003**, *42*, 790-793

[99] D. Peña, A. J. Minnaard, J. A. F. Boogers, A. H. M. de Vries, J. G. de Vries, B. L. Feringa, *Org. Biomol. Chem.*, **2003**, *1*, 1087-1089

[100] M. T. Reetz, G. Mehler, *Tetrahedron Letters*, **2003**, *44*, 4593-4596

[101] R. Hoen, J. A. F. Boogers, H. Bernsmann, A. J. Minnaard, A. Meetsma, T. D. Tiemersma-Wegman, A. H. M. de Vries, J. G. de Vries. B. L. Feringa, *Angew. Chem. Int. Ed.*, **2005**, *44*, 4209-4212

[102] J. A. F. Boogers, U. Felfer, M. Kotthaus, L. Lefort, G. Steinabauer, A. H. M. de Vries, J. G. de Vries, *Org. Process. Res. Dev.*, **2007**, *11*, 585-591

[103] T. Jerpaghnon, J.-L. Renaud, C. Bruneau, *Tetrahedron: Asymmetry*, **2004**, *15*, 2101-2111

[104] X. Jia, X. Li, L. Xu, Q. Shi, X. Yao, A. S. C. Chan, *J. Org. Chem*, **2003**, *68*, 4539-4541

[105] M. van den Berg, A. J. Minnaard, R. M. Haak, M. Leeman, E. P. Schudde, A. Meetsma, B. L. Feringa, A. H. M. de Vries, C. E. P. Maljaars, C. E. Willans, D. Hyett, J. A. F. Boogers, H. J. W. Henderickx, J. G. de Vries, *Adv. Synth. Catal.*, **2003**, *345*, 308-323

[106] M. van den Berg, R. M. Haak, A. J. Minnaard, A. H. M. de Vries, J. G. de Vries, B. L. Feringa, *Adv. Synth. Catal.*, **2002**, *344*, 1003-1007

[107] A. J. Minnaard, B. L. Feringa, L. Lefort, J. G. De Vries, *Acc. Chem. Res.*, **2007**, *40*, 1267-1277

[108] B.D. Vineyard, W.S. Knowles, M.J. Sabacky, G.L. Bachman, D.J. Weinkauff, *J. Am. Chem. Soc.*, **1977**, *99*, 5946-5952

[109] (a) A. Togni, C. Breutel, A. Schnyder, F. Spindler, H. Landert, A. Tijani, *J. Am. Chem. Soc.,* **1994**, *116*, 4062-4066 (b) J.P. Pye, K. Rossen, R. A. Reamer, N.N. Tsou, R.P. Volante, P.J. Reider, *J. Am. Chem. Soc.*, **1997**, *119*, 6207-6208

[110] E. Vervecken, M. Van Overschelde, T. Noël, Y. Gök, S. A. Rodríuez, S. Cogen, J. Van der Eycken, *Tetrahedron:* Asymmetry, **2010**, *21*, 2321-2328

NOVEL MONODENTATE BIFERROCENE-BASED DIAMIDOPHOSPHITE LIGANDS

"I have nothing to offer but blood, toil, tears and sweat"

Winston Churchill – 13 May 1940

4.1. Introduction

Diamidophosphite structures are a class of phosphorus containing compounds, in which this central atom is linked to an oxygen containing part and two nitrogen containing parts. It's general structure is shown as **4.01** in Figure 4.1 (a). In contrast to Feringa's well-known phosphoramidite ligands, diamidophosphites are much less applied as ligands for asymmetric transition metal catalysis. It is clear that these compounds have different properties because nitrogen substituents create more steric bulk around the central phosphorus atom. Moreover, the electron density on phosphorus is generally higher for diamidophosphites than phosphoramidites (or phosphites). However, diamidophosphites having electron-withdrawing sulfonamide substituents on nitrogen have also been published.[1] For the design of diamidophosphite ligands for asymmetric transition metal catalysis, chiral C_2-symmetric diamine backbones are frequently applied[1-6] (**4.02**, Figure 4.1 (b)). This allows to use a large library of achiral as well as chiral alcohols. The combination of a chiral amine and a chiral alcohol offers the possibility to have matched and mismatched combinations. Moreover, the use of a diol allows to prepare *P,P*-bidentate diamidophosphite ligands. All these features make that diamidophosphites are a highly modular ligand class and therefore deserve more interest in the field of asymmetric transition metal catalysis.

Figure 4.1 (a) Left: most general structure of a diamidophosphite **(b)** Right: general design for chiral diamidophosphite ligands

A concise overview of the most important diamidophosphite ligands reported in the field of asymmetric transition metal catalysis, with the exception of those used in the rhodium(I)-catalyzed hydrogenation, is described in this section. Diamidophosphite ligands used in the latter reaction are described in § 4.8 (*vide infra*).

In 1997, the research group of Buono reported already on the synthesis and use of chiral hybrid *P*,N*-type ligands characterized by a diamidophosphite substructure (Figure 4.2).[7] These ligands consisted of a chiral five membered 1,3,2-diazaphospholidine derived from 1-deoxy-2-phenylaminoprolinol in combination with different pyridine based alcohols. It can be seen that the central phosphorus atoms are chiral centers as well. The ligands were tested in a palladium-catalyzed asymmetric allylic alkylation which is a benchmark test reaction for *P,N*-type ligands. Best results were obtained with ligand **4.03**, which is nowadays well known as Quiphos (Figure 4.2).[8] Later on, this ligand was successfully applied by the same research group in palladium-catalyzed asymmetric allylic aminations[9,10], copper-catalyzed Diels-Alder reactions[11], copper-catalyzed conjugate addition of diethylzinc to enones[10,12-13] and palladium-catalyzed asymmetric allylic alkylation with formation of quaternary carbon centers on β-ketoesters.[13]

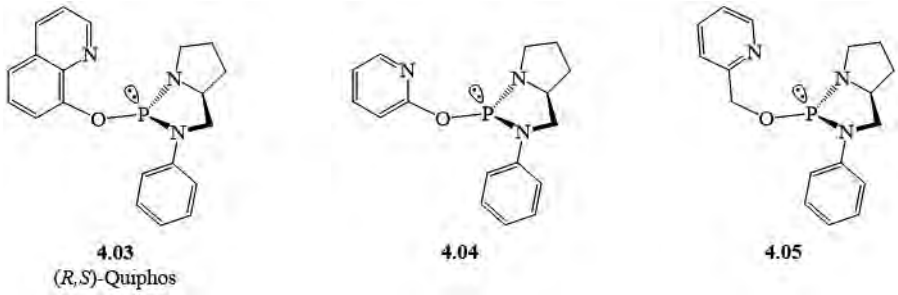

Figure 4.2 *P*,N*-type ligand with a diamidophosphite substructure reported by Buono *et al.*

In 2002, Nifant'ev *et al*. reported on the synthesis of some monodentate diamidophosphite ligands.[14] However, they were never able to isolate the target compounds due to their severe sensitivity towards oxidation. One year later, the research group of Reetz published a paper on the synthesis of novel monodentate binaphthyldiamine-based phosphorus containing ligands and their application in rhodium-catalyzed hydrogenation and rhodium-catalyzed hydroformylation reactions.[6] (More details are discussed in § 4.8, *vide infra*) Since these publications, a few research groups were able to prepare a variety of novel chiral diamidophosphite ligands and to test them in different transition metal catalyzed reactions.

One of the research groups that made a major contribution to the development of diamidophosphite ligands is the group of Gavrilov.[15-20] In 2004 they reported on new monodentate diamidophosphite ligands with a chiral C_1-symmetric diamine backbone.[16] As a consequence the central phosphorus is now a chiral center as well and important for chiral induction. Inclusion of the phosphorus atom in the five membered 1,3,2-diazaphospholidine ring is a key feature responsible for the stability against air and moisture. These *P**-chiral monodentate ligands were applied in palladium-catalyzed asymmetric allylic substitutions using different types of nucleophiles. Their best result, was obtained for the alkylation reaction of **4.06** with ligand **4.09** (Scheme 4.1). A conversion of 98% in combination with an enantiomeric excess of 97% were reported.

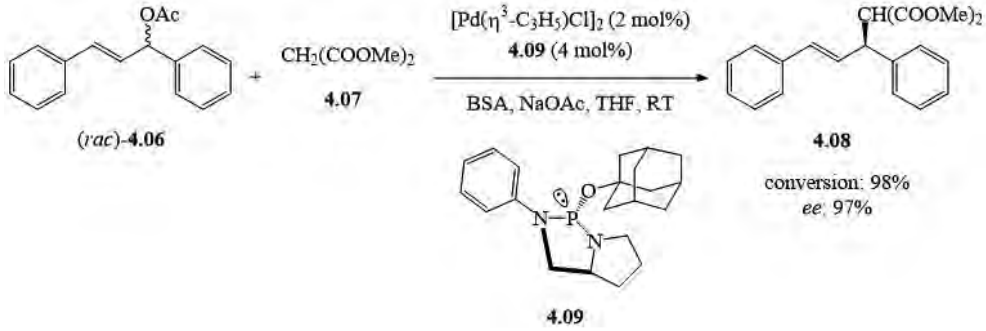

Scheme 4.1 Pd-catalyzed asymmetric allylic amination using a *P**-chiral monodentate diamidophosphite ligand

Later on, the research group of Gavrilov synthesized two diastereomeric *P**-chiral diamidophosphite ligands based on the same diamine backbone but with both enantiomers of the axial chiral *O*-methyl-binol substructure (**4.10**-**4.11**, Figure 4.3).[17] These ligands were successfully tested in benchmark palladium-catalyzed asymmetric allylic substitution reactions with S-, C- and N-nucleophiles, the palladium-catalyzed deracemisation of (*E*)-1,3-diphenylallyl carbonate and the rhodium-catalyzed asymmetric hydrogenation of dimethylitaconate. This library of *P**-chiral diamidophosphites was expanded in 2013 with different C_1-symmetric 1,2-diamine backbones, generally represented as **4.12** (Figure 4.3).[18] The effects of different substituents in the 1,3,2-diazaphospholidine cycle were studied in palladium-catalyzed asymmetric allylic substitution reaction with S-, C- and N-nucleophiles. Gavrilov *et al.* concluded that the success rate of enantio-induction depends on both the steric properties of the ligands and the nature of the nucleophile. Novel bidentate *P*,P**-chiral diamidophosphite ligands, **4.13**, with the classical 1,2-diamine backbone as shown in Figure 4.3 were syn-

thesized as well.[19] The chiral phosphorus centers were linked via two different diols. One of them was 1,1'-bis(hydroxymethyl)ferrocene. However, these ligands gave lower conversions and *ee*-values in palladium-catalyzed asymmetric substitution reactions. These ligands were also tested in the palladium-catalyzed desymmetrization of *N,N'*-ditosyl-*meso*-cyclopent-4-ene-1,3-diol bis carbamate (*vide supra* Chapter 5, § 5.1, Scheme 5.1) and a palladium-catalyzed allylic alkylation with the construction of quaternary stereocenters. In 2014, the research group of Gavrilov reported on the preparation of novel bidentate *P,P**-chiral phospine-diamidophosphite ligands again containing the 1,3,2-diazaphospholidine ring.[20] Just like the other bidentate ligands, these phosphine-diamidophosphite structures provided slightly lower *ee*-values than the monodentate ligands in the benchmark palladium catalyzed asymmetric allylic substitutions. As an extension on these ligands, in the same paper, the authors reported on the use of the 'mixed-ligand approach' in these palladium-catalyzed reactions. Nevertheless, the combination of a chiral monodentate diamidophosphite with triphenylphosphine afforded significantly lower conversions.

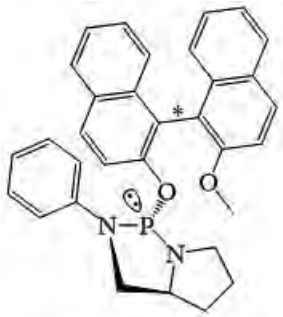

(R,S,S_a)-**4.10**
(R,S,R_a)-**4.11**

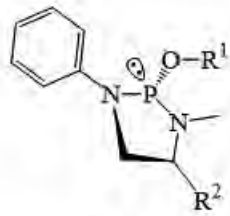

4.12:
R^1=Me, adamantyl
R^2=*i*-Pr, *t*-Bu, *s*-Bu, Ph, Bn

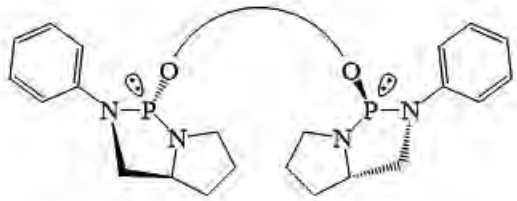

4.13

Figure 4.3 *P**-chiral diamidophosphite ligands developed by Gavrilov and co-workers

Another group that has been actively studying chiral diamidophosphite ligands for asymmetric transition metal catalyzed transformations is the research group of Rocamora and Muller.[2-5] In 2011, they reported for the first time on the synthesis and full characterization of a library of novel monodentate diamidophosphite ligands.[2] Different C_2-symmetric diamines with a variety of alcohols have been tested in the palladium-catalyzed asymmetric hydrovinylation of styrene. The best result for this benchmark test reaction was obtained for ligand **4.16** with an axial chiral dimethylbinaphthyldiamino based backbone in combination with borneol, as a chiral alcohol substituent (Scheme 4.2). A very good activity, TOF=595h^{-1} and enantioselectivity of 90% *ee* were obtained.

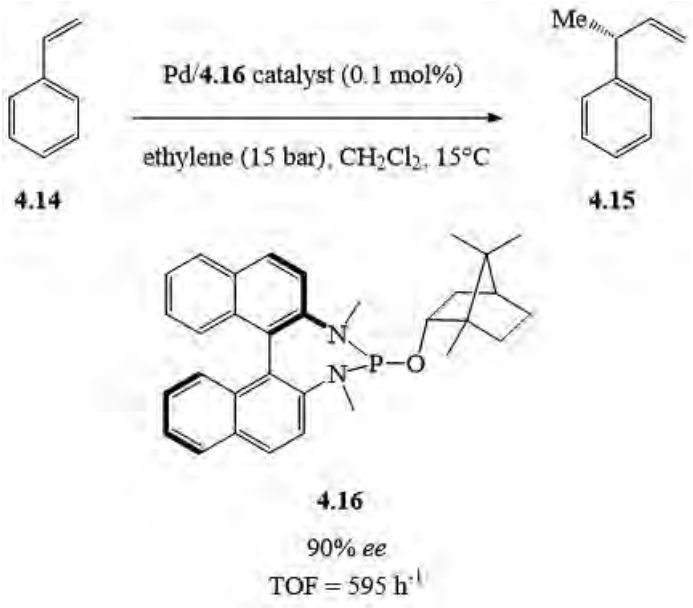

Scheme 4.2 Hydrovinylation of styrene using a Pd/**4.16** catalyst system

Since 2011, Rocamora and co-workers have published a few more papers on the application of diamidophosphite ligands. In 2014, they described the synthesis of two chiral ionic imidazolium-tagged diamidophosphite ligands **4.21** and **4.22**, their palladium coordination chemistry and their application in asymmetric allylic substitution reactions in neat ionic liquid as a solvent.[3] Best results were obtained using benzylamine as a nucleophile and benchmark substrate **4.06** (Scheme 4.3).

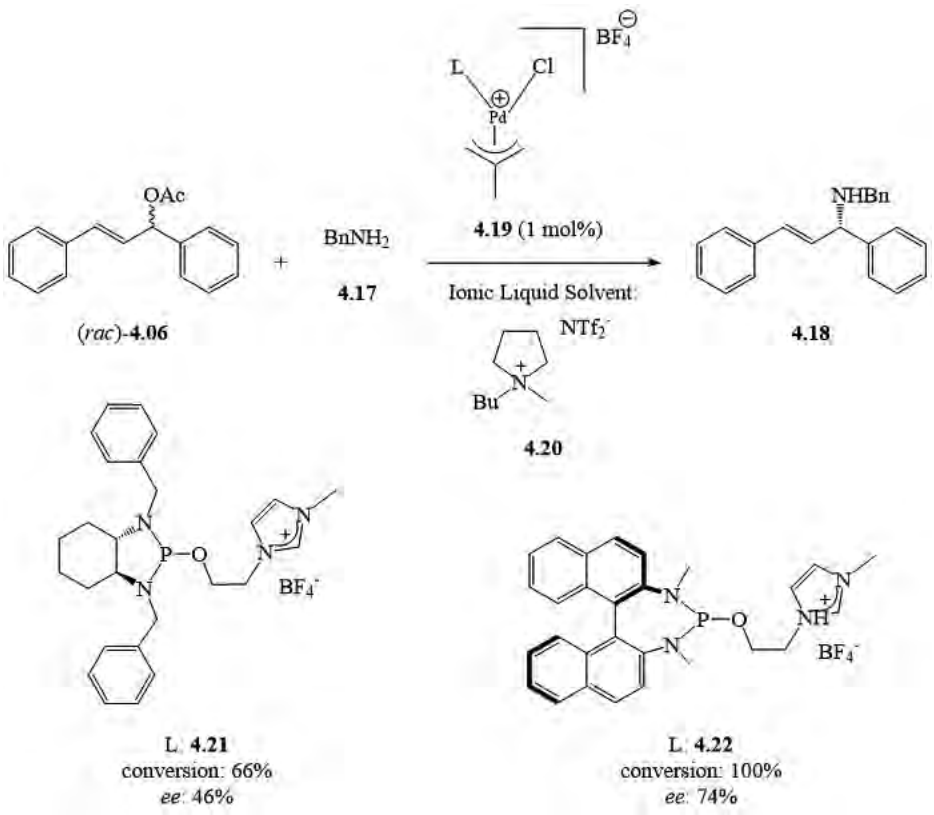

Scheme 4.3 Palladium-catalyzed asymmetric allylic amination using imidazolium tagged chiral diamidophosphite ligands in neat ionic liquids

Another paper was published in 2015, in which they successfully synthesized bidentate (bis)diamidophosphite ligands, with a bridging diol.[4] These ligands were tested in classical palladium-catalyzed asymmetric allylic substitution reactions with carbon nucleophiles as well as amines and in the rhodium-catalyzed hydroformylation of styrene. [4] For the allylic substitution reactions, benchmark substrate **4.06** was converted into the desired products with quantitative yields and enantioselectivities up to 83% *ee* for the alkylation reaction and up to 89% *ee* for the amination. For hydroformylation reactions, the best result was obtained for bidentate ligand **4.25**, however disappointing results were obtained: 46% conversion, 30% *ee* ((*R*)-product) and 68% regioselectivity (Scheme 4.4). Monodentate diamidophosphite ligand **4.16** provided better results for the latter reaction with a conversion of 44%, and an enantiomeric excess of 37% ((*S*)-product) and regioselectivity of 82%. However, it has to be noted that different conditions were applied.

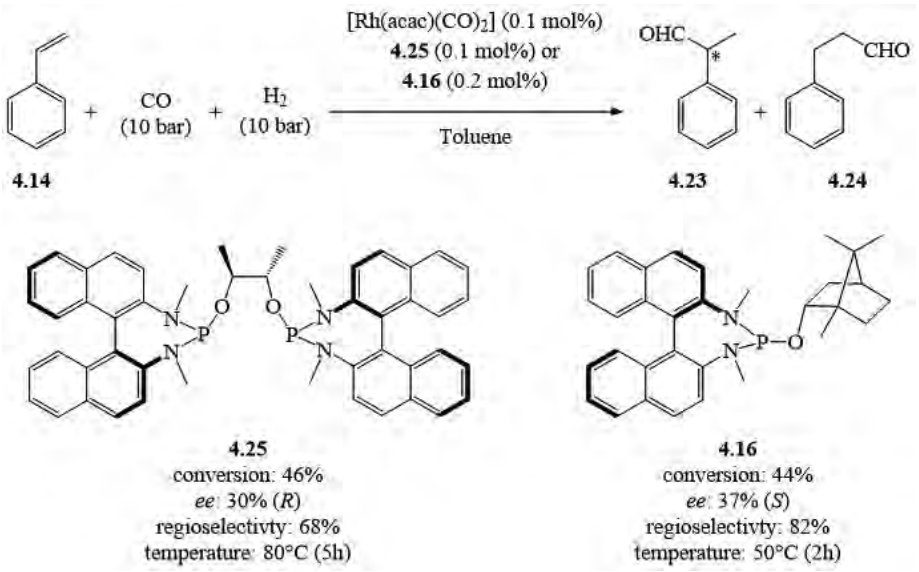

Scheme 4.4 Rhodium-catalyzed hydroformylation of styrene with bidentate and monodentate diamidophosphite ligands **4.25** and **4.16**

Diamidophosphite ligands have also been used by the renowned research group of Trost. They designed a small library of novel bidentate (bis)diamidophosphite ligands derived from (*S*,*S*)-*trans*-1,2-cyclohexanediamine and (2*R*,4*R*)-pentanediol.[21] These ligands were tested in a palladium-catalyzed asymmetric [3+2]-cycloaddition of vinyl-substituted trimethylenemethane (TMM) donor with α,β-unsaturated acyl imidazoles generating tetrasubstituted cyclopentanes bearing three stereocenters (Scheme 4.5).

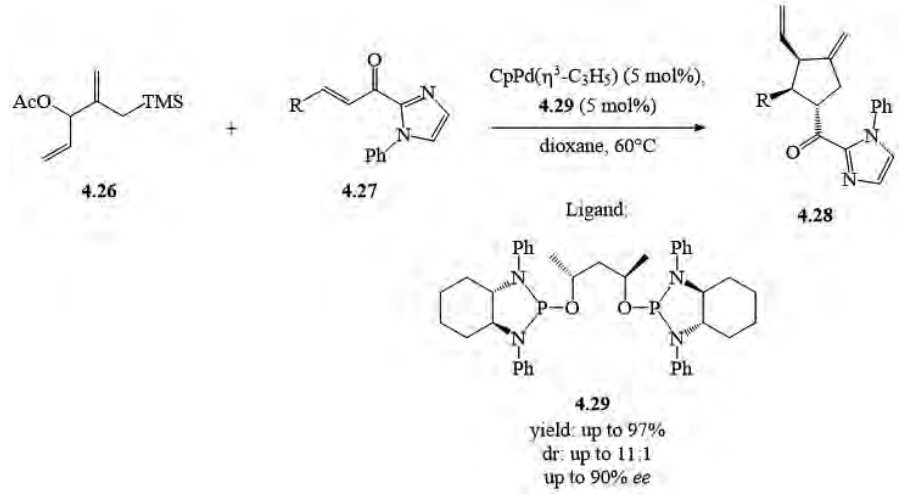

Scheme 4.5 Palladium-catalyzed asymmetric [3+2]-cycloaddition using bidentate diamidophosphite ligand **4.29**

Less successful were the *P**-chiral monodentate diamidophosphite ligands **4.30** and **4.31**, characterized by a binaphthyl aminoalcohol as axial chiral backbone, which have been prepared by Franciò *et al* (Scheme 4.6). [22] Only 4% conversion was obtained in the nickel-catalyzed hydrovinylation of styrene. Consequently, no *ee*-values were reported for these ligands. However, monodentate phosphoramidite **4.32** was successfully applied in this reaction with a conversion of 95% and enantiomeric excess of 95% favoring the (*S*)-product.

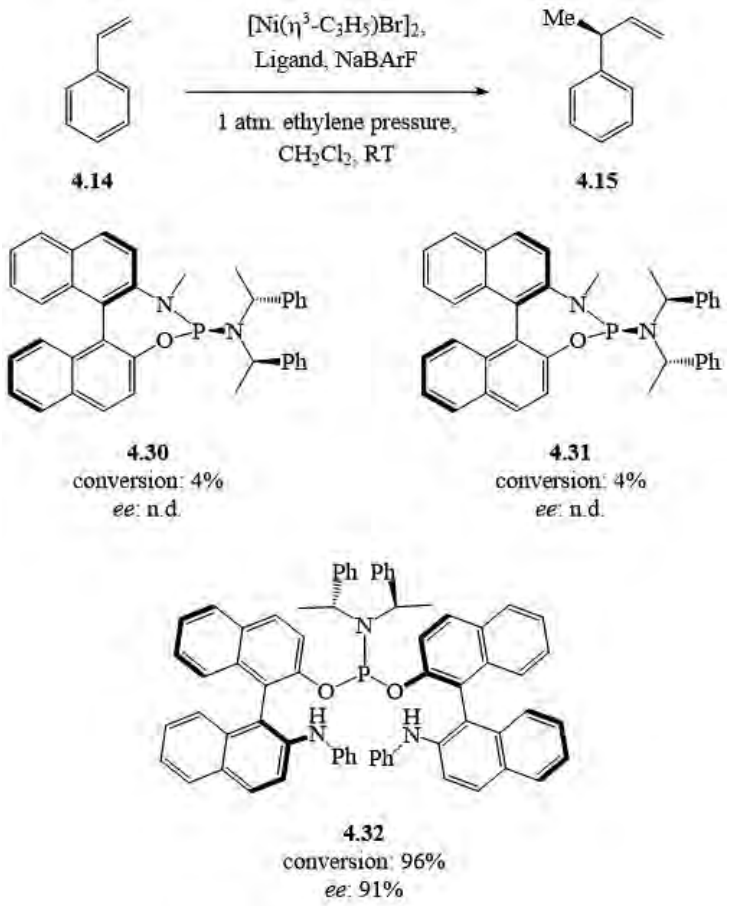

Scheme 4.6 Nickel-catalyzed hydrovinylation of styrene using *P**-chiral monodentate diamidophosphite ligands **4.30** and **4.31** and monodentate phosphoramidite ligand **4.32**

4.2. Retrosynthetic Analysis of Novel Diamidophosphite Ligands

The retrosynthetic analysis of the diamidophosphite ligand library **4.33** is shown in Scheme 4.7.

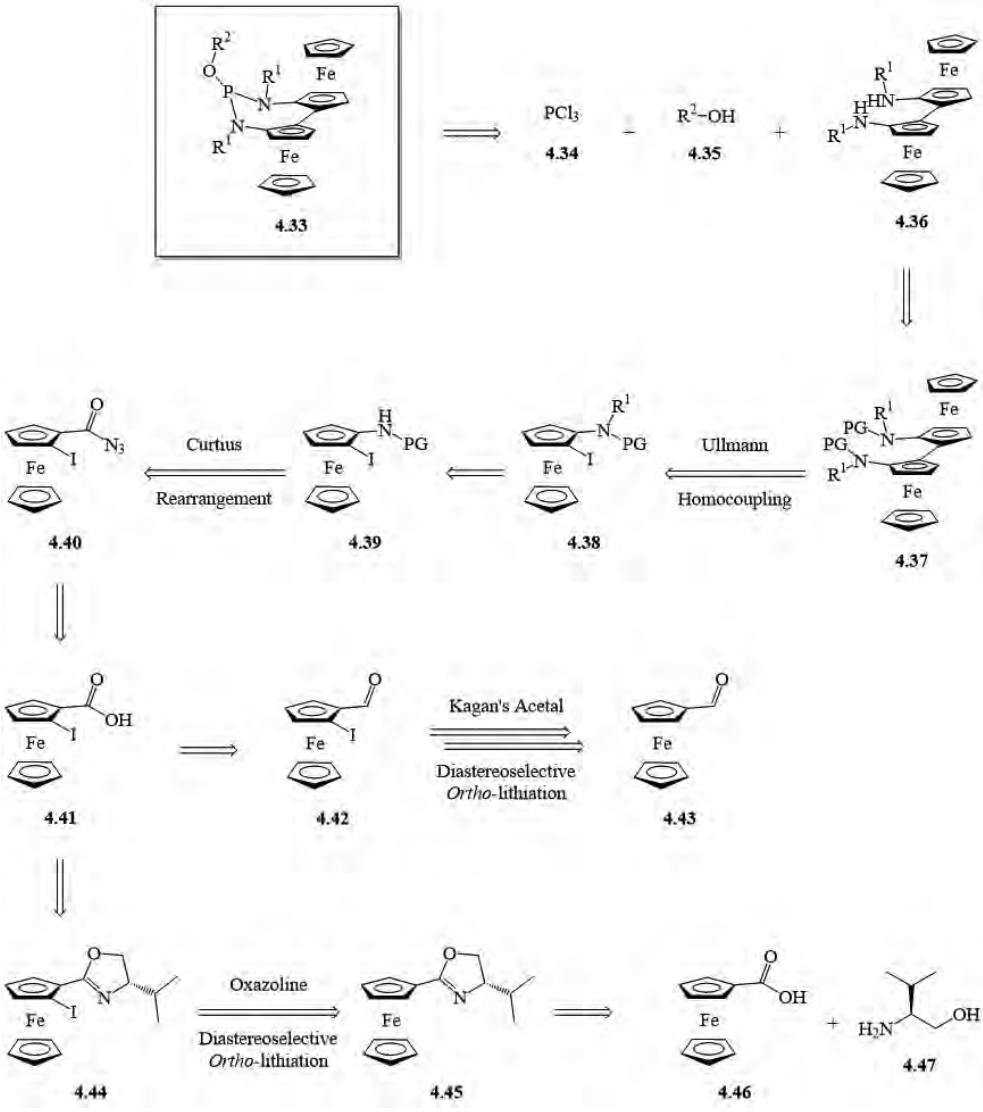

Scheme 4.7 Retrosynthetic analysis of the diamidophosphite ligand library **4.33**

The retrosynthetic analysis starts from disconnecting all bonds around phosphorus giving PCl_3, commercially available alcohols **4.35** and novel biferrocenyldiamines **4.36**.

Consequently, a synthetic route has to be developed for the latter building blocks. A copper mediated Ullmann homocoupling reaction, from ferrocenyliodide **4.39** is proposed for the formation of the biferrocene backbone. As stated earlier, 2,2'-disubstituted-1,1-biferrocenes are combining the elements of planar and axial chirality. As a consequence, the synthesis of a planar-chiral ferrocene moiety will form an important issue for the synthesis of the target diamidiophosphite ligands. To avoid substitutions of the iodine by hydrogen (dehalogenation) during this coupling, protection of the free amine is beneficial. Carbamates are a general and versatile type of protecting groups for amines. Due to the fact that amines are trivalent, the steric bulk can be modified by variation of the alkyl substituents on the nitrogen atom. Compound **4.39** can be obtained via a Curtius rearrangement from ferrocenoylazide **4.40** which can be synthesized from α-iodoferrocenecarboxylic acid **4.41**. Scheme 4.7 shows two potential routes towards this planar-chiral acid. The first one consists of a Pinnick oxidation from α-iodoaldehyde **4.42**, which can be obtained via Kagan's acetal procedure from ferrocenecarboxaldehyde **4.43**.[23] The second method involves hydrolysis of an oxazoline functional group, that will be used as an *ortho*-directing group for *ortho*-metallation to selectively synthesize planar-chiral α-iodoferrocenyloxazoline **4.44**. This methodology was developed independently by Richards[24-25], Sammakia[26-28] and Uemura[29] in 1995. Ferrocenyloxazoline **4.45** can be made in a three-step one-pot reaction via amide formation of ferrocenecarboxylic acid **4.46** and (*S*)-valinol (**4.47**).

4.3. Synthesis of (S_p)-α-Iodoferrocenecarboxylic Acid **4.41** Using Kagan's Chiral Acetal Approach

4.3.1. Synthesis of (S_p)-α-iodoaldehyde **4.42**

The synthesis of this compound is already mentioned in § 3.5.1 (*vide supra*). However, the origin and explanation of the stereo- and regioselectivity will be discussed in this chapter. The selectivity is the key to the successful synthesis of planar-chiral ferrocene-based ligands. A wide variety of protocols to introduce planar-chirality in ferrocene have been developed and recently an excellent review on this topic has been published by Schaarsmidt and Lang.[30] Diastereoselective *ortho*-directed metalation using

chiral auxiliaries is one of the best approaches to synthesize such compounds. One of these successful methods has been developed by Kagan *et al.*[23] A chiral auxiliary derived from malic acid is connected to ferrocenecarboxaldehyde to obtain the desired acetal **4.52** via a three-step procedure[21] (Scheme 4.9).

The chiral methoxy-methyl substituted dioxane will serve as a directing metalation group (DMG) in a selective directed *ortho*-metalation reaction (DoM). The outcome of such reactions is primarily governed by the metal coordination, inductive electron withdrawal and steric effects and is illustrated in Scheme 4.8.[31,32] This mechanism combines the principles of *complex-induced proximity effect*, which relies on pre-lithiation, followed by rate-determining metalation and *kinetically enhanced metalation*, which describes the simultaneous base complexation and proton abstraction.

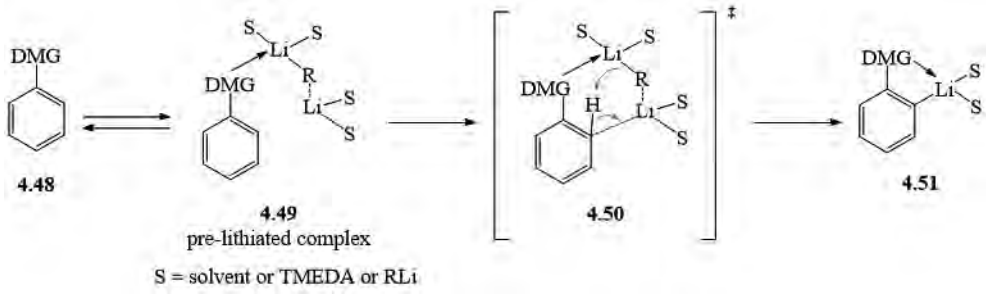

Scheme 4.8 Mechanism of diastereoselective *ortho*-lithiations as reported by Mortier *et al.*[31]

When *t*-BuLi is slowly added to chiral acetal **4.52** at -78°C (or -96°C), specific chelation of lithium by the methoxy group and one of the acetal oxygens occurs, resulting in the formation of a pre-lithiated complex which precipitates.[23b] The subsequent temperature increase dissolves the pre-lithiated species and promotes *ortho*-lithiation with formation of a new precipitate (**4.53-a** and **4.53-b**, Scheme 4.9).

21 The synthesis of the desired acetal **4.52** is discussed in § 3.5.1. In Chapter 3, this acetal is numbered as **3.99**.

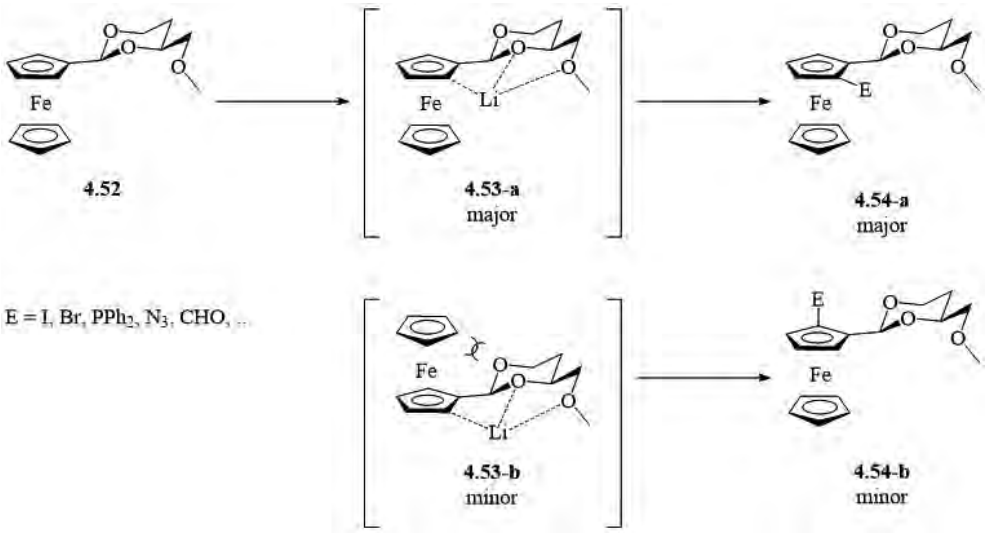

Scheme 4.9 Empirical model explaining the selectivity for the synthesis of planar-chiral disubstituted ferrocenes using Kagan's chiral acetal approach

The discussion of theoretical principles for the diastereoselective deprotonation starts with the assumption of the *cis*-1,3-structure of dioxane **4.52**, with 1,3-diequatorial substituents as most favorable conformation.[23] For the kinetically controlled deprotonation, two competing transition states **4.53-a** and **4.53-b** (Scheme 4.9) have to be considered. Based on molecular models, complex **4.53-b** is disfavored due to the *endo*-orientation of the acetal oxygen, not involved in the chelation. In complex **4.53-a**, this oxygen has an *exo*-orientation towards iron which is therefore the major diastereomeric complex.

Electrophilic quenching of the organo-lithium compound offers a reliable method to introduce a plethora of substituents. The stereoselectivity for the introduction of these substitutents was studied via ^{1}H-NMR by Kagan *et al.* and diastereomeric excess values of >98% are reported.[23] The introduction of the iodine substituent was achieved using 1,2-diodoethane as electrophile. Acetal hydrolysis was performed in a separate step with *para*-toluenesulfonic acid monohydrate (PTSA.H_2O), degassed water and dichloromethane. These conditions were repeated and the enantioselectivity in this thesis was studied via HPLC-analysis of (S_p)-α-iodoaldehyde **4.42** as described in § 3.5 and § 3.9 (*vide infra*). Aldehyde **4.42** could be isolated with reproducible *ee*-values of 93-96%. An alternative approach, in which the lithiation reaction with *t*-BuLi, the introduction of the iodine atom using 1,2-diiodoethane and the acetal hydrolysis were performed in

a one-pot reaction was also applied. The latter step was achieved via addition of a deoxygenated solution of PTSA.H_2O in water to the reaction mixture. Using this methodology, aldehyde **4.42** was obtained without loss in enantioselectiviy and a yield of 83%.

4.3.2. Synthesis of (S_p)-α-iodoferrocenecarboxylic **4.41** using the Pinnick oxidation

To prevent side- and decomposition reactions, the oxidation of ferrocenecarboxaldehydes into their corresponding ferrocenecarboxylic acids requires mild conditions. Therefore it is very challenging to obtain high yields in this type of transformations. However, the Pinnick oxidation affords a mild procedure for the transformation of aldehydes into carboxylic acids (Scheme 4.10).

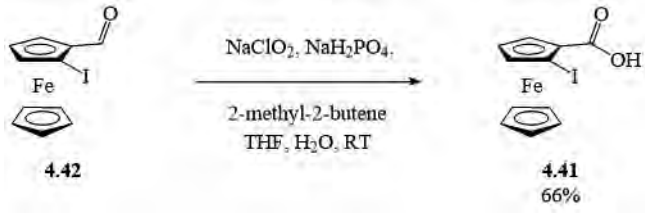

Scheme 4.10 Pinnick oxidation of aldehyde **4.42** to obtain ferrocene carboxylic acid **4.41**

The reaction uses $HClO_2$ as an oxidant which is formed in situ by $H_2PO_4^-$ and $NaClO_2$. During the oxidation reaction, HClO is formed, which is a stronger oxidant than $HClO_2$ itself. The addition of scavengers such as H_2O_2 and 2-methyl-2-butene is therefore recommended. However, when H_2O_2 was used, black reaction mixtures were obtained, indicating the formation of decomposition products. On the other hand, when 2-methyl-2-butene was used, the desired ferrocene carboxylic acid **4.41** was formed successfully. A solvent system that is often applied for the Pinnick reaction is a mixture of water and *t*-butanol. Normal work-up and purification procedures of classical Pinnick oxidations require extractions using strong acid (often 1 M HCl). This protocol, however, was dreadful for the preparation of **4.41** what resulted in the formation of decomposition products. Luckily, **4.41** could be extracted out of the aqueous phase without an extra acidification step. Removal of *t*-butanol generally calls for high temperatures, leading again to decomposition. Finally, the reaction was performed in H_2O/THF and removal of THF after work-up was possible at room temperature. This protocol allowed to isolate iodo-ferrocene carboxylic acid **4.41** with a yield of 66%. From these observa-

tions it is to be concluded that ferrocene carboxylic acid **4.41** is an unstable compound under specific conditions such as (strongly) oxidative conditions and higher temperatures (above 30°C).

4.4. Synthesis of (S_p)-α-Iodoferrocenecarboxylic Acid **4.41** Using the Chiral Oxazoline Approach

4.4.1. Synthesis of ferrocenecarboxylic acid **4.46**

Although ferrocenecarboxylic acid **4.46** is commercially available, it is more or less 500 times more expensive than ferrocene **4.56** itself.[22] Moreover carboxylic acid **4.46** can easily be prepared on a large scale with high yields via a two-step procedure published by Reeves and co-workers (Scheme 4.11).[33] Therefore, it was decided to start the synthesis towards the target ligands from ferrocene itself.

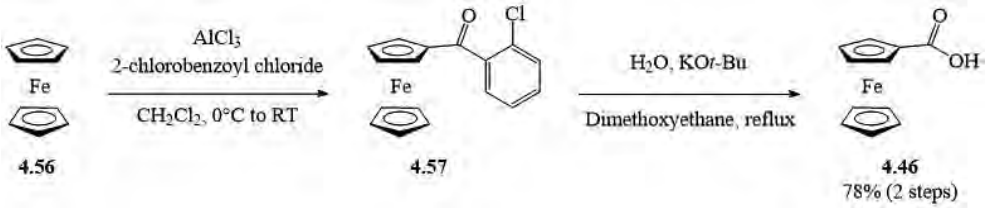

Scheme 4.11 Two-Step synthesis of ferrocenecarboxylic acid **4.46**

The first step is a Friedel-Crafts acylation with 2-chlorobenzoyl chloride and $AlCl_3$ as Lewis acid. Due to the high electron density of ferrocene, it reacts 10^6 times faster than normal benzene.[34-36] The second step is a hydrolysis reaction in which chlorobenzene is kicked out as a leaving group[37]. The conversion of non-enolizable ketones to carboxylic acids can be performed using KO*t*-Bu. The presence of the electron withdrawing *ortho*-chloro substituent on the phenyl ring, enhances the selective cleavage of the 2-chlorophenyl group. This procedure affords a simple methodology for the introduction of a carboxyl substituent onto aromatic rings and ferrocenes. Ferrocenecarboxylic acid **4.46** could be isolated with a yield of 78%. About 5% of ferrocene as well as 2-chlorophenyl ketone **4.57** could be recovered.

22 The price of ferrocenecarboxylic acid is € 58.3 per gram while ferrocene itself costs € 46.7 for 100 gram. (Sigma Aldrich, 04/09/2017).

4.4.2. Synthesis of (*S*)-(4-isopropyl-4,5-dihydrooxazol-2-yl)-ferrocene **4.45**

Ferrocenyl oxazoline **4.45** was synthesized from ferrocenecarboxylic acid **4.46** via a three step, one-pot procedure as published by Arnott *et al.* (Scheme 4.12).[38]

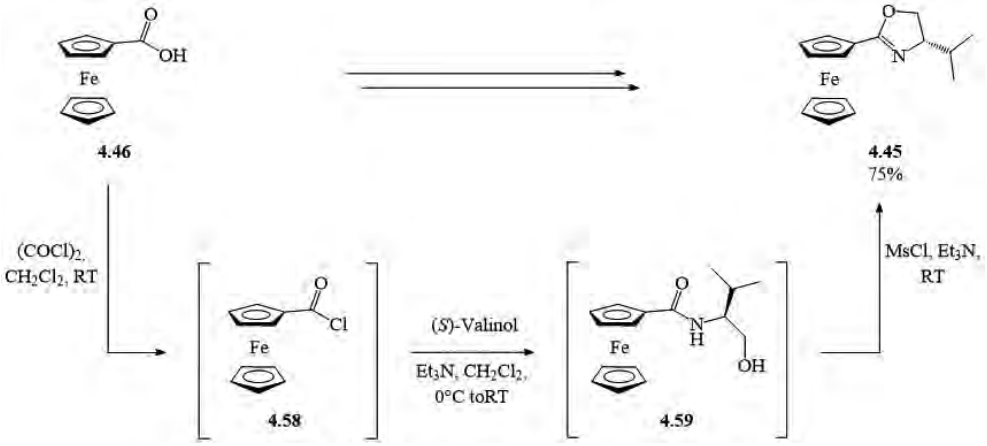

Scheme 4.12 Three-step synthesis of ferrocenyl oxazoline **4.45**

In the first step carboxylic acid **4.46** is converted into acid chloride **4.58**, using oxalyl chloride. Next, the formation of amide **4.59** via nucleophilic attack of the amine functional group of (*S*)-valinol in the presence of triethylamine was accomplished. The free alcohol is transformed into a good leaving group by adding mesylchloride. Under basic conditions (triethylamine), cyclization occurs with formation of oxazoline **4.45**. Using this methodology **4.45** was isolated with a yield of 75%.

Other methodologies for the synthesis of ferrocenyl oxazoline **4.45** are reported as well.[30] One of them is the one-step $ZnCl_2$ Witte-Seeliger condensation of cyanoferrocene and valinol.[29] Alternatives for the synthesis of amide **4.59** involve Weinreb amidation of ethoxycarbonylferrocene.[39] Cyclisation of amide **4.59** to oxazoline **4.45** using Appel conditions are reported as well.[24] In general, these alternatives provide lower yields or require extra purification steps compared to the synthesis procedure shown in Scheme 4.12.

The oxazoline will function as an alternative diastereoselective *ortho*-directing group for the synthesis of planar-chiral disubstituted ferrocene structures.

4.4.3. Synthesis of (S,S_p)-2-(α-iodoferrocenyl)-5-*iso*-propyloxazoline **4.44**

Before describing the experiments that were performed in in order to synthesize oxazoline **4.44**, more historical and theoretical background on the development of oxazolines as diastereoselective *ortho*-directing groups for the synthesis of planar-chiral ferrocene compounds is described.

1.4.1.1. *Historical and theoretical background of chiral oxazolines for the synthesis of planar-chiral ferrocene compounds*

In general, oxazolines have proven to be synthetically useful as directed *ortho*-metalating groups.[32] More specifically chiral oxazolines have shown to be effective as asymmetric inducing agents for a number of transformations.[40] In 1995, Richards[24-25], Sammakia[26-28] and Uemura[29] independently reported on diastereoselective *ortho*-lithiations using oxazolines as directing groups for the synthesis of planar-chiral 1,2-disubstituted ferrocenes.

A comprehensive study of the diastereoselectivity of different ferrocenyloxazolines was accomplished by Sammakia and co-workers.[26-28] In a first paper[26], the selectivity was investigated in function of steric effects via variation of the R-substituent of oxazoline **4.60** (Scheme 4.13). Based on these results, which are shown in Table 4.1, it seems that the diasteroselectivity is governed by steric effects: as the R-group on the oxazoline becomes larger, the selectivity increases, with the *t*-Bu group providing the highest selectivity. For all reactions *s*-BuLi was chosen as a base and there were no additives used. All reactions were carried out using THF as a solvent.

R-substitutent	Diastereoselectivity
Bn	3:1
Ph	6:1
i-Pr	8:1
t-Bu	36:1

Table 4.1 Selectivity values for the diastereoselective *ortho*-lithiation of ferrocenyloxazolines with different R-substituents

The stereochemical outcome of these reactions enforced Sammakia and co-workers to further examine whether the metalation is directed by nitrogen or oxygen.[27-28] Extra experiments with a conformationally constrained 1,1'-bridged-ferrocenyloxazoline showed that the nitrogen atom is responsible for the directive effects. This bridged-ferrocenyl-oxazoline does not allow free rotation around the ferrocene-oxazoline bond and therefore different planar-chiral ferrocenes are observed after trapping the lithiated species whether the nitrogen atom is responsible for the directing effect compared to the oxygen atom. Planar-chiral ferrocene structures derived from an oxygen-directed effect were not observed. These results indicate that lithiation of the unconstrained oxazolines proceeds via nitrogen coordination as well. Moreover, these results allowed to postulate an empirical model to explain the observed diastereoselectivity, which is shown in Scheme 4.13.[27-28] Later on, this model was acknowledged by Richards and Uemura as well.[24,41] Because of nitrogen-directed *ortho*-lithiation, two transition states **4.61-a** and **4.61-b** have to be considered. A first notification is that it seems reasonable to assume that the bulky lithium base approaches the acidic proton from the opposite face of the iron atom, away from the bulk of the ferrocene molecule. For transition state **4.61-b**, the substituent on the oxazoline ring is pointing away from the bulky ferrocene moiety, a favorable conformation at first sight (*cf.* Kagan's chiral acetal method § 4.3.1, *vide supra*). In contrast, for transition state **4.61-a** the substituent on the oxazoline is pointing towards ferrocene. However, the observed stereochemical outcome can only be explained if **4.61-a** is the major conformation in the transition state. On the other hand, in the transition state leading to the minor diastereomer **4.61-b**, there is a severe steric interaction between the alkyl group of the oxazoline and the buthyllitium base. This steric interaction is not observed in the diastereomeric transtition state leading to the major diastereomer since the alkyl group on the oxazoline points towards iron and away from the incoming base. The stereoselectivity is therefore not governed by the interaction between the substituent on the oxazoline and ferrocene but by the interaction of the (bulky) lithiating agent and the substituent on the oxazoline ring.

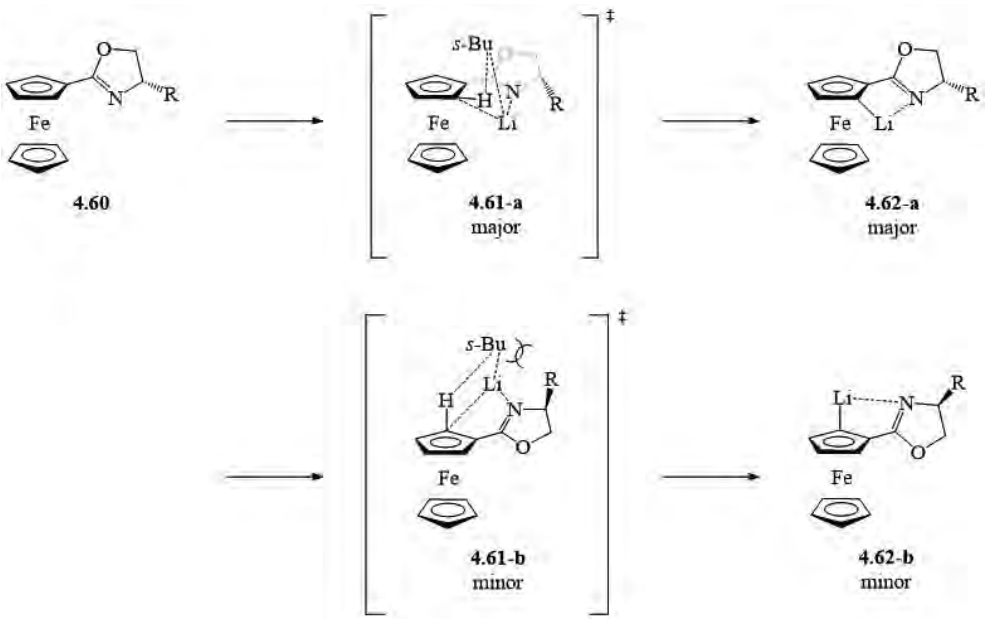

Scheme 4.13 Empirical model explaining the highly diastereoselective *ortho*-lithiation with chiral oxazolines as a directing group

Sammakia and co-workers reasoned that the binding of ligands to the alkyllithium reagent could influence the effective size of the metalating agent and provide greater selectivity. The results of this study are shown in Table 4.2.[27] When additives were used, the choice of solvent seemed to be a major concern: non-coordinating solvents such as hexanes and diethyl ether provided high selectivities whereas THF gave lower diastereoselectvities (entries 1-3). In the latter solvent, the effect of TMEDA (*N,N,N',N'*-tetramethylethylenediamine) is overwhelmed due to the formation of a lithium-solvent complex. Furthermore, for both *i*-Pr and *t*-Bu substituents high diastereoselectivities (>500:1) were obtained using *s*-BuLi as a base, TMEDA as additive and hexanes as solvent system (entry 4 and entry 7). When *n*-BuLi was used as lithiating agent the same diastereoselectivity was obtained for the *t*-Bu, substituent but a significantly lower selectivity was observed for the *i*-Pr substituent (entry 6 and entry 2). These results suggest that an increased steric interaction between the R substituent on the oxazoline and the lithiating agent, favors the major transition state **4.61-a** and can therefore increase the selectivity of the metalation. However, when *t*-BuLi was used as lithiating agent the diastereoselectivity drops for both the *i*-Pr and *t*-Bu substituent (entry 5 and entry 8). This can be attributed to severe steric hindrance between the bulky group of

the oxazoline and the *t*-Bu group of the lithium base preventing reaction via a nitrogen-directed pathway resulting in a reaction via an undirected pathway or oxygen-directed pathway.

Entry	R substituent	RLi	Solvent	Additive	Diastereoselectivity	Yield (%)
1	*i*-Pr	*n*-BuLi	Et_2O	TMEDA	100:1	80
2	*i*-Pr	*n*-BuLi	Hexanes	TMEDA	100:1	75
3	*i*-Pr	*n*-BuLi	THF	TMEDA	3:1	>75
4	*i*-Pr	*s*-BuLi	Hexanes	TMEDA	>500:1	94
5	*i*-Pr	*t*-BuLi	Hexanes	TMEDA	28:1	>75
6	*t*-Bu	*n*-BuLi	Hexanes	TMEDA	>500:1	>75
7	*t*-Bu	*s*-BuLi	Hexanes	TMEDA	>500:1	>75
8	*t*-Bu	*t*-BuLi	Hexanes	TMEDA	34:1	>75
9	Me	*n*-BuLi	Et_2O	TMEDA	>50:1	72
10	Bn	*s*-BuLi	Et_2O	-	93.5:6.5	56
11	Ph	*s*-BuLi	Et_2O	-	>99:1	55

Table 4.2 Optimization of diastereoselective *ortho*-lithiation of ferrocenyloxazolines by varying the R-substituent on the oxazoline

Table 4.2 shows the highest selectivities reported for other substituents as well. Richards and Mulvaney obtained a diastereoselectivity of >50:1 in combination with a yield of 72% for methyl substituted oxazoline **4.60** using *n*-BuLi as base, TMEDA as additive and Et_2O as solvent (entry 9).[24] Experiments with benzyl and phenyl substituents without an additive using *s*-BuLi as the lithiating agent and Et_2O as solvent were performed by Uemura and co-workers.[41] Selectivities of 93.5:6.5 and >99:1 were obtained for the benzyl and phenyl substituent respectively (entries 10-11). However, in both cases, the observed yields are significantly lower. In conclusion, oxazolines with an *i*-Pr and *t*-Bu substituent are excellent diastereoselective *ortho*-directing groups for the synthesis of planar-chiral ferrocenes. High yields and high selectivities were obtained for both substrates when *s*-BuLi was used as lithiating agent in combination with TMEDA as additive and ether or hexanes as solvents.

1.4.2.2. *Synthesis of (S,S$_p$)-2-(α-iodoferrocenyl)-5-*iso*-propyloxazoline **4.44***

Because L-*t*-leucinol is way much more expensive than L-valinol[23], oxazoline **4.45** with the *i*-Pr substituent, synthesized from L-valinol, was chosen for the synthesis of planar-chiral ferrocenes as precursors for the proposed biferreocene-based diamidophosphite ligands. Diastereoselective *ortho*-lithiation of oxazoline **4.45** was achieved using *s*-BuLi as a base and TMEDA as additive (Scheme 4.14). This reaction was performed in Et_2O at -78°C. Diiodoethane ($I(CH_2)_2I$) was again used as electrophile for the introduction of the iodine. Iodo-oxazoline **4.44** seemed to be sensitive towards light and special precautions were necessary (see § 4.9.4, *vide infra*). This allowed to synthesize **4.44** with a yield of 95% and very high diastereoselectivity.

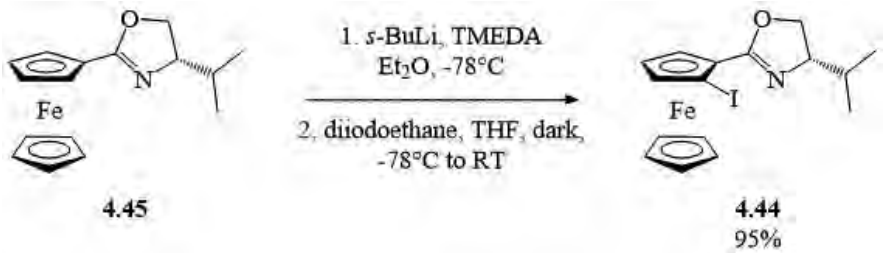

Scheme 4.14 Synthesis of 2-iodo-ferrocenyl oxazoline **4.44**

To study the diastereoselectivity, the reaction was also performed using *t*-BuLi in THF without TMEDA as an additive. Under these conditions a diastereoselectivity of approximately 91:9 was observed. Diastereoselectivities were measured via analytical reversed phase HPLC-MS. Figure 4.4 shows a chromatogram of the analysis of the reaction using *t*-BuLi and THF. Two signals at a retention time of 6.68 min. and 6.89 min. corresponding to both diastereomers ((*S,S$_p$*)-**4.44** and (*S,R$_p$*)-**4.63**) are noticed. Additionally, a single peak is observed using the standard procedure with *s*-BuLi, TMEDA in diethyl ether, illustrating the excellent diastereoselectivity (Figure 4.5).

23 The price for 5 grams of L-*t*-Leucinol and L-Valinol are respectively € 266.0 and € 97.6 (Sigma Aldrich, 04/09/2017).

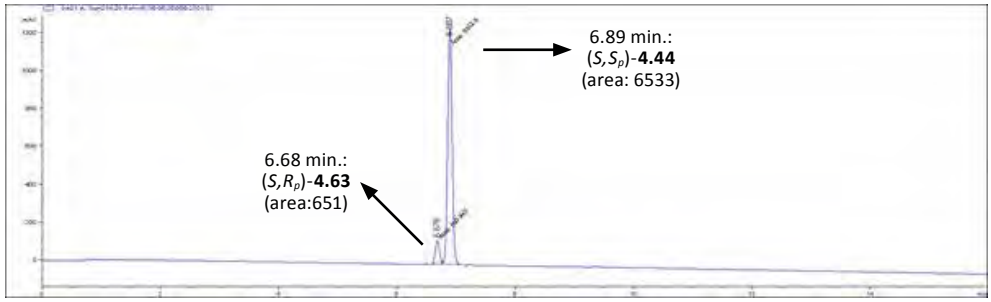

Figure 4.4 Chromatogram reversed-phase HPLC analysis of **4.44** synthesized via diastereoselective *ortho*-lithiation with *t*-BuLi in THF without TMEDA (diastereomeric ratio: 91:9) (Phenomenex Kinetex C18, solvent: method 6, flow rate = 1mL/min., T=35°C)[24]

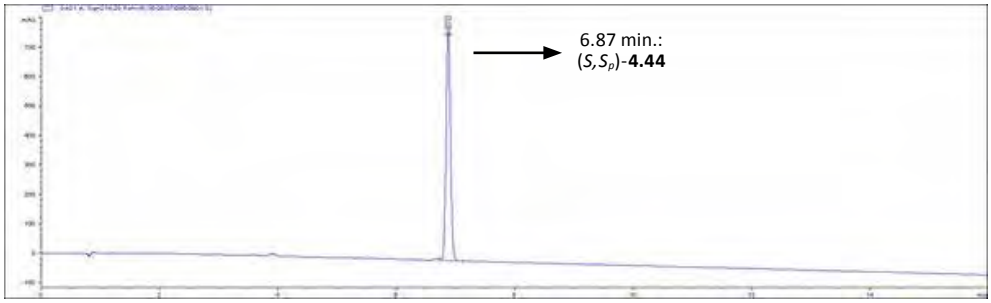

Figure 4.5 Chromatogram reversed-phase HPLC analysis of **4.44** synthesized via diastereoselective *ortho*-lithiation with *s*-BuLi and TMEDA in diethyl ether (single peak) (Phenomenex Kinetex C18, solvent: method 6, flow rate = 1mL/min., T=35°C)[24]

4.4.4. Synthesis of (S_p)-α-iodoferrocenecarboxylic acid **4.41** via hydrolysis of ferrocenyl oxazoline **4.44**

A few synthetic methods for the conversion of 1,2-disubstituted ferrocenyl oxazoline compounds into their corresponding ferrocenylcarboxylic acids have already been published.[42-46] A standard protocol involves a three-step procedure: ring-opening of the oxazoline using TFA and Na_2SO_4 in a solvent mixture of THF/H_2O, followed by acetylation of the primary amine and subsequent hydrolysis of the ester functional group under basic conditions. This method was originally developed for non-ferrocene containing oxazolines by Warshawsky and Meyers.[47] Scheme 4.15 shows the synthesis of ferrocenecarboxylic acid using this protocol. In a first step, ammonium salt **4.64** was formed, which was subsequently acetylated in a one-pot procedure using acetic an-

24 For experimental details see § 4.9.1 and § 4.9.5 (*vide infra*) and § 3.9.1 (*vide supra*).

hydride in the presence of pyridine. This allowed to obtain ferrocenylester-amide **4.65** with a yield of 94%. For the hydrolysis of the ester functional group, different bases such as NaOMe, NaOH and KO*t*-Bu, at different temperatures were successfully applied by different research groups.[28,42-45] In our experiments, a method developed by You and co-workers using NaOH in refluxing THF was applied. This allowed to isolate iodoferrocenecarboxylic acid **4.41** with a yield of 95% from **4.65.** The combined yield over three steps, starting from **4.44** was calculated as 89%.

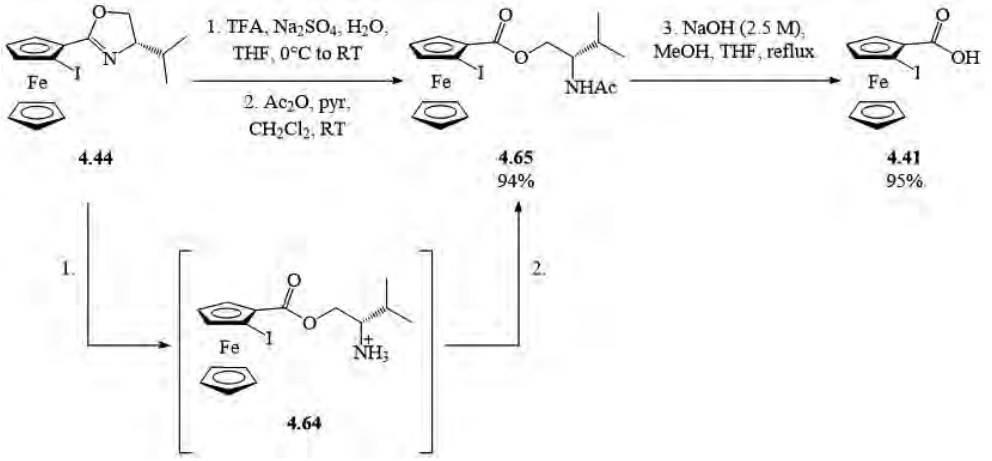

Scheme 4.15 Three-step hydrolysis of 2-iodo ferrocenyl oxazoline **4.44**

An alternative one-pot, two-step procedure, shown in Scheme 4.16, was reported by Ito *et al.* Treatment of iodo-ferrocenyloxazoline **4.44** with methyl trifluoromethanesulfonate (MeOTf) resulted in the formation of oxazolinium salt **4.66**. Subsequent hydrolysis with KOH in refluxing ethanol allowed to isolate iodoferrocenecarboxylic acid **4.41** with a yield of 87% over two steps.

Both methods described above allowed to obtain iodoferrocenecarboxylic acid **4.41** with similar and very good yields. The first method, which involves a three step procedure is somewhat more laborious because purification of intermediate **4.65** is necessary.

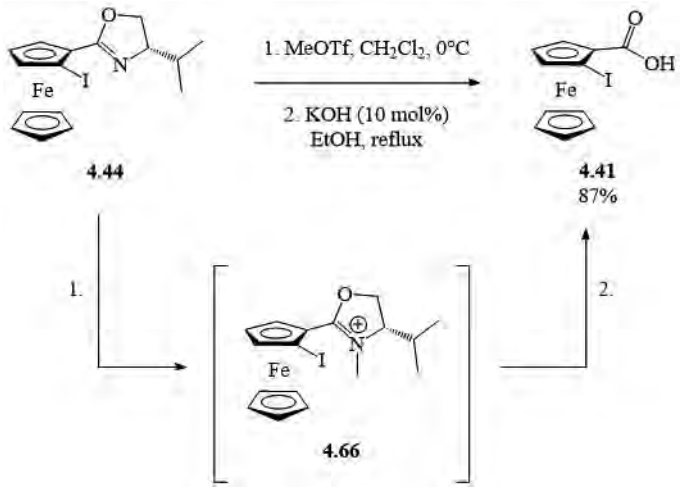

Scheme 4.16 Two-step hydrolysis of 2-iodo ferrocenyl oxazoline **4.44**

4.5. Conversion of (S_p)-α-Iodoferrocenecarboxylic Acid **4.41** into Alkylated Carbamates

Different procedures for the conversion of ferrocenecarboxylic acids into aminoferrocenes via ferrocenyl azide and ferrocenyl carbamate intermediates are already known in literature.[48-53] In general, ferrocenecarboxylic acids are transformed into acid chlorides using standard chlorinating agents like PCl_5, $(COCl)_2$ or $SOCl_2$, frequently activated via a catalytic amount of DMF.[50,53-54] Subsequently, these acid chlorides are reacted with NaN_3, occasionally in the presence of TBAB (tetra-*n*-butylammonium bromide) as a phase transfer catalyst to obtain the desired ferrocenyl azides. A Curtius rearrangement at elevated temperatures results in the formation of the corresponding isocyanates which can be trapped with an alcohol for the synthesis of the corresponding ferrocenyl carbamates. Although benzylalcohol is often used[49-51], other carbamates which function as latent amino groups are known as well.[52-53] Cleavage of these carbamates, via hydrogenolysis in case of benzyloxycarbonyl (cbz) protected amines, allows to obtain ferrocenylamines. However, these electron rich, strongly nucleophilic ferrocenylamines often seem to be air-sensitive compounds.[50]

4.5.1. Synthesis of ferrocenoyl azide **4.40**

Initial experiments for the synthesis of ferrocenoyl azide **4.40** were performed using a methodology described above and shown in Scheme 4.17. A first step involves transformation of carboxylic acid **4.41** is into acid chloride **4.67** using $(COCl)_2$ and a catalytic amount of DMF. Subsequently, **4.67** was reacted with sodium azide to obtain ferrocenoyl azide **4.40**. Unfortunately, low yields (10-25%) were achieved for this two-step procedure.

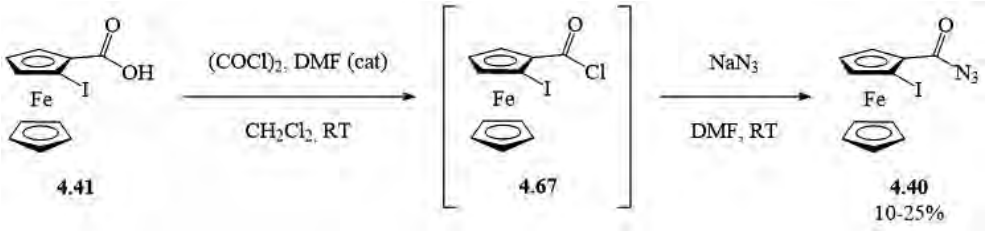

Scheme 4.17 Two-step synthesis of ferrocenoylazide **4.40** from ferrocenecarboxyl acid **4.41** via acid chloride **4.67**

Due to the observed low yields for the transformation of ferrocenecarboxylic acid **4.41** into ferrocenoyl azide **4.40** an alternative procedure had to be developed. A reliable method to convert carboxylic acids into their corresponding acyl azides in one step involves the addition of diphenyl phosphoryl azide (DPPA) in the presence of a base. Reaction of **4.41** with DPPA and Et_3N in acetonitrile allowed to obtain ferrocenoyl azide **4.40**, within 3 hours via a one-step procedure with an excellent yield of 96% (Scheme 4.18).

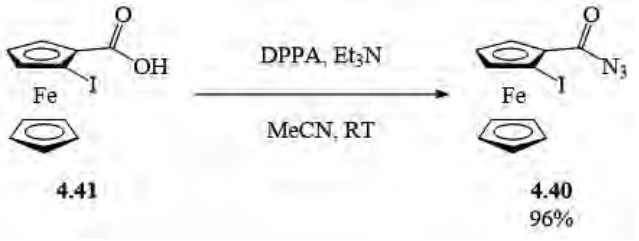

Scheme 4.18 Alternative synthesis of ferrocenoyl azide **4.40** using DPPA

4.5.2. Synthesis of ferrocene carbamate **4.68** via the Curtius rearrangement

The thermal decomposition (or pyrolysis) of acyl azides to the corresponding isocyanates, with loss of nitrogen gas is known as the Curtius rearrangement[55]. If the reaction is carried out in the presence of water, amines are formed via a decarboxylation reaction. Treatment of the *in situ* formed isocyanates with alcohols or amines allows to synthesize carbamates and ureas respectively. Scheme 4.19 illustrates the performed reaction for the formation of ferrocenyl carbamate **4.68** via a Curtius rearrangement. In a first step ferrocenoyl azide **4.40** is rearranged upon heating (105°C in toluene) into the corresponding isocyanate. After 10 to 15 min. the formation of nitrogen gas stopped and the reaction was quenched with 4-methoxybenzylalcohol. The reaction is fast and allows to synthesize **4.68** with a yield of 95% within only 4 hours.

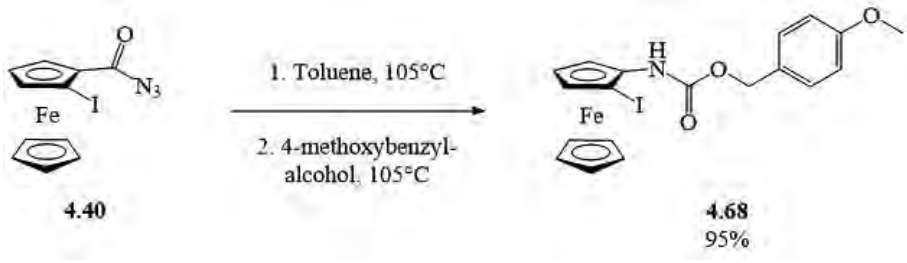

Scheme 4.19 Synthesis of ferrocenyl carbamate **4.68** via Curtius rearrangement and trapping with 4-methoxybenzylalcohol

Because ferrocenyl carbamate **4.68** is a highly stable molecule, it perfectly allows to compare the enantioselectivities obtained via Kagan's acetal procedure with those obtained via the chiral oxazoline approach. Moreover, this is the last step before a first diversification via the introduction of different R-groups on the nitrogen atom (*cf.* retrosynthetic analysis § 4.2, *vide supra*) towards a small ligand library. Chiral HPLC is the method of choice for the separation of enantiomers of planar-chiral ferrocene compounds. The chromatograms of ferrocenyl carbamate **4.68** obtained via the chiral acetal and chiral oxazoline approaches are shown in Figure 4.6 and Figure 4.7 respectively. The enantiomeric excess obtained via Kagan's chiral acetal diastereoselective *ortho*-lithiation is 93.3%, which is significantly lower than the one obtained via the oxazoline diastereoselective *ortho*-lithiation (>99%)

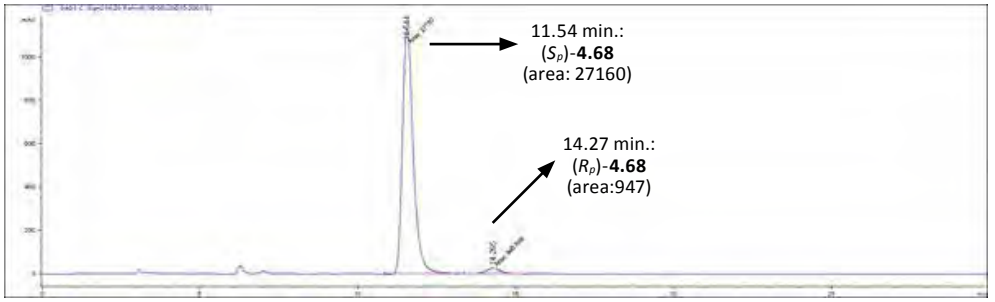

Figure 4.6 Chromatogram chiral HPLC analysis of ferrocenyl carbamate **4.68** obtained via Kagan's chiral acetal approach (Chiralcel OD-H column, solvent: *n*-hexane/EtOH (97:3), flow rate = 1mL/min, t = 30 min., T = 35°C)[25]

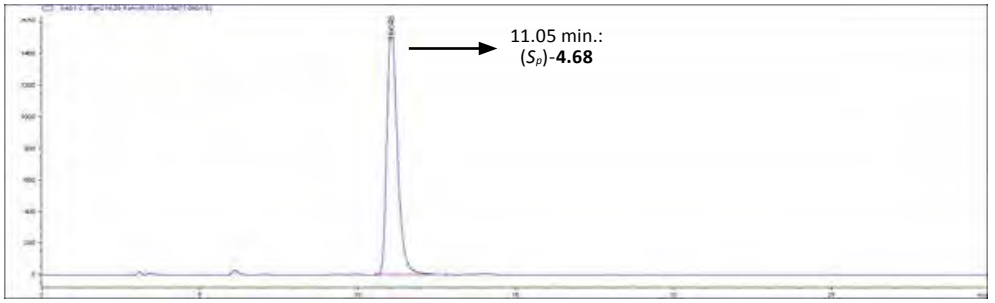

Figure 4.7 Chromatogram chiral HPLC analysis of ferrocenyl carbamate **4.68** obtained via the oxazoline approach (Chiralcel OD-H column, solvent: *n*-hexane/EtOH (97:3), flow rate = 1mL/min, t = 30 min., T = 35°C)[25]

4.5.3. Alkylations of ferrocene carbamate **4.68**

To study the influence of steric and electronic parameters regarding the central phosphorus donor atom in ligand series **4.33**, the introduction of certain substituents on nitrogen are proposed (Figure 4.8). The different alkyl chains will allow to explore the steric effects whereas the fluoroalkylsubstituents will significantly modify the electronic properties as well.

25 For experimental details see § 4.9.1 and § 4.9.8 and § 3.9.1

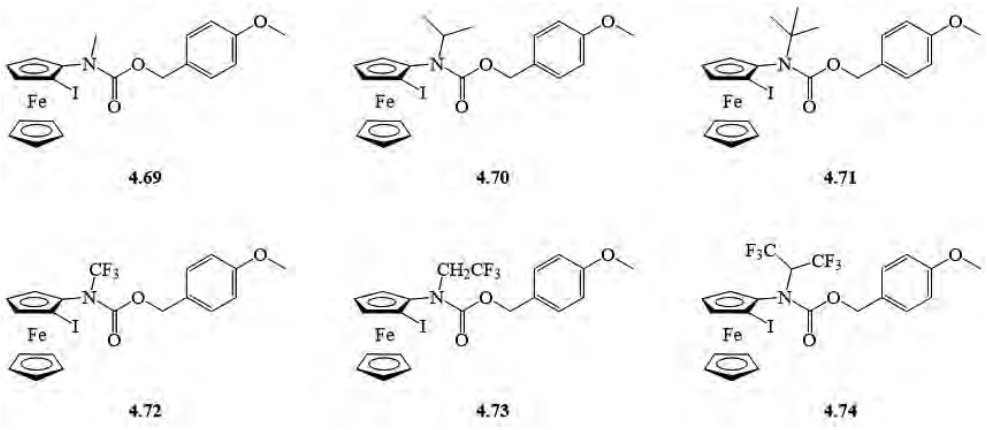

Figure 4.8 Proposed substituents to explore steric and electronic properties of the target ligands

Methylated ferrocenyl carbamate **4.69** could easily be synthesized via abstraction of the carbamate proton with sodium hydride and subsequent quenching with iodomethane in THF (Table 4.3). However, when these conditions were applied for the synthesis and of *i*-Pr and *t*-Bu carbamates **4.70** and **4.71**, no conversion was observed. Using DMF instead of THF made it possible to synthesize *i*-Pr substituted carbamate **4.70** with a yield of 55% (Table 4.3). It is important to note that the level of full conversion was not obtained using these conditions. Because it was impossible to separate *i*-Pr-carbamate **4.70** from starting material **4.68** via classical silica gel chromatography, the unreacted fraction of carbamate **4.68** in the obtained mixture was transformed into Me-carbamate **4.69** as described. Changing the solvent from THF to DMF for the synthesis of the severely sterically hindered ferrocenyl *t*-Bu-carbamate **4.71** did not succeed. This was mechanistically expected because S_N2-reactions with *tert*-butyl halides are not successful. As a consequence ferrocenyl carbamate **4.71** was not obtained.

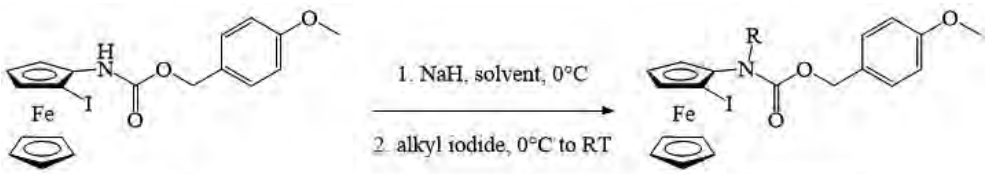

Target carbamate	Substituent	Solvent	Yield (%)
4.69	Me	THF	99
4.70	*i*-Pr	THF	0
4.71	*t*-Bu	THF	0
4.70	*i*-Pr	DMF	55
4.71	*t*-Bu	DMF	0

Table 4.3 Results for the alkylation of ferrocenyl carbamates **4.69-4.71**

The same methodology was applied for the introduction of fluoroalkyl groups on carbamate **4.68**: deprotonation with NaH and quenching with the corresponding fluoroalkyl iodides. For the introduction of the least-sterically hindered trifluoromethyl substituent, THF was chosen as a solvent, whereas DMF was applied for the most steric hexafluoropropan-2-yl substituent. Unfortunately no conversion was observed for both reactions, Table 4.4. Moreover, the introduction of a trifloroethyl group for the synthesis of ferrocenyl carbamate **4.73** was tested in THF as well as DMF, but for both reactions there was no conversion observed neither. Therefore, it is concluded that this methodology is not suitable for the introduction of the proposed fluoroalkyl substituents. Consequently, the influence of electronic effects was not studied in this research project.

Target carbamate	Substituent	Solvent	Conversion (%)
4.72	CF_3	THF	0
4.73	CH_2CF_3	THF	0
4.73	CH_2CF_3	DMF	0
4.74	$CH(CF_3)_2$	DMF	0

Table 4.4 Results for the fluroralkylations of ferrocenyl carbamates **4.72-4.74**

4.6. Synthesis of Biferrocene Carbamates **4.75** and **4.79**

As described in § 3.7.1 the Ulmann homocoupling reaction provides an excellent method for the synthesis of biferrocene structures. More specific, for small scale reactions, the homocoupling reaction using CuTC allowed to synthesize biferrocene dialdehyde **3.107** (§ 3.7.1, *vide supra*) with an acceptable yield of 59%. Similar to iodoaldehyde **4.42** (**3.96**, § 3.7.1), ferrocenyl carbamates **4.69** and **4.70** are characterized by a substituent possessing a lone-pair in the *ortho*-position which is beneficial for its reactivity.[56] However, the presence of a bulky group in the *ortho*-position tends to retard or inhibit the coupling reaction due to steric hindrance.[56] It should be mentioned that the homocoupling reaction of iodoferrocenes was initially optimized using carbamate **4.69** as a substrate. An overview of the applied conditions is shown in Table 4.5. When carbamate **4.69** was reacted with CuTC in NMP at room temperature, biferrocene carbamate **4.75** was isolated with a yield of 50% (entry 1). Nevertheless, the reaction went to full conversion and the formation of side products **4.76** and **4.77** (Figure 4.9) was observed.

Increasing the equivalents of CuTC, temperature and reaction time (entries 2-5) did not allow to increase the yield nor to suppress the formation of side products. Moreover, at 130°C (entry 6) there were no ferrocene compounds present in the reaction mixture based on TLC-analysis. Instead, black decomposition products were observed. Performing the reaction under microwave conditions was not beneficial either (entries 7-9).

There was no conversion obtained when the copper source was switched to CuI in DMF as solvent and a temperature of 70°C (entries 10 and 11). Decomposition products were again formed at 130°C (entry 12).

Nickel(0)-mediated homocoupling reactions, based on a procedure developed by Semmelhack for the synthesis of biaryl compounds[57], allowed to synthesize biferrocene carbamate **4.75** only in trace amounts at 40°C and 60°C using conventional heating and 0.5 equivalents of $Ni(cod)_2$ (entries 13-14). When this reaction was performed under microwave conditions at 70°C the yield increased to 35% (entries 15-16). Decomposition products were again formed at 130°C (entry 17).

The experiment using finely divided metallic copper at 70°C did not give any conversion (entry 18). However, when a similar reaction was performed at 105°C, dicarbamate

4.75 could be isolated with a good yield of 82% even though full conversion was not obtained (entry 19). A trace amount of dehalogenated side product **4.76** was identified via LC-MS. Again, the drawback of this methodology was the significantly lower yield obtained when the reaction was performed on small scale (generally less than 500 mg). Increasing the amounts of copper from 3 to 5 equivalents did not lead to an increased conversion (entry 20).

Dehalogenated side product **4.76** was generally formed in trace amounts and was identified via LC-MS. Its formation is explained by the presence of minimal amounts of protic impurities (solvents) in the reaction mixture. Application of the CuTC approach resulted in a maximum yield of 52% when fresh anhydrous NMP was used. However, it was experimentally observed that the amount of dehalogenated product **4.76** increases, with a higher amount of water present in the solvent. Consequently, the yield of the target product **4.75** decreases with a lower quality grade of NMP.

Side product **4.77** was isolated with a yield of 40-45% (entries 1-5 and 7-8) and was identified via LC-MS and ^{1}H-NMR. Its formation can be explained mechanistically. After oxidative addition of iodocarbamate **4.69** to CuTC, a copper(III) complex with ferrocenyl and thiophene carboxylate as organic ligands is formed. Reductive elimination enforced by the bulky ferrocenyl ligand structure results in the heterocoupling reaction of these ligands with formation of side product **4.77**. This step involves the formation of CuI.

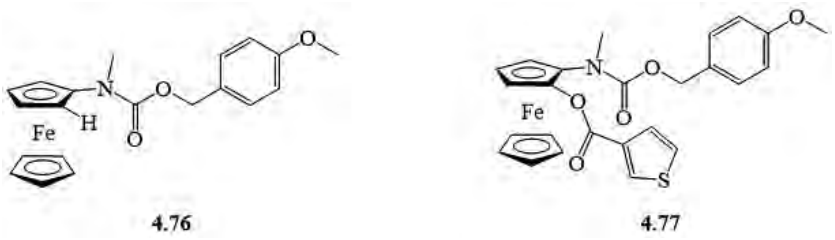

Figure 4.9 Side products identified for the Ullmann homocoupling reaction of substrate **4.69** to biferrocene dicarbamate **4.75**

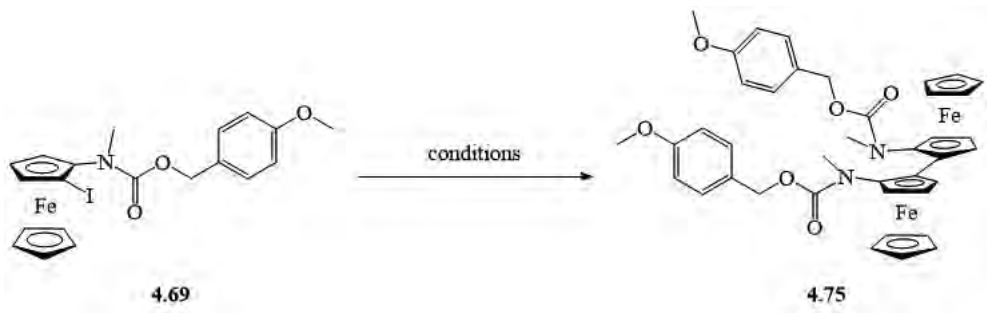

Entry	Metal source	eq	Solvent	Temperature (°C)	Time (h)	Microwave (250W)	Results
1	CuTC	3	NMP	20	3	No	50% yield + side products
2	CuTC	3	NMP	20	16	No	50% yield + side product
3	CuTC	5	NMP	20	3	No	50% yield + side products
4	CuTC	5	NMP	20	16	No	50% yield + side products
5	CuTC	3	NMP	70	16	No	50% yield + side products
6	CuTC	3	NMP	130	16	No	Decomposition
7	CuTC	3	NMP	70	4	Yes	50% yield + side products
8	CuTC	3	NMP	70	16	Yes	50% yield + side product
9	CuTC	3	NMP	130	16	Yes	Decomposition
10	CuI	3	DMF	70	4	Yes	No conversion
11	CuI	3	DMF	70	16	Yes	No conversion
12	CuI	3	DMF	130	4	Yes	Decomposition
13	$Ni(cod)_2$	0.5	DMF	40	24	No	Traces
14	$Ni(cod)_2$	0.5	DMF	60	24	No	Traces
15	$Ni(cod)_2$	0.5	DMF	70	4	Yes	35% yield + **4.69**
16	$Ni(cod)_2$	0.5	DMF	70	24	Yes	35% yield + **4.69**
17	$Ni(cod)_2$	0.5	DMF	130	4	Yes	Decomposition
18	Cu	3	/	70	16	No	No conversion
19	Cu	3	/	105	16	No	82% yield + **4.69** + **4.76**
20	Cu	5	/	105	16	No	82% yield + **4.69** + **4.76**

Table 4.5 Optimization table for the synthesis of biferrocene dicarbamate **4.75**

For the synthesis of biferrocenedialdehyde **3.107** a statistically inexplicable ratio of possible stereoisomers was formed and this intrinsic resolution was accepted as an important advantage for the synthesis of enantiopure monodentate phosphoramidite ligands (*cf.* 3.7.1, *vide infra*). Therefore, similar experiments were performed for the synthesis of biferrocene dicarbamate **4.77**. First, a racemic mixture of carbamate **4.69** was reacted with CuTC to obtain three stereoisomers: one achiral *meso*-isomer ((*R*$_p$,*S*$_p$)-**4.78**) and two enantiomers ((*R*$_p$,*R*$_p$)-**4.75** and ((*S*$_p$,*S*$_p$)-**4.75**). In contrast to the stereoisomers of dialdehyde **3.107** (and **3.110**), practical separation of the *meso*-compound from its two diastereomers was not possible via classical silica gel chromatography for dicarbamates **4.75** and **4.78**. Analytical chiral HPLC analysis allowed to separate those three isomers. Figure 4.10 shows a chromatogram of a chiral HPLC analysis of biferrocene dicarbamates **4.75** and **4.78**. It can be seen that the ratio of the isomers is approximately equal to the statistically expected 1/1/2 distribution. Therefore, an intrinsic resolution step as observed for the copper-mediated synthesis of dialdehyde **3.107** does not occur for the copper-mediated synthesis of dicarbamate **4.75**. Consequently, it is very important that biferrocene dicarbamates can be synthesized as enantiomerically pure compounds.

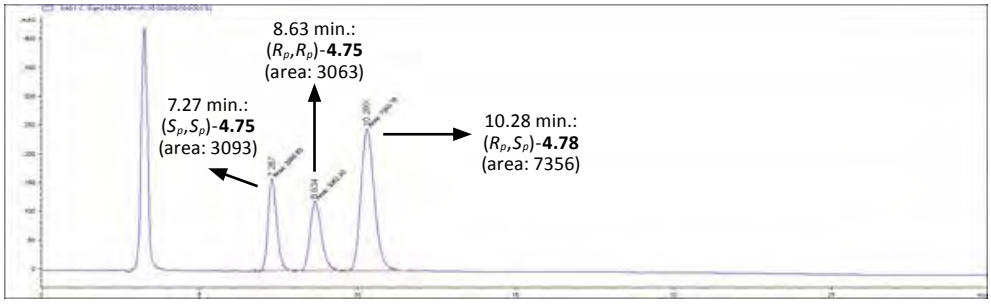

Figure 4.10 Chromatogram of a chiral HPLC analysis of biferrocene dicarbamates **4.75** and **4.79** starting from racemic **4.69**. A 1/1/2 ratio is observed. (Chiralcel OD-H column, solvent: *n*-hexane/EtOH (80:20), flow rate = 1mL/min, t = 30 min., T = 35°C)[26]

The chromatograms for the Ullmann couplings of ferrocenyl carbamate **4.69** synthesized via Kagan's chiral acetal approach and the diastereoselective *ortho*-lithiation using chiral oxazoline **4.45** are shown in Figure 4.11 and Figure 4.12 respectively. The first chromatogram shows that three isomers have been formed with (*R*$_p$,*R*$_p$)-**4.75** as the major compound. The isomeric ratio's for this compound have been calculated as 0.9/94.6/4.5.

26 For experimental details see § 3.9.1, § 4.9.1 and § 4.9.11.

These ratios are very close to those statistically expected for ferrocenyl carbamate **4.69** with an enantiomeric excess of 93-94%. In the second chromatogram there are only two peaks observed. The major compound is again (R_p,R_p)-**4.75** A very small signal corresponding to *meso*-compound (R_p,S_p)-**4.78** is noticed but there is no signal observed for isomer (S_p,S_p)-**4.75**. The ratio of the observed diastereoisomers has been calculated as 0.99/0.01. These results confirm that the chiral oxazoline approach is the method of choice for the synthesis of enantiomerically pure diamidophosphite ligands **4.33**.

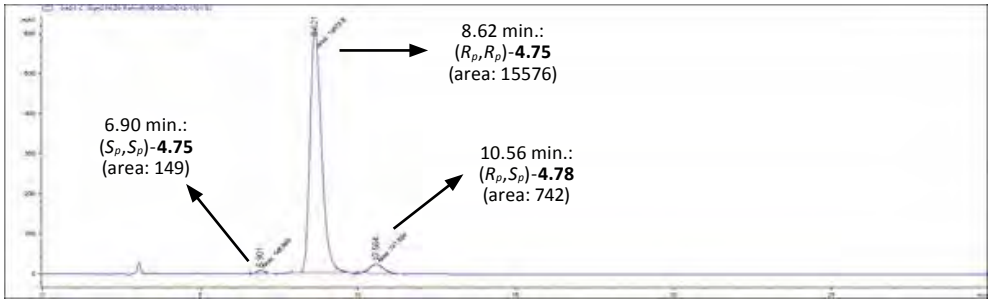

Figure 4.11 Chromatogram of a chiral HPLC analysis of biferrocene dicarbamates **4.75** and **4.78** starting from carbamate **4.69** obtained via Kagan's chiral acetal approach. (Chiralcel OD-H column, solvent: *n*-hexane/EtOH (80:20), flow rate = 1mL/min, t = 30 min., T = 35°C)[27]

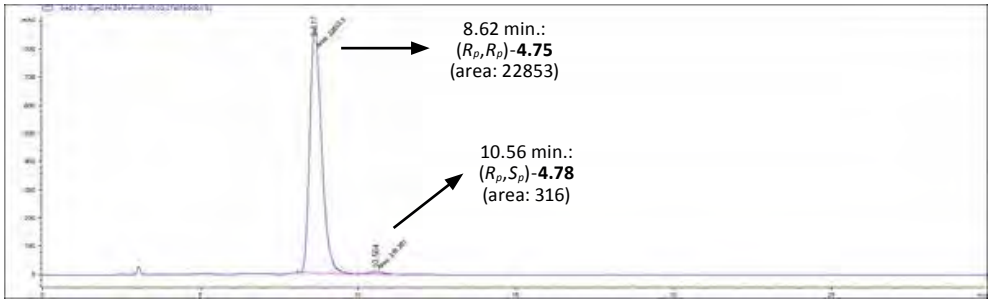

Figure 4.12 Chromatogram of a chiral HPLC analysis of biferrocene dicarbamates **4.75** and **4.78** starting from **4.69** obtained via the oxazoline approach. (Chiralcel OD-H column, solvent: *n*-hexane/EtOH (80:20), flow rate = 1mL/min, t = 30 min., T = 35°C)[27]

Previous experiments for the homocoupling of **4.69** have shown that two methods, one with CuTC and one with metallic copper, were practically useful for the synthesis of biferrocene dicarbamate **4.75**. Therefore these conditions were tested for the production of di-*iso*-propyl-dicarbamate biferrocene **4.79** starting from **4.70** (Scheme 4.20). Again, best yields, up to 72%, were obtained using metallic copper for larger scale reactions. For the procedure using CuTC at room temperature a yield of 48% was obtained.

27 For experimental details see § 3.9.1, § 4.9.1 and § 4.9.11.

Compared to the synthesis of biferrocene *N*-Me substituted dicarbamate **4.75**, *N*-*i*-Pr-substituted dicarbamate **4.79** was obtained in slightly lower yields. This can be explained by a more severe steric effect of the *i*-Pr group. In analogy with compounds **4.76** and **4.77** (Figure 4.9) side products **4.80** and **4.81** (Figure 4.13) were observed for this homocoupling reaction. The amount of ferrocenyl thiophene ester **4.81** was slightly higher compared to the formation of its *N*-Me substitued analogue **4.77** which is again explained by the steric effect of the *i*-Pr group.

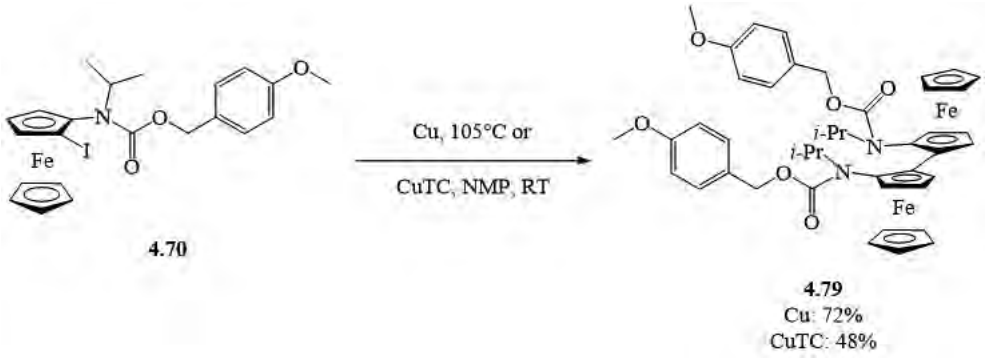

Scheme 4.20 Synthesis of biferrocene dicarbamate **4.79**

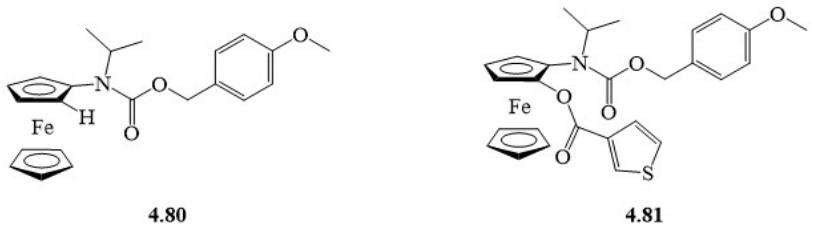

Figure 4.13 Side products identified for the Ulmann homocoupling of substrate **4.70** to biferrocene dicarbamate **4.79**

4.7. Two-step Synthesis of Diamidophosphite Ligand Series **4.33**

4.7.1. Carbamate deprotection for the synthesis of biferrocene diamines **4.82** and **4.83**

Biferrocene dicarbamates **4.75** and **4.79** were easily deprotected using TFA in dichloromethane (Scheme 4.21). *N*-Me substituted biferrocene diamine **4.82** was obtained in pure form, via trituration of the obtained crystals with a minimal amount of acetone

and a subsequent trituration with a minimal amount of diethyl ether, affording a yield of 67%. Unfortunately, this purification method was not successful for the synthesis of diamine **4.83**. Therefore, silica gel chromatography was necessary, which allowed to isolate **4.83** with a yield of 89%. In order to prevent decomposition of **4.83** it was important to add 2% triethylamine in the eluent system. It was also experimentally observed that biferrocene diamines **4.82** and **4.83** are sensitive towards degradation in air. This phenomenon was earlier noticed for other ferrocenylamines by Togni *et al.* as well.[50] It is also worthwhile to mention that diamines **4.82** and **4.83** are novel compounds, not described in scientific literature.

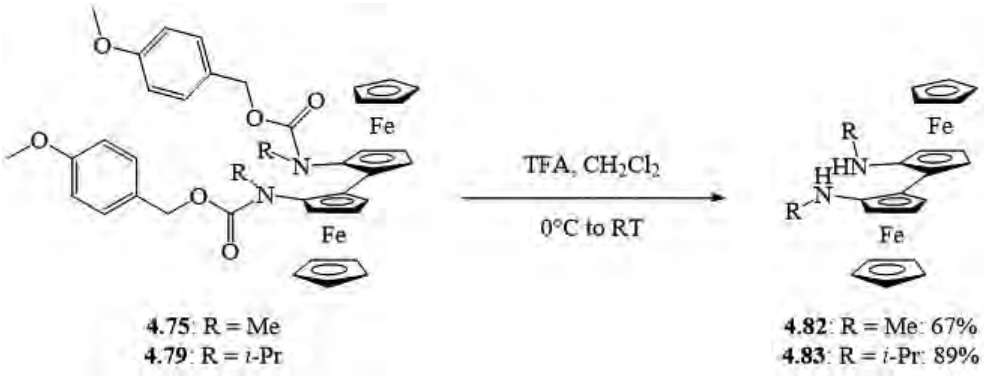

Scheme 4.21 TFA deprotection of biferrocene carbamates **4.75** and **4.79** for the synthesis of biferrocene diamines **4.82** and **4.83**

4.7.2. Alternative synthesis towards biferrocene diamines **4.82** and **4.83**

An alternative retrosynthetic analysis for biferrocene diamines **4.36** is illustrated in Scheme 4.22. This strategy involves the synthesis of iodo-ferrocenyl amines **4.84** as precursor for the Ulmann homocoupling reaction. This reaction will now be the last step before the synthesis of the diamidophosphite ligands. It is always strategically interesting to perform homocoupling reactions at the end of a synthetic sequence because partial transformations, with formation of troublesome side products will be avoided using this approach.

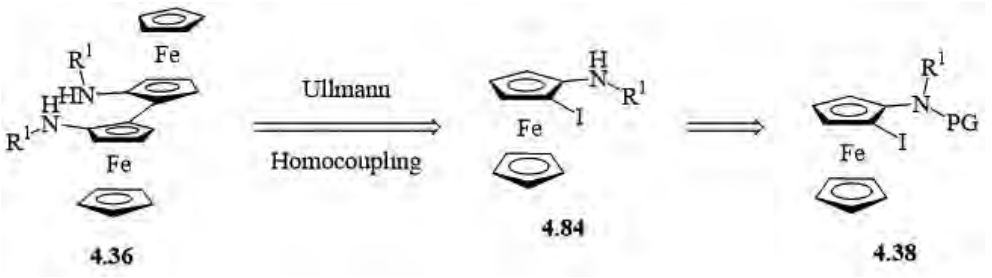

Scheme 4.22 Retrosynthetic analysis for the alternative synthesis of **4.36**

An attempt to synthesize iodo-ferrocenylamine **4.85** using the TFA/DCM procedure as described before is illustrated in Scheme 4.23. However, the formation of **4.85** was not observed and a black reaction mixture indicating the production of decomposition products was obtained.

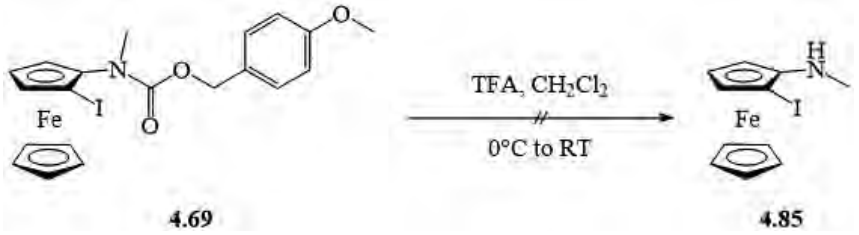

Scheme 4.23 Attempt to synthesize iodo-ferrocenyl amine **4.85**

In literature it is known that oxidative decomposition of highly electron rich ferrocenes, such as **4.85** and hydroxyferrocene, has hampered the use and synthesis of ligands possessing such properties.[50,58] Although hydroxyferrocene is stable under inert atmosphere, it was shown that radical decomposition occurs in the presence of oxygen with formation of Fe_xO_y and cyclopentadienone. In a similar way cyclopentaketimines are formed from ferrocenylamines. Similar experiments with *i*-Pr carbamate **4.70** were not performed but the formation of similar decomposition products is expected.

4.7.3. Synthesis of biferrocene-based diamidophosphite ligands

One of the goals of this research project is to synthesize a small library of different phosphoramidite ligands for both biferrocene diamine backbones **4.82** and **4.83** via variation of the alcohol substructure of the target ligand class family. In general, the methodology for the synthesis of diamidophosphites is the same as these for phospho-

ramidites, and three synthetic pathways are possible (*cf.* Chapter 3, § 3.7.4., Scheme 3.25). Two of these involve the use of PCl_3 as electrophilic phosphorus source in the presence of a base such as Et_3N or DIPEA in a suitable organic solvent, e.g. toluene. For the synthesis of the diamidophosphite ligands, initial experiments were performed according to method A, using *N*-Me substituted biferrocene diamine **4.82** as starting material. Solutions of Et_3N and PCl_3 were carefully added at 0°C, stirred for 2 hours at room temperature, followed by addition of *iso*-propanol (Scheme 4.24). Unfortunately, diamidophosphite ligand **4.87** was not formed but another remarkable ferrocene-based compound was isolated.

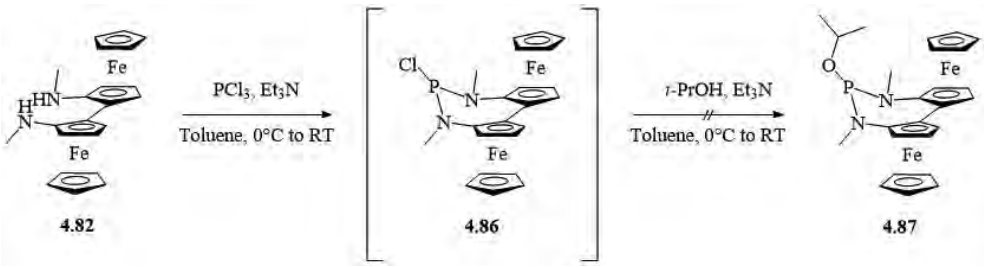

Scheme 4.24 Synthesis towards diamidophosphite ligand **4.87** using PCl_3, Et_3N and *i*-PrOH

In the decoupled ^{31}P-NMR spectrum one signal at 8.04 ppm was observed. This is a characteristic value for a $R(X)_2P{=}O$ double bond, where X is represents a heteroatom and R an alkyl group or hydrogen. More interesting is the ^{1}H-NMR spectrum, that is shown in Figure 4.14. The signals at 8.15 and 6.14 ppm are peculiar and each of these integrates for half a proton. Therefore it is assigned as a doublet, integrating for one proton, with a scalar coupling of 601 Hz. This is a typical value for a $^{1}J_{PH}$ which is the evidence for the presence of a P-H single bond in the molecule. Moreover, the sum of the integration for the peaks between 4.07 and 4.49 ppm is 16 protons. Ten of these are assigned as the protons of two non-substituted cyclopentadiene rings. Six of them belong to two cyclopentadiene rings, each with a 1,2-disubstitution pattern. Signals found between 3.04 ppm and 3.13 ppm integrate together for 6 protons and are assigned as two methyl substituents, one on each nitrogen atom. These signals are identified as two doublets (one at 3.06 ppm and one at 3.12 ppm), both with a $^{3}J_{PH}$ value of 8.67 Hz.

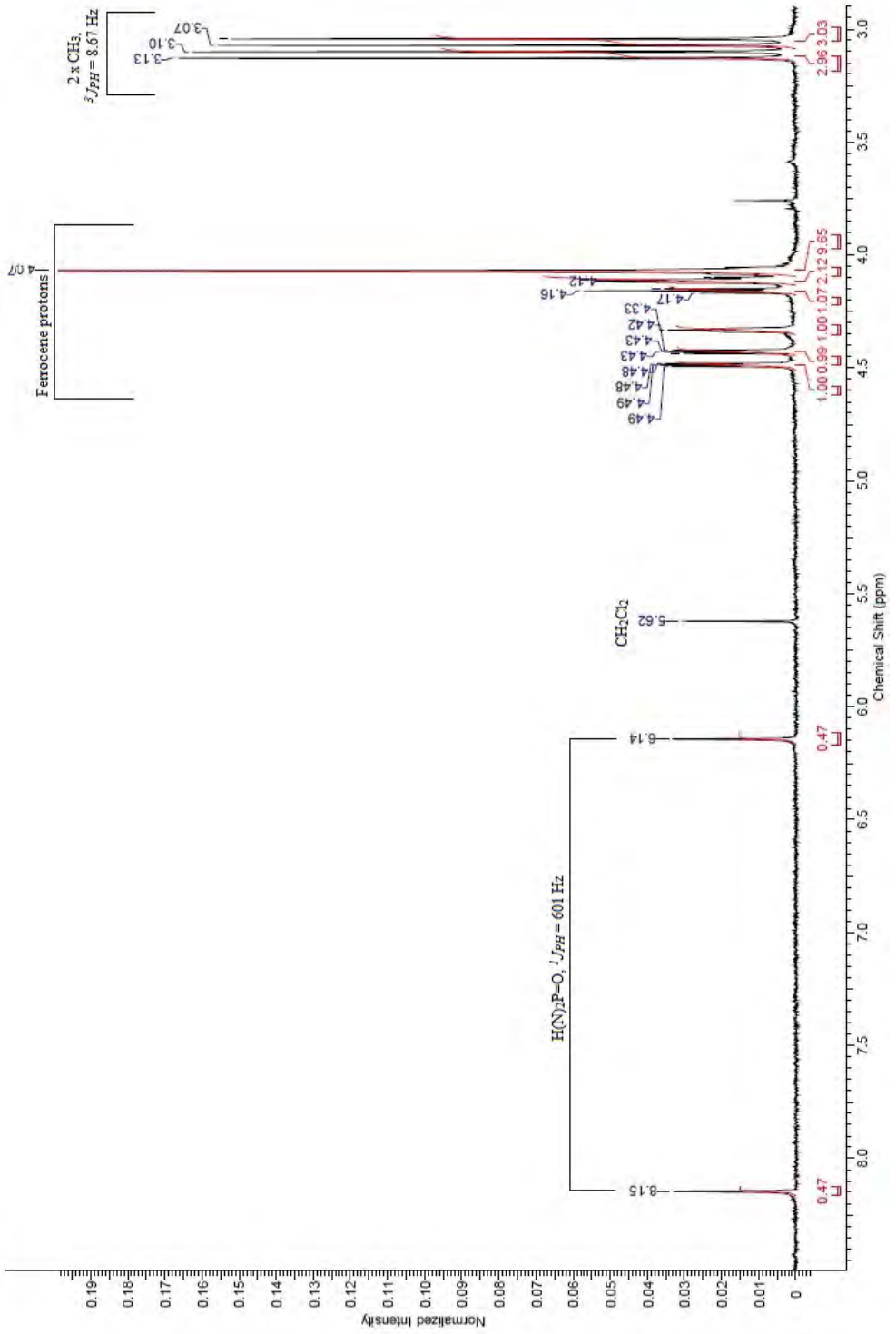

Figure 4.14 ^{1}H-NMR spectrum of the remarkable biferrocene-based compound **4.88** isolated from the reaction illustrated in Scheme **4.24**

Based on the analysis described above the side product formed from the reaction in Scheme 4.24 can be identified as DIAPHOX (diamino phosphineoxide) **4.88** which is shown in Figure 4.15. Extra evidence was obtained via an XRD experiment performed on a suitable single crystal obtained via slow evaporation of a 50/50 acetone/water mixture. The outcome is shown in Figure 4.15 via a three dimensional representation. Two explanations are possible for the formation of **4.88**. The first one is partial hydrolysis of PCl_3 with formation of $HP(O)Cl_2$, which itself reacts with biferrocene diamine **4.82**. An alternative explanation is the hydrolysis of intermediate **4.86** (Scheme 4.24).

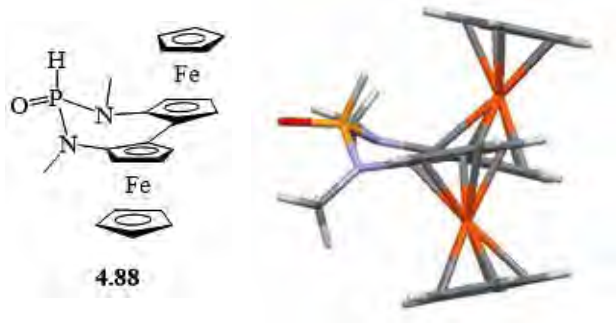

Figure 4.15 (a) Left: biferrocene DIAPHOX **4.88** formed as side-product via the reaction illustrated in Scheme 4.24 **(b)** Right: 3D representation of the X-ray diffraction structure of DIAPHOX **4.88**

The formation of side product **4.88** can be avoided using a methodology in analogy to pathway B of Scheme 3.25 (*cf.* Chapter 3, § 3.7.4, *vide supra*). This involves the synthesis of alkyldichlorophosphites via a reaction between (freshly distilled) PCl_3 and the desired alcohol in the presence of a base (e.g. Et_3N). Interestingly, methyldichlorophosphite ($(CH_3O)PCl_2$) and ethyldichlorophosphite ($(CH_3CH_2O)PCl_2$) are commercially available, what simplifies the practical synthesis protocol in the laboratory. When performing these experiments, high yields were obtained for the synthesis of *N,N'*-dimethyl-substituted ligands **4.89** and **4.90** (73% and 71% respectively, Scheme 4.25). However, low yields were obtained for *N,N'*-di-*iso*-propyl substituted ligands **4.91** and **4.92** (22% and 17% respectively). This significant difference can be explained by the severe sterical effect of the *iso*-propyl substituent. The yields obtained for the *O*-Et diamidophosphite ligands are also slightly lower compared to the obtained yields for the *O*-Me substituted ligands.

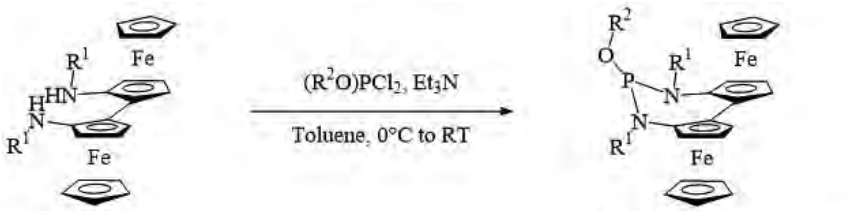

4.82: R^1 = Me
4.83: R^1 = *i*-Pr

4.89: R^1 = Me, R^2 = Me: 73.4%
4.90: R^1 = Me, R^2 = Et: 71.2%
4.91: R^1 = *i*-Pr, R^2 = Me: 22.1%
4.92: R^1 = *i*-Pr, R^2 = Et: 17.0%

Scheme 4.25 Successful synthesis of a small library of diamidophosphite ligands using methyl- and ethyldichlorophosphites instead of PCl_3

It was found that diamidophosphite ligands **4.89**-**4.92** are rather sensitive towards oxidation when exposed to air. This phenomenon was not observed for biferrocene-based phosphoramidite ligands **3.129**-**3.131** described in Chapter 3 (*cf.* Scheme 3.26, § 3.7.4, *vide supra*) and can be explained via the difference in electronic properties between both structure families. Phosphorus centers of phosphoramidites are relatively electron poor, due to the presence of two electron withdrawing oxygen atoms and only one electron donating nitrogen atom. In comparison, the phosphorus centers of diamidophosphites are relatively electron rich due to their bonding to two nitrogen atoms and only one oxygen atom. These observations are also confirmed when chemical shifts of decoupled ^{31}P-NMR spectra of biferrocene-based phosphoramidite ligands **3.129**-**3.131** are compared with those from biferrocene-based diamidophosphite ligands **4.89**-**4.92**. The phosphoramidite ligands, synthesized in Chapter 3, are characterized by a chemical shift value of approximately 145 ppm. Relatively large differencens are observed between *N,N'*-dimethyl substituted dimidophosphite ligands **4.89**-**4.90** and *N,N*-di-*iso*-propyl substituted diamidophosphite ligands **4.91**-**4.92**. Chemical shift values around 130 ppm and 105 ppm are observed respectively. Lower chemical shift values indicate a higher electron density on phosphorus and consequently, these compounds are more sensitive towards oxidation.

Single crystals suitable for X-ray analysis were easily obtained for diamidophosphite ligands **4.90** and **4.92** after chromatographic purification and removal of the solvents under reduced pressure. The three dimensional representation of *N,N'*-dimethyl substituted diamidophosphite **4.90** is shown in Figure 4.16 (a). More interesting is the crystal structure of *N,N'*-di-*iso*-propyl substituted diamidophosphite **4.92** shown in Figure 4.16

(b). Two conformationally different 3D structures are present in the crystal lattice. The differences are subtle and are mainly focused on the orientation of one of the unsubstituted cyclopentadiene rings of one ferrocene fragment. However, ^{1}H-NMR analysis revealed that the unsubstituted cyclopentadiene ring appears, as one regular singlet meaning that there is free rotation of this five-membered ring in solution.

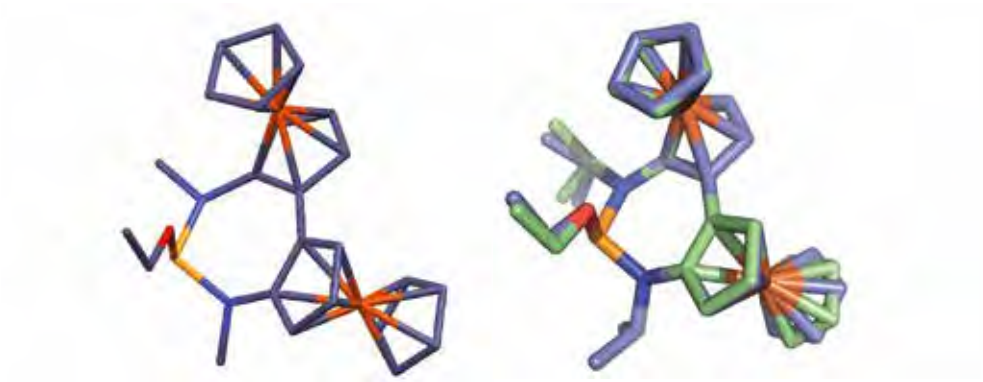

Figure 4.16 (a) Left: X-ray structure of biferrocene-based diamidophosphite ligand **4.90 (b)** Right: X-ray structure of biferrocene-based dimidophosphite ligand **4.92**. (Hydrogen atoms are omitted)

Further discussion of the conformational characteristics of both crystal structures will be performed based on ORTEP-drawings, shown in Figure 4.17. For *N,N'*-di-*iso*-propyl substituted diamidophosphite ligand **4.92** the 3D structure with an eclipsed ferrocene is selected because this one has the highest conformational similarity with the eclipsed ferrocene conformation observed in the crystal structure of *N,N'*-dimethyl substituted diamidophosphite ligand **4.90**. When both crystal structures are compared it can easily be seen that the *iso*-propyl substituents are effectively creating more steric bulk around the central phosphorus center because the hydrogen atom is oriented towards the ferrocene moiety or away from phosphorus. A second important observation is the nearly coplanar arrangement of the connected cyclopentadiene rings of **4.90** and **4.92**. Consequently, the coloured seven-membered ring systems in Figure 4.17 possess an envelope-like conformation with local C_1-symmetry. Furthermore, the ethoxy substituents on phosphorus are found in the axial position. Therefore, the conformational 3D structures of both biferrocene-based diamidophosphite ligands are very similar to the conformational 3D structures of biferrocene-based diazepine *P,N*-type ligands **3.61**-**3.71**, reported by Widhalm *et al.*, and discussed earlier in § 3.3 (*cf.* Figure 3.6, Figure 3.7 and Figure 3.8, *vide supra*).[59]

Despite these common properties of biferrocene structures containing a seven-membered ring system, some interesting remarks have to be made. A concise overview of some interesting (torsion) angles are shown in Figure 4.17 and Table 4.6.

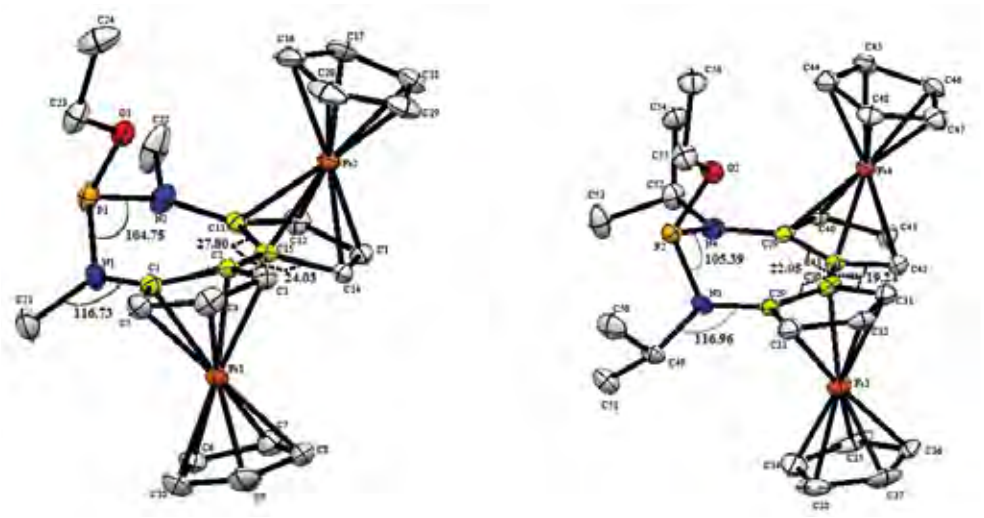

Figure 4.17 (a) Left: ORTEP drawing of diamidophosphite ligand **4.90 (b)** ORTEP drawing of diamidophosphite ligand **4.92** (Hydrogen atoms are omitted)

Ligand	Torsion Angle	(°)	Ligand	Torsion Angle	(°)
4.90	C1-C2-C15-C11	27.80	**4.92**	C29-C30-C43-C39	22.05
4.90	C3-C2-C15-C14	24.03	**4.92**	C31-C30-C43-C42	19.24
Ligand	**Angle**	**(°)**	**Ligand**	**Angle**	**(°)**
4.90	C1-N1-C21	116.73	**4.92**	C29-N3-C49	116.96
4.90	C1-N1-P1	121.71	**4.92**	C29-N3-P2	121.96
4.90	C21-N1-P1	117.73	**4.92**	C49-N3-P2	118.19
4.90	C11-N2-C22	115.39	**4.92**	C39-N4-C52	115.89
4.90	C11-N2-P1	127.21	**4.92**	C39-N4-P2	126.96
4.90	C22-N2-P1	113.96	**4.92**	C52-N4-P2	114.72
4.90	N1-P1-N2	104.75	**4.92**	N3-P2-N4	105.94
4.90	N1-P1-O1	101.93	**4.92**	N3-P2-O2	101.94
4.90	N2-P1-O1	97.64	**4.92**	N4-P2-O2	98.75

Table 4.6 Important torsion angles and angles measured from the crystal structures of **4.90** and **4.92**

First, the influence of the *N,N'*-dialkyl substituents on the torsion angles of the biferrocene fragments is unexpected. The torsion angle C1-C2-C15-C11 of *N,N'*-dimethyl substituted **4.90** (27.80°) is more than 5 degrees larger than the corresponding torsion angle C29-C30-C43-C39 of **4.92** with the more bulky *N,N'*-di-*iso*-propyl substituents (22.05°). It is obvious that a similar difference is observed when torsion angles C3-C2-C15-C14 and C31-C30-C43-C42 are compared, although both absolute values are slightly smaller than the torsion angles inside the seven membered ring-systems. Another interesting observation is the hybridization of the nitrogen atoms. As can be seen, all these values are almost similar to 120° indicating sp^2-hybridization. In contrast, the phosphorus centers of **4.90** and **4.92** are sp^3-hybridized with angles around 102°.

XRD-analysis provides incontestable evidence for the determination of the absolute stereochemistry. Based on the rules developed by Schlögl, all planar-chiral ferrocene fragments, illustrated in Figure 4.17 are assigned as R_p. Therefore, diamidosphosphite ligands can be labeled as (R_p,R_p)-**4.90** and (R_p,R_p)-**4.92**. Due to the torsion angles observed between the connected cyclopentadiene structures, biferrocene-based diamidophosphite ligands possess axial chirality. In literature, palladium- and ruthenium-bifep complexes, synthesized by the research group of Weissensteiner *et al.*, are assigned by stereodescriptors (*P*) and (*M*).[60] This assignment was possible due to the results obtained via XRD experiments. In analogy to their assignment, the biferrocene unit of ligands **4.90** and **4.92** adopts a (*P*)-shaped configuration which corresponds to the axial chiral (*S*)-configuration. This chirality axis is inherently related to the planar-chirality of the ferrocene units. It is worthwhile to have a discussion on the chiral aspects of the phosphorus coordination center based on Figure 4.18 as well. This center is not connected to four different atomic groups so the interchange of the lonepair (which is also considered as an atomic group) and the ethoxy group does not create a different isomer (structures **4.90** and **4.94** are the same molecules). Therefore this phosphorus center is astereogenic. But the mirror image of **4.90**, which is **4.93**, is not superposable on its original structure. Therefore, there is no S_n-axis present in this molecule, and the phosphorus atom is chirotopic.

In conclusion, diamidophosphite ligands **4.90** and **4.92** possess two planar-chiral ferrocene units with (R_p)-configuration, which are connected with the formation of a biferrocene axially-chiral substructure having the (*S*)-configuration (or (*P*)-shaped-configuration)) and the central phosphorus is a chirotopic, astereogenic center.

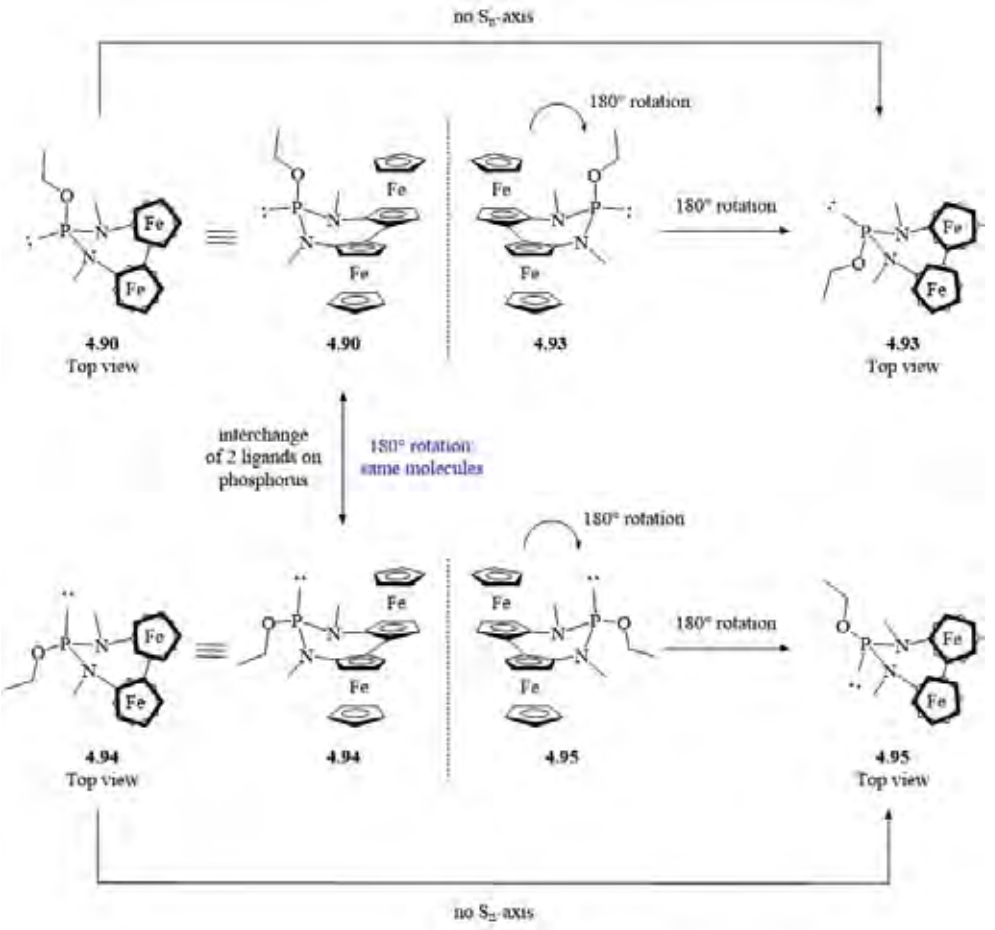

Figure 4.18 Elucidation of a chirotopic astereogenic phosphorus center in biferrocene diamidophosphite ligand **4.90**

4.8. Rhodium(I)-Catalyzed Asymmetric Hydrogenations

The general considerations, mechanistic aspects and origin of stereoselectivity for the rhodium-catalyzed asymmetric hydrogenation of prochiral olefins possessing a second coordinating group are explained in full detail in Chapter 3, § 3.8.1 (*vide supra*). In contrast to phosphoramidite ligands, diamidophosphites are much less frequently applied for this type of transformations. Therefore, a short overview of the diamidiphosphite ligands that were already tested in Rh-catalyzed hydrogenations of functionalized olefins is given in § 4.8.1. The results of the novel biferrocene-based diamidophosphite ligands developed in this thesis are discussed in § 4.8.2.

4.8.1. Reported diamidophosphite ligands used for the hydrogenation of prochiral olefins

In 2003 the research group of Reetz reported on the synthesis of a novel class of monodentate ligands characterized by a binapthyldiamine backbone.[6] These include the diamidophosphite ligands that are shown in Figure 4.19. Both ligands were tested in the hydrogenation of benchmark substrate dimethylitaconate **4.98** (Scheme 4.26). However, a very low conversion (<10%) was obtained with ligand **4.96** and an acceptable conversion of 80% in combination with a poor *ee*-value of 30% was achieved with ligand **4.97**. Based on his experiments, Reetz concluded that monodentate chiral ligands characterized by a binapthyldiamine backbone are considerably less active than their corresponding phosphites, phosphonites and phosphoramidites, with a binol-based backbone.

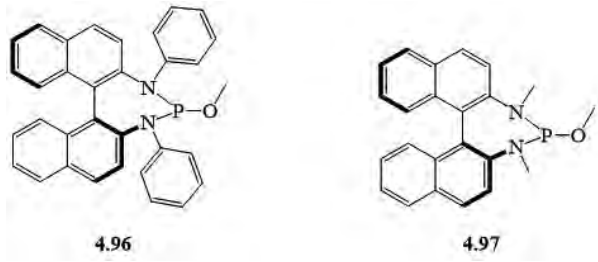

Figure 4.19 Monodentate diamidophosphite ligands synthesized by the research group of Reetz

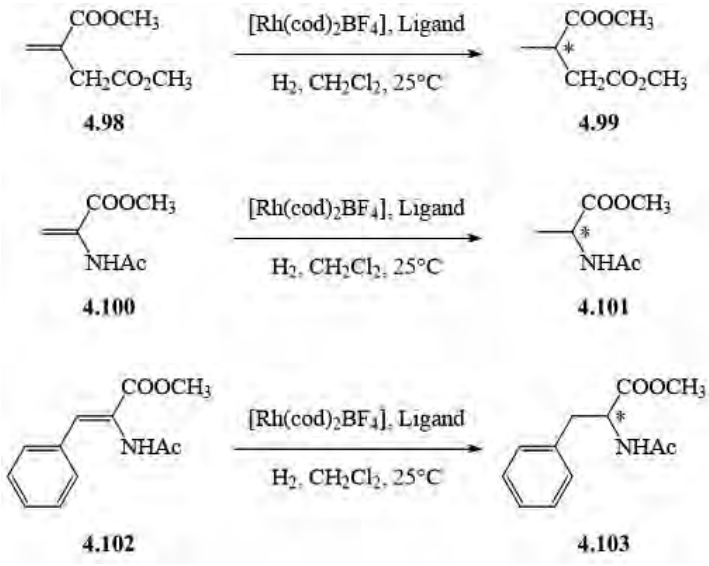

Scheme 4.26 Rhodium-catalyzed hydrogenations with benchmark substrates **4.98**, **4.100** and **4.102**

In 2010 Gavrilov *et al.* published a paper on the synthesis of novel *P**-monodentate diamidophosphite ligands, *P*,N*- and *P*,P**-bidentate diamidophosphite ligands (Figure 4.20). They applied these ligands in the rhodium-catalyzed hydrogenations of benchmark substrates, dimethyl itaconte **4.98** and methyl 2-acetamidoacrylate **4.100** (Scheme 4.26).[15] The results of these experiments are shown in Table 4.7. For both olefins best results were obtained with *P*,P**-bidentate diamidophosphite ligands **4.106** whereas extremely poor results were observed for both diastereomers of *P*,N*-bidentate ligands **4.105**. Monodentate ligand **4.104-a** provided a good selectivity of 60% *ee* for the hydrogenation of itaconate **4.98**, although a rather low conversion was observed (70%). In contrast, its diastereomeric ligand **4.104-b**, gave full conversion but a significantly lower selectivity was obtained (45% *ee*). While a good *ee*-value of 72% was obtained for the hydrogenation of substrate **4.100** with ligand **4.104-a**, only 11% *ee* was reported for ligand **4.104-b**. In conlusion, for both substrates **4.98** and **4.100**, the hydrogenation with monodentate ligands consisting of an (*S*)-binol based backbone gave higher enantioselectivities which is considered to be the matched situation. Interestingly, both diastereomers of *P**-monodentate diamidophosphite ligands **4.104** provide the (same) opposite enantiomer compared to the *P*,P*-bidentate diamidophosphite ligand **4.106**, although the configuration of the chiral phosphorus centers is identical for both ligands.

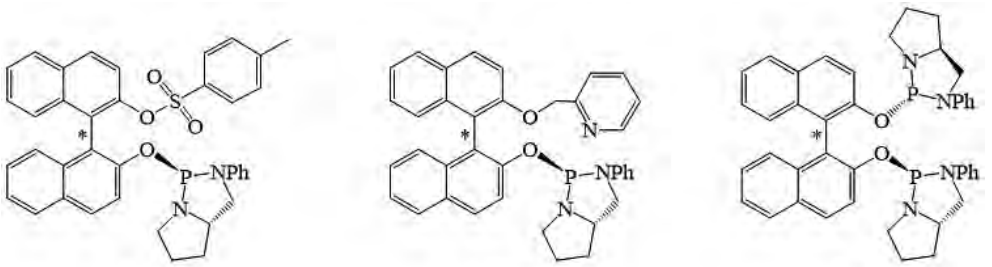

Figure 4.20 *P**-mono, *P*,N*- and *P*,P**-bidentate diamidophosphites ligands synthesized by the research group of Gavrilo

Substrate	Ligand	Ligand/Rh	Time (h)	H_2-pressure (bar)	Conversion (%)	*ee* (%)
4.98	**4.104-a**	2/1	20	1.3	70	60 (*S*)
4.98	**4.104-b**	2/1	20	1.3	100	45 (*S*)
4.98	**4.105-a**	1/1	20	1.3	20	0
4.98	**4.105-b**	1/1	20	1.3	100	4 (*R*)
4.98	**4.106-a**	1/1	20	1.3	100	>99 (*R*)
4.100	**4.104-a**	2/1	20	1.3	100	72 (*R*)
4.100	**4.104-b**	2/1	20	1.3	100	11 (*R*)
4.100	**4.105-a**	1/1	20	1.3	100	0
4.100	**4.105-b**	1/1	20	1.3	35	30 (*S*)
4.100	**4.106-a**	1/1	20	1.3	100	99 (*S*)

Table 4.7 Rh(I)-catalyzed asymmetric hydrogenation of dimethyl itaconate **4.98** and methyl 2-acetamidoacrylate **4.100** with *P**-mono, *P*,N*- and *P*,P**-bidentate diamidophosphite ligands

A third paper involving the use of diamidophosphite ligands in rhodium-catalyzed asymmetric hydrogenations was published by the research group of Muller in 2013.[5] A library of bidentate ligands **4.107**-**4.109** and monodentate ligand **4.16** (Figure 4.21) were prepared. These ligands were tested with three prochiral benchmark substrates: dimethylitaconate **4.98**, methyl 2-acetamidoacrylate **4.100** and methyl-(*Z*)-α-acetamidocinnamate **4.102** (Scheme 4.26). The most interesting results for matched combinations of different chiral ligand substructures are shown in Table 4.8.

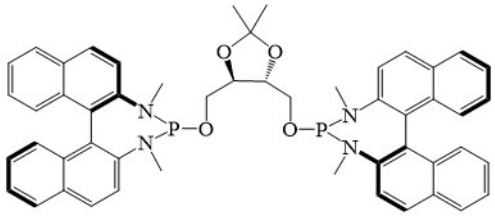

4.107

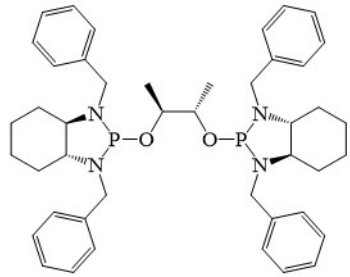

4.108

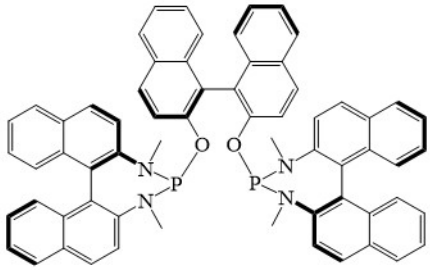

4.109

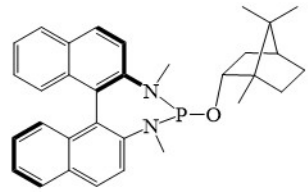

4.16

Figure 4.21 Diamidophosphite ligands prepared by the research group of Muller

Substrate	Ligand	Ligand/Rh	Time (h)	H_2-pressure (bar)	Conversion (%)	*ee*(%)
4.98	**4.107**	1/1	6	10	100	>99 (*R*)
4.98	**4.108**	1/1	6	10	70	97 (*S*)
4.98	**4.109**	1/1	6	10	92	75 (*R*)
4.98	**4.16**	2/1	6	10	100	78 (*S*)
4.100	**4.107**	1/1	6	10	100	>99 (*R*)
4.100	**4.108**	1/1	6	10	100	>99 (*R*)
4.100	**4.109**	1/1	6	10	100	>99 (*S*)
4.100	**4.16**	2/1	6	10	100	53 (*R*)
4.102	**4.107**	1/1	6	10	100	>99 (*S*)
4.102	**4.108**	1/1	6	10	100	95 (*R*)
4.102	**4.109**	1/1	6	10	100	96 (*S*)
4.102	**4.16**	2/1	6	10	100	79 (*R*)

Table 4.8 Rh(I)-catalyzed asymmetric hydrogenation of benchmark substrates **4.98**, **4.100** and **4.102** with bidentate diamidophosphite ligands **4.107**-**4.109** and monodentate diamidophosphite ligand **4.16**

The hydrogenation of substrate **4.98** with ligand **4.107** provided excellent results: full conversion and more than 99% *ee* favoring the (*R*)-enantiomer. The other ligands however were much less efficient. A very good selectivity of 97% of the (*S*)-enantiomer was obtained for ligand **4.108** but the conversion was only 70%. Ligand **4.109** gave almost full conversion (92%) with a moderate *ee*-value of 75% of the (*R*)-product. Monodentate ligand **4.16** provided full conversion in combination with a moderate enantiomeric excess of 78% favoring the (*S*)-product. For the hydrogenation of substrate **4.100** full conversion was obtained for the four ligands. Excellent enantioselectivities (>99%) were obtained for the bidentate ligands **4.107-4.109**, but monodentate ligand **4.16** provided an *ee*-value of only 53%. Only bidentate ligand **4.109** resulted in formation of the (*S*)-enantiomer of **4.101**. Remarkably, the (*R*)-product was formed with ligand **4.107**, a result counterintuitive compared to the other results. The hydrogenation of substrate **4.102** gave full conversion for the four ligands. The (*S*)-product was formed with very good enantioselectivities (>99% and 96% respectively) when ligands **4.107** and **4.109** were used. Bidentate ligand **4.108** provided the (*R*)-enantiomer also with a very good *ee*-value of 95%. Monodentate ligand **4.16** resulted in the formation of the (*R*)-enantiomer as well, however, a significantly lower enantiomeric excess of 79% was obtained.

Ligand **4.107** characterized by a (*R*)-binaphthyldiamine backbone in combination with (*R,R*)-(*O,O*)-*iso*-propylidenethreitol seemed to be superior because it reduced the three substrates with full conversion and each time with more than 99% *ee*. Monodentate diamidophosphite ligand **4.16**, however, provided the lowest selectivity for all substrates compared to the bidentate ligands. A remarkable result since it is generally accepted that monodentate ligands are the ligands of choice for this type of transformations.

4.8.2. Results of novel monodentate biferocene-based diamidophosphite Ligands **4.89**-**4.92**

The novel monodentate biferrocene-based diamidophosphite ligands, synthesized in this research project were also tested in the Rh-catalyzed asymmetric hydrogenation of enamide **4.102**. As well as the synthesis of novel phosphoramidite ligands **3.129**-**3.131** (§ 3.7.4, *vide supra*) only small amounts of diamidophosphite ligands **4.89-4.92** were obtained. Therefore only substrate **4.102** could be tested and a fully detailed, extensive study to optimize the enantioselectivities, TON or TOF is beyond the scope of this research project. However, initial test reactions were performed to gain a first impression

of the properties of the novel chiral diamidophosphite ligands **4.89-4.92**. The same reaction conditions as those described in chapter 3 were applied: 5 mol% $[Rh(cod)_2]BF_4$, 10 mol% ligand, 1 atmosphere H_2-pressure, room temperature and CH_2Cl_2 as solvent. The results are shown in Table 4.9.

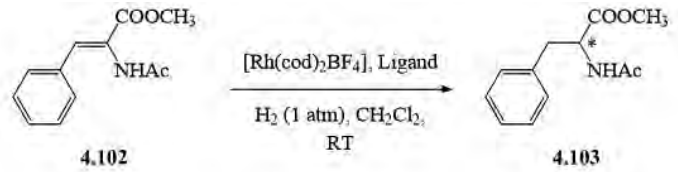

4.102 **4.103**

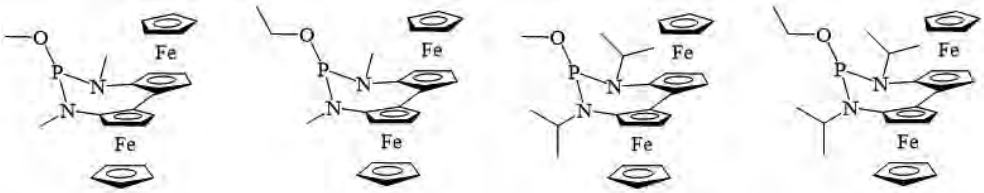

4.89 **4.90** **4.91** **4.92**

Substrate	Ligand	Time (h)	Conversion (%)	*ee* (%)
4.102	**4.89**	24	100	37.9 (*S*)
4.102	**4.90**	24	95	84.1 (*S*)
4.102	**4.91**	24	0	-
4.102	**4.92**	24	0	-
4.102	None (blanco)	24	0	-
4.102	(*rac*)-BINAP	24	80	0
4.102	(*R*)-MonoPhos	24	100	95.4 (*S*)

Table 4.9 Results for the Rh-catalyzed asymmetric hydrogenation of enamide **4.102** using novel biferrocene-based diamidophosphite ligands **4.89**-**4.92**

Excellent conversions were obtained for *N,N'*-dimethyl substituted ligand **4.89** and **4.90** (100% and 95% respectively). In contrast, there were no conversions observed for the *N,N'*-di-*iso*-propyl substituted analogs **4.91** and **4.92**. This can be explained by the increased steric bulk of these substituents preventing the formation of the required ligand-rhodium-complex. A relatively low *ee*-vaule was obtained with ligand **4.89** compared to ligand **4.90** (37.9% vs. 84.1%). Note that (R_p,R_p)-biferrocene-based ligands **4.89**

and **4.90** produce the same enantiomer of **4.103** as (*R*)-MonoPhos. However, the biferrocene-based diamidophosphite ligands cannot compete with Feringa's highly successful binol-based monodentate phosphoramidites ligands for the rhodium-catalyzed hydrogenation of enamide **4.102**.

4.9. Experimental

4.9.1. General

All experiments were performed according the general laboratory safety rules and personal protective equipment such as goggles, lab coat and gloves were always worn in the laboratory. All reactions, work-ups and purifications were performed in a well-ventilated fume hood. A detailed overview for the identification of the hazards of the most dangerous chemicals that were used in this chapter is given in Appendix I.

More information on general experimental details can be found in § 3.9.1 (*vide supra*). For the analytical separation of diastereomers (*S,S*$_p$)-**4.44** and (*S,R*$_p$)-**4.63** standard LC-MS experiments were performed as described earlier, but with a different solvent gradient system. The following conditions were used:

- **Method 6**
  Phenomenex Kinetex C18 column; 5 mM aqueous NH_4OAc/CH_3CN solvent system

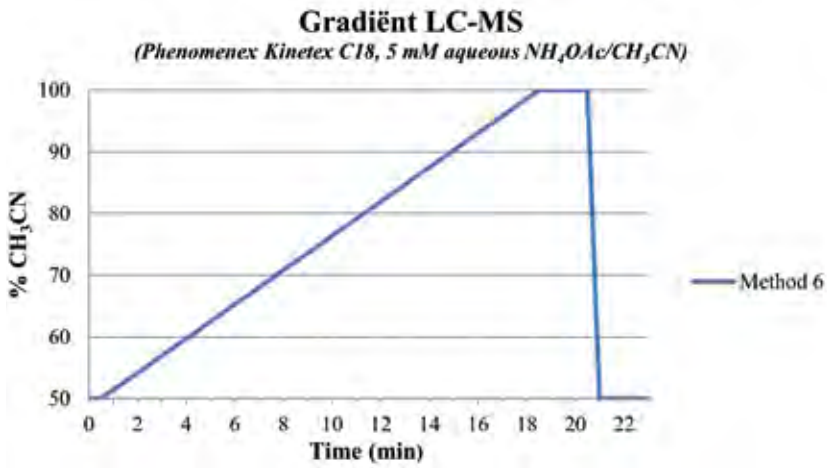

4.9.2. Synthesis of ferrocenecarboxylic acid **4.46**[33]

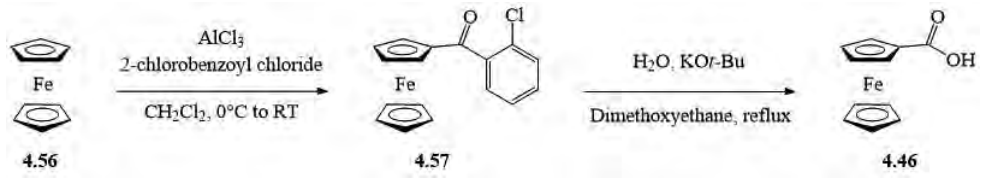

An oven-dried, 1 L two-neck, round-bottom flask was charged with a magnetic stirring bar, a gas-inlet tube which was connected to a Schlenk-line and put under an inert atmosphere of dry N_2. The flask was charged with ferrocene **4.56** (18.60 g, 0.100 mol), 2-chlorobenzoyl chloride (17.50 g, 0.100 mol, 1 eq) and CH_2Cl_2 (300 mL). The flask was cooled to 0°C using an ice-water bath. Afterwards anhydrous $AlCl_3$ (14.00 g, 0.105 mol, 1.05 eq) was added in small portions within 20 min. After stirring for an additional 30 min. at 0°C, the reaction was allowed to warm up to room temperature and stirred for an additional 2 h. The reaction mixture was cooled again to 0°C. Water (200 mL) was added cautiously and the resulting two-phase mixture was stirred vigorously for 30 min. After transferring the mixture into a separation funnel, the layers were separated and the aqueous layer was extracted two times with CH_2Cl_2 (100 mL). The combined organic solutions were washed with water (100 mL), twice with a 10 wt% aqueous NaOH solution (100 mL). The organic phase was dried over anhydrous $MgSO_4$, filtered and evaporated to dryness under reduced pressure. Crude (2-chlorobenzoyl)ferrocene **4.57** was obtained as a red solid with a yield of 93.6%

A 1 L round-bottom flask was charged with a magnetic stirring bar, **4.57** (30.4 g, 93.8 mmol), 1,2-dimethoxyethane (500 mL) and KO*t*-Bu (46.0 g, 411 mmol, 4.4 eq). While stirring, water (2.2 mL, 120 mmol, 1.3 eq) was added. The flask was equipped with a reflux condenser and the reaction was refluxed for 1 h. Afterwards the reaction was cooled and poured into water (1 L). The resulting solution was washed three times with Et_2O (400 mL). The combined organic solutions were back-extracted three times with a 10 wt% solution of NaOH (500 mL). The aqueous phases were combined and acidified with concentrated HCl until pH=1. The precipitate was filtered off and dried under reduced pressure. Ferrocenecarboxylic acid **4.46** was obtained as a yellow powder with a yield of 83.4%.

Formula: $C_{11}H_{10}FeO_2$ (230.04 g/mol)
R_f (pentane/EtOAc: 80/20): 0.44
^{1}**H-NMR** (Acetone-d_6, 500 MHz): δ = 4.21 (s, 5H), 4.44 (m, 2H), 4.75 (m, 2H) ppm.

^{13}**C-NMR** (Acetone-d_6, 125 MHz): δ = 70.5 (CH x5), 71.1 (CH x2), 72.1 (CH x2) ppm. (1 *C not observed*)

4.9.3. Synthesis of (*S*)-(4-*iso*-propyl-4,5-dihydrooxazol-2-yl)-ferrocene **4.45**[43]

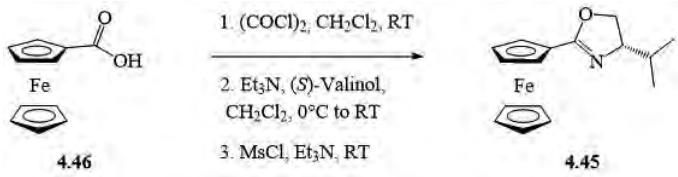

An oven-dried Schlenk tube was connected to a Schlenk-line and put under an inert atmosphere of dry N_2. This tube was charged with a magnetic stirring bar, ferrocenecarboxylic acid **4.46** (700 mg, 3.04 mmol), CH_2Cl_2 (21 mL) and oxalylchloride (0.70 mL, 9.1 mmol, 3 eq). The reaction mixture was stirred for 4 h at room temperature. CH_2Cl_2 and the excess of oxalylchloride were removed under reduced pressure, affording a red solid, which was taken up in fresh CH_2Cl_2 (20 mL). Et_3N (1.27 mL, 9.1 mmol, 3 eq) was added and the mixture was cooled to 0°C using an ice-water bath. Afterwards a solution of (*S*)-valinol (408 mg, 3.60 mmol, 1.3 eq) in CH_2Cl_2 (10 mL) was added. The reaction mixture was slowly warmed up to room temperature and stirred overnight. Mesylchloride (0.95 mL, 12.3 mmol, 2.6 eq) and Et_3N (1.27 mL, 9.1 mmol, 3 eq) were added and stirring was continued for an additional 3 h. The reaction was quenched with a saturated solution of $NaHCO_3$ (75 mL) and the layers were separated. The aqueous layer was extracted two times with CH_2Cl_2 (75 mL). The combined organic phases were dried over anhydrous $MgSO_4$ and filtered. The solvents were removed under reduced pressure and the resulting residue was purified by flash chromatography (petroleumether/EtOAc: 8/2) affording **4.45** as a red-orange solid with a yield of 75.0%.

Formula: $C_{16}H_{19}FeNO$ (297.17 g/mol)

R_f (pentane/EtOAc: 80/20): 0.44

^{1}**H-NMR** ($CDCl_3$, 500 MHz): δ = 0.94 (d, *J* = 6.9 Hz, 3H), 1.01 (d, *J* = 6.9 Hz, 3H), 1.86 (sptd, *J* = 6.9 Hz, *J* = 5.8 Hz, 1H), 3.99 (ddd, *J* = 9.5 Hz, *J* = 8.2 Hz, *J* = 5.8 Hz, 1H), 4.05-4.09 (m, 1H), 4.20 (s, 5H), 4.26-4.31 (m, 1H), 4.32 (ddd, *J* = 4.1 Hz, *J* = 2.4 Hz, *J* = 1.3 Hz, 1H, Fc), 4.33 (ddd, *J* = 4.1 Hz, *J* = 2.4 Hz, *J* = 1.3 Hz, 1H, Fc), 4.73 (dt, *J* = 2.4 Hz, *J* = 1.3 Hz, 1H, Fc), 4.77 (dt, *J* = 2.4 Hz, *J* = 1.3 Hz, 1H, Fc) ppm.

^{13}**C-NMR** ($CDCl_3$, 125 MHz): δ = 17.8 (CH_3), 19.0 (CH_3), 32.3 (CH), 69.0 (CH, Fc), 69.0 (CH, Fc), 69.3 (CH_2), 69.6 (CH x5), 70.1 (CH, Fc), 70.2 (CH, Fc), 70.6 (C), 72.3 (CH), 165.7 (C) ppm.

ESI-MS m/z (rel. intensity %): 298.1 (100) $[M+H]^+$, 299.1 (20), 296.2 (6)
Retention time HPLC: 6.52 min. (method 3), 1.72 min. (method 4).
Optical rotation: $[\alpha]_D^{20}$ = -91.5 (c 1.0, chloroform)
Melting point (°C): 68°C

4.9.4. Synthesis of (S,S_p)-2-(α-iodoferrocenyl)-5-*iso*-propyl-oxazoline **4.44**

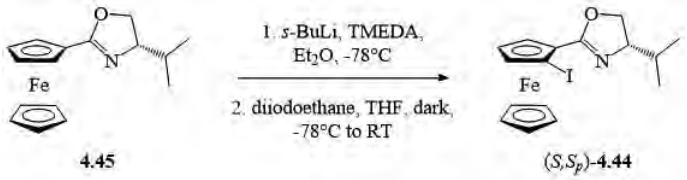

An oven-dried, 100 mL two-neck, round-bottom flask was connected to a Schlenk-line and put under an inert atmosphere of dry N_2. This flask was charged with a magnetic stirring bar, **4.45** (1.000 g, 3.37 mmol), Et_2O (40 mL) and TMEDA (656 µL, 4.37 mmol, 1.3 eq). The reaction mixture was cooled to -78°C and *s*-BuLi (1.4 M in cyclohexane 2.89 mL, 4.04 mmol, 1.2 eq) was added dropwise. The reaction was stirred for an additional h at this temperature. Afterwards a solution of diiodoethane[28] (1.423 g, 5.05 mmol, 1.5 eq) in THF (6.5 mL) was cautiously added and the reaction was stirred for 10 more min. at -78°C. The cooling bath was removed, the reaction flask was covered in aluminum foil and the reaction mixture was allowed to warm up to room temperature and stirred overnight. The reaction was quenched with water (70 mL). The aqueous layer was extracted 3 times with Et_2O (70 mL). The combined organic phases were washed with brine (50 mL), dried over anhydrous $MgSO_4$ and filtered. The solvents were removed under reduced pressure and the resulting residue was purified by flash chromatography (cyclohexane/EtOAc: 90/10) affording (S,S_p)-**4.44** as a brown-orange oil with a yield of 95.0%.

*Because compound **4.40** is light sensitive every step was covered as much as possible in aluminum foil. This involves reaction flasks, flasks on the rotavap, columns for chromatography and collection tubes (erlenmeyer flasks).*

Formula: $C_{16}H_{18}FeINO$ (423.07 g/mol)
$\mathbf{R}_f$ (cyclohexane/EtOAc: 7/3): 0.41

28 Diiodoethane was purified before use via the following procedure: 5.00 g of diiodoethane was dissolved in Et_2O (100 mL), washed 5 times with a saturated solution of $Na_2S_2O_3$ (25 mL) and one time with water (25 mL). The organic phase was dried over $MgSO_4$ and filtered. The solvents were removed under reduced pressure with the flask carefully covered in aluminum foil. Diiodoethane was obtained as white solid.

^{1}**H-NMR** ($CDCl_3$, 500 MHz): δ = 1.00 (d, *J* = 6.9 Hz, 3H), 1.06 (d, *J* = 6.9 Hz, 3H), 1.87 (sptd, *J* = 6.9 Hz, *J* = 5.8 Hz, 1H), 4.05 (ddd, *J* = 9.5 Hz, *J* = 7.2 Hz, *J* = 5.8 Hz, 1H), 4.10-4.14 (m, 1H), 4.21 (s, 5H), 4.28-4.33 (m, 1H), 4.37 (app t, *J* = 2.6 Hz, 1H), 4.62 (dd, *J* = 2.6 Hz, *J* = 1.5 Hz, 1H), 4.73 (dd, *J* = 2.6 Hz, *J* = 1.5 Hz, 1H) ppm.
^{13}**C-NMR** ($CDCl_3$, 125 MHz): δ = 18.1 (CH_3), 18.7 (CH_3), 32.6 (CH), 38.8 (C), 69.4 (CH_2), 69.5 (CH), 70.9 (CH), 72.1 (C), 72.5 (CH), 72.6 (CH x5), 78.4 (CH), 163.7 (C) ppm.
ESI-MS m/z (rel. intensity %): 424.0 (100) $[M+H]^+$, 425.0 (38), 422.0 (11)
Retention time HPLC: 6.68 min. for (*S*,R_p)-**4.44**, 6.89 min. for (*S*,S_p)-**4.44** (method 6)
Optical rotation: $[\alpha]_D^{20}$ = -119.5° (c 0.78, $CHCl_3$); literature: -131.0° (c 0.46, $CHCl_3$)[24]

Due to the fact that compound is light sensitive, full characterization could not be performed.

4.9.5. Synthesis of (S_p)-α-iodoferrocene carboxylic acid **4.41** via Pinnick oxidation of **4.42**

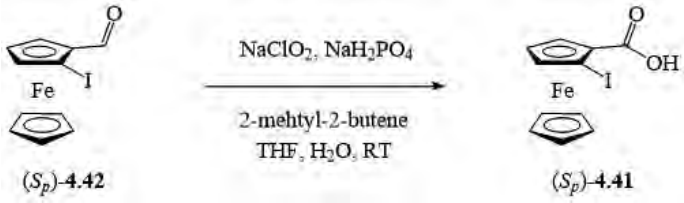

A 250 mL round-bottom flask was charged with a magnetic stirring bar, aldehyde (S_p)-**4.42** (1.421 g, 4.18 mmol), THF (30 mL), H_2O (30 mL), 2-methyl-2-butene (4.42 mL, 41.8 mmol, 10 equiv.), NaH_2PO_4 (2.88 g, 41.8 mmol, 5 eq) and $NaClO_2$ (1.51 g, 16.72 mmol, 4 eq) were added and the mixture was stirred overnight. The reaction was cooled to 0°C using an ice-water bath and quenched via dropwise addition of a saturated Na_2SO_3-solution (60 mL). The mixture was poured into a separation funnel and the aqueous layer was extracted three times with Et_2O (150 mL). The combined organic phases were dried over anhydrous $MgSO_4$ and filtered. The solvents were removed under reduced pressure. The brown crystals were triturated once with a minimal amount of acetone and twice with a minimal amount of Et_2O. Carboxylic acid (S_p)-**4.41** was obtained as an orange solid with a yield of 66.0%.

Formula: $C_{11}H_9FeIO_2$ (356.94 g/mol)
R$_f$ (*n*-hexane/acetone: 70/30): 0.26
^{1}**H-NMR** (Acetone-d6, 500 MHz): δ = 4.24 (s, 5H), 4.55 (dd, *J* = 2.3 Hz, *J* = 2.1 Hz, 1H), 4.75 (dd, *J* = 2.1 Hz, *J* = 1.5 Hz, 1H), 4.87 (dd, *J* = 2.3 Hz, *J* = 1.5 Hz, 1H), 10.96 (br. s,1H) ppm.

^{13}**C-NMR** (Acetone-d6, 125 MHz): δ = 40.1 (C), 71.4 (CH), 72.4 (C), 73.3 (CH), 73.6 (CH x 5), 80.8 (CH), 171.1 (C) ppm.

IR (HATR): ν_{max} = 3927, 3105, 2922, 2871, 2743, 2572, 1780, 1657, 1458, 1410, 1366, 1352, 1333, 1293, 1266, 1185, 1153, 1106, 1062, 1031, 1001, 943, 846, 822, 814, 776, 750 $cm^{-1.}$

ESI-MS m/z (rel. intensity %): 354.9 (100, $[M-H]^-$), 207.1 (17), 355.8 (14), 119.2 (12)

HRMS (ESI): calculated for $[M-H]^-$: 354.8997; found: 354.8930

Retention time HPLC: 4.12 min. (method 3)

Optical rotation: $[\alpha]_D^{20}$ = -51.1 (c 0.49, acetone, 75.3% *ee*)

4.9.6. Synthesis of (S_p)-α-iodoferrocene carboxylic acid **4.41** via hydrolysis of **4.44**

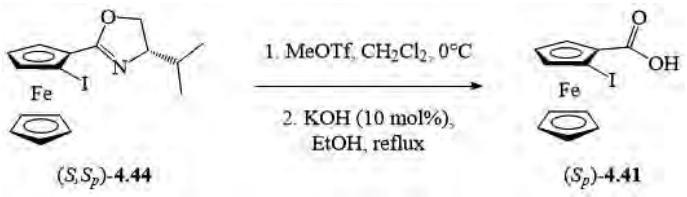

(S,S_p)-**4.44** (S_p)-**4.41**

An oven-dried, 25 mL round-bottom flask was charged with a magnetic stirring bar, (S,S_p)-**4.44** (300 mg, 0.71 mmol) and CH_2Cl_2 (15 mL). The solution was cooled to 0°C using an ice-water bath and MeOTf (160 µL, 1.4 mmol, 2 eq) was added. The reaction mixture was stirred for 1 h at 0°C. The solvents were removed under reduced pressure. The residu was taken up in EtOH (15 mL) and transferred in a two-neck 25 mL round-bottom flask. The solution was stirred at room temperature and a 10 mol% solution of KOH (15 mL) was added. Afterwards, the reaction mixture was heated to 80°C, stirred for 2 h and allowed to cool down to room temperature. The reaction mixture was poured into a separation funnel. Et_2O (50 mL) was added and the organic phase was extracted 3 times with a 10 mol% solution of KOH (25 mL). The combined aqueous phases was carefully acidified at 0°C with a 3 M HCl solution until pH=1 and extracted three times with 100 mL Et_2O. The combined organic phases were dried over anhydrous $MgSO_4$ and filtered. The organic solvents were removed under reduced pressure affording (S_p)-**4.41** as a yellow solid with a yield of 87.1%.

Formula: $C_{11}H_9FeIO_2$ (356.94 g/mol)

$\mathbf{R}_f$ (*n*-hexane/acetone: 70/30): 0.26

^{1}**H-NMR** (Acetone-d6, 500 MHz): δ = 4.24 (s, 5H), 4.55 (dd, *J* = 2.3 Hz, *J* = 2.1 Hz, 1H), 4.75 (dd, *J* = 2.1 Hz, *J* = 1.5 Hz, 1H), 4.87 (dd, *J* = 2.3 Hz, *J* = 1.5 Hz, 1H), 10.96 (br. s,1H) ppm.

^{13}**C-NMR** (Acetone-d6, 125 MHz): δ = 40.1 (C), 71.4 (CH), 72.4 (C), 73.3 (CH), 73.6 (CH x 5), 80.8 (CH), 171.1 (C) ppm.

IR (HATR): ν_{max} = 3927, 3105, 2922, 2871, 2743, 2572, 1780, 1657, 1458, 1410, 1366, 1352, 1333, 1293, 1266, 1185, 1153, 1106, 1062, 1031, 1001, 943, 846, 822, 814, 776, 750 cm$^{-1.}$

ESI-MS m/z (rel. intensity %): 354.9 (100, $[M-H]^-$), 207.1 (17), 355.8 (14), 119.2 (12)

HRMS (ESI): calculated for $[M-H]^-$: 354.8997; found: 354.8930

Retention time HPLC: 4.12 min. (method 3)

Optical rotation: $[\alpha]_D^{20}$ = -51.1 (c 0.49, acetone, 75.3% *ee*)

4.9.7. Synthesis of (S_p)-α-iodoferrocenoyl azide **4.40**

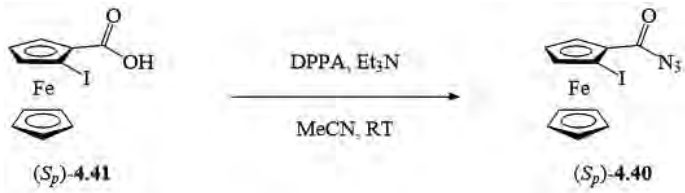

An oven-dried, 250 mL round-bottom flask was charged with a magnetic stirring bar, carboxylic acid (S_p)-**4.41** (787 mg, 2.205 mmol), anhydrous acetonitrile (55 mL), Et_3N (1.23 mL, 8.82 mmol, 4 eq) and DPPA (0.52 mL, 2.426 mmol, 1.1 eq). The reaction was stirred for 3 h at room temperature and quenched with a saturated solution of $NaHCO_3$ (75 mL). The aqueous phase was extracted 3 times with CH_2Cl_2 (75 mL). The combined organic phases were dried over anhydrous $MgSO_4$ and filtered. The solvents were removed under reduced pressure and the resulting residue was purified by flash chromatography (*n*-hexane/acetone: 99/1) affording (S_p)-**4.40** as a deep red oil with a yield of 95.7%.

Fomula: $C_{11}H_8FeIN_3O$ (380.95 g/mol)

R$_f$ (*n*-hexane/acetone: 70/30): 0.41

^{1}**H-NMR** (Acetone-d6, 500 MHz): δ = 4.32 (s, 5H), 4.67 (app t, *J* = 2.4 Hz, 1H), 4.85 (dd, *J* = 2.4 Hz, *J* = 1.4 Hz, 1H), 4.91 (dd, *J* =2.4 Hz, *J* = 1.4 Hz, 1H) ppm.

^{13}**C-NMR** (Acetone-d6, 125 MHz): δ = 39.2 (C), 61.0 (C), 71.8 (CH), 74.1 (CH x5), 74.6 (CH), 82.3 (CH), 176.0 (C) ppm.

IR (HATR): ν_{max} = 3098, 2927, 2870, 2262, 2198, 2131, 1688, 1424, 1385, 1369, 1352, 1324, 1256, 1240, 1181, 1123, 1107, 1079, 1042, 1011, 1002, 896, 821, 740 cm^{-1}.

ESI-MS m/z (rel. intensity %): 353.9 (100, $[M-N_2+H]^+$), 255.0 (13), 244.1 (9), 227.1 (6)

Retention time HPLC: 1.91 min. (method 4)

Chiral HPLC: Chiralcel OD-H column, solvent *n*-hexane/EtOH (98:2), flow rate = 1mL/min., t = 30 min., T = 35°C, retention times: 6.85 min. for (R_p)-**4.40**; 9.15 min. for (S_p)-**4.40**

Optical rotation: $[\alpha]_D^{20}$ = -87.26 (c 0.42, acetone, 75.3% *ee*)

4.9.8. Synthesis of 4-methoxybenzyl (*N*-(S_p)-α-iodoferrocenoyl) carbamate **4.68**

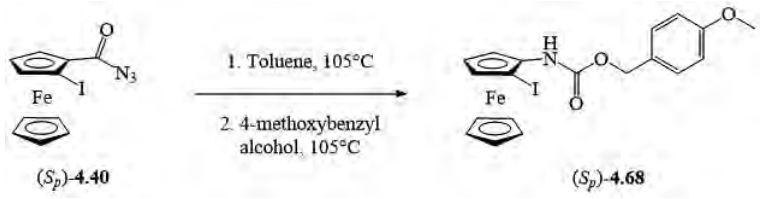

(S_p)-**4.40** (S_p)-**4.68**

An oven-dried, 50 mL round-bottom flask was charged with a magnetic stirring bar and ferrocenoyl azide (S_p)-**4.40** (728 mg, 1.91 mmol) and toluene (16 mL). The reaction mixture was heated to 105°C. When the formation of N_2-gas has stopped, 4-methoxybenzylalcohol (0.474 mL, 3.82 mmol, 2 eq) was carefully added and the reaction mixture was stirred for an additional 3 h at 105°C before it was allowed to cool down to room temperature. The mixture was poured into water (50 mL). The aqueous phase was extracted 3 times with CH_2Cl_2 (60 mL). The combined organic phases were dried over anhydrous $MgSO_4$ and filtered. The solvents were removed under reduced pressure and the resulting residue was purified via by flash chromatography (*n*-hexane/EtOAc: 80/20) affording (S_p)-**4.68** as an orange-brown viscous oil with a yield of 95.4%.

Formula: $C_{19}H_{18}FeINO_3$ (491.10 g/mol)

R_f (*n*-hexane/acetone: 70/30)**:** 0.35

^{1}**H-NMR**: (Acetone-d6, 300 MHz): δ = 3.79 (s, 3H), 4.15-4.21 (m, 2H), 4.20 (s, 5H), 4.33 (dd, *J* = 2.6 Hz, *J* = 1.4 Hz, 1H), 4.75 (br. s, 1H), 5.05 (d, *J* = 12.1 Hz, 1H, A part AB-system), 5.09 (d, *J* =12.1 Hz, 1H, B part AB-system), 6.90-6.98 (m, 2H), 7.30-7.39 (m, 2H) ppm.

^{13}**C-NMR**: (Acetone-d6, 75.4 MHz): δ = 55.6 (CH_3), 64.3 (C, Fc), 66.9 (CH, Fc), 67.1 (CH_2), 71.6 (CH, Fc), 72.7 (CH, Fc), 72.9 (CH x5), 96.8 (C, Fc), 114.6 (CH x2), 129.7 (C), 130.8 (CH x2), 155.5 (C, CO), 160.6 (C) ppm.

IR (HATR): ν_{max} = 3394, 3094, 2954, 2834, 2358, 2342, 1704, 1612, 1530, 1513, 1461, 1384, 1325, 1302, 1245, 1204, 1174, 1105, 1078, 1029, 1000, 949, 846, 819, 768, 735, 698 cm^{-1}.

ESI-MS m/z (rel. intensity %): 491.0 (31) $[M+H]^+$, 365.1 (100) $[M-I+H]^{\cdot+}$, 366.1 (21)
HRMS (ESI): calculated for $C_{19}H_{17}FeINO_3$.: 489.9680 $[M-H]^-$, found: 489.9624; calculated for $C_{19}H_{19}FeNO_3^{\cdot+}$: 365.0709 $[M-I+H]^{\cdot+}$, found: 365.0706
Retention time HPLC: 7.04 min. (method 3), 1.99 min. (method 4).
Chiral HPLC: Chiralcel OD-H column, solvent *n*-hexane/EtOH (97:3), flow rate = 1 mL/min., t = 30 min., T = 35°C, retention times: 10.97 min. for (S_p)-**4.68**; 13.51 min. for (R_p)-**4.68**
Optical rotation: $[\alpha]_D^{20}$ = -116.41 (c 0.1, acetone, 75.3% *ee*)

4.9.9. Synthesis of 4-methoxybenzyl (*N*-(S_p)-α-iodoferrocenoyl-*N*-methyl) carbamate **4.69**

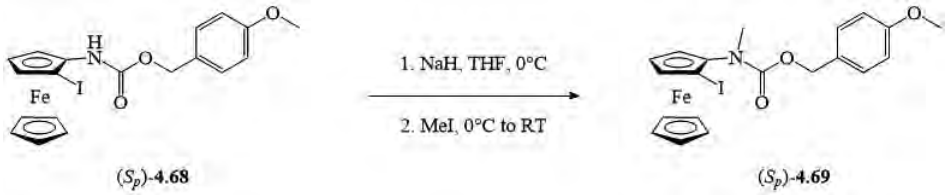

An oven-dried, 50 mL round-bottom flask was charged with a magnetic stirring bar and NaH (56.3 mg, 2.3 mmol, 1.5 eq). THF (1 mL) was added and the reaction flask was cooled to 0°C using an ice-water bath. A solution of (S_p)-**4.68** (728 mg, 1.91 mmol) in THF (10 mL) was added dropwise and stirred until the formation of hydrogen gas has stopped. Afterwards iodomethane (170 µL, 2.7 mmol, 1.7 eq) was carefully added. The reaction was stirred for an additional 10 min. at 0°C before it was allowed to warm up to room temperature and stirred overnight. The reaction was cooled to 0°C again and quenched with a saturated solution of NH_4Cl (25 mL). The aqueous phase was extracted 3 times with Et_2O (25 mL). The combined organic phases were dried over anhydrous $MgSO_4$ and filtered. The solvents were removed under reduced pressure and the resulting residue was purified by flash chromatography (*n*-hexane/EtOAc: 80/20) affording (S_p)-**4.69** as an orange-brown viscous oil with a yield of 99.0%.

Formula: $C_{20}H_{20}FeINO_3$ (505.13 g/mol)
R_f (*n*-hexane/EtOAc: 80/20): 0.20
^{1}**H-NMR** (Acetone-d6, 300 MHz): δ = 3.56 (s, 3H), 3.77 (s, 3H), 4.24 (app t, *J* = 2.6 Hz, 1H), 4.31 (s, 5H), 4.35 (dd, *J* = 2.6 Hz, *J* = 1.4 Hz, 1H), 4.45 (dd, *J* = 2.6 Hz, *J* = 1.4 Hz, 1H), 4.90 (d, *J* = 12.2 Hz, 1H, A part of AB-system), 5.01 (d, *J* = 12.2 Hz, 1H, B part of AB-system), 6.80-6.90 (m, 2H), 7.15-7.30 (m, 2H) ppm.

^{13}C-NMR (Acetone-d6, 75.4 MHz): δ = 41.5 (CH_3), 55.6 (CH_3), 66.5 (CH, Fc), 67.2 (CH, Fc), 67.6 (CH_2), 72.7 (CH, Fc), 72.8 (CH x5), 104.2 (C, Fc), 114.5 (CH x2), 129.9 (C), 130.4 (CH x2), 156.7 (C, C=O), 160.4 (C) ppm. *1 C (Fc) not observable in ATP*

IR (HATR): ν_{max} = 2954, 2932, 1699, 1612, 1586, 1513, 1461, 1430, 1414, 1379, 1338, 1302, 1245, 1165, 1137, 1108, 1032, 1003, 949, 931, 888, 820, 767, 673 cm^{-1}.

ESI-MS m/z (rel. intensity %): 505.9 (19) $[M+H]^+$, 504.9 (36), 379.1 (100) $[M-I+H]^{\cdot+}$, 380.1 (25)

HRMS (ESI): calculated for $C_{20}H_{21}FeNO_3^{\cdot+}$ $[M-I+H]^{\cdot+}$: 379.0865; found: 379.0852

Retention time HPLC: 7.14 min. (method 3), 2.25 (method 4)

Optical rotation: $[\alpha]_D^{20}$ = -81.57 (c 0.67, acetone, 75.3% *ee*)

4.9.10. Synthesis of 4-methoxybenzyl (*N*-(S_p)-α-iodoferrocenoyl-*N*-*iso*-propyl)carbamate **4.70** and 4-methoxybenzyl (*N*-(S_p)-α-iodoferrocenoyl-*N*-methyl)carbamate **4.69**

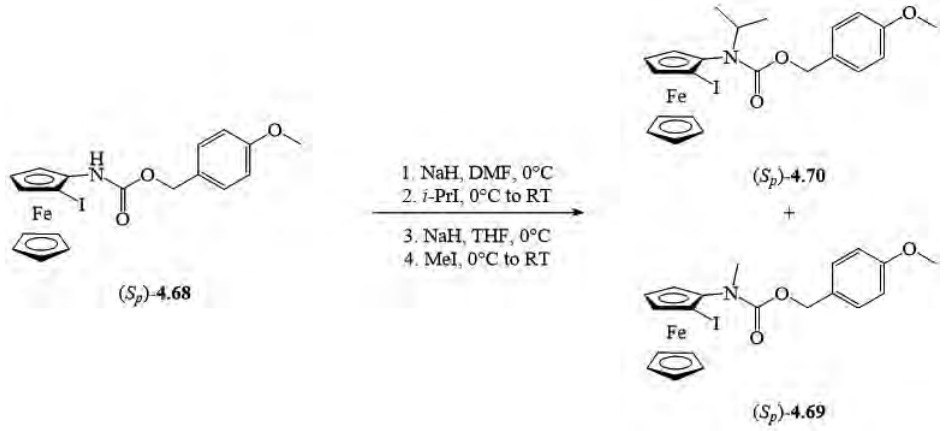

An oven-dried, 100 mL round-bottom flask was charged with a magnetic stirring bar and NaH (150 mg, 6.25 mmol, 2.0 eq). DMF (2 mL) was added and the reaction flask was cooled to 0°C using an ice-water bath. A solution of (S_p)-**4.68** (1.53 g, 3.13 mmol) in DMF (20 mL) was added dropwise and stirred until the formation of hydrogen gas has stopped. Afterwards 2-iodopropane (625 µL, 6.25 mmol, 2.0 eq) was carefully added. The reaction was stirred for an additional 10 min. at 0°C before it was allowed to warm up to room temperature and stirred overnight. The reaction was cooled to 0°C again and quenched with a saturated solution of NH_4Cl (50 mL). The aqueous phase was extracted 3 times with Et_2O (50 mL). The combined organic phases were washed twice with H_2O (50 mL), dried over anhydrous $MgSO_4$ and filtered. The solvents were removed under reduced pressure and the obtained dark-brown oil was filtered over sil-

ica gel (*n*-hexane/EtOAc: 80/20). The solvents were removed under reduced pressure. The obtained brown oil was dried on high vacuum, affording a mixture of (S_p)-**4.70** and (S_p)-**4.68**.

An oven-dried, 100 mL round-bottom flask was charged with a magnetic stirring bar and NaH (75 mg, 3.13 mmol, 1 eq). THF (2 mL) was added and the reaction flask was cooled to 0°C using an ice-water bath. The mixture of (S_p)-**4.70** and (S_p)-**4.68** was dissolved in THF (30 mL) and added dropwise. The reaction mixture was stirred until the formation of hydrogen gas has stopped. Afterwards iodomethane (195 µL, 3.13 mmol, 1 eq) was carefully added. The reaction was stirred for an additional 10 min. at 0°C before it was allowed to warm up to room temperature and stirred overnight. The reaction was cooled to 0°C again and quenched with a saturated solution of NH_4Cl (30 mL). The aqueous phase was extracted 3 times with Et_2O (30 mL). The combined organic phases were dried over anhydrous $MgSO_4$ and filtered. the solvents were removed under reduced pressure and the resulting residue was purified by flash chromatography (*n*-hexane/EtOAc: 80/20) affording (S_p)-**4.70** as a brown viscous oil with a yield of 55.0% and (S_p)-**4.69** as a brown viscous oil with a yield of 43.1%.

For full characterization of compound (S_p)-***4.69*** *see § 4.9.9*

Formula: $C_{22}H_{24}FeINO_3$ (533.18 g/mol)
R_f (*n*-hexane/EtOAc: 80/20): 0.27
^{1}**H-NMR** (500 MHz, Acetone-d6): δ = 1.51 (d, *J* = 6.8 Hz, 3H) 1.64 (d, *J* = 6.8 Hz, 3H) 3.76 (s, 3H), 4.21 (dd, *J* = 2.7 Hz, *J* = 1.4 Hz, 1H), 4.25 (app t, *J* = 2.7 Hz, 1H), 4.26 (s, 5H), 4.46 (dd, *J* = 2.7 Hz, *J* = 1.4 Hz, 1H), 4.53 (spt, *J* = 6.8 Hz, 1H), 4.86 (d, *J* = 12.3 Hz, 1H, A part of AB-system), 4.99 (d, *J* = 12.3 Hz, 1H, B part of AB-system), 6.83-6.86 (m, 2H), 7.17-7.21 (m, 2H) ppm.
^{13}**C-NMR** (125 MHz, Acetone-d6): δ = 20.8 (CH_3), 21.5 (CH_3), 43.8 (C, Fc), 55.5 (CH_3), 60.1 (CH), 65.6 (CH, Fc), 66.9 (CH_2), 67.0 (CH, Fc), 72.4 (CH, Fc), 72.9 (CH x5), 106.6 (C, Fc), 114.5 (CH x2), 129.9 (C), 130.3 (CH x2), 155.2 (C, C=O), 160.4 (C) ppm.
IR (HATR): ν_{max} = 3097, 2997, 2965, 2934, 2834, 1699, 1613, 1586, 1514, 1412, 1380, 1363, 1284, 1246, 1174, 1166, 1051, 1108, 1085, 1035, 1011, 928, 900, 918, 822, 768, 650 cm^{-1}.
ESI-MS m/z (rel. intensity %): 407.1 (100) $[M\text{-}I+H]^{\cdot+}$, 408.1 (26), 533.0 (8) $[M]^{\cdot+}$
HRMS (ESI): calculated for $C_{22}H_{25}FeNO_3^{\cdot+}$ $[M\text{-}I+H]^{\cdot+}$: 407.1184; found: 407.1167 calculated for $C_{22}H_{24}FeINO_3^{\cdot+}$ $[M]^{\cdot+}$: 533.0150; found: 533.0125

Retention time HPLC: 7.68 min. (method 3), 3.20 min.
Optical rotation: $[\alpha]_D^{20}$ = -88.8 (c 1.07, acetone, 75.3% *ee*)

4.9.11. Synthesis of (R_p,R_p)-2,2'-Bis[(4-methoxybenzyl)-*N*-methyl carbamate]-1,1'-biferrocene **4.75**

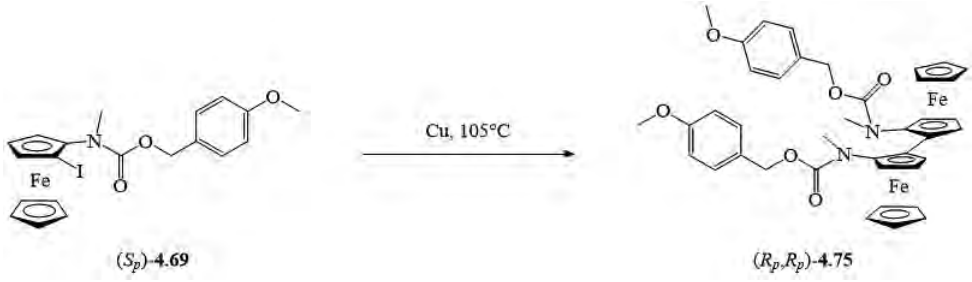

Carbamate (S_p)-**4.69** (522 mg, 0.64 mmol) was dissolved in a minimal amount of anhydrous CH_2Cl_2 and transferred into an oven-dried, 50 mL round-bottom flask. CH_2Cl_2 was evaporated using an Ar-flow from a balloon to have all the starting material on the bottom of the flask. 300 Mesh copper powder (122 mg, 1.92 mmol, 3 eq) was carefully added in such a way that all of the starting material was covered with copper. A heavy, egg-shaped stirring bar was carefully added. The reaction mixture was heated to 105°C and stirred overnight. The reaction mixture was taken up in a large amount of Et_2O and filtered over Celite. The solvent was removed under reduced pressure and the resulting residue was purified by flash chromatography (gradient *n*-hexane/EtOAc: 80/20 to *n*-hexane/EtOAc: 70/30) affording (R_p,R_p)-**4.75** as an orange solid with a yield of 82.0%.

Formula: $C_{40}H_{40}Fe_2N_2O_6$ (756.45 g/mol)
R_f (*n*-hexane/EtOAc: 80/20): 0.06
^{1}**H-NMR** (500 MHz, Acetone-d6): δ = 3.48 (s, 6H), 3.71 (s, 6H), 3.93 (app t, *J* = 2.7 Hz, 2H), 4.23-4.26 (m, 2H), 4.32 (s, 10), 4.63 (dd, *J* = 2.7 Hz, *J* = 1.4 Hz, 2H), 4.89 (d, *J* = 12.0 Hz, 2H, A part of AB-system), 5.01 (d, *J* = 12.0 Hz, 2H, B part of AB system), 6.76-6.84 (m, 4H), 7.17-7.25 (m, 4H) ppm.
^{13}**C-NMR** (125 MHz, Acetone-d6): δ = 39.8 (CH_3 x2), 55.5 (CH_3 x2), 59.6 (CH x2, Fc), 59.8 (CH x2, Fc), 62.2 (CH x2, Fc), 67.6 (CH_2 x2), 71.1 (CH x10), 93.5 (C x2, Fc), 110.1 (C x2, Fc), 114.5 (CH x4), 129.7 (C x2), 130.5 (CH x4), 156.0 (C x2, C=O), 160.2 (C x2) ppm.
IR (HATR): ν_{max} = 3095, 2970, 2869, 1698, 1612, 1586, 1513, 1499, 1443, 1412, 1384, 1356, 1326, 1302, 1246, 1224, 1171, 1142, 1106, 1091, 1058, 1032, 820, 767, 756, 736 cm^{-1}.

ESI-MS m/z (rel. intensity %): 757.1 (100) $[M+H]^+$), 756.1 (84), 758.0 (30), 755.1 (15), 754.1 (10), 759.1 (10), 636 (24), 592.1 (12), 713 (12)

HRMS (ESI): no identifiable ion-masses found in positive and negative mode

Retention time HPLC: 7.91 min. ((R_p,S_p)-**4.78** (*meso* compound): 7.73 min.) (method 3), 3.98 min. ((R_p,S_p)-**4.78** (*meso* compound): 3.46 min. (method 4)

CHIRAL HPLC: Chiralcel OD-H column, solvent *n*-hexane/EtOH 80:20, flow rate = 1 mL/min., T = 35°C, retention times: 7.28 min. for (S_p,S_p)-**4.75**; 8.63 min. for (R_p,R_p)-**4.75**; 10.28 min. for (R_p,S_p)-**4.78** (*meso* compound)

Optical rotation: $[\alpha]_D^{20}$ = -130.7 (c 0.47, acetone)

4.9.12. Synthesis of (R_p,R_p)-2,2'-Bis[(4-methoxybenzyl)-*N*-*iso*-propyl carbamate]-1,1'-biferrocene **4.79**

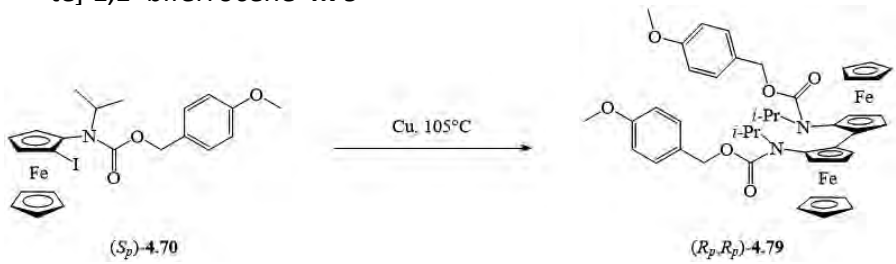

(S_p)-**4.70** (R_p,R_p)-**4.79**

Carbamate (S_p)-**4.70** (156 mg, 0.29 mmol) was dissolved in a minimal amount of anhydrous CH_2Cl_2 and transferred into an oven-dried, 50 mL round-bottom flask. CH_2Cl_2 was evaporated using an Ar-flow from a balloon to have all the starting material on the bottom of the flask. 300 Mesh copper powder (55 mg, 0.87 mmol, 3 eq) was arefully added in such a way that all the starting material was covered with copper. A heavy, egg-shaped stirring bar was carefully added. The reaction mixture was heated to 105°C and stirred overnight. The reaction mixture was taken up in a large amount of Et_2O and filtered over Celite. The solvent was removed under reduced pressure and the resulting residue was purified by flash chromatography (*n*-hexane/EtOAc: 80/20) affording (R_p,R_p)-**4.79** as an orange solid with a yield of 71.9%.

Formula: $C_{44}H_{48}Fe_2N_2O_6$ (812.55 g/mol)

$\mathbf{R}_f$ (*n*-hexane/EtOAc: 80/20): 0.14

^{1}**H-NMR**: (300 MHz, Acetone-d6): δ = 0.91 (d, *J* = 6.8 Hz, 6H), 1.37 (d, *J* = 6.8 Hz, 6H), 3.73 (s, 6H), 4.05 (app t, *J* = 2.6 Hz, 2H), 4.25 (dd, *J* = 2.6 Hz, *J* = 1.6 Hz, 2H), 4.27-4.40 (m, 2H), 4.38 (s, 10H), 4.47 (d, *J* = 12.3 Hz, 2H, A part of AB-system), 4.56 (dd, *J* = 2.6 Hz, *J* = 1.6 Hz, 2H), 5.12 (d, *J* = 12.3 Hz, B part of AB-system), 6.78-6.86 (m, 4H), 7.12-7.19 (m, 4H) ppm.

^{13}**C-NMR**: (75 MHz, Acetone-d6): δ = 20.6 (CH_3 x2), 20.7 (CH_3 x2), 55.5 (CH_3 x2), 60.4 (CH x2), 63.4 (CH x2, Fc), 66.2 (CH_2 x2), 70.5 (CH x10), 72.1 (CH x2, Fc), 72.2 (CH x2, Fc), 77.4 (C x2, Fc), 106.5 (C x2, Fc), 114.4 (CH x4), 130.3 (CH x4), 130.5 (C x2), 155.0 (C x2, C=O), 160.2 (C x2) ppm.

IR (HATR): ν_{max} = 3097, 2997, 2965, 2934, 2834, 1699, 1613, 1586, 1514, 1451, 1412, 1380, 1363, 1284, 1246, 1174, 1166, 1108, 1085, 1051, 1035, 1011, 822, 768 cm^{-1}.

ESI-MS m/z (rel. intensity %): 813.2 (100, $[M+H]^+$), 814.2 (60), 815.2 (16), 811.2 (14) 812.2 (12), 707.2 (14).

HRMS (ESI): calculated for $C_{44}H_{49}Fe_2N_2O_6$ $[M+H]^+$: 813.2211; founded: 813.2298

Retention time HPLC: 18.34 min. ((R_p,S_p)-**4.110** (*meso* compound): 17.94 min.) (method 2), 5.80 min., ((R_p,S_p)-**4.110** (*meso* compound): 5.54 min.) (method 4)

Optical rotation: $[\alpha]_D^{20}$ = -221.4 (c 0.5, acetone)

4.9.13. Synthesis of (R_p,R_p)-2,2'-Bis[*N*-methyl amine]-1,1'-biferrocene **4.82**

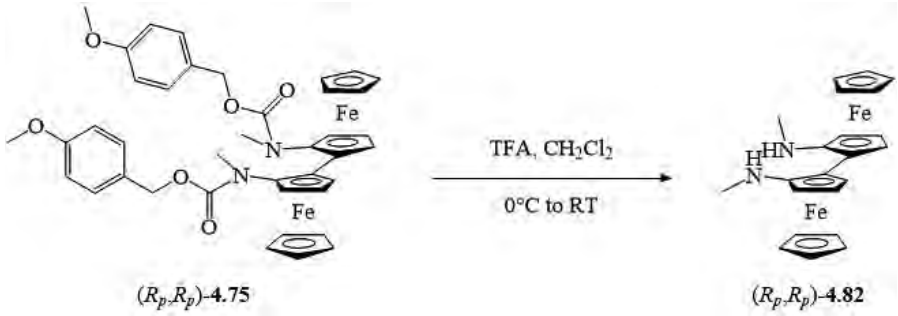

An oven-dried, 50 mL round-bottom flask was charged with a magnetic stirring bar, (R_p,R_p)-**4.75** (130 mg, 0.172 mmol) and CH_2Cl_2 (12 mL). The reaction flask was cooled to 0°C using an ice-water bath. TFA (132 µL, 1.72 mmol, 10 eq) was added dropwise. The reaction mixture was stirred for 15 min. at 0°C before it was allowed to warm up to room temperature and stirred for an additional hour. The reaction was cooled to 0°C again and quenched via dropwise addition of a solution of K_2CO_3 (713 mg, 5.16 mmol, 30 eq) in H_2O (20 mL). The aqueous phase was extracted 3 times with CH_2Cl_2 (30 mL). The combined organic phases were dried over anhydrous $MgSO_4$ and filtered. The solvents were removed under reduced pressure. The obtained brown crystals were triturated twice with a minimal amount of Et_2O. Diamine (R_p,R_p)-**4.82** was obtained as yellow-orange solid with a yield of 67.0%.

This compound was not bench stable.

Formula: $C_{22}H_{24}Fe_2N_2$ (428.13 g/mol)
R_f (*n*-hexane/acetone: 70/30): 0.35
^{1}**H-NMR** (Acetone-d6, 300 MHz): δ = 2.82 (s, 6H), 3.47 (br. s, 2H), 3.83-3.91 (m, 2H), 3.93-4.00 (m, 2H), 4.08-4.15 (m, 2H), 4.21 (s, 10H) ppm.
^{13}**C-NMR** (Acetone-d6, 75.4 MHz): δ = 33.8 (CH_3 x2), 53.9 (CH x2), 61.9 (CH x2), 65.7 (CH x2), 69.3 (CH x10), 171.06 (C) ppm. (1 *C not observed*)
ESI-MS m/z (rel. intensity %): 428.0 (100), 429.0 (100) $[M+H]^+$, 430.0 (18), 426.0 (12), 427.0 (11)
Retention time HPLC: 7.55 min. ((R_p,S_p)-**4.111** (*meso* compound): 7.76 min.) (method 3), 2.89 min. (method 4)

Due to the fact that compound is not bench stable, full characterization could not be performed.

4.9.14. Synthesis of (R_p,R_p)-2,2'-Bis[*N-iso*-propyl amine]-1,1'-biferrocene **4.83**

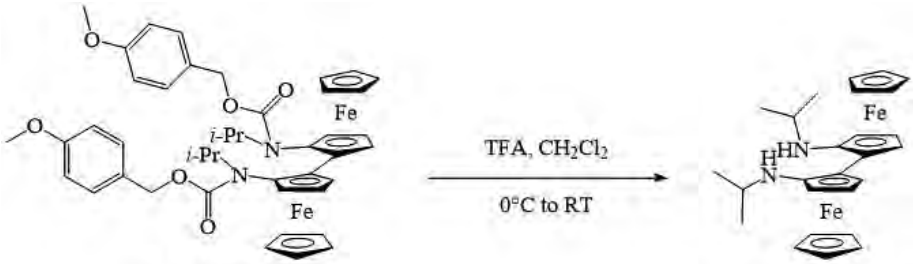

(R_p,R_p)-**4.79** (R_p,R_p)-**4.83**

An oven-dried, 50 mL round-bottom flask was charged with a magnetic stirring bar and (R_p,R_p)-**4.79** (140 mg, 0.172 mmol). CH_2Cl_2 (12 mL) was added and the reaction flask was cooled to 0°C using an ice-water bath. TFA (132 µL, 1.72 mmol, 10 eq) was added dropwise. The reaction The reaction mixture was stirred for 15 min. at 0°C before it was allowed to warm up to room temperature and stirred for an additional hour. The reaction was cooled to 0°C again and quenched via dropwise addition of a solution of K_2CO_3 (713 mg, 5.16 mmol, 30 eq) in of water (20 mL). The aqueous phase was extracted 3 times with CH_2Cl_2 (30 mL). The combined organic phases were dried over anhydrous $MgSO_4$ and filtered. The solvents were removed under reduced pressure and the resulting res-

idue was purified by flash chromatography on neutralized silica gel[29] (*n*-hexane/Et_2O/Et_3N: 88/10/2) affording (R_p,R_p)-**4.83** as a red solid with a yield of 88.6%.

This compound was not bench stable.

Formula: $C_{26}H_{32}Fe_2N_2$ (484.24 g/mol)
R_f (*n*-hexane/acetone 70:30): 0.59
^{1}**H-NMR** (Acetone-d6, 400 MHz): δ = 1.26 (d, *J* = 6.2 Hz, 6H), 1.44 (d, *J* = 6.2 Hz, 6H), 2.75-2.85 (m, 2H), 3.35-3.50 (m, 2H), 3.65-4.15 (m, 6H), 4.05 (s, 10H) ppm.
ESI-MS m/z (rel. intensity %): 484.8 (100), 485.8 (37) $[M+H]^+$
HRMS (ESI): calculated for $C_{26}H_{33}Fe_2N_2$ $[M+H]^+$: 485.1264; founded: 485.1318; calculated for $C_{26}H_{32}Fe_2N_2$ $[M]^{\cdot+}$: 484.1264; founded: 484.1259
Retention time HPLC: 6.40 min. ((R_p,S_p)-**4.112** (*meso* compound): 5.96 min.) (method 4)

Due to the fact that compound is not bench stable, full characterization could not be performed.

4.9.15. Synthesis of [N^2,$N^{2'}$-(dimethyl)-(1,1'-biferrocene)-2,2'-diamido]methyl phosphite **4.89**

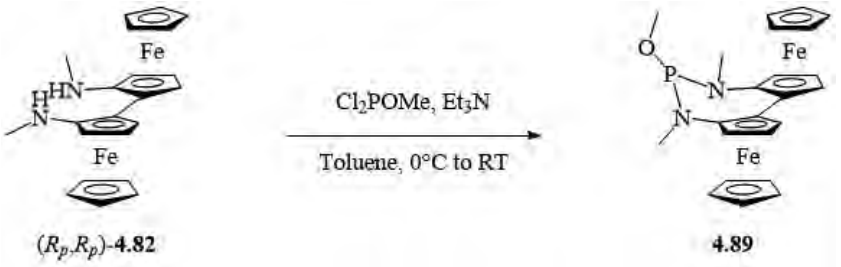

(R_p,R_p)-**4.82** **4.89**

An oven-dried, 25 mL round-bottom flask was charged with a magnetic stirring bar and (R_p,R_p)-**4.82** (110 mg, 0.26 mmol). The flask was cooled to 0°C using an ice-water bath. Deoxygenated toluene (2.5 mL) and deoxygenated Et_3N (360 µL, 0.64 mmol, 10 eq) were added followed by dropwise addition of a stock solution of Cl_2POMe in deoxygenated toluene (0.5 M, 570 µL, 0.29 mmol, 1.1 eq). The reaction was stirred for 15 min. at 0°C before it was allowed to warm up to room temperature and stirred overnight. The reaction was cooled to 0°C again and quenched with deoxygenated water (15 mL). The aqueous phase was extracted 3 times with deoxygenated CH_2Cl_2 (20 mL) under Ar flow.

29 Neutralized silica gel was obtained via washing with Et_2O/Et_3N (70/30) and eluens system before the column chromatographic separation was started.

The combined organic phases were dried over anhydrous $MgSO_4$ and filtered. The solvents were removed under reduced pressure and the resulting residue was purified by flash on neutralized silica gel29 (*n*-hexane/Et_2O/Et_3N: 97/2/1) affording **4.89** as an orange solid with a yield of 73.4%.

This compound was not bench stable.

Formula: $C_{23}H_{25}Fe_2N_2OP$ (488.12 g/mol)
R_f (*n*-hexane/EtOAc: 70/30): 0.61
^{1}**H-NMR** (Acetone-d6, 400 MHz): δ = 3.01 (d, *J* = 14.2 Hz, 3H), 3.16 (d, *J* = 12.9 Hz, 3H), 3.19 (d, *J* = 15.0 Hz, 3H), 3.89 (dd, *J* = 2.6 Hz, *J* = 1.6 Hz, 1H), 3.90 (app t, *J* = 2.6 Hz, 1H), 3.96 (s, 5H), 4.00 (dd, *J* = 2.6 Hz, *J* = 1.6 Hz, 1H), 4.01 (s, 5H), 4.07 (app t, *J* = 2.6 Hz, 1H), 4.34 (dd, *J* = 2.6 Hz, *J* = 1.6 Hz, 1H), 4.42 (dd, *J* = 2.6 Hz, *J* = 1.6 Hz, 1H) ppm.
^{13}**C-NMR** (Acetone-d6, 100 MHz): δ = 37.9 (d, *J* = 48.4 Hz, CH_3), 39.6 (d, *J* = 50.6 Hz, CH_3), 50.2 (d, *J* = 13.2 Hz, CH_3), 54.3 (CH), 56.5 (CH), 62.6 (CH), 64.4 (CH), 64.8 (CH), 66.2 (CH), 70.5 (CH x5), 70.8 (CH x5), 73.0 (C), 81.5 (C), 105.3 (d, *J* = 7.3 Hz, C), 105.8 (d, *J* = 11.0 Hz, C) ppm.
^{31}**P–NMR** (Acetone-d6, 121 MHz): δ = 130.30 ppm.
IR (HATR): ν_{max} = 3093, 2920, 2890, 2816, 1470, 1452, 1410, 1360, 1263, 1232, 1206, 1178, 1104, 1084, 1025, 999, 930, 864, 839, 815, 799, 789, 718, 680 cm^{-1}.
ESI-MS m/z (rel. intensity %): 489.0 (100) $[M+H]^+$, 488.0 (87) $[M]^{\cdot+}$, 490.0 (28)
HRMS (ESI): calculated for $C_{23}H_{26}Fe_2N_2OP$ $[M+H]^+$: 489.0403; found: 489.0439, calculated for $C_{23}H_{25}Fe_2N_2OP$ $[M]^{\cdot+}$: 488.0403; found: 488.0387
Retention time HPLC: 5.37 min. (method 4), 1.75 min. (method 5)
Optical rotation: $[\alpha]_D^{20}$ = -1457.9 (c 0.095, acetone)

4.9.16. Synthesis of [N^2,$N^{2'}$-(dimethyl)-(1,1'-biferrocene)-2,2'-diamido]ethyl phosphite **4.90**

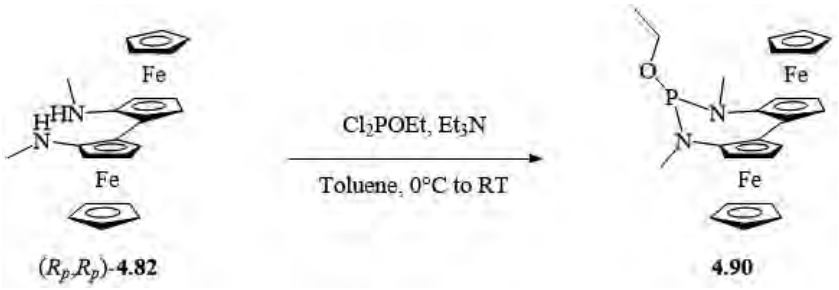

(R_p,R_p)-**4.82** **4.90**

An oven-dried, 25 mL round-bottom flask was charged with a magnetic stirring bar and (R_p,R_p)-**4.82** (110 mg, 0.26 mmol). The flask was cooled to 0°C using an ice-water bath. Deoxygenated toluene (2.5 mL) and deoxygenated Et_3N (360 µL, 0.64 mmol, 10 eq) were added followed by dropwise addition of a stock solution of Cl_2POEt in deoxygenated toluene (0.5 M, 570 µL, 0.29 mmol, 1.1 eq). The reaction was stirred for 15 min. at 0°C before it was allowed to warm up to room temperature and stirred overnight. The reaction was cooled to 0°C again and quenched with deoxygenated water (15 mL). The aqueous phase was extracted 3 times with deoxygenated CH_2Cl_2 (20 mL) under Ar flow. The combined organic phases were dried over anhydrous $MgSO_4$ and filtered. The solvents were removed under reduced pressure and the resulting residue was purified by flash on neutralized silica gel29 (*n*-hexane/Et_2O/Et_3N: 97/2/1) affording **4.90** as an orange solid with a yield of 71.2%.

This compound was not bench stable.

Formula: $C_{24}H_{27}Fe_2N_2OP$ (502.15 g/mol)
R$_f$ (*n*-hexane/EtOAc: 70/30): 0.62
^{1}**H-NMR** (Acetone-d6, 400 MHz): δ = 1.04 (app t, *J* = 7.0 Hz, 3H), 3.01 (d, *J* = 14.3 Hz, 3H), 3.18 (d, *J* = 14.9 Hz, 3H), 3.26-3.37 (m, 1H), 3.49-3.58 (m, 1H), 3.86 (dd, *J* = 2.6 Hz, *J* = 1.6 Hz, 1H), 3.90 (br s, 1H), 3.99 (s, 5H), 4.00 (br s, 1H), 4.01 (s, 5H), 4.07 (app t, *J* = 2.6 Hz, 1H), 4.35 (br s, 1H), 4.41 (dd, *J* = 2.6 Hz, *J* = 1.6 Hz, 1H) ppm.
^{13}**C-NMR** (Acetone-d6, 100 MHz): δ = 17.3 (d, J_{CP} = 7.3 Hz, CH_3), 37.9 (d, J_{CP} = 47.7 Hz, CH_3), 39.5 (d, J_{CP} = 50.6 Hz, CH_3), 54.2 (CH), 56.3 (CH), 59.2 (d, J_{CP} = 14.7 Hz, CH_2), 62.5 (CH), 64.4 (CH), 64.7 (CH), 66.2 (CH), 70.5 (CH x5), 70.9 (CH x5), 73.0 (C), 81.8 (C), 105.57 (d, J_{CP} = 7.3 Hz, C x2) ppm.
^{31}**P–NMR** (Acetone-d6, 162 MHz): δ = 128.32 ppm.

IR (HATR): ν_{max} = 3096, 2970, 2924, 2871, 2794, 1469, 1453, 1409, 1386, 1358, 1347, 1229, 1203, 1178, 1104, 1082, 1041, 1025, 997, 926, 915, 860, 837, 812, 794, 743, 708, 684 cm^{-1}.

ESI-MS m/z (rel. intensity %): 503.0 (100) $[M+H]^+$, 502.0 (87) $[M]^{\cdot+}$, 504.0 (28)

HRMS (ESI): calculated for $C_{24}H_{28}Fe_2N_2OP$ $[M+H]^+$: 503.0560; found: 503.0594, calculated for $C_{24}H_{27}Fe_2N_2OP$ $[M]^{\cdot+}$: 502.0560; found: 502.552

Retention time HPLC: 6.26 min. (method 4), 1.75 min. (method 5)

Optical rotation: $[\alpha]_D^{20}$ = -1200.0 (c 0.13, acetone)

4.9.17. Synthesis of [N^2,$N^{2'}$-(di-*iso*-propyl)-(1,1'-biferrocene)-2,2'-diamido] methyl phosphite **4.91**

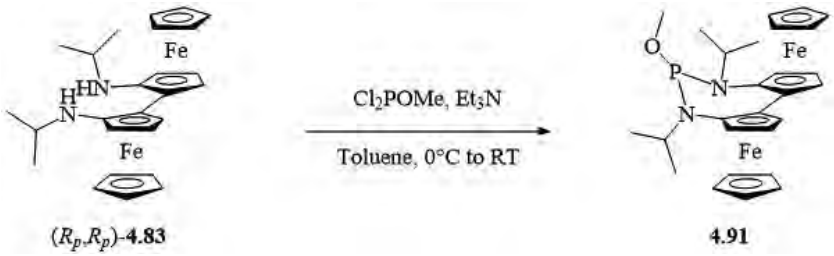

(R_p,R_p)-**4.83** **4.91**

An oven-dried, 25 mL round-bottom flask was charged with a magnetic stirring bar and (R_p,R_p)-**4.83** (110 mg, 0.26 mmol). The flask was cooled to 0°C using an ice-water bath. Deoxygenated toluene (2.5 mL) and deoxygenated Et_3N (360 µL, 0.64 mmol, 10 eq) were added followed by dropwise addition of a stock solution of Cl_2POMe in deoxygenated toluene (0.5 M, 570 µL, 0.29 mmol, 1.1 eq). The reaction was stirred for 15 min. at 0°C before it was allowed to warm up to room temperature and stirred overnight. The reaction was cooled to 0°C again and quenched with deoxygenated water (15 mL). The aqueous phase was extracted 3 times with deoxygenated CH_2Cl_2 (20 mL) under Ar flow. The combined organic phases were dried over anhydrous $MgSO_4$ and filtered. The solvents were removed under reduced pressure and the resulting residue was purified by flash on neutralized silica gel29 (*n*-hexane/Et_2O/Et_3N: 97/2/1) affording **4.91** as an orange solid with a yield of 22.1%.

This compound was not bench stable.

Formula: $C_{27}H_{33}Fe_2N_2OP$ (544.23 g/mol)

$\mathbf{R_f}$ (*n*-hexane/EtOAc: 80/20): 0.62

^{1}**H-NMR** ($CDCl_3$, 400 MHz): δ = 1.42 (d, *J* = 6.8 Hz, 3H), 1.46 (d, *J* = 6.8 Hz, 3H), 1.48 (d, *J*

= 6.8 Hz, 3H), 1.50 (d, *J* = 6.8 Hz, 3H), 3.15 (d, $J_{PH'}$ = 13.7 Hz, 3H), 3.55 (dd, *J* = 2.6 Hz, *J* = 1.5 Hz, 1H), 3.82 (dspt, J_{PH} = 22.5 Hz, *J* = 6.8 Hz, 1H), 3.91 (br s, 1H), 3.97 (s, 5H), 3.98 (s, 5H), 4.00 (app t, *J* = 2.6 Hz, 1H), 4.05-4.10 (m, 1H), 4.07 (dspt, J_{PH} = 22.5 Hz, *J* = 6.8 Hz, 1H), 4.26 (br s, 1H), 4.27 (dd, *J* = 2.6 Hz, *J* = 1.5 Hz, 1 H) ppm.

^{13}**C-NMR** ($CDCl_3$, 100 MHz): δ = 23.0 (d, J_{CP} = 14.7 Hz, CH_3), 23.7 (d, J_{CP} = 17.6 Hz, CH_3), 23.9 (d, J_{CP} = 8.8 Hz, CH_3), 24.5 (d, J_{CP} = 18.3 Hz, CH_3), 50.4 (d, J_{CP} = 16.9 Hz, CH_3), 52.3 (d, J_{CP} = 35.2 Hz, CH), 53.4 (CH), 54.0 (d, J_{CP} = 30.1 Hz, CH), 56.4 (CH), 61.4 (CH), 63.2 (CH), 63.8 (CH), 65.6 (CH), 69.8 (CH x5), 70.5 (CH x 5), 70.7 (C), 81.3 (C), 105.6 (d, J_{CP} = 6.6 Hz, C x2) ppm.

^{31}**P–NMR** ($CDCl_3$, 162 MHz): δ = 106.53 ppm.

ESI-MS m/z (rel. intensity %): 544.0 (100%) $[M]^{\cdot+}$, 545.0 (52) $[M+H]^+$, 542.0 (10)

HRMS (ESI): calculated for $C_{27}H_{34}Fe_2N_2OP$ $[M+H]^+$: 545.1029: found: 545.1058, calculated for $C_{27}H_{33}Fe_2N_2OP$ $[M]^{\cdot+}$: 544.1029 found: 544.1030

Retention time HPLC: 7.59 min. (method 4), 4.89 min. (method 5)

4.9.18. Synthesis of [N^2,$N^{2'}$-(di-*iso*-propyl)-(1,1'-biferrocene)-2,2'-diamido] ethyl phosphite **4.92**

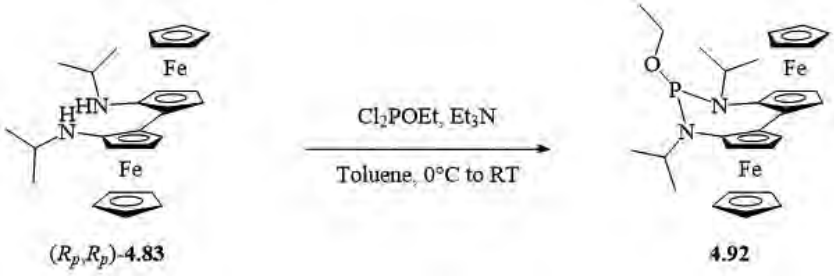

(R_p,R_p)-**4.83** **4.92**

An oven-dried, 25 mL round-bottom flask was charged with a magnetic stirring bar and (R_p,R_p)-**4.83** (110 mg, 0.26 mmol). The flask was cooled to 0°C using an ice-water bath. Deoxygenated toluene (2.5 mL) and deoxygenated Et_3N (360 µL, 0.64 mmol, 10 eq) were added followed by dropwise addition of a stock solution of Cl_2POEt in deoxygenated toluene (0.5 M, 570 µL, 0.29 mmol, 1.1 eq). The reaction was stirred for 15 min. at 0°C before it was allowed to warm up to room temperature and stirred overnight. The reaction was cooled to 0°C again and quenched with deoxygenated water (15 mL). The aqueous phase was extracted 3 times with deoxygenated CH_2Cl_2 (20 mL) under Ar flow. The combined organic phases were dried over anhydrous $MgSO_4$ and filtered. The solvents were removed under reduced pressure and the resulting residue was purified by

flash on neutralized silica gel29 (*n*-hexane/Et_2O/Et_3N: 97/2/1) affording **4.92** as an orange solid with a yield of 17.0%.

This compound was not bench stable.

Formula: $C_{28}H_{35}Fe_2N_2OP$ (558.25 g/mol)
R_f (*n*-hexane/EtOAc: 80/20): 0.63
^{1}**H-NMR** (Acetone-d6, 400 MHz): δ = 1.07 (t, *J* = 7.0 Hz, 3H), 1.40 (d, *J* = 6.8 Hz, 3H), 1.44 (d, *J* = 6.8 Hz, 3H), 1.47 (d, *J* = 6.8 Hz, 3H), 1.51 (d, *J* = 6.8 Hz, 3H), 3.26 (ddq, *J* = 17.0 Hz, J_{PH} = 14.2 Hz, *J* = 7.0 Hz, 1H), 3.52 (ddq, *J* = 17.0 Hz, J_{PH} = 14.2 Hz, *J* = 7.0 Hz, 1H), 3.59 (dd, *J* = 2.6 Hz, *J* = 1.5 Hz, 1H), 3.84-3.98 (m, 12H), 4.01 (app t, *J* = 2.6 Hz, 1H), 4.010-4.15 (m, 1H), 4.19 (dspt, J_{PH} = 22.5 Hz, *J* = 6.8 Hz, 1H), 4.32-4.41 (m, 2H) ppm.
^{13}**C-NMR** ($CDCl_3$, 100 MHz): spectrum not assignable due to decomposition
^{31}**P–NMR** ($CDCl_3$, 162 MHz): δ = 104.71 ppm.
IR (HATR): ν_{max} = 3092, 2965, 2925, 2867, 2357, 1459, 1438, 1380, 1361, 1250, 1224, 119, 1174, 1152, 1132, 1104, 1046, 1032, 998, 936, 915, 901, 882, 810, 749 cm^{-1}.
ESI-MS m/z (rel. intensity %): 558.1 (100) $[M]^{\cdot+}$, 559.1 (65) $[M+H]^+$, 560.1 (19)
HRMS (ESI): calculated for $C_{28}H_{36}Fe_2N_2OP$ $[M+H]^+$: 559.1186; found: 559.1199, calculated for $C_{28}H_{35}Fe_2N_2OP$ $[M]^{\cdot+}$: 558.1186; found: 558.1178
Retention time HPLC: 5.67 min. (method 5)

4.9.19. Synthesis of Methyl *Z*-2-acetamido-3-phenylacrylate **4.102**

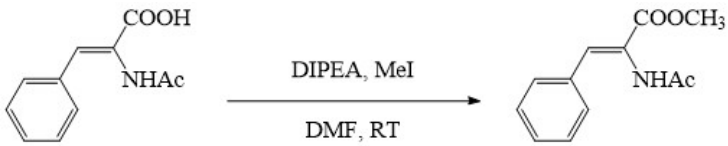

4.113 **4.102**

An oven-dried 50 mL round-bottom flask was charged with a magnetic stirring bar and α-acetamidocinnamic acid **4.113** (2.21 g, 10.7 mmol). Anhydrous DMF (20 mL), anhydrous DIPEA (3.7 mL, 21.5 mol, 2 eq) and iodomethane (2.7 mL, 43.1 mmol, 4 eq) were added. The reaction mixture was stirred overnight at room temperature, quenched with a saturated solution of NH_4Cl (100 mL) and extracted three times with EtOAc (100 mL). The combined organic phases were washed with a 10 mol% solution of $KHCO_3$ (100 mL) and a 10 mol% solution of citric acid (100 mL) and dried over Na_2SO_4. After filtration and removal of the organic solvents under reduced pressure, the obtained solid was

washed with Et_2O and *n*-hexane. Methyl *Z*-2-acetamido-3-phenylacrylate **4.102** was obtained as a white solid with a yield of 82.3%.

Formula: $C_{12}H_{13}NO_3$ (219.24 g/mol).
R_f (CH_2Cl_2/EtOAc: 85/15): 0.19
^{1}**H-NMR:** (400 MHz, $CDCl_3$): δ = 2.15 (s, 3H), 3.86 (s, 3H), 6.98 (br s, 1H), 7.10-7.7.85 (m, 6H) ppm.
^{13}**C-NMR:** (100 MHz, $CDCl_3$): δ = 23.5 (CH_3), 52.7 (CH_3), 124.2 (C), 128.6 (CH x 2), 129.5 (CH), 129.6 (CH x 2), 132.2 (CH), 133.7 (C), 165.7 (C), 168.7 (C) ppm.
ESI-MS m/z (rel. intensity %): 242.1 (100) $[M+Na]^+$, 220.1 (25) $[M+H]^+$.
Melting point: 123°C; literature: 122-124°C[61]

4.9.20. General procedure Rhodium(I)-catalyzed asymmetric hydrogenation of **4.102**

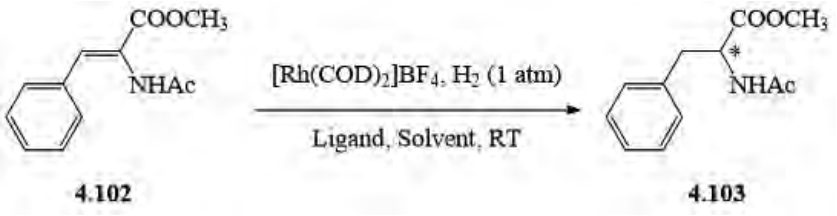

An oven-dried Schlenk tube was connected to an argon Schlenk line, charged with a magnetic stirring bar, $Rh(COD)_2BF_4$ (2.8 mg, 6.89 µmol, 1 mol%) and a ligand (**4.89**, **4.90**, **4.91**, **4.92**) (13.8 µmol, 2 mol%). Degassed[30] CH_2Cl_2 (3 mL) was added to the catalyst mixture and stirred for 30 min. at room temperature. Methyl *Z*-2-acetamido-3-phenylacrylate **4.102** (151 mg, 689 µmol) was added and hydrogen gas was bubbled through the reaction mixture for 10 min. The reaction was stirred overnight at room temperature under a hydrogen atmosphere using a balloon. The reaction mixture was filtered over a short plug of silica gel and eluted with EtOAc. The solvents were removed under reduced pressure and **4.103** was obtained as a white solid. Conversion and enantiomeric excess were determined by chiral LC analysis on a OD-H column. The absolute configuration of **4.103** was assigned via correlation of its specific rotation with literature values.[61,62]

30 Degassing was accomplished by bubling of H_2-gas through the solvent for 10 min. using a balloon.

Formula: $C_{12}H_{15}NO_3$ (221.25 g/mol).

R_f (CH_2Cl_2/EtOAc: 90/10): 0.18

^{1}**H-NMR:** (500 MHz, $CDCl_3$): δ = 1.98 (s, 3H), 3.09 (dd, *J* = 13.9 Hz, *J* = 5.8 Hz, 1H), 3.14 (dd, *J* = 13.9 Hz, *J* = 5.8 Hz, 1H), 3.73 (s, 3H), 4.83 (app dt, *J* = 7.8 Hz, *J* = 5.8 Hz, 1H), 5.95 (br s, 1H), 7.07-7.11 (m, 2H), 7.22-7.32 (m, 3H) ppm.

^{13}**C-NMR:** (125 MHz, $CDCl_3$): δ = 23.3 (CH_3), 38.0 (CH_2), 52.5 (CH), 53.2 (CH_3), 127.3 (CH), 128.4 (CH), 128.8 (CH), 135.9 (C), 169.8 (C), 172.2 (C) ppm.

ESI-MS m/z (rel. intensity %): 222.1 (74) $[M+H]^+$, 180.1 (92), 162.1 (100), 120.1 (50)

Retention time HPLC: 4.73 min. (method 3)

Chiral HPLC: Chiralcel OD-H column, solvent: *n*-hexane/EtOH (95:5), flow rate = 1mL/min, t = 30 min., T = 35°C, retention times: 11.20 min. for (*R*)-**4.103**, 12.80 min. (*S*)-**4.103** and 20.81 min. for starting material **4.102**.

Melting point: 64°C

4.10. References

[1] C. Markert, P. Rösel, A. Pfaltz, *J. Am. Chem. Soc.*, **2008**, *130*, 3234-3235

[2] I. Ayora, R. M. Ceder, M. Espinel, G. Muller, M. Rocamora, Serrano, *Organometallics*, **2011**, *30*, 115-128

[3] M. J. Bravo, I. Favier, N. Saffon, R. M. Ceder, G. Muller, M. Gómez, M. Rocamora, *Organometallics*, **2014**, *33*, 771-779

[4] M. J. Bravo, R. M. Ceder, A. Grabulosa, G. Muller, M. Rocamora, J. C. Bayón, *Organometallics*, **2015**, *34*, 3799-3808

[5] M. J. Bravo, R. M. Ceder, G. Muller, R. Rocamora, *Organometallics*, **2013**, *32*, 2632-2642

[6] M. T. Reetz, H. Oka, R. Goddard, *Synthesis*, **2003**, *12*, 1809-1814

[7] J. –M. Brunel, T. Constantieux, A. Labande, F. Lubatti, G. Buono, *Tetrahedron Lett.*, **1997**, *38*, 5971-5974

[8] J. –M. Brunel, T. Constantieux, G. Buono, *J. Org. Chem.*, **1999**, *64*, 8940-8942

[9] T. Constantieux, J. –M. Brunel, A. Labande, G. Buono, *Synlett*., **1998**, 49-50

[10] G. Delapierre, J. M. Brunel, T. Constantieux, *Tetrahedron: Asymmetry*, **2001**, *12*, 1345-1352

[11] J. –M. Brunel, B. Del Campo, G. Buono, *Tetrahedron Lett.*, **1998**, *39*, 9663-9666

[12] G. Delapierre, T. Constantieux, J. –M. Brunel, G. Buono, *Eur. J. Org. Chem.*, **2000**, 2507-2511

[13] J. –M. Brunel, A. Tenaglia, G. Buono, *Tetrahedron: Asymmetry*, **2000**, *11*, 3585-3590

[14] E. E. Nifant'ev, A. I. Zavalishina, E. I. Orzhekovskaya, N. M. Selezneva, L. K. Vasyanina, E. V. Vorontsov, A. I. Stash, V. K. Bel'skii, *Russian Journal of General Chemistry*, **2002**, *72*, 193-206

[15] K.N. Gavrilov, S. V. Zheglov, E. A. Rastorguev, N. N. Groshkin, M. G. Maksimova, E. B. Benetsky, V. A. Davankov, M. T. Reetz, *Adv. Synth. Catal.*, **2010**, *352*, 2599-2610

[16] V. N. Tsarev, S. E. Lyubimov, A. A.Shiryaev, S. V. Zheglov, O. G. Bondarev, V. D. Davankov, A. A. Kabro, S. K. Moiseev, V. N. Kalinin, K. N. Gavriolo, *Eur. J. Org. Chem.*, **2004**, 2214-2222

[17] K. N. Gavrilov, S. E. Lyubimov, S. V. Zheglov, E. B. Benetsky, P. V. Petrovskii, E. A. Rastorguev, T. B. Grishina, V. A. Davankov, *Adv. Synth. Catal.*, **2007**, *349*, 1085-1094

[18] K. N. Gavrilov, A.A. Shiyaev, S. V. Zheglov, O. Potapova, I. V. Chuchelkin, I. M. Novikov, E. A. Rastorguev, V. A. Davankov, *Tetrahedron: Asymmetry*, **2013**, *24*, 409-417

[19] K. N. Gavrilov, S. V. Zheglov, V. K. Gavrilov, I. V. Chuchelkin, I. M. Novikov, A. A. Shiryaev, A. N. Volov, I. A. Zamiltskov, *Tetrahedron: Asymmetry*, **2014**, *25*, 1116-1121

[20] K. N. Gavrilov, A. A. Shiryaev, S. V. Zheglov, V. K. Gavrilov, N. N. Groshkin, M. G. Maksimova, A. N. Volov, I. A. Zamiltskov, *Tetrahedron*, **2014**, *70*, 616-624

[21] B. M. Trost, T. M. Lam, *J. Am. Chem. Soc.*, **2012**, *134*, 11319-11321

[22] M. Schmitkamp, W. Leitner, G. Franciò, *Catal. Sci. Technol.*, **2013**, *3*, 589-594

[23] (a) O. Riant, O. Samuel, H.B. Kagan, *J. Am. Chem. Soc.*, **1993**, *115*, 5835-5836; (b) O. Riant, O. Samuel. T. Flessner, S. Taudine, H.B. Kagan, *J. Org. Chem.*, **1997**, *62*, 6733-6745

[24] C. J. Richards, A. W. Mulvaney, *Tetrahedron Asymmetry*, **1996**, *7*, 1419-1430

[25] C. J. Richards, T. Damaldis, D. E. Hibbs, M. B. Hursthouse, *Synlett*., **1995**, 74-76

[26] T. Sammakia, H. A. Latham, D. R. Schaad, *J. Org. Chem.*, **1995**, 60, 10-11

[27] T. Sammakia, H. A. Latham, *J. Org. Chem.*, **1995**, *60*, 6002-6003

[28] T. Sammakia, H. A. Latham, *J. Org. Chem.*, **1996**, *61*, 1629-1635

[29] (a) Y. Nishibashi, S. Uemura, *Synlett.*, **1995**, 79-81; (b) Y. Nishibayashi, K. Segawa, Y. Arikawa, K. Ohe, M. Hidai, S. Uemura, *J. Organomet. Chem.*, **1997**, *545-546*, 381-391

[30] D. Schaarsmidt, H. Lang, *Organometallics*, **2013**, *32*, 5668-5704

[31] D. Tilly, J. Magolan, J. Mortier, *Chem. Eur. J.*, **2012**, *18*, 3804-3820

[32] V. Snieckus, *Chem. Rev.*, **1990**, *90*, 879-933

[33] P. C. Reeves, *Org. Synt.*, **1977**, *56*, 28-31

[34] L.–X. Dai, X.–L. Hou, *Chiral ferrocenes in asymmetric catalysis*, Wiley-VCH Verlag GmbH & Co. KGaA, **2010**

[35] C. Elschenbroich, *Organometallics*, Wiley-VCH, **2006**

[36] L.-X. Dai, T. Tu. S.-L. You, W.-P. Deng, X.-L. Hou, *Acc. Chem. Res.*, **2003**, *36*, 659-667

[37] M. Derenberg, P. Hodge, *Tetrahedron Lett.*, **1971**, *41*, 3825-3828

[38] S. A. Herbert, D. C. Castell, J. Clayden, G. E. Arnott, *Org. Lett.*, **2013**, *15*, 3334-3337

[39] K. H. Ahn, C.-W. Cho, H.-H. Baek, J. Park, S. Lee, *J. Org. Chem.*, **1996**, *61*, 4937-4943

[40] K. A. Lutomski, A. I. Meyers, In *Asymmetric Synthesis*, Ed. J. D. Morisson, Academic Press: San Diego, **1984**, Vol 3, Part B, chapter 3

[41] Y. Nishibayashi, K. Segawa, Y. Arikawa, K. Ohe, M. Hidai, S. Uemura, *J. Organomet. Chem.*, **1997**, *545-546*, 381-398

[42] W. Zhang, T. Kida, Y. Nakatsjuji, I. Ikeda, *Tetrahedron Lett.*, **1996**, *37*, 7995-7998

[43] C. Bolm, K. Muñiz-Fernández, A. Seger, G. Raabe, K. Günther, *J. Org. Chem.*, **1998**, *63*, 7860-7867

[44] J. M. Longmire, B. Wang, X. Zhang, *Tetrahedron Lett.*, **2000**, *41*, 5435-5439

[45] S.-L. You, Y.-M. Luo, W.-P. Deng, X.-L. Hou, L.-X. Dai, *J. Organomet. Chem.*, **2001**, *637-639*, 845-849

[46] R. Kuwano, T. Uemura, M. Saitoh, Y. Ito, *Tetrahedron: Asymmetry*, **2004**, *15*, 2263-2271

[47] A. M. Warshawsky, A. I. Meyers, *J. Am. Chem. Soc.*, **1990**, *112*, 8090-8099

[48] A. Leonidova, T. Joshi, D. Nipkow, A. Frei, J-E. Penner, S. Konatschnig, M. Patra, G. Gasser, *Organometallics*, **2013**, *32*, 2037-2040

[49] S. Arimoto, A.C. Haven Jr., *J. Am. Chem. Soc.*, **1955**, *77*, 6295-6297

[50] A. Bertogg, F. Camponovo, A. Togni, *Eur. J. Inorg. Chem.*, **2005**, 347-356

[51] A. Sagi, J. Risphon, D. Shabat, *Anal. Chem.*, **2006**, *78*, 1459-1461

[52] M. Herberhold, M. Ellinger, W. Kremnitz, *J. Organomet. Chem.*, **1983**, *241*, 227-240

[53] D. C. D. Butler, C. J. Richards, *Organometallics*, **2002**, *21*, 5433-5436

[54] A. Arrieta, J. M. Aizpurua, C. Palomo, *Tetrahedron Lett.*, **1984**, *25*, 3365-3368

[55] L. Kürti, B. Czakó, *Strategic Applications of Named Reactions in Organic Synthesis*, Elsevier, **2005**, p 116-117

[56] L. Kürti, B. Czakó, *Strategic Applications of Named Reactions in Organic Synthesis*, Elsevier, **2005**, p 466-467

[57] (a) M. F. Semmelhack, P. M. Helquist, L. D. Jones, *J. Am. Chem. Soc.*, **1971**, *93*, 5908-5910 (b) M. F. Semmelhack, P. Helquist, L. D. Jones, L. Keller, L. Mendelson, L. S. Ryono, J. G. Smith, R. D. Stauffer, *J. Am. Chem. Soc.*, **1981**, *103*, 6460-6471

[58] J. Niemeyer, G. Kehr, R. Fröhlich, G. Erker, *Eur. J. Inorg. Chem.*, **2010**, 49, 680-684

[59] L. Xiao, W. Weissensteiner, K. Mereiter, M. Widhalm, *J. Org. Chem.*, **2002**, *67*, 2206-2214

[60] (a) L. Xiao, K. Mereiter, F. Spindler, W. Weissensteiner, *Tetrahedron: Asymmetry*, **2001**, *12*, 1105-1108 (b) G. Espino, L. Xiao, M. Puchberger, K. Mereiter, F. Spindler, B. R. Manzano, F. A. Jalón, W. Weissensteiner, *Dalton Trans.*, **2009**, 2751-2763

[61] B.D. Vineyard, W.S. Knowles, M.J. Sabacky, G.L. Bachman, D.J. Weinkauff, *J. Am. Chem. Soc.*, **1977**, *99*, 5946-5952

[62] (a) A. Togni, C. Breutel, A. Schnyder, F. Spindler, H. Landert, A. Tijani, *J. Am. Chem. Soc.,* **1994**, *116*, 4062-4066 (b) J.P. Pye, K. Rossen, R. A. Reamer, N.N. Tsou, R.P. Volante, P.J. Reider, *J. Am. Chem. Soc.*, **1997**, *119*, 6207-6208

NOVEL BIDENTATE BIFERROCENE-BASED TROST-TYPE LIGANDS

"De waarheid is nooit precies zoals je dacht dat hij zou zijn."

"The truth is never exactly as you thought it would be."

Johan Cruijff

5.1. Introduction

In 1992 Trost and Van Vranken published a paper in which they used a new type of chiral ligands for palladium-catalyzed asymmetric allylic alkylations.[1] These ligands, which are now known as Trost ligands, were diphenylphosphinobenzoyl derivatives of C_2-symmetric diamines. The most general Trost ligand, the DACH-phenyl ligand **5.01**, has a diaminocyclohexyl backbone and is shown in Figure 5.1.

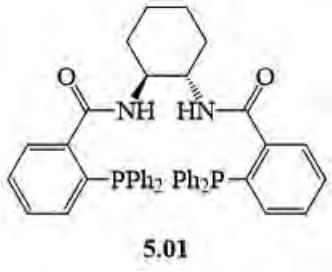

5.01

Figure 5.1 DACH-phenyl Trost ligand **5.01**

Scheme 5.1 shows the model asymmetric allylic amination reaction, tested for these types of bidentate diphosphine ligands. A yield of 97% and an *ee* of 78% were obtained for the DACH-phenyl Trost ligand. However, the best result in terms of *ee* was obtained with the ANDEN-phenyl ligand **5.04** (Figure 5.2), providing an *ee* of 88% (and a yield of 94%).

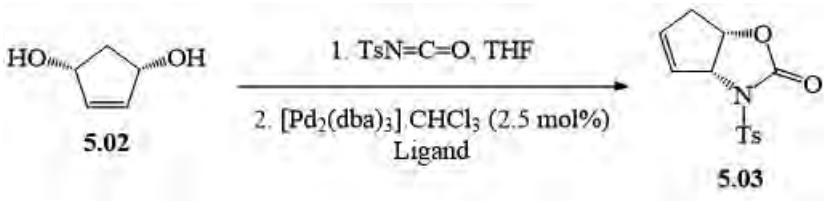

Scheme 5.1 First successful asymmetric transition metal catalyzed reaction using Trost ligands

Trost and Van Vranken synthesized a small library of this type of ligands by varying the chiral backbone. Ligand **5.05**, characterized by a 1,2-diphenyl-ethylenediamine substructure is another interesting diamide-diphosphine ligand. Replacement of the diamine by a diol allowed them to synthesize diester-diphosphine ligands **5.06** and **5.07**. However, these ligands showed to be less effective in terms of *ee* and yield in the model allylic amination reaction (Figure 5.2). Therefore the latter type of ligands is way much less exploited in the field of asymmetric transition metal catalysis.

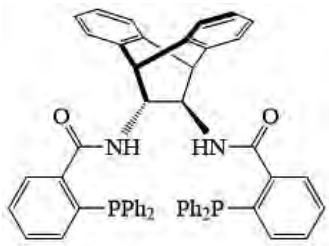

5.04 ANDEN-phenyl Trost
yield: 94%
ee: 88%

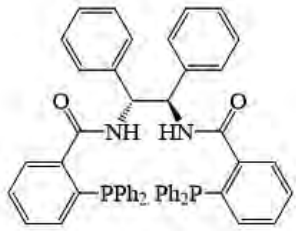

5.05
yield: 97%
ee: 80%

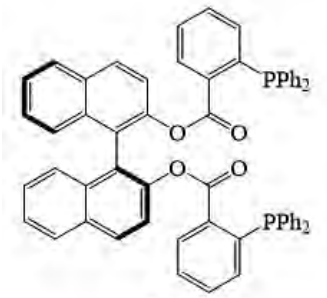

5.06
yield: 87%
ee: 40%

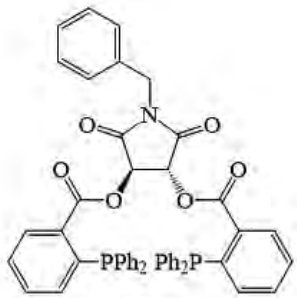

5.07
yield: 68%
ee: 75%

Figure 5.2 Other ligands published by Trost and Van Vranken that were tested in the model test reaction shown in Scheme 5.1

During the last decades more Trost-type ligands were developed by varying the 2-diphenylphosphinobenzoyl structure as well.[2-8] Some of these are straightforward like the DACH-naphthyl ligand **5.08** (Figure 5.3), which is characterized by a 2-diphenylphosphinonaphthyl substructure. Other ligands, such as the DACH-pyridyl ligand **5.09** where the nitrogen functions as a coordination center (instead of phosphorus) are totally different. As a consequence, the applications for this bidentate ligand are different as well. For example, the latter ligand showed good activity and enantioselectivity in a molybdenium-catalyzed asymmetric allylic alkylation for the synthesis of (-)-Δ^9-trans-tetrahydrocannabinol.[9]

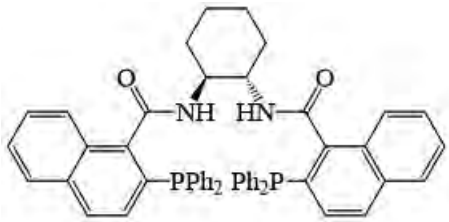

5.08 DACH-naphthyl

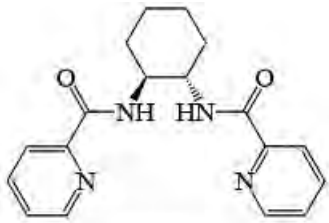

5.09 DACH-pyridyl

Figure 5.3 DACH-naphthyl Trost ligand **5.08** and DACH-pyridyl Trost ligand **5.09**

Two other interesting Trost-type ligands are **5.10** and **5.11** (Figure 5.4). The first one possesses an axial chiral binapthyldiamine backbone. The high success rate of BINAP has proven that axial chirality is an excellent chirality element to induce enantiocontrol. This ligand **5.10** was tested in the benchmark palladium-catalyzed desymmetrization of *meso*-cyclic carbamates of which an example is shown in Scheme 5.1.[4] However, low *ee*-values were obtained. In contrast, Bandini *et al.* used this ligand for the highly enantioselective synthesis of tetrahydro-γ-carbolines via intramolecular palladium-catalyzed allylic alkylation of indoles.[5] Enantioselectivities up to 93% in combination with a yield of 90% are reported. Due to the planar-chirality of the ferrocene substructure, ligand **5.11** has an extra element of chirality and therefore matched and mismatched situations are possible. Two diastereomers of this ligand type were first tested in the palladium-catalyzed asymmetric allylic alkylation of 2-cyclohexenyl esters and carbonates.[6] Enantioselectivities up to 92% in combination with 100% conversion and 91% yield were obtained for the matched situation. You *et al.* found that ligand **5.11** could be successfully used for the palladium-catalyzed asymmetric alkylation of ketone- enolates with enantioselectivities up to 95%.[7] One year later, the research group of Zhang

reported on the highly enantioselective silver-catalyzed [3+2]-cycloaddition of azomethine ylides with *ee*-values up to 96%.[8] The existence of this diversity of Trost-type ligands with possibility to fine-tune the steric and electronic properties of the diamine backbone as well as diphenylphosphinobenzoic acid substructure proves that this type of ligands are highly modular.

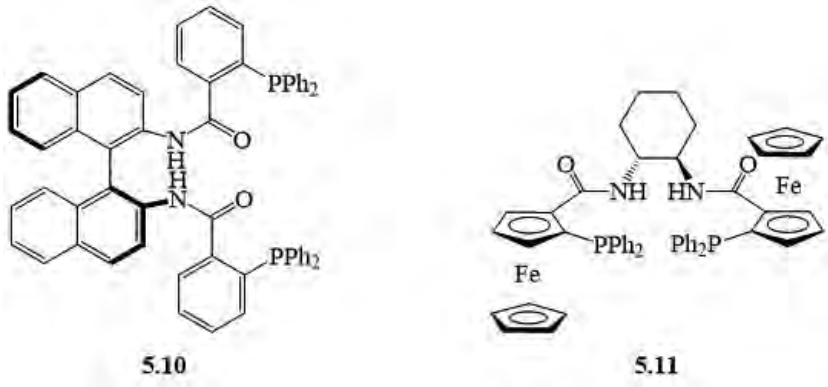

Figure 5.4 Interesting types of Trost ligands with axial chirality (**5.10**) and extra planar-chirality (**5.11**)

The Trost Modular Ligand series (TML series) has been successfully applied for a range of asymmetric allylic alkylations including reactions that have proven to be challenging for other chiral ligands, particularly those involving small cyclic allylic substrates.[10-15] It is generally accepted that the mechanism of the palladium-catalyzed reactions consist of four fundamental steps, which are shown in Scheme 5.2. These steps involve metal-olefin complexation, oxidative addition or ionization, nucleophilic addition and decomplexation. Every step of this catalytic cycle provides the opportunity for enantioselection.[16,17] Extensive mechanistic work demonstrates that ionization of palladium-olefin complex **5.14** occurs with inversion of stereochemistry, in an S_N2-like displacement of the leaving group by the incoming palladium 'nucleophile'.[18] The obtained η^3-bound (π-allyl)-palladium complex **5.16**, which functions as a key intermediate in the catalytic cycle, is in equilibrium with the corresponding η^1 derivatives. For these complexes there is the possibility for a rotation around a carbon-carbon bond. After rehybridization, a η^3-bound (π-allyl)-palladium complex is formed again. This π-σ-π interconversion may be involved with a *syn/anti* interconversion. Because the nucleophilic addition is the microscopic reverse of ionization, similar principles are valid. This also means that this step can be considered to be S_N2-like with palladium displaced by a nucleophile. To ensure an antiperiplanar trajectory, the nucleophile has to

approach the palladium-substrate complex in an *exo* sense (*vide infra*).[19] Besides enantioselectiviy, regioselectivity might be challenging as well. A combination of steric as well as electronic interactions determine at which carbon atom the nucleophilic addition will occur. These effects are dependent on the properties of the chiral ligands and the substrate itself.[16]

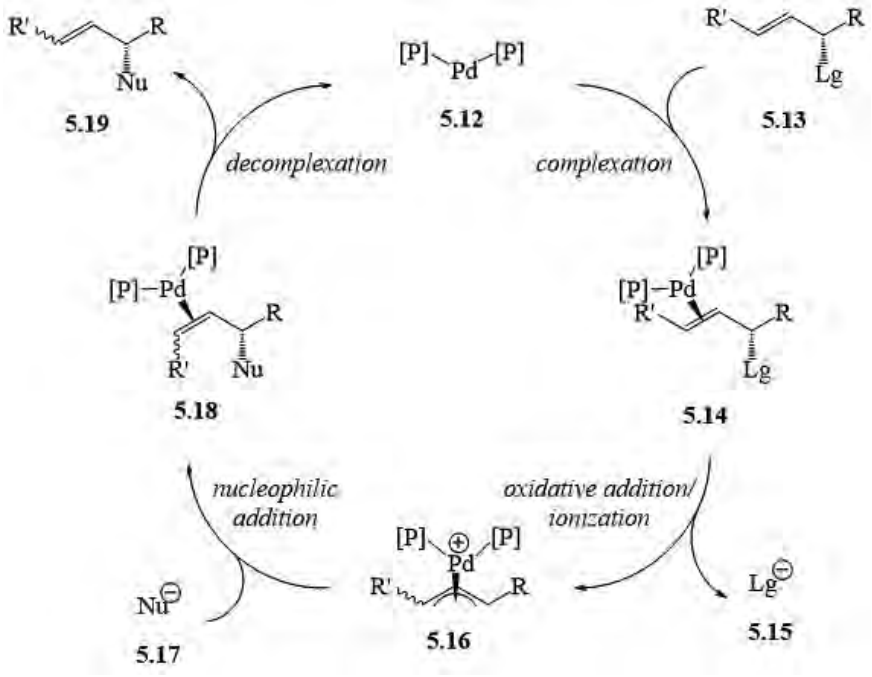

Scheme 5.2 Catalytic cycle of palladium-catalyzed asymmetric allylic substitution

Besides the chirality of the ligand, the choice of the transition metal (Pd, Ir, W, Mo, Rh) may also have an effect on the mechanism of enantioselectivity for allylic alkylation reactions.[20] Other parameters having an influence on the enantioselectivity are substrate, solvent, the nucleophile, escort ion (M^+), counter ion (X^-) additives and concentration of the reaction mixture.[21] Knowledge of the mode(s) of coordination of these bidentate diphosphine ligands to the metal is essential in any mechanistic explanation for this type of highly successful ligands. However, despite extensive efforts, crystals suitable for XRD-analysis of hypothetically catalytically active intermediates couldn't be obtained so far.[21-26] Instead, a working model has been proposed by Trost and co-workers to predict the stereochemistry of the palladium-catalyzed reactions with Trost-type ligands.[16,27] Having a closer look at the TML series, we see that all of

them are built of a chiral scaffold, two linkers (mostly amides), two coordinating phosphorus atoms and four bulky phenyl groups. It is generally assumed that the active ligand system consists of a bidentate diphosphine chelation to palladium forming a 13-membered ring. The working model, which is shown in Figure 5.5, considers only a time-averaged monomeric species in which the ligands coordinate in a C_2-symmetric manner.[16] Characteristic for these bisdiphenyldiphosphine ligands is the propeller-like arrangement of the phenyl groups to minimize sterical interactions between them. In this conformation, two phenyl rings are oriented approximately perpendicular to the plane of the allyl unit, pseudoaxially oriented, and acting as the 'walls'. The other two phenyl rings are oriented parallel according to the allyl plane, pseudoequatorially oriented and are known to be the 'flaps'. These walls and flaps are important for sterical reasons: they direct the way in which a substrate is oriented in the chiral cage: larger groups are oriented towards the flaps and smaller groups towards the walls. Moreover the walls are acting to selectively obstruct the egress of the leaving group (in the ionization step) and the entry of the nucleophile (in the nucleophilic addition step) in one front and one rear quadrant of the allyl substrate respectively. In S_N2-type reactions the preferred trajectory is one that places the leaving group at an angle of 180° to the approaching nucleophile. For the ionization reaction, palladium(0) can be considered as the nucleophile. For the nucleophilic addition, palladium(II) functions as the leaving group. Therefore, both ionization and nucleophilic addition should occur at an angle of 180°. According the working model proposed by Trost[21], the only reasonable accepted approach in the ionization step is that approach in which the leaving group is cleaved off at the side which bears the *syn*-substitutents of the π-allyl system. In the nucleophilic addition step, the nucleophile has to come in from this side as well. Moreover, for a matched situation, the leaving group and the nucleophile have to quit/enter the substrate under a raised flap for the ionization and nucleophilic addition step respectively. This cartoon 'wall' and 'flap' model has broad application in that it can be used to rationalize the outcome from nearly all the optimized reactions catalyzed by palladium in combination with a ligand form the TML series. In addition, it allows for the *a priori* prediction of the stereochemical outcome of a given allylic substitution with this type of ligands.[16,28] However, undeniable scientific evidence is missing and therefore this cartoon model has to be considered as a mnemonic.

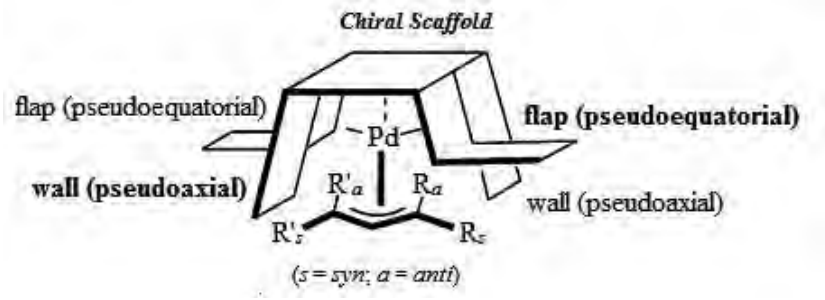

Figure 5.5 Cartoon 'Wall and Flap' model used to describe the palladium-ligand-allyl complex

In 2009, detailed NMR studies facilitated by isotopic labelling in combination with molecular-mechanics and DFT simulations were performed by a collaboration of different research groups.[29] For these experiments and calculations the authors chose to study the monomeric forms of two cationic palladium complexes both with standard DACH-phenyl Trost ligand **5.01**. The first complex consisted of a simple η^3-allyl substrate whereas a cyclic η^3-cyclohexenyl substrate was used for the second one. The results of these highly advanced experiments allowed to propose a new scientifically supported model. Extensive NMR studies proved some remarkable features. For both complexes, Trost ligand **5.01** forms a 13-membered chelate with palladium, in which the ligand creates a concave and convex surface around the palladium-allyl moiety (see also Figure 5.6). In this C_1-symmetric conformation, one amide NH is on the convex side and the other is on the concave, with the latter in close proximity to one allyl terminus. However, differences between both complexes are observed as well. For the Pd-**5.01**-allyl complex two isomers, which are called *endo* and *exo*, are present. These can interconvert into each other and isomerization involves inversion of the conformation such that the concave surface becomes convex and *vice versa*. For the cyclohexenyl substrate there is no isomerization between two conformations involved and it was found that the *exo* conformation was favored over the *endo* one. These results were also proven by the computational experiments. Molecular mechanics were used to select the conformationally most promising results which were further investigated by DFT calculations. Figure 5.6 shows the results of the DFT-optimized lowest energy conformers of both palladium(II)-complexes. For the η^3-allyl substrate complex the two isomers, *exo* and *endo*, are very similar in energy level. The *endo* structures of the η^3-cyclohexenyl substrate were significantly higher in energy and therefore irrelevant.

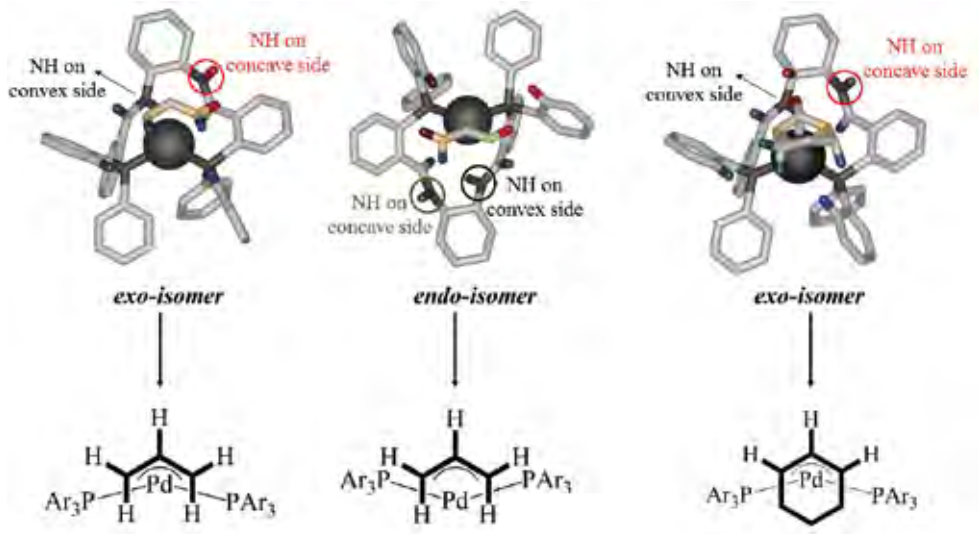

Figure 5.6 Optimized DFT lowest energy conformers of Pd(II)-DACH-phenyl Trost ligand complexes with η^3-allyl substrate (*exo* and *endo*) and η^3-cyclohexenyl substrate (only *exo*). The corresponding simplified schematic representations are shown below.

The progress of the reaction steps, ionization and nucleophilic addition, of the catalytic cycle were studied by DFT as well. Therefore (racemic) cyclohexenyl acetate was used as a substrate with different malonate nucleophiles. These DFT experiments reveal that starting from η^2-allyl complexes a hydrogen bond is formed for the (*S*)-enantiomer of the substrate between the acetate carbonyl of this substrate (acceptor) and the NH-amide hydrogen (donor) on the concave side of the (*R*,*R*)-chiral ligand. Such a hydrogen bond, which is responsible for an energetic stabilization, cannot be formed between the (*R*)-enantiomer of the substrate and the (*R*,*R*)-chiral ligand. Upon ionization, this energy difference increases due to the negative charge on the acetate. Figure 5.7 illustrates the results of the DFT-optimized transition state structures and here it can be seen that only one of the two enantiotopic acetate groups of the substrate can engage in hydrogen bonding with the amide what leads to selective ionization of the (*S*)-enantiomer. Therefore, ligands of this type are excellent discriminators for kinetic resolutions of chiral substrates.

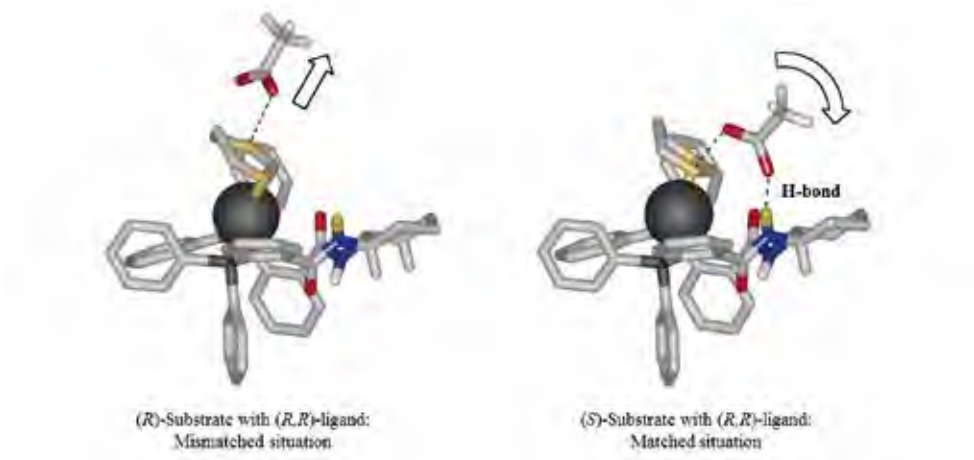

Figure 5.7 DFT-optimized transition state structures of the ionization process. Left: mismatched situation with (*R*)-cyclohexenyl acetate. Rigth: matched situation with (*S*)-cyclohexenyl acetate activated by the hydrogen bond formation.

Nucleophilic attack for different situations was also studied via DFT calculations. The results are represented in Figure 5.8. The first approach involves a simplified, hypothetical addition of free malonate without counter ion. Here, a hydrogen-bond interaction between the enolate oxygen of the malonate nucleophile and the amide NH of the ligand can be formed comparable to the hydrogen bond formed during the ionization step. It was found that this interaction was responsible for the highly selective attack at the *pro-S* terminus of the η^3-cyclohexenyl intermediate (*vide infra*). However, a second phenomenon, which is less important, was observed as well. A steric interaction between the η^3-cyclohexenyl substrate and one phenyl ring of the ligand causes a small counterclockwise rotation of the cyclohexenyl substrate which favors nucleophilic attack of the malonate anion at the *pro-R* terminus of the substrate. This phenomenon is known as *pro-R* torqueselectivity (Figure 5.8 (a)). It is the phenyl ring marked as **A** which is responsible for the counterclockwise rotation.

In order to obtain a more a more realistic representation, the counterion is taken into account in the second approach. 1,3-Dicarbonyl chelation of the metal ion (M^+) by the malonate resulted in attenuation of the hydrogen-bond interaction between the enolate and the amide. Simultaneously, a long-range dipole interaction between the metal ion and the concave-oriented amide carbonyl will also favore nucleophilic attack at the *pro-R* terminus of the substrate. Which of both stabilization factors, hydrogen bonding or ion-dipole interaction will be dominant is dependent on the coordina-

tion properties of the metal ion. For weakly coordinating counter metal ions (like Cs^+ or Bu_4N^+), the hydrogen bond interaction dominates, favoring *pro-S* nucleophilic attack. For strongly coordinating metal ions (like Li^+), the calculated energy difference for both paths is almost equal and racemic mixtures are likely to be expected. Figure 5.8 (a) and Figure 5.8 (b) illustrate the optimized transition states for the nucleophilic addition with Na^+ as counterion for respectively the *pro-R* approach caused by the ion-dipole interaction and *pro-S* approach caused by the hydrogen-bond interaction.

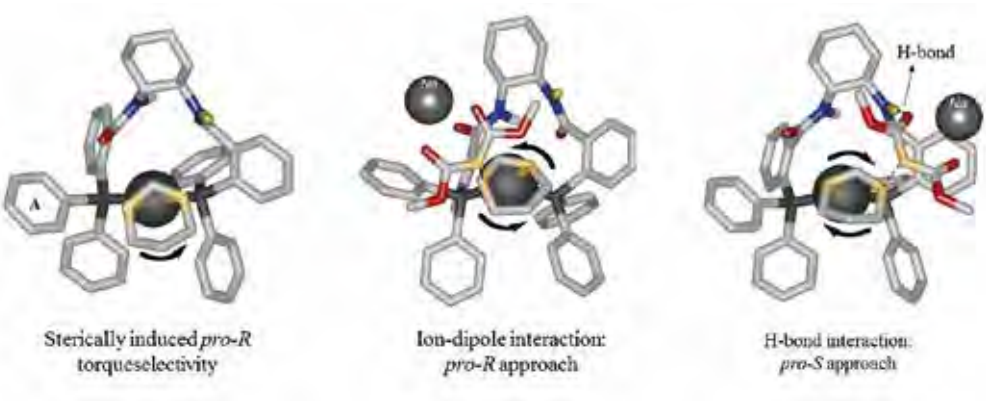

Figure 5.8 DFT results for the nucleophilic addition step. **(a)** Left: illustration of *pro-R* torqueselectivity caused by a sterical interaction between phenyl ring **A** and the substrate **(b)** Middle: illustration of the *pro-R* approach caused by the ion-dipole interaction with Na^+ as counterion **(c)** Right: illustration of the *pro-S* approach caused by the H-bonding interaction with Na^+ as counter ion.

In conclusion, a cartoon model to explain the selectivity mechanism was proposed.[29] This cartoon model, which is shown in Figure 5.9, consists of two pictures: one for the 'kinetic resolution in the ionization' and one for the asymmetric induction in the nucleophilic addition steps. Essential is the fact that the hydrogen-bonding interaction of the NH amide at the concave side of the complex can accelerate both the ionization step and the nucleophilic addition. Moreover, the high selectivity is obtained via selective favoring of one pathway and not by disfavoring of all undesired pathways. In addition, the acceleration is strongly dependent on the ligand conformation and only in a bidentate chelate complexation, will the structure exhibit a concave face with regioselectively placed activating amide groups.

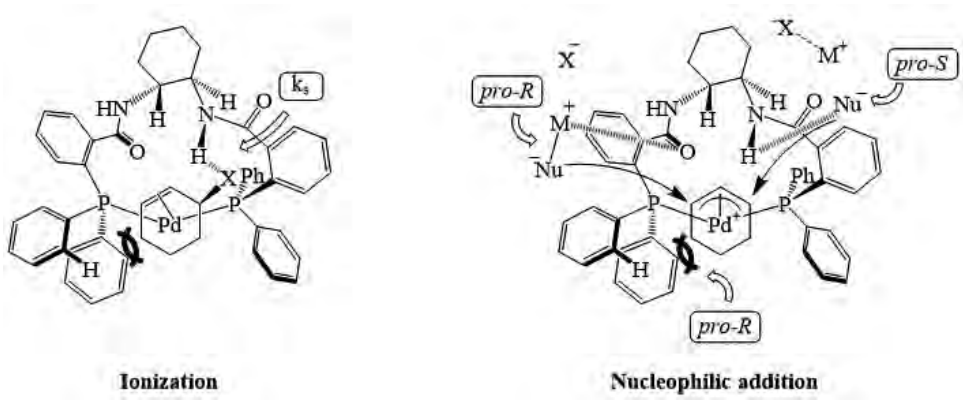

Figure 5.9 Proposed cartoon model for the kinetic resolution in the ionization step and the asymmetric induction in the nucleophilic addition

The aim of this project is to synthesise two Trost-type ligands which are shown in Figure 5.10. Similar to all other novel ligands proposed in this thesis, the targeted ligands **5.20** and **5.21** are characterized by a 1,1'-biferrocene backbone. The main goal of this research project is twofold. First, an optimal route to synthesize these ligand structures will be developed. Secondly, these novel ligands will be tested in a benchmark test reaction to explore the influence of this bulky diamine backbone. The decarboxylative asymmetric allylic alkylation (DAAA) for the synthesis of α-allyl-carbonyl compounds is such a reaction for which the Trost modular ligand series showed good yields and selectivities (Scheme 5.3).[28,30]

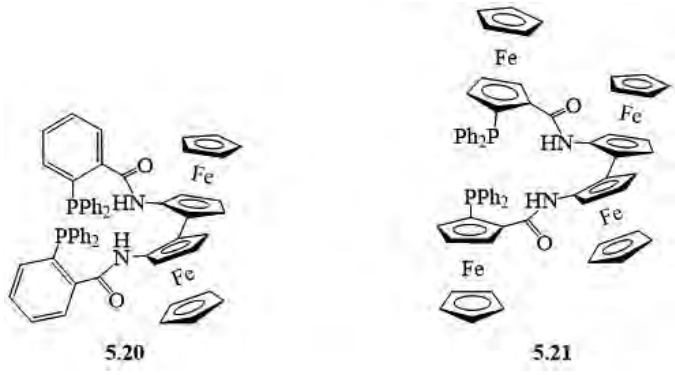

Figure 5.10 Novel Trost-type ligands **5.20** and **5.21** with a chiral biferrocene-based diamine backbone

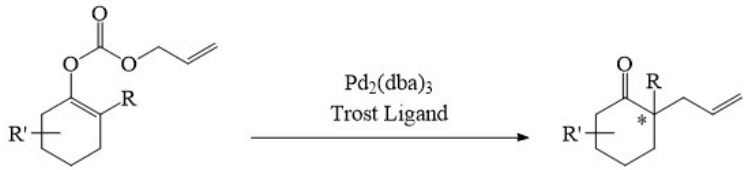

5.22 5.23

Scheme 5.3 Pd-catalyzed DAAA reaction for the synthesis of α-allyl-carbonyl compounds

5.2. Retrosynthetic Analysis of Novel Trost-Type Ligands

The retrosynthetic analysis for the novel Trost-type ligands are shown in Scheme 5.4 and Scheme 5.5, Ligand **5.20** can be synthesized from the commercially available carboxylic acid **5.24** whereas the planar-chiral ferrocene carboxylic acid **5.26** can be obtained via a procedure reported by Zhang and co-workers (*vide infra*).[6] For the coupling reaction between the diamine ligand precursor and the carboxylic acid building blocks, different options are available. These involve the condensation reaction between diamine **5.25** and the corresponding acid chlorides derived from carboxylic acids **5.24** and **5.26**, or the use of peptide coupling reagents such as DCC, HBTU, …

Because the novel diamine backbone **5.25** is very similar to the diamine backbones present in the biferocene-based diamidophosphite ligands **4.89**-**4.92** synthesized in Chapter 4 (Scheme 4.25, § 4.7.3, *vide supra*), the synthesis will be very comparable. Therefore the retrosynthetic analysis, shown in Scheme 5.5, will be restricted and simplified to compound **5.28**, with a *para*-methoxybenzyl-carbonyl as PG^1. This compound was already obtained for the synthesis of the biferrocene-based diamidophosphite ligand library as compound **4.68** (Scheme 4.19, § 4.5.2, *vide supra*). Two possible pathways for the synthesis of diamine **5.25**, in which the key step involves again a copper-mediated Ullmann reaction, are shown in Scheme 5.5. The first pathway, suggests a direct homocoupling of **5.28** to biferrocene **5.27**, followed by deprotection of the protecting group PG^1. The second pathway, involves the introduction of a second protecting group of the NH-carbamate proton. The rationale behind this latter approach is the avoidance of an undesirable dehalogenation reaction. Consequently, two protective groups have to be removed, preferably in one step or in two subsequent steps as shown in Scheme 5.5. The retrosynthetic analysis of iodocarbamate **5.28**/**4.68** is elucidated in § 4.2 (*vide supra*).

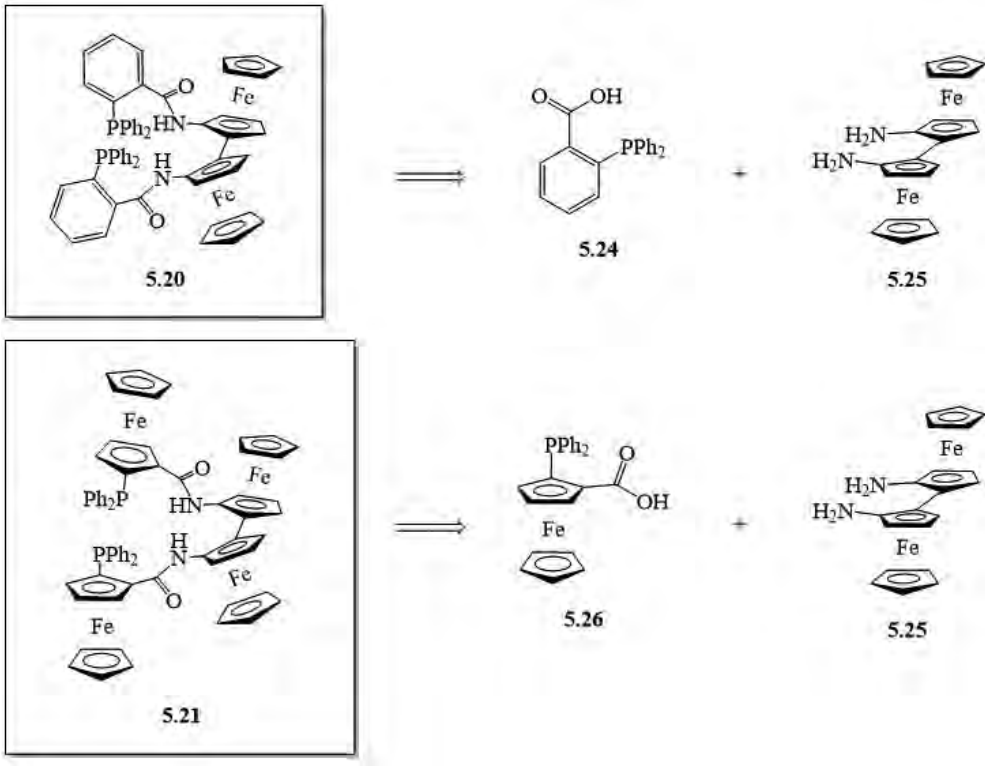

Scheme 5.4 First step of the retrosynthetic analysis for the novel biferrocene-based Trost-type ligands

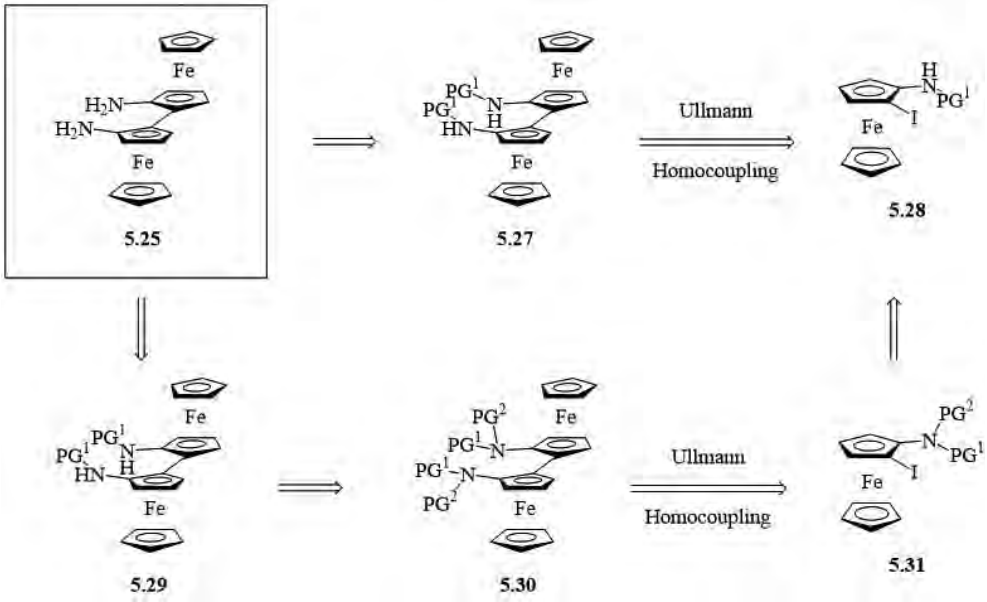

Scheme 5.5 Retrosynthetic analysis of biferrocene diamine **5.25** consisting of two pathways

The retrosynthetic analysis of planar-chiral α-diphenylphosphino ferrocenecarboxylic acid **5.26** as reported by Zhang and co-workers is shown in Scheme 5.6.[6] This compound can be synthesized via a three-step procedure, in a similar way as described in § 4.4.3 (*vide supra*), from the well-known chiral diphenylphosphino ferrocenyl oxazoline **5.32**. This compound itself can be obtained via a diastereoselective *ortho*-lithiation of oxazoline **5.33** as described in full detail in § 4.4.3.

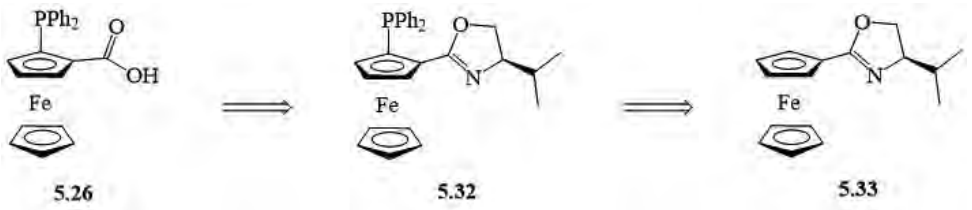

Scheme 5.6 Retroynthesis of planar-chiral phosphino ferrocenecarboxylic acid **5.26** as reported by Zhang and co-workers[6]

5.3. Synthesis of Biferrocene-Based Diamine **5.25**

Before the coupling of **5.28** to **5.27** was tested, different additional protective groups for the NH-carbamate were introduced onto **5.28**. Consequently, the copper mediated Ullmann-coupling could be tested on different substrates.

5.3.1. Protection of NH-carbamate with a Boc-, a benzyl- and an allyl-group

For the introduction of a second protecting group on iodoferrocene carbamate **5.28**, a Boc-, a benzyl- and an allyl group were chosen. The advantage of the Boc-group is that it can be cleaved simultaneously with the PMB-group using TFA in dichloromethane. Removal of the benzyl group can be obtained via catalytic hydrogenolysis using H_2-gas after removal of the PMB-group. The allyl group was chosen because it is less bulky compared to the other ones. Larger protecting groups can reduce the success rate of the Ullmann homocoupling. Removal of the allyl group can be accomplished using KO-*t*Bu in DMSO at 100°C. The synthesis of the Boc-, Bn- and allyl-protected carbamates is illustrated in Scheme 5.7. The Boc-group was introduced using Boc-anhydride and a catalytic amount of DMAP in the presence of Et_3N. Compound **5.34** could be obtained with a yield of 95%. The introduction of the benzyl and allyl group was accomplished via a one-pot, two-step procedure. After deprotonation of the acidic NH-carbamate

proton with NaH in THF, the reaction mixture was quenched with benzylbromide and allylbromide, respectively producing **5.35** and **5.36** with a yield of 97% and 95%.

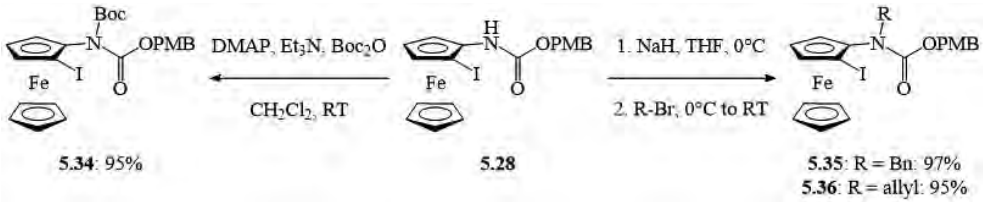

Scheme 5.7 Introduction of a Boc-, a benzyl-, and an allylgroup as protective groups for the NH-carbamate proton of **5.28**

5.3.2. Copper-mediated Ullmann-coupling of different α-iodoferrocene carbamates

For the homocoupling of double protected α-iodoferrocene carbamates **5.34**-**5.36** a metallic copper-mediated Ullmann reaction at 105°C was tested (Scheme 5.8). Unfortunately, complex reaction mixtures were obtained for the three reaction mixtures and biferrocenes **5.37**-**5.39** could not be identified via LC-MS.

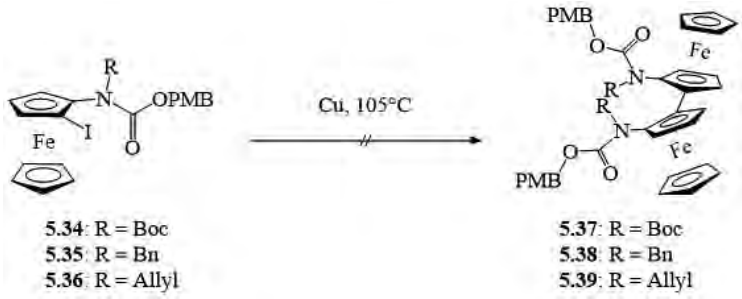

Scheme 5.8 Non-successful metallic copper-mediated Ullmann-coupling towards biferrocenes **5.37**-**5.39**

An alternative copper-source that was successfully applied at lower temperatures for the synthesis of biferrocene compounds is CuTC, (*cf.* Chapter 3, § 3.7.1 and Chapter 4, § 4.6). Boc-protected carbamate **5.34** was reacted with CuTC in NMP at room temperature and at 70°C. For both experiments, the formation of biferrocene **5.37** was not observed but ferrocenyl thiophene compound **5.40** was obtained (Scheme 5.9). This compound could be elucidated and identified based on ^{1}H-NMR and MS analysis. The ^{1}H-NMR spectrum of **5.40** and its assignment is illustrated in Figure 5.11. MS analysis showed a mass over charge ratio of 448 which represents the mass of [(**5.40**)-Boc+2H]$^{+}$.

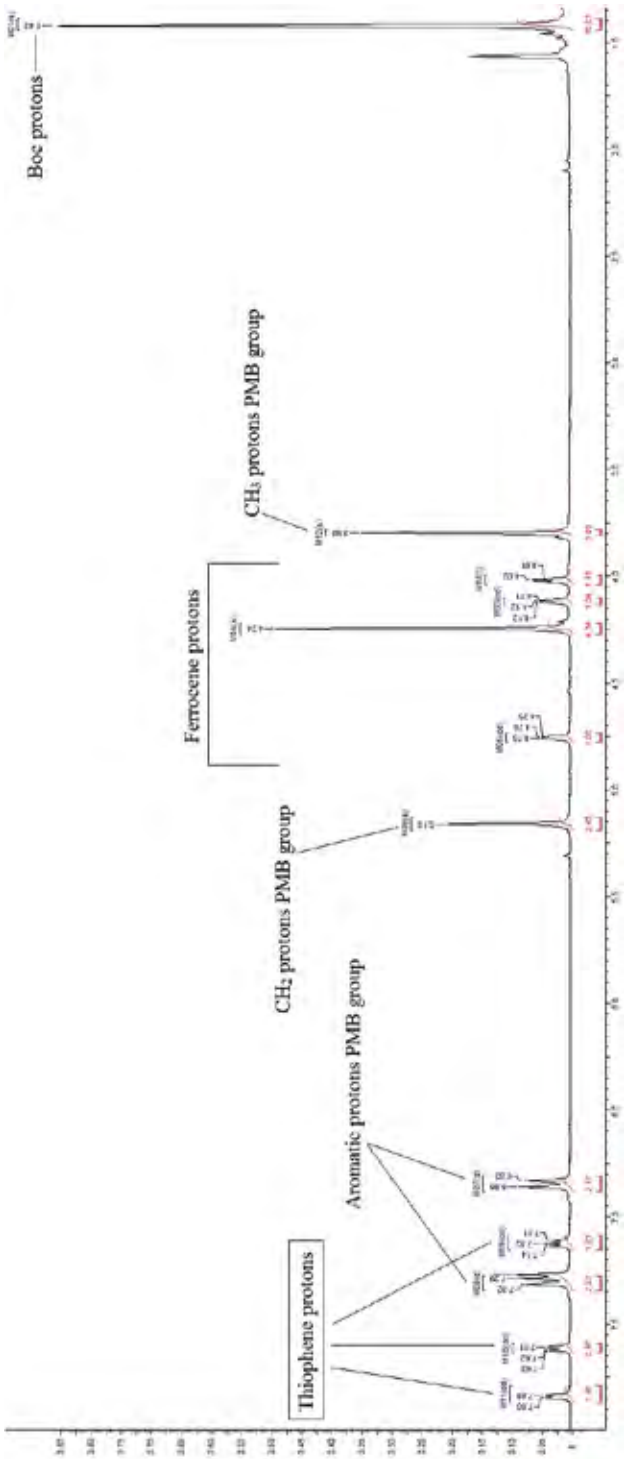

Figure 5.11 ^{1}H-NMR-spectrum of **5.40**

The formation of this side product can be explained by the presence of the bulky Boc-group at the α-position respective to the iodine. Mechanistically, a decarboxylation step has to occur after oxidative addition of iodocarbamate **5.34** and before, or during the reductive elimination step.

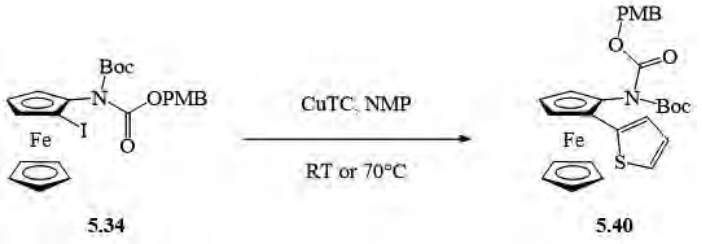

Scheme 5.9 Formation of side product **5.40** via Ullmann coupling of carbamate **5.34** with CuTC

Somewhat surprisingly, the copper-mediated Ullmann coupling of NH-carbamate **5.28** allowed to isolate biferrocene dicarbamate **5.27** with a yield of 76% (Scheme 5.10). In addition, the expected dehalogenated product **5.41** was formed in not more than 10% yield next to the isolation of starting material **5.28** (10% recovery).

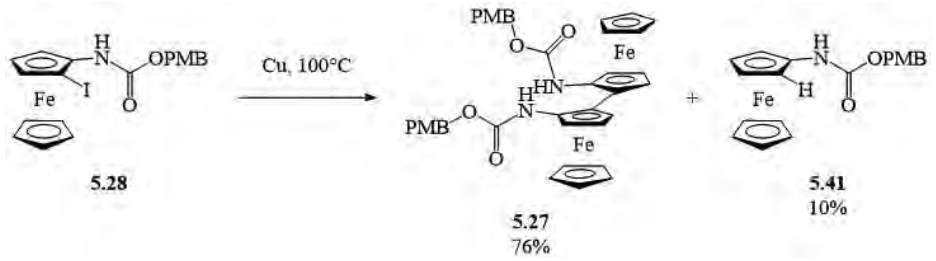

Scheme 5.10 Metallic copper-mediated Ullmann coupling of NH-carbamate **5.28**

The amount of dehalogenated side product **5.41** formed in the reaction described above is undoubtedly higher than the amount of the corresponding dehalogenated products formed for the copper-mediated synthesis of biferrocene compounds **4.75** and **4.79** (*cf.* Chapter 4, § 4.6)[31]. Scheme 5.11 illustrates a proposed mechanism for the formation of dehalogenated product **5.41**. Just like the classical Ullmann mechanism, the first step involves oxidative addition of metallic copper to α-iodoferrocene carbamate **5.28** what results in the formation of copper(II)-species **5.42**. At this point two reaction pathways are in competition with each other. Via a disproportionation and sub-

31 If Ullmann reactions of alkylated iodo-carbamates **4.69** and **4.70** were performed properly, what means that the starting materials had to be dried under high-vacuum in such a way all solvents were removed, the corresponding dehalogenated side products were not observed. If the starting materials were not completely dry, <5% of these side products were formed.

sequent steps of the classical Ullmann mechanism, biferrocene dicarbamate **5.27** will be formed. The other possible reaction step involves a proton transfer of the NH-carbamate proton to copper. This involves an increase of the oxidation level of copper to +III. As a consequence, a negative charge is formed on nitrogen which is resonance-stabilized via the adjacent CO double bond. In the reductive elimination a ferrocene-hydrogen bond is formed together with CuI. The last step involves protonation of the carbamate nitrogen which occurs during the work-up step.

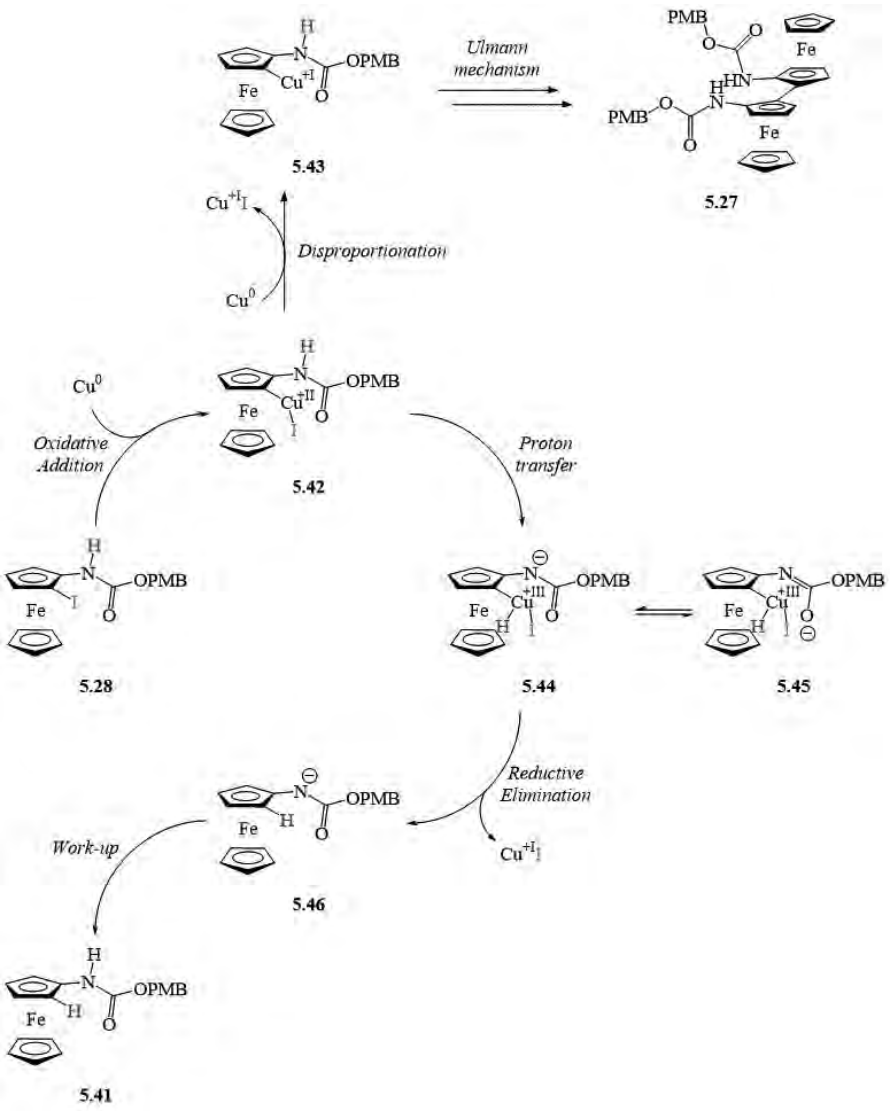

Scheme 5.11 Proposed mechanism for the formation of dehalogenated side product **5.41** in the Cu^0-mediated Ullmann reaction

5.3.3. Deprotection of biferrocene dicarbamate **5.27** – Synthesis of biferrocene diamine **5.25**

For the preparation of biferrocene diamine **5.25**, the same protocol as the one described in § 4.7.1, for the synthesis of biferrocene diamines **4.82** and **4.83** was applied. In practice, biferrocene dicarbamate **5.27** was deprotected using TFA in dichloromethane (Scheme 5.12). Just like diamines **4.82** and **4.83**, diamine **5.25** is a novel compound as well, not described in scientific literature. Another similiarity is that **5.25** is also found to be air-sensitive as and to prevent decomposition during the chromatographic purification on silica gel, triethylamine was added to the eluents. This allowed to isolate diamine **5.25** with a yield of 92%.

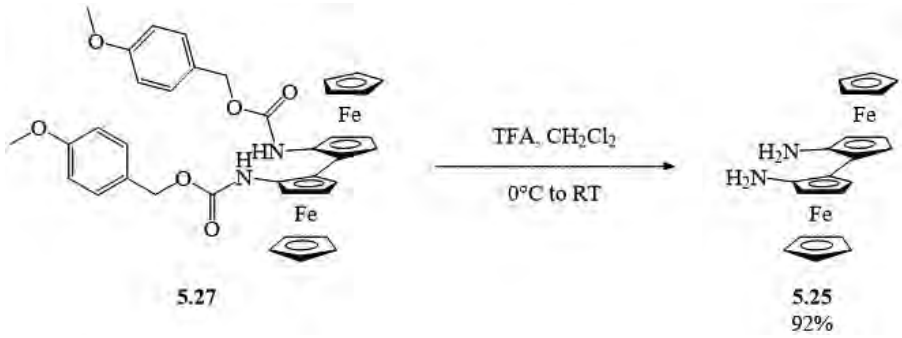

Scheme 5.12 Deprotection of dicarbamate **5.27** using TFA for the synthesis of biferrocene diamine **5.25**

5.4. Synthesis of Planar-Chiral Diphenylphosphino Ferrocene-carboxylic Acid **5.26**

5.4.1. Synthesis of **5.26** as reported by Zhang and co-workers[6]

Trost-type ligand **5.21** is peculiar because it is characterized by the presence of four chiral ferrocene substructures. All these ferrocene substructures possess planar-chirality and the ferrocene-ferrocene bond functions as a chirality axis. Therefore matched and mismatched situations are possible. Alteration of the planar-chirallity of the ferrocenecarboxylic acid ligand precursor is practically considered to be more straightforward than alteration of the chiral biferrocene backbone regarding the number of steps to obtain both

ligand building blocks. In this thesis only Trost-ligand **5.21** with (R_p)-diphenylphosphino ferrocenecarboxylic acid is presented. This compound can be obtained directly from chiral ferrocenyl oxazoline **5.33**, which itself is synthesized from (*R*)-valinol. Scheme 5.13 illustrates the synthetic pathway to obtain ferrocenecarboxylic acid **5.26** based on a method reported by Zhang and co-workers.[6] Ferrocenyl oxazoline **5.33** was synthesized in three steps in this research project from ferrocene carboxylic acid as described in § 4.4 with (*R*)-valinol (*vide supra*). Diastereoselective *ortho*-lithiation with *s*-BuLi and TMEDA and subsequent quenching with chlorodiphenylposphine allowed to obtain enantiopure planar-chiral diphenyl phosphino oxazoline **5.32** with a yield of 61%. The next transformation in the proposed synthesis of Zhang and co-workers is the three-step hydrolysis of the oxazoline functional group into the corresponding carboxylic acid. Therefore, the synthesis strategy is similar compared to the three-step hydrolysis as described in Scheme 4.15, § 4.4.4. However, TFAA (trifluoroacetic anhydride) was used instead of Ac_2O (acetic anhydride in the second step and also the third step was slightly different. Milder conditions with KO*t*-Bu at room temperature instead of NaOH in refluxing THF/MeOH were applied. Nevertheless, when the protocol of Zhang was repeated, the formation of diphenylphosphino carboxylic acid **5.26** was not observed.

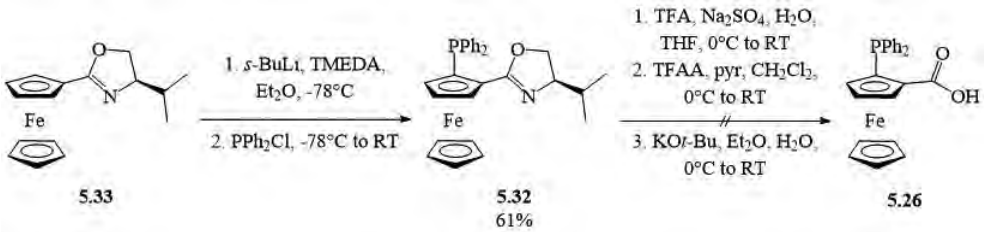

Scheme 5.13 Synthesis of planar-chiral diphenylphosphino ferrocenecarboxylic acid **5.26** as described by Zhang *et al.*[6]

5.4.2. Alternative synthesis of planar-chiral α-diphenylphosphino ferrocenecarboxylic acid **5.26**/**5.48** via a halogen-lithium exchange

An alternative synthetic protocol towards planar-chiral carboxylic acid, tested in this research project, is illustrated in Scheme 5.14. The reaction starts from enantiopure iodoferrocenecarboxylic acid **5.47** of which the synthesis is explained in full detail in § 4.3 and § 4.4 (*vide supra*). The proposed two-step reactions involves a halogen-lithium exchange and subsequent quenching with chlorodiphenylphosphine. Consequently, the

planar-chiral enantiomer of **5.26** is formed. Two equivalents of *n*-BuLi are necessary to form the lithiated ferrocenyl species.

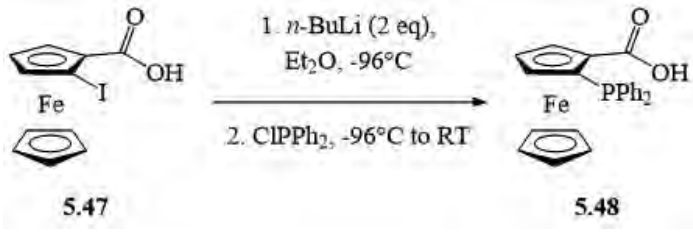

Scheme 5.14 Synthesis of **5.48** from iodoferrocenecarboxylic acid **5.47** via halogen-lithium exchange with two equivanlents *n*-BuLi and quenching with $ClPPh_2$

The first equivalent will abstract the carboxylic acid proton. Afterwards the second equivalent will perform the halogen-lithium exchange. After quenching the lithiated species with chlorodiphenylphosphine, the reaction mixture was studied via ^{31}P-NMR. In this spectrum a signal was observed at chemical shift value of -16.7 ppm, which might indicate the formation of **5.48**. To compare, Zhang and co-workers reported a comparable chemical shift value of -17.3 ppm.[8] The reaction seemed difficult to control, leading to unreproducible results and also the purification seemed to be very problematic. Therefore, it was impossible to obtain pure planar-chiral α-diphenylphosphino ferrocenecarboxylic **5.48** via the halogen-lithium exchange protocol neither.

5.5. Synthesis of Biferrocene-Based Trost-type Ligand **5.20**

Different synthetic protocols to obtain Trost-type ligands from carboxylic acids and diamines have been published.[6,8,10,23,24,31] The majority of them make use of the coupling reagents DCC (*N,N'*-dicyclohexylcarbodiimide) and EDCI (1-ethyl-3-(3-dimethylaminopropyl)carbodi-imide). Highly variable yields ranging from 30 up to 90% are reported. The research group of Lepoittevin observed that the order of the addition of the reagents has a high impact on the yield of the reaction.[10] Therefore, they highly recommend to add the coupling reagent DCC or EDCI and the nucleophilic catalyst DMAP to the carboxylic acid. Moreover, they found that it was most important to add the corresponding amine as the last reagent. Zhang and coworkers reported high yields (up to 84%) for the synthesis of ferrocene-based Trost-type ligand **5.11**. In their protocol they added the corresponding amine however before the coupling reagent EDCI.[6,8] An over-

view of the conditions that were applied, for the transformation of biferrocene diamine **5.25** into Trost-type ligand **5.20** is shown in Table 5.1.

Initial experiments (entry 1) using EDCI as coupling agent and DMAP as nucleophilic catalyst were performed according to the method reported by Zhang and co-workers. However, a complex reaction mixture was obtained and unfortunately biferrocene-based Trost-ligand **5.20** could not be identified. Changing the order of addition as recommended by Lepoittevin had no influence on the outcome of the reaction either. When the reaction was carried out with DCC (entry 2), similar results were obtained. Changing the synthesis strategy to a coupling reaction between diamine **5.25** and the acid chloride of carboxylic acid **5.24**, obtained via reaction of **5.22** with $(COCl)_2$ (oxalylchloride) led to black reaction mixtures, where no ferrocene compounds were observed via TLC analysis (entry 3). Performing the reaction with another type of coupling reagents like HBTU (hexafluorophosphate benzotriazole tetramethyl uronium), in the presence of Et_3N as a base resulted in the formation of complex reaction mixtures again (entry 4). ^{1}H-, ^{31}P-NMR analysis and LC-MS analysis showed that significantly different mixtures were obtained compared to those described in entries 1 and 2. The desired ligand **5.20** could also not be observed via a coupling strategy using DCC and HOBT (hydroxybenzotriazole) (entry 5) or CDI (1,1'-carbonyldiimidazole) and Et_3N (entry 6). The last test reaction (entry 7), involved 2-chloro-1-methylpyridinium iodide, a strongly electrophilic coupling agent also applied for the synthesis of esters from carboxylic acids and alcohols. However, neither this was able to convert **5.24** and **5.25** into **5.20** in a successful way.

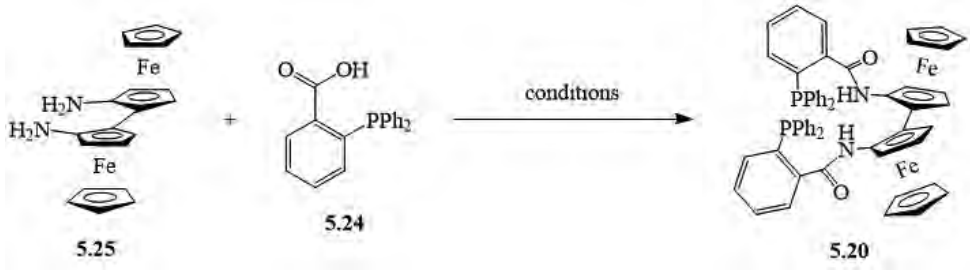

Entry	Conditions	Result
1	EDCI, DMAP, CH_2Cl_2	Complex reaction mixture
2	DCC, DMAP, CH_2Cl_2, RT	Complex reaction mixture
3	$(COCl)_2$, Et_3N, CH_2Cl_2, 0°C to RT	Decomposition ferrocene compounds
4	HBTU, Et_3N, DMF, RT	Complex reaction mixture
5	DCC, HOBT, CH_2Cl_2	**5.20** not identified
6	CDI, Et_3N, CH_2Cl_2	**5.20** not identified
7	2-chloro-1-methylpyridinium iodide, Et_3N, CH_2Cl_2, RT	**5.20** not identified

Table 5.1 Overview of the conditions for the transformation of biferrocene diamine **5.25** with diphenylphosphino benzoic acid into Trost-type ligand **5.20**

In conclusion, it was impossible to synthesize Trost-type ligands **5.20** and **5.21** via one of the described methods. Consequently it was also not possible to test them the palladium-catalyzed DAAA reaction as proposed.

5.6. Experimental

5.6.1. General

All experiments were performed according the general laboratory safety rules and personal protective equipment such as goggles, lab coat and gloves were always worn in the laboratory. All reactions, work-ups and purifications were performed in a well-ventilated fume hood. A detailed overview for the identification of the hazards of the most dangerous chemicals that were used in this chapter is given in Appendix I.

More information on general experimental details can be found in § 3.9.1 (*vide supra*).

5.6.2. Synthesis of (R_p,R_p)-2,2'-Bis[4-methoxybenzylcarbamate]-1,1'-biferrocene **5.27**

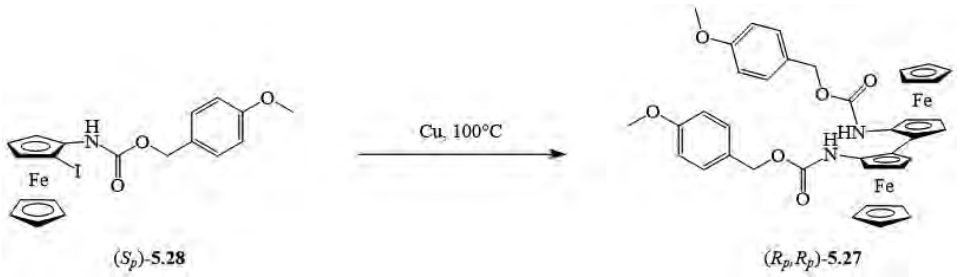

(S_p)-**5.28** (R_p,R_p)-**5.27**

(S_p)-**5.28** (800 mg, 1.62 mmol) was dissolved in a minimal amount of anhydrous CH_2Cl_2 and transferred into an oven-dried 50 mL, round-bottom flask. CH_2Cl_2 was evaporated using an argon-flow from a balloon to have all the starting material on the bottom of the flask. 300 Mesh copper powder (311 mg, 4.89 mmol, 3 eq) was added cautiously followed by careful addition of an egg shaped stirring bar of suitable size. The reaction was heated to 100°C and stirred overnight. The reaction mixture was taken up in a large amount of Et_2O and filtered over Celite. The solvent was removed under reduced pressure and the resulting residue was purified by flash chromatography (gradient cyclohexane/EtOAc: 90/10 to cyclohexane/EtOAc: 70/30) affording (R_p,R_p)-**5.27** as orange crystals with a yield of 75.9%.

Formula: $C_{38}H_{36}Fe_2N_2O_6$ (728.39 g/mol)
R$_f$ (cyclohexane/EtOAc: 80/20): 0.11
^{1}**H-NMR** ($CDCl_3$, 300 MHz): δ = 3.81 (s, 6H), 4.04 (dd, *J* = 2.5 Hz, *J* = 1.5 Hz, 2H), 4.08 (app

t, *J* = 2.5 Hz, 2H), 5.0-5.25 (m, 2H), 5.11 (d, *J* = 12.0 Hz, 2H, A part of AB-system), 5.18 (d, *J* = 12.0 Hz, 2H, B part of AB-system), 6.85-6.95 (m, 4H), 7.03 (br s, 2H), 7.30-7.40 (m, 4H) ppm.

ESI-MS m/z (rel. intensity %): 729.1 (16) $[M+H]^+$, 728.1 $[M]^+$ (35), 608.1 (100), 609.1 (36), 606.1 (10), 685.1 (35), 686.1 (15)

Retention time HPLC: 7.74 min. ((R_p,S_p)-**5.48** (*meso* compound): 7.57 min.) (method 3), 3.63 min. ((R_p,S_p)-**5.48** (*meso* compound): 3.15 min.) (method 4)

5.6.3. Synthesis of (R_p,R_p)-2,2'-biferrocenyldiamine **5.25**

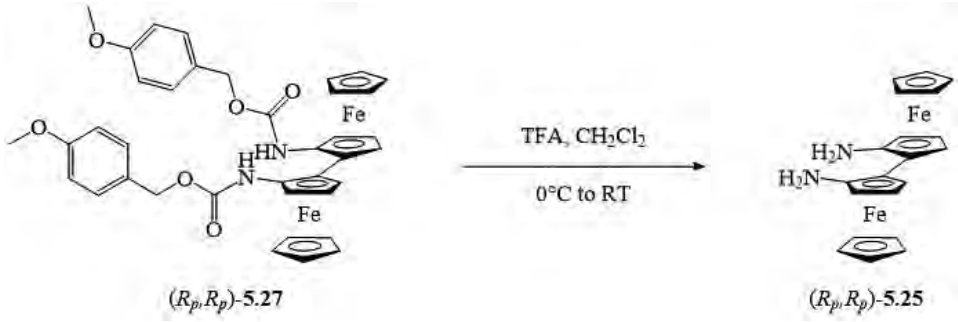

(R_p,R_p)-**5.27** (R_p,R_p)-**5.25**

An oven-dried, 25 mL round-bottom flask was charged with a magnetic stirring bar and (R_p,R_p)-**5.27** (100 mg, 0.137 mmol) and CH_2Cl_2 (8 mL). The reaction flask was cooled to 0°C using an ice-water bath. TFA (105 µL, 1.37 mmol, 10 eq) was added dropwise. The reaction mixture was stirred for 15 min. at 0°C before it was allowed to warm up to room temperature and stirred for an additional h. The reaction was cooled to 0°C again and quenched via dropwise addition of a solution of K_2CO_3 (568 mg, 4.11 mmol, 30 eq) in H_2O (15 mL). The aqueous phase was extracted 3 times with CH_2Cl_2 (25 mL). The combined organic phases were dried over anhydrous $MgSO_4$ and filtered. The solvents were removed under reduced pressure. The solvents were removed under reduced pressure and the resulting residue was purified by flash chromatography on neutralized silica gel[32] (*n*-hexane/Et_2O/Et_3N: 88/10/2) affording (R_p,R_p)-**5.25** as yellow-orange crystals with a yield of 92.1 %.

This compound was not bench stable.

32 Neutralized silica gel was obtained via washing with Et_2O/Et_3N (70/30) and eluens system before the column chromatographic separation was started.

Formula: $C_{20}H_{20}Fe_2N_2$ (400.08 g/mol)
R_f (cyclohexane/EtOAc: 60/40): 0.29
ESI-MS m/z (rel. intensiteit %): 401.0 (100) $[M+H]^+$, 400.1 (45), 402.1 (35), 399.1 (12)
Retention time HPLC: 6.37 min. (method 3), 1.56 min. (method 4)

Due to the fact that compound is not bench stable, full characterization could not be performed.

5.6.4. Synthesis of 4-methoxybenzyl (*N*-(S_p)-α-Iodoferrocenyl-*N*-*tert*-butyloxycarbonyl) carbamate **5.34**

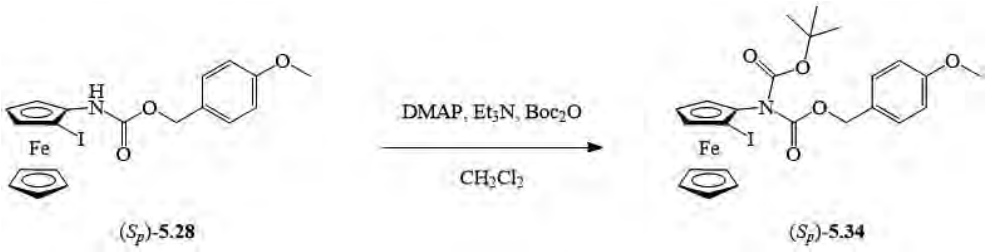

(S_p)-**5.28** (S_p)-**5.34**

An oven-dried, 10 mL round-bottom flask was charged with a magnetic stirring bar and (S_p)-**5.28** (397.1 mg, 0.809 mmol). CH_2Cl_2 (4.5 mL) was added, followed by DMAP (99.2 mg, 0.809 mmol, 1 eq), Boc_2O (388.2 mg, 1.779 mol, 2.2 eq) and Et_3N (113 µL, 0.809 mmol, 1 eq). The reaction was stirred for 15 h at room temperature. The solvents were removed under reduced pressure and the resulting residue was purified by flash chromatography (pentane/EtOAc: 85/15) affording (S_p)-**5.34** as an orange-brown oil with a yield of 95.0%.

Formula: $C_{24}H_{26}FeINO_5$ (591.02 g/mol)
R_f (pentane/EtOAc: 80/20): 0.44
^{1}**H-NMR** ($CDCl_3$, 400 MHz): δ = 1.46 (s, 9H), 3.82 (s, 3H), 4.18 (s, 5H), 4.22-4.27 (m, 2H), 4.41 (dd, *J* = 2.4 Hz, *J* = 1.6 Hz, 1H), 5.19 (d, *J* = 12.3 Hz, 1H, A part of AB-system), 5.23 (d, *J* = 12.3 Hz, 1H, B part of AB-system), 6.85-6.95 (m, 2H), 7.32-7.40 (m, 2H) ppm.
^{13}**C-NMR** ($CDCl_3$, 100 MHz): δ = 27.8 (CH_3 x3), 43.5 (C, Fc), 55.3 (CH_3), 64.9 (CH, Fc), 67.1 (CH, Fc), 68.7 (CH_2), 72.1 (CH, Fc), 72.7 (CH x5), 83.4 (C), 97.2 (C, Fc), 113.9 (CH x2), 127.3 (C), 130.3 (CH x2), 152.0 (C, C=O), 153.7 (C, C=O), 159.8 (C) ppm.

5.6.5. Synthesis of 4-methoxybenzyl (*N*-(S_p)-α-Iodoferrocenyl-*N*-benzyl) carbamate **5.35**

An oven-dried, 10 mL round-bottom flask was charged with a magnetic stirring bar and NaH (24.5 mg, 0.611 mmol, 1.5 eq). THF (0.200 mL) was added and the reaction flask was cooled to 0°C using an ice-water bath. A solution of (S_p)-**5.28** (200 mg, 0.407 mmol) in THF (2.7 mL) was added dropwise and stirred until the formation of hydrogen gas has stopped. Afterwards, benzylbromide (100 µL, 0.815 mmol, 2 eq) was carefully added. The reaction was stirred for an additional 10 min. at 0°C before it was allowed to warm up to room temperature and stirred overnight. The reaction was cooled to 0°C again and quenched with a saturated solution of NH_4Cl (20 mL). The aqueous phase was extracted 3 times with Et_2O (20 mL). The combined organic phases were washed with brine (50 mL), dried over anhydrous $MgSO_4$ and filtered. The solvents were removed under reduced pressure and the resulting residue was purified by flash chromatography (cyclohexane/EtOAc: 90/10) affording (S_p)-**5.35** as an orange viscous oil with a yield of 98.4%.

Formula: $C_{26}H_{24}FeINO_3$ (581.22 g/mol)

R_f (cyclohexane/EtOAc: 80/20): 0.32

^{1}**H-NMR** ($CDCl_3$, 400 MHz): δ = 3.80 (3H, s), 4.07 (5H, s), 4.16-4.23 (m, 2H), 4.46 (dd, *J* = 2.4 Hz, *J* = 1.6 Hz, 1H), 5.01 (d, *J* = 12.1 Hz, 1H, A part of AB-system), 5.06 (d, *J* = 12.1, 1H B part of AB-system), 5.08 (d, *J* = 16.2 Hz, 1H, A' part of A'B'-system), 5.37 (d, *J* = 16.2 Hz, 1H, B' part of A'B'-system), 6.80-6.82 (m, 2H), 7.12-7.14 (m, 2H), 7.28-7.32 (m, 1H), 7.39-7.40 (m, 4H) ppm.

^{13}**C-NMR** ($CDCl_3$, 100 MHz): δ = 42.3 (C, Fc), 55.2 (CH_3), 57.2 (CH_2), 65.8 (CH, Fc), 66.4 (CH, Fc), 67.4 (CH_2), 71.7 (CH, Fc), 71.7 (C, Fc), 72.0 (CH x5, Fc), 103.5 (C), 113.6 (CH x2), 126.2 (CH x2), 126.9 (CH), 128.5 (CH x2), 129.5 (CH x2), 138.73 (C), 156.31 (C, C=O), 159.2 (C) ppm.

5.6.6. Synthesis of 4-methoxybenzyl (*N*-(S_p)-α-Iodoferrocenyl-*N*-allyl) carbamate **5.36**

An oven-dried, 10 mL round-bottom flask was charged with a magnetic stirring bar and NaH (24.5 mg, 0.611 mmol, 1.5 eq). THF (200 µL) was added and the reaction flask was cooled to 0°C using an ice-water bath. A solution of (S_p)-**5.28** (200 mg, 0.407 mmol, 1 eq) in THF (2.7 mL) was added dropwise and stirred until the formation of hydrogen gas has stopped. Afterwards, allylbromide (70 µL, 0.815 mmol, 2 eq) was carefully added. The reaction was stirred for an additional 10 min. at 0°C before it was allowed to warm up to room temperature and stirred overnight. The reaction was cooled to 0°C again and quenched with a saturated solution of NH_4Cl (20 mL). The aqueous phase was extracted 3 times with Et_2O (20 mL). The combined organic phases were washed with brine (50 mL), dried over anhydrous $MgSO_4$ and filtered. The solvents were removed under reduced pressure and the resulting residue was purified by flash chromatography (cyclohexane/EtOAc: 90/10) affording (S_p)-**5.36** as an orange viscous oil with a yield of 98.6%.

Formula: $C_{22}H_{22}FeINO_3$ (531.16 g/mol)
R_f (cyclohexane/EtOAc: 80/20): 0.27
^{1}**H-NMR** ($CDCl_3$, 400 MHz): δ = 3.79 (3H, s), 4.18-4.21 (m, 2H), 4.23 (s, 5H), 4.44 (dd, *J* = 2.4 Hz, *J* = 1.8 Hz, 1H), 4.46 (app ddt, *J* = 16.4 Hz, *J* = 5.1 Hz, *J* = 1.6 Hz, 1H), 4.70 (app ddt, *J* = 16.4 Hz, *J* = 5.1 Hz, *J* = 1.6 Hz, 1H), 5.00 (d, *J* = 12.4 Hz, 1H, A part of AB-system), 5.05 (d, *J* = 12.4 Hz, 1H, B part of AB-system), 5.28 (app ddt, *J* = 10.2 Hz, *J* = 2.9 Hz, *J* = 1.6 Hz, 1H), 5.35 (app ddt, *J* = 17.2 Hz, *J* = 2.9 Hz, *J* = 1.6 Hz, 1H), 6.08 (app ddt, *J* = 17.2 Hz, *J* = 10.2 Hz, *J* = 5.1 Hz, 1 H), 6.80-6.87 (m, 2H), 7.15-7.25 (m, 2H) ppm.
^{13}**C-NMR** ($CDCl_3$, 100 MHz): δ = 42.5 (C, Fc), 55.2 (CH_3), 56.3 (CH_2), 65.5 (CH, Fc), 66.4 (CH, Fc), 67.2 (CH_2), 71.7 (CH, Fc), 72.02 (CH x5, Fc), 103.3 (C, Fc), 113.6 (CH x2), 115.7 (CH_2), 128.5 (C), 129.5 (CH x2), 134.6 (CH), 155.9 (C, C=O), 159.2 (C) ppm.

5.6.7. Synthesis of (R,R_p)-2-(α-diphenylphosphinoferrocenyl)-5-*iso*-propyl-oxazoline **5.32**

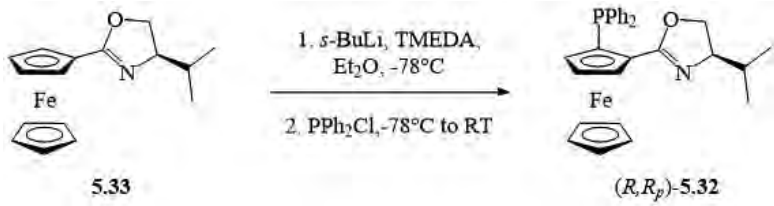

An oven-dried, 50 mL Schlenk-tube was connected to a Schlenk-line and put under an inert atmosphere of dry N_2. This tube was charged with a magnetic stirring bar, **5.33** (0.500 g, 1.68 mmol), Et_2O (17 mL) and TMEDA (326 µL, 2.19 mmol, 1.3 eq). The reaction mixture was cooled to -78°C and *s*-BuLi (2.89 mL, 4.04 mmol, 1.2 eq) was added dropwise. The reaction was stirred for an additional h at this temperature. Chlorodiphenylphosphine (482 mg, 393 µL, 2.19 mmol, 1.3 eq) was cautiously added and the reaction was stirred for 10 more min. at -78°C. The reaction mixture was allowed to warm up to room temperature and stirred overnight. The reaction was quenched with a saturated solution of $NaHCO_3$ (35 mL). The aqueous layer was extracted 3 times with CH_2Cl_2 (35 mL). The combined organic phases were washed with brine (50 mL), dried over anhydrous $MgSO_4$ and filtered. The solvents were removed under reduced pressure and the resulting residue was purified by flash chromatography (gradient cyclohexane/EtOAc: 100/0 to cyclohexane/EtOAc: 85/15 affording (R,R_p)-**5.32** with a yield of 61.0%.

Formula: $C_{28}H_{28}FeNOP$ (481.35 g/mol)

R_f (cyclohexane/EtOAc: 80/20): 0.42

^{1}**H-NMR** ($CDCl_3$, 300 MHz): δ = 0.74 (d, *J* = 6.7 Hz, 3H), 0.88 (d, *J* = 6.7 Hz, 3H), 1.71 (sptd, *J* = 6.7 Hz, *J* = 5.7 Hz, 1H), 3.66 (br s, 1H), 3.70-3.74 (m, 1H), 3.91 (ddd, *J* = 9.5 Hz, *J* = 8.1 Hz, *J* = 5.7 Hz, 1H), 4.27 (s, 5H), 4.29-4.33 (m, 1H), 4.41 (app t, *J* = 2.5 Hz, 1H), 5.03 (br s, 1H), 7.20-7.30 (m, 5H), 7.36-7.44 (m, 3H), 7.49-7.60 (m, 2H) ppm.

^{31}**P-NMR**: (121 MHz, $CDCl_3$): -16.88 ppm.

5.7. References

[1] B. M. Trost, D. L. Van Vranken, *Angew. Chem. Int. Ed. Engl.*, **1992**, *31*, 228-230

[2] B. M. Trost, R.C. Bunt, *Angew. Chem. Int. Ed. Engl*, **1992**, *35*, 99-102

[3] H. Adolfsson, C. Moberg, *Tetrahedron Asymmetry*, **1995**, *6*, 2023-2031

[4] C. W. Lim, S. Lee, *Tetrahedron*, **2000**, *56*, 5131-5136

[5] M. Bandini, A. Melloni, F. Piccinelli, R. Sinsi, S. Tommasi, A. Umani-Ronchi, *J. Am. Chem. Soc.*, **2006**, *128*, 1424-1425

[6] J. M. Longmire, B. Wang, X. Zhang, *Tetrahedron Lett.*, **2000**, *41*, 5435-5439

[7] S.-L. You, X.-L. Hou, L.-X. Dai, X.-Z. Zhu, *Org. Lett.*, **2001**, *3*, 149-151

[8] J. M. Longmire, B. Wang, X. Zhang, *J. Am. Chem. Soc.*, **2002**, *124*, 13400-13401

[9] B. M. Trost, K. Dogra, *Org. Lett.*, **2007**, *9*, 861-863

[10] S. Fuchs, V. Berl, J-P. Lepoittevin, *Eur. J. Org. Chem.*, **2007**, 1145-1152

[11] Z. Lu, S. Ma, *Angew. Chem. Int. Ed.*, **2008**, *47*, 258-297

[12] B. M. Trost, R. C. Bunt, *J. Am. Chem. Soc.*, **1994**, *116*, 4089-4090

[13] M. J. Moschitto, D. N. Caccarello, C. A. Lewis, *Ange. Chem. Int. Ed.*, **2015**, *54*, 2142-2145

[14] B. M. Trost, F.D. Toste, *J. Am. Chem. Soc.*, **2003**, *123*, 3090-3100

[15] B. M. Trost, G. Dong, *J. Am. Chem. Soc.*, **2006**, *128*, 6054-6055

[16] B. M. Trost, M. R.Machacek, A. Aponick, *Acc. Chem. Res.*, **2006**, *39*, 747-760

[17] B. M. Trost, D. L. Van Vranken. C. Bingel, *J. Am. Chem. Soc.*, **1992**, *114*, 9327-9343

[18] (a) B. M. Trost, L. Weber, *J. Am. Chem. Soc.*, **1975**, *97*, 1611-1612; (b) B. M. Trost, T. R. Verhoeven, *J. Am. Chem. Soc.*, **1976**, *98*, 630-632; (c) T. Hayashi, T. Haghira, M. Konishi, M. Kumada, *J. Am. Chem. Soc.*, **1983**, *105*, 7767-7768; (d) J. C. Fiaud, L. Y. Legros, *J. Org. Chem.*, **1987**, *52*, 1907-1911; (e) I. Stary, J. Zajicek, P. Kocovsky, *Tetrahedron*, **1992**, *48*, 7229-7250

[19] G. Helmchen, S. Kudis, P. Sennhenn, H. Steinhagen, *Pure Appl. Chem.*, **1997**, *69*, 513-518

[20] Mo: (a) B. M. Trost, M. J. Lautens, *J. Am. Chem. Soc.*, **1987**, *109*, 1469-1478; (b) B. M. Trost, I. Hachiya, *J. Am. Chem. Soc.*, **1998**, *120*, 1104-1105; W: (c) B. M. Trost, G. B. Tometzki, M. –H. Hung, *J. Am. Chem. Soc.*, **1987**, *109*, 2176-2177; (d) G. C. Lloyd-Jones, A. Pfaltz,, *Angew. Chem. Int. Ed. Engl.*, **1995**, *34*, 462-464; Rh: (e) P. A. Evans, J. D. Nelson, *J. Am. Chem. Soc.*, **1998**, *120*, 5581-5582; Ir: (f) R. Takeuchi, M. Kashio, *Angew. Chem. Int. Ed. Engl.*, **1997**, *36*, 263-265; (g) J. P. Janssen, G. Helmchen, *Tetrahedron Lett.*, **1997**, *38*, 8025-8026

[21] B. M. Trost, F. D. Toste, *J. Am. Chem. Soc.*, **1999**, *19*, 4545-4554

[22] G. C. Lloyd-Jones, S.C. Stephen, *Chem. Eur. J.*, **1998**, *4*, 2539-2549

[23] C. P. Butts, J. Crosby, G. C. Lloyd-Jones, S. C. Stephen, *Chem. Commun.*, **1999**, 1707-1709

[24] I. J. S. Fairlamb, G. C. Lloyd-Jones, *Chem. Commun.*, **2000**, 2447-2448

[25] G. C. Lloyd-Jones, S. C. Stephen, I. J. S. Fairlamb, A. Martorell, B. Dominguez, P. M. Tomlin, M. Murray, J. M. Fernandez, J. C. Jeffery, R. Riis-Johannessen, T. Guerziz, *Pure. Appl. Chem.*, **2004**,*76*, 589-601

[26] C. Amatore, A. Jutand, L. Mensah, L. Ricard, *J. Organomet. Chem.*, **2007**, *692*, 1457-1464

[27] B. M. Trost, D. J. Michaelis, J. Charpentier, J. Xu, *Angew. Chem. Int. Ed.*, **2012**, *51*, 204-208

[28] B. M. Trost, J. Xu, T. Schmidt, *J. Am. Chem. Soc.*, **2009**, *131*, 18343-18357

[29] C. P. Butts, E. Filali, G. C. Lloyd-Jones, P.-O. Norrby, D. A. Sale, Y. Schramm, *J. Am. Chem. Soc.*, **2009**, *131*, 9945-9957

[30] (a) R. Akula, R. Doran, P. J. Guiry, *Chem. Eur. J.*, **2016**, *22*, 9938-9942 (b) B. M. Trost, *Chem. Parm. Bull.*, **2002**, *50*, 1-14 (c) J. T. Mohr, B. M. Stoltz, *Chem. Asian J.*, **2007**, *2*, 1476-1491

[31] B. M. Trost, D. L. Van Vranken, R. C. Bunt, *US Patent*, **1998**, US5739396

CONCLUSION AND FUTURE PERSPECTIVES

"Research workers must stimulate one another intellectually. Research must be their hobby."

Dr. Paul Janssen – 1993

In this Ph.D. thesis three ligand classes have been studied, namely monodentate phosphoramidite ligands (*cf.* Chapter 3), monodentate diamidophosphite ligands (*cf.* Chapter 4) and bidentate Trost-type ligands (*cf.* Chapter 5). All of the proposed novel ligands are characterized by the presence of a chiral biferrocene ligand backbone. Besides the development of an optimal synthesis route, the testing of these ligands in a frequently used benchmark test reaction was aimed as well. Another purpose was the study of the spatial 3D-structure of the synthesized ligands based on XRD-analyses.

Scheme 6.1 illustrates the synthetic approach for the phosphoramidite ligands **6.06** that were initially proposed. These ligands are the biferrocene-based analogs of the privileged phosphoramidite ligands developed by the research group of Feringa.[1]

The synthesis of the chiral backbone structure is based on the synthesis of planar-chiral ferrocene subunits. Diastereoselective *ortho*-metallation reactions using a directing group, which functions as chiral auxiliary, is a frequently used procedure for the synthesis of enantiopure planar-chiral ferrocene compounds. One of these methods uses a chiral acetal, which is derived from malic acid.[2] The procedure starts with the five-step synthesis sequence of ferrocene carboxaldehyde **6.01** into planar-chiral iodoaldehyde **6.02** (Scheme 6.1). The latter one was obtained with a total yield of 57% and an enantiomeric excess of 96%. Subsequently, **6.02** was transformed into a diastereomeric mixture of alcohols **6.03**, via addition of methyl magnesium bromide (88% yield). Oxidation of this alcohol was possible with MnO_2 in chloroform under reflux conditions (83% yield). The subsequent transformation towards iodoester **6.05** via the proposed Baeyer-Villiger oxidation turned out to be problematic. Consequently, it was impossible to synthesize, test and study the proposed biferrocene-based monodentate phosphoramidite ligands **6.06.**

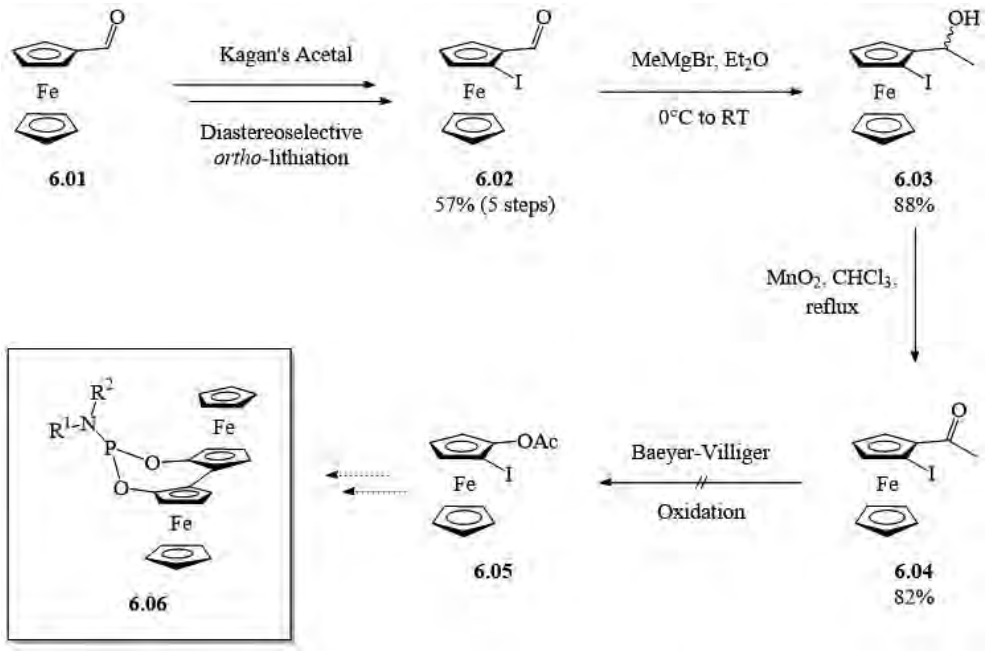

Scheme 6.1 Synthetic route for the initially proposed biferrocene-based monodentate phosphoramidite ligands **6.06**

Despite the fact that the initially proposed phosphoramidite ligands could not be synthesized, this led to new ideas concerning the design of novel biferrocene-based ligands. One of these implied that the biferrocene ligand backbone structure could be incorporated in the amine moiety of the phosphoramidite ligands. These structures are proposed as **6.10** in Scheme 6.2. A library of such ligands can be obtained by variation of the diol-based substructure. The use of an achiral diol allows to study the influence of the chiral biferrocene-backbone as such, whereas the combination of chiral amine and a chiral diol allows to explore the matched and mismatched situations. The synthetic route to obtain these ligands is shown in Scheme 6.2. It starts again from planar-chiral aldehyde **6.02**. The first step involves a homo-coupling towards biferrocene dialdehyde **6.07**. To this end, two procedures were applied. The first one is a classical Ullmann reaction, in which **6.02** reacts with metallic copper at high temperature (here 100°C). This allowed to synthesize dialdehyde **6.07** with a yield of 67%. An alternative procedure for the synthesis of biferrocene structures, at room temperature, was developed in this research project, based on a method reported by Liebeskind *et al.*[3] This method involves the use of copper thiophene-2-carboxylate (CuTC) in NMP.

Using this protocol, **6.07** was obtained with a yield of 50%. Reductive amination with allylamine, $NaBH_3CN$ and K_2CO_3 in dichloroethane resulted in biferrocene **6.08** with a yield of 76%. This methodology allowed to efficiently introduce the azepine substructure. Biferrocene-based azepine ligand precursor **6.09** was quantitatively obtained via a deprotection of the allylamine with KO*t*-Bu in DMSO at 100°C and mild acidic work-up using NH_4Cl. The final transformation of the synthesis sequence involved a two-step, one-pot reaction. In the first one, **6.09** was transformed in the corresponding dichloroaminophosphine using PCl_3, in the presence of Et_3N as a base. The desired phosphoramidite ligand **6.10** was obtained in a second step, via the addition of the corresponding diol and extra Et_3N. This allowed to synthesize ligands **6.13**-**6.15** (see also Scheme 6.3), which are characterized by the presence of an aromatic diol-based subunit, in variable yields between 29% and 44%. Despite different attempts to grow single crystals suitable for XRD-analysis, satisfying results were not obtained. Moreover, attempts to obtain copper- and rhodium-complexes of the synthesized ligands failed as well.

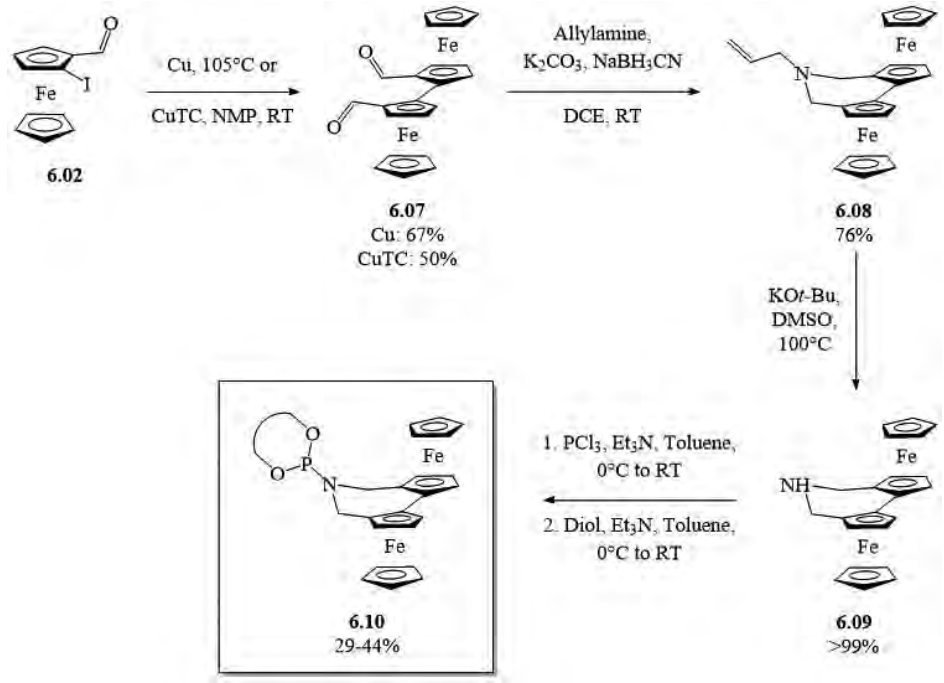

Scheme 6.2 Synthetic route towards the alternative monodentate phosphoramidite ligands **6.10** with a biferrocene azepine backbone structure

As shown in Scheme 6.3 ligands **6.13**-**6.15** were tested in the rhodium-catalyzed hydrogenation of enamide **6.11**. This reaction is one of the standard test reactions for the

evaluation of novel chiral monodentate ligands. The results are shown in Table 6.1. Full conversion and a modest *ee* of 26%, were obtained with ligand **6.11**, which consists of a chiral biferrocene backbone and bifenol as the diol substructure. Ligand **6.12**, characterized by the combination of the chiral biferrocene backbone and (*R*)-binol afforded a conversion of 95% and an enantiomeric excess of 68% (in favor of the (*S*)-enantiomer). This turned out to be the matched situation. On the other hand, ligand **6.13** synthesized from (*S*)-binol, is the mismatched combination with an *ee*-value of 4% (in favor of the (*R*)-enantiomer). Moreover, the conversion turned out to be lower for this ligand (84%).

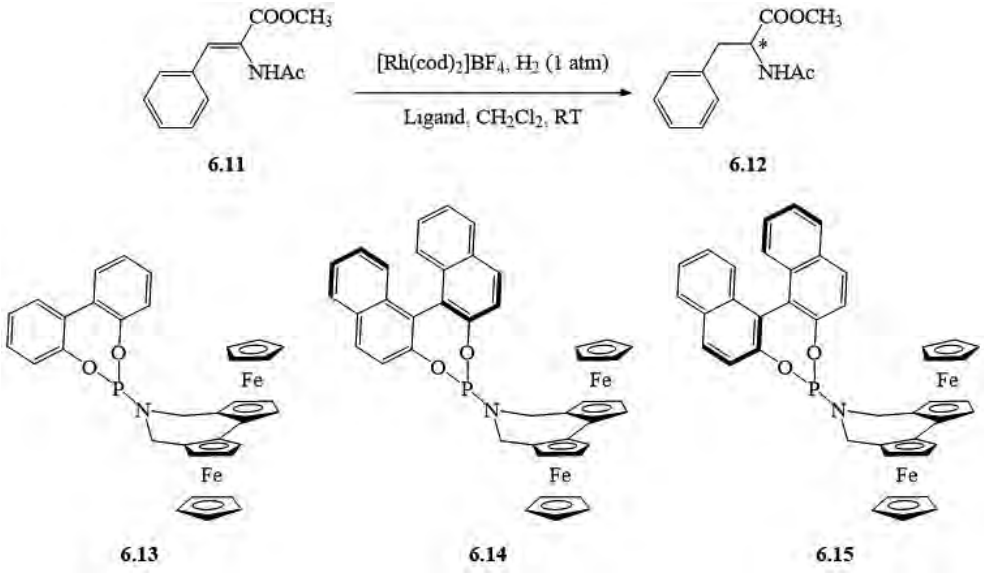

Scheme 6.3 Rhodium-catalyzed asymmetric hydrogenation of enamide **6.11** using novel biferrocene-based phosphoramidite ligands **6.13**-**6.15**

Substrate	Ligand	Time (h)	Conversion (%)	*ee* (%)
6.11	**6.13**	24	100	26 (*S*)
6.11	**6.14**	24	95	68 (*S*)
6.11	**6.15**	24	84	4 (*R*)

Table 6.1 Results for the rhodium-catalyzed asymmetric hydrogenation of enamide **6.11** with novel biferrocene-based phosphoramidite ligands **6.13**-**6.15**

The successful synthesis of biferrocene azepine ligand precursor **6.09** allows to expand the phosphoramidite ligand family as future perspectives. Some interesting examples are shown in Figure 6.1. Ligands **6.16**-**6.18** are characterized by an achiral, aliphatic diol

substructure. Further expansion of the library of phosphoramidite ligands by using chiral diols is an important future perspective as well. Therefore, ligands **6.19**-**6.22**, characterized by a taddol and spirodiol ligand backbone structure are proposed. Monodentate phosphoramidite ligands with these diol substructures have already been reported by the research groups of Feringa and Zhou respectively.[4] They applied these ligands in standard test reactions such as copper-catalyzed Michael additions with dialkylzinc reagents and rhodium-catalyzed hydrogenations of activated olefins such as esters of itaconic acid and enamide derivatives (inclusive olefin **6.11**). Therefore, it is interesting to test the biferrocene-based azepine phosphoramidite ligands in these reactions as well.

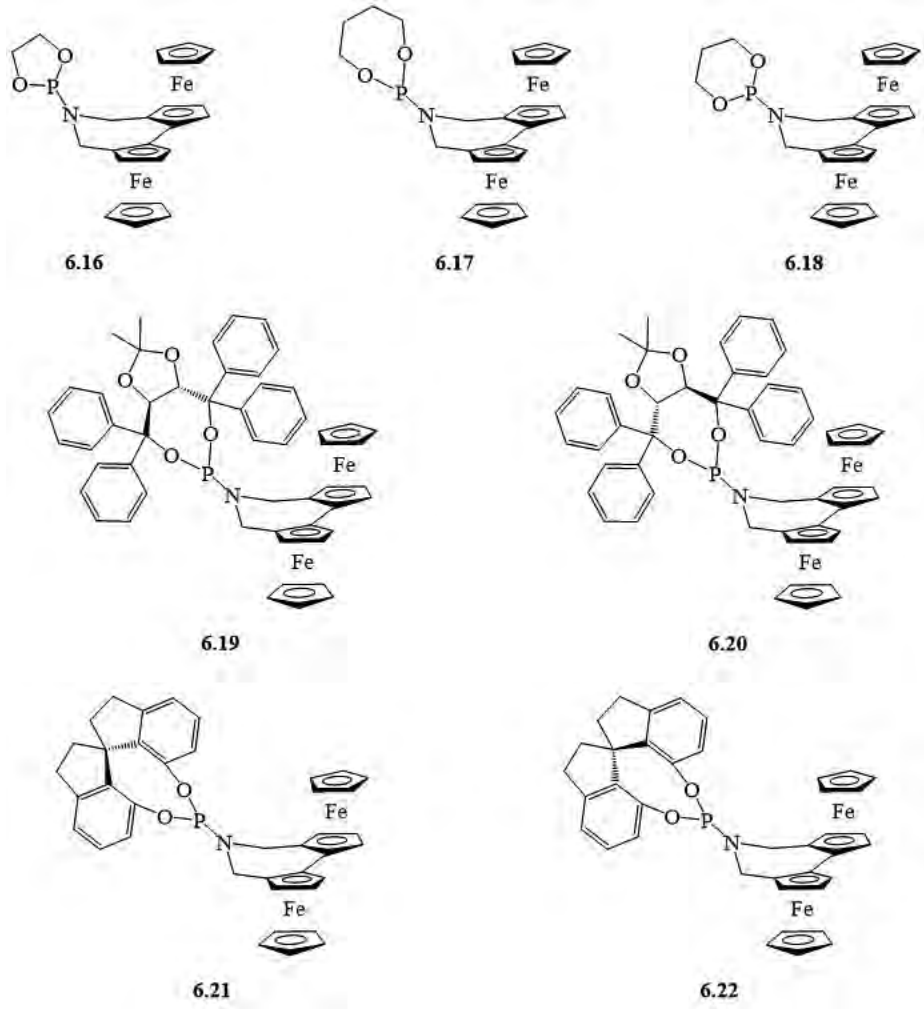

Figure 6.1 Expansion of phosphoramidite ligand library with the biferrocene-based azepine ligand backbone

Morover, these ligands also have to be tested in challenging asymmetric transition metal catalyzed reactions. Examples of such transformations are iridium-catalyzed hydrogenations of imines[5], rhodium-catalyzed Pauson-Khand tandem cycloaddition reactions[6] and palladium-catalyzed [3+2]-cycloaddition reactions[7] (Figure 6.2). The variety of transition metals that will be tested in these reactions will allow to study the coordination behavior of this ligand library. Finally, the request of XRD-analyses to examine the 3D-structure of these ligands and corresponding transition metal complexes remains an important future perspective as well.

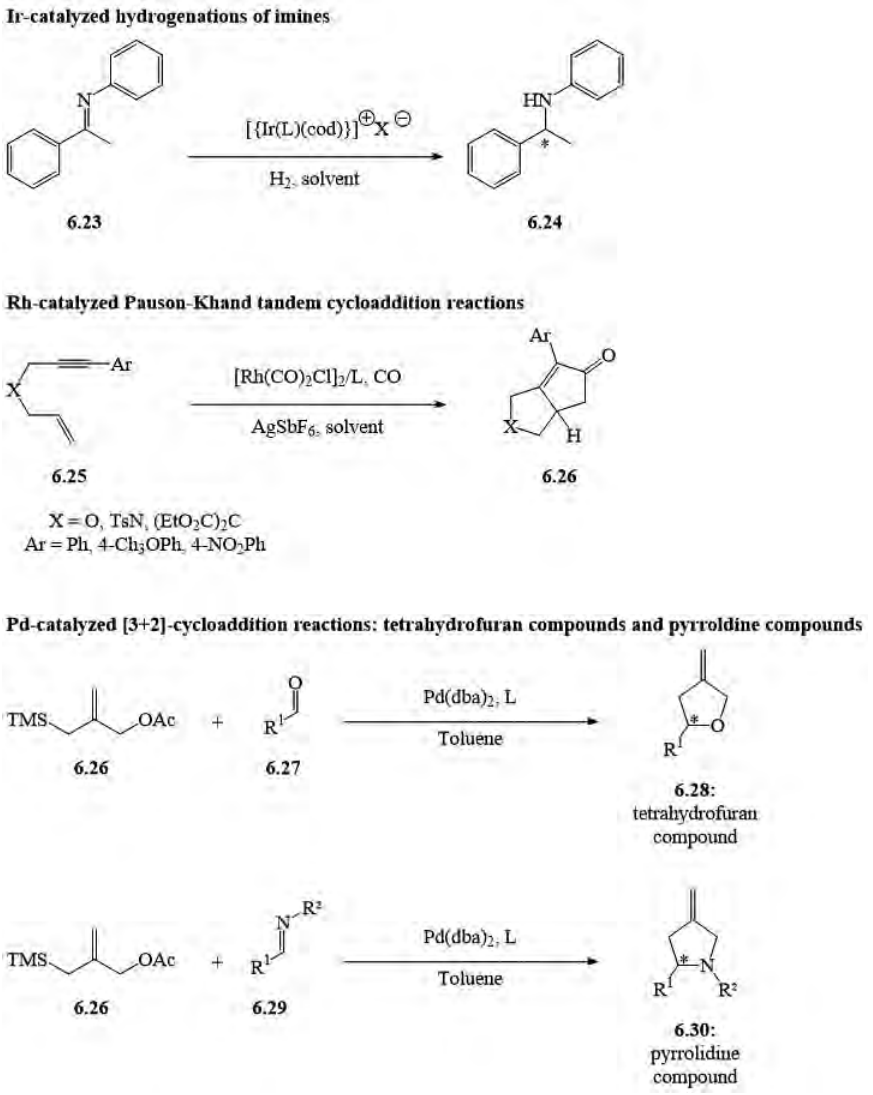

Figure 6.2 Challenging asymmetric transition metal catalyzed reactions for novel phosphoramidite ligands

Another idea originated from the unaccomplished synthesis of the initial phosphoramidite ligand library **6.06** consisted of exchanging the oxygen- and nitrogen atoms around the central phosphorus atom. This resulted in the development of the so-called diamidophosphite structure.[33] Despite the fact that some examples of this ligand family have been described in literature, the number of examples is way less extensive compared to the family of monodentate phosphoramidite ligands.[8] This can be explained by their sensitivity towards oxidation in air, which is a consequence of the significantly larger electron density around the central phosphorus atom. The essential building block for the synthesis of the novel biferrocene-based diamidophosphite ligands **6.44**-**6.47**, is planar-chiral iodo-carboxylic acid **6.35**. Two synthetic routes to obtain this compound have been investigated in this research project (Scheme 6.4). One of these methods involves oxidation of the well-known iodoaldehyde **6.02** via a mild Pinnick reaction, which allowed to isolate **6.35** with a yield of 66% (bottom left in Scheme 6.4).

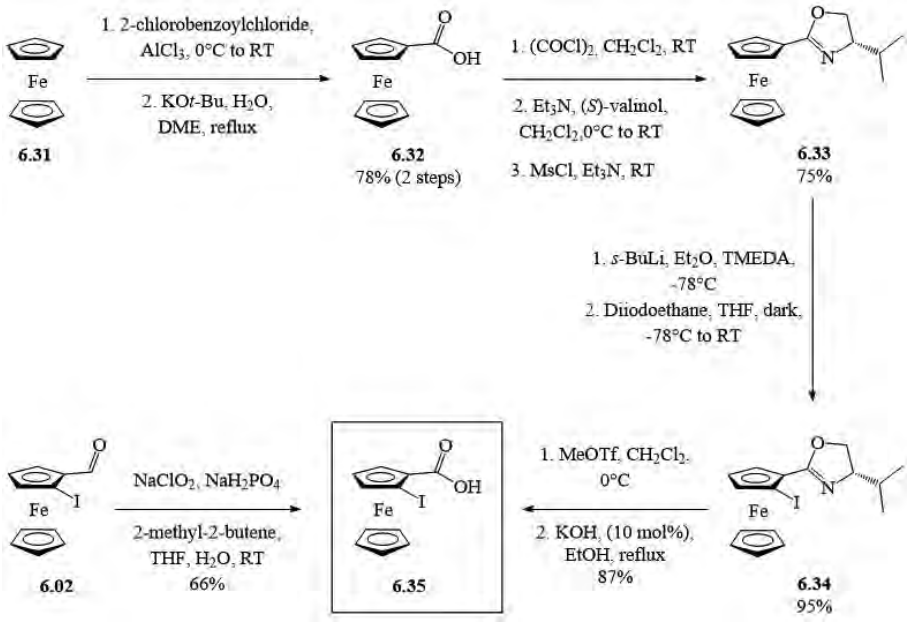

Scheme 6.4 Synthetic routes of key building block **6.35** for the synthesis of novel biferrocene-based monodentate diamidiophosphite ligands

The second synthetic route shown in Scheme 6.4, uses a chiral oxazoline, derived from (*S*)-valinol, as a diastereoselective *ortho*-directing group to synthesize enantiomerically pure planar-chiral ferrocene compounds. This frequently used method was de-

33 See also Scheme 6.5 (*vide infra*)

veloped independently by the research groups of Richards, Sammakia and Uemura.[9] The synthesis starts from commercially available ferrocene **6.31**. The latter was initially transformed into carboxylic acid **6.32** via a two-step process, described by Reeves *et al.*[10] Afterwards, **6.32** was converted in the desired oxazoline using a three-step, one-pot procedure via the initially formed acid chloride, reaction with (*S*)-valinol and subsequent cyclisation via mesylation in basic medium (75% yield). Diastereoselective *ortho*-lithiation with *s*-BuLi and TMEDA followed by reaction with electrophilic diiodoethane resulted in light sensitive, enantiomerically- and diastereomerically pure planar-chiral iodo-oxazoline **6.34** (95% yield). Methylation of the oxazoline-nitrogen atom with MeOTf followed by basic hydrolysis with KOH in ethanol under reflux conditions gave the desired building block, 2-iodo-carboxylic acid **6.35**, with a yield of 87%.

The subsequent part of the synthetic route towards the desired biferrocene-based diamidophosphite ligands starting from **6.35** is shown in Scheme 6.5. In a first reaction the latter compound is transformed into the corresponding acyl azide **6.36** using DPPA with a yield of 96%. A Curtius rearrangement at 105°C and subsequent reaction of the *in situ* formed isocyanate with 4-methoxybenzylalcohol resulted in the synthesis of carbamate **6.37** (95% yield). A first diversification of the target ligand library had to be implemented at this stage. This implied a mutually different substitution pattern at the nitrogen atoms of the diamidophosphite ligands. This is necessary to study the influence of the steric effects at this position. Therefore, two substituents were successfully introduced. Quantitative methylation was possible after deprotonation of the carbamate in THF, followed by addition of iodomethane. Introduction of the *i*-Pr substituent required the use of DMF as solvent (and a yield of only 55% was obtained). Other groups such as *t*-Bu and fluorinated alkyl groups could not be introduced using this methodology. For the homocoupling of planar-chiral iodocarbamates **6.38** and **6.39** two different procedures have been applied. The first one is again a classical metallic copper-mediated Ullmann reaction at 105°C, which allowed to obtain dicarbamates **6.40** and **6.41** with a yield of respectively 82% and 72%. The alternative procedure, which involved the use of CuTC at room temperature, gave the desired biferrocene structures with a yield of 50% for **6.40** and 48% for **6.41**. However, the formation of side products could not be excluded when this method was applied. Deprotection of the carbamate functional groups was possible via a standard procedure with TFA and allowed to isolate ligand precursors **6.42** and **6.43** with yields of respectively 76 and 89%. The final reaction consisted of a two-step transformation with PCl_3 and an alcohol, both in the

presence of Et_3N as a base. The huge diversity of commercially available alcohols theoretically allowed to synthesize an extensive library of ligands. However, methyl- and ethyl dichlorophosphite are two commercially available phosphorus precursors which allowed to significantly simplify the synthesis of the target diamidophosphite ligands. Biferrocene-based diamidophosphite ligands **6.44**-**6.47** were obtained with yields between 17% and 73%.

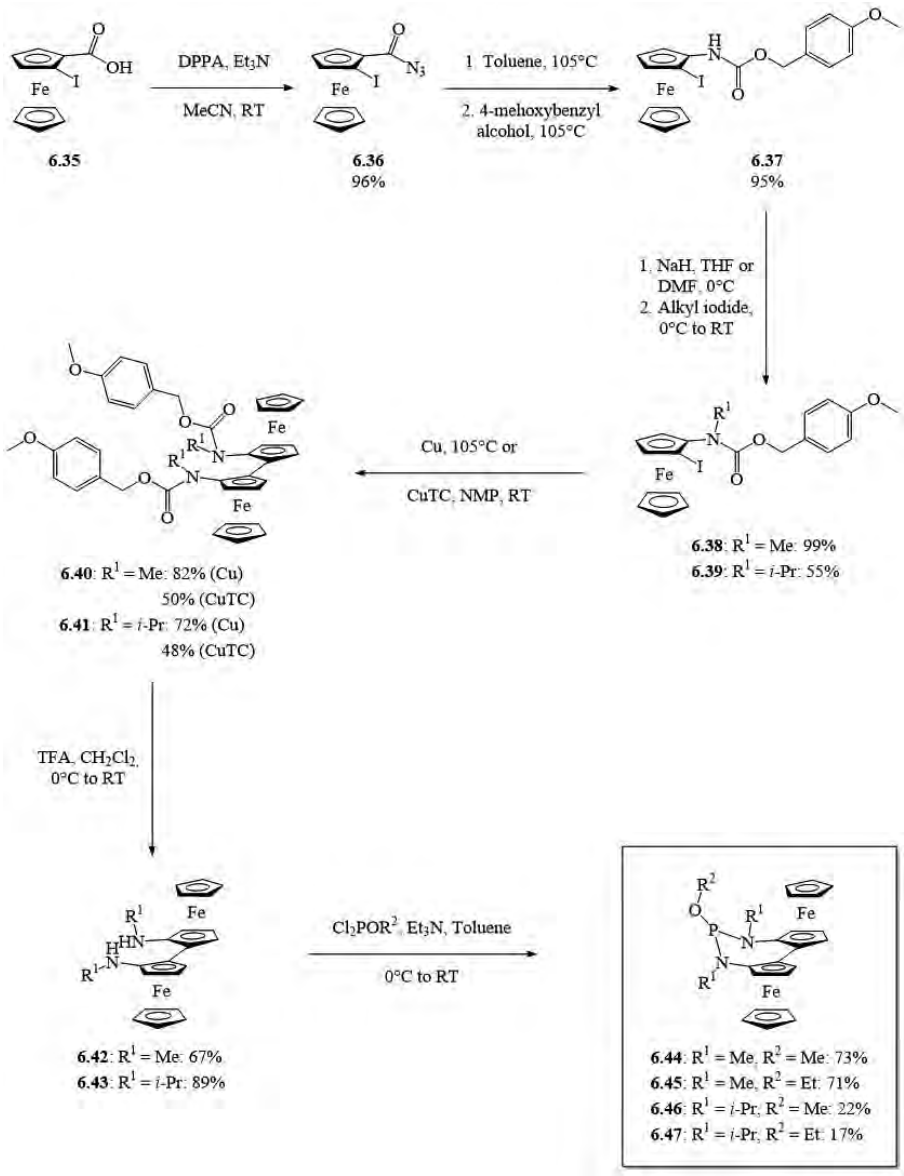

Scheme 6.5 Subsequent synthetic route towards the novel target monodentate biferrocene-based diamidophosphite ligands **6.44**-**6.47**

Just as phosphoramidite ligands **6.13-6.15**, biferrocene-based monodentate diamidophosphite ligands **6.44**-**6.47** were tested in the rhodium-catalyzed hydrogenation of enamide **6.11** (see also Scheme 6.3, *vide supra*). The results of these test reactions are shown in Table 6.2. Excellent conversions were obtained for *N,N'*-dimethyl substituted ligands **6.44** and **6.45** (100% and 95% respectively). In contrast, no conversions were obtained when *N,N'*-di-*iso*-propyl substituted ligands **6.46** and **6.47** were applied. This is explained by the larger steric effect caused by bulky *i*-Pr group, which makes the formation of the catalytically active rhodium-complex impossible. Ligand **6.45**, with ethoxy substituent on the central phosphorus atom, gave the highest enantiomeric excess, with an *ee*-value of 84% for the (*S*)-enantiomer. A significantly lower enantiomeric excess of 38% was obtained for ligand **6.44** characterized by a methoxy substituent at phosphorus. These results indicate that a small difference between two substituents can be responsible for a significant difference in terms of enantiomeric excess.

Substrate	Ligand	Time (h)	conversion (%)	*ee* (%)
6.11	**6.44**	24	100	38 (*S*)
6.11	**6.45**	24	95	84 (*S*)
6.11	**6.46**	24	0	-
6.11	**6.47**	24	0	-

Table 6.2 Results for the rhodium-catalyzed hydrogenation of enamide **6.11** with novel biferrocene-based diamidophosphite ligands **6.44**-**7.47**

In contrast to biferrocene-based phosphoramidite ligands **6.13**-**6.15** (Scheme 6.3, *vide supra*), crystals of ligands **6.45** and **6.47** suitable for XRD-analysis were easily obtained (Figure 6.3). It can be seen that the bulky *i*-Pr substituents cause significantly more sterical hindrance around the central phosphorus atom, which prohibits complexation with transition metals. It is correctly stated that for both structures **6.45** and **6.47**, the two connected cyclopentadiene rings adopt a (nearly) co-planar orientation with respect to each other. Consequently, the seven-membered heterocyclic ring system adopts an envelope-like conformation with local C_1-symmetry. Finally it has to be mentioned that the ethoxy-substituent has an axial orientation. These results are consistent with those reported by Widhalm for other seven-membered, heterocyclic biferrocene compounds.[11]

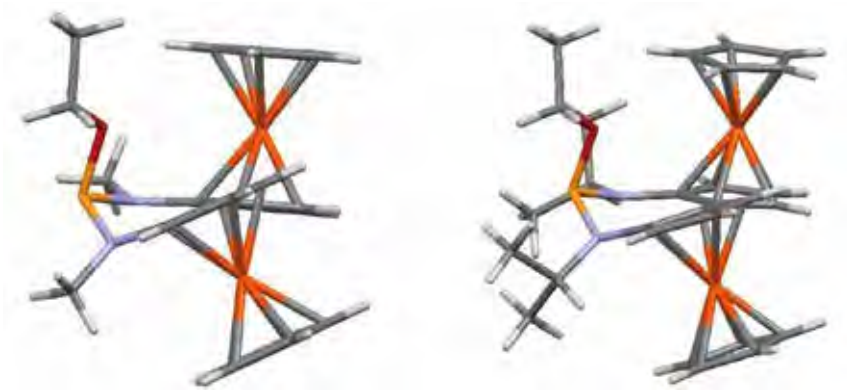

Figure 6.3 Crystal structures of biferrocene-based monodentate diamidophosphite ligands **6.45** (left) and **6.47** (right)

As for the biferrocene-based monodentate phosphoramidite ligands, the future perspectives for the diamidophosphite ligands are numerous as well. First, there is the opportunity to expand this ligand family. Examples of novel biferrocene-based diamidophosphite ligands are shown in Figure 6.4. The use of (distilled) PCl_3, Et_3N and different chiral as well as achiral alcohols allows to synthesize an extensive and diverse library of novel chiral ligands. This will make it possible to perform a detailed study of the alkoxy substituent (R^2, Scheme 6.5). Based on the performed experiments, it is proposed to synthesize te corresponding dichlorophosphites in a first step. The second step involves then the addition of the biferrocene-diamine. Expansion of this class of ligands is also possible via variation of the substituent on nitrogen (R^1, Scheme 6.5). Interesting options are the ethylsubstituent (**6.50**) and a benzylsubstituent (**6.51**), because these can theoretically be introduced using the methodology as described above. Electron deficient benzyl substituents (e.g. NO_2-substituents, **6.52**) may allow to improve the stability towards ligand oxidation.

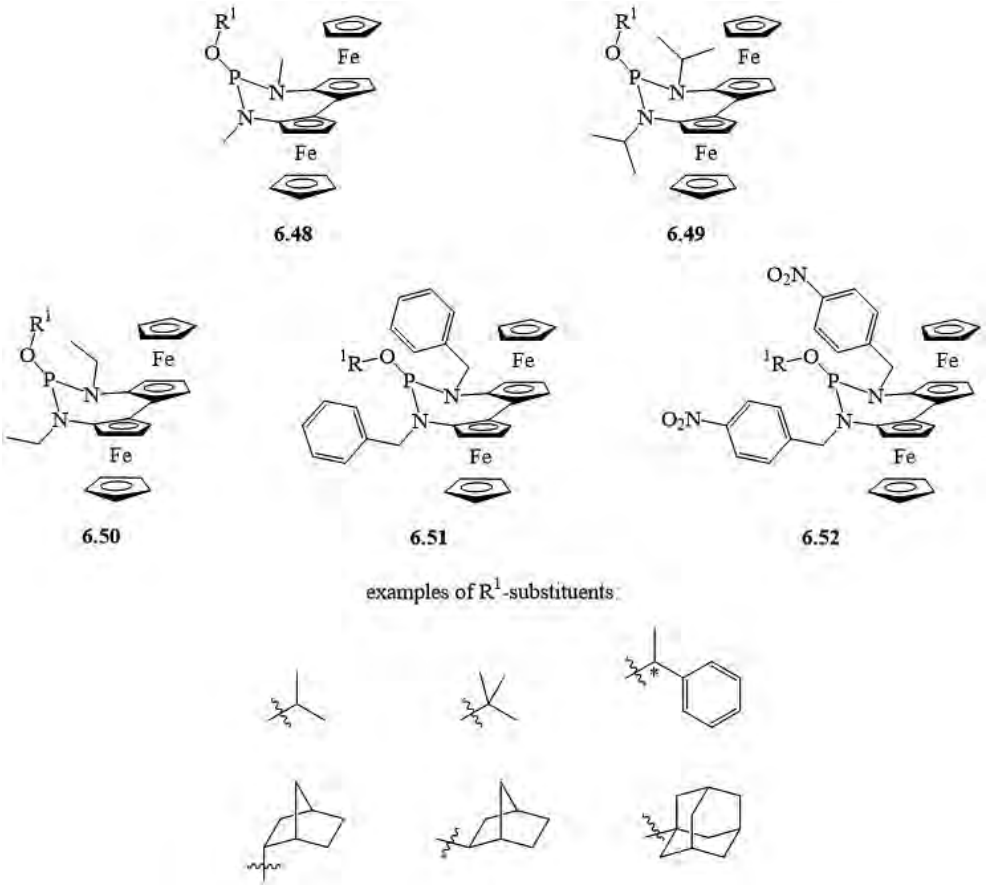

Figure 6.4 Expansion of diamidophosphite ligands: examples of novel biferrocene-based ligands

Benchmark test reactions for monodentate diamidophosphite ligands are rhodium-catalyzed hydrogenations of olefins such as enamide derivatives and esters of itaconic acid, palladium-catalyzed asymmetric allylic substitutions and palladium- or nickel-catalyzed hydrovinylations of styrene. These test reactions will give more insight in the coordination behavior of these ligands because different transition metals will be used. Beside these benchmark test reactions, it is important to explore the properties and characteristics of this ligand family in challenging reactions like those mentioned for the phosphoramidite ligands (*cf.* Figure 6.2, *vide supra*). Despite the fact that crystal structures of two ligands were already obtained, XRD-analyses of transition metal complexes are still missing.

The successful synthesis of the diamidophosphite ligands and the corresponding biferrocene diamines **6.42** and **6.43** have been inspiring for the development of a synthetic

route for novel analogs of another renowned ligand class. Trost-type ligands are characterized by the presence of a chiral diamine backbone as well. A variety of this type of bidentate ligands has already been synthesized and tested in multiple reactions by different research groups.[12,13] Therefore, biferrocene diamine **6.54** (Scheme 6.6) was proposed as a novel strategic chiral ligand backbone structure. Its synthetic route starts form building block **6.37**, which was already prepared for the synthesis of the diamidophosphite ligands **6.44**-**6.47** (*cf.* Scheme 6.5, *vide supra*). A copper mediated Ullmann homocoupling at 100°C was (again) chosen for the synthesis of the biferrocene substructure. This resulted in dicarbamate **6.53** with a yield of 76%. Removal of the protecting groups was again possible via the standard procedure using TFA, and biferrocene diamine **6.54** was obtained with a yield of 92%.

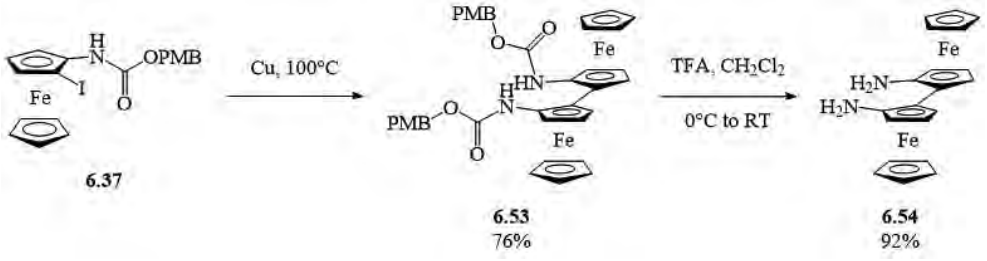

Scheme 6.6 Synthesis of the biferrocne-diamine backbone structure **6.54** for the target Trost-type ligands

Subsequent coupling with commercially available diphenylphosphino carboxylic acid **6.55**, as proposed in Scheme 6.7, appeared to be less straightforward. Different procedures were tested but target Trost-type ligand **6.56** could not be synthesized. The second target biferrocene-based Trost-type ligand **6.58** consists of two extra (identical) planar-chiral ferrocene substructures. In contrast to **6.55**, diphenylphosphino carboxylic acid **6.57** is not commercially available and had to be synthesized.

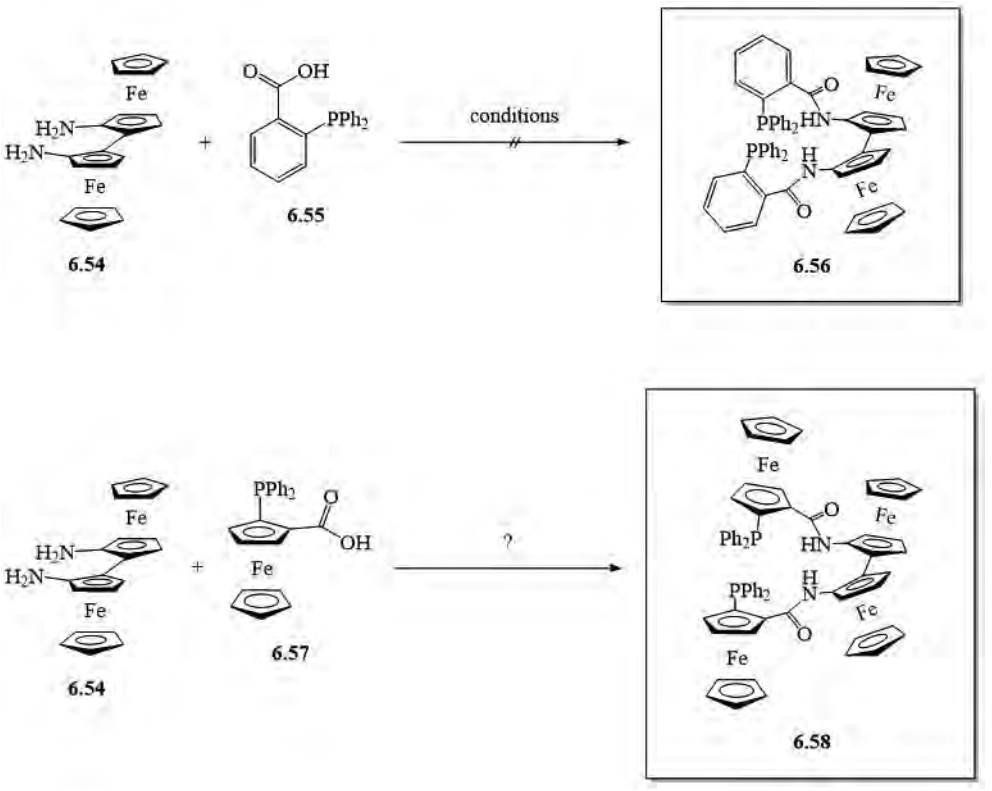

Scheme 6.7 Novel proposed Trost-type ligands **6.56** and **6.58** starting from biferrocene diamine **6.54**

The synthesis of **6.57** has been described by the research group of Zhang and is shown in Scheme 6.8.[13] This procedure uses the methodology of the chiral ferrocenyl oxazoline as *ortho*-directing group as well. Compound **6.59** was obtained in the same way as its enantiomer **6.33** (Scheme 6.4, *vide supra*). The first reaction of Scheme 6.8 involves the introduction of the diphenylphosphino group via diastereoselective *ortho*-lithiation and subsequent quenching with chlorodiphenylphosphine as electrophile. Planar-chiral ferrocene compound **6.60** was obtained with a yield of 61%. However, the three-step transformation of oxazoline **6.60** in the corresponding carboxylic acid **6.57** as described by Zhang could not be reproduced. An alternative procedure, which involved the halogen-lithium exchange of 2-iodocarboxylic acid **6.35** with two equivalents *n*-BuLi and subsequent quenching with chlorodiphenylphosphine to obtain the planar-chiral enantiomer of **6.57** was not successful either. Consequently, target biferrocene-based Trost ligand **6.58** (or its diastereomer) could not be accessed neither.

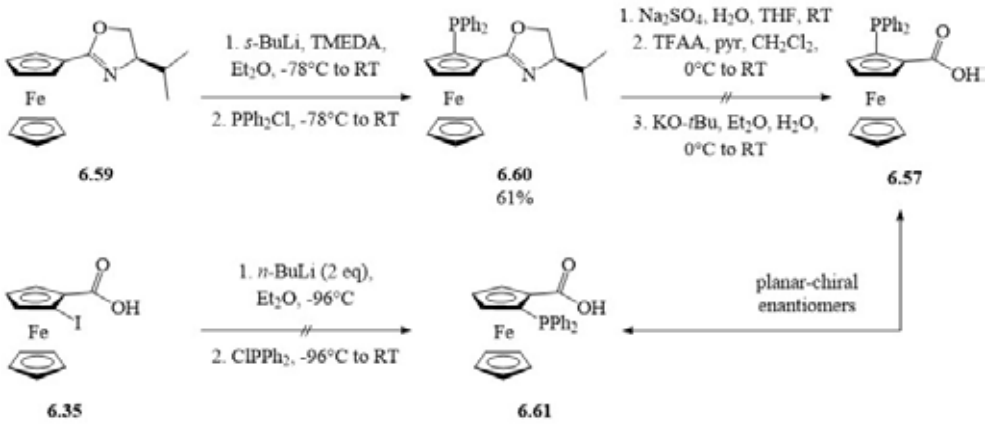

Scheme 6.8 Synthesis of planar-chiral 2-diphenylphosphino carboxylic acid **6.57** according to a procedure reported by Zhang[13] and the alternative synthesis of its planar-chiral enantiomer **6.61** via a halogen-lithium exchange starting from **6.35**

6.1. References

[1] (a) A. H. M. de Vries, A. Meetsma, B. L. Feringa, *Angew. Chem. Int. Ed.*, **1996**, *35*, 2374-2376; (b) M. van den Berg, R. M. Haak, A. J. Minnaard, A. H. M. de Vries, J. G. de Vries, B. L. Feringa, *Adv. Synth. Catal.*, **2002**, *344*, 1003-1007; (c) A. J. Minnaard, B. L. Feringa, L. Lefort, J. G. De Vries, *Acc. Chem. Res.*, **2007**, *40*, 1267-1277; (d) J. F. Teichert, B. L. Feringa, *Angew. Chem. Int. Ed.*, **2010**, *49*, 2486-2528

[2] (a) O. Riant, O. Samuel, H.B. Kagan, *J. Am. Chem. Soc.*, **1993**, *115*, 5835-5836; (b) O. Riant, O. Samuel. T. Flessner, S. Taudine, H.B. Kagan, *J. Org. Chem.*, **1997**, *62*, 6733-6745

[3] S. Zhang, D. Zhang, L. S. Liebeskind, *J. Org. Chem.*, **1997**, *62*, 2312-2313

[4] (a) E. Keller, J. Maurer, R. Naasz, T. Schader, A. Meetsma, B. L. Feringa, *Tetrahedron: Asymmetry*, **1998**, *9*, 2409-2413; (b) Y. Fu, J.-H. Xie, A.-G. Hu, H. Zhou, L.-X. Wang, Q.-L. Zhou, *Chem. Commun.*, **2002**, 480-481; (c) A.-G. Hu, Y. Fu, J.-H. Xie, H. Zhou, L.-X. Wang, Q.-L. Zhou, *Angew. Chem. Int. Ed.*, **2002**, *41*, 2348-2350

[5] (a) S. F. Zhu, J. B. Xie, Y. Z. Zhang, S. Li, Q. L. Zhou, *J. Am. Chem. Soc.*, **2006**, *128*, 12886-12891; (b) S. Zhou, S. Fleisscher, K. Junge, S. Das, D. Addis, M. Beller, *Angew. Chem. Int. Ed.*, **2010**, 49, 8121-8125

[6] B.-M. Fan, J.-H. Xie, S. Li, Y.-Q. Tu, Q.-L. Zhou, *Adv. Synth. Catal.*, **2005**, *347*, 759-762

[7] (a) B. M. Trost, S. M. Silverman, J. P. Stambuli, *J. Am. Chem. Soc.*, **2007**, *129*, 12398-12399; (b) B. M. Trost, D. A. Bringley, S. M. Silverman, *J. Am. Chem. Soc.*, **2011**, *133*, 7664-7667

[8] (a) M. T. Reetz, H. Oka, R. Goddard, *Synthesis*, **2003**, 1809-1814; (b) M. J. Bravo, R. M. Ceder, A. Grabulosa, G. Muller, M. Rocamora, J. C. Bayón, *Organometallics*, **2015**, *34*, 3799-3808; (c) K. N. Gavrilov, A. A. Shiryaev, S. V. Zheglov, V. K. Gavrilov, N. N. Groshkin, M. G. Maksimova, A. N. Volov, I. A. Zamiltskov, *Tetrahedron*, **2014**, *70*, 616-624; (d) B. M. Trost, T. M. Lam, *J. Am. Chem. Soc.*, **2012**, *134*, 11319-11321; (e) M. Schmitkamp, W. Leitner, G. Franciò, *Catal. Sci. Technol.*, **2013**, *3*, 589-594; and references therein

[9] (a) C. J. Richards, T. Damaldis, D. E. Hibbs, M. B. Hursthouse, *Synlett.*, **1995**, 74-76; (b) C. J. Richards, A. W. Mulvaney, *Tetrahedron Asymmetry*, **1996**, *7*, 1419-1430; (c) T. Sammakia, H. A. Latham, D. R. Schaad, *J. Org. Chem.*, **1995**, 60, 10-11; (d) T. Sammakia, H. A. Latham, *J. Org. Chem.*, **1995**, *60*, 6002-6003; (e) T. Sammakia, H. A. Latham, *J. Org. Chem.*, **1996**, *61*, 1629-1635; (f) Y. Nishibashi, S. Uemura, *Synlett.*, **1995**, 79-81; (g) Y. Nishibayashi, K. Segawa, Y. Arikawa, K. Ohe, M. Hidai, S. Uemura, *J. Organomet. Chem.*, **1997**, *545-546*, 381-391

[10] P. C. Reeves, *Org. Synt.*., **1977**, *56*, 28-31

[11] L. Xiao, W. Weissensteiner, K. Mereiter, M. Widhalm, *J. Org. Chem.*, **2002**, *67*, 2206-2214

[12] (a) B. M. Trost, D. L. Van Vranken, *Angew. Chem. Int. Ed. Engl.*, **1992**, *31*, 228-230; (b) B. M. Trost, R.C. Bunt, *Angew. Chem. Int. Ed. Engl*, **1992**, *35*, 99-102; (c) H. Adolfsson, C. Moberg, *Tetrahedron Asymmetry*, **1995**, *6*, 2023-2031; (d) C. W. Lim, S. Lee, *Tetrahedron*, **2000**, *56*, 5131-5136

[13] J. M. Longmire, B. Wang, X.Zhang, *Tetrahedron Lett.*, **2000**, *41*, 5435-5439

CONCLUSIE EN TOEKOMSTPERSPECTIEVEN

"Research workers must stimulate one another intellectually. Research must be their hobby."

Dr. Paul Janssen – 1993

In deze doctoraatsstudie werden drie ligandklassen bestudeerd, namelijk monodentaat fosforamidiet liganden (*cf.* Hoofdstuk 3), monodentaat diamidofosfiet liganden (*cf.* Hoofdstuk 4) en bidenaat Trost-type liganden (*cf.* Hoofdstuk 5). Alle nieuwe liganden die voorgesteld worden in deze doctoraatsthesis, worden gekenmerkt door de aanwezigheid van een chirale biferroceen ruggengraatstructuur. Naast de ontwikkeling van een optimale syntheseroute, werd tevens als doel gesteld om deze liganden te testen in een veelvuldig gebruikte transitiemetaal gekatalyseerde testreactie. Daarnaast werd ook getracht om de ruimtelijke 3D-structuur van de gesynthetiseerde liganden te bestuderen aan de hand van XRD-analyses.

Schema 7.1 toont de syntheseroute van de initieel voorgestelde monodentaat fosforamidiet liganden **7.06**. Deze liganden gelden als biferroceen-gebaseerde analogen van de geprivilegieerde fosforamidiet liganden, die ontwikkeld werden door de onderzoeksgroep van Feringa.[1]

De synthese van de chirale ruggengraatstructuur berust op de synthese van planair-chirale ferroceeneenheden. Diastereoselectieve *ortho*-metallatie reacties met behulp van een richtende groep, die bovendien als chirale hulpstof fungeert, is een veelgebruikte procedure voor de synthese van enantiomeer zuivere planair-chirale ferroceenverbindingen. Één van deze methodes maakt gebruik van een chiraal acetaal afgeleid van appelzuur.[2] Deze procedure start uitgaande van ferroceen carboxaldehyd **7.01** (Schema 7.1), dat via een vijf-stappen sequentie omgezet wordt in het planair-chirale jood-aldehyd **7.02**. Dit resulteerde in een totaal rendement van 57% en een enantiomere overmaat van 96%. Vervolgens werd **7.02** omgezet in een diastereomeer mengsel van alcohol **7.03**, door toevoegen van het methyl Grignard reagens (88% rendement). Oxidatie van dit alcohol was mogelijk met MnO_2, in chloroform onder reflux condities (83%

rendement). Verdere omvorming tot jood-ester **7.05** via de voorgestelde Baeyer-Villiger oxidatie bleek problematisch. Hierdoor was het onmogelijk om de vooropgestelde biferroceen-gebaseerde monodentaat fosforamidiet liganden **7.06** te synthetiseren, te testen en te bestuderen.

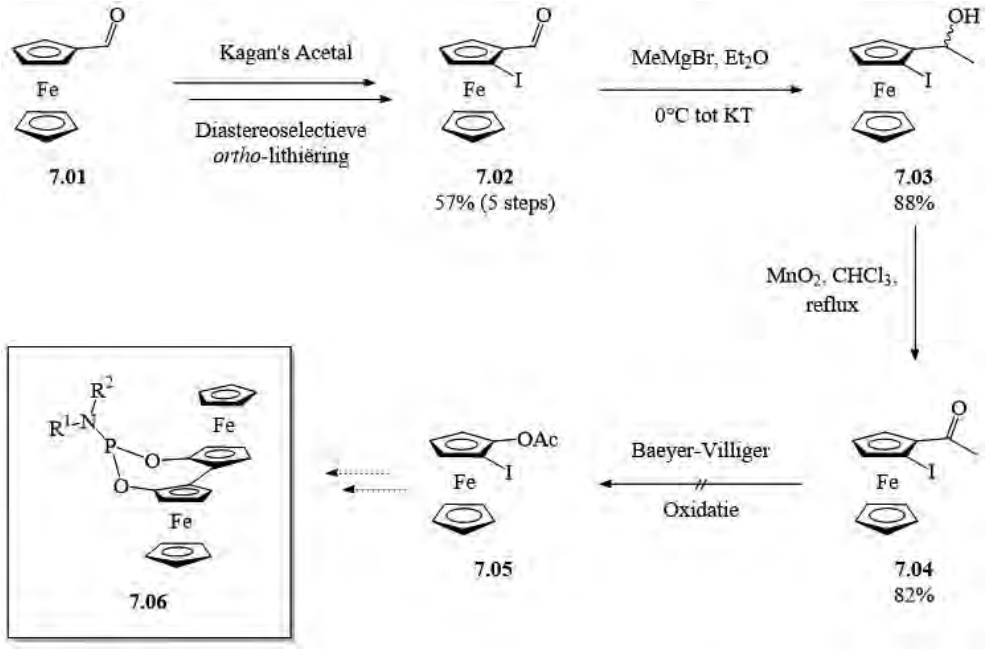

Schema 7.1 Syntheseroute voor de initieel voorgestelde biferroceen-gebaseerde monodentaat fosforamidiet liganden **7.06**

Ondanks het feit dat de initieel vooropgestelde fosforamidiet liganden niet gesynthetiseerd konden worden leidde dit tot nieuwe ideeën betreffende het ontwerpen van andere, nieuwe biferroceen-gebaseerde liganden. Één van deze ideeën impliceerde dat de biferroceen ligandstructuur kon ingebouwd worden in het amine gedeelte van de fosforamidiet liganden. Deze structuren kunnen algemeen voorgesteld worden als **7.10** in Schema 7.2. Een bibliotheek van liganden kan bekomen worden door variatie van het diol-gebaseerde gedeelte. Het gebruik van achirale diolen laat toe om de invloed van de chirale biferroceen-gebaseerde azepine structuur te bestuderen. Aanwending van chirale diolen laat toe om *'matched and mismatched'* situaties te onderzoeken. De synthesesequentie van deze ligandbibliotheek wordt weergegeven in Schema 7.2. Ze start eveneens vanuit het planair-chirale jood-aldehyd **7.02**. De eerste stap is de homokoppeling tot bifferoceen dialdehyd **7.07**. Hiervoor werden twee procedures aangewend.

De eerste is een klassieke Ullmann reactie waarbij **7.02** reageert met metallisch koper in een solventvrije reactie bij verhoogde temperatuur (hier 100°C). Dialdehyd **7.07** kon op deze manier bekomen worden met een rendement van 67%. Een alternatieve procedure voor de synthese van biferroceen structuren, bij kamertemperatuur, werd ontwikkeld in dit onderzoeksproject, op basis van een methode gepubliceerd door Liebeskind *et al.*[3] Deze methode impliceert het gebruik van koperthiofeen carboxylaat (CuTC) in NMP waarmee biferroceen **7.07** verkregen kon worden met een rendement van 50%. Reductieve aminering met allylamine, $NaBH_3CN$ en K_2CO_3 in dichloorethaan resulteerde in biferroceen **7.08** met een rendement van 76%. Op deze wijze kon de azepine-eenheid efficiënt geïntroduceerd worden. Synthese van de biferroceen-gebaseerde azepine ligand precursor **7.09** gebeurde kwantitatief via klassieke ontscherming van de allylaminefunctie met KO*t*-Bu in DMSO bij 100°C en een mild zure afwerkingsstap (NH_4Cl). De laatste transformatie van de synthesesequentie bestond uit een twee-staps, 1-pot reactie. Tijdens de eerste stap werd **7.09** omgezet in het overeenkomstige dichloroaminephosphine door gebruik van PCl_3 in de aanwezigheid van Et_3N. Het gewenste fosforamidiet **7.10** werd bekomen tijdens de tweede stap door het overeenkomstig diol en extra Et_3N toe te voegen. Op deze manier was het mogelijk om liganden **7.13-7.15** (zie ook Schema 7.3), welke gekarakteriseerd worden door een aromatische diol-gebaseerde subeenheid, te synthetiseren met rendementen variërende tussen 29% en 44%. Niettegenstaande dat er verschillende pogingen ondernomen werden voor het bekomen van kristallen, geschikt voor XRD-analyses bleven de vereiste resultaten uit. Dit geldt eveneens voor de experimenten omtrent het bekomen van koper- en rhodium-complexen van de voorgestelde liganden.

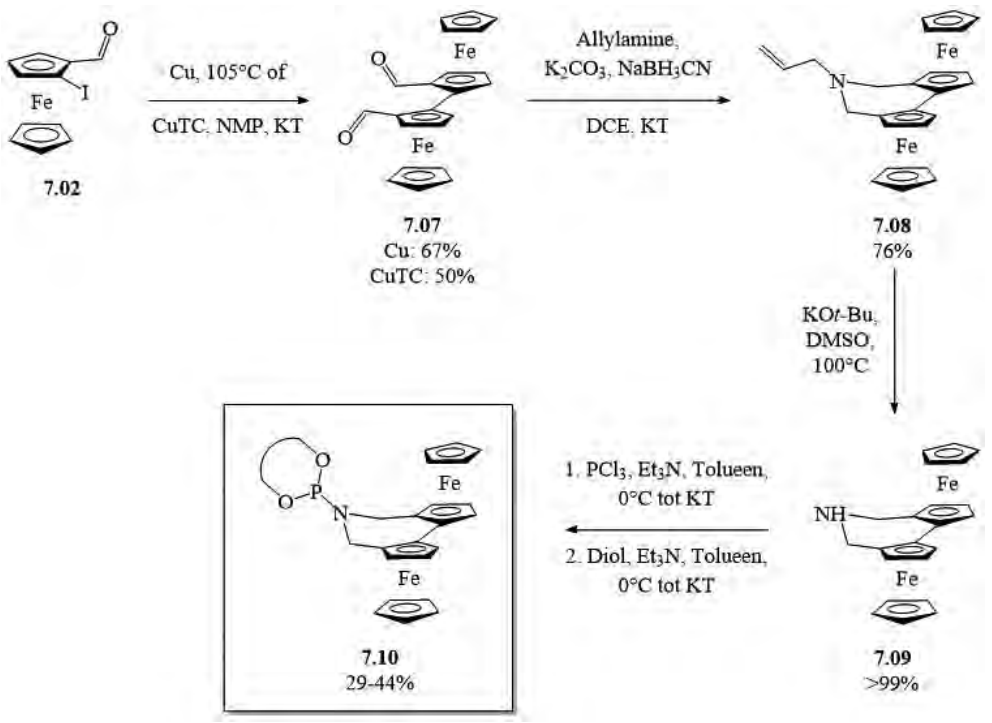

Schema 7.2 Syntheseroute voor de alternatieve monodentaat fosforamidiet liganden **7.10** met een biferroceen azepine ruggengraat structuur

Zoals getoond in Schema 7.3 werden Liganden **7.13-7.15** getest in de rhodium-gekatalyseerde hydrogenatie van enamide **7.11**. Deze reactie geldt als een standaard testreactie voor de evaluatie van nieuwe chirale monodentaat liganden. De resultaten worden getoond in Tabel 7.1. Volledige conversie en een bescheiden *ee*-waarde van 26% werden bekomen met ligand **7.11**, bestaande uit een chirale biferroceen substructuur en het achirale bifenol. Ligand **7.12** dat bestaat uit de combinatie van de chirale biferroceen ruggengraatstructuur en (*R*)-binol resulteerde in 95% conversie en een enantiomere overmaat van 68% (van het (*S*)-enantiomeer). Deze combinatie geldt dan ook als de *'matched'* ligandstructuur. Anderzijds geldt ligand **7.13**, gesynthetiseerd met (*S*)-binol, als de *'mismatched'* situatie waarmee een *ee*-waarde van slechts 4% (van het (*R*)-enantiomeer) bekomen werd. Bovendien bleek ook de conversie lager voor dit ligand (84%).

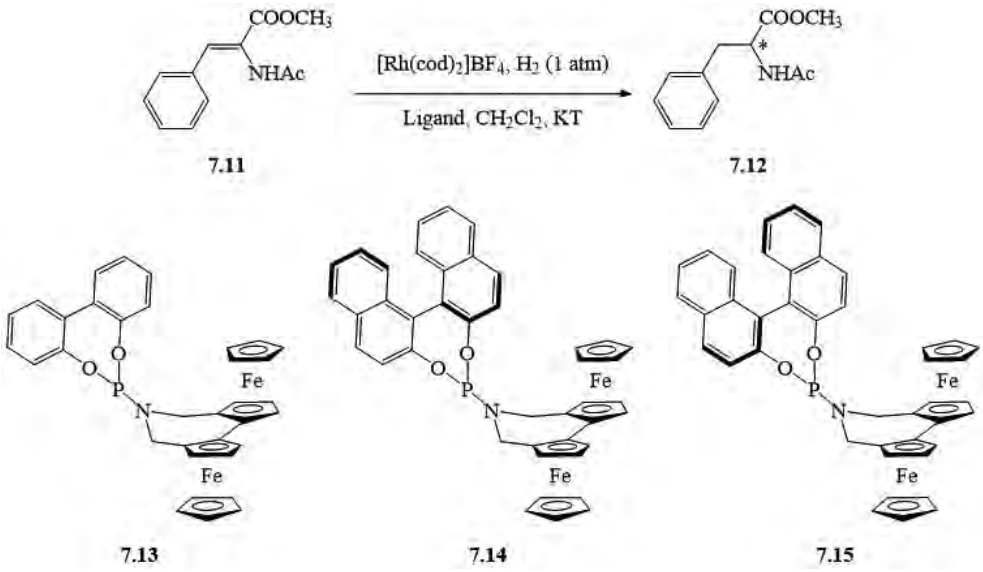

Schema 7.3 Rhodium-gekatalyseerde asymmetrische hydrogenatie van enamide **7.11** met nieuwe biferroceen-gebaseerde fosforamidiet liganden **7.13**-**7.15**

SUBSTRAAT	Ligand	TIJD (U)	ConversiE (%)	*ee* (%)
7.11	**7.13**	24	100	26 (*S*)
7.11	**7.14**	24	95	68 (*S*)
7.11	**7.15**	24	84	4 (*R*)

Tabel 7.1 Resultaten voor de rhodium-gekatalyseerde asymmetrische hydrogenaties van enamide **7.11** met nieuwe biferroceen-gebaseerde fosforamidiet liganden **7.13**-**7.15**

De succesvolle synthese van de biferroceen azepine ligand precursor **7.09** laat toe om de bibliotheek van fosforamidiet liganden in de toekomst verder uit te breiden. Enkele interessante voorbeelden worden getoond in Figuur 7.1. Liganden **7.16**-**7.18** worden gekenmerkt door een achirale, alifatische diol substructuur. Verdere uitbreiding van de fosforamidiet ligandfamilie via het gebruik van chirale diolen vormt eveneens een belangrijk toekomstperspectief. Daarom worden liganden **7.19**-**7.22**, gekarakteriseerd door een taddol en spirodiol ligand ruggengraatstructuur, voorgesteld. Andere monodentaat fosforamidiet liganden gekenmerkt door deze diol substructuren werden eerder al gerapporteerd door de onderzoeksgroepen van respectievelijk Feringa en Zhou.[4] Zij bestudeerden deze liganden in standaard testreacties zoals koper-gekatalyseerde Michaeladditities met dialkylzink reagentia en rhodium-gekatalyseerde hydrogenaties van geactiveerde olefines zoals esters van itaconzuur en enamide derivaten (inclusief

olefine **7.11**). Op basis hiervan is het interessant om de voorgestelde biferroceen-azepine fosforamidiet liganden eveneens in deze reacties te testen.

Daarnaast dienen deze liganden getest te worden in meer uitdagende asymmetrische transitiemetaal gekatalyseerde reacties. Hiertoe behoren onder meer iridium-gekatalyseerde hydrogenaties van imines[5], rhodium-gekatalyseerde Pauson-Khand tandem cycloadditiereacties[6] en palladium-gekatalyseerde [3+2]-cycloadditiereacties[7] (Figuur 7.2). De verscheidenheid aan transitiemetalen die op deze manier ingezet zullen worden, zal toelaten om het coördinatiegedrag van deze ligand biblioteek te bestuderen. Tot slot blijft de nood aan XRD-analyses, voor de studie van de 3D-strucutuur, van deze liganden en bijhorende transitiemetaalcomplexen een belangrijk toekomstperspectief.

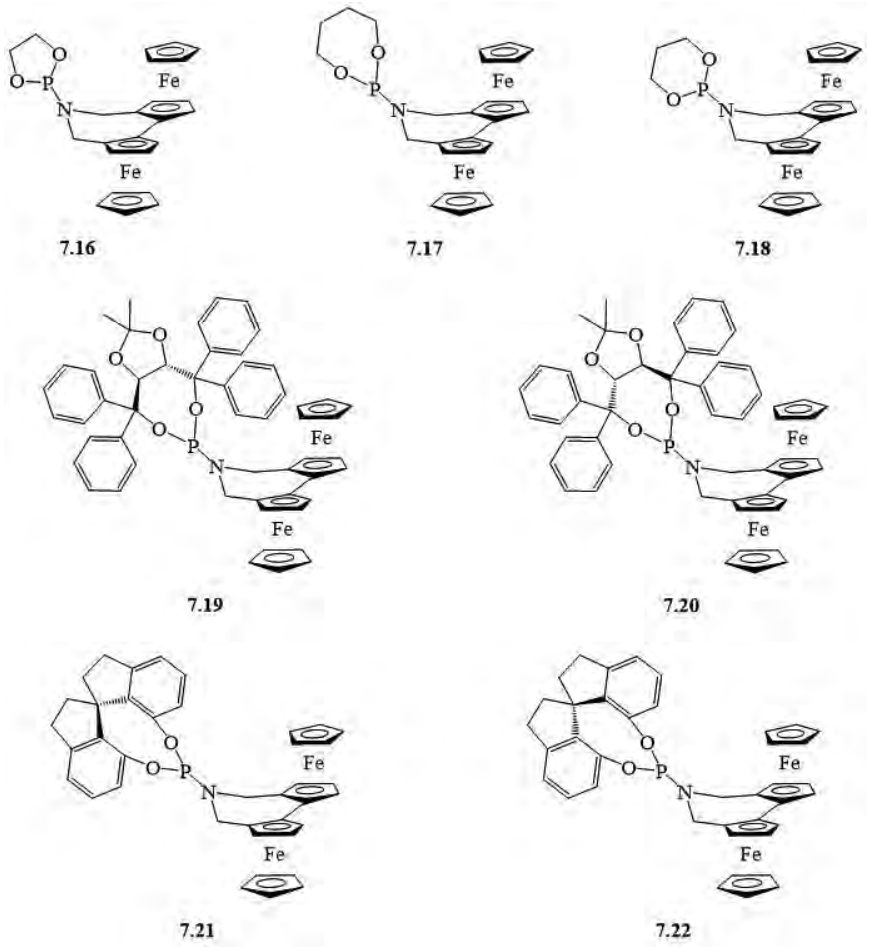

Figuur 7.1 Uitbreiding van de bibliotheek van fosforamidiet liganden met de biferroceen-azepine ligand ruggengraatstructuur

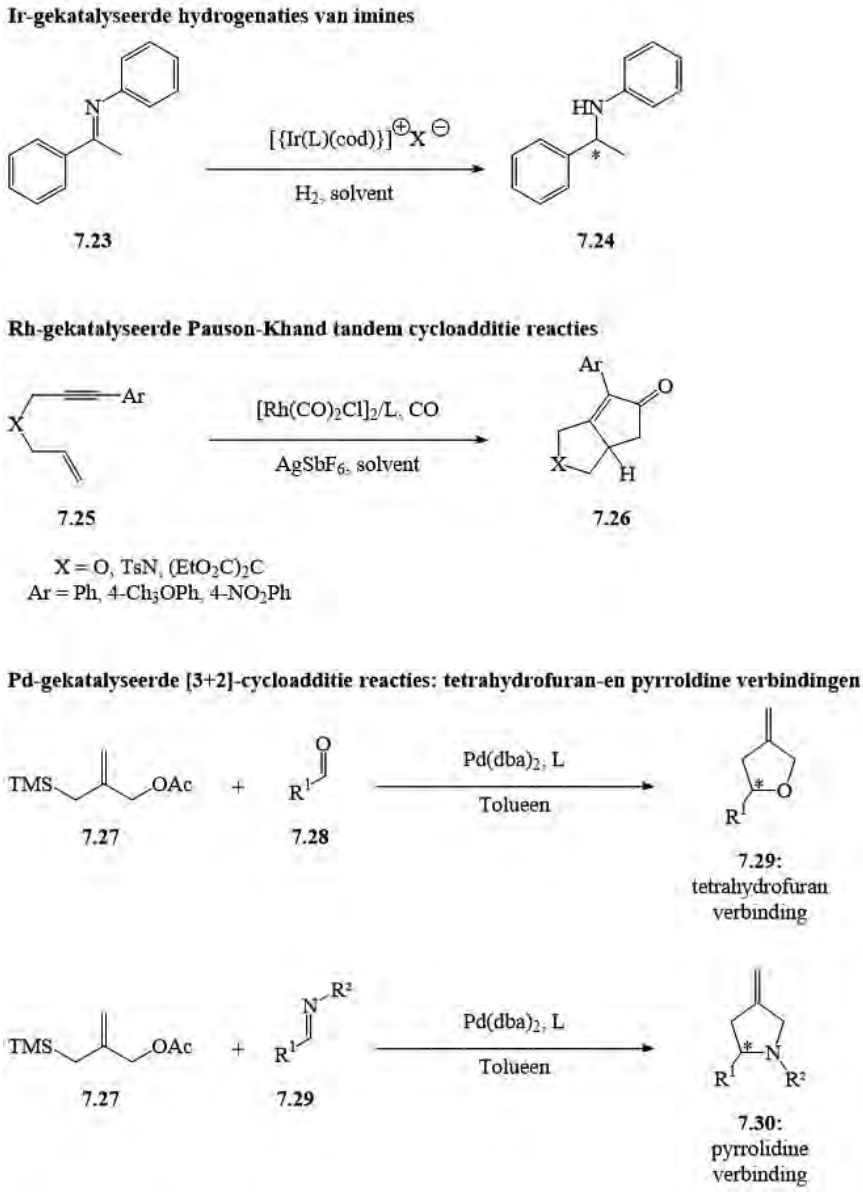

Figuur 7.2 Uitdagende asymmetrische transitiemetaal gekatalyseerde reacties voor fosforamidiet liganden

Een ander idee dat ontstond uit de onvoltooide synthese van de initiële fosforamidiet liganden **7.06** bestond uit het omwisselen van de zuurstof- en stikstofatomen rond het centrale fosforatoom. Op deze manier wordt de zogeheten diamidofosfiet structuur bekomen.[34] Ondanks het feit dat er reeds voorbeelden van deze ligandfamilie beschre-

34 Zie eventueel ook Schema 7.5 (*vide infra*).

ven zijn in de literatuur, is deze bibliotheek veel minder uitgebreid ten opzichte van de familie van fosforamidiet liganden.[8] Bovendien worden ze veel minder frequent aangewend in asymmetrische transitiemetaal gekatalyseerde reacties. Dit valt toe te schrijven aan hun gevoeligheid voor oxidatie, wanneer ze blootgesteld worden aan de lucht. Deze instabiliteit wordt verklaard door de grotere elektronendensiteit rond het centrale fosforatoom. De centrale bouwsteen voor de synthese van de nieuwe biferroceen-gebaseerde diamidofosfietliganden **7.44-7.47**, is het planair-chirale jood-carbonzuur **7.35**. Hiervoor werden twee syntheseroutes onderzocht (Schema 7.4). Één van deze methodes impliceert oxidatie van het gekende jood-aldehyd **7.02** via een milde Pinnick reactie, wat toeliet om **7.27** te isoleren met een rendement van 66% (links onder in Schema 7.4).

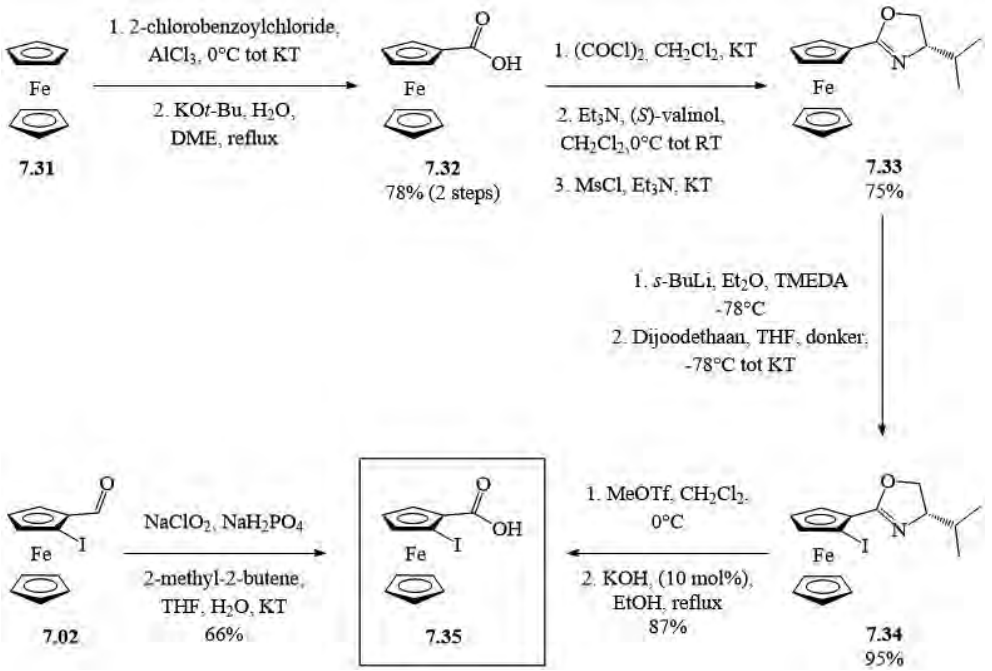

Schema 7.4 Syntheseroutes voor de centrale bouwsteen **7.35** voor de synthese van nieuwe biferroceen-gebaseerde monodentaat diamidofosfiet liganden

De tweede syntheseroute maakt gebruik van een chiraal oxazoline, afgeleid van (*S*)-valinol, als diastereoselectieve *ortho*-richtende groep voor het bekomen van enantiomeer zuivere planair-chirale ferroceen verbindingen. Deze veelvuldig gebruikte methode werd onafhankelijk ontwikkeld door de onderzoeksgroepen van Richards, Sammakia en Uemura.[9] De synthese start vanuit het commercieel beschikbare ferroceen **7.31**. Dit

werd initieel omgezet in carbonzuur **7.32**, via een twee-staps proces beschreven door Reeves *et.al*.[10] Het gewenste oxazoline **7.33** werd daarna bekomen via een drie-staps, één-pot procedure via het intermediair gevormde zuurchloride, gevolgd door reactie met (*S*)-valinol en navolgende cyclisatie via mesylatie in basisch milieu (75% rendement). Diastereoselectieve *ortho*-lithiëring met *s*-BuLi en TMEDA gevolgd door reactie met het electrofiele dijoodethaan resulteerde in het lichtgevoelige, enantio- en diastereomeer zuivere planair-chirale jood-oxazoline **7.34** (95% rendement). Methylatie van het oxazoline-stikstofatoom met MeOTf gevolg door basische hydrolyse met behulp van KOH in ethanol onder reflux condities leverde de gewenste bouwsteen **7.35** op met een rendement van 87%.

De verdere syntheseroute tot de gewenste biferroceen-gebaseerde diamidofosfiet liganden, uitgaande van **7.35** wordt getoond in Schema 7.5. In een eerste reactie wordt deze omgezet in het overeenkomstig acylazide **7.36** met behulp van DPPA (96% rendement). Curtius omlegging bij 105°C en reactie van het *in situ* gevormde isocyanaat met 4-methoxybenzylalcohol resulteerde in carbamaat **7.37** (95% rendement). Een eerste diversificatie voor de beoogde ligandbibliotheek diende te gebeuren tijdens de volgende stap. Dit impliceerde een verschillend substitutiepatroon op de stikstofatomen van de diamidofosfiet liganden zodat de invloed van sterische effecten op deze positie bestudeerd kon worden. Hiervoor werden twee groepen succesvol geïntroduceerd. Kwantitatieve methylering was mogelijk na deprotonatie van het carbamaat in THF, gevolgd door reactie met joodmethaan. Introductie van de *i*-Pr substituent vereiste het gebruik van DMF als solvent. Bovendien leverde dit (slechts) een rendement op van 55%. Andere groepen, zoals *t*-Bu en fluoroalkyl groepen konden niet volgens deze methodologie geïntroduceerd worden. Voor de homokoppeling van beide planair-chirale jood ferroceen carbamaten **7.38** en **7.39** werden eveneens twee procedures aangewend. De eerste was opnieuw een klassieke Ullmann reactie waarbij **7.38** en **7.39** telkens reageerden met metallisch koper bij verhoogde temperatuur (105°C). Dicarbamaten **7.40** en **7.41** konden op deze manier bekomen worden met een rendement van respectievelijk 82% en 72%. De alternatieve procedure bij kamertemperatuur met behulp van CuTC leverde ook de gewenste biferroceen structuren op (50% en 48% voor respectievelijk **7.40** en **7.41**). De vorming van nevenproducten kon echter niet uitgesloten worden wanneer de laatstgenoemde methode toegepast werd. Ontscherming van de carbamaat functionele groepen was mogelijk via een standaardprocedure met TFA waardoor de vereiste ligand precursoren bekomen werden (67% en 89% voor respec-

tievelijk **7.42** en **7.43**). De laatste transformatie bestaat uit een twee-staps reactie met PCl_3 en een alcohol, telkens in aanwezigheid van Et_3N als base.

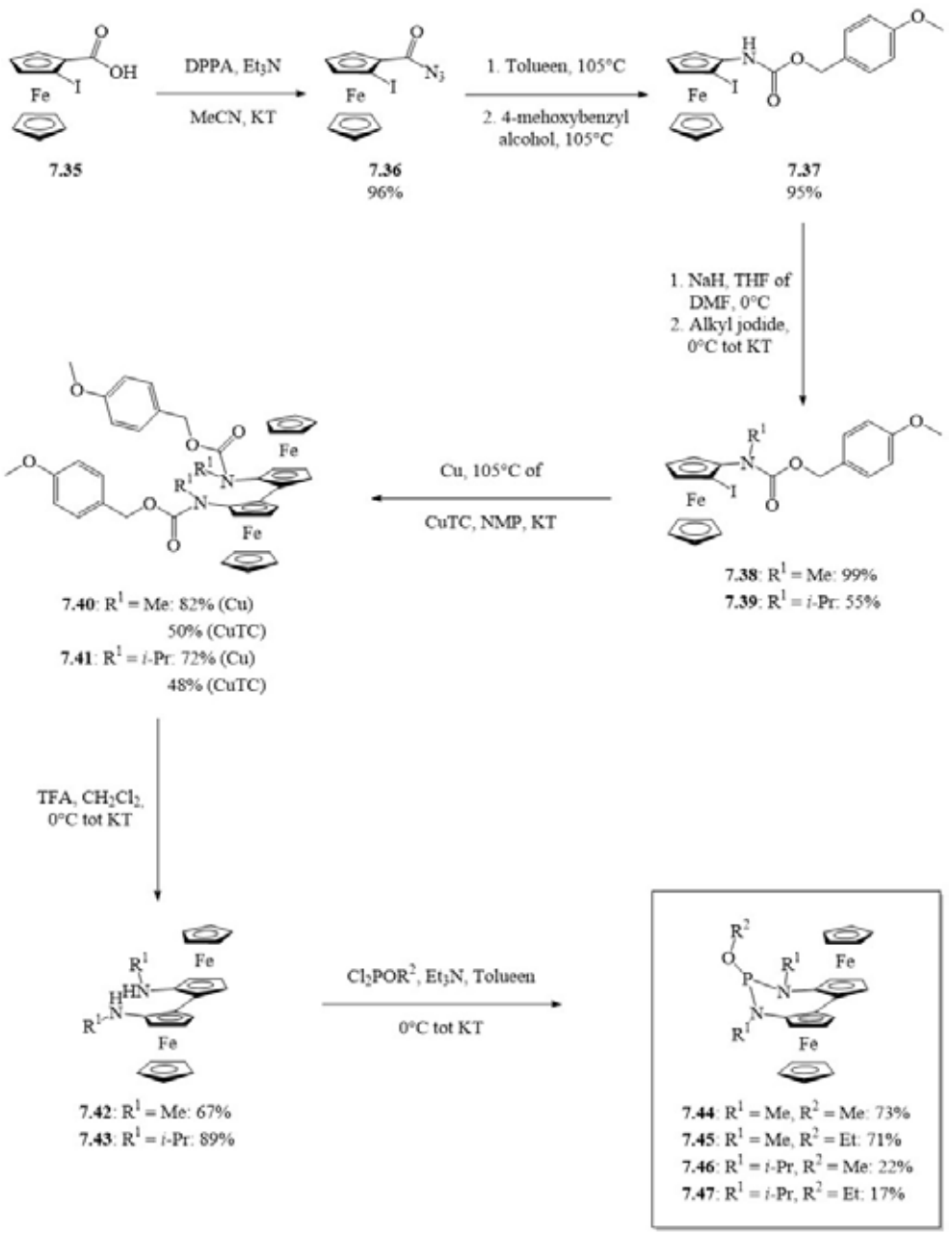

Schema 7.5 Vervolg syntheseroute voor de beoogde, nieuwe monodentaat biferroceen-gebaseerde diamidofosfiet liganden **7.44**-**7.47**

De grote verscheidenheid aan commercieel beschikbare alcoholen impliceert dat een zeer uitgebreide bibliotheek van liganden gesynthetiseerd kan worden. Echter, methyl dichloorfosfiet en ethyl dichloorfosfiet zijn twee commercieel beschikbare fosforprecursoren die de synthese van de beoogde diamidofosfiet liganden praktisch sterk vereenvoudigden. Dit liet toe om de beoogde biferroceen-gebaseerde liganden **7.44**-**7.47** te bekomen met een rendement variërende tussen 17% en 73%.

Net zoals de fosforamidietliganden **7.13-7.15**, werden de biferroceen-gebaseerde monodentaat diamidofosfiet liganden **7.44-7.47** eveneens getest in de rhodium-gekatalyseerde hydrogenatie van enamide **7.11** (zie ook Schema 7.3, *vide supra*). De resultaten van deze testreacties worden weergegeven in Tabel 7.2. Zeer goede conversies werden bekomen voor *N,N'*-dimethylgesubstitueerde liganden **7.44** en **7.45** (respectievelijk 100% en 95%). In tegenstelling hiermee werd er geen conversie waargenomen wanneer *N,N'*-di-*iso*-propyl gesubstitueerde liganden **7.46** en **7.47** aangewend werden. Dit wordt toegeschreven aan de stericiteit van deze substituenten waardoor het onmogelijk wordt geacht om het gewenste catalytisch actieve rhodium-complex te vormen. Ligand **7.45**, met ethoxy subsituent op het centrale fosforatoom leverde de hoogste *ee*-waarde op (84% voor het (*S*)-enantiomeer). Een significant lagere enantiomere overmaat van 38% werd waargenomen voor ligand **7.44**, met de methoxysubstituent. Deze resultaten tonen aan dat een klein onderling verschil tussen twee substituenten verantwoordelijk kan zijn voor een significant verschil in enantiomere overmaat.

Substraat	Ligand	TIJD (U)	conversie (%)	*ee* (%)
7.11	**7.44**	24	100	38 (*S*)
7.11	**7.45**	24	95	84 (*S*)
7.11	**7.46**	24	0	-
7.11	**7.47**	24	0	-

Tabel 7.2 Resultaten voor de rhodium-gekatalyseerde hydrogenatie van enamide **7.11** met nieuwe biferroceen-gebaseerde diamidofosfiet liganden **7.44**-**7.47**

In tegenstelling tot bovenvermelde biferroceen-gebaseerde fosforamidiet liganden **7.13-7.15** (Schema 7.3, *vide supra*) werden voor liganden **7.45** en **7.47** wel geschikte kristallen gevormd voor XRD-analyse (Figuur 7.3). Het is duidelijk te zien dat de volumineuze *i*-Pr substituenten significant meer sterische hinder veroorzaken rondom het centra-

le fosforatoom waardoor complexatie bemoeilijkt wordt. Bovendien geldt voor beide structuren dat, de twee verbonden cyclopentadieen ringen (bij benadering) een co-planaire oriëntatie hebben ten opzichte van elkaar. Bijgevolg neemt de hetereocyclische zevenring een enveloppe conformatie aan die gekenmerkt wordt door een C_1-symmetrie. Tot slot valt op dat de ethoxysubstituent voor beiden structuren de axiale oriëntatie aanneemt. Deze bevindingen zijn conform met de resultaten gepubliceerd door Widhalm voor andere biferroceen structuren met een heterocyclische zevenring.[11]

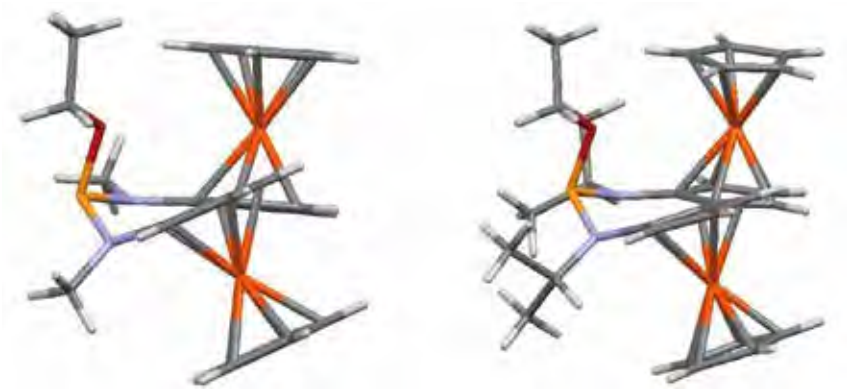

Figuur 7.3 Kristalstructuren van biferroceen-gebaseerde monodentaat diamidofosfiet liganden **7.45** (links) en **7.47** (rechts)

In overeenstemming met de biferroceen-gebaseerde monodentaat fosforamidiet liganden zijn de toekomstperspectieven deze diamidofosfiet liganden eveneens legio. Ten eerste is er de mogelijkheid tot verdere uitbreiding van deze ligandklasse. Voorbeelden van nieuwe biferroeen-gebaseerde diamidofosfietliganden worden getoond in Figuur 7.4. Gebruik van (gedestilleerd) PCl_3, Et_3N en verscheidene chirale en achirale alcoholen laat toe om een zeer omvangrijke en diverse bibliotheek te synthetiseren. Dit zal het mogelijk maken om de invloed van de alkoxy substituent (R^2, Schema 7.5) nauwgezet te bestuderen. Op basis van de uitgevoerde experimenten is de meest aangeweze methode deze waarbij de corresponderende dichlorofosfieten gesynthetiseerd worden in een eerste stap. Tijdens de tweede stap wordt het gewenste biferroceen-diamine toegevoegd. Uitbreiding van deze ligandklasse is eveneens mogelijk door extra variatie van de stikstofsubstituenten (R^1, Schema 7.5). Interessante opties zijn de ethylsubstituent (**7.50**) en de benzylsubstituent (**7.51**) omdat het theoretisch mogelijk is om deze op bovenvermelde wijze te introduceren. Elektronzuigende benzylsubstitu-

enten (bijvoorbeeld NO_2-substituenten, **7.52**) laten mogelijks toe om de oxidatiegevoeligheid te verbeteren.

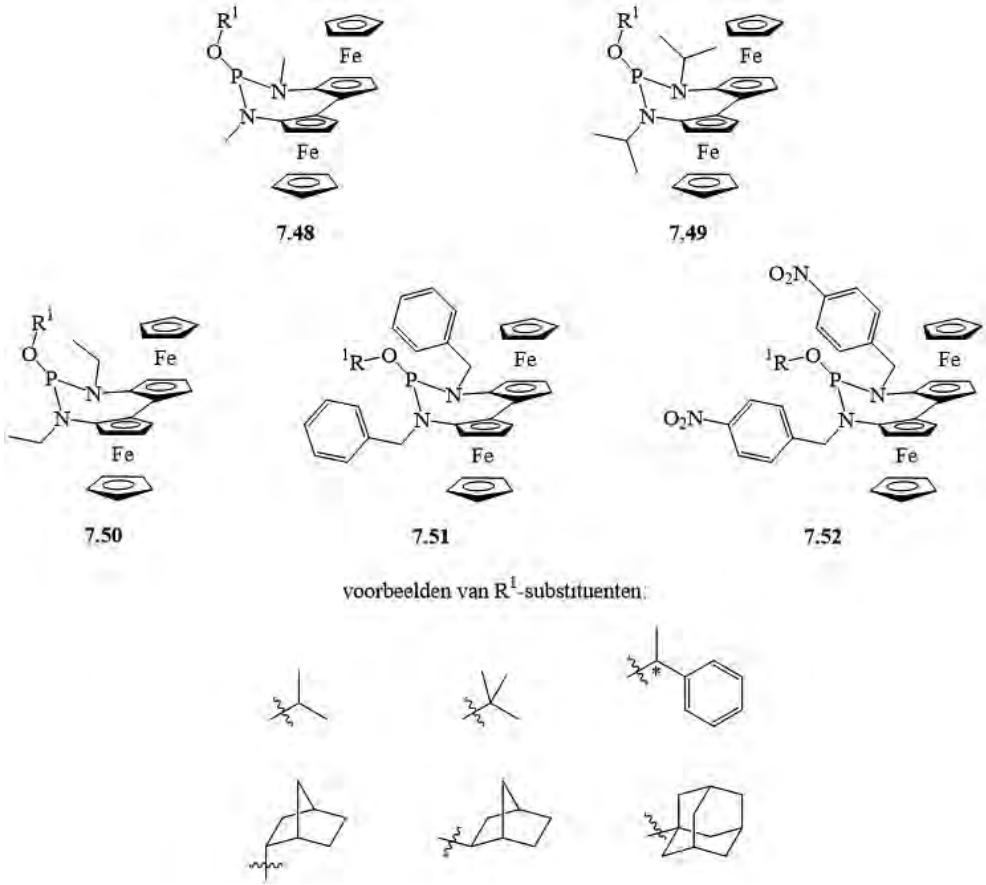

Figuur 7.4 Uitbreiding van diamidofosfiet liganden: voorbeelden van nieuwe biferroceen-gebaseerde liganden

Standaard testreacties voor monodentaat diamidofosfiet liganden zijn (eveneens) rhodium-gekatalyseerde hydrogenaties van olefines zoals enamide derivaten en esters van itaconzuur, palladium-gekatalyseerde asymmetrische allylische substituties en palladium- of nikkel-gekatalyseerde hydrovinylering van styreen. Aangezien verschillende transitiemetalen bij deze reacties aan bod zullen komen, zullen deze testen meer inzicht geven over het coördinatiegedrag van de biferroceen-gebaseerde diamidofosfiet liganden. Daarnaast vormt het onderzoek van het gedrag van deze liganden in meer uitdagende testreacties, zoals deze genoemd bij de fosformadietliganden, eveneens een belangrijk toekomstperspectief (*cf.* Figuur 7.2, *vide supra*). Ondanks het feit dat

kristalstructuren van twee van deze liganden reeds bekomen werden, ontbreken er nog XRD-analyses van de bijhorende transitiemetaalcomplexen.

De succesvolle synthese van bovenstaande diamidofosfiet liganden en biferroceen diamines **7.42** en **7.43** inspireerden op hun beurt tot de ontwikkeling van een syntheseroute voor nieuwe analogen van een andere befaamde ligandklasse. Trost-type liganden zijn namelijk eveneens afgeleid van diamines, die de chirale ruggengraatstructuur vormen. Verscheidene varianten van deze bidentaat liganden werden reeds succesvol gesynthetiseerd en getest door verschillende onderzoeksgroepen.[12,13] Biferroceen diamine **7.54** (Schema 7.6) werd daarom voorgesteld als nieuwe strategische chirale ruggengraatstructuur. De syntheseroute start vanuit bouwsteen **7.37**, welke reeds bereid werd voor de synthese van de diamidofosfietliganden **7.44**-**7.47** (*cf.* Schema 7.5, *vide infra*). Een Ullmann homokoppeling met metallisch koper bij 100°C werd (opnieuw) aangewend voor de synthese van de biferroceen substructuur **7.53**. Hierbij werd een rendement van 76% bekomen. Verwijderen van de beschermgroepen was opnieuw mogelijk via de standaardprocedure met TFA, wat diamine **7.54** opleverde met een rendement van 92%.

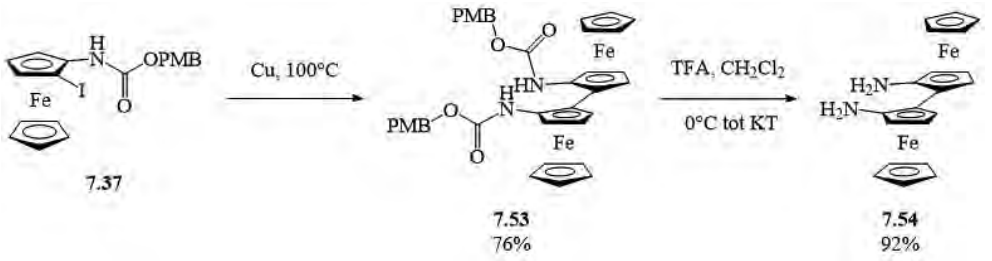

Schema 7.6 Synthese van de biferroceen-diamine ruggengraatstructuur **7.54** voor de beoogde Trost-type liganden

Verdere koppeling met commercieel beschikbaar diphenylphosphino carbonzuur **7.55**, zoals voorgesteld in Schema 7.7, bleek minder evident. Verscheidene procedures werden getest maar het beoogde Trost ligand **7.56** kon niet gesynthetiseerd worden. Het tweede beoogde biferroceen-gebaseeerde Trost ligand **7.58** is opgebouwd met twee extra (identieke) planair-chirale ferroceen eenheden. Het diphenylphosphino carbonzuur **7.57** is niet commercieel beschikbaar en diende daarom gesynthetiseerd te worden.

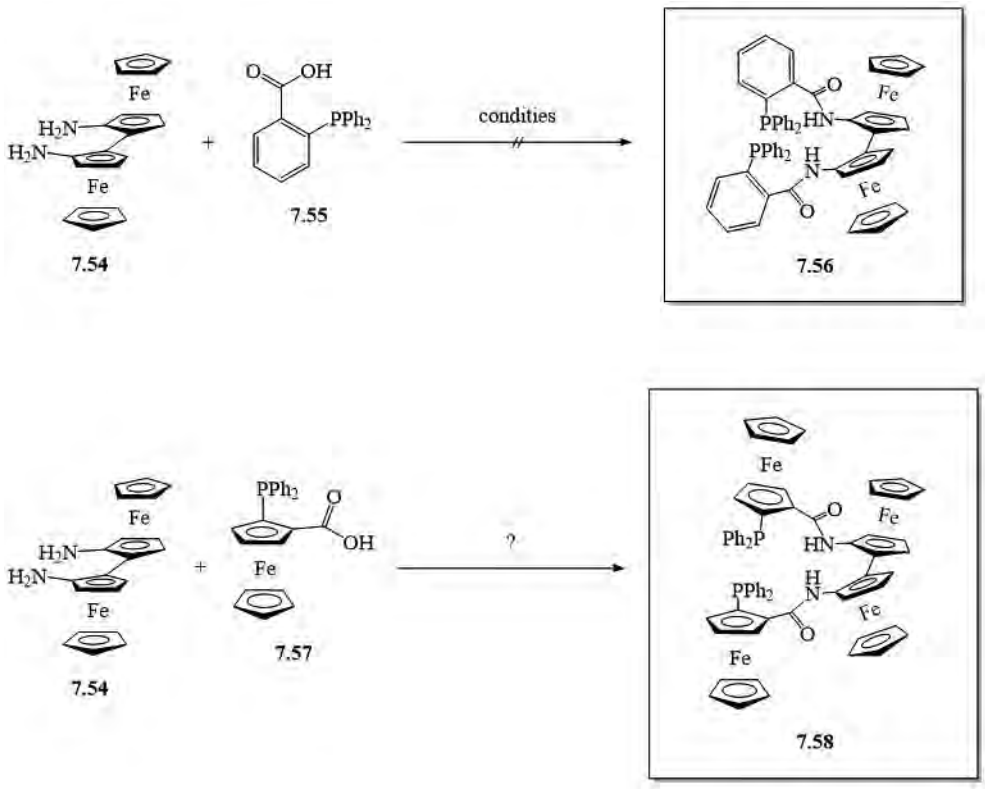

Schema 7.7 Nieuwe voorgestelde Trost liganden **7.56** en **7.58** uitgaande van biferroceen diamine **7.54**

De syntheseprocedure voor **7.57** werd wel reeds beschreven door de onderzoeksgroep van Zhang en wordt voorgesteld in Schema 7.8.[13] Deze procedure maakt eveneens gebruik van de methodologie van het chirale oxazoline. Planair-chiraal ferrocenyl oxazoline **7.59** werd op gelijkaardige wijze bekomen als zijn enantiomere vorm **7.33** (Schema 7.4, *vide supra*). De eerste stap, voorgesteld in Schema 7.8 bestaat uit het invoeren van de diphenylphoshino groep via diastereoselectieve *ortho*-lithiëring, gevolgd door toevoegen van chlorodiphenylphosphine als electrofiel. Op deze manier kon de planair-chirale ferroceen component **7.60** bekomen worden met een rendement van 61%. De drie-staps transformatie van oxazoline **7.60** in het overeenkomstige carbonzuur **7.57**, zoals beschreven door Zhang kon echter niet gereproduceerd worden. Een alternatieve procedure, bestaande uit de lithium-halogeen uitwisseling van jood carbonzuur **7.35** met twee equivalenten *n*-BuLi, gevolgd door afvangen van het reactiemengsel met chlorodiphenylphosphine, voor het bekomen van het planair-chirale enantiomeer van **7.57**, was eveneens niet succesvol. Bijgevolg kon ook het beoogde biferroceen-gebaseerde Trost ligand **7.58** (of het diastereomeer) niet bekomen worden.

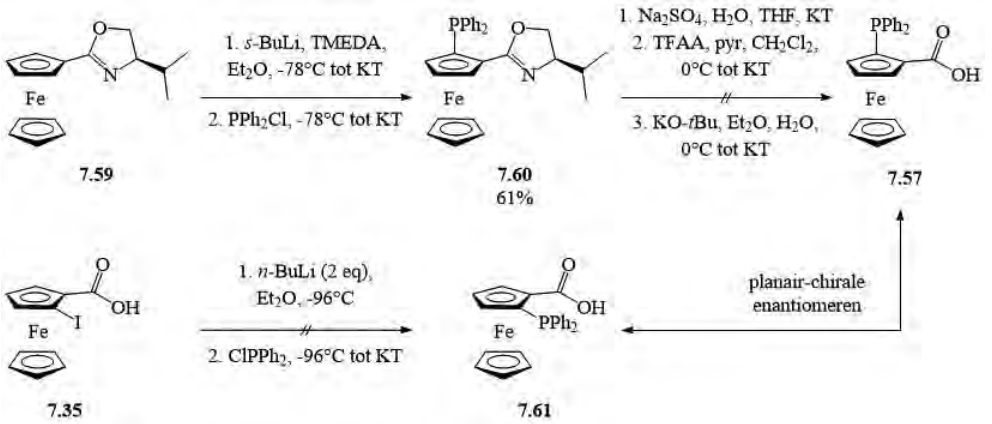

Schema 7.8 Synthese van het planair-chiraal diphenyl phosphinocarbonzuur **7.57** volgens de procedure van Zhang[13] en de alternatieve synthese van het planair-chiraal enantiomeer **7.61** via lithium-halogeen uitwisseling uitgaande van **7.35**

7.1. Referenties

[1] (a) A. H. M. de Vries, A. Meetsma, B. L. Feringa, *Angew. Chem. Int. Ed.*, **1996**, *35*, 2374-2376; (b) M. van den Berg, R. M. Haak, A. J. Minnaard, A. H. M. de Vries, J. G. de Vries, B. L. Feringa, *Adv. Synth. Catal.*, **2002**, *344*, 1003-1007; (c) A. J. Minnaard, B. L. Feringa, L. Lefort, J. G. De Vries, *Acc. Chem. Res.*, **2007**, *40*, 1267-1277; (d) J. F. Teichert, B. L. Feringa, *Angew. Chem. Int. Ed.*, **2010**, *49*, 2486-2528

[2] (a) O. Riant, O. Samuel, H.B. Kagan, *J. Am. Chem. Soc.*, **1993**, *115*, 5835-5836; (b) O. Riant, O. Samuel. T. Flessner, S. Taudine, H.B. Kagan, *J. Org. Chem.*, **1997**, *62*, 6733-6745

[3] S. Zhang, D. Zhang, L. S. Liebeskind, *J. Org. Chem.*, **1997**, *62*, 2312-2313

[4] (a) E. Keller, J. Maurer, R. Naasz, T. Schader, A. Meetsma, B. L. Feringa, *Tetrahedron: Asymmetry*, **1998**, *9*, 2409-2413; (b) Y. Fu, J.-H. Xie, A.-G. Hu, H. Zhou, L.-X. Wang, Q.-L. Zhou, *Chem. Commun.*, **2002**, 480-481; (c) A.-G. Hu, Y. Fu, J.-H. Xie, H. Zhou, L.-X. Wang, Q.-L. Zhou, *Angew. Chem. Int. Ed.*, **2002**, *41*, 2348-2350

[5] (a) S. F. Zhu, J. B. Xie, Y. Z. Zhang, S. Li, Q. L. Zhou, *J. Am. Chem. Soc.*, **2006**, *128*, 12886-12891; (b) S. Zhou, S. Fleisscher, K. Junge, S. Das, D. Addis, M. Beller, *Angew. Chem. Int. Ed.*, **2010**, 49, 8121-8125

[6] B.-M. Fan, J.-H. Xie, S. Li, Y.-Q. Tu, Q.-L. Zhou, *Adv. Synth. Catal.*, **2005**, *347*, 759-762

[7] (a) B. M. Trost, S. M. Silverman, J. P. Stambuli, *J. Am. Chem. Soc.*, **2007**, *129*, 12398-12399; (b) B. M. Trost, D. A. Bringley, S. M. Silverman, *J. Am. Chem. Soc.*, **2011**, *133*, 7664-7667

[8] (a) M. T. Reetz, H. Oka, R. Goddard, *Synthesis*, **2003**, 1809-1814; (b) M. J. Bravo, R. M. Ceder, A. Grabulosa, G. Muller, M. Rocamora, J. C. Bayón, *Organometallics*, **2015**, *34*, 3799-3808; (c) K. N. Gavrilov, A. A. Shiryaev, S. V. Zheglov, V. K. Gavrilov, N. N. Groshkin, M. G. Maksimova, A. N. Volov, I. A. Zamiltskov, *Tetrahedron*, **2014**, *70*, 616-624; (d) B. M. Trost, T. M. Lam, *J. Am. Chem. Soc.*, **2012**, *134*, 11319-11321; (e) M. Schmitkamp, W. Leitner, G. Franciò, *Catal. Sci. Technol.*, **2013**, *3*, 589-594; and references therein

[9] (a) C. J. Richards, T. Damaldis, D. E. Hibbs, M. B. Hursthouse, *Synlett*., **1995**, 74-76; (b) C. J. Richards, A. W. Mulvaney, *Tetrahedron Asymmetry*, **1996**, *7*, 1419-1430; (c) T. Sammakia, H. A. Latham, D. R. Schaad, *J. Org. Chem.*, **1995**, 60, 10-11; (d) T. Sammakia, H. A. Latham, *J. Org. Chem.*, **1995**, *60*, 6002-6003; (e) T. Sammakia, H. A. Latham, *J. Org. Chem.*, **1996**, *61*, 1629-1635; (f) Y. Nishibashi, S. Uemura, *Synlett*., **1995**, 79-81; (g) Y. Nishibayashi, K. Segawa, Y. Arikawa, K. Ohe, M. Hidai, S. Uemura, *J. Organomet. Chem.*, **1997**, *545-546*, 381-391

[10] P. C. Reeves, *Org. Synt.*., **1977**, *56*, 28-31

[11] L. Xiao, W. Weissensteiner, K. Mereiter, M. Widhalm, *J. Org. Chem.*, **2002**, *67*, 2206-2214

[12] (a) B. M. Trost, D. L. Van Vranken, *Angew. Chem. Int. Ed. Engl.*, **1992**, *31*, 228-230; (b) B. M. Trost, R.C. Bunt, *Angew. Chem. Int. Ed. Engl*, **1992**, *35*, 99-102; (c) H. Adolfsson, C. Moberg, *Tetrahedron Asymmetry*, **1995**, *6*, 2023-2031; (d) C. W. Lim, S. Lee, *Tetrahedron*, **2000**, *56*, 5131-5136

[13] J. M. Longmire, B. Wang, X.Zhang, *Tetrahedron Lett.*, **2000**, *41*, 5435-5439

APPENDIX I: SAFETY NOTES

All experiments were performed according the general laboratory safety rules and personal protective equipment such as goggles, lab coat and nitrile rubber gloves were always worn in the laboratory. All reactions, work-ups and purifications were performed in a well-ventilated fume hood. A detailed overview for the identification of the hazards of the 50 most dangerous chemicals that were used in this thesis is given below (page 314 – page 318, *vide infra*). This overview of safety aspects includes Hazard (H) an Precautionary (P) statements, Globally Harmonized System (GHS) safety pictograms, signal word and National Fire Protection Association (NFPA) 704 safety square (fire diamond).

The explanation of the Hazard and Precautionary statement numbers and the GHS-symbols is found below the overview of the hazardous chemicals.

The NFPA 704 or Standard System for the identification of the Hazards of Materials for Emergency Response is a labeling system published by the National Fire Protection Association of the United Stades of America. The 'safety square' or 'fire diamond' allows the emergency personnel to quickly and easily identify the risks proposed by hazardous materials. However, it has proven to be usefull for chemists as well because it shows the potential health-, flammability- and reactivity risks of a chemical. The label consists of four diamonds, each of which is color coded and represents a differtent type of hazard. Blue stands for health hazard (left), red for flammability (top), yellow for chemical instability (right) and the white diamond involves special precautions (bottom). Each Diamond (with exception of the white one) contains a number which corresponds to a level of danger. The numbers range from zero to four and the lower the number, the lower the hazard. The white diamond can be empty (in case no special precautions are necessary) but can also contain an abbreviation inidicating some special hazards. An 'empty' NFPA 704 safety diamond and the rating explanation guide are shown below.

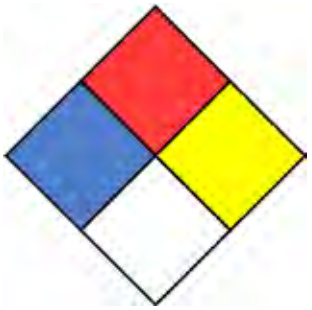

NFPA-rating Symbol	Special Hazard (White)
ALK	Alkaline
ACD	Acidic
COR	Corrosive
OX	Oxidizing
☢	Radioactive
W	Reacts violently or explosive with water
W OX	Reacts violently or explosive with water and oxidizing

NFPA-rating number	Health Hazard (Blue)	Flammability Hazard (Red)	Instability Hazard (Yellow)
4	Can be lethal	Will vaporize and readily burn at normal temperatures	May explode at normal temperatures and pressures
3	Can cause serious or permanent injury	Can be ignited under almost all ambient temperatures	May explode at high temperature or shock
2	Can cause temporary incapacitation or residudal injury	Must be heated or high ambient temperature to burn	Violent chemical change at high temperatures or pressures
1	Can cause significant irriation	Must be preheated before ignition can occur	Normally stable. High temperatures make unstable
0	No Hzard	Will not burn	Stable

Certain chemical reagents and products need to have a little more discussion on safety aspects. The chemicals used in theis research project that are labelled with NFPA rating number 4, 'can be lethal' in the Health Hazard diamond are: $(COCl)_2$, DCC, DPPA, MsCl, $NaClO_2$, NaN_3 and PCl_3. Special attention with respect to safety precautions was paid when handling these chemicals.

The buthyllithium solutions that were used have to be handled carefully according the following procedure:

- Always clamb the reagent bottle to prevent it from moving or falling over.
- Always clamb the receiving vessel to prevent it from moving or falling over.
- Connect the bottle to an inert gas source and keep the needle tip above the liquid level. Ensure that the bottle is not over-pressurized.
- Use a syringe with a tight seal to prevent leakages between the plunger and the syrince body.
- Ensure the needle is firmly attached to the syringe.
- Flush your syringe at least 3 times with inert gas to avoid contact with water
- Pull the plunger gently to draw liquid into the syringe.
- If the desired amount is drawn into the syringe, collect some inert gas to empty any liquid from the needle. (This will avoid the needle dripping when transferring the liquid to the recipient vessel)
- When transferring the liquid into the recipient vessel always hold the needle syringe connection. Transfer the liquid gently into the recipient vessel, preferrably dropwise.
- Clean the needle and syringes with hexane first and 2-propanol second. Afterwards, the syringes can be washed with water and acetone if necessary.
- Fire extinguishers to be used in case of a buthyllithium fire: dry chemical powder.
- Fire extinghuishers unsuitable in case of a buthyllithium fire: water.

In Chapter 4, § 4.5.1, NaN_3 and DPPA were used for the preparation of ferrocenoyl azide **4.40**. Organic azides are potentially explosive substances, sensitive to decomposition with the slightest input of energy from an external source (heat, light, pressure). Therefore the following safety precautions have to be taken into account when working with this class of compounds:

1. Store organic azides at low temperature (-18°C) and protected from light.

- Organic azide waste should be placed in a separate, explicitly-labeled container. Make sure, azide waste cannot come into contact with acids, avoiding formation of highly toxic HN_3.
- The carbon to nitrogen ratio is indicative for the stability of organic azides and the following equation helps to evaluate whether a specific azide is stable to work with or not: A specific azide is safe tho work with if:

$$\frac{N_C + N_O}{N_N} \geq 3$$

with

N_C = number of carbon atoms in the molecule

N_O = number of oxygen atoms in the molecule

N_N = number of nitrogen atoms in the molecule

When this equation is applied for ferrocenoyl azide **4.40** and DPPA with brutoformulas $C_{11}H_8FeIN_3O$ and $C_{12}H_{10}O_3P$ ratio's of respectively 4 and 5 are calculated. Consequently, both azides are safe to work with (on a laboratory scale, up to 20g). Evapaoration of solvent using a rotavapor during work-up and purification was possible when the temperature of the heating bath was kept at 30°C.

The use of NaN_3 involves some safety precautions as well:

- Azide ion as a high toxicity (similar to cyanide ion). Always were the correct gloves when weighing azido salts. (Correct gloves are nitrile rubber gloves. Make sure the gloves are sufficiently thick, use double gloves if necessary).
- NaN_3 reacts violently with common laboratory organics: bronstead acids, heavy metals and their salts, bromine and CS_2.
- Chlorinated solvents are strictly forbidden in combination with NaN_3 due to the formation of very explosive comopounds: CH_2Cl_2 and $CHCl_3$ will result in the formation of di- and tri-azidomehane respectively.
- (Heavy) metals form shock and pressure sensitive compounds with azide anions. Consequently metal spatulas may not be used for weighing.

Chemical	Hazard Statements	Precautionary Statements	GHS Safety Pictograms	Signal word	NFPA 704 Safety Square
α-Acetamidocinnamic acid	315, 319	264, 280, 280, 302 + 352, 305 + 351 + 338, 332 + 313, 337 +313, 362		Warning	
$AlCl_3$	314	260, 280, 301 + 330 +331, 303 + 361 + 353, 305 + 351 + 338 + 310		Danger	
Allyl bromide	225, 301, 314, 318, 340, 351, 400	201, 202, 210, 233, 240, 241, 242, 243, 264, 270, 273, 280, 281, 301 + 310 + 330, 301 + 330 + 331, 303 + 361 + 353, 304 + 340 + 310, 305 + 351 + 338 + 310, 308 + 313, 363, 370 + 378, 391, 403 + 235, 405, 501		Danger	
Benzyl bromide	227, 315, 319, 335	210, 264, 271, 280, 302 + 352, 304 + 340 + 312, 305 + 351 + 338, 332 + 313, 337 +313, 362, 370 + 378, 403 + 233, 403 + 235, 405, 501		Warning	
Binol	301, 315, 319	264, 270, 280, 301 + 310 + 330, 302 + 352, 305 + 351 + 338, 332 + 313, 337 + 313, 362, 405, 501		Danger	

Chemical	Hazard Statements	Precautionary Statements	GHS Safety Pictograms	Signal word	NFPA 704 Safety Square
Boc_2O	226,315, 317, 318, 330, 335	210, 233, 240, 241, 242, 243, 260, 264, 271, 272, 280, 284, 303 + 361 + 353, 304 + 340 + 310, 305 + 351 + 338 + 310, 333 + 313, 362, 370 + 378, 403 + 233, 403 + 235, 405, 501		Danger	
t-BuI	225, 315, 319, 335, 410	210, 233, 240, 241, 242, 243, 261, 264, 271, 273, 280, 303 + 361 + 353, 304 + 340 + 312, 305 + 351 + 338		Danger	
n-BuLi-Solution (1.6 M in hexanes)	225, 250, 261, 304, 314, 318, 336, 361, 373, 411	201, 202, 210, 222, 223, 231 + 232, 233, 240, 241, 242, 243, 260, 264, 271, 273, 280, 281, 301 + 310, 301 + 330 + 331, 302 + 334, 303 + 361 + 353, 304 + 340 + 310, 305 + 351 + 338 + 310, 308 + 313, 335 + 334		Danger	

Chemical	Hazard Statements	Precautionary Statements	GHS Safety Pictograms	Signal word	NFPA 704 Safety Square
s-BuLi-Solution (1.4 M in cyclohexane)	225, 250, 260, 304, 314, 318, 336, 400	210, 222, 223, 231 + 232, 233, 240, 241, 242, 243, 261, 264, 271, 273, 280, 301 + 310, 301 + 330 + 331, 302 + 334, 303 + 361 + 353, 304 + 340 + 310, 305 + 351 + 338 + 310, 335 + 334, 363, 370 + 378, 391, 402 + 404, 403 + 233, 403 + 235, 405, 422		Danger	
t-BuLi-Solution (1.7 M in hexanes)	225, 250, 260, 304, 314, 336, 411	210, 280, 231 + 232, 301 + 310 +331, 301 + 330 + 331, 303 + 361 + 353, 370 + 378 305 + 351 + 338 + 310,		Danger	
CDI	302, 314, 360	201, 202, 260, 264, 270, 280, 301 + 312 + 330, 301 + 330 + 331, 304 + 340 + 310, 305 + 351 + 338 + 310, 308 + 313, 363, 405, 501		Danger	

Chemical	Hazard Statements	Precautionary Statements	GHS Safety Pictograms	Signal word	NFPA 704 Safety Square
CF_3CH_2I	319, 335	261, 264, 271, 280, 280, 302 + 352, 304 + 340 + 312, 305 + 351 + 338, 332 + 313, 337 + 313, 362, 403 + 233, 405, 501		Warning	
CF_3I	280, 341	201, 202, 280, 308 + 313, 405, 410, 403, 501		Warning	
$CHCl_3$	302, 315, 319, 331, 351, 361d, 372	302 + 352, 304 + 340, 305 + 351 + 338, 308 + 310		Danger	
CH_3CO_3H	226, 242, 271, 290, 314, 400	210, 220, 221, 233, 234, 240, 241, 242, 243, 264, 273, 280, 283, 301 + 330 + 331, 303 + 361 + 353, 304 + 340 + 310, 305 + 351 + 338 + 310, 306 + 360, 363, 370 + 378, 371 + 380 + 375, 390, 391, 405, 406, 410, 411 + 235, 420, 501		Danger	
2-chlorobenzoyl chloride	314, 335	280, 301 + 330 + 331, 303 + 361 + 353, 305 + 351 + 338 + 310		Danger	

Chemical	Hazard Statements	Precautionary Statements	GHS Safety Pictograms	Signal word	NFPA 704 Safety Square
$(COCl)_2$	225, 260, 314, 331, 335	210, 231 + 232, 280, 303 + 361 + 353, 304 + 340 + 310, 305 + 351 + 338		Danger	
*m*CPBA	242, 271, 315, 317, 319, 335	210, 220, 221, 234, 261, 264, 271, 272, 280, 283, 302 + 352, 304 + 340, 305 + 351 + 338, 306 + 360 312, 321, 333 + 313, 362, 370 + 378, 371 + 380 + 375, 403 + 233, 405, 410, 411 + 235, 420, 501		Danger	
CuTC	411	273, 391, 501		None	
DCC	302, 311, 317, 318	261, 264, 270, 272, 280, 301 + 312 + 330, 302 + 352 + 312, 305 + 351 + 338 + 310, 333 + 313, 362, 405, 501		Danger	
DCE	225, 302, 304, 315, 319, 331, 335, 350	202, 210, 301 + 312, 303 + 361 + 353, 305 + 351 + 338, 308 + 313		Danger	

Chemical	Hazard Statements	Precautionary Statements	GHS Safety Pictograms	Signal word	NFPA 704 Safety Square
$ClPPh_2$	290, 302, 314, 412	234, 264, 270, 273, 280, 301 + 312 + 330, 301 + 361 + 353, 304 + 340 + 310, 305 + 351 + 338 + 310, 363, 390, 405, 406, 501		Danger	
DMAP	301, 310, 315, 319, 335	261, 262, 264, 270, 271, 280, 301 + 310 + 330, 302 + 350 + 310, 302 + 352, 304 + 340 + 312, 305 + 351 + 338, 332 + 313, 337 + 313, 362, 403 + 233, 405, 501		Danger	
DMF	226, 312 + 332, 319, 360D	201, 280, 305 + 351 + 338, 308 + 313		Danger	
diiodoethane	315, 319, 335	302 + 352, 305 + 351 + 338		Warning	
DIPEA	225, 302, 318, 331, 335	210, 301 + 312 + 330, 304 + 340 + 311, 305 + 351 + 338 + 310		Danger	

Chemical	Hazard Statements	Precautionary Statements	GHS Safety Pictograms	Signal word	NFPA 704 Safety Square
DPPA	301 + 311 + 331, 315, 319, 335	280, 301 + 310 + 330, 302 + 352 + 312, 304 + 340 + 311, 305 + 351 + 338		Danger	
EDCI	302, 311, 315, 317, 318, 373, 410	260, 264, 270, 272, 273, 280, 301 + 312 + 330, 302 + 352 + 312, 305 + 351 + 338 + 310, 314, 333 + 313, 362, 391, 405, 501		Danger	
Ethyl dichloro-phosphite	225, 314	210, 280, 305 + 351 + 338, 310		Danger	
Et_3N	225, 302, 311 + 331 314, 335	210, 280, 301 + 330 + 331, 303 + 361 + 353, 304 + 340 + 311, 305 + 351 + 338 + 310		Danger	
$Fe(acac)_3$	302, 319	264, 270, 280, 301 + 312 + 330, 305 + 351 + 338, 337 + 313, 501		Warning	

Chemical	Hazard Statements	Precautionary Statements	GHS Safety Pictograms	Signal word	NFPA 704 Safety Square
H_2	220, 280	210, 381, 410 + 403		Danger	
HBTU	315, 317, 319, 334, 335	261, 264, 271, 272, 280, 285, 302 + 352, 304 + 340 + 312, 305 + 351 + 338, 333 + 313, 337+ 313, 342 + 311, 362, 403 + 233, 405, 501		Danger	
H_2O_2	302, 314, 335, 401, 412	261, 264, 270, 271, 273, 280, 301 + 312 + 330, 301 + 330 + 331, 304 + 340 + 310, 305 + 351 + 338 + 310, 363, 403 +233, 405, 501		Danger	
HOBT.H_2O	228, 319, 412	210, 240, 241, 264, 273, 280, 305 + 351 + 338, 337 + 313, 370 + 378, 501		Warning	
i-PrI	226, 302	210, 233, 240, 243, 261, 264, 271, 280, 403 + 233		Warning	

Chemical	Hazard Statements	Precautionary Statements	GHS Safety Pictograms	Signal word	NFPA 704 Safety Square
KOH	290, 302, 314, 402	234, 260, 264, 270, 273, 280, 301 + 312 + 330, 301 + 330 + 331, 303 + 361 + 353, 304 + 340 + 310, 305 + 351 + 338 + 310, 363, 390, 405, 406, 501		Danger	
KO*t*-Bu	228, 260, 314	210, 231+ 232, 260, 280, 303 + 361 + 353, 305 + 351 + 338		Danger	
MeI	226, 301 + 331, 312, 315, 319, 335, 351, 410	201, 210, 273, 280, 301 + 310 + 330, 302 + 352 + 312,		Danger	
MeOTf	226, 314	260, 280, 301 + 330 + 331 + 310, 303 + 361 + 353 + 310 + 363, 304 + 340 + 310, 305 + 351 + 338 + 310		Danger	
Methyl dichloro-phosphite	226, 314, 335	261, 280, 310 305 + 351 + 338		Danger	

Chemical	Hazard Statements	Precautionary Statements	GHS Safety Pictograms	Signal word	NFPA 704 Safety Square
MsCl	301 + 311, 314, 317, 330, 335	280, 301 + 310 + 330, 301 + 330 + 331, 304 + 340 + 310, 305 + 351 + 338		Danger	
$NaBH_3CN$	228, 314, 410, 300 + 310 + 330	210, 260, 280, 303 + 361 + 353, 304 + 340 + 310, 305 + 351 338		Danger	
$NaClO_2$	271, 301, 310, 314, 373, 410	210, 260, 280, 301 + 310 + 330, 303 + 361 + 353, 305 + 351 + 338		Danger	
NaH	228, 260, 290, 314	210, 231 + 232, 260, 280, 303 + 361 + 353, 305 + 351 + 338 + 310		Danger	

Chemical	Hazard Statements	Precautionary Statements	GHS Safety Pictograms	Signal word	NFPA 704 Safety Square
NaN_3	300 + 310 + 330, 373, 410	262, 273, 280, 301 + 310 + 330, 302 + 352 +310, 304 + 340 + 310		Danger	
NMP	315, 319, 335, 360FD	201, 202, 261, 302 + 352, 305 + 351 + 338		Danger	
PCl_3	300, 314, 331, 373	260, 280, 314 303 + 361 + 353, 304 + 340 + 310, 305 + 351 + 338		Danger	
$[Rh(COD)_2]BF_4$	228, 314	210, 280, 305 + 351 + 338, 310		Danger	
TFA	225, 302, 315, 319	210, 301 + 312 + 330, 302 + 352, 305 + 351 + 338		Danger	
TFAA	314, 332, 412	261, 264, 271, 273, 280, 301 + 330 + 331, 303 + 361 + 353, 304 + 340 + 310, 305 + 351 + 338 + 310, 363, 405, 501		Danger	

Chemical	Hazard Statements	Precautionary Statements	GHS Safety Pictograms	Signal word	NFPA 704 Safety Square
TMEDA	225, 302 + 332 314	210, 280, 301 + 330 + 331, 303 + 361 + 353, 304 + 340 + 312, 305 + 351 + 338		Danger	
Toluene	225, 361d, 304, 373, 315, 316	210, 243, 280, 260, 202, 301 + 310, 331, 308 + 313, 303 + 361 + 353, 304 + 340		Danger	
$ZrCl_4$	314	234, 260, 264, 280, 301 + 330 + 331, 303 + 361 + 353, 304 + 340, 305 + 351 + 338, 310, 321, 363, 390, 405, 406, 501		Danger	

The EU-GHS Hazard Statements

H200	Unstable explosives.
H201	Explosive; mass explosion hazard.
H202	Explosive, severe projection hazard.
H203	Explosive; fire, blast or projection hazard.
H204	Fire or projection hazard.
H205	May mass explode in fire.
H220	Extremely flammable gas.
H221	Flammable gas.
H222	Extremely flammable aerosol.
H223	Flammable aerosol.
H224	Extremely flammable liquid and vapour.
H225	Highly flammable liquid and vapour.
H226	Flammable liquid and vapour.
H228	Flammable solid.
H229	Pressurised container: May burst if heated.
H230	May react explosively even in the absence of air.
H231	May react explosively even in the absence of air at elevated pressure and/or temperature.
H240	Heating may cause an explosion.
H241	Heating may cause a fire or explosion.
H242	Heating may cause a fire.
H250	Catches fire spontaneously if exposed to air.
H251	Self-heating: may catch fire.
H252	Self-heating in large quantities; may catch fire.
H260	In contact with water releases flammable gases which may ignite spontaneously.
H261	In contact with water releases flammable gases.
H270	May cause or intensify fire; oxidizer.

H271	May cause fire or explosion; strong oxidizer.
H272	May intensify fire; oxidizer.
H280	Contains gas under pressure; may explode if heated.
H281	Contains refrigerated gas; may cause cryogenic burns or injury.
H290	May be corrosive to metals.
H300	Fatal if swallowed.
H301	Toxic if swallowed.
H302	Harmful if swallowed.
H304	May be fatal if swallowed and enters airways.
H310	Fatal in contact with skin.
H311	Toxic in contact with skin.
H312	Harmful in contact with skin.
H314	Causes severe skin burns and eye damage.
H315	Causes skin irritation.
H317	May cause an allergic skin reaction.
H318	Causes serious eye damage.
H319	Causes serious eye irritation.
H330	Fatal if inhaled.
H331	Toxic if inhaled.
H332	Harmful if inhaled.
H334	May cause allergy or asthma symptoms or breathing difficulties if inhaled.
H335	May cause respiratory irritation.
H336	May cause drowsiness or dizziness.
H340	May cause genetic defects *<state route of exposure if it is conclusively proven that no other routes of exposure cause the hazard>*.
H341	Suspected of causing genetic defects *<state route of exposure if it is conclusively proven that no other routes of exposure cause the hazard>*.

H350	May cause cancer *<state route of exposure if it is conclusively proven that no other routes of exposure cause the hazard>.*
H351	Suspected of causing cancer *<state route of exposure if it is conclusively proven that no other routs of exposure cause the hazard>.*
H360	May damage fertility or the unborn child *<state specific effect if known > <state route of exposure if it is conclusively proven that no other routes of exposure cause the hazard>.*
H361	Suspected of damaging fertility or the unborn child *<state specific effect if known> <state route of exposure if it is conclusively proven that no other routes of exposure cause the hazard>.*
H362	May cause harm to breast-fed children.
H370	Causes damage to organs *<or state all organs affected, if known> <state route of exposure if it is conclusively proven that no other routes of exposure cause the hazard>.*
H371	May cause damage to organs *<or state all organs affected, if known> <state route of exposure if it is conclusively proven that no other routes of exposure cause the hazard>.*
H372	Causes damage to organs *<or state all organs affected, if known>* through prolonged or repeated exposure *<state route of exposure if it is conclusively proven that no other routes of exposure cause the hazard>.*
H373	May cause damage to organs *<or state all organs affected, if known>* through prolonged or repeated exposure *<state route of exposure if it is conclusively proven that no other routes of exposure cause the hazard>.*
H300 + H310	Fatal if swallowed or in contact with skin.
H300 + H330	Fatal if swallowed or if inhaled.
H310 + H330	Fatal in contact with skin or if inhaled.
H300 + H310 + H330	Fatal if swallowed, in contact with skin or if inhaled.
H301 + H311	Toxic if swallowed or in contact with skin.
H301 + H331	Toxic if swallowed or if inhaled.
H311 + H331	Toxic in contact with skin or if inhaled.
H301 + H311 + H331	Toxic if swallowed, in contact with skin or if inhaled.

H302 + H312	Harmful if swallowed or in contact with skin.
H302 + H332	Harmful if swallowed or if inhaled.
H312 + H332	Harmful in contact with skin or if inhaled.
H302 + H312 + H332	Harmful if swallowed, in contact with skin or if inhaled.
H400	Very toxic to aquatic life.
H410	Very toxic to aquatic life with long lasting effects.
H411	Toxic to aquatic life with long lasting effects.
H412	Harmful to aquatic life with long lasting effects.
H413	May cause long lasting harmful effects to aquatic life.
H420	Harms public health and the environment by destroying ozone in the upper atmosphere.

The EU-GHS Precautionary Statements

P101	If medical advice is needed, have product container or label at hand.
P102	Keep out of reach of children.
P103	Read label before use.
P201	Obtain special instructions before use.
P202	Do not handle until all safety precautions have been read and understood.
P210	Keep away from heat, hot surfaces, sparks, open flames and other ignition sources. No smoking.
P211	Do not spray on an open flame or other ignition source.
P220	Keep/Store away from clothing/…/combustible materials.
P221	Take any precaution to avoid mixing with combustibles…
P222	Do not allow contact with air.
P223	Do not allow contact with water.
P230	Keep wetted with…

P231	Handle under inert gas.
P232	Protect from moisture.
P233	Keep container tightly closed.
P234	Keep only in original container.
P235	Keep cool.
P240	Ground/bond container and receiving equipment.
P241	Use explosion-proof electrical/ventilating/lighting/…/ equipment.
P242	Use only non-sparking tools.
P243	Take precautionary measures against static discharge.
P244	Keep valves and fittings free from oil and grease.
P250	Do not subject to grinding/shock/…/friction.
P251	Do not pierce or burn, aven after use.
P260	Do not breathe dust/fume/gas/mist/vapours/spray.
P261	Avoid breathing dust/fume/gas/mist/vapours/spray.
P262	Do not get in eyes, on skin, or on clothing.
P263	Avoid contact during pregnancy/while nursing.
P264	Wash … thoroughly after handling.
P270	Do no eat, drink or smoke when using this product.
P271	Use only outdoors or in a well-ventilated area.
P272	Contaminated work clothing should not be allowed out of the workplace.
P273	Avoid release to the environment.
P280	Wear protective gloves/protective clothing/eye protection/ face protection.
P282	Wear cold insulating gloves/face shield/eye protection.
P283	Wear fire/flame resistant/retardant clothing.
P284	[In case of inadequate ventilation] wear respiratory protection.
P231+ P232	Handle under inert gas. Protect from moisture.

P235+ P410	Keep cool. Protect from sunlight.
P301	IF SWALLOWED:
P302	IF ON SKIN:
P303	IF ON SKIN (or hair):
P304	IF INHALED:
P305	IF IN EYES:
P306	IF ON CLOTHING:
P308	IF exposed or concerned:
P310	Immediately call a POISON CENTER/doctor/…
P311	Call a POISON CENTER/doctor/….
P312	Call a POISON CENTER/doctor/…/ if you feel unwell.
P313	Get medical advice/attention.
P314	Get medical advice/attention if you feel unwell.
P315	Get immediate medical advice/attention.
P320	Specific treatment is urgent (see … on this label).
P321	Specific treatment (see … on this label).
P330	Rinse mouth.
P331	Do NOT induce vomiting.
P332	If skin irritation occurs:
P333	If skin irritation or rash occurs:
P334	Immerse in cool water/wrap in wet bandages.
P335	Brush off loose particles from skin.
P336	Thaw frosted parts with lukewarm water. Do no rub affected area.
P337	If eye irritation persists:
P338	Remove contact lenses, if present and easy to do. Continue rinsing.
P340	Remove person to fresh air and keep comfortable for breathing.

P342	If experiencing respiratory symptoms:
P351	Rinse cautiously with water for several minutes.
P352	Wash with plenty of water/…
P353	Rinse skin with water/shower.
P360	Rinse immediately contaminated clothing and skin with plenty of water before removing clothes.
P361	Take off immediately all contaminated clothing.
P362	Take off contaminated clothing.
P363	Wash contaminated clothing before reuse.
P364	And wash it before reuse.
P370	In case of fire:
P371	In case of major fire and large quantities:
P372	Explosion risk in case of fire.
P373	DO NOT fight fire when fire reaches explosives.
P374	Fight fire with normal precautions from a reasonable distance.
P375	Fight fire remotely due to the risk of explosion.
P376	Stop leak if safe to do so.
P377	Leaking gas fire: Do not extinguish, unless leak can be stopped safely.
P378	Use … to extinguish.
P380	Evacuate area.
P381	Eliminate all ignition sources if safe to do so.
P390	Absorb spillage to prevent material damage.
P391	Collect spillage.
P301 + P310	IF SWALLOWED: Immediately call a POISON CENTER/doctor/….
P301 + P312	IF SWALLOWED: Call a POISON CENTER/ doctor/…/ if you feel unwell.
P301 + P330 + P331	IF SWALLOWED: rinse mouth. Do NOT induce vomiting.

P302 + P334	IF ON SKIN: Immerse in cool water/wrap in wet bandages.
P302 + P352	IF ON SKIN: Wash with plenty of water/…
P303 + P361 + P353	IF ON SKIN (or hair): Take off immediately all contaminated clothing. Rinse skin with water/shower.
P304 + P340	IF INHALED: Remove person to fresh air and keep comfortable for breathing.
P305 + P351 + P338	IF IN EYES: Rinse cautiously with water for several minuts. Remove contact lenses, if present and easy to do. Continue rinsing.
P306 + P360	IF ON CLOTHING: rinse immediately contaminated clothing and skin with plenty of water before removing clothes.
P308 + P311	IF exposed or concerned: Call a POISON CENTER/doctor/…
P308 + P313	IF exposed or concerned: Get medical advice/attention.
P332 + P313	If skin irritation occurs: Get medical advice/attention.
P333 + P313	If skin irritation or rash occurs: Get medical advice/attention.
P335 + P334	Brush off loose particles from skin. Immerse in cool water/ wrap in wet bandages.
P337 + P313	If eye irritation persists: Get medical advice/attention.
P342 + P311	If experiencing respiratory symptoms: Call a POISON CENTER/doctor/…
P361 +P364	Take off immediately all contaminated clothing and wash it before reuse.
P362+ P364	Take off contaminated clothing and wash it before reuse.
P370 + P376	In case of fire: Stop leak if safe to do so.
P370 + P378	In case of fire: Use … to extinguish.
P370 + P380	In case of fire: Evacuate area.
P370 + P380 + P375	In case of fire: Evacuate area. Fight fire remotely due to the risk of explosion.
P371 + P380 + P375	In case of major fire and large quantities: Evacuate area. Fight fire remotely due to the risk of explosion.
P401	Store …
P402	Store in a dry place.

P403	Store in a well-ventilated place.
P404	Store in a closed container.
P405	Store locked up.
P406	Store in corrosive resistant/… container with a resistant inner liner.
P407	Maintain air gap between stacks/pallets.
P410	Protect from sunlight.
P411	Store at temperatures not exceeding …°C/…°F.
P412	Do not expose to temperatures exceeding 50°C/ 122°F.
P413	Store bulk masses greater than … kg/… lbs at temperatures not exceeding …°C/…°F.
P420	Store aways from other materials.
P422	Store contents under …
P402 + P404	Store in a dry place. Store in a closed container.
P403 + P233	Store in a well-ventilated place. Keep container tightly closed.
P403 + P235	Store in a well-ventilated place. Keep cool.
P410 + P403	Protect from sunlight. Store in a well-ventilated place.
P410 + P412	Protect from sunlight. Do not expose to temperatures exceeding 50°C/ 122°F.
P411 + P235	Store at temperatures not exceeding …°C/…°F. Keep cool.
P501	Dispose of contents/container to …
P502	Refer to manufacturer/supplier for information on recovery/ recycling.

The GHS Symbols

GHS Symbol	Explanations GHS symbol
	Explosives: substances and preparations which may explode (very fast combustion, even without the participation of oxygen.
	Flammables: collective term for different categories of flammable chemicals (gas, aerosol, liquid, vapor and solid).
	Oxidizers: substances and mixtures which, in contact with other substances and/or mixtures (especially flammable substances), can cause or contribute to fire.
	Gasses under pressure: this group comprises compressed gases, liquefied gases, refrigerated liquefied gases and dissolved gases.
	Corrosives: substances that are corrosive to metals and skins, as well as substances that can cause eye damage
	Acute toxicity: substances and mixtures which, even in low quantities, may cause harm or death within a few hours or a day if inhaled or absorbed via the mouth or skin.
	Irritants/Sensitizers/Other Hazards: substances and mixtures which, in direct prolonged or repeated contact with the skin or mucous membranes, can cause inflammation. This group also comprises narcotic and skin-sensitising substances. These are substances which, absorbed through the skin, may give rise to such a reaction of hypersensitisation (hypersensitivity) that subsequent exposure to the substance or preparation will cause characteristic adverse effects.
	Long-term health Hazards: this includes carcinogenic, mutagenic and reprotoxic substances which may cause cancer, give rise to hereditary genetic disorders or have an effect on the fertility of men and/or women or which harm the unborn child (signal word Danger) or which are suspected of having such effects (signal word Warning). This group also includes respiratory sensitizers, substances with aspiration hazard and substances with specific target organ toxicity.
	Environmental Hazard: substances that present or may present immediate or delayed danger to animals and/or nature.

WIM KIMPE

In 2007, Wim decided to study chemistry at the faculty of Sciences at the University of Ghent. Five years later obtained his degree as *Master of Science in Chemistry*. In January 2013 he started a PhD under the supervision of Professor Dr. Johan Van der Eycken. In his research he designed, synthesized and tested novel chiral biferrocene-based ligands for asymmetric transition metal catalysis. In September 2015 Wim temporarily left the university of Ghent to spent eight months at the research group of Professor Dr. Patrick Guiry at University College Dublin (Ireland), where he worked on the same research topics. After this short-term exchange Wim came back to Ghent to finish his PhD-project. After his PhD, he started working as a research scientist at Ecosynth where he is involved with continuous flow chemistry projects.

GHENT
UNIVERSITY